


# University of Oxford

# A transcriptomic and electrophysiological characterisation of the rat stellate ganglia in health and disease

**Harvey Davis**

**Green Templeton college**

**Thesis submitted for the degree of Doctor of Philosophy (DPhil) in Ion channels and disease**

**Supervisors: Professor David Paterson and Associate Professor Neil Herring**

**Hilary term**

**2021**

# Abstract

Hypertension represents a major health burden in both the developed and developing world. A significant component of hypertension is abnormal activation of the sympathetic nervous system, which is associated with a wide spectrum of serious co-morbidities. However, the molecular mechanisms behind this are poorly understood, as are the biophysical properties underlying heightened cardiac sympathetic activity in the prehypertensive state. This thesis utilised large-scale transcriptomics, combined with patch-clamp electrophysiology and live-cell imaging to investigate the molecular mechanisms behind the sympathetic hyperactivity observed in hypertension.

**Chapter 1** introduces the sympathetic nervous system in the context of arterial blood pressure control. This chapter also introduces hypertension, the contemporary pharmacopeia of hypertensive treatments and sympathetic dysfunction in hypertension. Finally, ion channel biophysics is covered here to enable further discussion.

**Chapter 2** explains the methodologies used in the following data chapters. Particular focus is given to whole-cell and perforated patch-clamp electrophysiology which feature heavily throughout this thesis. The results provided a target discovery framework for subsequent chapters.

**Chapter 3** provides single-cell and bulk RNA-sequencing datasets describing the transcriptomic profile of the cardiac innervating stellate ganglia from normotensive and spontaneously hypertensive rats. This chapter also discusses the methodology behind RNA-sequencing analysis.

**Chapter 4**, with supporting data from chapter 3, highlighted a downregulation in M-current subunit encoding *KCNQ5* in stellate ganglia neurons from prehypertensive rats. This chapter demonstrated that the decrease in KCNQ5 transcript expression led to a functional decrease in M-Current, with the conclusion that it is likely to cause the electrical hyperactivity observed in prehypertensive stellate ganglia neurons. Further, these data suggested that selective inhibition of several $Na_V$ subunits was sufficient to restore a normotensive electrical phenotype in prehypertensive neurons.

**Chapter 5** demonstrated that sympathetic stellate ganglia neurons could sense $Na^+$ with a similar potency to central sodium sensing regions in the brain. This argued that this may have important implications for the correlation between $Na^+$ sensitivity and blood pressure control.

**Chapter 6** investigated the ability for sympathetic stellate ganglia neurons to respond to sensory signals via transient receptor potential channels or via G-protein coupled receptors. These data revealed functional TRPV2 signalling in stellate ganglia neurons, although they did not produce robust responses to any of the inflammatory transmitters. Finally, this chapter investigated the ability for cardiomyocytes to communicate with sympathetic neurons via retrograde signalling. This study identified that prehypertensive neurons co-cultured with normotensive cardiomyocytes exhibited a phenotype similar to that in normotensive neurons.

**Chapter 7** is a concluding discussion which places these results into a physiological context and suggests new molecular and intercellular mechanisms for the targeting of the stellate ganglia neurons in states of sympathetic dysautonomia.

# Acknowledgements

I would like to thank the Wellcome Trust OXION programme and the University of Oxford Medical Sciences Doctoral Training Centre for funding my DPhil, and Professor Stephen Tucker for constant support and career advice during my time with OXION. Additionally, I would like to thank members of the wider OXION community for providing me with technical advice and pointing me in the right direction with my work. In particular, I would like to thank Dr. Michael Puljing, Samuel Usher, Dr. Linus Conrad, Associate Professor Paolo Tammaro, Dr. Kathryn Acheson, Associate Professor Maike Glitsch and Professor Anant Parekh.

To Professor David Paterson, I want to thank you for putting your faith in me. For allowing me to explore my interests and for constantly challenging my assumptions and scientific outlook. I believe my time with your group has been a formative experience, and that I am indebted to you for your constant advice within and outside of science. I am grateful for your constant patience as I have discovered who I am as a scientist and as an individual, and for supporting the various directions that I have taken throughout my time working in your laboratory. The small advances made within this thesis wouldn't have been possible without your open-minded approach to new technology and theories, and your encouragement to pursue new angles of research.

To Associate Professor Neil Herring, thank you for your constant scientific guidance and for encouraging me to assess problems from a clinical perspective as well as a scientific one. Your ability to digest problems from both your clinical background but also your strong fundamental understanding of science was invaluable throughout my DPhil and has undoubtedly changed my perspective of how science should be conducted. Your persistent encouragement, honesty and faith has made my DPhil a more enjoyable experience and I am grateful for the enthusiasm you have shown for my projects throughout.

To both Professor David Paterson and Associate Professor Neil Herring, I would like to thank you for leading by example and showing me that a strong work ethic and an inquisitive mind is the key to success in life. Thank you for sharing your hard-earned experience with me, and for teaching me in a collaborative and welcoming partnership between your research groups. Thank you both for always making the time to meet with me, often on short notice, throughout my DPhil and for the lively discussions and debates on scientific problems. Last, but certainly not least you have both shown me a kinder approach to science, away from the confrontation and competition that is often seen as a hallmark of the modern scientist. I have enjoyed my time in your groups and wish you both the best for your future endeavours.

Thank you to members of the Paterson and Herring groups for being friends and colleagues during my DPhil. Thank you to Oliver Neely, Dr. Dan Li, Dr. Kun Lui, Dr. Perry Green, Dr. Nikita Ved and Dr. Thomas Gibbs for your constant support and friendship over the past four years. Even if for many of you this involved a few too many after work beers. To all of you, I appreciate all the help you have given me in various forms over the course of my DPhil and I hope we stay in touch in the future. Thank you to my FHS student Ayesha, your hard work and inquisitive nature are a credit to you, and I wish you all the best for what I'm sure will be a bright future.

Thank you to my thesis examiners Professor Bennett and Professor Shah for your constructive and fair comments and for taking the time to read my thesis and perform the thesis viva. Thank you both for making it an enjoyable experience. Thank you also to Professor Swietach for the helpful comments in both my transfer and confirmation examinations.

In addition to those made through work, thank you to the various friends I've made over the course of my DPhil, and for making the long days spent in the lab bearable. In particular, thank you to Max, Sam, Brad, Severin, Linus, Luke and Mike. Finally, as always thank you to my friends from before Oxford, especially Tom, Sam, Derek, Kyle, Mark, Carl, Jack and Owen who I appear to be stuck with no matter how far I move away from home. I would also like to thank my parents, for teaching me the value of hard work and for supporting me as I've followed my interests.

. Last but certainly not least, I would like to thank my partner Tonia. You have been my rock throughout my DPhil, and I hope you know how much I appreciate you. Thank you for everything and for making being a supportive and caring person look effortless. Thank you for listening to my problems and ideas, and for encouraging me throughout. Long days in the lab would have been a lot bleaker if I didn't have you to come home to.

**Abstract** 1
**Acknowledgements** 2
**Abbreviations** 8
**Chapter 1: Introduction** 9
**1.1 The sympathetic nervous system** 12
**1.1.1 Sympathetic control of the heart and vasculature** 14
**1.1.2 Sympathetic control of the kidney** 17
**1.1.3 Sympathetic neurotransmission** 19
**1.2 Hypertension** 23
**1.2.1 Hypertension and the sympathetic nervous system** 27
**1.2.2 Animal models of hypertension** 29
**1.3 Neuronal electrophysiology** 33
**1.3.1 The neuron in the basal state** 33
**1.3.2 General properties of voltage-gated ion channels** 35
**1.3.3 Passive neuronal properties** 37
**1.3.4 The neuronal action potential** 39
**1.3.5 Neurotransmitter release** 40
**1.3.6 Neuronal firing properties** 42
**1.4 Ion channel subtypes** 44
**1.4.1 Voltage-gated sodium channels** 45
**1.4.2 Voltage-gated potassium channels** 47
**1.4.2.1 A-type $K_v$ current** 48
**1.4.2.2 Delayed rectifier $K_V$ currents** 49
**1.4.2.3 M-current** 49
**1.4.3 Hyperpolarisation-activated cyclic nucleotide-gated channels** 52
**1.4.4 Voltage-gated $Ca^{2+}$ channels** 54
**1.4.5 Calcium-activated Cl- channels** 56
**1.4.8 $K_{Ca}$ channels** 57
**1.4.9 $K_{Na}$ channels** 59
**1.5 Summary** 60
**Chapter 2: Methods** 62
**2.1 Animal experiments** 63
**2.2 Cell culture** 64
**2.3 Patch clamp electrophysiology** 65
**2.3.1 Perforated patch-clamp theory** 75
**2.3.2 Whole-cell patch clamp electrophysiology – methodology** 76
**2.3.3 Perforated patch clamp electrophysiology – methodology** 77
**2.3.4 Analysis** 78
**2.3.5 Example recordings** 78
**2.4 Live cell $Ca^{2+}$ imaging** 85
**2.4.1 Fura-2 AM methodology** 87
**2.5 Immunohistochemistry** 88
**2.5.1 Immunohistochemistry protocol** 89

2.6 Two-step reverse transcriptase quantitative real-time PCR (RT-qPCR) Statistics 90
2.7 Co-culture 92
2.8 Statistics 94
Chapter 3: Transcriptomics of the stellate ganglia 95
3.1 Introduction 96
3.1.1 Single-cell and bulk RNA-sequencing 96
3.2 Methods 99
3.2.1 Alignment 99
3.2.2 Prefiltering single-cell RNA-sequencing data 99
3.2.3 Clustering 104
3.2.4 Dimensionality reduction 105
3.2.5 Differential expression analysis 107
3.2.6 Gene ontology and KEGG analysis 107
3.2.7 Trajectory inference analysis 108
3.2.8 Single-cell RNA-sequencing 109
3.2.9 Bulk RNA-sequencing 110
3.3 Results 114
3.3.1 Single-cell RNA-sequencing 114
3.3.1.1 Neurons 117
3.3.1.1.1 Neuronal gene expression changes in the SHR 125
3.3.1.1.2 Neuronal gene ontology and KEGG analysis 129
3.3.2 Bulk RNA-sequencing 133
3.3.2.1 Differential expression 133
3.3.2.2 Gene ontology 138
3.4 Discussion 140
3.4.1 The heterogeneity of the stellate ganglia 140
3.4.2 Two populations of sympathetic neurons? 142
3.4.3 Other populations 146
3.4.4 Comparison with Bulk RNA-sequencing 147
3.4.5 Limitations 151
3.4.6 Future work 153
Chapter 4: The role of M-current in the SHR phenotype 156
4.1 Introduction 157
4.2 Methods 159
4.2.1 Patch clamp electrophysiology 159
4.2.2 Single-cell and bulk RNA-sequencing 160
4.2.3 Immunohistochemistry 160
4.2.4 Human tissue 161
4.2.5 RT-qPCR 162
4.2.6 Statistics 162
4.3 Results 162
4.3.1 SHR stellate ganglia neuron phenotype 162
4.3.2 Single-cell RNA-sequencing 169

4.3.3 Confirmation of differential M-current expression and function 166
4.3.4 Phenotypic recapitulation 175
4.3.5 $Na_v$ as alternate targets 180
4.3.6 $Na_v1.8$ in stellate ganglia neurons? 183
4.3.7 Physiological role of $Na_v$ and M-current 185
4.3.8 Other channels 189
4.4 Discussion 195
4.4.1 The phenotype of SHR stellate ganglia neurons 195
4.4.2 M-current as the putative mechanism for SHR hyperexcibitality 196
4.4.3 Evidence for alternate mechanisms of SHR pathology 199
4.4.4 The role of $Na_v$ subunits 201
4.4.5 Stellate ganglia neuron $Na_v1.8$? 204
4.4.6 Other channels in the stellate ganglia neuron 206
4.4.7 The stellate ganglia neuron 211
4.4.8 Do these data fit well with the human phenotype? 213
4.4.9 SNPs in the SHR 213
4.4.10 Study limitations 214
4.4.11 Future work 216
Chapter 5: Sodium sensing in stellate ganglia neurons 217
5.1 Introduction 218
5.1.1 NaCl sensing – Na+ or osmolarity? 218
5.1.2 Central mechanisms of Na+ sensing 219
5.1.3 $Na_x$ - the molecular sodium sensor 222
5.1.4 Renal NaCl response 223
5.1.5 Sympathetic $Na_x$? 225
5.2 Methods 226
5.2.1 Cell-culture and long-term ion adjustments 226
5.2.2 Whole-cell patch-clamp electrophysiology 227
5.2.3 Immunohistochemistry 227
5.2.4 Fura-2 Imaging 228
5.2.5 Statistics 228
5.3 Results 229
5.3.1 NaCl response in sympathetic neurons 229
5.3.2 $Na^+$ dependence 233
5.3.3 $Na_x$ in stellate ganglia neurons 234
5.3.4 Exclusion of other $Na^+$ dependent mechanisms 236
5.3.5 $Ca^{2+}$ independence 241
5.3.6 Transient receptor potential channel independence 242
5.3.7 Osmolarity independence 244
5.3.8 Effects of long term NaCl 248
5.4 Discussion 249
5.4.1 Ganglia-specific effects 253
5.4.2 $Na_x$ as the candidate mechanism 255

5.4.3 The feasibility of a sympathetic $Na^+$ sensor 256
5.4.4 Limitations of $Na_x$ as a $Na^+$ sensor 258
5.4.5 Long-term effect of high NaCl 259
5.4.6 Limitations of pharmacology 260
5.4.7 Future work 261
Chapter 6: Novel signalling pathways 263
6.1 Introduction 264
6.1.1 Transient receptor potential channels 264
6.1.2 Stellate ganglia neuron response to the "inflammatory soup" 266
6.1.3 Glutamatergic receptors 271
6.1.4 The effect of post-synaptic cardiomyocytes upon the neuronal phenotype 273
6.2 Methods 275
6.2.1 Single-cell RNA-sequencing 275
6.2.2 Whole-cell and perforated patch-clamp 275
6.2.3 Calcium imaging 276
6.2.4 siRNA knockdown 276
6.2.5 Immunohistochemistry 277
6.2.6 Co-culture 277
6.3 Results 278
6.3.1 TRP channels 278
6.3.2 Response to the inflammatory soup 292
6.3.3 Is there functional evidence for the glutamatergic receptors? 299
6.3.4 Can cardiomyocytes signal to sympathetic neurons? 302
6.4 Discussion 307
6.4.1 Observations on TRP channels 307
6.4.2 Observations on sensory G-protein coupled receptors 311
6.4.3 Observations on glutamatergic receptors 314
6.4.4 Observations on co-culture 316
6.4.5 Summary 318
Chapter 7: Concluding discussion 319
7.1 Aim 1 320
7.2 Aim 2 325
7.3 Aim 3 327
7.4 Future work and concluding remarks 329
Appendix 330
References 360

# Abbreviations

**$[Ca^{2+}]_i$** Intracellular calcium concentration

**ATP** Adenosine triphosphate

**BK** Large-conductance $K_{Ca}$

**CaCC** Calcium-activated $Cl^-$ channels

**$Ca_v$** Voltage-gated calcium channel

**cAMP** 3',5'-Cyclic adenosine monophosphate

**DNA** Deoxyribonucleic acid

**GPCR** G-protein coupled receptor

**HCN** Hyperpolarisation-activated cyclic nucleotide-gated

**IK** Intermediate conductance $K_{Ca}$

**$K_v$** Voltage-gated potassium channel

**mRNA** messenger RNA

**$Na_v$** Voltage-gated sodium channel

**$[Na^+]_i$** Intracellular sodium concentration

**RMP** Resting membrane potential

**RNA** Ribonucleic acid

**RT-qPCR** Real-time quantitative PCR

**$R_s$** Series resistance

**SCG** Superior cervical ganglia

**ScRNAseq** Single-cell RNA-sequencing

**SGN** Stellate ganglia neuron

**SK** Small conductance $K_{Ca}$

**SNA** sympathetic nerve activity

# CHAPTER 1

## Introduction

Cardiovascular disease is the biggest global killer (Lozano *et al.*, 2012). At a staggering toll of an estimated 17.9 million deaths per year (Roth *et al.*, 2017), there is a desperate clinical need to treat this collection of diseases. Of these deaths over 85% result from heart attacks or stroke, with the primary risk factors including diabetes mellitus, smoking, high blood pressure, blood cholesterol, body weight and patient genetics (Virani *et al.*, 2020). Whilst the majority of these factors are linked to poor lifestyle choices (Beilin *et al.*, 1999), and therefore are most likely to be curbed by an effective public health intervention, high blood pressure (hypertension) presents a more complicated situation since it is a "silent killer" where the patient is often unaware of having the pathology (Zhou *et al.*, 2019).

Hypertension presents as either secondary hypertension, where an identified organ dysfunction, for example chronic renal disease, renal artery stenosis or endocrine dysfunction, leads to a rise in blood pressure, or essential (primary) hypertension, with an unknown aetiology (Bolívar, 2013). Essential hypertension represents the majority of hypertension cases (Carretero & Oparil, 2000) and is a multi-factorial disease involving the heart, kidney, vasculature, central and peripheral nervous system, with an even murkier origin.

Hypertension is an ever growing problem, where an estimated >1.5 billion people will be afflicted by 2025 (Kearney *et al.*, 2005). Sympathetic hyperactivity is a known hallmark of hypertension (Grassi, 2009). This is clinically important as long-term cardiac sympathetic input is both hypertrophic and arrhythmogenic, thereby contributing to the numerous deadly comorbidities associated with hypertension (Herring *et al.*, 2019). Unfortunately, we currently have an incomplete understanding of the how cardiac projecting neurons, which mostly originate in the stellate ganglia (Rajendran *et al.*, 2019), function in health and disease. This thesis investigated the

stellate ganglia neuron (SGN) and its role in the hypertensive phenotype. To this end, this thesis investigated three primary aims:

1) Characterise the stellate ganglia neuron in terms of its transcriptome and unidentified signalling pathways.
2) Characterise cellular and molecular pathways underpinning sympathetic hyperactivity in an animal model of hypertension.
3) Assess *ion channel targets* to counteract sympathetic hyperactivity.

This chapter will introduce the overview of literature on the sympathetic nervous system, the heart, hypertension, and sympathetic end organs affected by hypertension. For clarity, it has been divided this introduction into four sections; 1) The sympathetic nervous system, 2) Hypertension, 3) Neuronal electrophysiology and transmitter release and 4) Ion channels.

## 1.1 The sympathetic nervous system



***Figure 1.1 Early drawings of human lumbar sympathetic neurons by Fernando de Castro*** *The first drawings of the sympathetic neuron were produced by Fernando de castro (1923). Here neurons from the human lumbar ganglia were stained by the Cajal method, and drawn by hand.*

The sympathetic nervous system (SNS), and the autonomic nervous system to which it belongs, is a major mediator of bodily homeostasis. The term "*autonomic nervous system*" was originally proposed by John Langley to describe the "*sympathetic system and the allied nervous system of the cranial and sacral nerves and for the local nervous system of the gut*" (Langley, 1898). The SNS is responsible for the "fight or flight" response (Cannon, 1915) and is in direct opposition to the parasympathetic nervous system (PNS) (Cannon, 1911) and its "rest and digest" response. Together these two systems provide excitatory and inhibitory input to the various organs of the body.

Both the PNS and SNS are arranged in a relay system of pre- and post-ganglionic neurons (Bankenahally & Krovvidi, 2016). However, the PNS and SNS differ in how this system is arranged. Preganglionic sympathetic neurons originate in the intermediolateral column of the spinal cord, where they project to post-ganglionic sympathetic neurons (**Figure 1.1**) arranged in ganglia along the spinal cord in the "sympathetic chain" (Rocco *et al.*, 1995). Whereas preganglionic parasympathetic neurons originate from the dorsal motor nucleus, nucleus solitarius and the nucleus ambiguus of the medulla oblongata, with the majority of the preganglionic parasympathetic neurons being arranged into the vagus nerve (Câmara & Griessenauer, 2015).

There are three sympathetic ganglia that are important to this study; the stellate ganglia, the superior cervical ganglia (SCG), and the coeliac ganglia. Of these ganglia, the stellate ganglia provide most of the cardiac sympathetic innervation (Rajendran et al., 2019) and is the primary focus of this work. Other end-organ targets of the stellate ganglia include the vasculature (Arbab *et al.*, 1988) and lungs (Kummer *et al.*, 1992).

The role of the SCG in cardiac innervation is debated, with studies reporting nil (Janes *et al.*, 1986) or very little involvement in cardiac innervation (Armour & Hopkins, 1981). The majority of SCG projections are instead to structures in the head and neck such as the salivary glands (Luebke *et al.*, 1992), eye (McDougal & Gamlin, 2015) and cerebral artery (Edvinsson *et al.*, 1989). Whilst physiologically important, they are not relevant to study here. However, an awareness of the SCG is important given that most work on the SNS has focussed upon these ganglia.

Renal sympathetic innervation is primarily mediated by the coeliac (Gattone *et al.*, 1986) and superior mesenteric ganglia (Barajas *et al.*, 1992) ganglia. As the

coeliac ganglia and superior mesenteric ganglia are co-localised in the same complex (Hamer & Santer, 1981), they are often studied as one.

### 1.1.1 Sympathetic control of the heart and the vasculature

The heart is densely innervated (**Figure 1.2**) by both sympathetic and parasympathetic neurons (Rajendran *et al.*, 2019). The SNS causes an increase in the beating rate of the heart and force of contraction (Ng *et al.*, 2001; Brack *et al.*, 2006; Rajendran *et al.*, 2019) through the action of noradrenaline (Euler & Hillarp, 1956) (Nobel Prize, 1970) and adrenaline (Elliott, 1905). This effect can be replicated by electrical or optogenetic stimulation of the stellate ganglia (Wallace & Sarnoff, 1964; Rajendran *et al.*, 2019).

Increased contractile force is achieved by direct action upon cardiomyocytes, whereas the increase in heart rate follows transmission to two specialised multicellular systems in the heart, the sinoatrial node and cardiac conduction system (Herring & Paterson, 2018). Sinoatrial node cells have an intrinsic pace-making ability (Flack, 1910; Lewis *et al.*, 1910; Cramer *et al.*, 1977) which is accelerated upon sympathetic input (Flack, 1910).

The cardiac conduction system includes the atrioventricular node, purkinje fibres and the bundle of his, which together facilitate electrical conduction between the atria and ventricles (Herring & Paterson, 2018). Of these structures the atrioventricular node is stimulated by the SNS, increasing conduction velocity and thereby decreasing the latency between atrial and ventricular contraction to facilitate a faster the heart rate (Wallace & Sarnoff, 1964; Vargas *et al.*, 1975). An increase in heart rate is further supported by a sympathetic mediated reduction in the period of cardiomyocyte relaxation (Hicks *et al.*, 1979).

On the other hand, vagal nerve simulation decreases cardiac contractility and heart rate (Rajendran *et al.*, 2019) primarily via acetylcholine, the main parasympathetic transmitter (Loewi, 1921; Loewi & Navratil, 1926; Dale & Dudley, 1929; Dale *et al.*, 1936)(Nobel Prize, 1936). Both the PNS (Parker *et al.*, 2001; Baker *et al.*, 2018) and SNS (Beck, 1958; Zimmerman *et al.*, 1960; Tucker, 1985; Baker *et al.*, 2018) contribute to the basal heart rate and are therefore activate under baseline conditions.

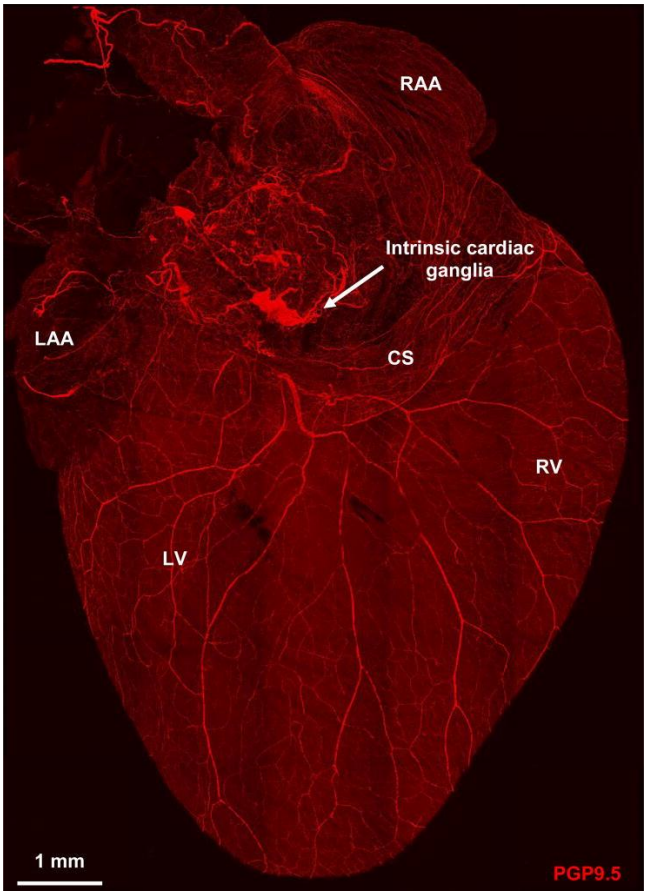



***Figure 1.2 A visual demonstration of the complexity of cardiac innervation*** *using immunohistochemical staining for the pan-neuronal marker PGP9.5. Originally from* (Hanna *et al.*, 2017)*. Here LAA and RAA refer to left atrial appendage and right atrial appendage respectively. LV and RV refer to right left ventricle and right ventricles.*

Cardiac sympathetic innervation is dictated by the pattern of coronary veins within the heart (Nam *et al.*, 2013). This provides the tree like pattern of innervation observed in **Figure 1.2**. Sympathetic neuron axon outgrowth follows the release of nerve growth factor by vascular smooth cells (Nam *et al.*, 2013), which is also required for sympathetic neuron survival (Ruit *et al.*, 1990).

The vasculature is also heavily innervated by the SNS, where the major component of innervation favours major arteries, precapillary arterioles and veins (Sheng & Zhu, 2018). The SNS causes vasoconstriction through the release of multiple neurotransmitters (Marshall, 1982; Huidobro-Toro & Donoso, 2004) (Expanded upon in 1.1.3). Most of the sympathetic control of blood pressure occurs through the restriction of the so called resistance vessels (Levy *et al.*, 2001). Basal sympathetic activity maintains a degree of vascular constriction, and so ganglionic blockade reduces both vascular tone and blood pressure (Haas & Goldblatt, 1960). One notable exception is the coronary vasculature, where sympathetic innervation causes vasodilation (Klocke *et al.*, 1965).

Sympathetic control of the heart and vasculature is regulated by a range of central and peripheral mechanisms. However, of these the baroreflex and central mechanisms are most relevant to this thesis. Central mechanisms are covered in chapter 5. The baroreflex is mostly mediated by aortic (Min *et al.*, 2019) and carotid sinus sensory nerve terminals (Yokoyama *et al.*, 2019), where changes in pressure are transduced to sensory nerve firing in real time (Bronk & Stella, 1932; Seagard *et al.*, 1990). Pressure is transduced by piezo2 channels in both baroreceptor populations (Zeng *et al.*, 2018; Min *et al.*, 2019). This change in firing is then integrated into brainstem autonomic control centres (Dampney, 2016). If arterial pressure rises, the PNS is subsequently activated and the SNS inhibited, and vice

versa. This directly modifies the heart rate and contractility of the heart by modifying cardiac nerve function (Lanfranchi & Somers, 2002). More importantly for blood pressure regulation, it also alters innervation to the vasculature, causing changes in peripheral resistance. This system has a several second lag (Borst & Karemaker, 1983), but is supported by a faster nitric oxide based system. If blood pressure rises, stretch induced vascular nitric oxide release causes vasodilation, thereby reducing peripheral resistance (Just *et al.*, 1994). Together these systems provide continuous control of the SNS, but are both dysregulated in hypertension permitting increased sympathetic nerve activity (SNA) (Head, 1994; Grassi *et al.*, 1998; Li *et al.*, 2015).

### 1.1.2 Sympathetic control of the kidney

The kidney, alongside representing the body's filtration system, has a key role in blood pressure regulation via pressure natriuresis, prostaglandin synthesis and the hormonal renin-angiotensin-aldosterone system. Additionally, the kidney has a key role in the control of SNS by renal afferents (Frame *et al.*, 2016) and is in turn strongly regulated by the SNS (Lohmeier *et al.*, 1998). Both factors are important for blood pressure control and hypertension. The contribution of the arginine-vasopressin system is introduced in chapter 5.

Pressure natriuresis refers to the relationship between renal arterial pressure and sodium excretion. At high renal arterial pressures, sodium excretion is favoured and vice versa (Hall *et al.*, 1988). Increased sodium excretion reduces plasma volume via diuresis, which in turn reduces cardiac output and blood pressure (Granger *et al.*, 2002). The set point of this relationship can be altered by renal sympathetic input (Kubota *et al.*, 1993), whereby increased sympathetic input decreases urinary sodium excretion (Lohmeier *et al.*, 1998).

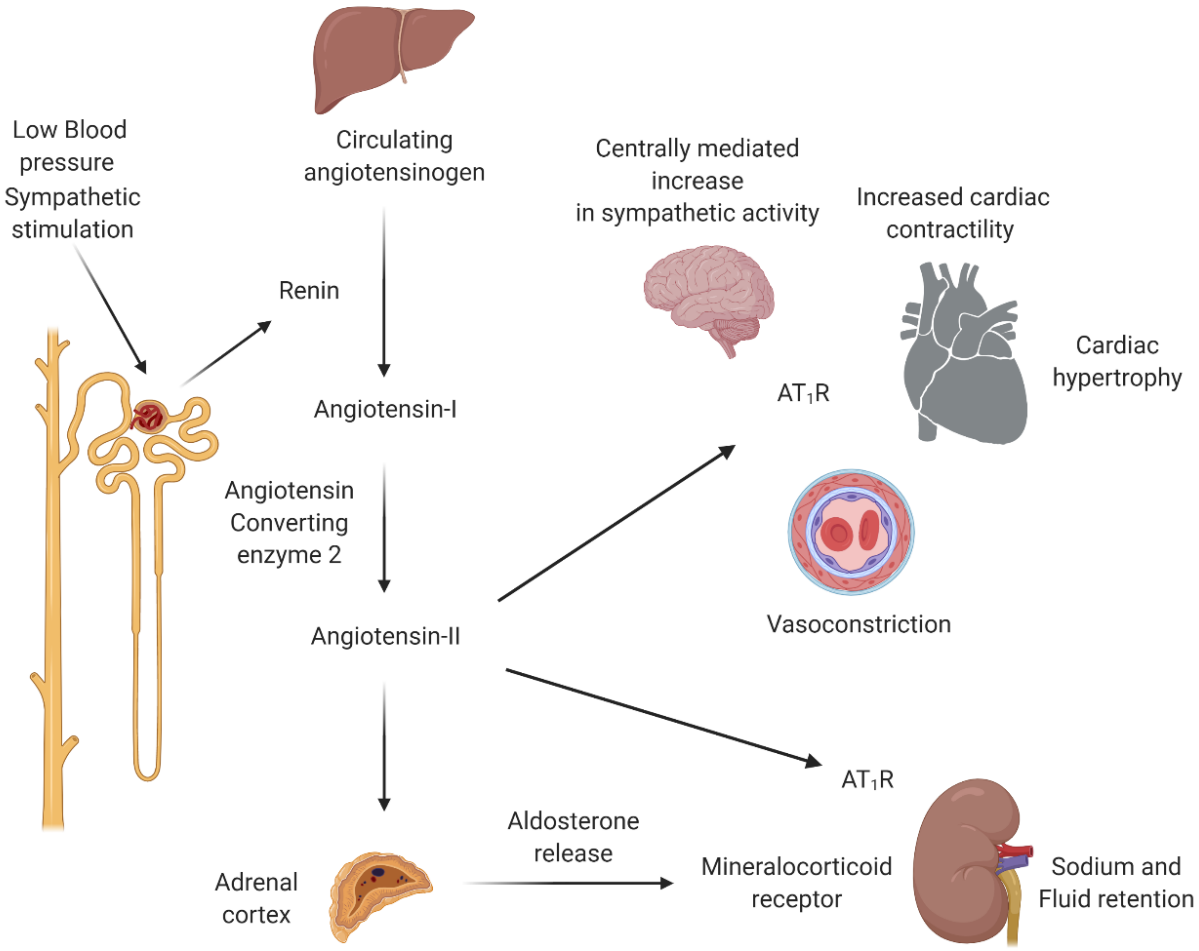



***Figure 1.3 Simple schematic of the renin angiotensin aldosterone system (RAAS)*** *Renin is released from the juxtaglomerular apparatus in response to reduced blood pressure, sympathetic stimulation or low renal blood flow. Renin catalyses the conversion of angiotensin, which is produced by the liver, to angiotensin I. Angiotensin I is converted to the biologically active angiotensin-II. Angiotensin II then elicits several tissue dependent pathways, including peripheral vasoconstriction, an increase in sympathetic activity via central pathways and decreased natriuresis via direct action and through aldosterone.*

The RAAS (**Figure 1.3**) has a two-way relationship with the SNS. Sympathetic input stimulates renin secretion (Gordon *et al.*, 1967; Lohmeier *et al.*, 2000), and resultant angiotensin-II activates central sympathetic pathways (Garcia-Sevilla *et al.*, 1979; Ogawa *et al.*, 2011). Notably, the activation of the SNS by central angiotensin-II is sufficient to dramatically increase blood pressure (Fink *et*

*al.*, 1980). There is also experimental evidence supporting the direct excitation of sympathetic neurons by angiotensin-II (Lewis & Reit, 1965; Castrén *et al.*, 1987; Xiuying *et al.*, 2001; Fernandez *et al.,* 2003) putatively through M-current inhibition (Constanti & Brown, 1981; Shapiro *et al.*, 1994; Zaika *et al.*, 2006), and by direct elevations in free intracellular $Ca^{2+}$ concentration ($[Ca^{2+}]_i$), although the latter mechanism is controversial (Shapiro *et al.*, 1994; Fernandez *et al.,* 2003).

Renal chemo- and mechanoreceptor afferents provide strong feedback to the SNS via central pathways. This can be either be in the form of the inhibitory reno-renal reflex, where high blood pressure is sensed in the kidney, as increased renal arterial pressure and the SNS is inhibited to compensate, or the excitatory reno-renal reflex, whereby the SNS is overactivated. The excitatory reflex occurs during experimental delivery of inflammatory transmitters (Katholi *et al.*, 1983; Smits & Brody, 1984; Barry & Johns, 2015) (Which are expanded upon in chapter 6), or following renal pathology (Esler *et al.*, 1986), and causes an associated increase in blood pressure and SNA (Barry & Johns, 2015).

### 1.1.3 Sympathetic Neurotransmission

The primary neurotransmitter released from sympathetic nerve terminals is noradrenaline, as first demonstrated by Von Euler (Euler & Hillarp, 1956) (Nobel Prize, 1970). Following release of noradrenaline, its effect is limited by reuptake into the presynaptic cell by the noradrenaline transporter (NET) (Mandela & Ordway, 2006), a mechanism proposed by Julius Axelrod (Axelrod *et al.*, 1962) (Nobel Prize, 1970). Release is further regulated by noradrenergic $G_{i/o}$-coupled $\alpha_2$-autoreceptors on the presynaptic terminal, which serve to inhibit calcium entry and thus reduce transmitter release (Delmas *et al.*, 1999). Additionally, somatic β-receptors are

present (Armour & Butler, 1989), which generally appear to have an excitatory effect upon SGN function (Armour & Butler, 1989; Berg, 2014; Bardsley *et al.*, 2018b). However, it remains unknown if these receptors are responsive to noradrenaline spill-over *in situ*.

Several co-transmitters have been well-established in the SNS including adenosine triphosphate (ATP) (Su *et al.*, 1971), Neuropeptide Y (NPY) (Lundberg *et al.*, 1982; Kummer, 1987; Warner & Levy, 1990), Galanin (Kummer, 1987). ATP and NPY release has been demonstrated to be dependent upon high frequency stimulation (Lundberg *et al.*, 1989; Burnstock, 2004). Co-transmitter release is also reduced by autoinhibition (Brock & Tan, 2004).

On the postsynaptic cell, neurotransmitters activate either ligand-gated ion channels (Katz & Miledi, 1972) or G-protein coupled receptors (GPCRs) (May *et al.*, 1985; Dohlman *et al.*, 1987) (Nobel Prizes, 1994 and 2012). Ligand-gated ion channels are activated, and typically also quickly inactivated, upon binding their specific neurotransmitter, and provide fast electrical stimulation (Del Castillo & Katz, 1954) or inhibition (Coombs *et al.*, 1955) of the post-synaptic cell. GPCRs generally have a slower excitatory/inhibitory role (Marrion *et al.*, 1989; Craig & McBain, 2014). GPCRs are coupled to a range of intracellular signalling pathways based upon the identity of the associated G-protein (**Figure 1.4**). GPCRS display a degree of promiscuity between these subunits (Sandhu *et al.*, 2019), and can also associate with β-arrestin signalling pathways (Luttrell & Lefkowitz, 2002), However, here G-protein signalling will generally refer to their canonical pathways with the assumption that this is their primary signalling mode of function.

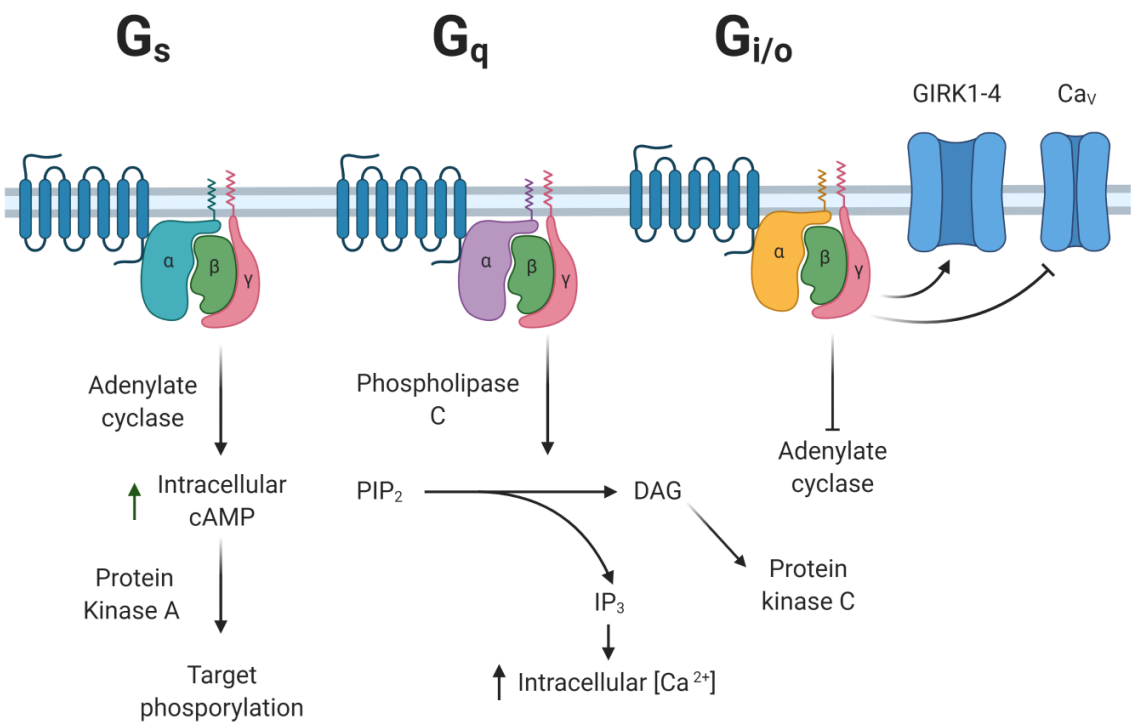



***Figure 1.4 Simplified schematic of G-protein signalling*** *Canonical pathways for G-protein signalling are visually highlighted.*

In the heart, post-synaptic receptors of the sympathetic synapse typically $G_s$-coupled (Green *et al.*, 1992) $\beta_1$-receptors (Myagmar *et al.*, 2017), $G_{s-}$ (Green *et al.*, 1992), and occasionally $G_i$-coupled (Chen-Izu *et al.*, 2000) $\beta_2$-receptors (Myagmar *et al.*, 2017) and $G_q$-coupled (Graham *et al.*, 1996) $\alpha_{1A,B,D}$ receptors (O'Connell *et al.*, 2013). Of these $\beta_1$- (Bristow *et al.*, 1986) and $\alpha_{1B}$-receptors (Myagmar *et al.*, 2017) are the predominant isoforms in the cardiomyocyte. In addition, cardiomyocytes have been demonstrated to express NPY receptors (Nicholl *et al.*, 2002), P2X ATP receptors (Yang & Liang, 2012) (Expanded upon in chapter 6) and galanin receptors (Parsons & Merriam, 1993).

In cardiomyocytes, $\beta_1$-receptor activation leads to protein kinase A phosphorylation of cardiomyocyte L-type voltage-gated calcium channels ($Ca_v$) (Reuter & Scholz, 1977; Mikala *et al.*, 1998). This is mediated by a compartmentalised increase in 3',5'-cyclic adenosine monophosphate (cAMP) (Rall

& Sutherland, 1958; Sutherland *et al.*, 1968) (Nobel prize, 1971) downstream of $G_s$-signalling (Zaccolo & Pozzan, 2002). The net effect of this mechanism is to increase the contractile force with which the cardiomyocyte beats (Xiao & Lakatta, 1993). Additionally, noradrenergic β-receptor signalling at the sinoatrial node serves to increase firing rate, and therefore increased heart rate, through enhanced $Ca^{2+}$ signalling (Ju & Allen, 1999). In addition, cAMP dependent gating of HCN4 channels appears to be important (Noma & Irisawa, 1976; Alig *et al.*, 2009). Finally, the atrioventricular node of the cardiac conduction system noradrenergic β-receptor signalling increases conduction velocity (Vargas *et al.*, 1975). In the rat, noradrenergic $\alpha_1$-receptors also increase intracellular $Ca^{2+}$ thereby augmenting cardiomyocyte contractility (Jensen *et al.*, 2011), although the overall contribution of these receptors in humans is controversial due to relatively low expression (Steinfath *et al.*, 1992). $NPY_1R$ and $\alpha_1$-receptors are also involved in cardiomyocyte hypertrophy (Millar *et al.*, 1994; Jensen *et al.*, 2011). Whilst P2X ATP receptors are present in the cardiomyocyte and promote increased contractility (Mei & Liang, 2001).

The nature of the sympathetic neuron to cardiomyocyte synapse remains controversial (Zaglia & Mongillo, 2017). Noradrenaline is released from varicosities along the axon of the sympathetic neuron (Koh & Hille, 1997) which reside in close opposition (<200nm) to cardiomyocytes and exhibit a high density of vesicles (Choate *et al.*, 1993). Notably, this is still a large distance relative to either the neuromuscular junction (Slater, 2017) or neuron to neuron synapses (Schikorski & Stevens, 1997) When this synapse is studied *in vitro* the opposing postsynaptic cardiomyocyte also forms post-synaptic densities of adrenergic receptors and synaptic scaffolding proteins (Shcherbakova *et al.*, 2007).

On the other hand, the post-ganglionic sympathetic neuron receives cholinergic input from preganglionic sympathetic neurons. In this synapse, acetylcholine activates the sympathetic neuron via cholinergic nicotinic (Feldberg & Gaddum, 1934; Cuevas *et al.*, 2000) and muscarinic receptors (Brown, 1967). Nicotinic receptors are ligand-gated ion channels (Katz & Miledi, 1972) with a permeability to $Na^+$ and $Ca^{2+}$ and are believed to mediate the main fast excitatory input into sympathetic neurons (Tapia *et al.*, 2007). In sympathetic neurons, postsynaptic $G_q$-coupled $M_1$-receptors elicit a decrease in an non-inactivating $K_v$ current termed M-current (Marrion *et al.*, 1989), which causes sufficient excitation to initiate neurotransmitter release from SCG neurons (Lechner *et al.*, 2003) and cardiac nerves (Brown, 1967; Flacke & Gillis, 1968).

## 1.2 Hypertension

Hypertension, has been understood in crude terms for a staggering period of time, with descriptions of treatments for “hard pulse disease” being recorded as early as around 2600 BC, and early descriptions of hypertension occurring in many subsequent ancient cultures (Esunge, 1991). Current estimates suggest that greater than one billion people suffer from hypertension worldwide (Zhou *et al.*, 2017). In the contemporary clinical setting hypertension is defined as a blood pressure of 140/90 mmHg (NICE, 2019). Hypertensive patients can be grouped into three broader categories; prehypertensive in the 120-139 mmHg systolic (or 80-89 mmHg diastolic) blood pressure bracket, Stage 1 hypertensives in the 140-159 mmHg systolic (or 90-99 mmHg) blood pressure bracket, and stage 2 ≥160 mmHg systolic pressure (or ≥100 mmHg pressure) (Nguyen *et al.*, 2010). Hypertension can be further categorised as either secondary or primary in origin. Secondary

hypertension results as a co-morbidity of an established pathology, and can be the result of endocrine, renal, or vascular dysfunction amongst others (Rimoldi *et al.*, 2014). Primary hypertension has no known cause but represents the overwhelming majority of hypertensive patients (Carretero & Oparil, 2000).

There are many suggested causes of primary hypertension, of several are listed here. To give an idea of hypertensions complexity, single nucleotide polymorphisms (SNPs) in over 900 loci have been associated with hypertension so far (Evangelou *et al.*, 2018). A well-known example is the INTERSALT study which found a significant association between sodium consumption and hypertension (Rose *et al.*, 1988; Elliott *et al.*, 1996). Although this received criticism for its statistical approach (Freedman & Petitti, 2001), it is well-supported by additional studies (Forte *et al.*, 1989; Poulter *et al.*, 1990; Denton *et al.*, 1995; He *et al.*, 2013). This relationship between sodium and hypertension is explored further in chapter 5. Obesity is also an established risk factor for hypertension, where obese adolescents were more sensitive to high-salt induced blood pressure changes than their normal weight peers (Rocchini *et al.*, 1989). Meanwhile, work based stress significantly increases the probability of hypertension (Karasek *et al.*, 1981). In addition, there is a significant renal component to human hypertension. For example, age-matched normotensive patients have a higher nephron number than their hypertensive counterparts (Hollenberg, 2003; Rule, 2011), although it is unknown if this is causative or correlative. Finally, intermittent hypoxia (e.g. obstructive sleep apnoea) leads to the development of hypertension, which is abolished by selective ablation of carotid body chemoreceptor populations (Peng *et al.*, 2014). Whilst this list is by no means exhaustive, it does show the diversity of disease-causing mechanisms in hypertension.

The clinical burden of primary hypertension is extremely high, indeed Hypertension is the second biggest cause of disability adjusted life years globally (Alcocer & Cueto, 2008). This is due in part to high incidence of comorbidities. For example, 49.3% of hypertensives in the ATRIA trial presented with atrial fibrillation (Go *et al.*, 2001) and hypertension preceded the development of heart failure in a staggering 91% of tested heart failure patients (Levy *et al.*, 1996) Whilst successful management of hypertension limits the development of further cardiovascular diseases (Neal *et al.*, 2000; Devereux *et al.*, 2002; Klingbeil *et al.*, 2003; Manolis *et al.*, 2014), only 53% of identified hypertensives in the US have reached target blood pressures (Go *et al.*, 2013).

The first line current treatments for hypertension include angiotensin converting enzyme (ACE) inhibitors, angiotensin receptor blockers, calcium channel blockers and thiazides (NICE, 2019; Sinnott *et al.*, 2020). ACE inhibitors reduce blood pressure by reducing the conversion of angiotensin-I to angiotensin-II by the enzyme ACE (Raia Jr *et al.*, 1990). Similarly, angiotensin receptor blockers act as antagonists for angiotensin-II $AT_1$-receptors (Burnier & Brunner, 2000). Both have a comparable effect on blood pressure (Sinnott *et al.*, 2020), primarily by inducing vasodilation (Ray-Chaudhuri *et al.*, 1993) and reducing sympathetic excitability (Guido *et al.*, 1997). Thiazide diuretics inhibit the renal $Na^+/Cl^-$ cotransporter (Velazquez & Wright, 1986), but are believed to decrease blood pressure through an unidentified mechanism of peripheral resistance reduction (Rapoport & Soleimani, 2019). Alternatively, calcium channel blockers inhibit L-type $Ca_v$, thereby reducing the contractility of the heart, causing vasodilation and thereby reducing peripheral resistance (Knight *et al.*, 1985) and increasing renal blood flow (Navar *et al.*, 1986) thereby increasing natriuresis (Krishna *et al.*, 1991). It is possible that they

will also effect sympathetic neurons through the control of gene transcription by neuronal L-type channels (Gomez-Ospina & Dolmetsch, 2008), though this has not been explored.

It is notable that treatment with these first-line drugs reduces blood pressure on average to around 140 mmHg (Sinnott *et al.*, 2020). Whilst this is the current NICE target (NICE, 2019), it is notable that this is above the current recommendations of the American college of cardiology (Whelton *et al.*, 2018). Further, a recent metanalysis highlights that even blood pressures in the 130-140 mmHg range increase the risk of adverse cardiovascular events in young adults (Luo *et al.*, 2020). Finally, the cohort of patients who are resistant to all current treatment regimens is estimated to be ~15.3% (Sim *et al.*, 2013), and there is therefore a clear unmet need for novel treatments.

Drugs that directly target sympathetic function such as α-blockers, β-blockers and α2-agonists are used as secondary treatments for resistance hypertension (NICE, 2019). α-blockers inhibit post-synaptic $\alpha_1$-receptors in the vasculature, thereby causing vasodilation and reduce peripheral resistance (Mancia *et al.*, 1980). Unfortunately, some α-blockers have been reported to increase the risk of cardiovascular co-morbidities (Furberg *et al.*, 2002), and their use has been limited. β-blockers can be competitive antagonists, or partial agonists of post-synaptic β-receptors (Wong *et al.*, 2014), which are activated by sympathetic transmitter noradrenaline (Euler & Hillarp, 1956). β-receptors are primarily held to reduce blood pressure through a decline in cardiac output (Conway, 1983), altered baroreflex sensitivity (Floras *et al.*, 1988) and reduced renin secretion (Blumenfeld *et al.*, 1999). Whilst effective at reducing blood pressure, they are no longer used as first-line therapy since they do not reduce patient mortality or stroke incidence (Wiysonge

*et al.*, 2017). This may be due to the involvement of co-transmitters in sympathetic neurotransmission (Herring, 2015). These co-transmitters are not inhibited by β-blockers, but also play a key role in cardiac pathologies (Millar *et al.*, 1994; Kalla *et al.*, 2020). $\alpha_2$-agonists cause a reduction in blood pressure (MacDougall *et al.*, 1970) through activation of inhibitory auto-receptors on sympathetic neurons (Hein *et al.*, 1999), and through central inhibition of sympathetic activity (Buerkle & Yaksh, 1998). However, severe hypertension follows cessation (Mehta & Lopez, 1987), limiting use. Finally, reserpine inhibits the vesicular monoamine transporter-2 (Henry *et al.*, 1997), preventing catecholamine transport into pre-synaptic vesicles (Kirshner, 1962), thereby preventing sympathetic noradrenaline release (Shafi *et al.*, 2000). Although it is efficacious for reducing blood pressure, there is limiting data assessing the effect on patient outcome (Shamon & Perez, 2016). Together, these treatments demonstrate the potential of the SNS as a drug targets in hypertension.

### 1.2.1 Hypertension and the sympathetic nervous system

Human hypertension is known to have a significant autonomic component. Although it is difficult to separate this aspect of the pathology from end-organ dysfunction this will be attempted here. Sympathetic dysfunction manifests as increased SNA (Anderson *et al.*, 1989; Grassi *et al.*, 1998; Greenwood *et al.*, 1999; Flaa *et al.*, 2006), increased cardiac noradrenaline spill-over (Esler *et al.*, 1986), renal noradrenaline spill-over (Esler *et al.*, 1986; Schlaich *et al.*, 2003) and plasma noradrenaline (Esler *et al.*, 1986; Rocchini *et al.*, 1989). Interestingly, this dysfunction has been reported to occur at the level of a single sympathetic fibre (Greenwood *et al.*, 1999). In addition, individuals who are more sensitive to blood

pressure rises with high dietary salt are more susceptible to sympathetic overactivity (Yatabe *et al.*, 2010), which is explored in chapter 5.

The removal of the sympathetic chain was once proposed as a treatment for hypertension, and whilst effective clinically (Evans & Bartels, 1949), it was burdened with severe side effects which include a poor cerebrovascular outcome (Peet & Isberg, 1949). More recent studies have utilised renal denervation to attempt to reduce blood pressure in treatment resistant humans (Esler *et al.*, 2010*a*; Bhatt *et al.*, 2014). This is based upon a number of observations, for example intrarenal perfusion of noradrenaline causes sustained hypertension (Osborn *et al.*, 1997), renal denervation in animals reduces blood pressure in animal models of hypertension (Katholi, 1983) and a prevailing theory for the contribution of renal afferents to hypertensive pathology (Frame *et al.*, 2016). Unfortunately, whilst this approach encountered initial success (Krum *et al.*, 2009; Esler *et al.*, 2010*b*), it subsequently failed in a large multi-centre trial (Bhatt *et al.*, 2014). Whilst more recent clinical trials have provided more positive results, these trials reported only a meagre reduction in blood pressure (5-7 mmHg) (Kandzari *et al.*, 2018; Böhm *et al.*, 2020) relative to promising early studies reporting decreases in blood pressure in excess of 30 mmHg (Esler *et al.*, 2012; Christian *et al.*, 2013; Krum *et al.*, 2014). This perhaps suggests that a greater understanding of the SNS in physiology and hypertensive pathology is required.

Hypertensive pathology is known to have a significant cardiac sympathetic component. Cardiac sympathetic denervation, via removal of the bottom half of the stellate ganglia and first two thoracic ganglia, has been demonstrated to be efficacious for the treatment of ventricular arrythmia (Irie *et al.*, 2017; Meng *et al.*, 2017) and appears to have positive effects on atrial fibrillation (Zhou *et al.*, 2013)

and myocardial infarction (Xiong *et al.*, 2018) in large animal models. Further, cardiac sympathetic activity correlates with left ventricular hypertrophy in man (Schlaich *et al.*, 2003). As these are all sympathetic associated common co-morbidities of hypertension, reducing stellate ganglia activity *in vivo* would be beneficial for patient outcomes in treatment resistant hypertension. However, cardiac sympathetic denervation is an invasive procedure with a high error rate and off target effects (eg. Horner's syndrome) (Herring *et al.*, 2019). Currently, there is a fundamental lack of understanding of the basic properties of the SGN in health and disease. By expanding this knowledge new pharmacological targets can be identified to avoid this invasive procedure.

### 1.2.2 Animal models of hypertension

In this work, the inbred spontaneously hypertensive rat (SHR) model of essential hypertension (Okamoto & Aoki, 1963) was used as a surrogate for dysautonomia. The SHR was developed via the selective inbreeding of outbred Wistar rodents which exhibited a phenotype of elevated blood pressure (Okamoto & Aoki, 1963; St Lezin *et al.*, 1992). Currently the SHR remains the most commonly used model of essential hypertension (Lerman *et al.*, 2019). An inbred control strain was later developed in the Wistar Kyoto rat, by inbreeding normotensive Wistar rodents from the same animal facility in Kyoto (Louis & Howes, 1990). However, the use of this inbred control is limited based upon its financial cost and questions around its validity. Criticism has focussed upon the significant time period of outbreeding between the development of the SHR and WKY models (approximately 12 years) (Louis & Howes, 1990) and the genetic divergence between these strains that has developed over this period or subsequent decades of independent

inbreeding (Johnson *et al.*, 1992). For these reasons, the outbred Wistar strain is used as a control here instead.

The SHR exhibits sympathetic hyperactivity (Schramm & Chornoboy, 1982; Caplea *et al.*, 2002), atrial fibrillation (Lau *et al.*, 2013), ventricular arrhythmia (Pahor *et al.*, 1989), endothelial dysfunction (Puzserova *et al.*, 2014), cardiac hypertrophy (McCrossan *et al.*, 2004), progressive renal dysfunction (Griffin *et al.*, 2001) and eventual heart failure (Bing *et al.*, 1995). Prehypertension in the SHR begins at around 4-5 weeks of age which develops into hypertension at around 6-12 weeks (Minami *et al.*, 1989; Dickhout & Lee, 1998). Importantly, the hallmarks of sympathetic hyperactivity occur during prehypertension from around four weeks of age (Li *et al.*, 2012; Shanks *et al.*, 2013), thereby replicating the prehypertensive phenotype observed in man (Anderson *et al.*, 1989). In addition, the SHR mirrors the delayed and varied occurrence of hypertensive co-morbidities seen in patients (Kannel *et al.*, 1998; Oh & Cho, 2020). For example, in the SHR complications such as heart failure (>20 months old) (Conrad *et al.*, 1995) and arrythmia (>3 months old) (Pahor *et al.*, 1989) occur in a limited cohort and at a later timepoint than hypertension development. Finally, the SHR responds to clinical pharmacology in a similar way to essential hypertensive patients (Tabei *et al.*, 1970; Harrap *et al.*, 1990; Penney & Robinson, 1990; You *et al.*, 2005). Phenotypically it is therefore a solid model for the human phenotype of human hypertension.

The key issues with the SHR are the use of rodent physiology, and the neurological phenotype of the SHR, which includes attention deficit disorder (Sagvolden *et al.*, 1992). However, the use of an inbred rodent model is unavoidable due to, the cost and lack of availability for large animal models for hypertension (Lerman *et al.*, 2019), and limited access to well-controlled human hypertensive

tissue. Further, the neurological phenotype does not preclude study of this model *ex vivo* as performed here but should be considered for longitudinal *in vivo* study.

A wide spectrum of alternate hypertension models are used and will be discussed briefly here for comparison. Specifically, the Dahl-salt sensitive rat, deoxycorticosterone acetate (DOCA) rat, angiotensin-II perfusion rats and environmental models of hypertension. Less common inbred models of spontaneous hypertension such as the New Zealand (Smirk & Hall, 1958), Prague (Heller *et al.*, 1993), Lyon (Vincent *et al.*, 1978) and Milan (Trippodo & Frohlich, 1981) hypertensive rat strains will not be discussed here as these models do not benefit from the breadth of research performed upon the SHR and provide no phenotypic benefit.

The Dahl-salt sensitive rat, and its salt-insensitive control, are an alternate inbred model of hypertension, where hypertension induced by a relatively low dietary salt intake (Rapp & Dene, 1985). Later work revealed that this occurred through mutations in the loci for *ACE* (Angiotensin converting enzyme) and *NPPA* (Atrial natriuretic peptide) (Deng & Rapp, 1992). The development of these rodent strains was based upon the observation that blood pressure in outbred rat strains was linearly dependent upon dietary salt intake, but with significant variation between individuals. This model has a comparable phenotype to the SHR but does not benefit from the depth of study in the SHR model.

In DOCA salt rats, DOCA, a synthetic mineralocorticoid, is infused alongside NaCl following unilateral nephrectomy (Basting & Lazartigues, 2017). This model replicates elements of human hypertension such as elevated SNA (Takeda & Buñag, 1980) cardiac fibrosis, cardiac (Karam *et al.*, 1996) and vascular hypertrophy (Deng & Schiffrin, 1992) and endothelial dysfunction (Nunes *et al.*,

2000). However, this model uses an extreme methodology for hypertension induction and given the use of surgical renal damage it is difficult to argue that this model represents primary and not secondary hypertension.

Continuous perfusion of angiotensin-II causes hypertension, with associated increases in renal SNA (Guild *et al.*, 2012). This model is currently the most common, with the most recent metanalysis finding that 50% of NIH-funded hypertension studies used it (Galis *et al.*, 2013). This model is based upon the rationale that the expression of the angiotensin producing enzyme, angiotensin converting enzyme increases in hypertension (Furuhashi *et al.*, 2015; Li *et al.*, 2017). Similarly, L-NAME infusion induces hypertension by inhibiting nitric oxide synthase (Bryant *et al.*, 1995), limiting nitric oxide induced vasodilation and reducing renal glomerular filtration rate. This leads to an increase in vascular resistance and thereby blood pressure (Bryant *et al.*, 1995). Neither model represents the complexity of hypertension, but they are useful for observing the impacts of sustained blood pressure on end-organ function.

Finally, environmental models involve extreme environmental conditions or psychological stressors (Spruill, 2010). For example, maintaining rats at 5$^{o}$C for 3 weeks induces hypertension (Fregly, 1954) with a catecholaminergic phenotype (Russ *et al.*, 1991) similar to that observed in humans who develop hypertension in cold geographical regions (Fares, 2013). Whilst these environmental models are of scientific interest, their clinical utility is likely very narrow. Further, rodent models of psychological stress are unlikely to represent human stress, where blood pressure increases are largely-dependent upon work-related stress (Karasek *et al.*, 1981).

## 1.3 Neuronal electrophysiology and transmitter release

This thesis focusses upon SGN electrophysiology, however, SGNs have received limited study, despite their physiological importance as a major centre for cardiac innervation. Therefore, unless specified these data will typically refer to the SCG.

### 1.3.1 The neuron in the basal state

Electricity in biological processes is mediated by charged ions. $Na^+$, $K^+$, $Cl^-$ and $Ca^{2+}$ are the most important ions to metazoan cell function, with some notable contributions of $Mg^{2+}$ ions. The lipid membrane encompassing the cell is largely impermeable to these ions and so provides a physical barrier to ion movement between the intracellular cytoplasm and extracellular fluid (Papahadjopoulos *et al.*, 1972). This allows for the establishment of concentration gradients between the intracellular and extracellular compartments of the cell. The establishment of ion gradients in a resting cell requires the movement of ions against their electrical and chemical gradients, therefore this is an energetically expensive process, which is achieved by a range of active transporters. These transporters use the dephosphorylation of the biochemical energy currency ATP, to facilitate this process. Indeed, most of a neurons ATP and therefore energy, expenditure is on ion transport (Vergara *et al.*, 2019). The importance of this process is perhaps best demonstrated by the initiation of excitotoxic cell death upon the depletion of intracellular ATP (Eguchi *et al.*, 1997).

The most important of these ion transporters is the $Na^+/K^+$ ATPase (Skou, 1957) (Nobel prize, 1997), which utilises ATP to transport simultaneously co-transport 2 $K^+$ in to the cell for every 3 $Na^+$ channels out. This process is thus electrogenic,

causing a net negative charge on the intracellular side of the membrane due to imbalanced charge movement.

If ion movement is permitted, for example of $K^+$ or $Na^+$, then a potential is generated across the membrane. During this movement, the actual number of ions that move is very small, and so this has a minimal effect upon the macroscopic concentrations on either side. The equilibrium potential ($V_{Eq}$) for individual ions, can be derived using the Nernst equation (**Equation 1.1**). From this equation we can observe, that in a system permeable to only one ion species *X*, the membrane potential would reach the equilibrium potential $V_{eq}$.

***Equation 1.1 The Nernst equation*** *At V Where R indicates the universal gas constant, T is the temperature in Kelvin, z the valence of the ion under question and F faradays constant.*

$$V_{\text{eq.}} = \frac{RT}{zF} \ln \frac{[X]_{\text{o}}}{[X]_{\text{i}}}$$

As mentioned, the membrane has a very low permeability to ions and so ion channels are required to permit the fast diffusion of one or multiple ion species across the membrane through their pore like structure (Doyle *et al.*, 1998). These proteins can be open or closed, thereby limiting or facilitating ion conductance across the membrane (Rubinstein, 2017).

The neuronal resting membrane potential (RMP) is largely maintained by $K^+$ efflux and as such the RMP is generally close to $E_K$. $E_k$ is negative in the metazoan cell due to the role of $Na^+/K^+$ ATPase maintaining an extremely high intracellular [$K^+$] relative to extracellular [$K^+$]. The role of $K^+$ is best demonstrated by early experiments demonstrating that elevated extracellular KCl causes a dramatic shift

in membrane potential to the new value of $E_K$. This can be explained by the large number of potassium channels which are open around the RMP. These $K^+$ selective channels include members of the voltage-gated delayed rectifier and $K_v7$ families alongside the "leak" potassium two-pore ion channel family (Enyedi & Czirják, 2010). However, in a typical neuron the RMP is not equal to the $E_k$ and is instead typically depolarised relative to $E_K$ (Wright, 2004). This is because of a smaller leak conductance to $Na^+$ and $Cl^-$ through channels such as the Sodium Leak Channel (NALCN) (Ren, 2011), and Chloride channel 2 (Jentsch *et al.*, 2005). The reversal potential for this complicated situation can be calculated via a variant of the Nernst equation, the Goldman–Hodgkin–Katz equation (**Equation 1.2**).

***Equation 1.2 The Goldman-Hodgkin-Katz equation*** *Here $P_X$ refers to the permeability of a ion X, R to the universal gas constant, T temperature in kelvin and F to faradays constant. In a typical neuron, $P_K$ is high, and $P_{Na}/P_{Cl}$ low.*

$$V_m = \frac{RT}{F} \ln\left( \frac{p_K[K^+]_o + p_{Na}[Na^+]_o + p_{Cl}[Cl^-]_i}{p_K[K^+]_i + p_{Na}[Na^+]_i + p_{Cl}[Cl^-]_o} \right)$$

### 1.3.2 General properties of voltage-gated ion channels

Voltage-gated ion channels are found throughout nature, from the humble virus to complex multi-cellular organisms (Moran *et al.*, 2015), and are critical to metazoan life. Due to the diversity of ions involved in signalling, a varied family of ion channels have evolved to conduct them. These channels differ widely in their ion selectivity, structures, kinetics, and mechanisms of regulation and channel-specific nuances will be covered in detail later.

Voltage-gated ion channels are activated by changes in membrane potential. For most of these channels, activation results from a depolarisation of the

membrane potential (Hodgkin & Huxley, 1952*a*-d) (Nobel Prize, 1963). A combination of molecular dynamics simulations, structural biology and biophysical study have gradually uncovered the mechanisms behind the mechanism behind voltage-gating (Kim & Nimigean, 2016). Voltage-gated channels possess a transmembrane region with a high density of positive charges in their fourth transmembrane helix (Noda *et al.*, 1984). Changes in membrane potential cause the movement of this S4 domain (Mannuzzu *et al.*, 1996). As hypothesised by Hodgkin and Huxley (1952*a*) this movement can be measured as a gating current (Armstrong & Bezanilla, 1973; Logothetis *et al.*, 1992; Mannuzzu *et al.*, 1996; Aggarwal & MacKinnon, 1996). Movement of the S4 domain leads to an associated conformational change in the overall protein structure and subsequent channel activation (Guy & Seetharamulu, 1986; Yang & Horn, 1995; Mannuzzu *et al.*, 1996; Catterall, 2010). Upon hyperpolarisation these channels will then deactivate to a closed state (Hodgkin & Huxley, 1952*a-d*). Some voltage-gated channels also exhibit inactivation, where the channel enters a non-conductive inactivated state following activation. Inactivation is typically by hyperpolarisation (Hodgkin & Huxley, 1952*a-d*; Kuo & Bean, 1994), to allow subsequent channel reactivation.

The current flow through an ion channel can be summarised as shown in **equation 1.3**, where for a voltage-gated channel the conductance will increase when more channels are in the open state (Hodgkin & Huxley, 1952*a*).

***Equation 1.3 Relationship between membrane current, ionic conductance and the potential difference between the membrane potential and ionic reversal potential***

$$I_X = g_x.(E_M - E_x)$$

### 1.3.3 Passive neuronal properties

Both the intracellular and extracellular solutions function as conductors of electricity, due to the presence of dissolved ions in solution, and the plasma membrane behaves as a leaky insulator. Under this arrangement, the plasma membrane behaves as a capacitor. The capacitance of the membrane is typically assumed to be constant at around 1-1.3 μF/cm$^2$ based upon early work on the squid giant axon (Curtis & Cole, 1938; Hodgkin & Huxley, 1952*a*), however more recently this has been estimated to vary between neuronal subtypes (Major *et al.*, 1994; Thurbon *et al.*, 1998; Gentet *et al.*, 2000) and between differing areas of protein distribution in the membrane (Fernández *et al.*, 1982).

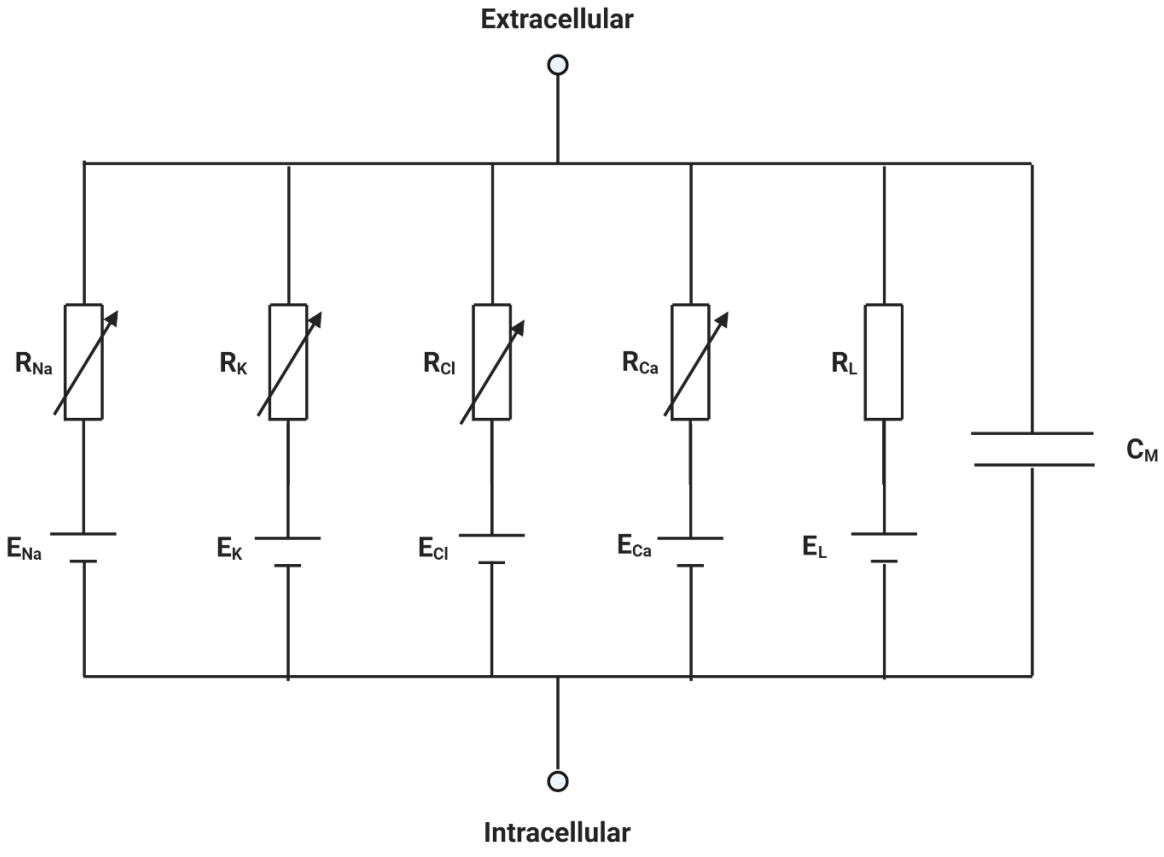



***Figure 1.5 A simplified model of the neuronal membrane, where voltage-gated channels are grouped by ion species*** *This figure is adapted from the work of Hodgkin and Huxley (1952). Here leak current is assumed to be ohmic, and therefore have a fixed resistance. Voltage-gated channels are grouped by ion species, and are shown to have a variable resistance, based upon their voltage dependence. Resistance is the inverse of the conductance for each ion. $E_x$ is the reversal potential for each ion.*

The membrane channels can also be said to behave as resistors (Hodgkin & Huxley, 1952*a*), where the resistance is the inverse of ionic conductance across the membrane resulting from the sum ion channel conductance. By this relationship, as ion channels activate and conduct ions, the membrane resistance decreases. By ohms law this means that a cell with a greater $R_M$ will be more responsive to smaller current injections than a cell with a low $R_M$. The relationship between different ionic currents and the membrane resistance is therefore the sum of the different ion channels in series (**Figure 1.5**)**.** The input resistance at rest is largely a property of the leak current (**Figure 1.5**) and is often used as a measure of the passive membrane properties (Spruston & Johnston, 1992).

Together the combined membrane resistance $R_M$ and $C_M$ form an RC circuit with time constant $T_M$ (Rall, 1969) (**Equation 1.4**). A greater $C_M$ and/or $R_M$ will mean that the membrane takes longer to respond to a change in membrane current injection, therefore slowing the propagation of electrical activity throughout the neuron (Rall, 1969). Whilst the delay to membrane loading is clearly observable in experimental recordings, its physiological relevance is debated (Koch *et al.*, 1996).

***Equation 1.4 Equation determining the membrane time constant*** *$T_M$ indicates the membrane time constant. $C_M$ the membrane capacitance, and $R_M$ the membrane resistance, which at rest is assumed to equal $R_L$ (Figure 2) (The inverse of the leak conductance).*

$$T_M = C_M . R_M$$

### 1.3.4 The neuronal action potential

The action potential is an excitatory depolarisation of the membrane potential exhibited by a range of animal, fungi (Adamatzky, 2018) and plant cells (Abe *et al.*, 1980), in mammals this includes neurons (Bean, 2007), myocytes (Grant, 2009) and endocrine (Stojilkovic, 2012) cells. “Animal electricity” had been theorised since the work of Luigi Galvani, but it wasn’t until 1865 that the first recording of an action potential’s time course was made by Julius Bernstein (Schuetze, 1983). This remarkable early achievement was theoretically expanded by Bernstein in 1902 (Carmeliet, 2019), who cemented an early theory of the action potential and RMP. The role of $Na^+$ remained veiled until the work of Hodgkin & Katz (1949). These pioneering studies made way for the Hodgkin-Huxley model of the action potential time course (Hodgkin & Huxley, 1952*a*), which is still frequently adapted for modern neuronal modelling (Hines & Carnevale, 2001; Stimberg *et al.*, 2019).

In the simplest terms, a typical action potential can be summarised in terms of $Na^+$ and $K^+$ (Hodgkin & Huxley, 1952*a*). An action potential is evoked through an initial stimulus causing membrane depolarisation. This subsequently leads to an increase in the probability of voltage-gated sodium channel opening ($P_{Na}$) and a resultant influx of $Na^+$ through voltage-gated sodium channels ($Na_v$). This causes further membrane depolarisation and positive hyperpolarisation towards the potential of $E_{Na}$ (~55 mV). This sudden large influx of $Na^+$ is relatively short lived, and $Na_v$ subsequently inactivate. The membrane depolarisation also causes $P_k$ of voltage-gated $K^+$ channels ($K_v$) to increase, albeit with activation kinetics that are significantly slower than in $Na_v$ channels.

In a real neuron, voltage-gated calcium channel ($Ca_v$) probability of opening ($P_{Ca}$) also increases during membrane depolarisation leading to $Ca^{2+}$ influx (Helton

*et al.*, 2005), which activates $Ca^{2+}$-dependent intracellular signalling cascades. In the somata, this could be $Ca^{2+}$-dependent processes such as regulation of gene transcription (Berridge *et al.*, 2000; Bengtson & Bading, 2012) or in the presynaptic axon terminal, neurotransmitter release (Katz & Miledi, 1967; Llinás & Nicholson, 1975; Koester & Johnston, 2005).

### 1.3.5 Neurotransmitter release

During neurotransmission vesicles of one or more neurotransmitter are released across the small gap separating the pre- and postsynaptic cell (Del Castillo & Katz, 1954) (Nobel Prize, 1970) thereby evoking a postsynaptic response (Brock *et al.*, 1952; Coombs *et al.*, 1953) (Nobel Prize, 1963). Neurotransmission is heavily entwined with the action potential, as the probability of vesicular release is $Ca^{2+}$-dependent (Katz & Miledi, 1967; Dodge Jr & Rahamimoff, 1967). $Ca^{2+}$ enters the presynaptic terminal via $Ca_V$ during an action potential as measured by voltage-clamp (Llinás *et al.*, 1981; Charlton *et al.*, 1982; Augustine *et al.*, 1985) or $Ca^{2+}$ imaging (Llinás & Nicholson, 1975; Sabatini & Regehr, 1996). The subsequent transmitter release can be artificially recapitulated via direct injection of $Ca^{2+}$ into the presynaptic terminal (Miledi, 1973). There is a significant variation in the probability of release between synapses (Branco & Staras, 2009), but at least for neuron to neuron synapses this appears to be constrained by the identity of the post-synaptic cell (Koester & Johnston, 2005).

Under typical voltage-clamp recordings, the majority of the inward $Ca^{2+}$ conductance occurs during the tail current where driving force is greatest (Augustine *et al.*, 1985), however, in physiology this relates to the repolarisation of the action potential (Llinás *et al.*, 1981; Sabatini & Regehr, 1996). This provides the largest

delay to synaptic release with $Ca^{2+}$ influx beginning approximately 1 ms after action potential initiation (Llinás *et al.*, 1981; Sabatini & Regehr, 1996). At least in central synapses, the time-frame of the subsequent steps is extremely quick, with $Ca^{2+}$-induced vesicular release occurring approximately 60 µs after $Ca^{2+}$ influx (Sabatini & Regehr, 1996), which is followed by a post-synaptic potential within the post-synaptic neuron roughly 200 µs after the initial calcium influx (Llinás *et al.*, 1981; Sabatini & Regehr, 1996).

The mathematical relationship between extracellular [$Ca^{2+}$] and transmitter release (Dodge Jr & Rahamimoff, 1967), was established to be dependent upon the mechanisms of vesicular release rather than channel conductance (Augustine & Charlton, 1986). $Ca_v$ are directed to the pre-synaptic active zone thereby providing a local source of $Ca^{2+}$ (Kaeser *et al.*, 2011). Raised $[Ca^{2+}]_i$ in the axon terminal is sensed by the vesicular-membrane associated $Ca^{2+}$-sensor synaptotagmin (Brose *et al.*, 1992; Davletov & Südhof, 1993) which signals for the initiation of vesicular fusion, and thereby transmitter release (Geppert *et al.*, 1994). There are multiple isoforms of synaptotagmin, which alter the kinetics of vesicular release (Xu *et al.*, 2007).

Vesicles of transmitters are first chaperoned to the presynaptic active zone and primed for release (Südhof, 2013). Vesicles are then held in place by the SNARE-complex (Söllner *et al.*, 1993*a*; Sutton *et al.*, 1998), which includes the vesicular associated protein synaptobrevin (VAMP) (Trimble *et al.*, 1988) and plasma membrane associated syntaxin-I (Bennett *et al.*, 1992) alongside cytosolic SNAP-25 (Söllner *et al.*, 1993*b*). This complex associates together with Munc-18 via syntaxin (Hata *et al.*, 1993; Dulubova *et al.*, 2007). Vesicular synaptotagmin associates with this complex and upon $Ca^{2+}$ binding to synaptotagmin vesicular

fusion is triggered and thereby transmitter release is facilitated (Fernandez-Chacon *et al.*, 2001) via zippering of the primed SNARE complex (Hanson *et al.*, 1997). The contributions of Sudhof, Rothman and Schekman were acknowledged by the 2013 Nobel Prize in Physiology or Medicine.

### 1.3.6 Action potential firing properties

The pattern of action potential firing is generally considered to be the most important aspect of neuronal action potential firing (Bean, 2007), and in this view represents a digital all or none method of communication. This observation is important given that increased sympathetic firing in hypertension occurs at a single neuron level (Yarowsky & Weinreich, 1985; Greenwood *et al.*, 1999).

In general, the frequency of firing is both stimulation dependent and cell-type dependent, but in the SNS neurons fire either single action potentials (Phasic 1), time resolved bursts of action potentials (Phasic 2) or continuously (Tonic) (Wang & McKinnon, 1995). Whilst the relationship between these firing patterns and transmitter release has not been directly established in the sympathetic neuron. In central neurons, it is well established that increased neuronal firing leads to increased calcium entry in the soma (Smith *et al.*, 1983; Harding *et al.*, 2020) and axon (Mackenzie *et al.*, 1996; Kreitzer *et al.*, 2000), and the latter is directly coupled to transmitter release (Mackenzie *et al.*, 1996). The number of responsive axonal varicosities also increases with increased neuronal firing (Mackenzie *et al.*, 1996). However, even a single presynaptic action potential can evoke an excitatory response in the post-synaptic cell (Llinás *et al.*, 1981; Sabatini & Regehr, 1996; Koester & Johnston, 2005). There is also a demonstrated relationship between the frequency of sympathetic nerve stimulation and transmitter release (Buttgereit *et al.*,

2016). Finally, co-transmitter release is affected by the frequency of firing (Burnstock, 2004).

Action potential shape can not only influence the speed of neuronal firing, but can also alter calcium entry into the somata (Park & Dunlap, 1998) and axon terminal (Sabatini & Regehr, 1996, 1997; Geiger & Jonas, 2000). In this sense action potentials are also an analogue form of information. Multiple studies have reported that the shape of the presynaptic action potential strongly impacts terminal calcium influx and transmitter release (Sabatini & Regehr, 1997; Borst & Sakmann, 1999; Geiger & Jonas, 2000). However, axonal terminal action potential waveforms are observably different from those recorded in the soma (Kole *et al.*, 2007), due to differing ion channel complements in the axon relative to the soma (Kole *et al.*, 2007; Kole & Cooper, 2014; Hu & Bean, 2018). It should also be noted that consecutive and repetitive firing can also broaden the action potentials shape and this can have profound effects upon neuronal function (Bean, 2007). For example, action potential broadening in the mossy fibre bouton increases calcium influx, and enhances synaptic transmission (Geiger & Jonas, 2000).

The action potential also functions as a lossless format to transmit information across the plasma membrane. As an action potential spreads across the membrane, a new action potential will be generated, in this sense the action potential behaves as a binary information system. The conduction velocity of action potentials along the axon can vary based upon axon diameter (Cragg & Thomas, 1957), and the degree of myelination (Arancibia-Cárcamo *et al.*, 2017). Conduction speed increases with axon diameter (Cragg & Thomas, 1957). Lipid rich myelin insulates sections of the axon, promoting saltatory conduction (Arancibia-Cárcamo

*et al.*, 2017) and in the case of neurons which require extremely fast conduction, the soma too can be myelinated (Wise *et al.*, 2017).

The overwhelming majority of sympathetic axons are not myelinated (Orimo *et al.*, 2011), but sympathetic axons *in situ* are wrapped in non-myelinating Schwann cells (Choate *et al.*, 1993; Luff, 1996). The role of these cells in the function of the SNS is unexplored. It is unknown why this system favours a lack of myelination. This is especially surprising given the relatively long distance between the sympathetic ganglia and their targets (Bankenahally & Krovvidi, 2016), and the higher energy cost of energy transmission in unmyelinated neurons (Wang *et al.*, 2008).

The threshold for action potential firing can be determined by the rheobase. The rheobase refers to the minimal threshold current injection of infinite duration which reaches the threshold of action potential firing (Noble & Stein, 1966). In practice, a finite recording stimulation is used of around one second. This allows for the membrane to charge to a constant potential, and therefore limits the effect of the membrane time constant on the estimated threshold.

### 1.4 Ion channel subtypes

There is a known dysfunction of neuronal firing properties in hypertension in sympathetic nerves (Greenwood *et al.*, 1999) and cultured SCG neurons (Yarowsky & Weinreich, 1985). Current work implicates A-type potassium channels (Robertson & Schofield, 1999) or SK channels (Jubelin & Kannan, 1990), although this is not firmly established. This section will provide a brief description of ion channels focussed upon in chapter 4 of this thesis.

### 1.4.1 Voltage-gated $Na^+$ channels

$Na_v$ characteristically display extremely fast activation, and equally fast inactivation, such that the process of activation and inactivation can occur within ms at physiological temperatures (Hodgkin & Huxley, 1952*a*; Bennett *et al.*, 2019). Currently, 9 $Na_v$ α-subunits have been identified, $Na_v$1.1-1.9, which each have their own unique expression patterns and kinetic profile. Previous studies have highlighted $Na_v$1.7 (Toledo-Aral *et al.*, 1997) and $Na_v$1.6 (Xie *et al.*, 2015) expression in sympathetic ganglia, and $Na_v$1.8 inhibitors have been shown to inhibit stellate ganglia function (Yu *et al.*, 2017). Although $Na_v$ are mostly selective to $Na^+$, $Na_v$ are also permeable to $Ca^{2+}$ (Hille, 1972; Akaike & Takahashi, 1992), which has been observed to play a role in neuronal calcium signalling (Hanemaaijer *et al.*, 2020).

$Na_v$ channels are mostly closed at a neuron's physiological membrane potential, and activate at around -40 to -30 mV (Noda *et al.*, 1986), which is quickly followed by inactivation. Physiological removal of inactivation is achieved upon membrane hyperpolarisation following neuronal firing, thereby facilitating a ready pool of $Na_v$ channels for additional action potentials. Some $Na_v$ subunits do not completely inactivate, which allows them (Smith *et al.*, 1998; Rugiero *et al.*, 2003; Mantegazza *et al.*, 2005) to conduct a small non-inactivating inward current, known as the persistent $Na_v$ current (Crill, 1996).

In many neuronal populations $Na^+$ channel opening at hyperpolarised potentials following recovery from inactivation has also been reported, known as the resurgent $Na^+$ current, and this property is believed to be conferred by associated $Na_v$ $\beta_4$-subunits(Aman *et al.*, 2009; Bant & Raman, 2010; Lewis & Raman, 2011). Here the $\beta_4$-subunit blocks the $Na^+$ channel pore at positive membrane potentials,

and in so doing inactivates the channel whilst preventing binding of the actual inactivation gate. Upon hyperpolarisation, the $\beta_4$-subunit dissociates allowing channel conductance (Grieco *et al.*, 2005). These observations are reinforced by a reduction of resurgent $Na_v$ currents following $Na_v$ $\beta_4$ subunit knockdown (Bant & Raman, 2010).

Alongside, conducting a rapidly inactivating inward conductance of $Na^+$ ions, a second smaller non-inactivating conductance state termed the persistent sodium current ($Na_P$) is also observed in physiological measurements of $Na_v$ (Stafstrom et al., 1982, 1985). Based upon single-channel recordings $Na_P$ appears to primarily result from both short bursts of late $Na_v$ opening and a second gating modality in which a small population of $Na_v$ channels fail to inactivate and exhibit sustained firing (Alzheimer et al., 1993). The low probability of these gating events explains the small size of $Na_P$ relative to transient $I_{Na}$. At hyperpolarised membrane potentials, $Na_v$ window currents also contribute to $Na_P$ (Attwell et al., 1979).

Whilst $Na_P$ is present in currents recorded from heterologously expressed pore-forming $Na_v$ α-subunits (Aman et al., 2009), $Na_P$ is significantly larger when α-subunits are co-expressed with $\beta_3$ (Qu et al., 2001) and $\beta_4$-subunits (Aman et al., 2009), and like resurgent current $Na_P$ is reduced following $\beta_4$-subunit knockdown (Bant & Raman, 2010). Conversely, co-expression of $Na_v$ $\beta_1$ subunits inhibits the $\beta_4$ associated increase in persistent current (Aman et al., 2009). In addition to the differences in persistent current amplitude conferred by $Na_v$ β subunits, the identity of the Nav α-subunit itself also appears to influence the size of the persistent current. For example, heterologously expressed $Na_v1.6$ α-subunits conduct a larger persistent current than $Na_v1.2$ α-subunits (Chen et al., 2008).

### 1.4.2 Voltage-gated potassium channels

Potassium channels represent the largest mammalian family of ion channels with 145 associated channels, 40 of which belong to the $K_v$ family (Ranjan *et al.*, 2019). This makes the $K_v$ family the largest of the voltage-gated ion channel families. $K_v$ channels are further divided into 12 sub-families, $K_V1$-$K_v12$. $K_v$ have seen a particularly large share of biophysical research, in part because they are especially selective for their preferred ion species, $K^+$, when compared to other voltage-gated families (Dudev & Lim, 2009).

$K_v$ are tetrameric channels, and heteromeric subunit co-assembly can occur, for example within subunits of the $K_v1$ family (Isacoff *et al.*, 1990; Ruppersberg *et al.*, 1990; Wang *et al.*, 1999), $K_v2$ family (Kihira *et al.*, 2010) and $K_v7$ family (Wang *et al.*, 1998) as well as between $K_v$ sub-families (Gayet-Primo *et al.*, 2018). Diversity within the $K_v$ family is increased further by RNA-editing of $K_v$ transcripts via extensive alternative splicing (Xie & McCobb, 1998; Pan *et al.*, 2001; Zandany *et al.*, 2015) and enzymatic deamination of adenosine residues by adenosine deaminase acting on RNA (ADAR) (Patton *et al.*, 1997). These modifications independently alter key $K_v$ characteristics such as cell surface expression and channel kinetics. The evolutionary importance of these processes is emphasised by their conservation across invertebrate (Patton *et al.*, 1997; Rosenthal & Bezanilla, 2002; Hoopengardner *et al.*, 2003; Garrett & Rosenthal, 2012; Zandany *et al.*, 2015) and vertebrate (Pan *et al.*, 2001; Hoopengardner *et al.*, 2003; Bhalla *et al.*, 2004) species.

Protein phosphorylation of $K_v$ subunits, and association of $K_v$ auxiliary subunits such as $K_v\beta_{1\text{-}3}$ provide further modification of $K_v$ function. For example, $K_v\beta_{1\text{-}2}$ were shown to increase $K_v4.3$ plasma membrane expression (Yang *et al.*,

2001) and $K_v\beta_1$ confers inactivation kinetics onto $K_v1$ family members (Rettig *et al.*, 1994)(See **1.4.2.1**).

The remarkable diversity of the $K_v$ family allows for a varied kinetic profile, examples of which are described in **1.4.2.1-1.4.2.3** for $K_v$ family members of particular importance to this thesis. Through tissue and cell specific patterns of $K_v$ expression and function, these channels confer a wide range of action potential kinetics and firing properties to excitable cells (Humphries & Dart, 2015), alongside contributing to a plethora of physiological processes including renal potassium secretion (Carrisoza-Gaytán *et al.*, 2010) and hormone secretion (Yan *et al.*, 2004).

### 1.4.2.1 A-type $K_v$ current

A-type $K^+$ current refers to a family of $K_v$ which share similar kinetics, namely fast activation and fast inactivation (Hagiwara *et al.*, 1961; Connor & Stevens, 1971; Neher, 1971; Thompson, 1977). The pharmacology of A-type current has long been used to identify it, 4-amino pyridine (4-AP) is a classical A-type inhibitor, but it is insensitive to $K^+$ current inhibitor tetraethylammonium (TEA) (Thompson, 1977). The channels that conduct A-type current include $K_v1.4$, $K_v3.3$-$3.4$ and $K_v4.1$-$4.3$ (Zemel *et al.*, 2018). In addition, association of $K_v\beta1$ confers A-type kinetics on $K_v$ subunits which do not otherwise show inactivation (Rettig *et al.*, 1994). Prior work in SCG neurons highlights two A-type currents, with faster and slower kinetics (Malin & Nerbonne, 2000). The authors further suggest that $K_v4.2$ (*KCND2*) and $K_v1.5$ (*KCNA5*) are the primary $K_v$ subunits responsible for fast A-type potassium current in these neurons (Malin & Nerbonne, 2000, 2001).

A-type channels activate between -60 mV and -45 mV and begin to undergo voltage-dependent steady-state inactivation from -80 mV to full inactivation at -40

mV (Amberg *et al.*, 2003). They are mostly inactive around the RMP due to this steady-state inactivation. Physiologically reversal of the inactivation is achieved by action potential afterhyperpolarisations (Connor & Stevens, 1971), which has an important functional role in determining neuronal firing. As A-type activates between -60 and -45 mV, removal of steady state inactivation during the after-hyperpolarisation leads to A-type activation. This in turn delays membrane depolarisation and causes a lag between action potentials, thus decreasing the neuronal firing rate (Connor & Stevens, 1971).

#### 1.4.2.2 Delayed rectifier $K^+$ currents

Delayed rectifier potassium current ($K_{DR}$) is characterised by its slow activation and lack of voltage-dependent inactivation (Hodgkin & Huxley, 1952*a*; Hutter & Noble, 1960; Noble & Tsien, 1969; Blaine & Ribera, 2001). In SCG neurons, $K_v2$ channels contribute the majority of delayed rectifier current (Malin & Nerbonne, 2002; Liu & Bean, 2014). Inhibition of these channels decreases SCG neuron firing rate (Liu & Bean, 2014). In other cell types, $K_v3.1$ and $K_v3.2$ subunits also contribute to the delayed rectifier current (Itri *et al.*, 2005).

#### 1.4.2.3 M-current

M-current, is a non-inactivating $K_v$ which exhibits slow activation and deactivation kinetics and lacks voltage-dependent inactivation (Brown & Adams, 1980). M-current was originally described in sympathetic neurons where it was notable for its inactivation by the neurotransmitter muscarine (Brown & Adams, 1980; Adams *et al.*, 1982). Due to its lack of inactivation M-current plays a role in determining the RMP (Brown & Adams, 1980), alongside neuronal input resistance

(Shah *et al.*, 2008), rheobase (Martinello *et al.*, 2019), and firing rate (Aiken *et al.*, 1995; Peters *et al.*, 2005).

$K_v7.2$ and $K_v7.3$ heteromers from the archetypal M-current conducting channel (Wang *et al.*, 1998), however $K_v7.4$ and $K_v7.5$ also form viable M-current conducting constructs (Lerche *et al.*, 2000; Selyanko *et al.*, 2000; Schroeder *et al.*, 2000*a*; Wickenden *et al.*, 2001; Shah *et al.*, 2002). $K_v7.5$ can form functional homomers alone, or heteromers in combination with $K_v7.3$ (Schroeder *et al.*, 2000) and $K_v7.4$ (Brueggemann *et al.*, 2014). Subunit differences confer alternate pharmacology and activation kinetics. For example, whilst $K_v7.2$ containing channels are sensitive to TEA (Wang *et al.*, 1998), $K_v7.5$ containing hetereomers are relatively TEA insensitive (Schroeder *et al.*, 2000). Additionally, M-current conducted by $K_v7.5$ subunit containing channels activates more slowly (Schroeder *et al.*, 2000) than M-currents conducted by $K_v7.2$ containing channels (Biervert *et al.*, 1998).

M-current is dependent upon membrane $PIP_2$, and $PIP_2$ depletion leads to an inhibition of M-current conducting channels (Suh & Hille, 2002; Zhang *et al.*, 2003; Suh *et al.*, 2006; Robbins *et al.*, 2006). $G_q$ signalling appears to dramatically reduce membrane $PIP_2$ activity (Suh *et al.*, 2006) and therefore inhibits M-current (Brown & Passmore, 2009).

Alongside $PIP_2$ regulation of M-current, there is also evidence of calmodulin-dependent $Ca^{2+}$ regulation of both M-current (Gamper & Shapiro, 2003; Gamper *et al.*, 2005; Kosenko & Hoshi, 2013) and $K_v7$ subunit trafficking (Alaimo *et al.*, 2009). Raised intracellular $Ca^{2+}$ inhibits M-current in a $PIP_2$ independent manner (Martinello *et al.*, 2015). Currently a direct $Ca^{2+}$-binding site has not been identified on KCNQ subunits, and heterologously expressed KCNQ subunits appear to have

little sensitivity to intracellular $Ca^{2+}$ (Gamper & Shapiro, 2003). Upon co-expression of KCNQ subunits with calmodulin, M-current becomes extremely sensitive to intracellular $Ca^{2+}$ elevations (Gamper & Shapiro, 2003). Calmodulin is also believed to be involved in the intracellular trafficking of KCNQ2 subunits, whereby association with calmodulin is required for KCNQ2 transport out of the endoplasmic reticulum (Etxeberria *et al.*, 2008). Co-expression of a $Ca^{2+}$-insensitive variant of calmodulin increased endoplasmic reticulum accumulation of KCNQ2, suggesting that this process is $Ca^{2+}$-dependent (Alaimo *et al.*, 2009).

Whilst most reports are in agreement on these mechanisms, a recent study suggests M-current activation following $M_1$ activation in dentate gyrus granule neurons (Carver & Shapiro, 2019). In this work, the authors suggest that $M_1$ activation leads to an increased synthesis of $PIP_2$ synthesis, thereby eliciting an increase in M-current. This is reported to be downstream of an $M_1$ mediated increase in TRPC $Ca^{2+}$ influx, which subsequently stimulates $PIP_2$ synthesis. These data are in disagreement with the contemporary understanding of $M_1$ mediated depletion of $PIP_2$ in neurons, and ignores the inhibitory effect of elevated $Ca^{2+}$ on M-current (Selyanko & Brown, 1996; Martinello *et al.*, 2015). Additionally, these data are in direct contradiction with prior work, which demonstrates that $M_1$-mediated increases dentate gyrus granule neuronal excitability downstream of a $Ca^{2+}$-dependent inhibition of M-current (Martinello *et al.*, 2015). Further confirmation is needed before this proposed mechanism is credible, for example a direct measurement of changes in subcellular compartment $PIP_2$ levels following $G_q$ signalling. However, based upon the earlier work of Martinello *et al.* (2015) it seems unlikely that the mechanism described by Carver & Shapiro (2019) is correct.

Finally, M-current is also directly activated by the endogenous neurotransmitter, γ-aminobutyric acid (GABA) in a KCNQ subunit-specific manner (Manville *et al.*, 2018). However, currently the evidence for a physiological role for this phenomenon in neurotransmission is lacking.

### 1.4.3 Hyperpolarisation cyclic nucleotide activated channels

Hyperpolarisation cyclic-nucleotide activated (HCN) channels (Noma & Irisawa, 1976) are cation selective ion channels present in a range of neuronal populations (Paál *et al.*, 2003; Notomi & Shigemoto, 2004; Mobley *et al.*, 2010; Gao *et al.*, 2012), as well as in pacemaking cells of the heart (Noma & Irisawa, 1976; Difrancesco, 1986). HCN channels are gated by both voltage and intracellular cyclic nucleotides. Characteristically HCN channels display very unusual voltage-dependent activation, in that they begin to activate at potentials more hyperpolarised than -50 mV. Due to their permeability to $K^+$ and $Na^+$, HCN channels have a reversal potential between -25 mV and -40 mV (Biel *et al.*, 2009), resulting in membrane depolarisation from a typical RMP. HCN channels appear to have very low conductance, at around 1 pS (Difrancesco, 1986; Kole *et al.*, 2006), although this is disputed (DiFrancesco, 2005; Simeone *et al.*, 2005).

Four HCN genes and corresponding subunits have currently been identified, *HCN1-4* (Ludwig *et al.*, 1998; Santoro *et al.*, 1998), with each of these subunits exhibiting different kinetics and nucleotide binding affinities. All four HCN subunits are expressed in central neuron populations, with region specific subunit expression (Notomi & Shigemoto, 2004). HCN1-4 are all expressed in homogenised SCG tissue (Kullmann *et al.*, 2016), although stellate ganglia expression and function is unknown.

HCN channels do not inactivate, and due to being activated at typical neuronal membrane potentials, influence RMP and input resistance. This is best demonstrated by membrane polarisation hyperpolarisation and increased input resistance observed following inhibition of HCN via either selective pharmacological inhibitors (Yamada-Hanff & Bean, 2015; Hu & Bean, 2018) or $Cs^+$ mediated inhibition (Magee, 1998).

Intracellular cyclic nucleotides bind directly to the c-terminus of HCN channels (DiFrancesco & Tortora, 1991; Zagotta *et al.*, 2003), which causes a depolarising shift in channel kinetics, resulting in channel activation around physiological membrane potentials. Equally, decreases in intracellular cyclic nucleotide levels cause a hyperpolarising shift in HCN kinetics reducing current at typical membrane potentials. Either cAMP or cGMP can bind to HCN channels to enact shifts in activation kinetics (Ludwig *et al.*, 1998), with a markedly higher sensitivity to cAMP than cGMP.

HCN1-4 have varied activation kinetics, where HCN1 is the fastest activating subunit and HCN 4 the slowest (Biel *et al.*, 2009), with HCN3 (Stieber *et al.*, 2005) and HCN2 displaying intermediate kinetics. However, even HCN1 activation kinetics are relatively slow relative to other voltage-gated channels (Ishii *et al.*, 2001). HCN1 has a very weak shift in activation $V_{0.5}$ following cAMP binding in the order of 2–10 mV (Santoro *et al.*, 1998), whilst HCN2 and 4 see much larger (20-30 mV) shifts in activation $V_{0.5}$ (Ludwig *et al.*, 1999). HCN3 on the other hand appears to be cAMP insensitive (Stieber *et al.*, 2005). Further functional variation occurs due to the formation of HCN heteromers which significantly alter the kinetics of the final HCN channel (Altomare *et al.*, 2003).

### 1.4.4 Voltage-gated $Ca^{2+}$ channels

The $Ca_v$ family has several key roles in neurons including neuronal excitability, neurotransmitter release and control of transcription. Under physiological conditions $Ca_v$ conduct an excitatory inwards current, with an approximately >500-fold higher selectivity for $Ca^{2+}$ than $Na^+$ in normal physiological solutions (Sather & McCleskey, 2003).

Ten $Ca_v$ α subunits have been identified $Ca_v$1.1-1.4, $Ca_v$2.1-2.3 and Cav3.1-3.3, but discussion here will be limited to neuronal $Ca_v$, which include $Ca_v$1.2-1.3, $Ca_v$2.1-2.3 and $Ca_v$3.1-3.3. Of these neuronal subunits, $Ca_v$1.2-1.3 are termed L-type, $Ca_v$2.1 P/Q-type, $Ca_v$2.2 N-type, $Ca_v$2.3 R-type and $Ca_v$3.1-3.3 T-type (Nowycky *et al.*, 1985; Dolphin, 2016).

In addition, these channels are often grouped in low voltage activated (LVA) and high voltage activated (HVA) channels based upon the membrane potentials upon which they activate (Carbone & Lux, 1984). T-type $Ca_v$ are activated at -50 mV and therefore belong to the LVA family, whilst remaining channels belong to the HVA family and are activated at around -20 mV(Hagiwara *et al.*, 1975; Bean, 1985). Both HVA and LVA channels can inactivate, although the degree to which this occurs depends upon the $Ca_V$ subunit. Notably, whilst both HVA and LVA channels possess voltage dependent inactivation, only HVA $Ca_V$ channels have been shown to exhibit $Ca^{2+}$ dependent inactivation, where rises in $[Ca^{2+}]_i$ reduce channel function.

L-type encoding subunits are primarily present on the neuronal somato-dendritic compartment (Di Biase *et al.*, 2008; Jenkins *et al.*, 2010), and are so named due to the initial description their long-lasting and relatively large currents (Hess *et al.*, 1984; Nowycky *et al.*, 1985). Neuronal L-type channels alter the action

potential waveform (Bean, 2007), and couple neuronal activity to transcriptional changes (West *et al.*, 2001). L-type $Ca_v$ currents have been previously identified in sympathetic neurons (Lipscombe *et al.*, 1988).

P/Q-type $Ca_v$ are localised within the presynaptic terminal of a range of neurons, but has been pharmacologically excluded from SCG neurons (Mintz *et al.*, 1992*a*), although a later reports suggests that they are present in the stellate ganglia (Kukwa *et al.*, 1998; Fuller *et al.*, 2004*a*). P-type are so named due to their high expression in Purkinje neurons of the cerebellum (Hillman *et al.*, 1991), whereas Q-type channels are splice variants of the P-type channel (Bourinet *et al.*, 1999) with a lower sensitivity to P-type antagonist Omega-agatoxin-IVA (Mintz *et al.*, 1992*b*; Randall & Tsien, 1995).

N-type is present in sympathetic neurons (Lipscombe *et al.*, 1988), and are so named for being non L-type or T-type and neuronal in Tsien's original characterisation (Nowycky *et al.*, 1985). Like P/Q type channels, N-type current is involved in synaptic transmission, but N-type $Ca_v$ are favoured in peripheral neurons including sympathetic neurons (Lipscombe *et al.*, 1988; Fuller *et al.*, 2004*b*).

R-type is so named due to being the residual current after the application of common $Ca_v$ inhibitors at the time of characterisation, and is thus relatively resistant to pharmacological manipulation (Randall & Tsien, 1995). R-type $Ca_v$ channels are poorly understood comparison to other members of the $Ca_v$ family, but are known to have a relatively wide expression in central neurons, with pre- and post-synaptic expression patterns (Parajuli *et al.*, 2012). Limited experimental work has revealed a role for R-type $Ca_v$ in determining sensory neuron activity (Matthews *et al.*, 2007) and neurotransmitter release (Terashima *et al.*, 2013), but further work is required.

T-type $Ca_v$ are LVA and named for their “transient” and ”tiny” current (Nowycky *et al.*, 1985). T-type $Ca_v$ require only a small depolarisation to roughly -60 mV to activate, a small deviation from typical neuronal RMP. As the name suggests, T-type $Ca_v$ exhibit relatively fast activation and inactivation for $Ca_v$ (Carbone & Lux, 1984; Perez-Reyes, 2003). However, the activation and inactivation kinetics of all $Ca_v$ are such that there are a range of potentials where incomplete inactivation and high activation leads to a steady state window current. This is especially relevant in T-type $Ca_v$, where the window current is typically only slightly depolarised from the RMP (Perez-Reyes, 2003). This uniquely allows T-type $Ca_v$ to conduct a steady-state $Ca^{2+}$ current near to the RMP.

### 1.4.5 Calcium-activated $Cl^-$ channels

Calcium-activated $Cl^-$ channels (CaCC) are a family of $Cl^-$ conducting channels, which exhibit voltage-dependence (Xiao *et al.*, 2011). Further, these channels exhibit outward rectification at low $[Ca^{2+}]_i$ which is diminished at higher $[Ca^{2+}]$ (Xiao *et al.*, 2011). CaCCs are encoded by *ANO1* and *ANO2*, encoding TMEM16A (Caputo *et al.*, 2008; Schroeder *et al.*, 2008; Yang *et al.*, 2008) and TMEM16B (Stöhr *et al.*, 2009) respectively. The mechanism of $Ca^{2+}$ sensitivity in CaCCs is speculated to be via direct binding (Tien *et al.*, 2014; Dang *et al.*, 2017), although the exact binding site is still unproven.

Unlike most other physiologically important ions, intracellular $[Cl^-]$ is maintained at drastically different concentrations amongst different cell populations (Koncz & Daugirdas, 1994; Kuner & Augustine, 2000; Kaneko *et al.*, 2002), which through shifting the Nernst potential for $Cl^-$ can make $Cl^-$ channels either excitatory or inhibitory (Tyzio *et al.*, 2006). So in neurons CaCCs can cause

afterdepolarisations (Mayer, 1985), or shorten action potential duration and dampen neuronal excitability (Huang *et al.*, 2012).

### 1.4.6 $K_{Ca}$ channels

$K_{Ca}$ channels are activated by elevations in $[Ca^{2+}]_i$, although the exact nature of this process varies between $K_{Ca}$ subtypes. Small conductance (SK) channels ($K_{Ca}$2.1-2.3), encoded by *KCNN1-3* (Köhler *et al.*, 1996), sense rises in $[Ca^{2+}]_i$ indirectly by through an associated calmodulin protein (Xia *et al.*, 1998). A similar mechanism is exhibited by intermediate conductance (IK) channels ($K_{Ca}$3.1), encoded by *KCNN4* (Morales *et al.*, 2013). Alternatively, large conductance (BK) channels $K_{Ca}$1.1, encoded by *KCNMA1* (Butler *et al.*, 1993), directly bind $Ca^{2+}$ at two C-terminal binding sites (Xia *et al.*, 2002). Whilst only one BK encoding gene is known, 12 splice variants of this channel have been identified (Saleem *et al.*, 2009). Further, the properties of BK channels are modulated through association of one of four β-subunits (Wallner *et al.*, 1999).

The high $Ca^{2+}$ sensitivity of SK and IK via allows them to sense $Ca^{2+}$ changes from a range of $Ca^{2+}$ sources within the same microdomain. BK channels are less sensitive to elevations in $[Ca^{2+}]_i$ and require elevations of >10 µM to shift voltage-dependent activation into a physiological range (Rothberg & Magleby, 2000). This relatively large increase in $Ca^{2+}$ is most frequently observed in $Ca^{2+}$ nanodomains, near $Ca^{2+}$ sources, where $Ca^{2+}$ can rise to as high as 100 µM on a microsecond timescale (Neher, 1998; Augustine *et al.*, 2003). For this reason, BK channels are found in functional and physical association with $Ca^{2+}$ channels, perhaps most elegantly demonstrated by inhibition of BK conductance with high-affinity $Ca^{2+}$ chelator, BAPTA (Berkefeld *et al.*, 2006).

Further functional differences occur between these channel types. SK and IK channels have no voltage-dependence (Stocker, 2004), but BK channels exhibit voltage dependence via a similar mechanism to other $K_v$ (Yang *et al.*, 2015). SK channels, whilst not voltage-dependent in a classical sense do display inward rectification at positive membrane potentials by physiologically plausible concentrations of $Mg^{2+}$ and $Ca^{2+}$ (Soh & Park, 2001).

SK channels undergo fast activation in response to calcium with an activation time constant of 5-15 ms (Xia *et al.*, 1998). BK channels activate with an even faster and more complicated $Ca^{2+}$ and voltage-dependent time constant which varies dependent upon cell type and location. One estimate places activation between the range of 1.4-4.5 ms (Sun *et al.*, 2004). Notably this difference is due to differing channel kinetics and not the differing $Ca^{2+}$ sources, as even microdomain level changes occur in milliseconds (Neher, 1998; Augustine *et al.*, 2003). SK channels deactivate relatively slowly upon the removal of $Ca^{2+}$ (Berkefeld *et al.*, 2006), whereas BK channel deactivation is extremely rapid (Li & Aldrich, 2004). As suggested by their nomenclature, SK channels have a relatively low single channel conductance of 9-10 pS (Köhler *et al.*, 1996), IK have a relatively intermediate conductance of 39 pS (Ishii *et al.*, 1997; Joiner *et al.*, 1997; Logsdon *et al.*, 1997) and BK channels a large conductance of 100-300 pS (Marty, 1981; Yang *et al.*, 2015). It is worth noting that further variance in channel kinetics occurs for all $K_{Ca}$ channels based upon the association of auxiliary subunits (Li & Yan, 2016), although this is beyond the scope of this work.

Together these properties ensure that SK and IK channels have a different functional role to that of BK channels. SK kinetics mean that in neurons they are involved in the generation of the medium after-hyperpolarisation, determining firing

rate, temporal precision and are involved in the generation of more complicated firing behaviours such as burst firing neurons (Stocker, 2004). In SCG neurons, SK channel inhibition increased firing rate (Kawai & Watanabe, 1986). Which is similarly observed in central neurons (Hallworth *et al.*, 2004), where SK activation can reverse this effect (Cingolani *et al.*, 2002). IK channels are often expressed in non-neuronal cell types, where they regulate membrane potential and provide negative feedback for $Ca^{2+}$ signalling (Kshatri *et al.*, 2018). BK channels in neurons, with their faster kinetics, contribute to action potential width and neuronal firing rate (Kshatri *et al.*, 2018).

### 1.4.7 $K_{Na}$ channels

The $K_{Na}$ family, are a family of $K^+$ channels which are directly regulated by $Na^+$ (Yuan *et al.*, 2003). Two channels have been identified within this family, “Sequence like an intermediate conductance K channel” (slick) and “Sequence like A calcium-activated K channel” (slack), encoded by the genes *KCNT2* and *KCNT1* respectively. The presence of $K_{Na}$ was first highlighted in cardiomyocytes (Kameyama *et al.*, 1984), but has since been documented in a variety of peripheral (Dryer, 1991; Bischoff *et al.*, 1998) and central neurons (Schwindt *et al.*, 1989).

Both slick and slack are activated by rises in intracellular $Na^+$ concentration ($[Na^+]_i$), but slack has a two-fold higher affinity for $[Na^+]_i$ (Bhattacharjee *et al.*, 2003). Macroscopic ion concentrations remain relatively constant, but transient increases in $[Na^+]_i$ follow sustained activation of persistent $Na_v$ current (Rose & Ransom, 1997) and $Na^+$ permeable ligand-gated receptors (Kiedrowski *et al.*, 1994). Slack channels are normally inhibited by intracellular $Ca^{2+}$, however slack subunits can form

intermediate conductance $Ca^{2+}$-activated heteromers with BK subunits (Joiner *et al.*, 1998).

## 1.5 Summary

The SNS is part of a complex physiological network, and thereby is normally under strict control during physiological conditions. However, this is perturbed during hypertension. Cardiac and renal sympathetic neurons play a critical role in hypertensive physiology (Schlaich *et al.*, 2003), yet both are poorly understood. Recent attempts at renal denervation have failed to improve patient outcomes (Bhatt *et al.*, 2014). Targeting sympathetic innervation at postsynaptic β-receptors is efficacious for reducing blood pressure, but not at reducing mortality which may be due to incomplete block of neuronal co-transmitter action (Herring, 2015). This thesis attempts to identify new mechanisms for targeting presynaptic sympathetic neurons through regulating neuronal activity.

Neuronal firing properties are important determinants of neuronal function, which are coupled to neurotransmitter release (Mackenzie *et al.*, 1996; Kreitzer *et al.*, 2000) and therefore post-synaptic function (Koester & Johnston, 2005). This property is a direct product of ion channel function, which can be regulated by many processes including GPCR dependent mechanisms (Altier & Zamponi, 2011) and gene expression changes (Roden & Kupershmidt, 1999). This thesis sets out to identify how ion channels underpinning SGN firing properties are perturbed in hypertension. It also expands on the knowledge of how the firing property of these neurons can be regulated by novel signalling pathways to increase the repertoire of available targets.

Chapter 3 describes the transcriptomic phenotype of rodent SGNs cultured from normotensive and hypertensive rodents using a combination of single-cell and bulk RNA-sequencing. In chapter 4, a description of a putative mechanism of sympathetic hyperactivity is made using perforated patch-clamp, alongside identifying alternate targets for the ablation of this hyperactivity**.** Chapter 5 investigated the ability for sympathetic neurons to sense extracellular sodium via $Na_x$. Finally, chapter 6 investigated SGN signalling through transient receptor potential channels, sensory receptors and glutamatergic receptors, alongside retrograde signalling by cardiomyocytes.

# Chapter 2

## Methods

# Methods

## 2.1 Animal experiments

Animal use complied with the University of Oxford Local Ethical Guidelines and was in accordance with the Guide for the Care and Use of Laboratory Animals published by the US National Institutes of Health (Publication No. 85-23, revised 2011) and the Animals (Scientific Procedures) Act 1986 (United Kingdom). Experiments were performed under British Home Office Project License (PPL 30/3131 [D.J.P.] and P707EB251 [D.J.P.]). All animals were purchased from Envigo, UK. Animals were house in the local animal facility in open top conventional cages at 20-24ºC with 55% Relative Humidity on a 12-hour day-night cycle. Air within the housing room was cycled approximately 60 times per hour. Water was changed 3-4 times per week. Animals were socially housed generally in groups of 2-4, and their cages were changed once per week. Nesting material was provided in the form of Sizzlenest and woodchip. Animals were provided with one plastic enrichment item; either a red plastic house or a red plastic tunnel and one cardboard enrichment item; either a cardboard house or a cardboard tunnel. To cull the animals, they were first anaesthetised via isoflurane, and then euthanized via an intraperitoneal overdose of pentobarbitone and confirmed via exsanguination according to Schedule 1 of the Animals (Scientific Procedures) Act 1986 (United Kingdom). Male normotensive Wistar rats and male prehypertensive SHRs were culled at 5 to 6 weeks of age, at which age SHRs possess a phenotype unaffected by prolonged hypertension as found in older animals (Minami *et al.*, 1989; Dickhout & Lee, 1998). Additionally, in this age range postnatal ion channel expression is believed to have mostly stabilised in rodent sympathetic ganglia (Hadley *et al.*, 2003). Animals were all handled before culling by a male experimenter.

## 2.2 Cell culture

The following protocol is from Davis *et al.* (2020), and was adapted from existing culture protocols in order to improve cell viability and yield. Bilateral stellate ganglia were visually dissected from a minimum of two euthanised five to six-week old male rats, before being immediately transferred to ice-cold HEPES buffered L-15 media (L1518, Thermofisher, US). Contaminating tissue was removed from the stellate ganglia alongside the fibrous outer sheath covering the ganglia. The cleaned stellate ganglia were then cut into roughly 2 mm sections using surgical scissors to increase the surface area of the tissue. The resultant tissue pieces were then enzymatically digested at 37$^{o}$C using 1 mg/ml Collagenase IV (Worthington, US) in L15 for 25 minutes, followed by 30 minutes in 2 mg/ml Trypsin (Worthington, US) in $Ca^{2+}$ and $Mg^{2+}$ free Hanks buffered salt solution (Thermofisher, US) with 0.1 mg/ml DNAase I (Fischer, 1982) to limit cell aggregation (Reichard & Asosingh, 2019). Collagenase activity was then inhibited using two washes of a blocking solution **Table 2.1**. The digested tissue suspension was resuspended in a Neurobasal plus based plating media (**Table 2.2**) and mechanically disrupted using a sterilised fine-tipped glass pipette. The cell suspension was then plated onto Poly-D-lysine precoated Fluorodish 35 mm dishes (WPI, US) which had been pre-incubated for two hours with 1 ug/ml laminin. The concentration of laminin was chosen to limit neuronal outgrowth whilst still promoting cell survival (Buettner & Pittman, 1991). Cell containing dishes were subsequently incubated at 37 $^{o}$C with 95% oxygen and 5% CO2 for a period of one to five days *in vitro*.

*Table 2.1 Blocking media*

| | **Blocking media** |
|---|---|
| **L-15** (L1518, Thermofisher, US) | 95 mL |
| **Fetal bovine serum** (Sigma Aldrich, US) | 2 mL |
| **Penicillin-streptomycin (10,000 U/mL)** (Thermofisher, US) | 1000 µL |

*Table 2.2 Neuronal plating media used for the majority of culture-based experiments*

| | **Plating media** (Neurobasal plus based) |
|---|---|
| **Neurobasal plus media** (Thermofisher, US) | 97.15mL |
| **B27 plus** (Thermofisher, US) | 2 mL |
| **2.5s NGF (100ug/ml)** (Merck Millipore, US) | 100 µL |
| **Glutamax** (Thermofisher, US) | 250 µL |
| **Penicillin-streptomycin (10,000 U/mL)** (Thermofisher, US) | 500 µL |

## 2.3 Patch-clamp electrophysiology

Patch-clamp refers to a range of electrophysiological techniques which facilitate the study of ion channel function from single ion channels to recordings of an entire cell's electrical properties. The general methodology was invented (Neher & Sakmann, 1976; Hamill *et al.*, 1981; Sakmann & Neher, 1984) (Nobel prize, 1991), as a low-noise approach that offered significant advancement over previous electrophysiological techniques such as the intracellular perfusion (Kostyuk, 1984) and intracellular sharp recording methods (Parkington & Coleman, 2012). The use of low-resistance fine

tipped glass micropipettes, with fire polished tips alongside inward pressure allowed for the formation of a tight physical seal between the pipette tip and the membrane of the cell (Hamill *et al.*, 1981). This tight seal has an electrical resistance ≥1 GΩ, which facilitates a low-noise recording of channels positioned under the pipette tip (Hamill *et al.*, 1981). This original configuration is known as the cell-attached configuration and allows for records of one or several channels depending upon the size of the pipette tip and the channel distribution of the cell (Maki *et al.*, 2014). Several further variations of this technique exist and are covered in **Figure 2.1**.

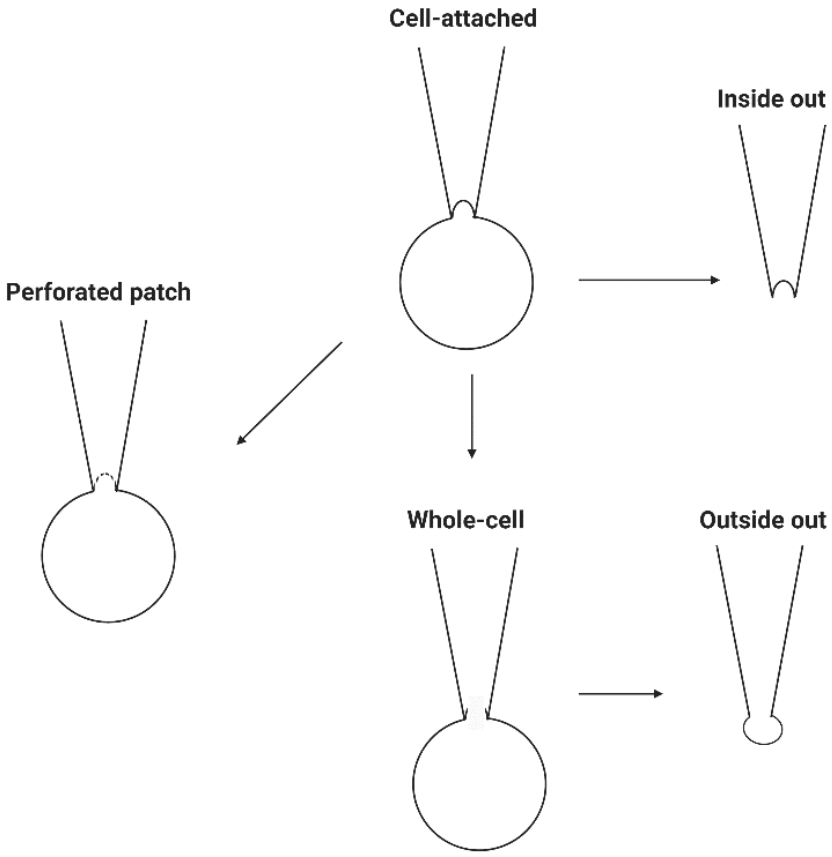



***Figure 2.1 Simple diagram of the primary methods of patch-clamp electrophysiology*** *The cell attached confirmation refers to the pipette being sealed onto the whole cell. The inside-out configuration refers to a detached piece of membrane with the intracellular facing side of the membrane exposed to the bath solution. This is achieved via retracting the pipette from the cell once in the cell-attached confirmation. Whole-cell refers to a state in which there is complete electrical and physical access to the inside of the cell following the rupture of the membrane under the pipette by negative pressure. Outside-out patch refers to a membrane patch with the extracellular membrane side facing the bath solution. This is achieved by retracting the pipette from the cell in the whole-cell configuration. The perforated patch-clamp configuration is a variation of whole-cell, where electrical access is achieved via the use of pore-forming perforating agents.*

Whole-cell configuration of patch-clamp remains the principle methodology for recording the electrophysiological properties of an entire cell (Hamill *et al.*, 1981; Sakmann & Neher, 1984; Segev *et al.*, 2016). In this technique, a ≥1 GΩ seal is formed as above, but sharp inward pressure is applied to facilitate direct electrical access to

the inside of the cell by rupturing the cells membrane under the pipette tip (**Figure 2.1**; Hamill *et al.*, 1981).

Whole-cell recordings can be performed in two electrical configurations, voltage-clamp and current-clamp. In voltage-clamp, the aim is to set the cells potential to a user-defined command potential and then measure the current movement across the membrane potential (Hamill *et al.*, 1981; Sakmann & Neher, 1984). This is measured as the current injected by the amplifier to reach the command potential and will in theory equal in size and opposite in polarity to any currents evoked by a change in the command potential or exposure to an exogenous ligand (Hamill *et al.*, 1981; Sakmann & Neher, 1984). Whole-cell voltage-clamp is used primarily to measure macroscopic ion channel currents. In whole-cell current-clamp the voltage is instead recorded, and the user controls the size and waveform of the current injected (Hamill *et al.*, 1981; Sakmann & Neher, 1984). Current-clamp is therefore typically used to measure the cells membrane potential, action potential kinetics, firing properties and the input resistance. An example picture of a SGN in the whole-cell configuration is shown in **figure 2.2**.

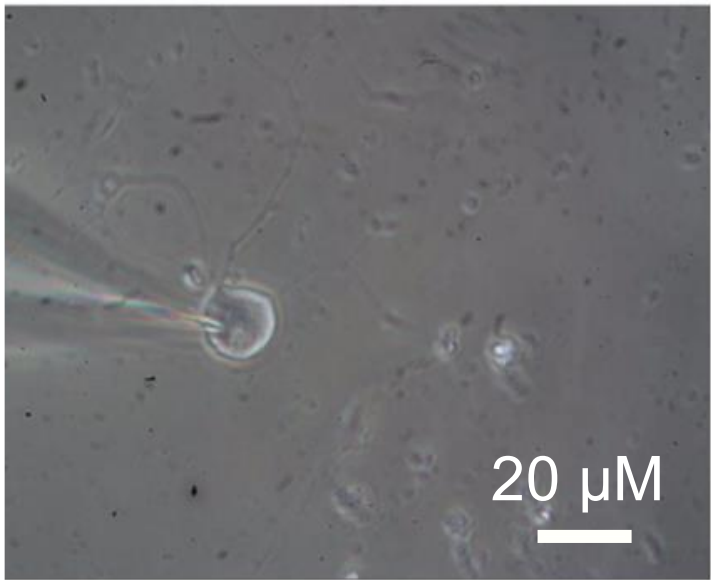



***Figure 2.2 A whole-cell patch-clamp recording of a cultured stellate ganglia neuron after two days in culture.***

By achieving electrical access to the inside of the cell in this manner, the ruptured membrane also facilitates perfusion of the inside of the cell with the solution on the inside of the pipette (Fenwick *et al.*, 1982). As the reservoir of solution within the glass pipette is many times larger than within the cell, the net effect of this is to replace the diffusible components of the intracellular solution with that of the recording electrode (Fenwick *et al.*, 1982; Oliva *et al.*, 1988). This allows the user to control the intracellular solution but can also result in channel rundown due a loss of intracellular factors or proteins over time. For example, this is apparent in whole-cell voltage-clamp $Ca_v$ recordings (Sarantopoulos *et al.*, 2004).

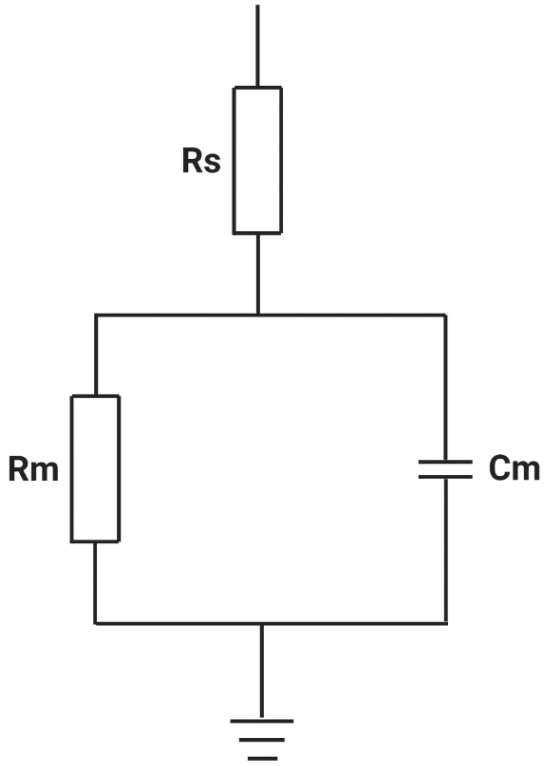



***Figure 2.3 Simplified circuit diagram of the pipette resistance in series with the membrane resistance and capacitance*** *Where $R_S$ indicates series resistance, $C_M$ the cell capacitance and $R_M$ the membrane resistance.*

A primary consideration during a whole-cell voltage-clamp recording is the contribution of the micropipette resistance to the electrical circuit between the electrode and the cell (Sigworth, 1995). This is referred to as the *series resistance* ($R_s$), as it is in series with the resistance and the capacitance of the cell's membrane (**Figure 2.3**) (Sigworth, 1995). $R_s$ primarily affects the recording in three ways; by filtering the recording, causing a delay in the membrane potential reaching the command potential, and finally causing a voltage drop (Sigworth, 1995).

The $R_s$ along with the $C_M$ forms a RC circuit, with time constant T (**Equation 2.1**). This RC circuit also causes a low-pass filter with a frequency cut-off as determined in **Equation 2**. For a cell with a $C_M$ value of 22-30 pF and a pipette with a $R_s$ value of 10 MΩ this causes a frequency cut-off of 530-723 Hz which can affect recordings of fast currents such as voltage-gated sodium currents. This low pass filter can also attenuate even low frequency signals if $R_s$ is large, thus limiting the cells ability to reach the desired command potential. Finally, this RC circuit is also responsible for the delay in achieving the command potential, as the amplifier must first charge the capacitor via the $R_s$, thus causing an initial lag.

***Equation 2.1 Equation determining time constant of the RC circuit affecting voltage-clamp patch-clamp circuitry*** *Where T is the time constant, $C_M$ is the membrane capacitance and $R_s$ is the series resistance.*

$$T = C_M . R_s$$

***Equation 2.2 Equation for the frequency cut-off of the low-pass filter formed by an RC circuit*** *Here* T *represents the time constant of the RC circuit, as determined in equation 1 or equation 4.* fc *refers to the frequency cut-off*.

$$f_c = \frac{1}{2.\pi.T}$$

Alongside the artefact introduced by the RC low-pass filter, an additional voltage drop can be determined by ohms law, as $R_s$ is in series with the cell (**Figure 2.3**) any current travelling through the pipette must cross the $R_s$. Thus, a voltage potential forms as shown in equation 2.3:

***Equation 2.3 Ohmic relationship between expected voltage-drop, pipette current and series resistance in patch-clamp*** *Where $V_p$ indicates the voltage-drop over the pipette, $I_p$ represents the current flowing through the pipette electrode and $R_s$ indicates the series resistance.*

$$V_p = I_p.R_s$$

If the $R_s$ value is large, or the current is large, the voltage-error, or voltage-drop, will be extremely large. For example, a 5 nA current across a 10 MΩ $R_s$ will cause a voltage-drop of 50 mV. The amplifier cannot distinguish between this voltage error (**Equation 2.2**) and the cell membranes voltage potential, and thus will measure the combination of the cell's potential and this voltage error. This is a function of the circuit behaving as a voltage divider (**Figure 2.3**), where the voltage is divided over the $R_s$

and the $R_M$. This makes the ratio of $R_M/R_s$ important, which should be at least 10, to ensure that most of the recorded voltage is due to current flow through $R_M$ not $R_s$.

These $R_s$ dependent effects can be limited via using low $R_s$ pipettes, limiting current sizes to reduce the voltage drop and through electronic $R_s$ compensation. For electronic compensation, the $R_s$ must first be estimated. To achieve this, the pipette and cell capacitances are first cancelled. The pipette capacitance ($C_{pip}$) is calculated in the cell-attached configuration and is cancelled by the user. This is a superficial process, as the circuitry does not affect the signal observed by the cell. The $C_M$ and $R_s$ are calculated from the remaining capacitive transients in whole cell. The $C_M$ is cancelled via similar circuitry to the pipette capacitance. An estimate of the $R_s$ can be calculated as the command voltage divided by peak of the RC current. $R_s$ compensation effectively reduces $R_s$ by a certain percentage, by injecting additional current with a slight delay. As this is a positive feedback mechanism over-compensation will typically lead to cell death. Thus, $R_s$ compensation is usually limited to percentages below 90%.

Physiological cells typically have multiple physical and/or electronic compartments and can be relatively large in size (Williams & Mitchell, 2008). True voltage-clamp only occurs in an area proximal to the patch pipette and this can therefore affect the voltage reading in distal parts of a complex cell (Bar-Yehuda & Korngreen, 2008; Williams & Mitchell, 2008). Indeed experimental evidence suggests that in neurons, voltage-clamp is only achieved in the neuronal soma (Williams & Mitchell, 2008). This should be considered when interpreting whole-cell voltage-clamp data.

In current clamp the $R_s$ dependent voltage-drop can be relatively simply accounted for using a process known as bridge balancing. The calculated ohmic (linear) voltage-error (**Equation 2.2**) across the pipette is subtracted from the recorded voltage potential. This change is purely cosmetic and does not affect the current injected by the cell, but it does results in a more accurate voltage output.

In current-clamp recordings, $R_s$ also has a second effect upon the recording, this time in concert with the parasitic capacitance ($C_p$). The parasitic capacitance refers to pipette capacitance, and capacitance from elements within the head stage and amplifier. Together these form a RC circuit (**Equation 2.4**), and this causes a low-pass filter upon the data as represented in **Equation 2.2**. In the typical range of parasitic capacitances (5-10 pF) with a typical $R_s$ (10 MΩ) this can result in a frequency cut-off of 1.6 KHz to 3.2 KHz as calculated by **Equations 2.2** and **2.4**.

***Equation 2.4 Time constant for RC circuit formed by parasitic capacitance and series resistance*** *$T_P$ stands for time constant for parasitic capacitance. $C_p$ is the parasitic capacitance. $R_s$ is the series resistance.*

$$T_p = C_p . R_s$$

In addition, during voltage changes the cell charges the $C_P$ instead of charging only the $C_M$ as would occur in physiology. By drawing current from the cell, this will affect the cells electrophysiological characteristics. This can be at least partially resolved by capacitance neutralisation, where the amplifier charges the $C_P$ rather than the cell. However, this capacitance neutralisation circuitry is not present in many

amplifiers and is very rarely neutralised. These effects must therefore be considered when viewing current clamp data.

Liquid junction potentials cause a static voltage-offset for both voltage-clamp and current-clamp recordings. Liquid junction potentials form between two contacting solutions with differing ion concentrations and are based upon the ion mobilities and concentrations. When the pipette and bath solutions have differing ionic compositions a liquid junction potential form between them. The electrode voltage is zeroed prior to patch-clamping a cell, and whilst this removes electrical artefacts, this liquid junction potential is also removed. During a whole cell recording, the junction potential is no longer present, but the correction for the liquid junction potential is still in effect. The observed potential is therefore the membrane potential plus the correction for the liquid junction potential. This can be corrected by either calculating (Barry, 1994) or measuring the junction potential experimentally, and subtracting this value from the voltage-clamp potential or $V_M$ measured in current clamp.

Whole-cell patch-clamp presents as the superior methodology for measuring the electrical properties of a cell relative to the primary alternatives; intracellular recordings, voltage dye recordings and measurement of $[Ca^{2+}]_i$ as a proxy for electrical activity. Intracellular recordings are inferior to whole cell for several reasons. Whole-cell patch-clamp provides a lower $R_s$, and therefore better electrical access, (Staley et al., 1992) with a stronger seal (Li et al., 2004) than intracellular sharp recordings. Voltage sensitive dyes are relatively cytotoxic, have distorted outputs and have a limited sampling frequency relative to microelectrode techniques (Preuss & Stein, 2013; Bando et al., 2019; Strack, 2019). Voltage-sensitive dyes and calcium dyes also do not allow for voltage-clamp or current-clamp, but instead only provide output from the cell (Preuss & Stein, 2013; Bando et al., 2019; Strack, 2019; Ali & Kwan, 2020).

Calcium dyes are a passable proxy for cell firing in vivo, but calcium imaging does not capture the nuisances of cellular electrophysiology such as well-resolved patterns of neuronal firing (Ali & Kwan, 2020).

### 2.3.1 Perforated patch clamp – theory

Whole-cell recordings can also be performed using ion-permeable perforating agents (Horn & Marty, 1988). In this methodology, a perforating agent such as nystatin, gramicidin, amphotericin or β-escin are dissolved in the intracellular recording period and integrate into the cell membrane whilst the cell is in the cell-attached configuration (Horn & Marty, 1988; Rae *et al.*, 1991; Linley, 2013). When this process is complete, electrical access to the inside of the cell is achieved, with a similar $R_s$ range similar to that observed in whole-cell recordings (Rae *et al.*, 1991; Linley, 2013). This limits the loss cell dialysis which occurs in whole-cell, and so is beneficial for recordings of cell processes which exhibit run-down due to the loss of intracellular factors (Horn & Marty, 1988). Different permeating agents have different advantages, for example, Nystatin, amphotericin-B and gramicidin-D are all $Ca^{2+}$ impermeant and so allow for relatively undisturbed intracellular $Ca^{2+}$ dynamics (Ishibashi *et al.*, 2012). Whereas β-escin is calcium permeable and so allows the user to determine the $[Ca^{2+}]_i$ (Fan & Palade, 1998; Sarantopoulos *et al.*, 2004). Gramicidin is $Cl^-$ impermeable and so allows for the determination and/or maintenance of physiological intracellular $[Cl^-]$ (Myers & Haydon, 1972). The major disadvantages of perforated patch-clamp are the increased difficulty and time require for recordings, as well as $R_s$ which tend to be slightly larger than in whole-cell (Ishibashi *et al.*, 2012).

### 2.3.2 Whole-cell patch clamp electrophysiology – methodology

Current-clamp recordings with a $R_s$ greater than >20 MΩ were discarded. For voltage-clamp recordings cells with a $R_s$ >12 MΩ were discarded. For $Na_v$ voltage-clamp recordings, recordings with a $R_s$ >8 MΩ were discarded. Recordings where the $R_s$ changed by more than 20% were discarded for voltage clamp. $R_s$ compensation of 70% was used for most voltage clamp recordings. For voltage-gated sodium channel recordings 80% $R_s$ compensation was used. For current-clamp recordings with a $R_s$ change greater than 30% were discarded. Cells with a leak current >90 pA were discarded. Cells were allowed to equilibrate for a period of 30 seconds, or until stable before recording was commenced.

External recording solutions are outlined in **Table 2.3**. The internal solution for whole-cell recordings featured in the main thesis contained: 130 mM K+ -Gluconate, 10 mM KCl, 10 mM HEPES, 10 mM Na+ -Phosphocreatine, 4 mM MgATP, 0.3 mM Na2GTP. Internal pH was adjusted to 7.3 with KOH. For $K_v$ and $Na_v$ recordings using TTX subtraction used the standard internal solution and the external solution in **Table 2.3**. For HCN recordings the external solution used in described in **Table 2.4**. For $Na_v$ isolating solutions the external solution in outlined in **Table 2.5**, and the internal in **Table 2.6**. For $K_v$ isolating solutions the external composition was: **Table 2.7** and the internal solution as above. All recordings were performed at room temperature. Pipettes with a tip resistance of 2-4 MΩ were used. A KCl agar salt bridge was used for the bath electrode. Data were acquired using WinWCP (Versions 5.4.0-5.5.4) and recorded via a Multiclamp 700B amplifier (Molecular Devices, US) and an axon digidata 1550A (Molecular devices, US) digitizer.

### 2.3.3 Perforated patch clamp electrophysiology – methodology

The perforating agent amphotericin (Rae *et al.*, 1991), at a concentration of 0.48 mg/ml was used for all perforated patch clamp recordings in this thesis. Full perforation took around 15-20 minutes. Following perforation $R_s$ was monitored for a period of 5 minutes to ensure stability before recording. Cells were held at -50 mV during seal formation as electronegative potentials aid seal formation and maintenance (Suchyna *et al.*, 2009; Segev *et al.*, 2016). Cells where immediate electrical access occurred were discarded, as they likely represented spontaneous whole cell recordings. This concentration allowed for consistent high-quality recordings with a good stability and low $R_s$ (<20 MΩ). Pipettes with a tip resistance of 2-4 MΩ were used. For perforated patch-clamp recordings, the internal solution contained the following: 145 mM $K^+$-Aspartate, 2.2 mM EGTA, 10 mM HEPES, 1 mM MgCl2. Internal pH was adjusted to 7.3 using KOH. For voltage-gated calcium recordings the external solution the external solution is described in **Table 2.8**. The internal solution was the standard perforated internal. For current-clamp perforated patch-clamp experiments cells with a $R_s$ >30 MΩ were discarded. For voltage clamp, recordings with a $R_S$ >12 MΩ were discarded. Voltage clamp recordings also employed 70% $R_s$ compensation. For both recording protocols $R_s$ was monitored at the beginning and ending of the recording, and changes greater than 20% were discarded. Liquid junction potentials were corrected in chapter 4 based upon an estimation of 24.3 mV by JPCalc (Barry, 1994) in Clampex (v11.0.3) (Molecular Devices, US), which was subtracted from the recorded membrane potential in current-clamp. An Ag/Cl pellet was used for the bath electrode. Data were acquired using WinWCP (Versions 5.4.0-5.5.4) and recorded via a Multiclamp 700B amplifier (Molecular Devices, US) and an axon digidata 1550A (Molecular devices, US) digitizer.

### 2.3.4 Analysis

Maximum firing rate was measured as the highest firing rate between 0-200pA current injections. Rheobase was taken as the smallest amplitude 1000ms positive current injection that could elicit an action potential. Input resistance was calculated as described previously (**Figure 2.5**; Spruston & Johnston, 1992). Voltage-clamp recordings analyses and drug subtractions were performed in Clampfit (Version 11.1) (Molecular devices, US). Otherwise analysis was performed within WinWCP.

### 2.3.5 Example recordings

Example current-clamp and voltage-clamp recordings are shown in **Figures 2.4-2.6**. All example recordings were performed with standard internals outlined in text and the physiological external solution in **Table 2.3**.

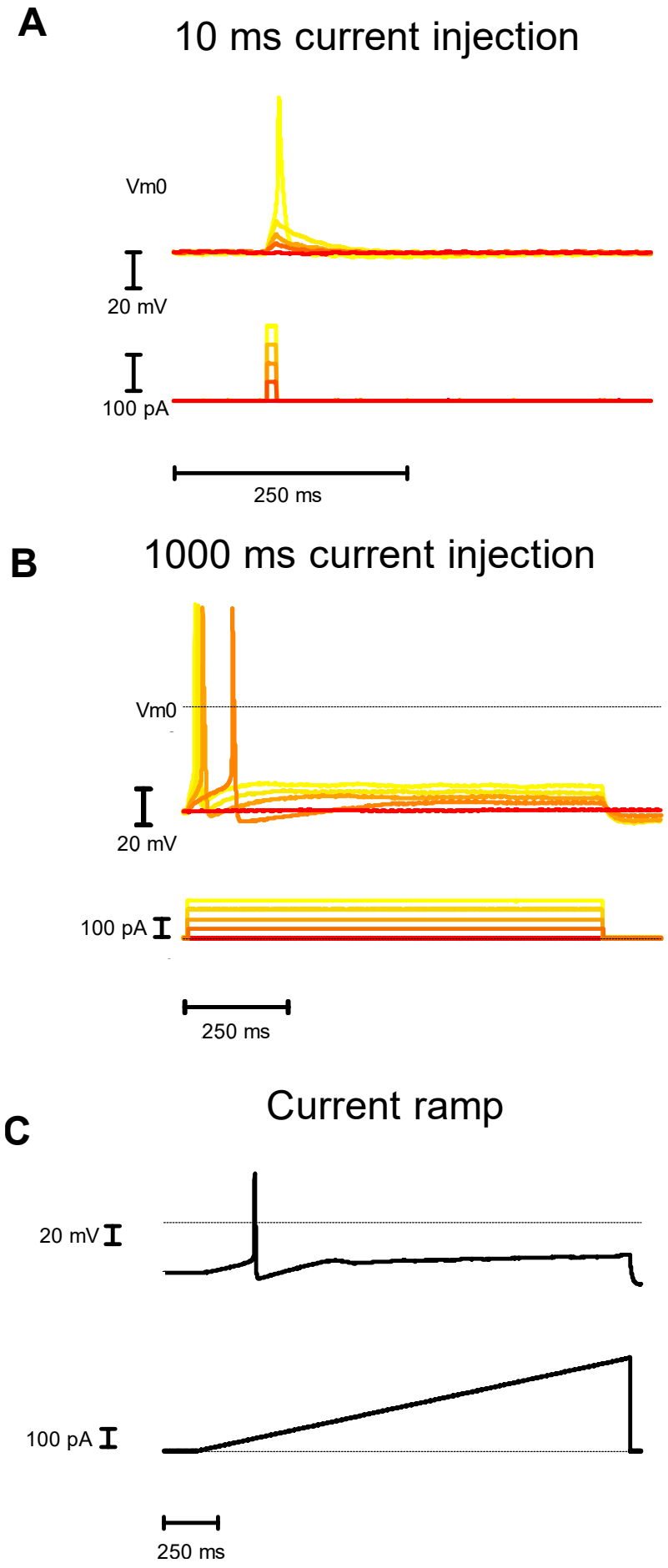



***Figure 2.4 Example current clamp recordings from Wistar stellate ganglia neurons***

*(A) A single action potential (Top trace) evoked by a 10 ms positive current injection (Bottom trace). The strength of this current injection was increased by 50pA until an action potential was evoked. Both set of traces are colour-coded to indicate the strength of the current injection. Here a lighter colour indicates a stronger current injection.*

*(B) Neuronal firing evoked by a 1000ms current injection. In this case, a single action potential was evoked (Top trace) following a 1000ms current injection of increasing amplitude (Bottom trace). For clarity, traces are shown as 50pA intervals. The data shown here covers 0-200pA. These data are colour coded in a similar manner to (A).*

*(C) A neuronal firing response to a slow current ramp. Here a single action potential was evoked in response to a gradual increase in injected current from 0pA to 200pA*

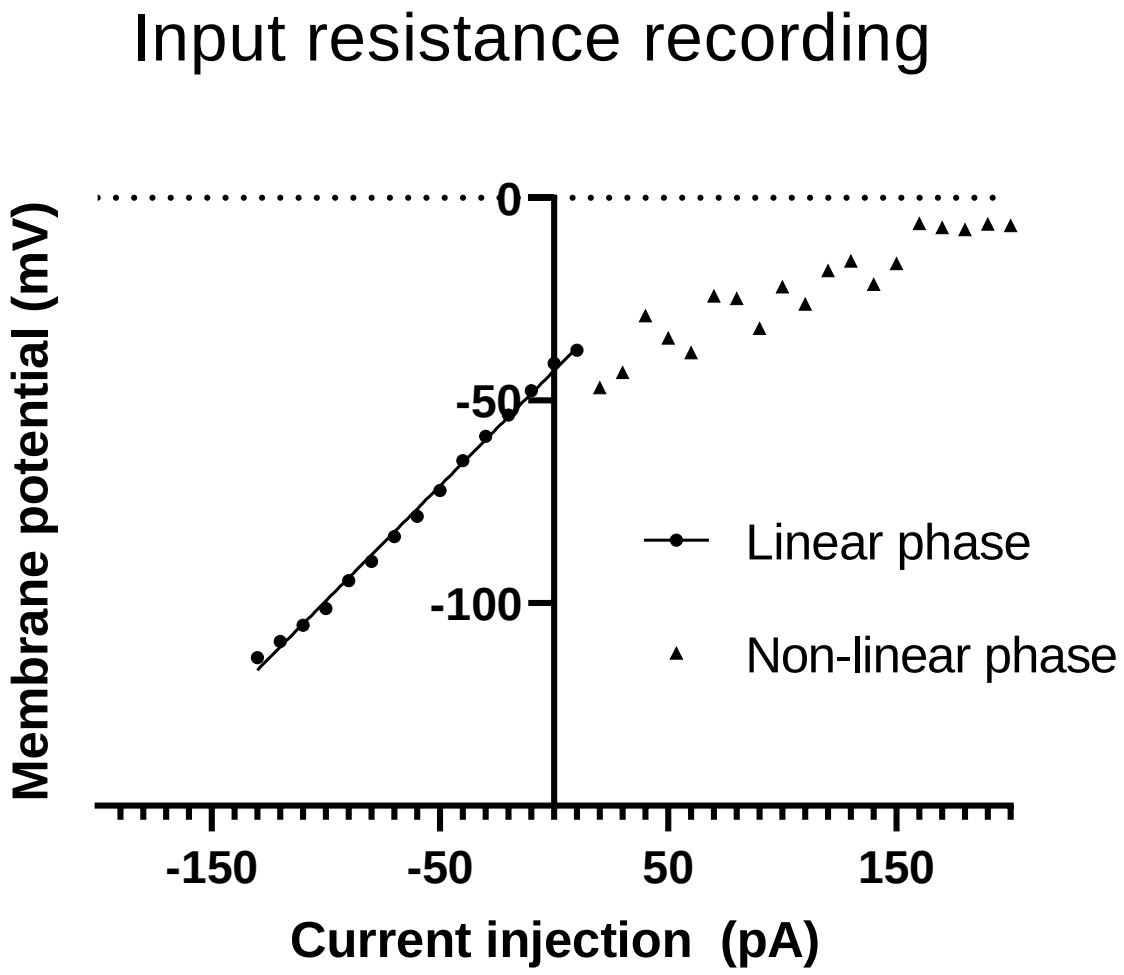



***Figure 2.5 Example input resistance measurement*** *The data here represents a randomly chosen perforated patch-clamp recording of a tonic Wistar neuron, which received both positive and negative current injections as shown on the x-axis. Between -130pA and +10pA there is a clear linear relationship between injected current and voltage. The gradient of this relationship can then be used to calculate the passive input resistance of the cell. For this cell, current injections below 130pA caused fluctuations in voltage and so were not included in the analysis.*

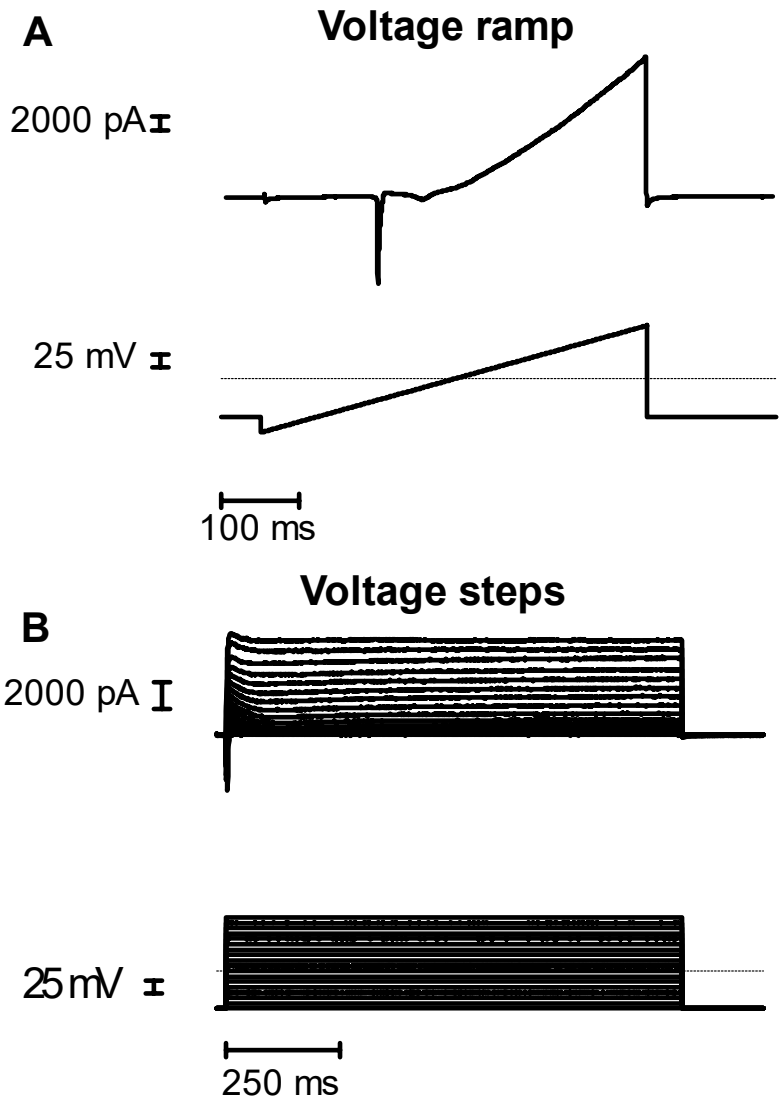



***Figure 2.6 Example voltage-clamp recordings*** *Example voltage ramp (A) and voltage step (B) protocols from whole-cell recordings of stellate ganglia neurons. These recordings illustrate the validity of the preparation.*

*(B) Example action potential waveform clamp recording where a pre-recorded action potential was used as a voltage protocol (Top trace). To illustrate the technique a TTX subtraction protocol is shown. Here, the current following an action potential is shown in the middle trace before (black) and after (blue) addition of $Na_V$ inhibitor TTX. The difference between these currents is shown in red (middle trace). This current represents the sodium current during an action potential (bottom trace), which exhibits both transient and persistent properties.*

*Table 2.3 Patching external solution (Tyrodes)*

| | **Patching external solution** |
|---|---|
| **KCl** | 5.2 mM |
| **NaCl** | 140 mM |
| **MgCl2** | 1 mM |
| **CaCl2** | 1.8 mM |
| **HEPES** | 10 mM |
| **Glucose** | 10 mM |
| pH adjusted to 7.4 with NaOH | |

*Table 2.4 HCN recording external solution*

| | **Patching external solution** |
|---|---|
| **KCl** | 5.2 mM |
| **NaCl** | 140 mM |
| **MgCl2** | 1 mM |
| **CaCl2** | 1.8 mM |
| **HEPES** | 10 mM |
| **Glucose** | 10 mM |
| **Tetrodotoxin** | 1 µM |
| **TEACl** | 10 mM |
| **4-Aminopyridine** | 1 mM |
| **$CdCl_2$** | 0.1 mM |
| pH adjusted to 7.4 with NaOH | |

*Table 2.5 $Na_v$ external recording solution*

| | Patching external solution |
|---|---|
| **NaCl** | 35 mM |
| **MgCl2** | 5 mM |
| **CaCl2** | 0.1 mM |
| **HEPES** | 10 mM |
| **Glucose** | 10 mM |
| **NMDG-Cl** | 65 mM |
| **TEACl** | 30 mM |
| pH adjusted to 7.4 with TEAOH | |

*Table 2.6 $Na_v$ internal recording solution*

| | Patching external solution |
|---|---|
| **NaCl** | 5 mM |
| **MgCl2** | 2 mM |
| **CaCl2** | 1 mM |
| **EGTA** | 11 mM |
| **HEPES** | 10 mM |
| **TEACl** | 40 mM |
| **Cs-methanosulphate** | 20 mM |
| **CsCl** | 80 mM |
| pH adjusted to 7.3 with TEAOH | |

*Table 2.7 Voltage-gated potassium channel recording solution*

| | **Patching external solution** |
|---|---|
| **MgCl2** | 5 mM |
| **CaCl2** | 0.1 mM |
| **HEPES** | 10 mM |
| **Glucose** | 10 mM |
| **NMDG-Cl** | 140 mM |
| **Tetrodotoxin** | 1 uM |
| pH adjusted to 7.4 with NaOH | |

*Table 2.8 Voltage-gated calcium channel recording solution*

| | **Patching external solution** |
|---|---|
| **TEACl** | 160 mM |
| **$BaCl_2$** | 2 mM |
| **HEPES** | 10 mM |
| **4-Aminopyridine** | 1 mM |
| **Tetrodotoxin** | 300 nM |
| pH adjusted to 7.4 with TEAOH | |

## 2.4 Live-cell Calcium imaging

Calcium imaging uses small molecular or genetically encoded protein sensors for calcium to measure $[Ca^{2+}]_i$. These $Ca^{2+}$ sensors function report changes in $[Ca^{2+}]_i$ through a change in their fluorescent properties upon binding $Ca^{2+}$ (Lock *et al.*, 2015).

The molecular $Ca^{2+}$ sensor Fura-2 was used in this thesis, due to its ease of use, reliability and required hardware being established in the group. Upon binding $Ca^{2+}$ the peak excitation wavelength changes from 380 nm to 340 nm, with both the $Ca^{2+}$ bound and $Ca^{2+}$ unbound molecules emitting at ~505-512 nm (Grynkiewicz *et al.*, 1985). By sequentially stimulating 340 nm and 380 nm, changes in $Ca^{2+}$ binding can be measured as the relative strength of the emission at 510 nm. This is typically presented as the ratio of emission following stimulation at 340/380 nm, whereby an increase in $Ca^{2+}$ causes an increase in the 340/380 nm ratio (Grynkiewicz *et al.*, 1985). Ratiometric dyes minimise the effects of photobleaching and dye unloading (Paredes *et al.*, 2008), however, the need to stimulate or record at two wavelengths enforces a technical on the acquisition speed (Lock *et al.*, 2015). Further, as fura-2 has a high affinity for calcium, it alters the amplitude and kinetics of the observed $Ca^{2+}$ response (Stout & Reynolds, 1999). The use of Fura-2 remains valid here as it is not used to study the kinetics, comparative amplitude or time course of intracellular $Ca^{2+}$ responses in this work. The acetoxymethyl ester of Fura-2, Fura-2AM was used here, which renders the dye cell permeable. However, upon entering the cell the ester group is hydrolysed, and the dye is effectively trapped inside the cell (Tsien, 1981). Fura-2AM can accumulate inside intracellular organelles (Malgaroli *et al.*, 1987; Steinberg *et al.*, 1987), however, the assumption is that the majority of the fluorescence measured is cytosolic (Roe *et al.*, 1990).

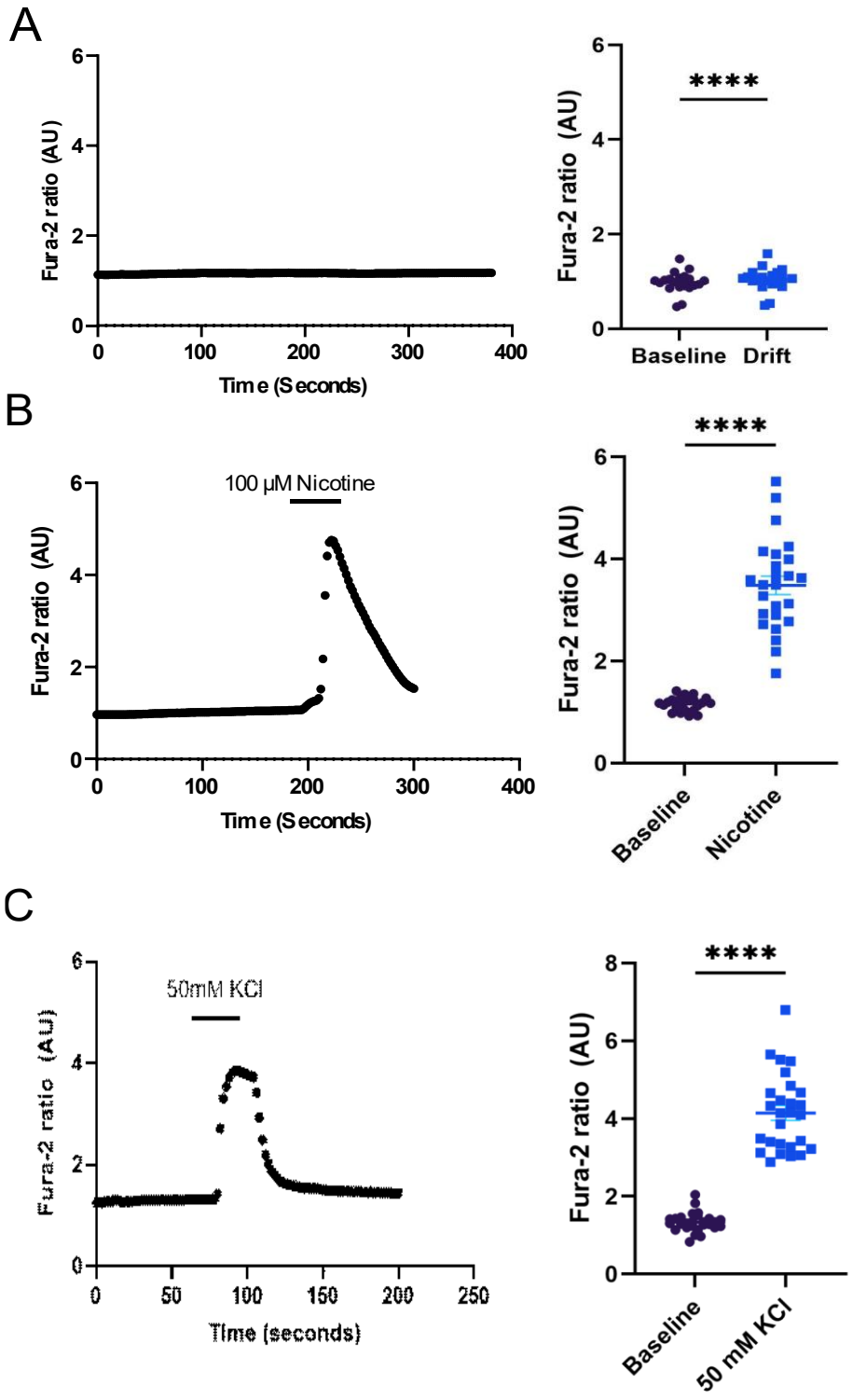



***Figure 2.7 Example Fura-2AM $[Ca^{2+}]_i$ imaging recordings*** *Example datasets for Fura-2AM based imaging. (A) A slight drift in Fura-2 ratio occurs over time in baseline Tyrode's solution (0.06 ± 0.01) (n = 20; Paired t-test, p<0.0001) (B) 100 µM nicotine elicited responses in all tested neurons (2.25 ± 0.20) (n = 20; Paired t-test, p<0.0001) (C) 50mM KCl evoked a large intracellular calcium response in all tested neurons (2.81 ± 0.20) (n = 27; Paired t-test, p<0.0001). Recordings were performed at 37°C in Tyrode's solution (**Table 2.9**).*

### 2.4.1 Fura-2AM - methodology

For Fura-2 AM imaging cells were cultured on 1 mg/ml poly-d-lysine and 1 µg/ml laminin coated nitric acid washed glass coverslips. Cells were incubated for 30 minutes at 37$^{o}$C in 2 µM Fura-2 AM dissolved in Tyrode's solution. Following incubation with Fura-2, cells were washed three times in imaging Tyrode's solution (**Table 2.9**). Cells were recorded in a 100 µL chamber. The recording chamber was maintained at 36°C±0.5°C via an inline heater under constant gravity-fed perfusion at a rate of 5-6 ml/minute. Images were acquired with a QICLICK digital CCD camera (Photometrics, US). Fura-2 was alternatively stimulated at emission wavelengths 355 nM and 380 nM and emission was detected at 510 nM. Images were acquired via a x40 oil immersion objective on an inverted Nikon microscope. Recordings were discarded where there was significant drift in the baseline ratio, or the baseline Fura-2 ratio was differed by more than 1.5 x the interquartile range for all baseline values from a given project. Whole cell fluorescence was averaged, and background fluorescence subtracted. Baseline was taken as the average ratio over a 30 second period prior to drug perfusion. Average responses were measured as an average of at least five points. An example recording of a stable baseline recording, nicotine and KCl response are shown in **Figure 2.7**

*Table 2.9 Calcium imaging external solution (Tyrode's)*

| | Calcium imaging external solution |
|---|---|
| **KCl** | 4.5 mM |
| **NaCl** | 135 mM |
| **MgCl2** | 1 mM |
| **CaCl2** | 2 mM |
| **HEPES** | 20 mM |
| **Glucose** | 10 mM |
| pH adjusted to 7.4 with NaOH | |

## 2.5 Immunohistochemistry

Immunohistochemistry combines the high specificity of antibody-antigen binding, with fluorescence imaging to highlight specific protein targets within the cell (Coons *et al.*, 1942). The basic principle behind the methodology is shown in **Figure 2.8**, however, it is worth noting several additional points.

First, recombinant and monoclonal methods produce a pure population of antibodies which theoretically recognise only one epitope, whereas polyclonal antibodies recognise multiple epitopes on the same antigen. Monoclonal antibodies are generally more consistent. On the other hand, polyclonal antibodies are typically cheaper to produce, and more tolerant to changes in the structure of the antigen (Lipman *et al.*, 2005). In reality, antibody choices are often limited to be the best reviewed, or only available antibodies for the antigen of interest. Secondly, the secondary antibody is directed against the host species of the primary antibody. Therefore, to limit off-target immunofluorescence primary antibodies raised in a different species than the antigen are chosen, and when targeting multiple antigens, primary antibodies are chosen from different host species (Evilsizor *et al.*, 2015).

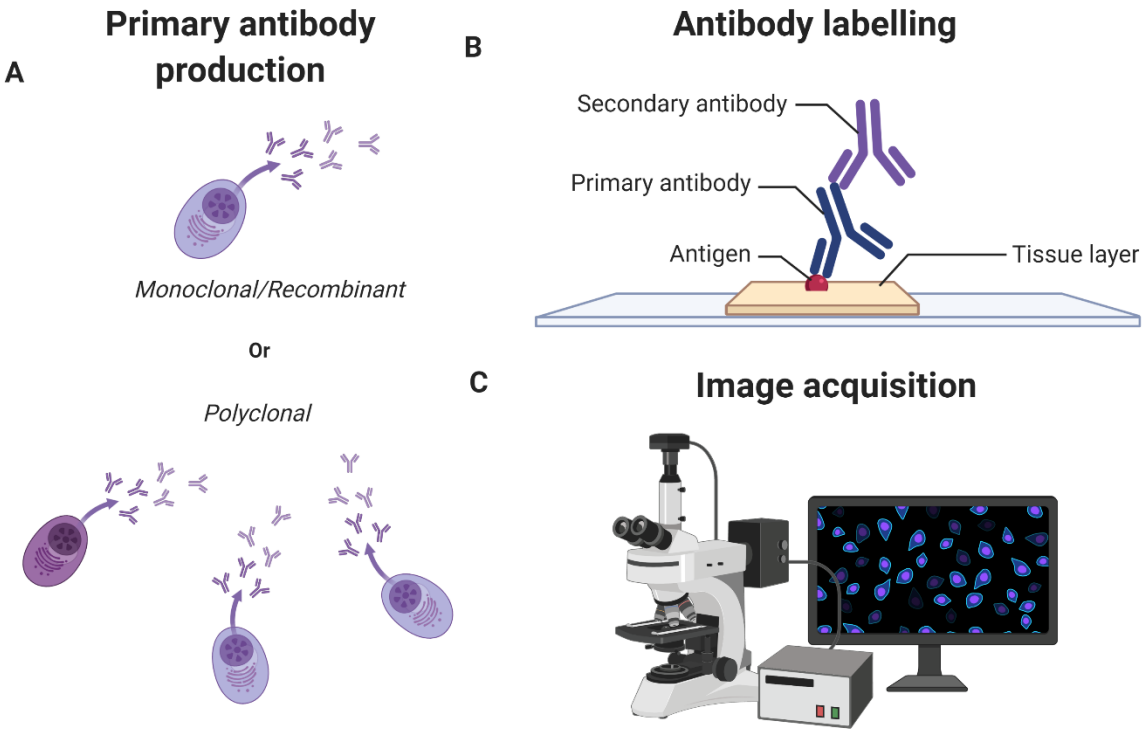



***Figure 2.8 Diagram illustrating the basic points of immunohistochemistry*** *(A) The primary antibody is specific to the protein of interest, and are can be polyclonal or monoclonal. Differences between monoclonal, recombinant and polyclonal antibodies arise from their respective methods of production (B) The primary antibody is bound to the antigen of interest within fixed tissue or cells. A fluorophore conjugated secondary antibody is bound to the primary antibody (C) A fluorescence capable microscope is used to acquire still images of the bound secondary antibodies' fluorescence. The choice of secondary antibody fluorophores is dictated by the filter-set and excitation wavelengths of the microscope used for image acquisition. When multiplexing antibodies to target several antigens, overlap between the emission and excitation wavelengths of the chosen secondary antibody fluorophores must also be considered.*

### 2.5.1 Immunohistochemistry protocol

For immunohistochemistry of cultured cells, cells were cultured by the protocol described in 2.1. After 48 hours in culture, neurons were fixed for 10 minutes in 4% paraformaldehyde, before being washed three times in phosphate buffered saline (PBS). Cells were then blocked and permeabilised in 0.1% triton-x, with donkey serum and 3% BSA for 30 minutes. Cells were subsequently washed three times in PBS. Cells were incubated with primary and secondary antibodies as described in the results chapters.

## 2.6 Two-step reverse transcriptase quantitative real-time PCR (RT-qPCR)

RT-qPCR is a fast and accurate methodology for quantifying the expression of messenger ribonucleic acid (mRNA) (Holland *et al.*, 1991; Higuchi *et al.*, 1993). The key principles underlying RT-qPCR are demonstrated in **Figure 2.9**. Within this thesis, Taqman RT-qPCR technology (Thermofisher, US) was used.

Total RNA was extracted using a RNeasy minikit (Qiagen, US) from whole flash frozen human or rat stellate ganglia. RNA samples were then stored immediately in liquid nitrogen before immediate cDNA library preparation. A low volume sample was separated prior to freezing and the purity and quantity of the mRNA sample was assessed via a nanodrop (Desjardins & Conklin, 2010). Frozen samples RNA were then converted to complementary DNA (cDNA) via Superscript IV VILO with ezDNase genomic DNA depletion (Thermofisher, US), limiting further degradation of the sample by ribonucleases (Houseley & Tollervey, 2009). Samples of cDNA were then stored at -80$^{o}$C for a period of <3 months. For RT-qPCR reactions reagents were made to a total volume of 20 µL as per the standard protocol for Taqman RT-qPCR. An initial starting cDNA quantity of 2ng was used, which was found to produce the desired cycle threshold value <30 for target genes of interest (Taylor *et al.*, 2019). An ABI Prism 7000 (Thermofisher, US) was used to perform quantitative PCR. A cycle threshold of 0.2 was used.

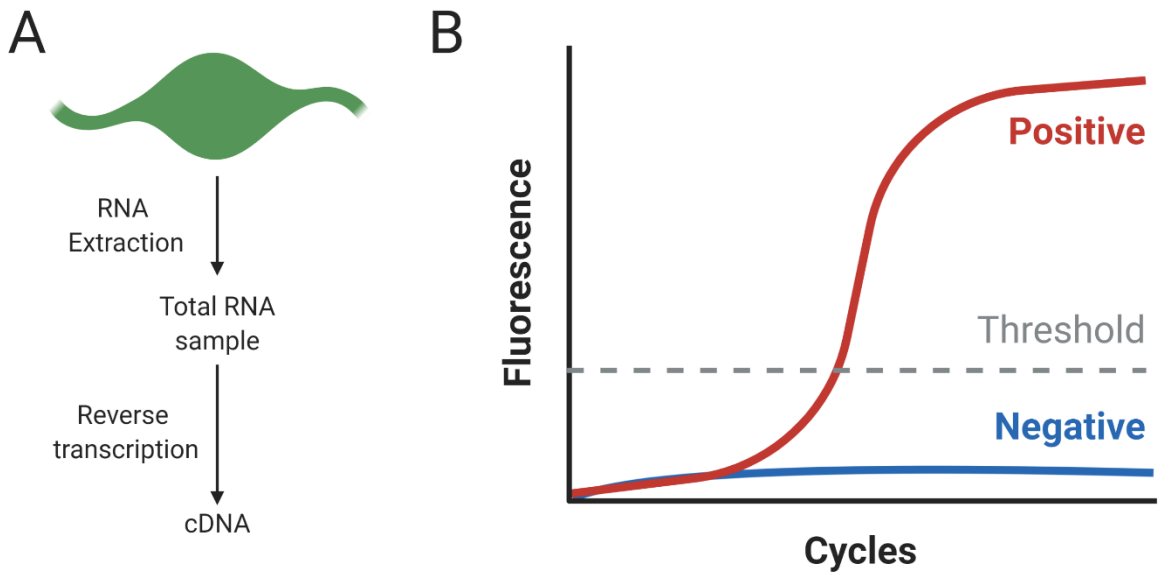



***Figure 2.9 Schematic of the principles underlying reverse transcriptase quantitative real-time PCR (RT-qPCR)*** *(A) RNA is extracted from a cell, collection of cells or tissue, in this case a nerve (Green). RNA is subsequently converted to cDNA via a reverse transcriptase enzyme. (B) Quantitative real-time PCR relies upon thermocycling as shown here. Following, two Initial temperature steps to 50°C (two minutes), 95°C (ten minutes), temperature is subsequently repeatedly cycled between 95°C and 60°C, where 95°C facilitates DNA synthesis by a thermostable taq DNA polymerase* (Saiki *et al.*, 1988)*. With each 95°C cycle Taq DNA Polymerase activity is facilitated which enables DNA synthesis and thereby amplification of the sequence of interest. Taqman utilises a Förster resonance energy transfer (FRET)* (Förster, 1948; Fernandez & Berlin, 1976) *based mechanism. Here, a dual-fluorophore probe binds to a specific cDNA sequence located between the primers. Before second strand synthesis, fluorescence from the measured fluorophore is quenched due to the proximity of the adjacent quencher fluorophore. Upon second strand synthesis, the probe is cleaved (Holland* et al.*, 1991), and fluorescence is measured. If the sequence of interest is expressed at a higher level, the initial cDNA quantity will be greater, thereby the fluorescence emitted during DNA amplification will cross a predetermined threshold at a lower number of cycles. A lower cycle threshold value refers to higher expression levels for the sequence of interest in the original reaction mixture.*

## 2.7 Co-culture

Neonatal ventricular cardiomyocytes were cultured by Dr. Dan Li, Dr. Kun Lui and Dr. Ni Li. Wistar rats were culled at 1-2 days of age. Hearts were dissected from the neonatal rat's post-mortem, and the atria and aorta were discarded. The ventricles were subsequently mechanically disrupted using scissors into ~1 $mm^3$ pieces. These were then enzymatically digested in 0.45 mg/ml collagenase and 1.25 mg/ml pancreatin solution for a period of 5 minutes at 37$^oC$. After the first 5 minutes of digestion, the supernatant was discarded, and fresh collagenase solution was added. 9 ml of cell-containing supernatant was then removed every 20 minutes and replaced with a fresh 9mls of collagenase solution. The supernatant was combined with 1 ml of new calf serum to inactivate collagenase. Cells were transferred to M1 media (**Table 2.10**), and then plated at 300,000 cells/ml. On the second day of culturing media was changed to M2 media (**Table 2.11**). On the third day, media was changed to 50:50 M2 and Plating media. Dissociated neurons were prepared as previously and were suspended in 50:50 M2 and Plating media before being added directly to the dish containing cultured cardiomyocytes.

***Table 2.10 Cardiomyocyte medias for co-culture*** *Both media's are shown as the ingredients for 100 ml.*

| | **Medium 1** | **Medium 2** |
|---|---|---|
| **DMEM with 25mM HEPES** (42430025, Invitrogen, US) | 67 ml | 75 ml |
| **Medium 199** (31150022, Invitrogen, US) | 17.5 ml | 17 ml |
| **Horse serum** (Thermofisher, US) | 10 ml | 5 ml |
| **Newborn calf serum** (Thermofisher, US) | 5 ml | 0.5 ml |
| **200 mM Glutamine** (Thermofisher, US) | 1 ml | 1 ml |
| **Penicillin-streptomycin (10,000 U/mL)** (Thermofisher, US) | 100 µL | 100 µL |

***Table 2.11 Neuron media for co-culture*** *Media is shown as the ingredients for 100 ml.*

| | **Plating media** (L-15 based) |
|---|---|
| **L-15 media** (L5520, Sigma Aldrich, US) | 90 ml |
| **NaHCO3** (Sigma Aldrich, US) | 201.6mg (24 mM) |
| **Glucose** (Sigma Aldrich, US) | 684mg (38 mM) |
| **Penicillin-Strepomycin (10,000U/mL)** (Thermofisher, US) | 0.5 ml |
| **2.5s NGF (100ug/ml)** (Merck Millipore, US) | 50 uL |
| **Fetal bovine serum** (Thermofisher, US) | 10 mL |
| pH adjusted to 7.6 with HCl | |

## 2.8 Statistics

Statistics were performed in either GraphPad Prism (Graphpad software, US), or within R (v4.0.0). Firing rate and rheobase data are discontinuous data, and therefore are not normally distributed and do not meet a parametric assumption. Firing rate data is technically count data and should ideally be tested via poisson regression. However, poission regression is technically difficult and is poorly adopted in medical sciences research.

Instead firing rate data was analysed here using non-parametric statistics which more accurately models count data than parametric and in some cases Poisson regression (Wang & Qiu, 2018). Rheobase was also treated via non-parametric statistics due to non-parametric. To test for normality in other, continuous datasets, several methodologies were used including; QQ plots, an Anderson-Darling, D'Agostino and Pearson, Kolmogorov-Smirnov. If assumptions were met, then a parametric statistical test was used.

# Chapter 3

## Transcriptomics of the stellate ganglia

# 3.1 Introduction

Recent years have seen the rapid advancement of large-scale genomic and transcriptomic techniques, allowing for broad exploratory studies of genomes and transcriptomes. In particular, next generation sequencing has facilitated the fast and unbiased transcriptomic characterisation of cells and tissues in models of pathology and physiology.

This chapter outlines the findings of a scRNAseq dataset comparing Wistar and SHR sympathetic stellate ganglia. The intention of this study was to identify dysregulated neuron-specific ion channel encoding genes that might explain the phenotype of sympathetic hyperactivity in hypertension (Manolis *et al.*, 2014). In addition, these data were used to aid in the characterisation of neuron-specific ion channels and GPCR expression in the stellate ganglia. Single-cell RNA-sequencing (scRNAseq) is also useful for characterising cell heterogeneity and used here to assess how different neuronal populations would affect subsequent functional analysis. These data are referenced throughout the following chapters of this thesis, and as such this chapter serves as both a methods and data chapter. These data are then compared with an additional study utilising bulk RNA-sequencing.

## 3.1.1 Single-cell and bulk RNA-sequencing

The two primary methods of RNA-sequencing are bulk and scRNAseq. Bulk RNA-sequencing refers to the sequencing of an ribonucleic acid (RNA) sample normally derived from a whole tissue lysate, and thus provides the average gene expression from all cells that make up the RNA sample. Conversely, scRNAseq

involves the sequencing of RNA from individual cells which are typically sorted from a cell suspension via microfluidics (**Figure 3.1**) (Tang *et al.*, 2019).

The process for bulk RNA-sequencing is as follows. First, total RNA extracted from the tissue of interest is reverse transcribed into cDNA. These cDNA constructs are then fragmented and 5' and 3' adapters are ligated onto the cDNA sequences. Next, the sequences are amplified by polymerase chain reaction. These cDNA molecules are then sequenced using a next generation sequencing technology such as Illumina Hiseq 4000. This process produces reads of short sequences of bases (typically around 75 base pairs), which are stored as digital information.

The process is relatively similar for scRNAseq (Baran-Gale *et al.*, 2018), except that reverse transcription primers will also contain unique molecular identifiers and cell barcodes. These markers allow for a sequence to be attributed to an exact messenger RNA (mRNA) molecule and cell. cDNA is then amplified, and the process continues in a similar manner to that described for bulk RNA-sequencing.

This chapter employed scRNAseq to compare Wistar and SHR stellate ganglia cell populations. Specifically, it demonstrates cluster analysis of scRNAseq, highlights the top differentially expressed genes between Wistar and SHR stellate ganglia and significantly overrepresented gene ontology groups. Moreover, it establishes a molecular framework for functional work laid out in chapters 4-6.

Finally, key differentially expressed genes are compared to an existing bulk RNA sequencing dataset for which I performed the analysis (Davis *et al.*, 2018; Bardsley *et al.*, 2018*a*).

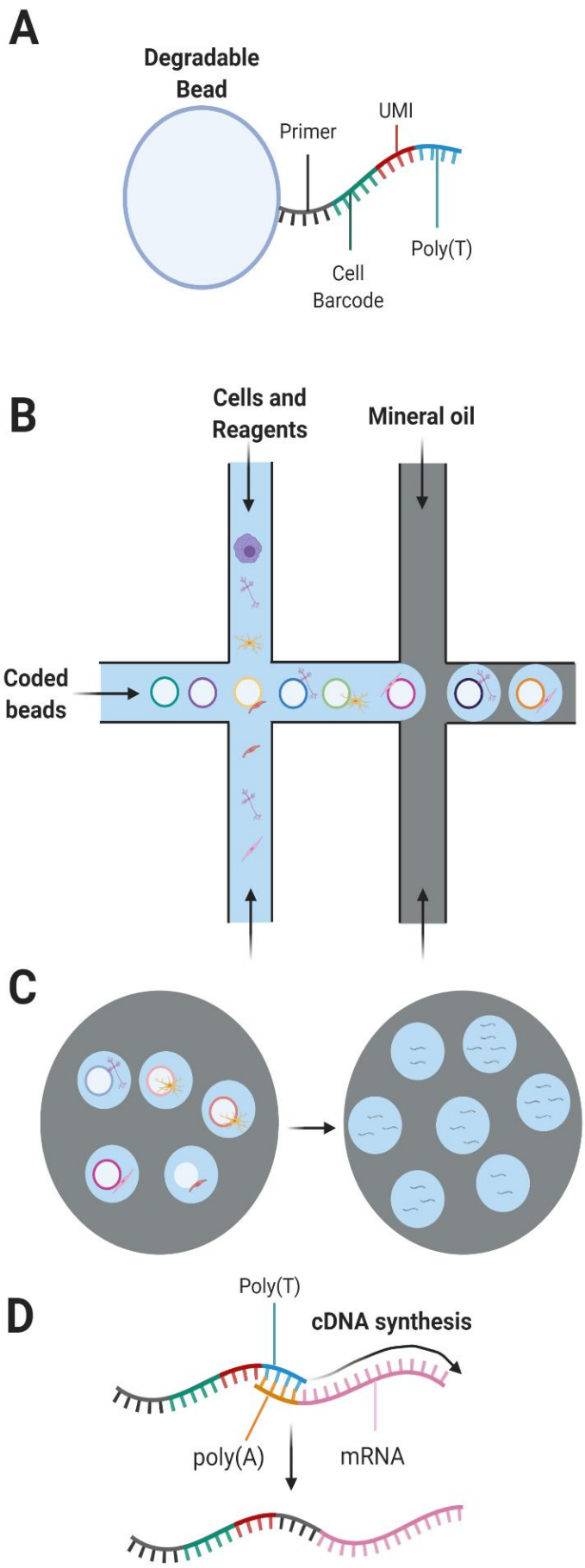



***Figure 3.1 Visual breakdown of Single-cell RNA-sequencing by 10X genomics*** *10X genomics functions by a process known as gel bead in emulsion, which is outlined here. This diagram summarises the content of Zheng et al. (2017).*

*(A) Barcoded beads are key to the 10X genomics process. Degradable gel beads are attached to multiple DNA strands containing several regions of interest. An example strand is shown here, which contains a primer and sequencing adapter sequence. In addition, this strand contains a 14 base-pair barcode unique to this gel bead and therefore any cell associated with this gel bead. Each individual strand also contains a 10 base-pair unique molecular identifier (UMI) sequence which is unique to each strand of DNA. Finally, a terminal 30 base-pair poly(T) sequence allows for association with mRNA poly(A) tails.*

*(B) Coded beads (as shown in A) are combined with cells and reagents, with most gel beads associating with a single cell. These gel-bead and cell conjugates are then encapsulated in oil and thereby isolated from other gel-bead and cell combinations.*

*(C) Isolated in an oil emulsion, the gel bead degrades, thereby releasing its attached oligonucleotides. In addition, the cell is lysed thereby releasing its mRNA content.*

*(D) mRNA molecules from the lysed cells associate with the DNA barcoded oligonucleotides via binding between the poly(A) tail at the 3' end of the mRNA molecule, and the poly(T) sequence of the barcoded sequence. This mRNA sequence is reverse transcribed into the barcoded sequence as cDNA. These sequences can then be amplified through PCR via the incorporated primer sequence before downstream sequencing.*

## 3.2 Methods

The full process for sample isolation and analysis for scRNAseq and bulk RNA-sequencing is shown in **Figure 3.2**. Sequencing was performed by the Wellcome Trust Centre for Human Genetics.

### 3.2.1 Alignment

To interpret data produced during sequencing, reads need to be mapped onto a known genome or transcriptome during a process called alignment. When alignment is performed onto a transcriptome rather than a genome, this process is known as quasi-mapping (Patro *et al.*, 2017). For the scRNAseq technique used here, 10x genomics, this process is relatively simple and can be performed within 10x genomics own pipeline (Zheng *et al.*, 2017) using a star-based alignment methodology (Dobin *et al.*, 2013), which performs extremely well for scRNAseq alignment (Du *et al.*, 2020). In this pathway, correctly mapped reads are then placed into groups dependent upon their cell barcode, unique molecular identifier code and the associated gene from genome alignment. For bulk RNA-sequencing, reads are quasi-mapped onto the rat transcriptome using *Salmon* (Patro *et al.*, 2017), which has the advantage of being fast and accurate, but with limited information on novel genes and splice variants.

### 3.2.2 Prefiltering single-cell RNA-sequencing data

The R package *Seurat* (Stuart *et al.*, 2019), was used for scRNAseq analysis. Data are first filtered by gene count, which removes cells or debris where minimal

gene expression is detected. The user then determines the number of highly variable genes to be carried forward for clustering.

At this stage, covariates such as variation in read counts between cells and the percentage of mitochondrial genes can be regressed out of the downstream clustering analysis. By regressing out the difference in read counts between cells, the user limits the effect of cell size or technical variation upon the clustering process (Buettner *et al.*, 2015). High mitochondrial gene expression can occur following cell lysis during cell dissociation, where cytosolic mRNA is depleted, and mitochondrial encoded RNA is preserved. Thus, the relative amount of mitochondrial encoded RNA is enriched relative to the depleted mRNA levels (Ilicic et al., 2016).

To reduce the complexity of the dataset further, the user must then determine the number of principal components which account for variance in this population of variable genes (Stuart *et al.*, 2019). Principal components are mathematically derived variables generated *de novo* from the original dataset. These new variables are generated in a manner that attributes the greatest variation to the first principal component, and subsequent principal components represent less and less variation. This methodology thereby aims to decrease the dimensionality of the original dataset, with minimal information loss, by explaining the variation within the dataset through a smaller number of variables (Pearson, 1901; Hotelling, 1933). Therefore, when the user determines the number of principal components used for downstream analysis, choose the minimal number of principal components that can still explain most of the variation within the dataset. To this end, two alternative methodologies are typically employed to determine the number of principal components, a jackstraw plot, and an elbow plot. In a jackstraw plot, individual principal components are statistically and graphically compared to a linear null

distribution (Macosko *et al.*, 2015). A jackstraw plot for this dataset is shown in **Figure 3.3A**.

On the other hand, an elbow plot visually highlights the variation conferred by each principal component. An elbow plot for these data is provided in **Figure 3.3B**. Here, the elbow plot was more informative than the jackstraw plot, with a plateau of low variability between principal components 18-20. Based upon the elbow plot, a principal component cut-off of 19 was chosen. There appears to be some additional variation in the jackstraw plots, however this was not corroborated by the elbow plot. To ensure that the choice of 19 was sound, principal components of 25 and 30 were also tested and had little effect upon the downstream clustering (Data not shown).

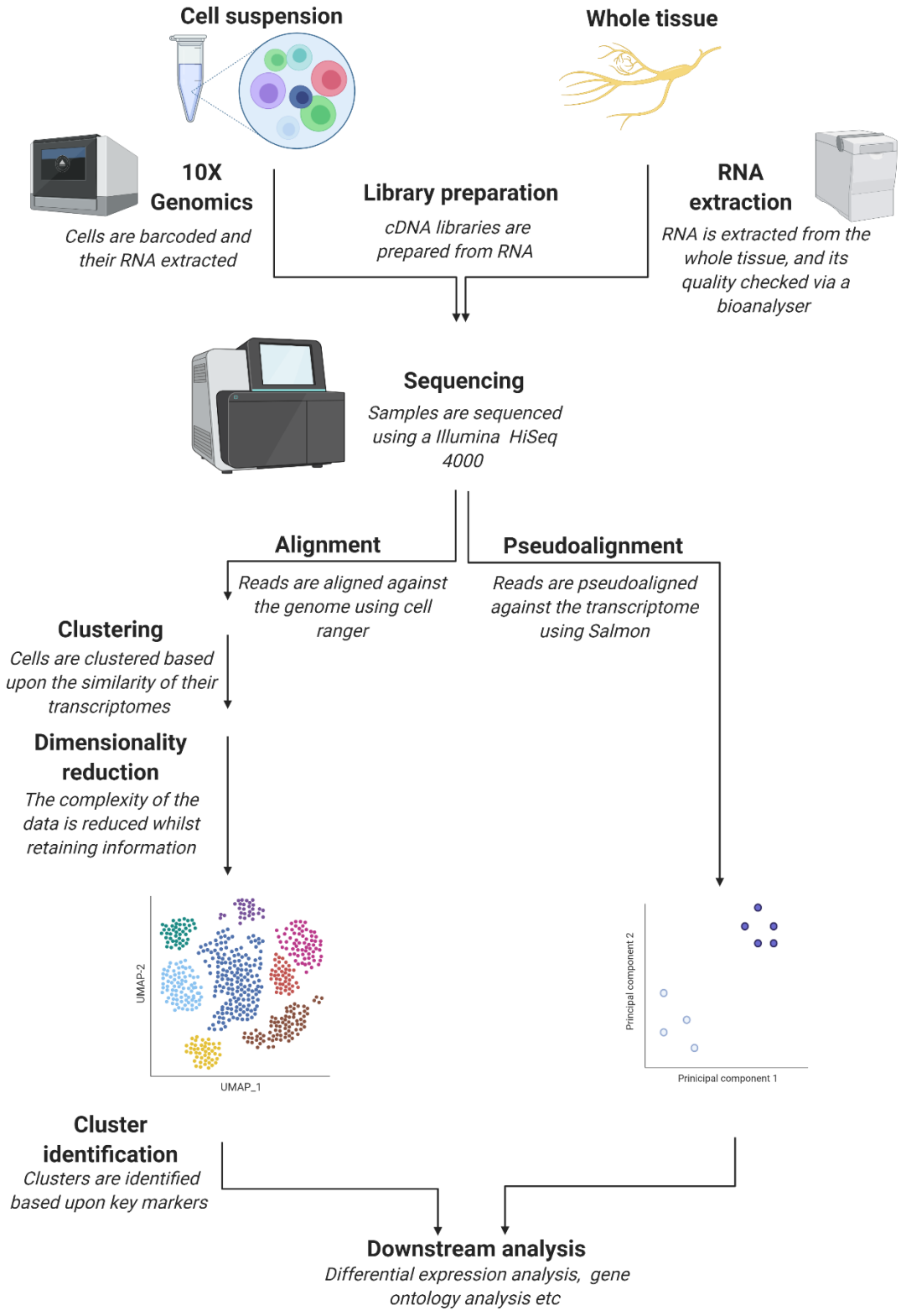



***Figure 3.2 Experimental pipelines for single-cell and bulk RNA-sequencing as used in this chapter*** *This diagram visually demonstrates the steps described in the methods section of this chapter.*

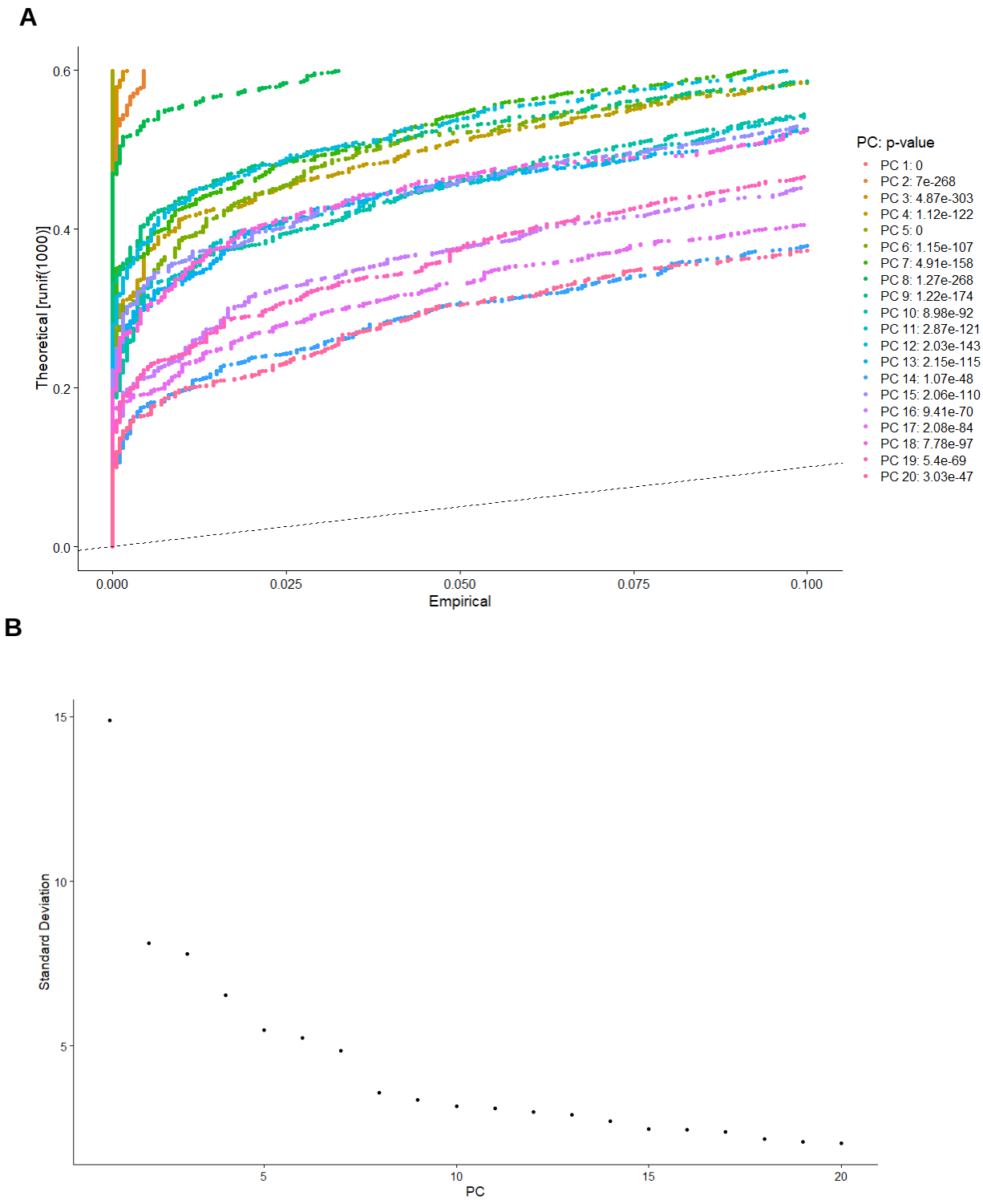



***Figure 3.3 A jackstraw plot and elbow plot for the stellate ganglia single-cell RNA-sequencing dataset*** *(A) Jackstraw plot testing the difference between the variance explained by each principal component and the null distribution (dashed line). (B) Elbow plot, showing the standard deviation explained by each principal component. Here three plateaus are observed, around 10-12, 15-18 and 19-20. At the 19-20 plateau, very little variation is explained by these principal components and so these are chosen as the cut-off point. 19 principal components were chosen for further analysis.*

### 3.2.3 Clustering

Clustering refers to the reorganisation of scRNAseq datasets into groups of cells with similar transcriptomic identities, often representing cell populations or subpopulations (Zhang *et al.*, 2020). In *Seurat*, data is clustered in three stages; first a K-nearest neighbours' graph is produced, this is then converted to a shared nearest neighbours' graph and finally, clusters are identified by the Louvain method. A K-nearest neighbours algorithm determines the classification of a cell based upon the classification of its nearest k neighbours (Zhang, 2016). The number of neighbours assigned to each cell is therefore defined by the value of k (default = 20). This produces a graph where each cell is connected only to their k-nearest neighbours. These data are then converted to a shared nearest neighbours (SNN) graph. Briefly, the more shared neighbours between two cells indicates a stronger association, and this connection is weighted accordingly. The number of shared neighbours is determined by how many of each cells K-nearest neighbours are identical, for the two cells under comparison. This process is repeated, and the connections between cells exhibiting weak shared neighbours' connections are depleted. This produces a similar graph to k-nearest neighbours, but here cells only remain connected to their k-nearest neighbours with a larger number of shared neighbours.

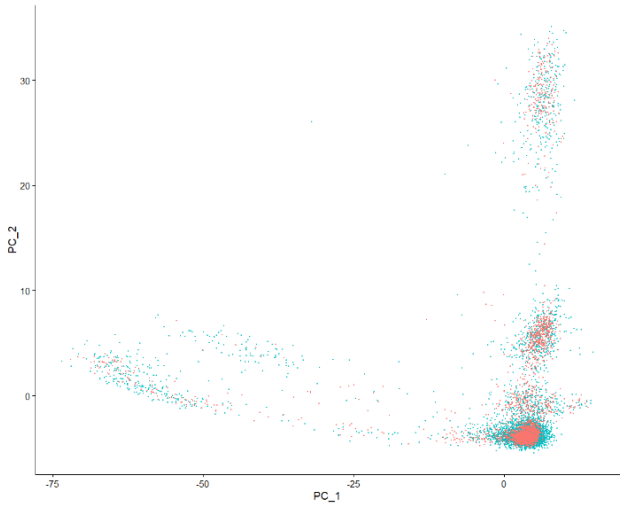
Clusters are then identified used a community-detection Louvain algorithm. Here the user can define the resolution, effectively controlling the granularity of the clustering. The Louvain algorithm assesses the density of connections between cells within a putative cluster of cells versus cells in a random network, then using a "bottom up" approach partitions cells with dense shared networks together (Blondel *et al.*, 2008). This process is then repeated for each cell in turn, with the

process continuing until the partitions cannot be further optimised. In the next step, these partitions are then merged to form cell clusters. The strength of the connections between cell clusters is then determined by the same process. This is calculated as the summed strength of the connections between cells in either cluster. Together these steps provide a robust clustering methodology, allowing for the clear identification of cell clusters for downstream analysis (Stuart *et al.*, 2019).

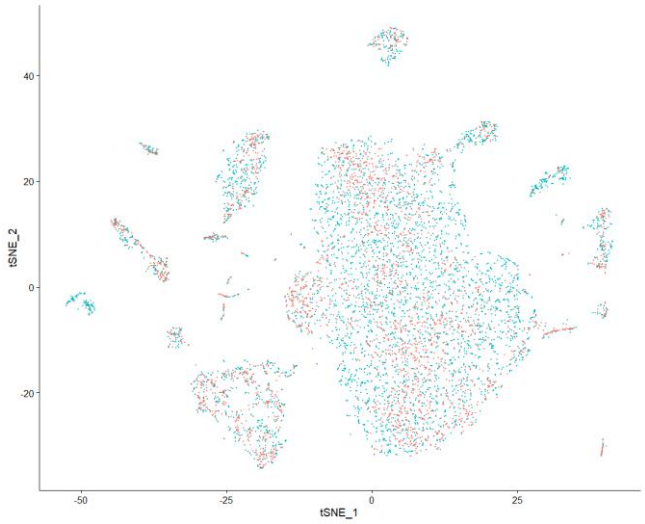
### 3.2.4 Dimensionality reduction

Dimensionality reduction is the mathematical transformation of data to allow simplified graphical representation of high-dimensional data, such as scRNAseq data, in a 2D graphical form. ScRNAseq generally uses one of three methodologies for dimensionality reduction: principal component analysis (PCA) (Pearson, 1901), t-distributed Stochastic Neighbour Embedding (t-SNE) (Van Der Maaten & Hinton, 2008), or Uniform Manifold Approximation and Projection (UMAP) (McInnes *et al.*, 2018). Of these three methodologies, UMAP and t-SNE visually separate populations in a similar manner and maintain local structures (clusters), but UMAP is considerably faster and less computationally demanding (Becht *et al.*, 2019). UMAP also preserves global structure of the dataset to a greater degree than t-SNE (Becht *et al.*, 2019), which is useful for viewing clusters in relation to each other. Both methods outperformed PCA in most measures (Becht *et al.*, 2019). A comparison of the three dimensionality reduction methodologies is shown for this dataset in **Figure 3.4**.

**A**




**B**




**C**

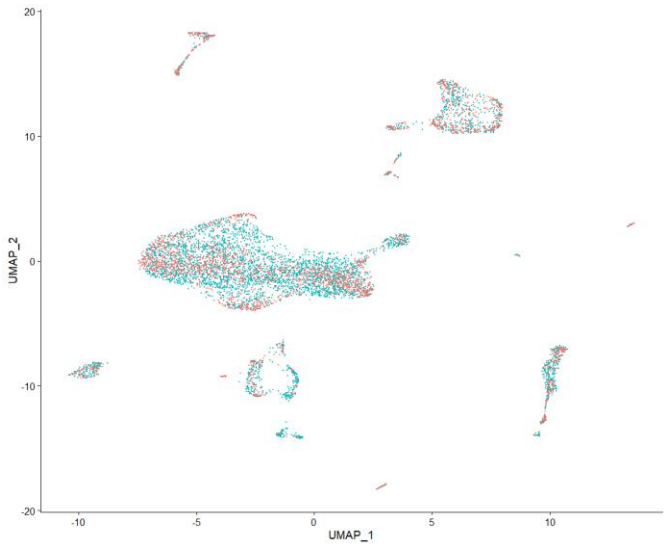



***Figure 3.4 Demonstration of the three typical methods of data visualisation in single-cell RNA-sequencing using the stellate ganglia single-cell RNA-sequencing dataset***

*This figure visualises the three methods of dimensionality reduction employed in single-cell RNA-sequencing analysis. The data shown here is from the stellate ganglia Wistar and SHR single-cell RNA-sequencing datasets. Blue indicates Wistar cells, red indicates SHR cells. This dataset is published as part of a larger study (Davis et al., 2020). The cell identities are expanded upon in* ***figure 3.6****.*

*As can be observed, PCA derived clustering (A), produces poor clustering, whilst TSNE (B) and UMAP (C), lead to more robust and easily distinguishable clusters. However, overall UMAP (C) has a superior global structure with denser clustering and better cluster separation. This aids with identifying groups of similar cell types and distinguishing physiologically relevant clusters from technical artefacts.*

### 3.2.5 Differential expression analysis

Differential expression analysis is used to detect changes in gene expression between two conditions, or in the case of scRNAseq can also be used to detect differences between clusters. There are a number of available methodologies for both bulk and scRNAseq differential expression analyses (Wang *et al.*, 2019). The selection of differential expression analysis methods is a trade-off between accurate detection of true changes, and the methodologies false positive rate. For scRNAseq the *MAST* (Finak *et al.*, 2015) method was used, which has an extremely high precision and low false positive rate, but with an ensuing high false negative rate (Wang *et al.*, 2019). For bulk RNA-sequencing, *DESeq2* (Love *et al.*, 2014) was used where it is comparable to other available methodologies (Baik *et al.*, 2020).

All differential expression methodologies employ a type of p value adjustment due to the large number of multiple corrections that are typical in RNA-sequencing datasets. For *MAST* analysis performed in *Seurat*, this was achieved by a Bonferonni correction (Stuart *et al.*, 2019), and for *DESeq2* this was by a Benjamini-Hochberg correction (Love *et al.*, 2014). Bonferonni reduces all input p-values equally (Haynes, 2013*a*), whereas Benjamini-Hochberg correction adjusts p-values based upon their rank (Haynes, 2013*b*).

### 3.2.6 Gene ontology and KEGG analysis

The gene lists produced by differential expression analysis can often be expansive and difficult to interpret. To resolve this issue, differentially expressed genes can be summarised by biological categories, such as function, disease association, or localisation within a cell compartment. Two primary classification

systems, Gene ontology (Carbon *et al.*, 2019) and Kyoto Encyclopedia of Genes and Genomes (KEGG) (Kanehisa *et al.*, 2016) exist for this purpose, and were used in this chapter to summarise transcriptional changes in sympathetic neurons. Genes that were significantly differentially expressed at the $p<0.05$ are grouped into either KEGG or gene ontology terms based upon their known physiological functions. These ontology terms are then tested for over-representation (Boyle et al., 2004). Significantly over-represented gene ontology groups will contain many differentially expressed genes relative to the wider dataset (Yu et al., 2012). For gene ontology analysis, multiple overlapping terms are limited by using the Simplify command of *clusterProfiler* (Yu et al., 2012).

### 3.2.7 Trajectory inference analysis

Trajectory inference analysis is a broad term covering multiple different methodologies, which generally aim to find development or transitional pathways between cell populations (Saelens *et al.*, 2019). These methodologies differ in their mathematical approach, the amount of guidance provided, their accuracy and the shapes of the trajectories the software can infer (Saelens *et al.*, 2019). The technique employed here, *Slingshot* (Street *et al.*, 2018), utilises preidentified clusters to identify linear, bifurcation, multifurcation or tree like trajectories between clusters using a minimum scanning tree approach. The use of predefined clusters is shared amongst many of these methodologies, and one of the advantages for the end-user is that this makes the data more readily interpretable due to existing knowledge of the cluster's transcriptomes and identities. Slingshot was also the best overall tree-based method for trajectory inference, and the most accurate method

overall when the most common methods were compared on biological and simulated datasets (Saelens *et al.*, 2019).

## Protocols

### 3.2.8 Single-cell RNA-sequencing

Left and right stellate ganglia were dissected from six 5-6 week male Wistar and six 5-6 week male SHR. Ganglia were then pooled per strain, and cells were dissociated by enzymatic and mechanical disruption of the tissue as described for culture experiments. The resulting cell suspensions were then transported in ice-cold PBS and sequenced. Up to 10000 events were then labelled and sequenced by 10x Genomics chromium *v3* (10x genomics, US) (Zheng *et al.*, 2017) single-cell preparation and *Illumina Hiseq 4000* (Illumina, US) based sequencing. Before subsequent filtering, these steps achieved 66-72k mean reads per cell, with a 53-55% sequencing depth per cell.

Data were then analysed using 10x Genomics' *Cell ranger* pipeline (v3.0.2) with default settings and the rat Rnor6.0 genome. Data were then filtered and analysed in *Seurat* (v3.0). Cells with a count number lower than 4000, or cells with 30% or more mitochondrial gene expression, were excluded. 10000 features and the variance-stabilizing transformation (VST) (Hafemeister & Satija, 2019) setting were used for the identification of variable features by FindVariableFeatures (Stuart *et al.*, 2019).

Differential expression analysis was performed via *MAST* (v1.14.0) (Finak *et al.*, 2015) within *Seurat* (v3.0) (Stuart *et al.*, 2019). Adjusted p-values of 0.05 were used as a cut-off for significance. The MAST methodology used throughout this chapter is relatively conservative (Wang *et al.*, 2019). However, using the Wistar

and SHR all neuron dataset as a comparison, both *MAST* (Finak *et al.*, 2015) and a Wilcoxon summed ranks test, the default for *Seurat* (Stuart *et al.*, 2019) identified 474 gene expression changes at an adjusted p-value cut-off of <0.05 (**Table 3.3**), which was comparable to the 606 changes detected by the “bimod” method (McDavid *et al.*, 2013). A fourth methodology, *DESeq2* (Love *et al.*, 2014) suggested 1523 significant changes with the same criteria. The *MAST* and the Wilcoxon summed ranks test are in agreement and in close alignment with bimod, whilst the number of changes by *DESeq2* were extremely large implying a large number of false positives, as has been previously reported (Wang *et al.*, 2019). Therefore, *MAST* was deemed an appropriate methodology to continue with. Gene ontology and KEGG analysis were performed via *clusterProfiler* (v3.16.1) (Yu *et al.*, 2012). Trajectory inference analysis was performed via slingshot (v1.6.1) (Street *et al.*, 2018).

### 3.2.9 Bulk RNA-sequencing

RNA extraction and quality control were performed by Dr. Emma Bardsley. Whole right stellate ganglia were dissected from 15-16 week Wistar and SHR, following which the ganglia were mechanically disrupted in RNeasy RLT buffer, after which RNA was extracted using an RNeasy micro kit (Qiagen, CA, US). RNA quality was assessed using a Bioanalyzer 2100 (Agilent Technologies, CA, US), and samples with RNA integrity below 8.5 were discarded.

Four samples each of whole stellate ganglia Wistar and SHR RNA were then sequenced using an Illumina Hi-Seq 4000, with an llumina TruSeq Stranded mRNA Library Prep Kit (Illumina, CA, USA). A paired-end 75 base pair protocol was used.

SMARTer (Clontech, US) amplification was used due to the low mRNA content of individual stellate ganglia. As this methodology involves amplification, this methodology biases towards highly expressed genes (Shanker *et al.*, 2015). *FastQC* was then used to quality control the data produced (Zhang *et al.*, 2017). A slight GC bias was detected in the data, which was corrected during analysis. Subsequently, the *Salmon* package was used (Version 0.8.2) (Patro *et al.*, 2017) to quasi-map reads against the UCSC Rnor6.0 transcriptome. GC bias and positional bias corrections were employed for this process. In this manner, a mapping rate of 68.5-78.7% (**Table 3.1**) was achieved across the 8 samples. The *tximport* package (Soneson *et al.*, 2016) was used to import the quasi-mapped reads into R. Differential expression analysis was performed using *DESeq2* (Version 1.16.1) (Love *et al.*, 2014) and benjamin-hochberg adjusted p-values less than 0.05 were taken as significant. The relationship between significance, the size of the $\log_2$ fold change and the mean of normalised count is shown in **Figure 3.5**. As expected, genes with low expression require a larger fold change to achieve significance, thereby limiting false positives from genes with low expression.

Finally, genes that were significantly differentially expressed were assessed via gene ontology and KEGG analysis. This was performed by *clusterProfiler* (Yu *et al.*, 2012) as described for scRNAseq.

***Table 3.1 Bulk RNA-sequencing mapping rate and read numbers per sample***
*Mapping rates are shown for each of the eight samples following quasi-mapping via Salmon.*

| Subjects | Mapping rate | Number of mapped reads |
|---|---|---|
| Wistar 1 | 78.66% | 35509076 |
| Wistar 2 | 75.57% | 30112270 |
| Wistar 3 | 78.38% | 34634784 |
| Wistar 4 | 75.18% | 33764576 |
| SHR 1 | 70.63% | 31194868 |
| SHR 2 | 78.47% | 25820298 |
| SHR 3 | 68.50% | 32573670 |
| SHR 4 | 72.60% | 34026720 |

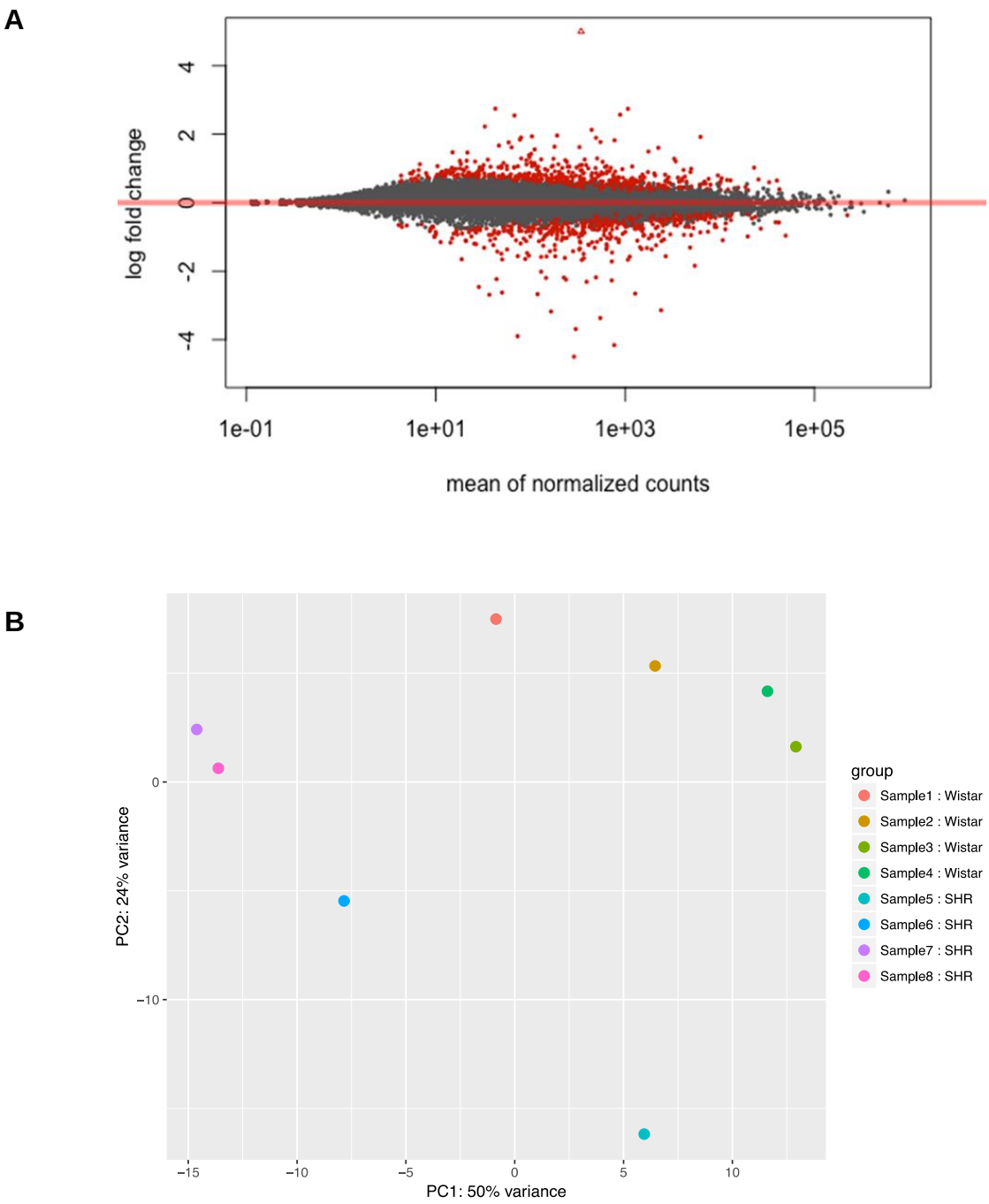



***Figure 3.5 Graphs summarising the bulk RNA-sequencing dataset*** *(A) A plot showing the relationship between gene average expression, the $log_2$ fold change between Wistar and SHR samples, and significance. Each dot indicates a gene. Red indicates p<0.05, grey indicates non-significant. The data can be seen to taper with average expression so that highly expressed genes require smaller changes in expression to achieve significance. This limits the effects of false positives in genes with low expression. (B) PCA plot demonstrating separation of the eight samples across the datasets first and second principal components. Each dot indicates an individual sample. The SHR samples are generally separated from the Wistar samples along the first principal component, as would be expected if the wistar and SHR samples had an altered transcriptome in the SHR.*

# 3.3 Results

## 3.3.1 Single cell RNA-sequencing

The scRNAseq dataset contained 4402 cells for Wistar and 2879 cells for SHR, following the removal of contaminants such as cells with a high percentage of mitochondrial gene expression and cells with low gene counts during filtering as described in the methods section.

Of these remaining cells, six primary populations were identified (**Figure 3.6**). Additionally, several small populations were identified, however these populations were too small to adequately analyse and for the purpose of this thesis were termed “other”. In addition, the distribution of Wistar and SHR cells amongst these clusters is shown in **Figure 3.7**. As expected, the Wistar and SHR populations were well distributed throughout each of these six populations, thereby facilitating direct comparison between these strains. This chapter focuses upon SGNs, given their demonstrated role in the hypertensive phenotype in the SHR (Shanks *et al.*, 2013; Larsen *et al.*, 2016*b*, 2016*a*). Data on the five other populations are provided in the appendix.

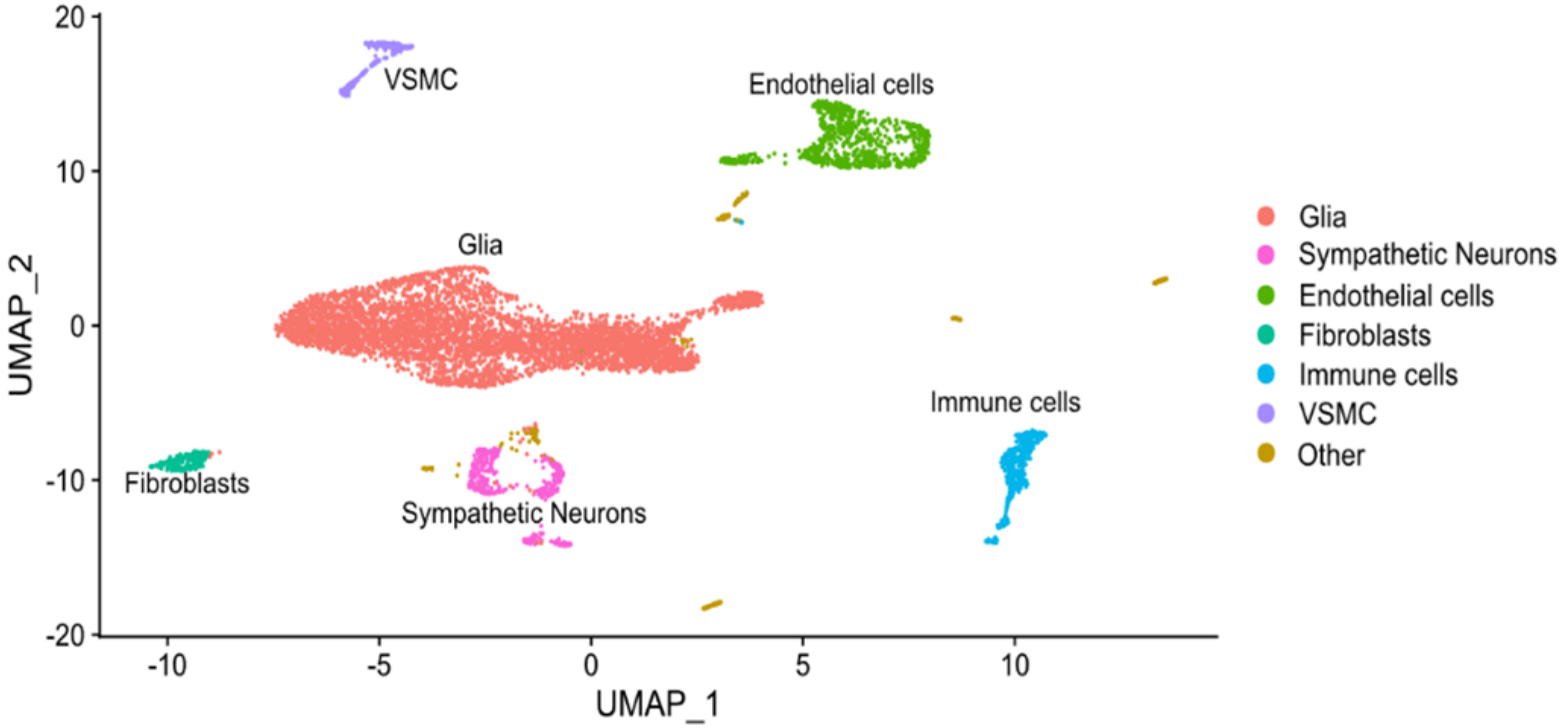



***Figure 3.6 UMAP representations of identified cell populations*** *Identified cell clusters are highlighted in the stellate ganglia. Each population is colour coded as stated in the legend. Populations are also labelled on the graph. VSMC indicates vascular smooth muscle cells. Here UMAP refers to Uniform Manifold Approximation and Projection.*

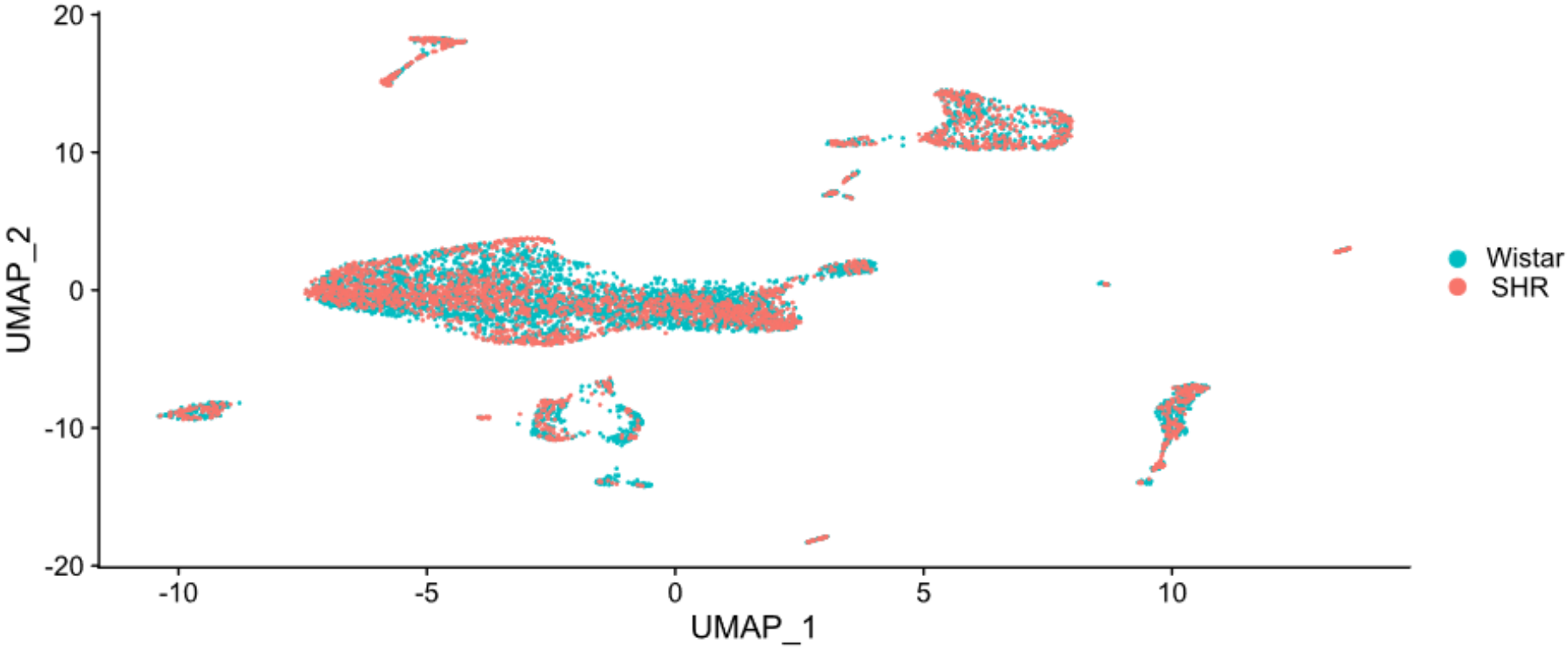



***Figure 3.7 UMAP representations the distribution of Wistar and SHR cells amongst these populations***. *The distribution of Wistar and SHR cells highlighted across the clusters identified in figure 1. Wistar cells are indicated in blue, SHR cells are indicated in red. Here UMAP refers to Uniform Manifold Approximation and Projection.*

### 3.3.1.1 Neurons

Sympathetic neurons were first characterised to facilitate downstream analysis. Sympathetic neurons were identified as cell clusters expressing the markers highlighted in **Figure 3.8**. These markers are well documented identifiers of sympathetic neurons and/or peripheral neurons and have been previously characterised in SGNs and SCG neurons (Larsen *et al.*, 2016*a*; Raba *et al.*, 2016; Pirzgalska *et al.*, 2017; Ernsberger & Rohrer, 2018).

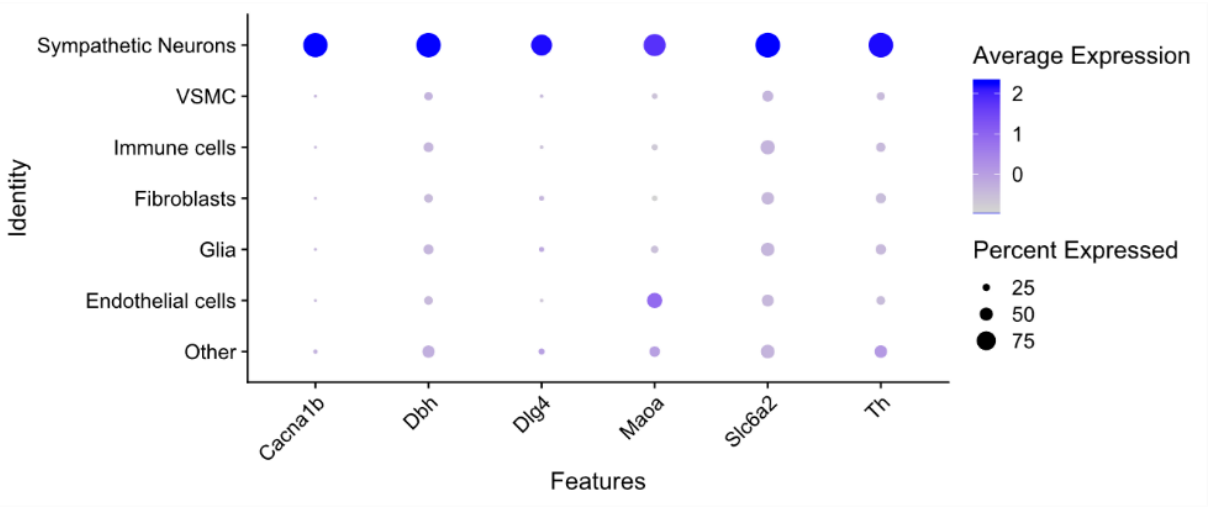



***Figure 3.8 The sympathetic neuron population expresses key sympathetic markers*** *The stated markers were used to identify neuron populations based on previous functional and qualitative descriptions of sympathetic neurons. (Cacna1b, Cav2.2; Dbh, dopamine-β-hydroxylase; Dlg4, PSD-95; Maoa, monoamine oxidase A; Slc6a2, Norepinephrine transporter; Th, Tyrosine hydroxylase)*

Heterogeneity amongst these populations was also of interest, given the effect this would have on functional analysis. The sympathetic neuron cluster was subdivided into six smaller clusters (**Figure 3.9A**). Of these clusters, neuronal clusters 1 and 2 (align with sympathetic subpopulations in the SCG which have

previously been identified using either immunohistochemistry (Li & Horn, 2006) or an *NPY*-GFP reporter line (Sikora *et al.*, 2017).

Neuronal clusters 1 and 2 both expressed the full range of sympathetic markers (**Figure 3.9B**), but can be differentiated, into an NPY (Neuropeptide Y) positive population, and an NPY negative population (**Figure 3.9C**). Interestingly, these populations also diverged in the expression of *CHRM2* **(Figure 3.9C**). *CHRM2* encodes the $M_2$ cholinergic receptor which has previously been associated with direct inhibition of sympathetic neurons by the PNS (Löffelholz & Muscholl, 1969; Vanhoutte, 1974; Habermeier-Muth & Muscholl, 1988). The difference in expression of CHRM2 and NPY between these populations was statistically significant (**Table 3.2;** *CHRM2, Average natural log(Ln) Fold change=0.53, p=4.13E-29*). These two markers are referred to here as markers of an *NPY* low, *CHRM2* low population, termed “Sympathetic neurons 1” and an *NPY* high, *CHRM2* high population, termed “Sympathetic neurons 2” (**Figure 3.9C**).

Beyond the differences in expression highlighted by these analyses, it was important to assess further differences between neuronal clusters 1 and 2. There were 285 differentially expressed genes (**Figure 3.12**) between these two populations, the top 25 of which are shown in **Table 3.2**. As the presence of two sympathetic neuron populations could confound later functional studies on cultured neurons, the difference in ion channel α encoding genes (**Figure 3.9C**), and other key genes related to chapters 4-6 was assessed. None of these genes were significantly differentially expressed. Of note, *KNCNMB4* was upregulated in neuron population 2 (NPY *high*/CHRM2 *high*) (**Table 3.2**) a channel briefly explored in chapter 4.

In addition, there were physiologically interesting differences in enzymes concerned with noradrenaline release, uptake and synthesis (*TH*, Ln fold change=-0.37, Adjusted p-value=1.913193e-15; *SLC6A4*, Ln fold change=0.60, Adjusted p-value=1.462122e-37; *MAOA*, Ln fold change=0.83, Adjusted p-value=2.096857e-62; *SYT2*, Ln fold change=0.7, p=6.977858e-43; *SYT4*, Log fold change=-0.54, p= 1.761248e-15; *SYT5*, Ln fold change=-0.26, p=1.7e-07; *SYN2*, Log fold change=-0.4, p=8.775311e-26), as well as GPCRS (*ADRA2A*, Ln fold change -0.31, Adjusted p-value=1.282618e-10; *ADRB2*, Ln fold change=0.41, Adjusted p-value=1.957442e-17; *HTRA1*, Ln fold change=0.83, Adjusted p-value=1.166253e-41; *DRD2*, Ln fold change=0.60, Adjusted p-value=2.421206e-36).

Of the four additional neuronal clusters identified (**Figure 3.9A**), clusters 4 and 6 had atypical expression of sympathetic markers (**Figure 3.9B**). Neuron cluster 6 may present as a dopaminergic neuron population, given high expression of *DDC* (Dopa Decarboxylase) and *TH* (Tyrosine hydroxylase), but minimal expression of noradrenaline producing *DBH* (Dopamine Beta-hydroxylase) (**Figure 3.9B**). For this reason, cluster 6 was excluded from the downstream analysis, where this chapter focusses upon sympathetic neurons only. Cluster 4 had a low cell count and low expression of the chosen sympathetic markers (**Figure 3.9B**) and was therefore also excluded from downstream analysis.

The identity of the final neuron clusters, 3 and 5, was more ambiguous. The predetermined sympathetic markers were present in cluster 3, but with relatively low expression for key makers such as *DDC* and *TH* (**Figure 3.9C**). Neuron cluster 5 had only sporadic expression of key sympathetic neuron markers but was not clearly visually separated from neuron cluster 3 (**Figure 3.9A**). Given this ambiguity, the Wistar neuronal clusters 1-3 and 5 were separated from clusters 4 and 6, and from

the SHR neurons. The analysis pathway was then repeated on these isolated clusters (**Figure 3.10**) in order to clearly identify the identity of clusters 3 and 5. By this analysis there were only two major populations, again separated into *NPY* and *CHRM2* low and high clusters (**Figure 3.10**). No populations resembling clusters 3 and 5 were present.

Trajectory inference analysis was performed via the *slingshot* package (**Figure 3.11**) (Street *et al.*, 2018). Trajectory inference analysis attempts to find pathways between similar cell clusters, and in doing so defines the similarity or developmental pathways between clusters. Here, this methodology was used to identify whether neuron clusters 1 and 2 were more similar to each other than to neuronal clusters 3 and 5. It was hypothesised that if populations 3 and 5 were indeed transitory states as indicated by **Figure 3.10**, then trajectory analysis would support this. In agreement with this hypothesis, the trajectory analysis data (**Figure 3.11**) suggest that neuronal clusters 1 and 2 are closer to 3 and 5 than each other, and that the trajectory is through clusters 3 and 5.

Based upon the data, neuronal clusters 3 and 5 were included in analyses referring to sympathetic neurons, but only neuronal clusters 1 and 2 were treated as physiologically relevant subpopulations. To prevent confusion, references to scRNAseq beyond this chapter will to the combined clusters 1-3 and 5 as sympathetic neurons.

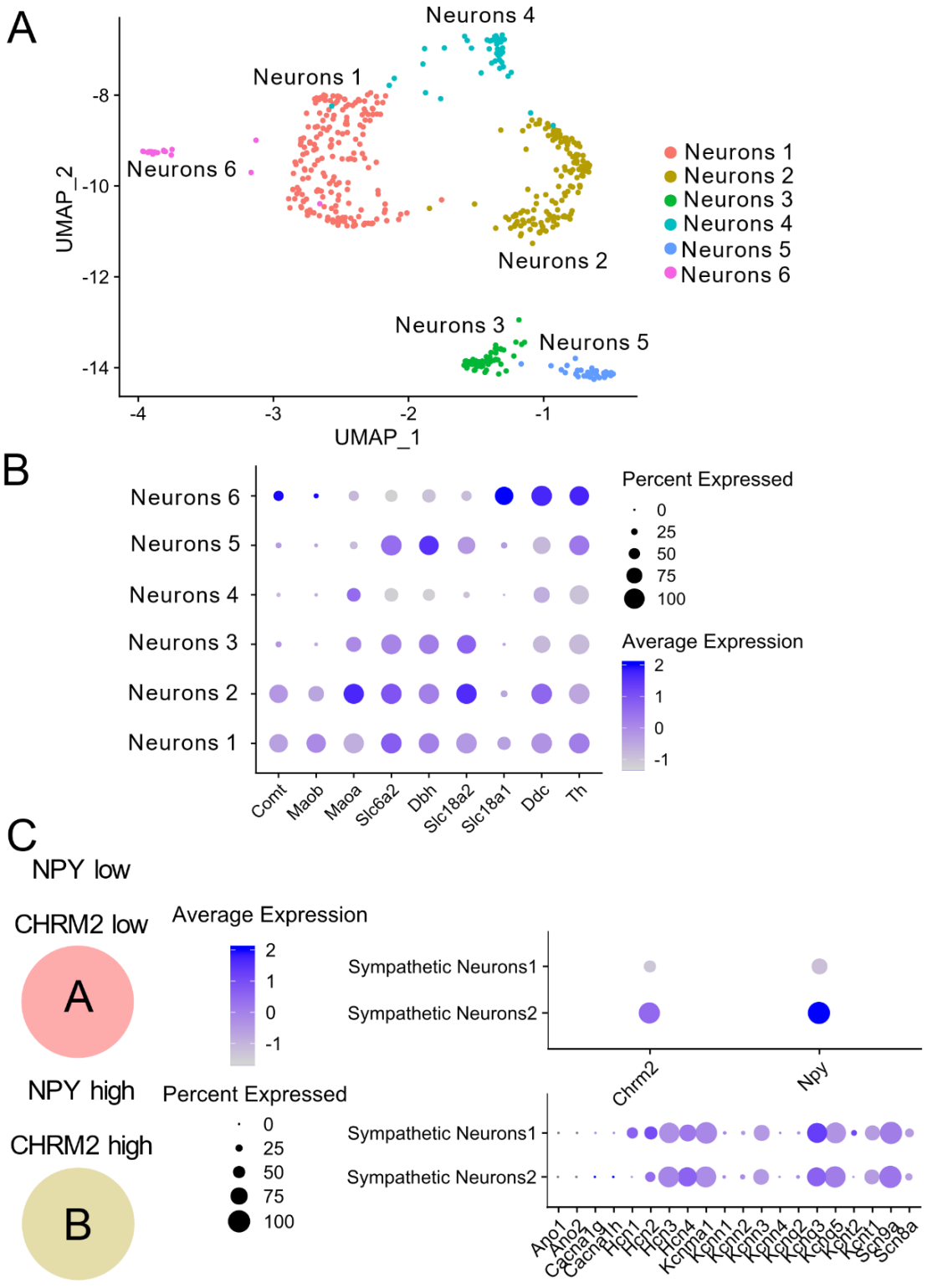



***Figure 3.9 The identification of 2 putative neuronal clusters and their sympathetic markers*** *6 Neuronal clusters were identified (A), although only populations 1 and 2 clearly expressed all sympathetic markers (B), from this we identified 2 neuronal clusters that are likely to represent physiological populations, clusters 1 and 2. (C) Clusters 1 and 2 can be differentiated based upon their expression of NPY and CHRM2. Notably, neither population differentially expressed transcripts for voltage-gated ion channel α subunits.*

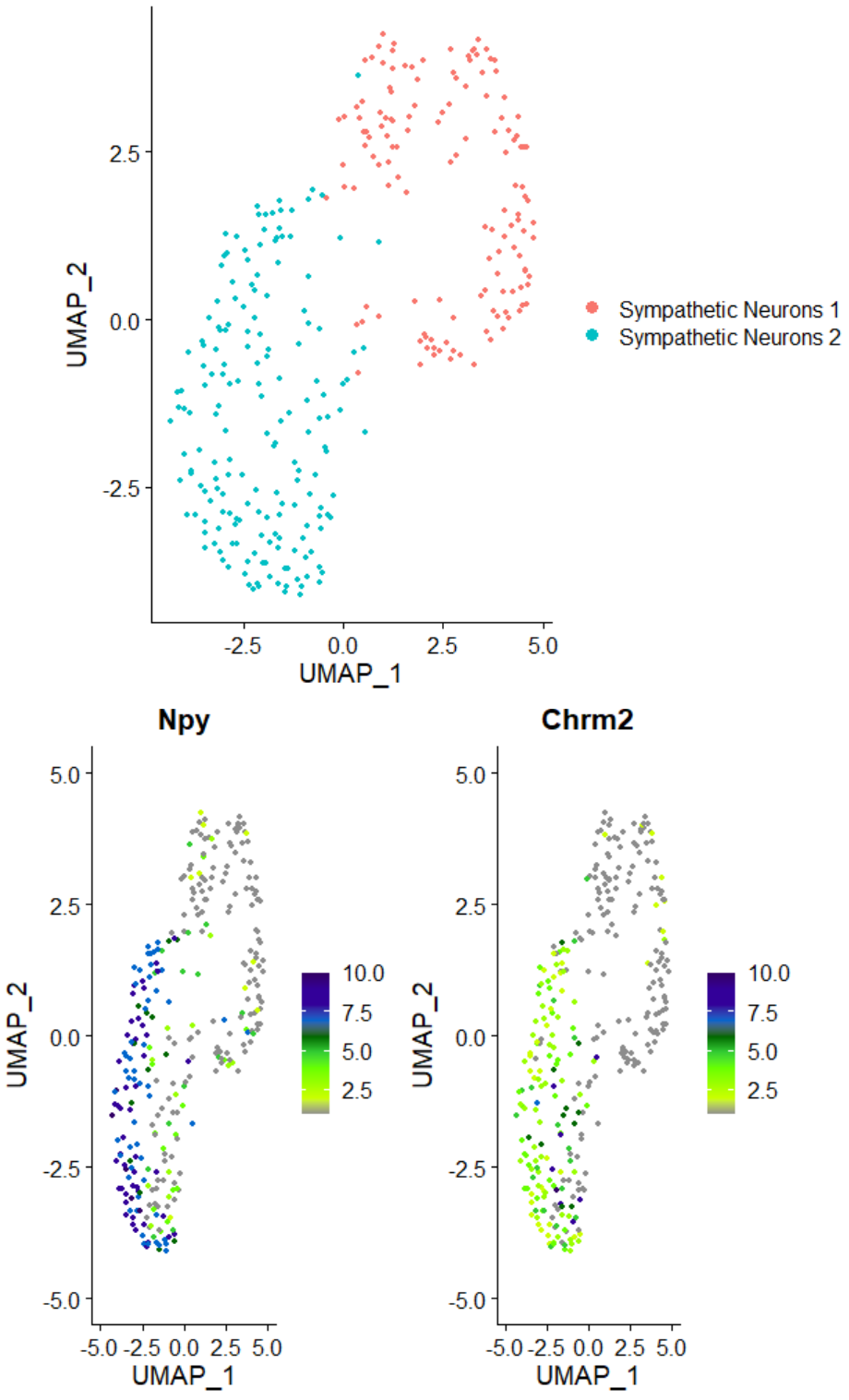



***Figure 3.10 Clustering of Wistar neurons alone suggests 2 populations of sympathetic neurons*** *Wistar sympathetic neurons were subset, and re-clustered to assess the number of potential neuronal subpopulations. This resulted in two neuronal populations with distinct expression patterns of NPY and CHRM2 which are similar to the Sympathetic neuron clusters 1 and 2 highlighted by clustering of the combined Wistar and SHR datasets.*

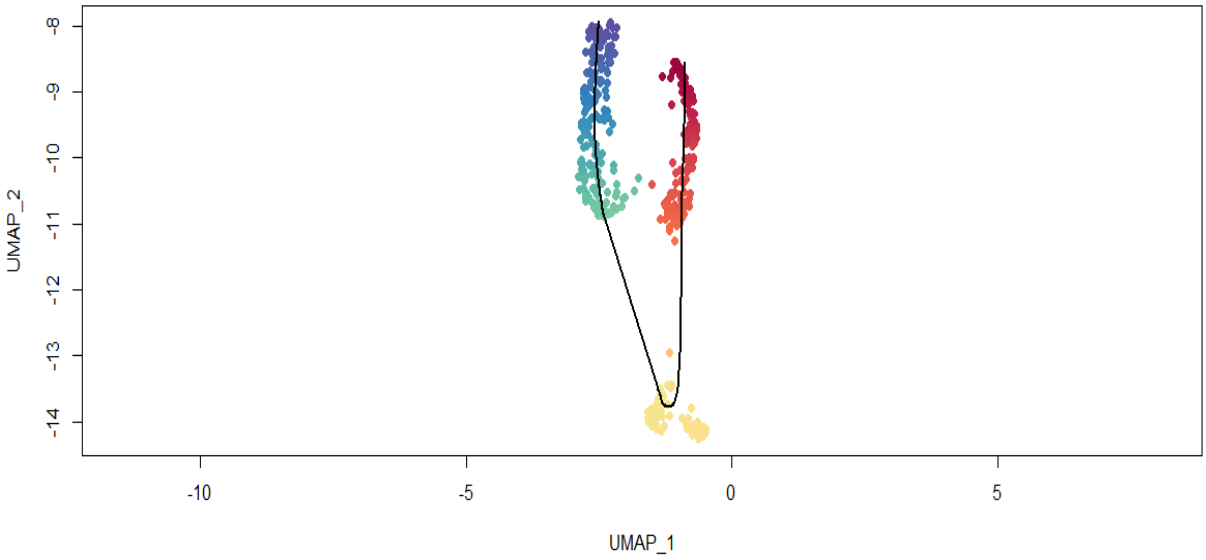



***Figure 3.11 Trajectory inference analysis suggests that neuron clusters 3 and 5 are transitory states*** *Slingshot trajectory inference analysis highlights a pathway where clusters 3 and 5 are intermediary between clusters 1 and 2, supporting the notion of two primary sympathetic neuron clusters. Colours here are used to indicate distinct clusters of cells.*




***Figure 3.12 Summary of differential expression analysis between neuron clusters 1 and 2*** *In Wistar neuron cluster 2 (NPY high/CHRM2 high). 166 genes were upregulated and 119 downregulated relative to neuron cluster 1 (NPY low/CHRM2 low).*

***Table 3.2 Top 25 genes that are differentially expressed in Wistar sympathetic neuron population 2 (NPY high/CHRM2) high relative to Sympathetic Neuron population 1 (NPY low/CHRM2 low)*** *Mast differential expression analysis detected 285 genes with significantly different expression in Sympathetic neuron population 2 relative to Sympathetic neuron population 1.*

| Gene | Name | Ln Fold change | Adjusted P Value |
|---|---|---|---|
| **Epha5** | EPH Receptor A5 | 1.18 | 6.13E-72 |
| **Dgkb** | Diacylglycerol Kinase Beta | 0.99 | 1.38E-68 |
| **Kcnmb4** | Potassium Calcium-Activated Channel Subfamily M Regulatory Beta Subunit 4 | 0.94 | 3.08E-68 |
| **Ncald** | Neurocalcin Delta | 1.12 | 4.28E-67 |
| **Npy** | Neuropeptide Y | 1.58 | 8.67E-67 |
| **Fxyd5** | FXYD Domain Containing Ion Transport Regulator 5 | 1.23 | 1.26E-62 |
| **Maoa** | Monoamine oxidase A | 0.83 | 2.10E-62 |
| **Mcub** | Mitochondrial Calcium Uniporter Dominant Negative Subunit Beta | 0.92 | 6.53E-62 |
| **Pcp4** | Purkinje Cell Protein 4 | 2.04 | 1.76E-60 |
| **Dync1i2** | Cytoplasmic dynein 1 intermediate chain 2 | 0.73 | 5.90E-59 |
| **Alcam** | Activated Leukocyte Cell Adhesion Molecule | 1.31 | 9.52E-59 |
| **Olfm2** | Olfactomedin 2 | 1.00 | 9.31E-55 |
| **Aqp1** | Aquaporin 1 | 1.07 | 3.84E-54 |
| **Lgals3** | Galectin 3 | -1.30 | 9.04E-52 |
| **Galnt16** | Polypeptide N-Acetylgalactosaminyltransferase 16 | 0.91 | 2.07E-50 |
| **Zbtb20** | Zinc Finger And BTB Domain Containing 20 | 0.75 | 2.37E-49 |
| **Brinp2** | BMP/Retinoic Acid Inducible Neural Specific 2 | 0.97 | 1.57E-48 |
| **Nrp2** | Neuropilin 2 | -0.60 | 2.97E-48 |
| **Csrp1** | Cysteine and glycine-rich protein 1 | -0.80 | 7.10E-48 |
| **Pcdh7** | Protocadherin 7 | 0.47 | 1.06E-46 |
| **Fst** | Follistatin | 0.61 | 6.28E-46 |
| **Bcam** | Basal cell adhesion molecule | -0.87 | 8.27E-46 |
| **Nrp1** | Neuropilin-1 | 0.73 | 5.15E-44 |
| **St3gal5** | ST3 Beta-Galactoside Alpha-2,3-Sialyltransferase 5 | 0.79 | 7.54E-44 |
| **Tenm2** | Teneurin-2 | 0.72 | 5.95E-43 |

### 3.3.1.2 Neuronal gene expression changes in the SHR

A key aim of this study is to facilitate functional studies through identifying neuron-specific differences in gene expression in the SHR. To this end, neuronal gene expression was compared between Wistar and SHR neuron clusters using MAST (Finak *et al.*, 2015). Differential expression analysis was performed between all sympathetic neurons (**Figure 3.13**; **Table 3.3**) and in separate analyses for Sympathetic Neurons 1 (*NPY* low, *CHRM2* low) (**Figure 3.14**; **Table 3.4**), and Sympathetic Neurons 2 (*NPY* high, *CHRM2* high) (**Figure 3.15**; **Table 3.5**). For completeness, the remaining sympathetic neuron clusters, 3 and 5, were also analysed. No significant differences in gene expression between Wistar and SHR neuron clusters 3 and 5 were observed.




***Figure 3.13 Summary of gene expression changes between Wistar and SHR neurons at 5-6 weeks of age*** *There were 474 differentially expressed genes between Wistar and SHR neurons. 246 of which were upregulated and 228 were downregulated in the SHR population.*

***Table 3.3 Top 25 differentially expressed genes between Wistar and SHR neuron clusters*** *MAST differential expression highlighted 474 differentially expressed genes between Wistar and SHR stellate ganglia neuron clusters at the adjusted p < 0.05 cut-off level.*

| Gene | Name | Ln Fold change | Adjusted P Value |
|---|---|---|---|
| **Gsta4** | Glutathione S-Transferase A4 | 0.49 | 1.20E-52 |
| **Jund** | Transcription Factor Jun-D | 1.51 | 2.11E-46 |
| **AABR07043389.1** | | -0.70 | 1.14E-21 |
| **Slc12a3** | Na-Cl Cotransporter | -0.66 | 2.64E-21 |
| **Clic3** | Chloride Intracellular Channel 3 | 0.44 | 3.09E-21 |
| **Ube2s** | Ubiquitin-Conjugating Enzyme E2 S | 0.45 | 4.82E-21 |
| **Avil** | Advillin | -0.81 | 5.72E-21 |
| **Tnpo1** | Transportin 1 | -0.68 | 6.79E-21 |
| **AC134224.1** | | -1.19 | 2.36E-20 |
| **Lgals3** | Galectin 3 | 0.74 | 2.37E-20 |
| **Gch1** | GTP Cyclohydrolase 1 | 0.31 | 4.01E-20 |
| **Nrsn1** | Neurensin-1 | 0.44 | 5.15E-20 |
| **Fxyd6** | FXYD Domain Containing Ion Transport Regulator 6 | 0.45 | 1.81E-19 |
| **Rps25** | Ribosomal Protein S25 | 0.58 | 9.26E-19 |
| **Pcp4** | Purkinje Cell Protein 4 | -0.89 | 1.10E-18 |
| **Prkg2** | Protein Kinase CGMP-Dependent 2 | -0.54 | 5.53E-18 |
| **RT1-A1** | RT1 class I, A1 | 0.55 | 1.45E-17 |
| **Gria2** | Glutamate Ionotropic Receptor AMPA Type Subunit 2 | -0.74 | 2.29E-17 |
| **Lgals1** | Galectin 1 | 0.57 | 3.48E-17 |
| **Pdxp** | Pyridoxal Phosphatase | 0.33 | 3.82E-17 |
| **Macf1** | Microtubule Actin Crosslinking Factor 1 | -0.62 | 9.69E-17 |
| **Rgs10** | Regulator of G-Protein Signalling 10 | 0.64 | 3.44E-16 |
| **Ddc** | Dopa Decarboxylase | -0.60 | 3.54E-16 |
| **Sema5a** | Semaphorin 5A | 0.26 | 4.12E-16 |
| **Arhgap21** | Rho GTPase Activating Protein 21 | -0.50 | 1.66E-15 |

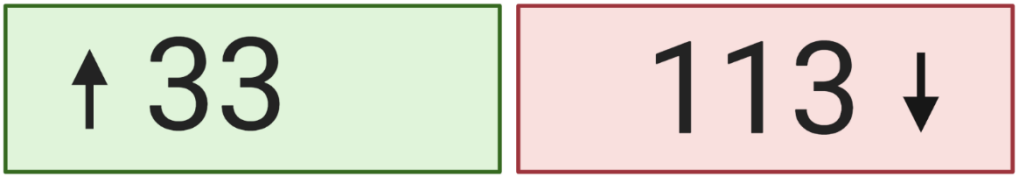



***Figure 3.14 Summary of differential expression between Wistar and SHR neuron population (NPY low/CHRM2 low)*** *In SHR neuron population 1 33 genes were upregulated and 113 downregulated relative to Wistar neuron population 1.*

***Table 3.4 Top 25 differentially expressed genes between Wistar and SHR neuron cluster 1 (NPY low/CHRM2 low)*** *MAST differential expression highlighted 146 differentially expressed genes between Wistar and SHR stellate ganglia neuron cluster 1 at the adjusted p < 0.05 cut-off level.*

| Gene | Name | Ln Fold change | Adjusted P Value |
|---|---|---|---|
| **Jund** | Transcription Factor Jun-D | 1.52 | 7.62E-68 |
| **Gsta4** | Glutathione S-Transferase Alpha 4 | 0.58 | 1.72E-35 |
| **Avil** | Advillin | -0.97 | 1.39E-30 |
| **Nudt17** | Nudix Hydrolase 17 | -0.29 | 1.59E-25 |
| **Prkg2** | Protein Kinase CGMP-Dependent 2 | -0.49 | 1.03E-20 |
| **Ddc** | Dopa Decarboxylase | -0.64 | 1.65E-20 |
| **Dnah6** | Dynein Axonemal Heavy Chain 6 | 0.27 | 6.93E-19 |
| **AABR07043389.1** | | -0.69 | 1.07E-17 |
| **Csrp1** | Cysteine And Glycine Rich Protein 1 | -0.49 | 2.41E-17 |
| **Gria2** | Glutamate Ionotropic Receptor AMPA Type Subunit 2 | -0.49 | 2.61E-17 |
| **Mal2** | Mal, T Cell Differentiation Protein 2 | -0.44 | 3.48E-17 |
| **RT1-A1** | RT1 class I, A1 | 0.48 | 6.89E-15 |
| **AC134224.1** | | -0.79 | 1.21E-12 |
| **Lmbrd1** | LMBR1 Domain Containing 1 | -0.36 | 2.38E-12 |
| **Thy1** | Thy-1 Cell Surface Antigen | -0.46 | 5.06E-12 |
| **Kif5b** | Kinesin Family Member 5B | -0.40 | 5.16E-12 |
| **Tnpo1** | Transportin 1 | -0.36 | 7.16E-12 |
| **Rps25** | Ribosomal Protein S25 | 0.56 | 2.45E-11 |
| **Pcp4** | Purkinje Cell Protein 4 | -0.62 | 3.38E-11 |
| **Clic3** | Chloride Intracellular Channel 3 | 0.35 | 8.61E-11 |
| **Mustn1** | Musculoskeletal Embryonic Nuclear Protein 1 | -0.51 | 1.59E-10 |
| **Fuca2** | Alpha-L-Fucosidase 2 | -0.29 | 1.85E-10 |
| **RT1-CE4** | RT1 class I, CE4 | -0.39 | 2.10E-10 |
| **Rgs10** | Regulator Of G-Protein Signaling 10 | 0.60 | 4.87E-10 |
| **Pdxp** | Pyridoxal Phosphatase | 0.27 | 8.59E-10 |




***Figure 3.15 Summary of differential expression between Wistar and SHR neuron population (NPY high/CHRM2 high)*** *In SHR neuron population 2 16 genes were upregulated and 25 downregulated relative to Wistar neuron population 2.*

***Table 3.5 Top 25 differentially expressed genes between Wistar and SHR neuron cluster 2 (NPY high/CHRM2 high)*** *MAST differential expression highlighted 41 differentially expressed genes between Wistar and SHR stellate ganglia neuron cluster 2 at the adjusted p < 0.05 cut-off level.*

| Gene | Name | Ln Fold change | Adjusted P Value |
|---|---|---|---|
| **Jund** | Transcription Factor Jun-D | 1.27 | 8.20E-24 |
| **RT1-A1** | RT1 class I, A1 | 0.95 | 2.44E-18 |
| **Mal2** | Mal, T Cell Differentiation Protein 2 | -0.50 | 2.19E-14 |
| **Ddc** | Dopa Decarboxylase | -0.76 | 6.78E-12 |
| **Arpc1b** | Actin Related Protein 2/3 Complex Subunit 1B | 0.46 | 1.40E-07 |
| **Lgals3** | Galectin 3 | 0.54 | 2.64E-07 |
| **AABR07043389.1** | | -0.75 | 1.31E-06 |
| **Actb** | Actin Beta | -0.66 | 1.92E-05 |
| **RT1-CE10** | | -0.53 | 2.00E-05 |
| **Rtn4** | Reticulon 4 | -0.43 | 9.67E-05 |
| **Ssr2** | Signal Sequence Receptor Subunit 2 | -0.35 | 1.97E-04 |
| **Scg5** | Secretogranin V | -0.50 | 2.34E-04 |
| **Ndfip1** | Nedd4 Family Interacting Protein 1 | -0.44 | 2.37E-04 |
| **Cpe** | Carboxypeptidase E | -0.40 | 9.50E-04 |
| **Ngdn** | Neuroguidin | 0.26 | 1.07E-03 |
| **Tmem59l** | Transmembrane Protein 59 Like | -0.33 | 1.23E-03 |
| **Ilf3** | Interleukin Enhancer Binding Factor 3 | 0.28 | 1.53E-03 |
| **Laptm4a** | Lysosomal Protein Transmembrane 4 Alpha | -0.50 | 2.68E-03 |
| **Bsg** | Basigin (Ok Blood Group) | -0.43 | 3.11E-03 |
| **Lrpap1** | LDL Receptor Related Protein Associated Protein 1 | -0.47 | 3.21E-03 |
| **Csrp1** | Cysteine And Glycine Rich Protein 1 | -0.40 | 4.10E-03 |
| **Hadhb** | Hydroxyacyl-CoA Dehydrogenase Trifunctional Multienzyme Complex Subunit Beta | -0.29 | 4.52E-03 |
| **Rps25** | Ribosomal Protein S25 | 0.50 | 5.03E-03 |
| **Vamp1** | Vesicle Associated Membrane Protein 1 | 0.50 | 8.09E-03 |
| **Ndufa10l1.1** | NADH dehydrogenase (ubiquinone) 1 alpha subcomplex 10-like 1 | -0.28 | 8.83E-03 |

### 3.3.1.3 Neuronal gene ontology and KEGG analysis

Differential expression analysis is useful for providing a comprehensive list of changes, but the large volume of changes (i.e. **Table 3.3**) can prove difficult to interpret. Predefined semantic groupings of genes such as gene ontology and KEGG terms allow these differential expression changes to be summarised into biological processes. This was implemented via *clusterProfiler* (Yu *et al.*, 2012).

A directed acyclic graph groups significantly over-represented gene ontology terms by their shared differentially expressed genes (**Figure 3.16**). Gene ontology analysis is subdivided into terms associated with biological processes, cell components and molecular function (Carbon *et al.*, 2019). This figure displays all significantly over-represented “cell component” gene ontology terms. Edges were drawn between gene ontology terms with shared differentially expressed genes, thereby suggesting similarity. This allows for clusters of relevant gene ontology terms to be identified. For example, a cluster of gene ontology terms in the lower left-hand side of **figure 3.16** contains a cluster multiple overrepresented gene ontology groups associated with mitochondrial function (eg. “respiratory chain complex”, “mitochondrial protein complex”) indicating dysregulation of genes associated with this wider process in the SHR. For clarity, only a directed acyclic graph for significantly overrepresented “cell components” terms is provided here (**Figure 3.16**), however, similar graphs for “biological process” and “molecular function” gene ontology terms are shown in appendix figures 1-4**.**

From the over-represented “cell component” gene ontology terms in **Figure 3.16**, the terms “Neuron to Neuron synapse”, “Post-synaptic density”, “Cation channel complex” and “Transporter complex” were of interest for understanding

SHR neuron electrophysiology and so were expanded upon in **Figure 3.17**. In **Figure 3.17**, each of these over-represented gene ontology terms is linked by an edge to the differentially expressed genes associated with that term. These edges are colour coded to represent each ontology group. Despite reducing overlap through *cluster-Profiler*'s simplify command, (Yu *et al.*, 2012) these gene ontology terms still overlap. Therefore, some genes are linked to multiple ontology groups, and are connected to multiple coloured edges. **Figure 3.17** highlights differential expression of *KCNQ5*, *SCN2A*, *SCN9A* and *GRIA2* which were investigated in chapter 4 and 6.

These analyses were repeated for KEGG terms in appendix figures 5-6. In contrast to gene ontology, KEGG orthology terms (Kanehisa *et al.*, 2016) are not subdivided and tend to cover broader areas.

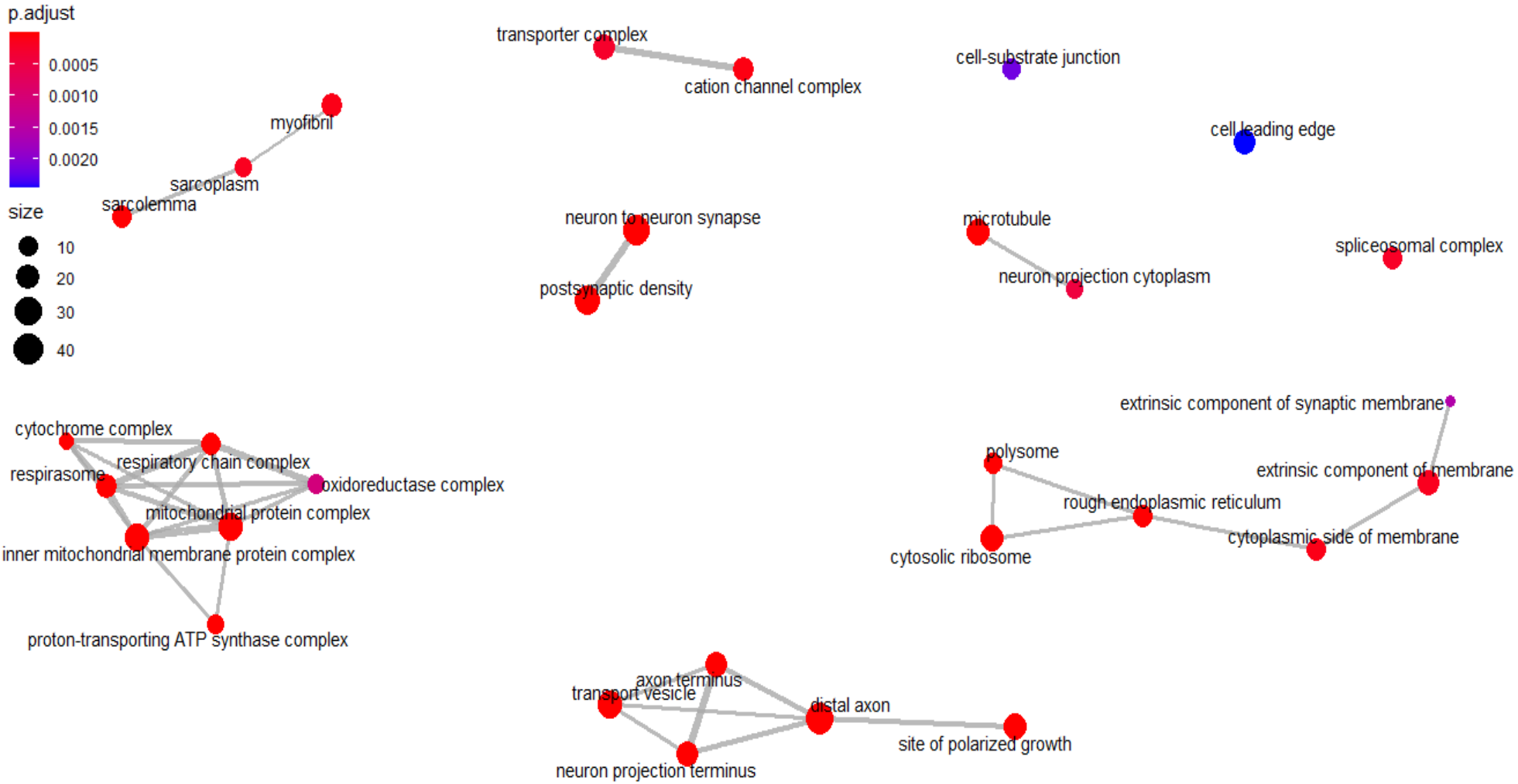



***Figure 3.16 Over-represented "cell component" gene ontology groups in SHR neurons*** *Gene ontology over-representation analysis highlighted multiple "Cell-component" gene ontology terms with a larger than expected number of dysregulated genes. Here the colour of each dot is scaled by the adjusted p value for the over-representation of each gene ontology group. The dot sizes indicate the number of differentially expressed genes per gene ontology group. Edges between dots indicate shared differentially expressed genes between gene ontology groups. The thickness of these lines is scaled by the number of shared differentially expressed genes.*

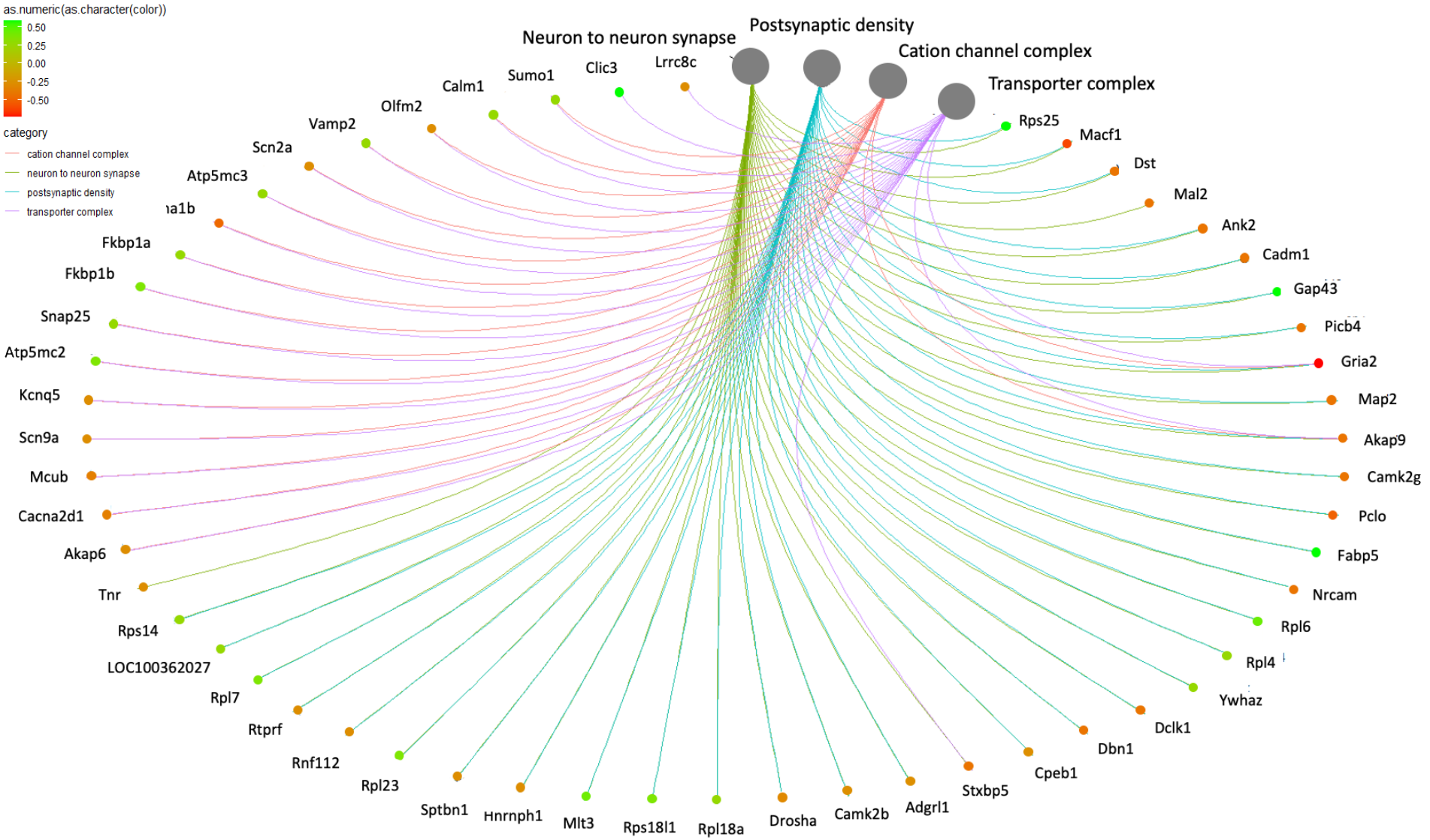



***Figure 3.17 A visual breakdown of gene expression changes underpinning 4 physiologically interesting over-represented "Cell component" gene ontology terms*** *The differentially expressed genes from the over-represented gene-ontology groups "neuron to neuron synapse", "postsynaptic density", "cation channel complex" and "transporter complex" are graphically represented here. Lines are colour coded to the gene ontology term of origin. Circles representing genes are coloured based upon the difference in expression between Wistar and SHR neurons, where green indicates an increase in SHR neurons and red indicates a decrease.*

### 3.3.2 Bulk RNA-sequencing

Bulk RNA-sequencing was performed on 16-week-old Wistar and SHR right whole stellate ganglia. At this age, the SHRs present with symptoms of established hypertension (Minami *et al.*, 1989). As these animals are older, and these data are contaminated by non-neuronal populations, references to this dataset remain limited throughout the thesis. This dataset is publicly available from NCBI Sequence Read Archive (SRP132271) and published in various forms in three manuscripts (Davis *et al.*, 2018; Bardsley *et al.*, 2018*a*-*b*). The comparison presented in **Figure 3.20** between scRNAseq and Bulk RNA-sequencing data are unpublished. The bulk RNA-sequencing dataset was previously validated by RT-qPCR (Davis *et al.*, 2018), and so we use these data to observe whether the differential expression observed in whole ganglia, replicate those observed by scRNAseq.

#### 3.3.2.1 Differential expression

Differential expression analysis was performed between Wistar and SHR whole ganglia RNA, and the top 25 differentially expressed genes, as sorted by adjusted p-value, are shown in **Table 3.6.** There were 768 differentially expressed genes in the bulk RNA-sequencing dataset (**Figure 3.18**). This was similar to the summed total of 737 unique differentially expressed genes across each of the six populations identified by scRNAseq (**Figure 3.19**). However, only 77 of these changes were reported by both methodologies and only 38 of the neuron-specific changes detected by scRNAseq were detected by bulk RNA-sequencing (**Figure 3.19**).

For most differentially expressed genes reported by scRNAseq, bulk RNA-sequencing reported a similar direction of change (**Figure 3.20A**). However, for the remaining genes, the smaller effect size observed by bulk RNA-sequencing appears to limit the number of statistically significant differentially expressed genes (**Figure 3.20B**). It is noteworthy that the Wistar datasets appear relatively similar when correlated, although RNA expression is higher in the bulk RNA-sequencing dataset (**Figure 3.20C**). This is to be expected given the technical differences between these methodologies, and the differences in normalisation strategy between the analysis pathways.

Despite these differences, when the datasets were compared for the 25 largest differentially expressed genes in neurons by scRNAseq, the datasets appeared to be well correlated (**Figure 3.21**).




***Figure 3.18 Summary of differential expression between Wistar and SHR whole stellate ganglia by bulk RNA-sequencing*** *350 genes were upregulated and 418 downregulated in the SHR stellate ganglia relative to the Wistar stellate ganglia at 16 weeks.*

***Table 3.6 Top 25 gene expression changes from bulk RNA-sequencing of 16 week Wistar and SHR stellate ganglia*** *Bulk RNA-sequencing highlights 768 changes between Wistar and SHR 16 week homogenised stellate ganglia tissue* (Davis *et al.*, 2018)**.**

| Gene | Name | Ln Fold change | Adjusted P value |
|---|---|---|---|
| **Synpr** | Synaptoporin | -4.16 | 1.20E-80 |
| **Nudt17** | Nudix Hydrolase 17 | -3.69 | 2.84E-80 |
| **Pxmp4** | Peroxisomal membrane protein 4 | 2.74 | 6.99E-67 |
| **Gsta4** | Glutathione S-Transferase Alpha 4 | 2.57 | 1.85E-65 |
| **Nudt3** | Nudix Hydrolase 3 | 1.92 | 4.53E-48 |
| **Lrsam1** | Leucine-rich repeat and sterile alpha motif-containing protein 1 | -3.14 | 7.34E-47 |
| **LOC363337** | Takusan domain-containing protein | -1.84 | 3.46E-46 |
| **LOC103689947** | Selenium-binding protein 1 | -3.37 | 1.01E-41 |
| **Mfsd14b** | Major facilitator superfamily domain containing 14B | 1.90 | 7.96E-36 |
| **Perp** | P53 Apoptosis Effector Related to PMP22 | -2.31 | 5.86E-32 |
| **Ptgr1** | Prostaglandin reductase 1 | 1.82 | 1.74E-31 |
| **Tnni1** | Troponin I1, Slow Skeletal Type | -3.18 | 3.95E-31 |
| **Camk2d** | Calcium/Calmodulin Dependent Protein Kinase II Delta | -2.27 | 6.06E-31 |
| **Hba-a1** | Hemoglobin alpha, adult chain 1 | -4.50 | 4.53E-30 |
| **Fxyd7** | FXYD Domain Containing Ion Transport Regulator 7 | -1.72 | 6.57E-29 |
| **Fbxw8** | F-Box And WD Repeat Domain Containing 8 | -1.67 | 6.56E-28 |
| **Cela1** | Chymotrypsin Like Elastase 1 | -2.67 | 7.41E-27 |
| **Selenbp1** | Selenium Binding Protein 1 | 5.51 | 1.38E-26 |
| **Elk3** | ETS Transcription Factor ELK3 | -1.62 | 2.39E-26 |
| **Bdkrb2** | Bradykinin Receptor B2 | 2.13 | 4.55E-26 |
| **Tatdn3** | TatD DNase Domain Containing 3 | -1.46 | 4.58E-26 |
| **Pcdhga1** | Protocadherin Gamma Subfamily A, 1 | -2.19 | 2.26E-25 |
| **RT1-Bb** | RT1-Bb RT1 class II | -2.66 | 5.24E-25 |
| **Nt5dc1** | 5'-Nucleotidase Domain Containing 1 | -1.67 | 1.95E-24 |
| **Ttc39a** | Tetratricopeptide Repeat Domain 39A | -1.35 | 2.55E-24 |

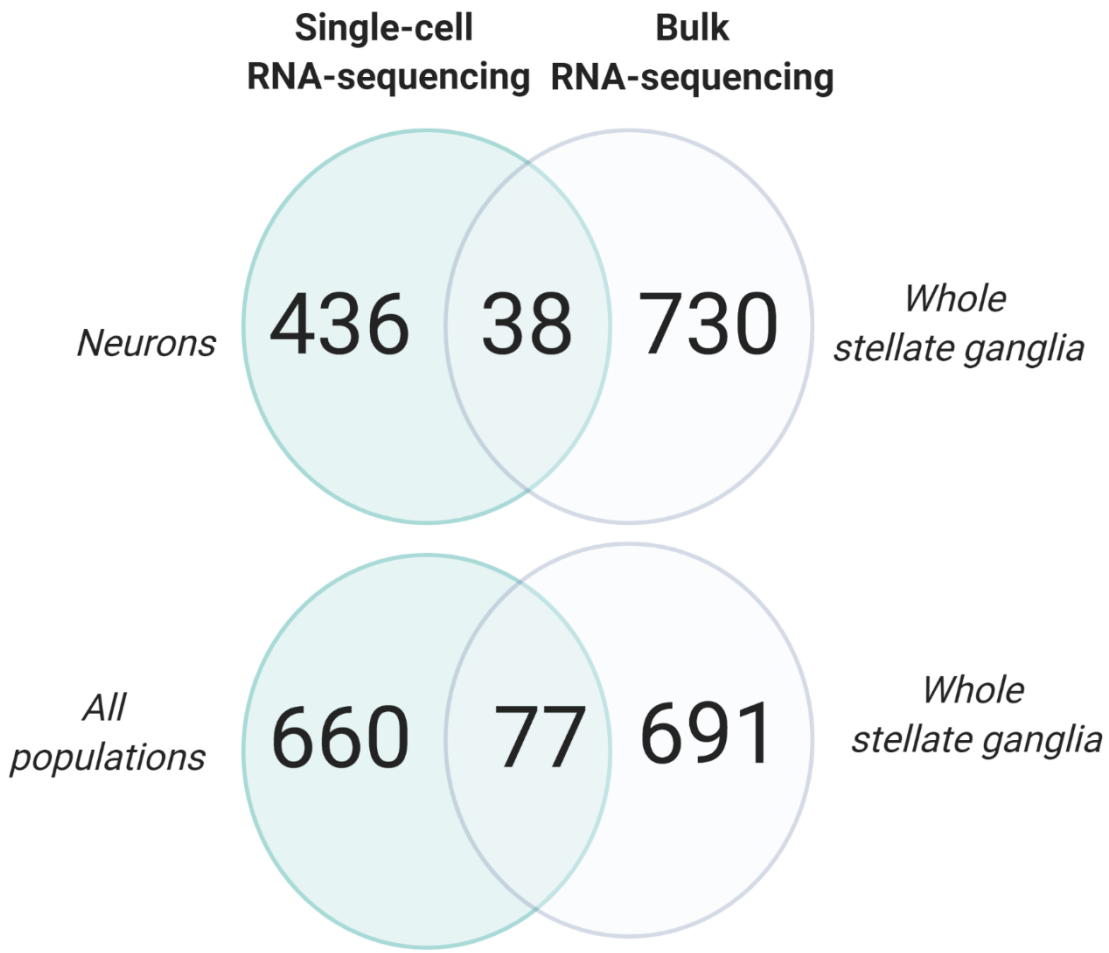



***Figure 3.19 Venn diagrams summarising changes observed by bulk and single-cell RNA-sequencing datasets*** *(A) Highlights that of the 474 differentially reported genes reported by single-cell RNA-sequencing, only 38 were also reported by bulk RNA-sequencing. Likewise, 730 gene expression changes were reported by bulk RNA-sequencing that are not present in the single-cell RNA-sequencing dataset. Additionally, it should be noted that of the 468 neuronal changes in reported in the single-cell RNA-sequencing dataset, 76 of these were not found to be expressed by bulk RNA-sequencing. (B) 77 gene expression changes were shared between identified populations by RNA-sequencing and whole stellate ganglia. 737 unique genes which were differentially expressed were detected across all six stellate ganglia cell populations.*

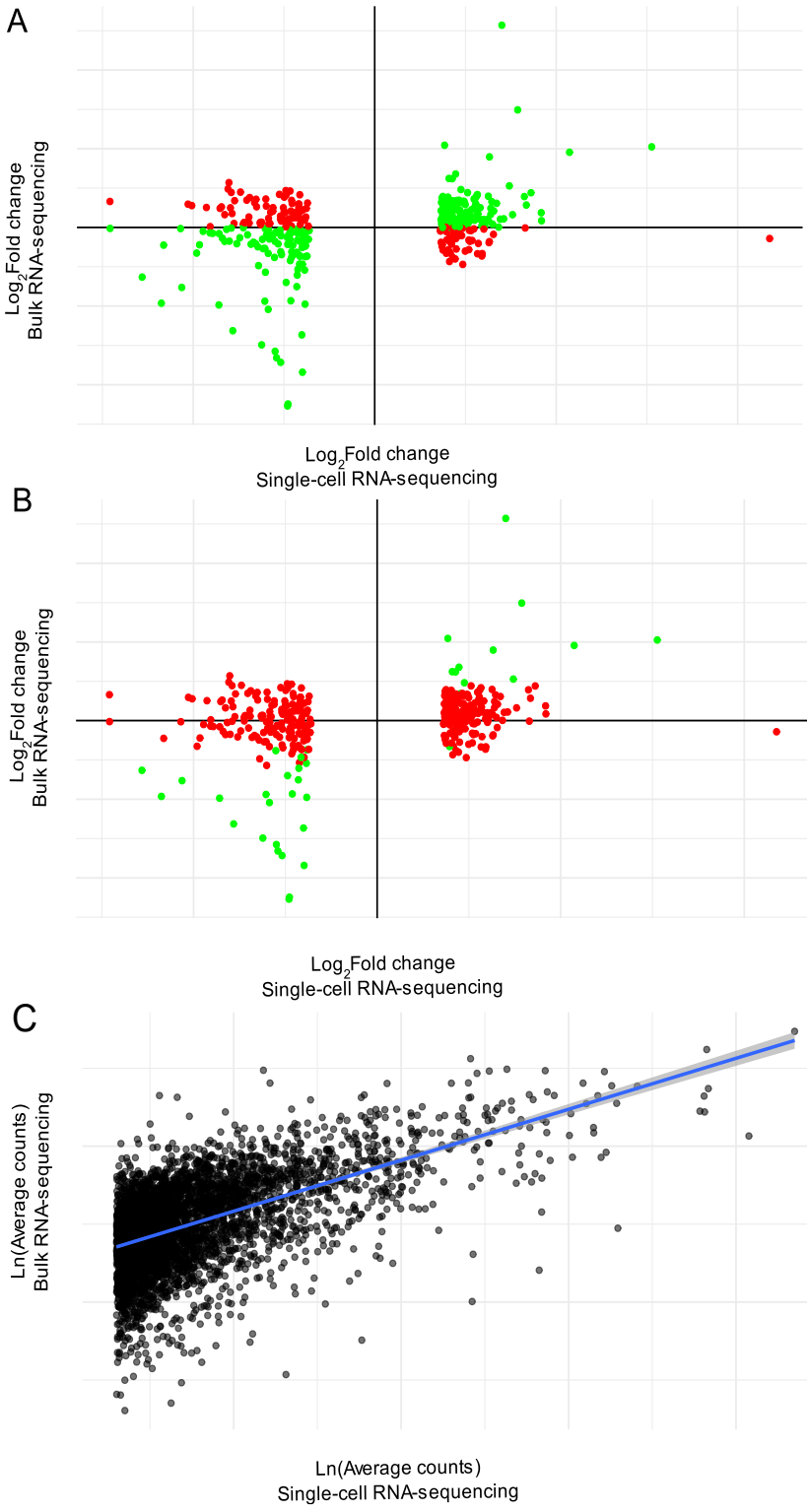



**Figure 3.20 Comparison of differential expression and Wistar expression data between bulk RNA-sequencing and pseudo-bulk analysis of the single-cell RNA-sequencing dataset**

Single-cell RNA-sequencing expression data was averaged across the neuronal population creating a "pseudo-bulk" dataset to compare to the bulk RNA-sequencing dataset.

(A)(B) The $Log_2$ fold change between Wistar and SHR neurons is shown on the x axis as derived from bulk RNA-sequencing. The y axis highlights the size of the differential expression for whole stellate ganglia by the bulk RNA-sequencing dataset. The 398 genes were selected based upon being differentially expressed in the single-cell RNA-sequencing dataset and also expressed in the bulk RNA-sequencing dataset. In (A) genes with the same direction of change are highlighted in green (258 genes), and with alternate directions of change in red (140 genes). In (B) genes which were differentially expressed in both the bulk RNA-sequencing and single-cell RNA-sequencing datasets are shown in green, red points indicate statistical significance in the single-cell RNA-sequencing dataset only.

In (C) a correlation between bulk RNA-sequencing and single-cell RNA-sequencing is shown in Wistar ($R^2$ = 0.32, r = 0.56). All genes with an expression greater than Ln(0.3) across either the averaged bulk RNA-sequencing Wistar samples, or the average Wistar neuronal population from the single-cell RNA-sequencing were included in this analysis.

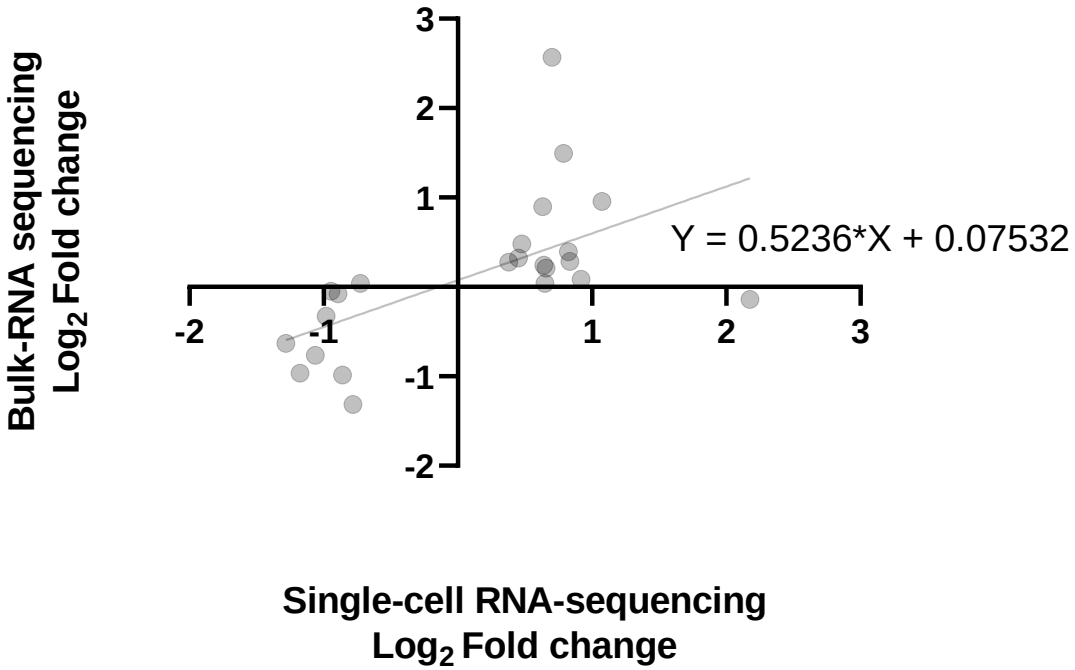



***Figure 3.21 Comparison of single-cell and bulk RNA-sequencing derived differential expression changes*** *The top 25 differentially expressed genes from the single-cell RNA-sequencing neuronal cluster were compared with bulk RNA-sequencing of the whole stellate ganglia. The $Log_2$ Fold changes were correlated with a $R^2$ value of 0.35 (r = 0.59). Both datasets have been previously published separately* (Davis *et al.*, 2018, 2020).

### 3.3.2.2 Gene ontology

To facilitate comparison with scRNAseq, bulk RNA-sequencing dataset was then studied via gene ontology analysis. As before, over-represented "cell component" gene ontology groups are visually highlighted in **Figure 3.22,** and similar analysis for "molecular function" and "biological process" groups can be found in appendix figures 12-13. In mimicry of the scRNAseq dataset, terms associated with synaptic transmission and ion channels were over-represented, including "postsynaptic membrane", "ion channel complex" and "neurotransmitter receptor complex".

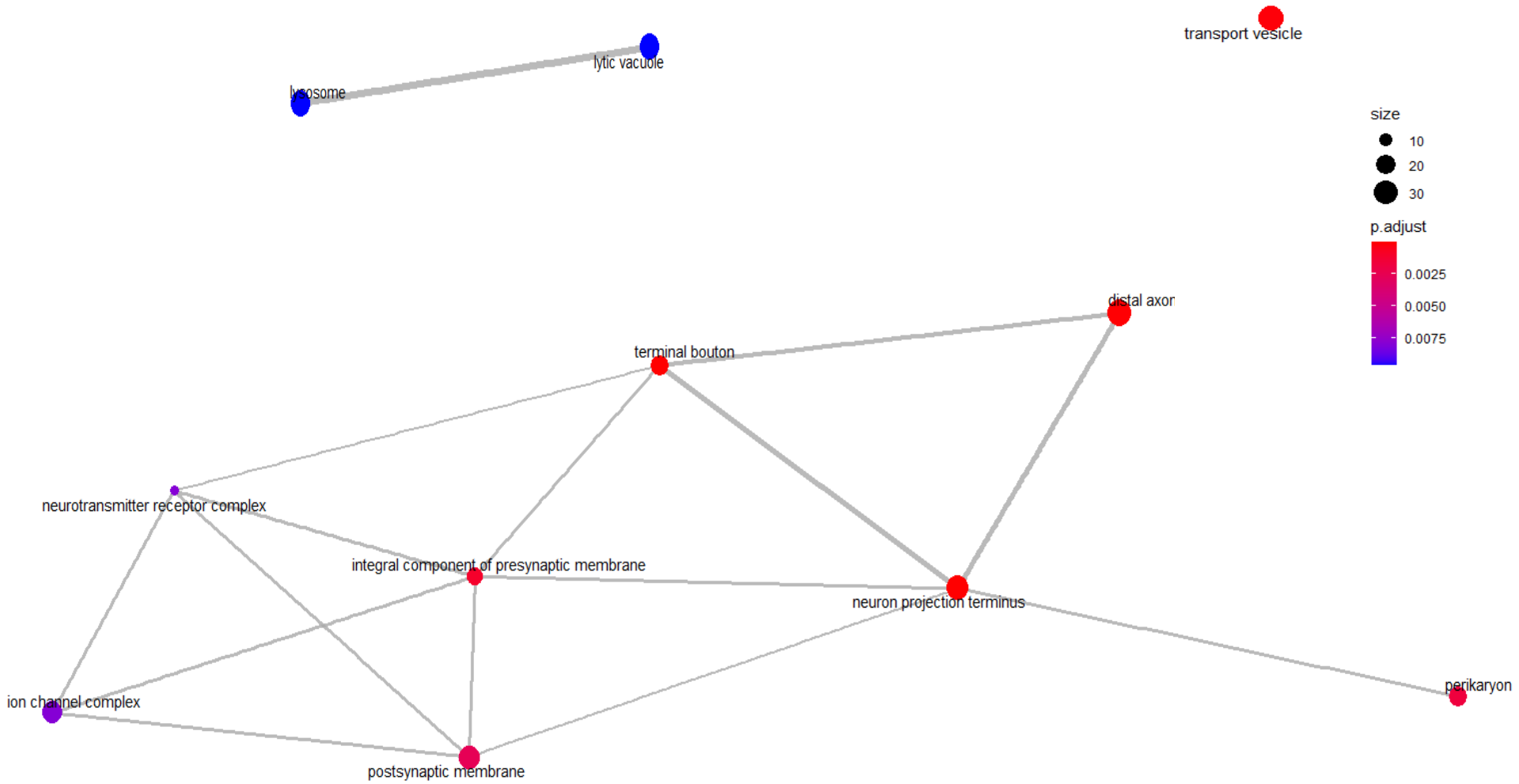



***Figure 3.22 Significantly overrepresented "cell component" gene ontology groups in SHR tissue*** *Gene ontology over-representation analysis highlighted multiple "Cell-component" gene ontology terms with a larger than expected number of dysregulated genes. Here the colour of each dot is scaled by the adjusted p value for the over-representation of each gene ontology group. The dot sizes indicate the number of differentially expressed genes per gene ontology group. Edges between dots indicate shared differentially expressed genes between gene ontology groups. The thickness of these lines is scaled by the number of shared differentially expressed genes.*

## 3.4 Discussion

This chapter provides a broad overview of a scRNAseq dataset which is heavily referenced in subsequent functional chapters. These data represent the first scRNAseq study of the Wistar and SHR stellate ganglia as well as the first scRNAseq study of the isolated stellate ganglia. These data provide evidence for significant cellular heterogeneity within the stellate ganglia, indicating multiple cell populations which have previously been largely ignored. Further, these data highlighted that two sympathetic subpopulations are present in the stellate ganglia, with a large number of transcriptional differences between them. The scRNAseq study provided an insight into transcriptional changes in the stellate ganglia at the critical time points of prehypertension. Several similar changes were observed in a bulk RNA-sequencing dataset of the 16-week SHR. However, these datasets differed when directly compared. Together these data provide a framework for future study on both SGNs and other populations in the stellate ganglia.

### 3.4.1 The heterogeneity of the stellate ganglia

The stellate ganglia appear to be a very heterogenous tissue (**Figure 3.6**), with many prominent non-neuronal cell populations. Whilst undocumented, this is not controversial, given that throughout the central and peripheral nervous system, neurons are supported by a range of other cell types. Vascular smooth muscle cell populations and vascular endothelial cell populations were expected given that sympathetic ganglia are vascularised tissues (Chungcharoen *et al.*, 1952) and as such would be expected to host a complement of associated cell types. Similarly glia cells have been reported in the SCG (Hanani, 2010), although the size and

heterogeneity of the population was surprising (**Figure 3.6**). In terms of immune cell populations, macrophages have been reported in the SCG (Pirzgalska *et al.*, 2017), and as the animals used in these experiments were not perfused prior to stellate ganglia dissection, circulating immune cells are also likely to be present. Fibroblasts have been visually identified in sympathetic cultures and fibronectin, a product of fibroblasts, has been immunohistochemically confirmed in SCG culture (Roufa *et al.*, 1986).

Furlan et al. (2016), report only neuronal clusters by their own scRNAseq study. These authors dissociate both the stellate ganglia and a large proportion of the thoracic sympathetic chain (T1-T12) but excluded contaminating populations during analysis. It is therefore not possible to comment on non-neuronal cell identities from this dataset.

In addition, these data highlight that glia, not neurons, represent the largest population in the stellate ganglia by this methodology (**Figure 3.6**), which since has been reported in the mouse stellate ganglia (van Weperen *et al.*, 2020). However, this may result from the dissociation protocol and not be a true reflection of the proportions found physiologically. Whilst these data would need to be confirmed *in situ,* they at least suggest that glia may represent a larger population than previously expected.

The presence of other cell types is often ignored when assessing sympathetic function and pathology. Historically, molecular biology studies of sympathetic ganglia neurons have been performed on whole tissue RNA samples or homogenates, with the assumption that neurons were the predominant population. This is reflected in our adoption of bulk RNA-sequencing. These data

could have wider implications into how sympathetic research is conducted. It would be interesting to follow up the relationships between these intra-ganglia populations and observe whether any of these cell types play a role in neuronal function or pathology.

### 3.4.2 Two populations of sympathetic neurons?

Two primary populations of sympathetic neurons were identified (**Figures 3.5-3.7**), with 285 differentially expressed genes between them (**Table 3.1**). The presence of NPY positive and negative sympathetic neuron populations (**Figure 3.9-3.10**) has previously been described but this has so far only been correlated with axonal conduction velocity and *in situ* neuronal morphology (Li & Horn, 2006). A prior study succeeded in isolating NPY positive cells from the SCG using a NPY reporter line, but failed to capitalise upon this advance through an effective transcriptomic or functional follow-up (Sikora *et al.*, 2017).

NPY release from sympathetic ganglia requires high frequency and prolonged stimulation relative to noradrenaline (Lundberg *et al.*, 1989). This has led authors to suggest that NPY sympathetic neurons in SCG represent a “high-threshold” population, with differing electrophysiological properties than NPY negative neurons. This theory is derived from intracellular and extracellular recording based descriptions of NPY positive and negative SCG neurons (Li & Horn, 2006, 2008). By comparing NPY positive and NPY negative populations, the authors report altered postganglionic neuron afterhyperpolarisation half-width, and a higher threshold response to presynaptic neuron stimulation as measured by extracellular recordings (Li & Horn, 2008). They reported no differences in input

resistance, action potential width, afterhyperpolarisation amplitude or RMP. In support of these data no change in the expression of ion channel α subunits was observed between the two neuronal populations (**Figure 3.9C**), despite a remarkable 285 other differentially expressed genes between these populations.

A difference in threshold could also arise from differences in firing rate, however, firing rate was not measured in these previous studies (Li & Horn, 2006, 2008). Differences in M-current (Wang & McKinnon, 1995; Luther & Birren, 2009) and $Na_V$ current (Luther & Birren, 2009) have previously been reported between SCG neurons with different firing properties. However, given that there was no difference in voltage-gated channel α subunit expression between these populations (**Figure 3.9C**), it is unlikely these changes correlate with *NPY* expression. Prior reports in other neuronal populations suggest that electrophysiological differences often arrive through stochastic differences in channel expression amongst populations of neurons (Schulz *et al.*, 2006; Scala *et al.*, 2020), rather than strictly defined groups. It seems likely that this explains a large part of the divergent firing properties in sympathetic neurons (Wang & McKinnon, 1995), rather than expression differences between two populations.

Instead, the change in the BK channel beta subunit, *KCNBM4*, reported in **Table 3.4**, might confer subtle changes in electrophysiological properties. This change might explain the variation in afterhyperpolarisation half-width observed in SCG neurons (Li & Horn, 2008). In support of this hypothesis, in hippocampal dentate granule neurons knockout of *KCNBM4* was associated with an increase in neuronal excitability and an altered afterhyperpolarisation (Brenner *et al.*, 2005).

However, alongside altered expression of *KCNMB4*, this analysis provides several alternative explanations for differences in NPY release. For example, the two neuronal populations differentially express 3 synaptotagmin isoforms, *SYT2*, *SYT4* and *SYT5*, alongside Synapsin 2 (SYN2). Notably, NPY is released from dense core vesicles rather than synaptic vesicles (Walch-Solimena *et al.*, 1993), which may explain these differences. From prior functional studies (Li & Horn, 2006, 2008), and the data presented here it is not possible to conclude what confers a higher threshold to NPY release. Further work is required to resolve whether the molecular mechanism behind the high threshold for NPY release is linked to synaptic release machinery, *KCNBM4* or an alternate mechanism.

There are further interesting differences between these populations, *NPY* positive neurons also have a high expression of *ADRB2*, *CHRM2*, *MAOA*, *HTRA1*, *DRD2* and *SLC6A4*, whilst *NPY* negative neurons have a higher expression of *ADRA2A* and *TH*. This could have wider implications for our understanding of sympathetic neuron function. For example, Muscarinic $M_2$ receptors (*CHRM2*) have been previously reported in SGNs (Yang *et al.*, 2006), and are known to mediate inhibition of the SNS following activation of the parasympathetic nervous. Therefore, if they are only present in *NPY* positive neurons, or expressed to a greater degree in *NPY* positive neurons, does this mean that only these neurons are inhibited by the PNS? And if so, does this preferentially inhibit NPY release? In addition, differential expression of excitatory β-receptors (*ADRB2*) or inhibitory (*ADRA2A*) receptors could indicate differing roles of presynaptic control by noradrenaline between these two populations. This hypothesis is supported by a prior study, which suggests that noradrenaline has an inhibitory effect upon the electrophysiological properties of NPY-negative, but not NPY-positive SCG neurons (Li & Horn, 2008).

The preferential expression of *DRD2* and *HTRA1*, also suggests that *NPY* positive neurons may be modulated by dopamine and serotonin in a way that *NPY* negative neurons are not. Finally, *NPY* positive neurons exhibit lower expression of *TH,* which encodes the rate limiting enzyme for noradrenaline synthesis (Kobayashi & Nagatsu, 2012), tyrosine hydroxylase, but exhibits higher expression of noradrenaline degrading enzyme *MAOA* and noradrenaline reuptake enzyme *SLC6A4*. Could these data indicate that *NPY* positive neurons are less catecholaminergic, or that noradrenaline release from these neurons is better regulated? These questions are all exciting proposals that require further functional investigation.

Finally, Furlan et al. (2016) report five separate sympathetic neuron clusters in their study of the combined stellate and thoracic ganglia, in contradiction with the two reported here (**Figure 3.9-3.10**). For the clusters reported by these authors, two populations were *NPY* positive, and three *NPY* negative. This study was pioneering in its early adoption of single-cell RNA sequencing but suffers from several limitations. Firstly, by combining a large section of the sympathetic chain (T1-T12) with the stellate ganglia, it is possible that these populations arose due to variation between sympathetic ganglia, which has previously been described in functional studies (Wang & McKinnon, 1995; Jobling & Gibbins, 1999; Shanks *et al.*, 2013). Sympathetic ganglia from male and female mice were combined for this study, which may introduce further variation due to established gender differences in sympathetic function (Bayles *et al.*, 2019) and transcript expression (Bayles *et al.*, 2018). In addition, whilst NPY positive and NPY groups are clearly separated in their analyses, the five putative sympathetic identities show minimal separation between clusters. Finally, a number of the neuronal groups reported appear to contain very

few cells, and it is therefore difficult to draw a definitive conclusion on their identity.

### 3.4.3 The diseased stellate ganglia neuron

In line with previous functional reports from SGNs and other sympathetic neuron populations (Li *et al.*, 2012; Shanks *et al.*, 2013; Larsen *et al.*, 2016*a*; Bardsley *et al.*, 2018*b*) this scRNAseq study reports that many (474) genes are differentially expressed in the SHR SGN. Sympathetic neurons had the largest number of differentially expressed genes, which reaffirms the contemporary assumption that a significant proportion of SHR sympathetic nerve dysfunction occurs at the level of the sympathetic neuron. This is reinforced by a widespan of published literature, which suggest multiple impairments of SHR sympathetic neuronal function (Yarowsky & Weinreich, 1985; Robertson & Schofield, 1999; Li *et al.*, 2012; Shanks *et al.*, 2013; Larsen *et al.*, 2016*b*; Bardsley *et al.*, 2018*b*).

Several physiologically interesting targets will be briefly discussed here. Two differentially expressed genes, *CLIC3* and *SLC12A3*, point to a dysregulation in intracellular $Cl^-$ homeostasis (**Table 3.3).** *SLC12A3* encodes for the sodium-chloride transporter (NCC) and is typically associated with renal ion transport (Gamba, 2012). Mutations in *SLC12A3* have previously associated with hypertension (Ji *et al.*, 2008), but have been associated with renal function. The role of *SLC12A3* is currently unknown in sympathetic neurons. *CLIC3* encodes the nuclear $Cl^-$ channel chloride intracellular channel protein 3 (Qian *et al.*, 1999). As NET is also Na and $Cl^-$ dependent (De Felice, 2016), changes in intracellular [$Cl^-$] could have implications for noradrenaline reuptake.

*DDC* and *DBH* expression decreased in the SHR neuron population (**Table 3.3**), which may initially appear contradictory with the increased plasma noradrenaline observed in prehypertensive patients (Dominiak & Grobecker, 1982). However, as part of a previous study we demonstrated that whilst total catecholamine content was decreased in SHR stellate ganglia lysates, catecholamine release was increased (Bardsley *et al.*, 2018*b*).

*VAMP1*, *VAMP2* and *SNAP25* (**Table 3.3; Figure 3.17**) are all upregulated in SHR SGNs. As these genes are associated with proteins facilitating neurotransmitter vesicular release (Rizo & Xu, 2015), their upregulation may have important implications for noradrenaline release from sympathetic neurons in the SHR. It is possible that this could contribute to the increased noradrenaline release observed in this disease model (Bardsley *et al.*, 2018*b*).

Numerous mitochondrial genes were dysregulated in the SHR SGN population (**Figure 3.16**), which fits with prior reports of mitochondrial dysfunction in other tissues in the SHR (De Cavanagh *et al.*, 2006; Smith *et al.*, 2013; Collett *et al.*, 2013; Silva *et al.*, 2019). Further, *GSTA4*, which encodes the antioxidant enzyme glutathione S-Transferase alpha 4, was upregulated in the SHR by both bulk RNA-sequencing (**Table 3.6**) and scRNAseq (**Table 3.3**). Together, these results suggest that there may be a metabolic element to SHR SGN dysfunction.

### 3.4.4 Comparison with Bulk RNA-sequencing

Inconsistencies between the bulk and scRNAseq datasets (**Figure 3.19-3.20**) in this chapter could have arisen for a number of reasons including; technical differences between these methodologies, age-related differences between the

samples and the inherent difference between the RNA complement of a whole ganglia containing multiple cell types and a dissociated clusters of cells.

Additionally, it is currently unknown whether the sizes of the cell populations in the stellate ganglia are constant between the Wistar and SHR. Given that there are multiple development differences between the SHR and Wistar strains (Gattone, 1986), this consistency cannot be assumed. Any changes in cell population abundances could confound the bulk RNA-sequencing dataset but have a limited effect upon the scRNAseq datasets.

Despite the inconsistencies it was reassuring to observe that at least some of the changes observed in the 5-week SHR SGNs are conserved in 16-week animals and were detected by the bulk RNA-sequencing analysis (**Figure 3.19-3.20**). Additionally, these data suggest that at least some changes in neuronal expression are detectable through techniques using whole tissue lysates. Further, there is an observable trend between the level of expression in Wistar stellate ganglia and Wistar SGNs (**Figure 3.20C**).

Further analysis could build upon the pseudo-bulk analysis performed here (**Figure 3.20**), however, this analysis will always be limited by the technical differences and age-related differences between these datasets. For this reason, a conservative approach was taken here.

For balance, it is worth acknowledging that bulk RNA-sequencing detected 691 changes that were not observed by scRNAseq (**Figure 3.19**). An advantage of bulk RNA-sequencing is that the larger volume from a lysed sample permits deeper sequencing than is achieved for each individual cell in scRNAseq. This could explain the discrepancy, as previously reported for other tissues (Hoffman *et al.*,

2020). It is therefore difficult to work with the differentially expressed genes in this dataset, especially as neurons may not be the predominant cell type.

Gene ontology analysis, which is more tolerant to variance amongst gene to gene-level expression changes given its grouping of genes into biological themes, appeared to provide a more robust comparison between these datasets. For example, when compared via “cell component” gene ontology groups, both methodologies report changes in terms associated with “ligand-gated ion channels”, and “neuronal projection“ (**Figure 3.16**; **Figure 3.22**). However, a striking difference observed by gene ontology analysis was the over-representation of a cluster of mitochondria-associated “cell component” gene ontology groups in the scRNAseq dataset (**Figure 3.16**), which were not observed by bulk RNA-sequencing (**Figure 3.22**).

The differentially expressed mitochondria associated genes from the scRNAseq dataset are mostly restricted to the neuronal clusters (Data not shown). Therefore, the bulk RNA-sequencing may not have detected these changes due to the contamination of the total RNA sample by other stellate ganglia cell populations (**Figure 3.6**). Alternatively, these changes may reflect the difference in age between the samples used for bulk RNA-sequencing (16 weeks) and scRNAseq (5-6 weeks).

In addition, many differentially expressed mitochondria-related genes were not reported in the Wistar or SHR bulk RNA-sequencing datasets (Appendix table 6), which may have limited the discovery of mitochondrial dysfunction in the bulk RNA-sequencing set. This may arise from misalignment. Briefly, RNA molecules are fragmented during the sequencing process, and only short lengths of RNA are sequenced. When multiple genes with similar DNA sequences are present, these

RNA fragments can be misattributed to a similar gene sequence, an error known as misalignment (Conesa *et al.*, 2016). *Salmon* typically attributes reads which can map to multiple sites within the transcriptome to a gene with higher read counts, thereby limiting read misalignment to inappropriate targets which are not expressed in the tissue sample (Patro *et al.*, 2017). This is a common issue during RNA-sequencing alignment (Conesa *et al.*, 2016; Raplee *et al.*, 2019).

Finally, scRNAseq involves cell dissociation, and any resulting broken cells may over express both mitochondrial encoded transcripts, and transcripts associated with mitochondrial function, apoptosis or membrane scaffolding (Ilicic *et al.*, 2016). If either Wistar or SHR SGNs contained a larger proportion of broken cells, then this may cause a change in these groups of genes. These analyses reported differential expression of only one mitochondria associated transcript *MT-ND3* (**Table 3.3**) of the 37 known mitochondria encoded genes (Taanman, 1999), whereas previous work suggests that multiple mitochondria encoded genes are upregulated in broken cells (Ilicic *et al.*, 2016). Further, the transcriptome was used to quasi-map the bulk RNA-sequencing reads (Patro *et al.*, 2017) and genes encoded by mitochondrial DNA were excluded and would not be detected in the bulk RNA-sequencing dataset (Appendix table 6).

Over-represented ontology groups related to both membranes and mitochondria are reported in this scRNAseq dataset (**Figure 3.16**), however, these changes are restricted to discrete functional processes. For example, over-represented mitochondria related ontology groups and their associated differentially expressed genes are almost all related to ATP synthesis (**Figure 3.16**; Individual genes not shown) and differentially expressed membrane proteins were generally associated with ligand gated ion channels (**Figures 3.16-3.17**). In this manner these

data do not reflect generalised changes as reported in broken cells (Ilicic *et al.*, 2016). Further, apoptosis associated gene ontology groups were not over-represented. From a technical standpoint, mean counts per cell (Δ6k), and sequencing depth, (Δ3%) also did not differ massively between samples suggesting a similar sample quality. In addition, tissue from both strains simultaneously underwent the same dissociation protocol and so neither sample is likely to contain more broken cells.

Overall, there is a large disparity between the bulk and scRNAseq datasets. Given the advantages of focussing upon a dissociated neuronal population, the scRNAseq dataset was taken forward as the primary method for studying gene expression changes. The use of scRNAseq also reflects an acknowledgement that the tissue and neurons themselves might express heterogeneity, as confirmed in this chapter.

### 3.4.5 Limitations

Whilst a powerful technique, scRNAseq has several key restrictions. First, the low quantity of RNA per cell leads to variable data with a large amount of technical noise. Further, this relatively low RNA quantity can also lead to dropouts, where a gene is detected in one or several cells within a cluster due to low expression levels. To a certain extent, these limitations can be resolved by obtaining a high sequencing depth as was achieved here, but this has a significant financial cost and will not completely resolve the issue. Computational methods also act to counteract the issues of low RNA yield. For example, highly variable genes are selected, and dimensionality reduction is employed for this purpose (Brennecke *et*

*al.*, 2013). This approach has proven to be remarkably effective, but by preselecting genes for clustering, the user is excluding genes with low expression from the clustering process. Finally, it isn't possible to prove an absence of gene expression via scRNAseq due to the low mRNA content of individual cells (Kim *et al.*, 2020). However, the dataset presented here appears to have detected many physiologically expected genes and will likely have detected the majority of medium-highly expressed genes.

ScRNAseq is reliant upon cell dissociation, so we cannot infer relative population sizes from these data. For example, whilst the glial population was large, it may be that glia preferentially survived the process of dissociation. Equally, it is difficult to exclude smaller populations from the stellate ganglia which may not have survived dissociation. This limitation of course applies to all methodologies downstream of dissociation and so confirmation of relative population sizes would have to be performed *in situ*.

ScRNAseq and bulk RNA-sequencing are, like all transcriptomic techniques, limited in that they focus upon transcript and not protein expression, and therefore may not represent protein levels in the cell or lysate of interest. In addition, proteins are typically extensively trafficked, phosphorylated and otherwise modified (Dalbey & von Heijne, 2002) and so expression levels may not represent function. Finally, these techniques capture a snapshot of the transcriptome, which may be constantly in flux. Trajectory analysis attempts to provide relationships between cell populations in "pseudo-time" (Reid & Wernisch, 2016), but this is of course suboptimal.

Like many computational methods, trajectory inference analysis can produce data without biological relevance. It should therefore only be used if there is a suspected developmental pathway, or clusters representing intermediate states. When employed here, there were suspected intermediate clusters (Neuronal clusters 3 and 5). Finally, *slingshot* cannot detect cyclic trajectories between clusters, due to its adoption of a minimum scanning tree methodology (Saelens *et al.*, 2019), however, a cyclic relationship (as with the cell-cycle) was not suspected for either of the datasets analysed here.

### 3.4.6 Future work

This study used stellate ganglia from the left and right side of the rat and restricted analysis to male rodents. As left and right ganglia appear to innervate different areas of the heart, and as there appears to be a gender divide in sympathetic function (Bayles *et al.*, 2018), it would have been interesting to separate analysis and comparison of left-right and male-female differences in SGN expression. Finally, it would be interesting to compare expression differences of SGNs in the SHR with other hypertensive models, and ideally with human SGNs.

The stellate ganglia innervates multiple tissues beyond the heart (Bankenahally & Krovvidi, 2016), and so it would have been useful to separate cardiac and non-cardiac neurons to be sequenced and compared. However, to achieve this, one must either use retrograde labelling of cardiac innervating neurons and cell sorting to separate these neurons, or visually identify the area of the stellate ganglia which predominantly innervates the heart. Both methodologies suffer from a similar limitation, that it is extremely unlikely to achieve a pure non-cardiac

population. For the labelling strategy it is not possible to achieve complete retrograde labelling and for physical isolation of the cardiac neurons, whilst this area has been identified (Mo *et al.*, 1994; Rajendran *et al.*, 2019) it is not trivial to dissect this region in isolation, and even harder to prove specificity.

Finally, it was originally my intention to use fluorescence-activated cell sorting to isolate $Ca_v2.2$ positive neurons from Wistar and SHR stellate ganglia and, in collaboration with Novo Nordisk, run scRNAseq and RT-qPCR on this purified neuronal population. This would allow for the sequencing of a much larger neuronal population than that achieved here, due to non-neuronal cells using a large proportion of the maximum cell count. Regrettably, COVID lock-down prevented these data from being collected. This would still serve as an interesting future experiment, to confirm and further investigate the different neuronal subpopulations.

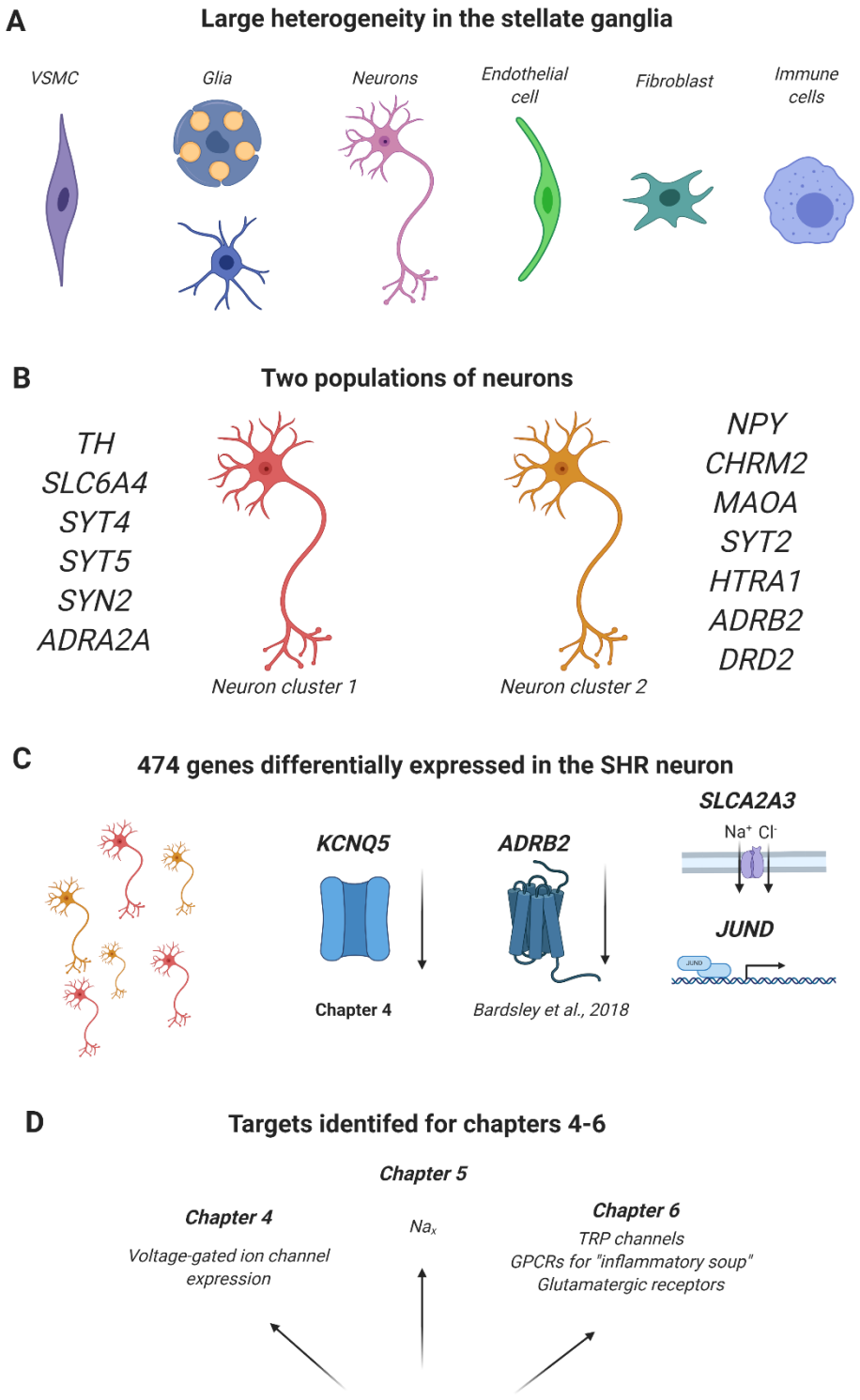



***Figure 3.23 Graphical summary of chapter 3*** *(A) Single-cell RNA-sequencing highlighted significant cellular heterogeneity in the dissociated stellate ganglia. (B) Two primary populations of sympathetic neurons were identified, termed neuron cluster 1 and 2 here. These populations differed by the expression of 285 genes a select few of which are shown here. The genes shown on the left are significantly higher in neuronal cluster 1 and on the right are significantly higher in neuronal cluster 2. (C) 474 genes were differentially expressed between Wistar and SHR stellate ganglia neurons. Four of which are shown here. (D) Wistar data from this dataset was used to aid in functional studies in the subsequent chapters 4-6.*

# Chapter 4

## The role of M-current in the SHR phenotype

## 4.1 Introduction

Aberrant SNA is a known hallmark of many cardiovascular diseases including hypertension (Herring *et al.*, 2019; Guyenet *et al.*, 2020). During the development and maintenance of hypertension, pathological sympathetic activity contributes to raised arterial blood pressure (Guyenet, 2006) and commonly associated co-morbidities (Herring *et al.*, 2019). These co-morbidities are often serious, including cardiovascular pathologies such as left ventricular hypertrophy (Schlaich *et al.*, 2004), heart failure (Zhang & Anderson, 2014) and arrhythmia (Meng *et al.*, 2017). However, despite the large body of work supporting the importance of this phenotype in this disease, the underlying cause of elevated SNA is still unknown.

In human hypertension, SNA increases at both a single-unit and multi-unit level (Grassi *et al.*, 1998; Greenwood *et al.*, 1999), implying that dysfunction may occur at the level of individual sympathetic neurons. Unfortunately, the ability to study this phenotype in human hypertensive tissue is limited, and we are instead reliant upon animal models of hypertension. The SHR model of hypertension, replicates the phenotype of sympathetic hyperactivity *in vivo* (Thoren & Ricksten, 1979), and replicates co-morbidities found in human's with hypertension, including hypertrophy (Li *et al.*, 2019), heart failure (Itter *et al.*, 2004) and arrhythmia (Lau *et al.*, 2013; Nguyen *et al.*, 2016).

Prior studies utilising intracellular recordings of SHR SCG neurons have highlighted increased neuronal excitability at a cellular level (Yarowsky & Weinreich, 1985; Jubelin & Kannan, 1990). However, these studies failed to uncover a convincing molecular mechanism for this phenotype and did not provide methods of modulating or ablating this activity. Further, the SCG provides only a small

proportion of the cardiac sympathetic innervation. It otherwise innervates tissues in the head and neck (Bankenahally & Krovvidi, 2016) which are not believed to be directly implicated in either the pathology of hypertension or resulting pathologies. This is especially important, given that previous work suggests that sympathetic ganglia differ significantly in their functional and electrophysiological profiles (Wang & McKinnon, 1995; Jobling & Gibbins, 1999).

The majority of cardiac sympathetic innervation originates from the stellate ganglia, a poorly studied ganglia, whose electrical phenotype has not been well characterised in hypertension. A disease phenotype has already been observed in rodent SGNs in the form of elevated somatic $Ca^{2+}$ signalling (Li *et al.*, 2012; Larsen *et al.*, 2016), decreased noradrenaline transport (Shanks *et al.*, 2013) and dysregulated cyclic nucleotide homeostasis (Li & Paterson, 2016). Whilst these phenotypes are likely to contribute to the elevated noradrenaline spill-over observed in hypertension (Manolis *et al.*, 2014), these do not explain the elevated cardiac SNA observed in both patients and animal models.

Whilst this study was guided and supported by the scRNAseq dataset provided in chapter 3, there were multiple *a priori* ion channel targets that are known to have a strong role in the control of neuronal firing in sympathetic and other neuron populations. Several ion channels have been implicated, but not proven, to cause SCG neuron hyperactivity in hypertension. Previous studies have primarily suggested a role for SK channels (Jubelin & Kannan, 1990) and A-type potassium current (Robertson & Schofield, 1999).

Alongside these *a priori* targets other ion channels have been implicated in SCG sympathetic neuron firing and will also be studied here. These include CaCC

(Martínez-Pinna *et al.*, 2002) and $Na_v$ channels (Luther & Birren, 2009). In addition T-type $Ca_v$ (Dolphin, 2016), HCN channels (Shah, 2014) and $K_{Na}$ (Kaczmarek, 2013) channels have a demonstrated role in regulating neuronal firing in non-sympathetic neuronal populations and will also be covered within this chapter.

This chapter aims to dissect the electrical phenotype of SGNs in health and hypertension. In addition, this chapter provides molecular and functional evidence for the mechanism of electrophysiological dysfunction in SHR SGNs. Finally, data here suggests alternate pharmacological targets to reduce the aberrant activity observed in sympathetic neurons during hypertension. These data also provide important functional validation of the single-cell sequencing dataset described in chapter 3.

## 4.2 Methods

### 4.2.1 Patch clamp electrophysiology

Patch-clamp recordings were performed by amphotericin perforated patch (0.48 mg/ml) (Rae *et al.*, 1991), except for $Li^+$ substitution experiments listed in **Table 4.3** which were performed by whole-cell recordings. Unless stated otherwise, patch-clamp recordings used the previously outlined extracellular Tyrode's solution (Chapter 2). Internal solutions and more detailed methods are provided in chapter 2. For $Ca^{2+}$ free experiments (**Table 4.3**), $CaCl_2$ was omitted from the external solution and EGTA was added to chelate any remaining $Ca^{2+}$. For $Li^+$ substitution experiments, 140mM LiCl was substituted for NaCl to block $K_{Na}$. In these experiments external pH was adjusted by LiOH rather than NaOH. Liquid junction potentials were corrected based upon an estimation of 24.3 mV by JPCalc (Barry,

1994) in Clampex (v11.0.3) (Molecular Devices, US), which was subtracted from the recorded membrane potential. M-current deactivation was recorded by a similar to that protocol described in Linley *et al.*, (2008). With the exception of LiCl and XE-991, which were perfused for 10 minutes, all remaining drugs were perfused for 5 minutes at 4-6ml/min.

### 4.2.2 Single-cell and bulk RNA-sequencing

Single-cell and bulk RNA-sequencing utilised the pre-existing dataset and analysis described in chapter 3.

### 4.2.3 Immunohistochemistry

The following methods are adapted from a previous publication where these data are published (Davis *et al.*, 2020). Stellate ganglia were dissected, and immediately transferred to 4% paraformaldehyde for a period of one to two hours. The tissue was then incubated in 20% sucrose-PBS overnight at 4 $^{o}$C. Subsequently, tissue was embedded in OCT compound (TissueTek, US). Embedded tissue was frozen and stored at -80 $^{o}$C for < two weeks. The frozen tissue was then cryosectioned in 12 µm sections. These 12 µm tissue sections were then permeabilized in 0.3% triton-X for 30 minutes at room temperature. Following permeabilization, the sections were then incubated in PBS based blocking buffer (1% BSA, 5% donkey serum) for 2 hours. Tissue sections were then incubated with primary antibodies for 24 hours at 4 $^{o}$C, followed by five repeated five-minute washes in PBS and a further two hours incubation with secondary antibodies. Primary antibodies used were as follows: mouse TH (66334-1-Ig) (ProteinTech, US), rabbit KCNQ2 (ab22897)

(Abcam, UK), rabbit KCNQ3 (ab66640) (Abcam, UK) or rabbit KCNQ5 (ab66740) (Abcam, UK). For secondary antibodies, 1:200 Donkey anti-mouse Alexa Fluor 555 (A-31570) and 1:200 Donkey anti-rabbit AlexaFluor 488 (A32790) were used (Invitrogen, US). Cells were nuclear stained with DAPI (ab228549) (Abcam, UK). Finally, sections were imaged on a Zeiss LSM 880 Airy Scan Upright laser-scanning confocal microscope with a Plan-Apochromat 20x/0.8 M27 objective.

### 4.2.4 Human tissue

The following statement is adapted from the published manuscript associated with this paper (Davis *et al.*, 2020). Stellate ganglia were collected from patient organ donors at the time of organ procurement as approved by the University of California Los Angeles institutional review board: 12-000701. Written informed consent was provided by the patient or appropriate designee. This study complies with the Declaration of Helsinki.

Patients represent a mixed cohort, with tissue obtained from organ donors as well as patients undergoing stellectomy for sympathetic dysfunction. These samples were used as part of a larger study (Liu *et al.*, 2018). The clinical characteristics of the patients/donors were: Sample ID 19, Male, 77 years old, 30-35% left ventricular ejection fraction, non-ischemic cardiomyopathy and ventricular fibrillation; Sample ID 20, Female, 61 years old, Hypertension and hypothyroidism; Sample ID 23, Male, 19 years old, left ventricular ejection fraction 55-60%, normal cardiac function; Sample ID 24, Male, 62 years old, left ventricular ejection fraction 50%, polymorphic ventricular tachycardia.

### 4.2.5 RT-qPCR

The following primer sets were used: KCNQ2 (Rn00591249_m1), KCNQ3 (Rn00580995_m1), KCNQ5 (Rn01512013_m1) and normalised to GAPDH (Rn01775763_g1) or B2M (Rn00560865_m1). Changes in expression were measured by the ΔΔCT method (Livak & Schmittgen, 2001).

### 4.2.6 Statistics

For the comparison of the qualitative data in **Figure 4.2** a Pearson's $\chi^2$ test was performed in R. However, for further comparisons of phenotypes trends were underpowered, and are instead shown as case studies due to low n for qualitative statistics. For quantitative data, firing rate and rheobase were treated as non-parametric. Other variables were tested for normality as described in chapter 2.

## 4.3 Results

### 4.3.1 SHR stellate ganglia neuron phenotype

It was first prudent to investigated whether SGNs cultured from prehypertensive SHR displayed increased neuronal excitability. This was achieved via perforated patch-clamp recordings from the somata of age-matched Wistar and SHR neurons, between one and five days in vitro. SHR neurons had an increased median firing rate, over the tested stimulation range of 0-200 pA 1 second current injections, and stimulated neuronal firing was less time-resolved in SHR neurons

than in Wistar neurons (**Figure 4.1**). These quantitative data were reinforced by a qualitative description of the firing rate phenotypes in these neurons (**Figure 4.2**).

Meanwhile, SHR neuronal membrane potentials were significantly depolarised in SHR neurons, -64.97±0.78 mV, relative to Wistar neurons, -68.04±0.81 mV, and had a significantly decreased rheobase (Median; Wistar, 50 pA; SHR, 30 pA), and a trend towards increased input resistance Wistar 218.2 MΩ, SHR 251.2 MΩ (**Figure 4.3**).

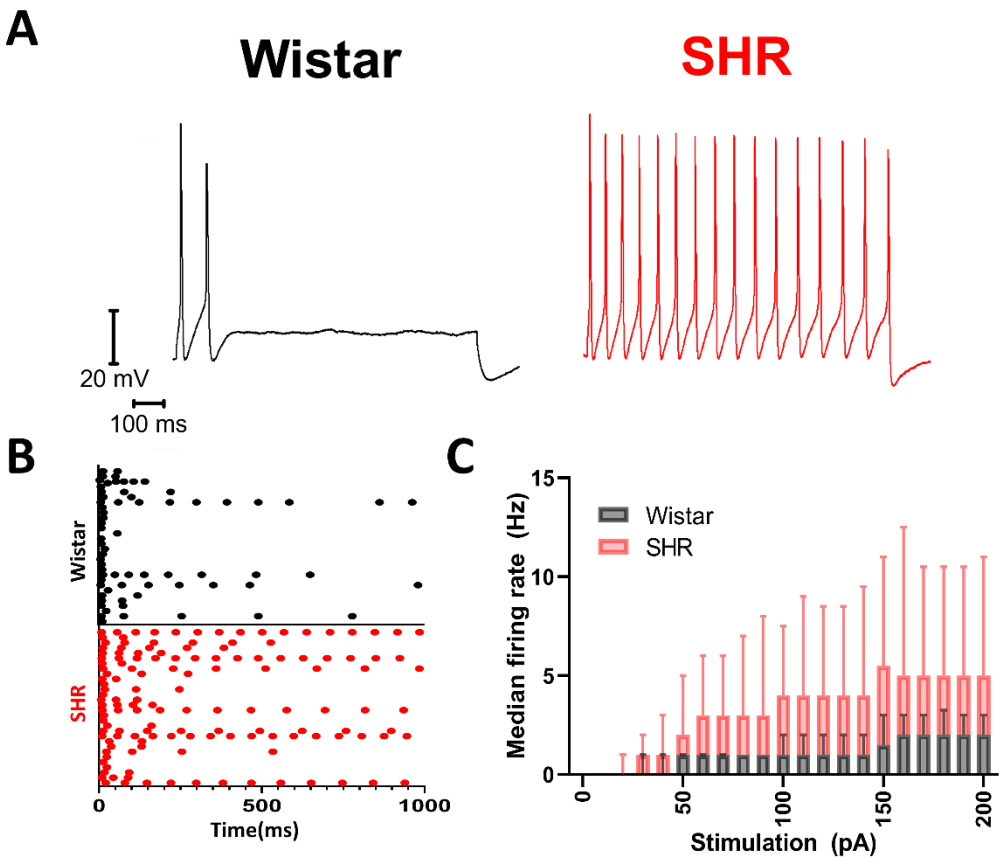



***Figure 4.1 Perforated patch-clamp revealed increased electrical activity in prehypertensive stellate ganglia sympathetic neurons*** *Current clamp recordings highlighted increased firing in response to 1 second current injections betweenthe range 10-200 pA in sympathetic stellate ganglia neurons of the SHR. These data are shown as (A) raw example traces following a 150 pA current injection, (B)raster plots revealing the patterns of neuronal firing in either strain (Wistar, n=30; SHR, n=30), and (C) frequency input-relationships (Wistar, n=66; SHR, n=70) (Median±IQR). When assessed as a frequency-input relationship, SHR neurons were found to be more excitable. Here n refers to cell number, where a minimum culture n of 4 was used, with each culture using a minimum of 2 animals.*

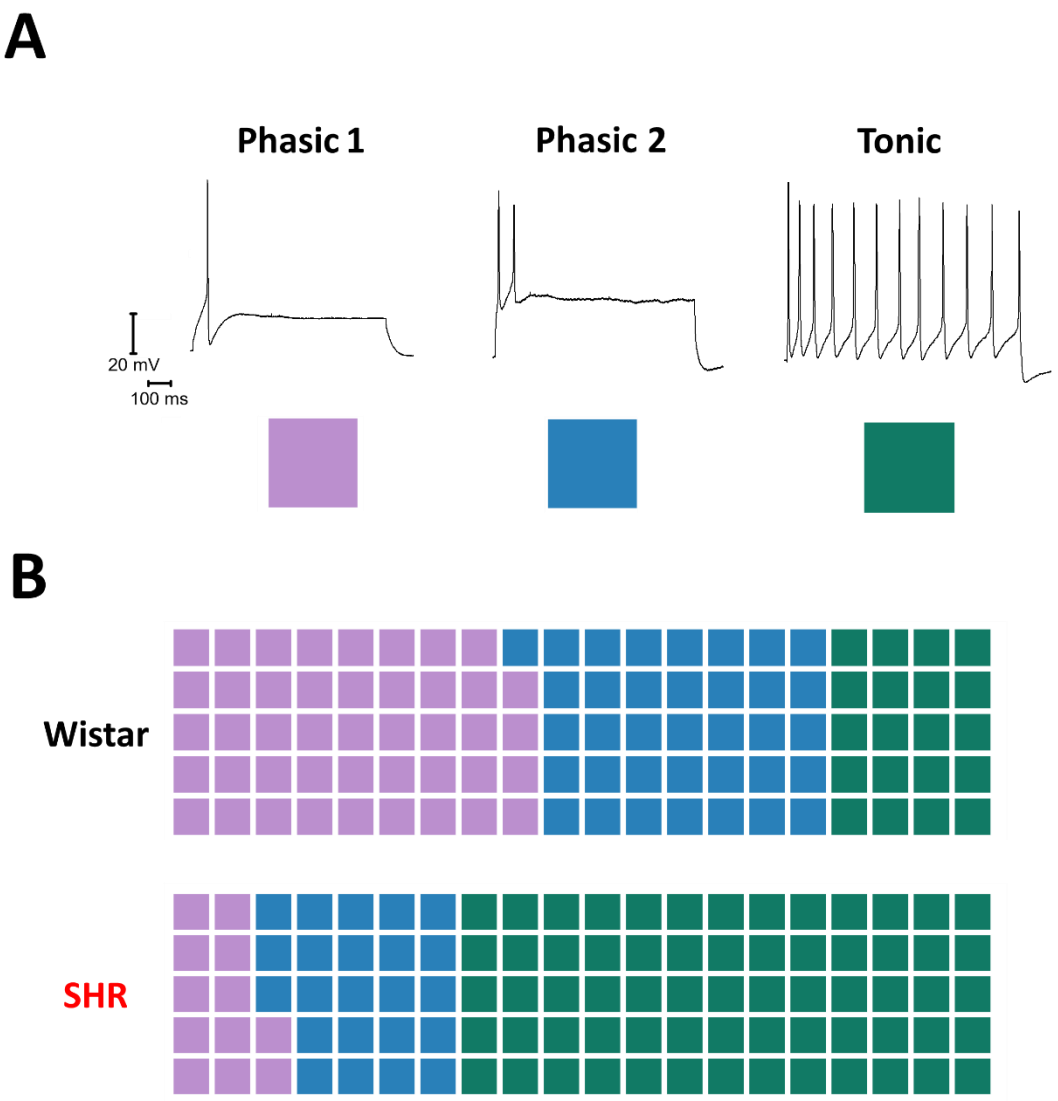



***Figure 4.2 The SHR phenotype has a higher proportion of tonic firing neurons than in wistar*** *(A)The schema for the phasic 1, phasic 2 and tonic firing types; phasic 1 represent single firing neurons, phasic 2 neurons fire up to 5 times in a manner restricted to the first 500 ms, and tonic neurons that fire continuously over the 1000 ms recoridng, or <5 times. (B) The proportion of phasic 1, phasic 2 and tonic neurons identified with 0-200 pA current injections Wistar and SHR neurons and is significantly different between these phenotypes (Wistar, n=66; phasic 1, n=29; phasic 2, n=24; tonic, n=13; SHR, n=73; phasic 1, n=9; phasic 2, n=17; tonic, n=47; $\chi 2=12.37$, df=2, p=0.002). The SHR has a higher number of tonic firing neurons. Here n refers to cell number, where a minimum culture n of 8 was used, with each culture using a minimum of 2 animals.*

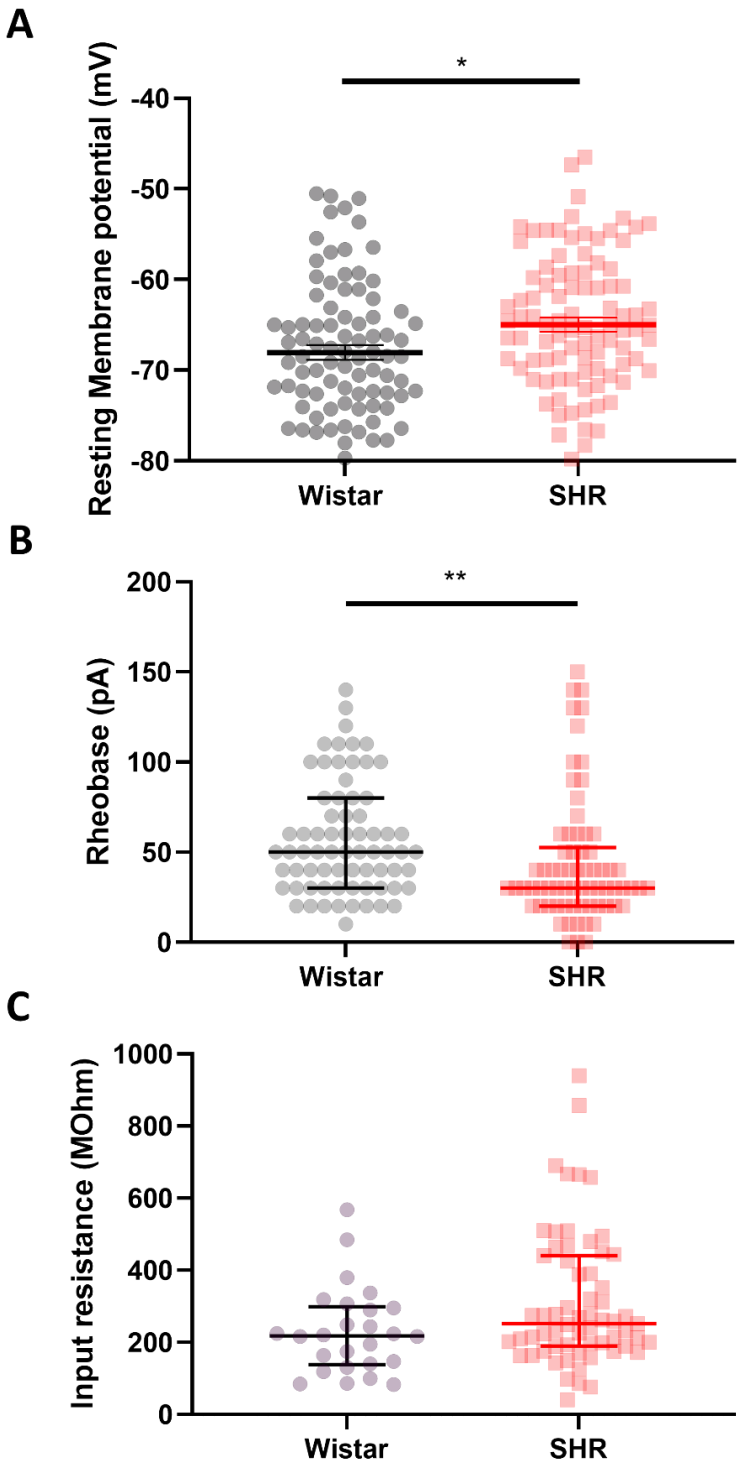



***Figure 4.3 SHR neurons exhibit other measures of neuronal excitability*** *(A) Prehypertensive SHR stellate ganglia neurons are significantly more depolarised than Wistar neurons (Mean±SEM; Wistar, -68.04±0.81 mV; SHR, -64.97±0.78 mV) (n=89, n=97; Unpaired t-test; p=0.007). (B) SHR stellate ganglia neurons also exhibit a decreased neuronal rheobase (Median±IQR) (Median; Wistar, 50 pA; SHR, 30 pA) (n=70, n=70; Mann-Whitney test; p=0.001). (C) SHR neurons display a non-significant trend towards increased input resistance (Median±IQR) (Median; Wistar 218.2 MΩ, SHR 251.2 MΩ)* (n=26, *n=63; Mann-Whitney test; p=0.066). Here n refers to cell number, where a minimum culture n of 8 was used, with each culture using a minimum of 2 animals.*

To confirm that membrane depolarisation was correlative and not causative of the increase in induced neuronal firing described in **Figures 4.1-4.2**, a current clamp protocol was utilised to hyperpolarise the RMP of SHR neurons, prior to injecting +150 pA of current (**Figure 4.4**). This protocol had no effect upon the neuronal firing rate of SHR neurons across the tested range of current injections (0 to -100 pA).

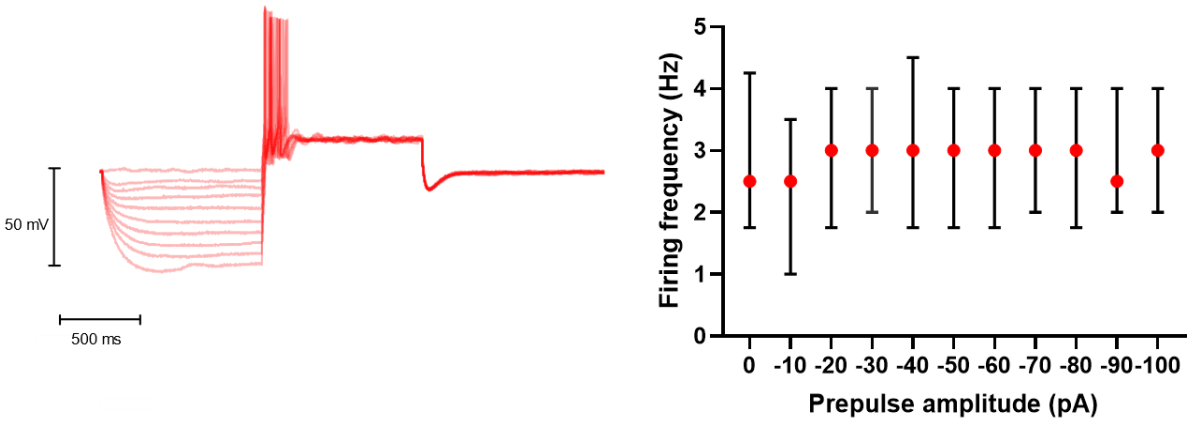



***Figure 4.4 The increased neuronal firing is independent of membrane potential depolarisation*** *SHR neurons were hyperpolarised by a 1 second negative current injection between 0 to -100 pA prior to a postive 150 pA current injection to induce neuronal firing. Example trace of a typical recording (Left). SHR neurons firing rates were not altered by the negative current step (Right) (n=26; Friedman test; p=0.16). Here n refers to cell number, where a minimum culture n of 3 was used, with each culture using a minimum of 2 animals.*

As these comparisons were made between two unpaired populations of neurons, it was especially important to exclude the influence of other variables upon these recordings. To this end, **Figure 4.5** assesses the relationship between the number of days in vitro, and the maximum neuronal firing in Wistar and SHR neurons, where no significant effect was found between these measures for either strain. In **Figure 4.5** the relationship between maximum firing rate and capacitance

was also assessed in both Wistar and SHR neurons. No relationship between capacitance and firing rate was found in either Wistar or SHR neurons. Finally, the median number of days in vitro (**Figure 4.6**) and the average cell capacitance (**Figure 4.7**) for was compared between Wistar and SHR, confirming that there was no bias between Wistar and SHR neurons.

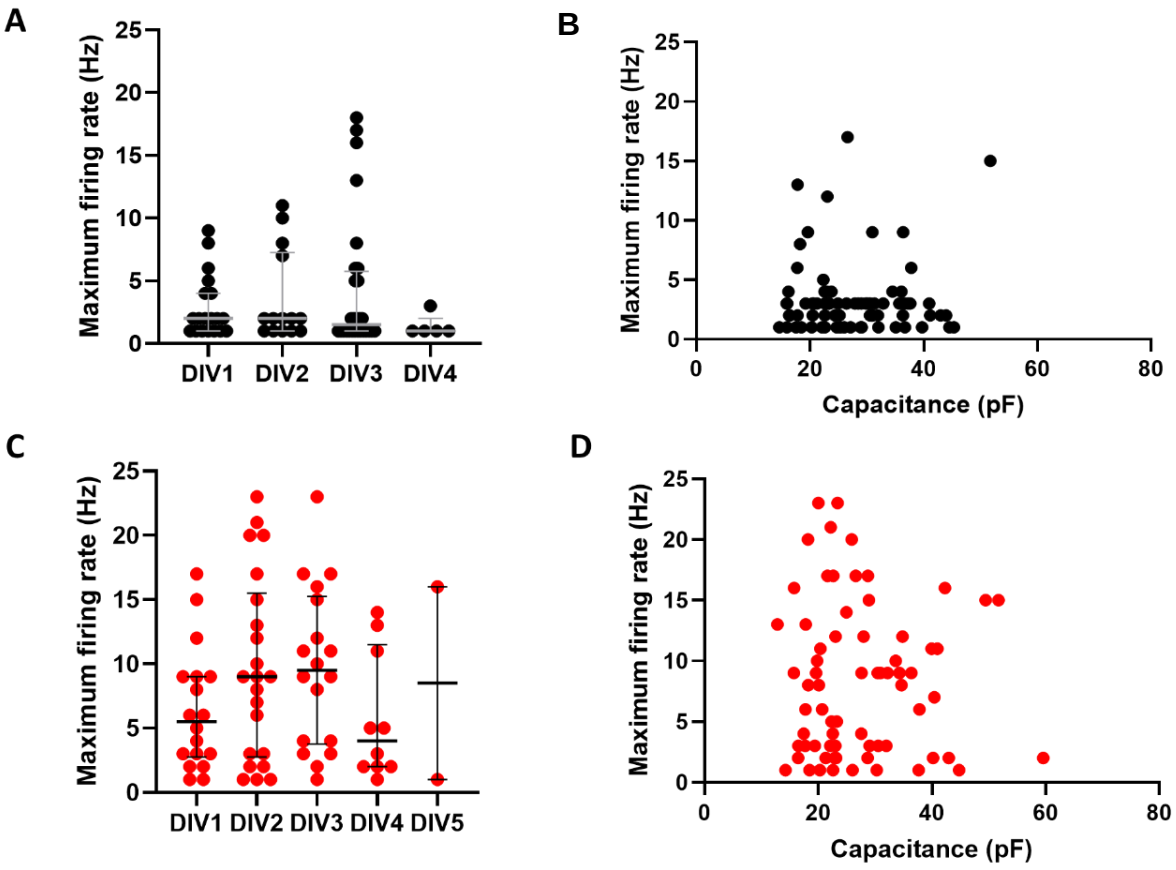



***Figure 4.5 The firing rate phenotype didn't vary with the number of days in vitro (DIV) or cell capacitance*** *There was no significant difference between maximum firing rate and the number of days in vitro for Wistar (A) (Median±IQR) (Kruskal-Wallis test; p=0.48) amd SHR (C) (Median±IQR) (Kruskal-Wallis test; p=0.35). There was no correlation between maxmimum firing rate and capacitance in either Wistar (n=66; r=0.023; $R^2$=0.0005) or SHR (n=70; r=-0.021; $R^2$=0.0004) neurons as assessed by linear regression. Here n refers to cell number, where a minimum culture n of 8 was used, with each culture using a minimum of 2 animals.*

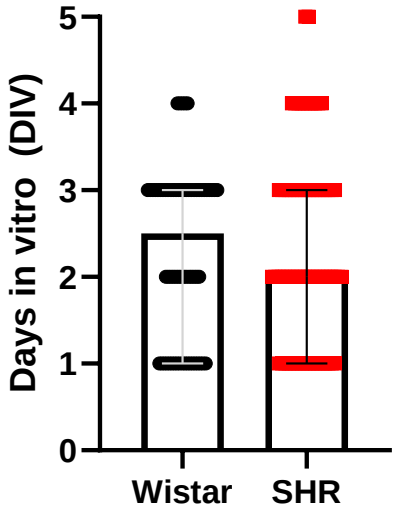



***Figure 4.6 The median number of days in vitro for recorded cells did not vary between Wistar and SHR neurons*** *When assessed by a Mann-Whitney test (Median; Wistar, 2.5 days in vitro; SHR, 2 days in vitro) (n=66, n=70; Mann-whitney test; p=0.83) their was no bias in terms of days in vitro between either strain. Here n refers to cell number, where a minimum culture n of 8 was used, with each culture using a minimum of 2 animals.*

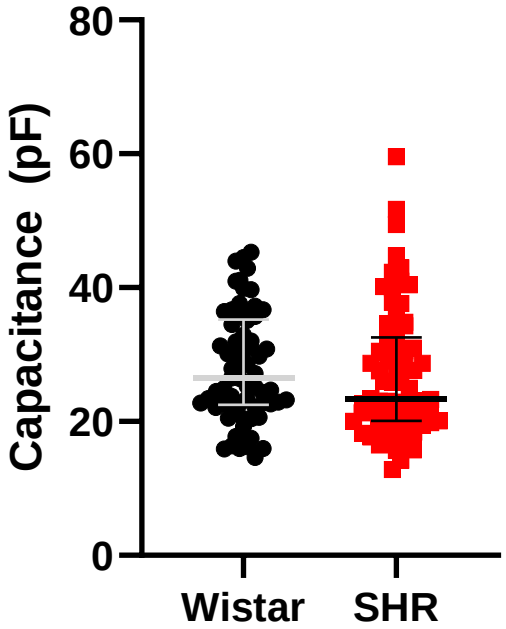



***Figure 4.7 Cell capacitance did not signficantly vary between either strain*** *There was no significant difference beween the cell capacitance of either strain (Mean±SEM; Wistar, 28.05±1 pF; SHR, 27.23±1.56 pF) (Wistar, n=66; SHR, n=70; Mann Whitney test; p=0.59). Here n refers to cell number, where a minimum culture n of 8 was used, with each culture using a minimum of 2 animals.*

### 4.3.2 Single-cell RNA-sequencing

It was important to identify putative mechanisms that might cause an increase in neuronal firing, membrane depolarisation, decreased rheobase and a loss of time resolved firing patterns. Single-cell RNA sequencing was used to provide an unbiased insight into any transcriptional changes in the expression of ion channel encoding genes in the previously identified neuronal population. Significant differential expression between Wistar and SHR neuron populations was investigated via the MAST differential expression package, and four ion channel alpha subunit encoding genes were revealed **Table 4.1**.

KCNQ5 was highlighted as a key target of interest based upon its previously highlighted role in forming M-current conducting channels (Lerche *et al.*, 2000; Schroeder *et al.*, 2000; Wickenden *et al.*, 2001; Shah *et al.*, 2002), which determine neuronal firing, RMP and rheobase (Shah *et al.,* 2008; Martinello *et al.,* 2019; Brown & Passmore, 2009). To support these data scRNAseq was used to highlight the expression of the two alternate M-current encoding genes, KCNQ2 and KCNQ3, in SGNs (**Figure 4.8**). Next, protein expression of $K_v7.2$, $K_v7.3$ and $K_v7.5$ was confirmed using immunohistochemistry in cryosections of Wistar stellate ganglia tissue (**Figure 4.9**).

***Table 4.1 Single-cell RNA-sequencing revealed a decrease in the expression of several ion channel subunits in SHR neurons*** *Differentially expressed ion channel subunits between Wistar and SHR neurons as highlighted by MAST differential expression analysis reveals 5 genes of interest.*

| Gene | Name | Scaled average $Log_2$Fold change | Adjusted p Value |
|---|---|---|---|
| **Cacna1b** | $Ca_v2.2$ | -0.69 | <0.001 |
| **Kcnq5** | $K_v7.5$ | -0.42 | <0.001 |
| **Scn1a** | $Na_v1.1$ | -0.42 | <0.001 |
| **Scn2a** | $Na_v1.2$ | -0.49 | <0.001 |
| **Scn9a** | $Na_v1.7$ | -0.43 | <0.001 |

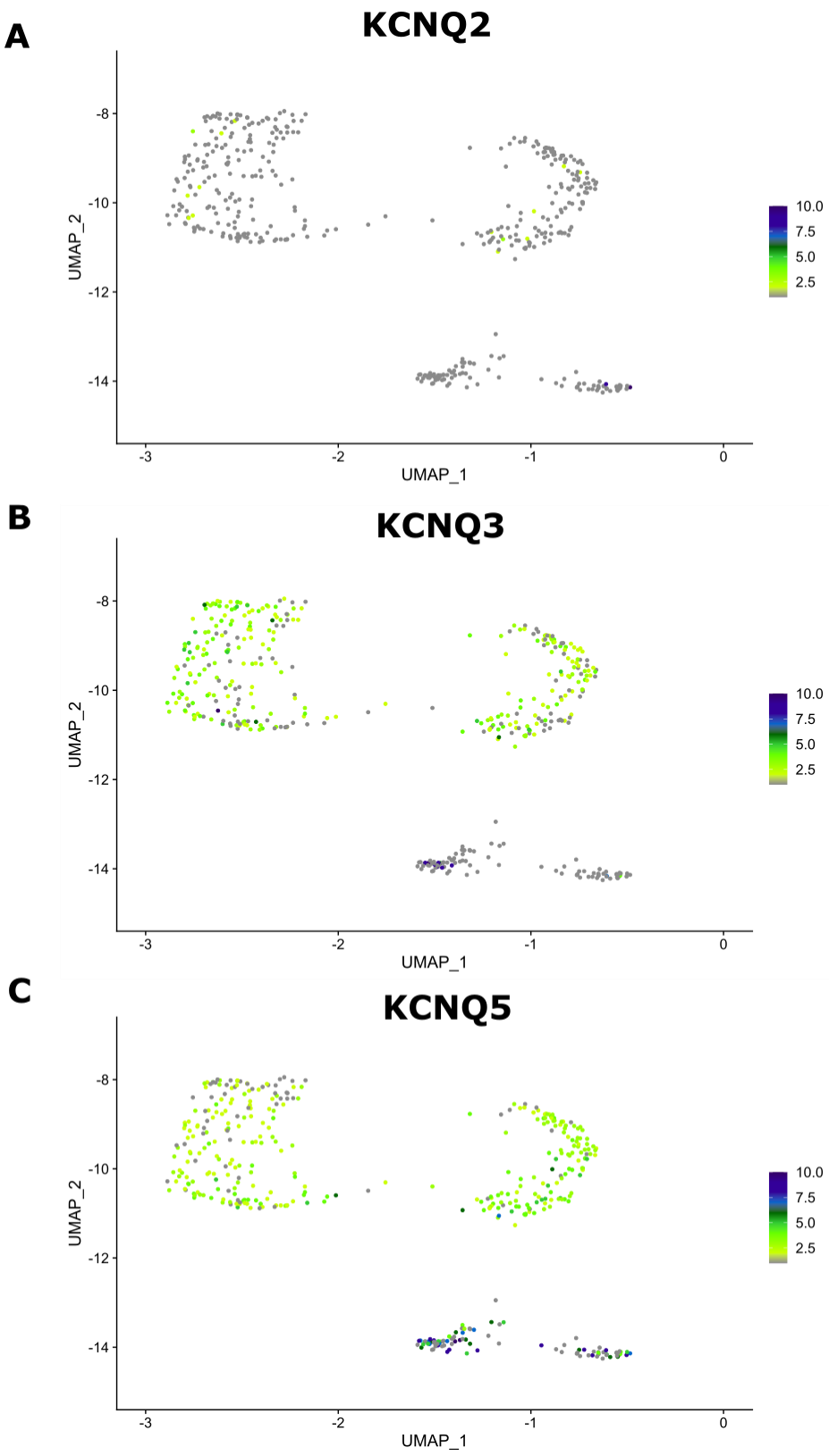



***Figure 4.8 Single-cell RNA-sequencing highlights KCNQ2,3 and 5 expression in all major neuronal populations identified by single-cell RNA-sequencing***
*UMAP refers to uniform manifold approximation and projection. These data are an alternate visualisation of the single-cell RNA-sequencing dataset featured in chapter 3.*

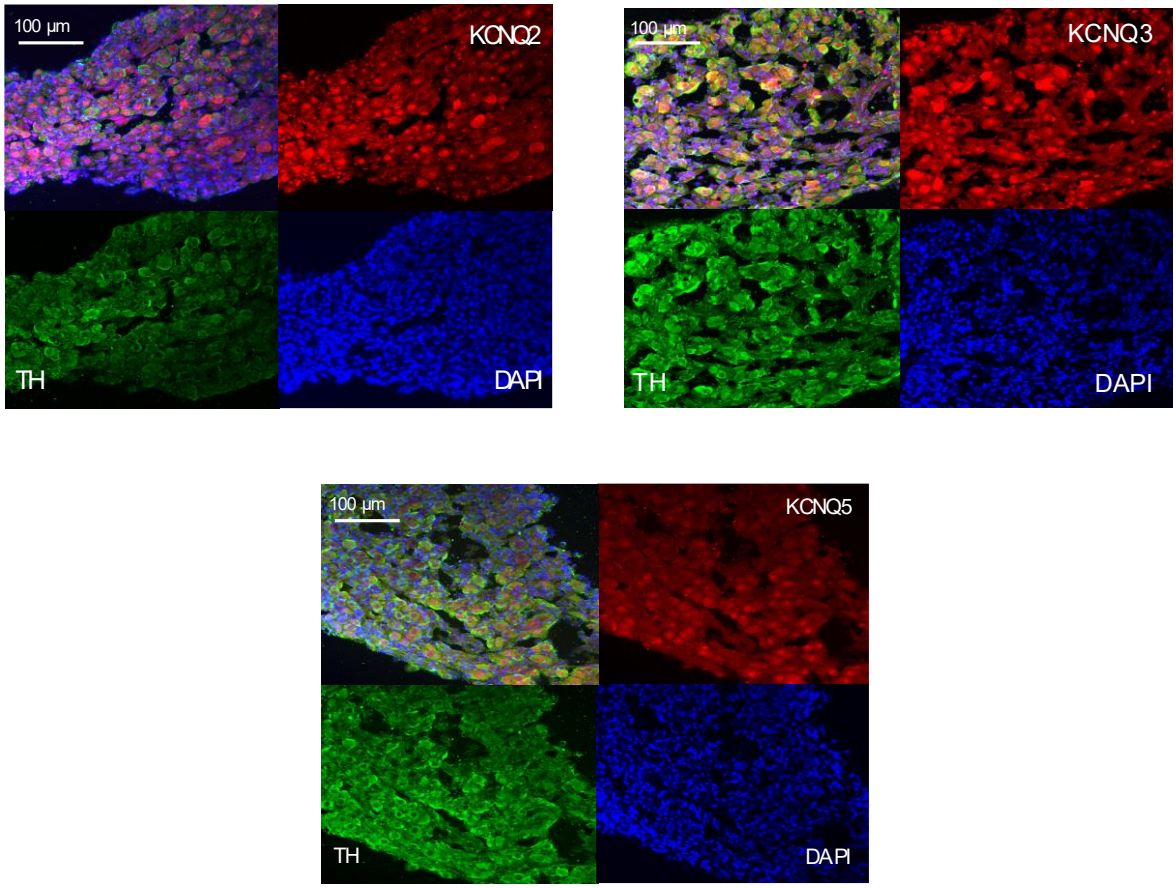



***Figure 4.9 Immunohistochemistry highlights the expression of M-current forming KCNQ2, KCNQ3 and KCNQ5 subunits in Wistar stellate ganglia cryosections.***

### 4.3.3 Confirmation of differential M-current

Based upon the electrical phenotype identified in **Figure 4.1**, and the decrease in *KCNQ5* transcript expression identified in **Table 4.1**, changes in M-current were further investigated. Differential expression was then confirmed via RT-qPCR using homogenates of whole Wistar and SHR stellate ganglia (**Figure 4.10A**), alongside the presence of KCNQ2, KCNQ3 and KCNQ5 in whole homogenised patient stellate ganglia samples (**Figure 4.10B**). Finally, any changes in M-current density between Wistar and SHR were elucidated using an M-current deactivation protocol with pharmacological subtraction of XE-991 sensitive current (Linley *et al.*, 2008). Briefly, cells were voltage-clamped at -25 mV, before a brief 1 second hyperpolarisation to -55 mV. The difference in current following the initial

ohmic change, and the steady-state current towards the end of the step were used as a measurement of deactivating M-current. To ensure that the measured current was primarily M-current, only current sensitive to 10 µM XE-991 was analysed. M-current density was significantly decreased from 4.03 pA/pF in Wistar SGNs to 1.77 pA/pF in SHR SGNs (**Figure 4.10C**). Finally, bulk RNA-sequencing of 15-16 week old Wistar and SHR revealed a similar pattern of gene expression changes. In these data*KCNQ5* expression significantly decreased when assessed by non-adjusted p-value, but not by adjusted p-value (**Table 4.2**).

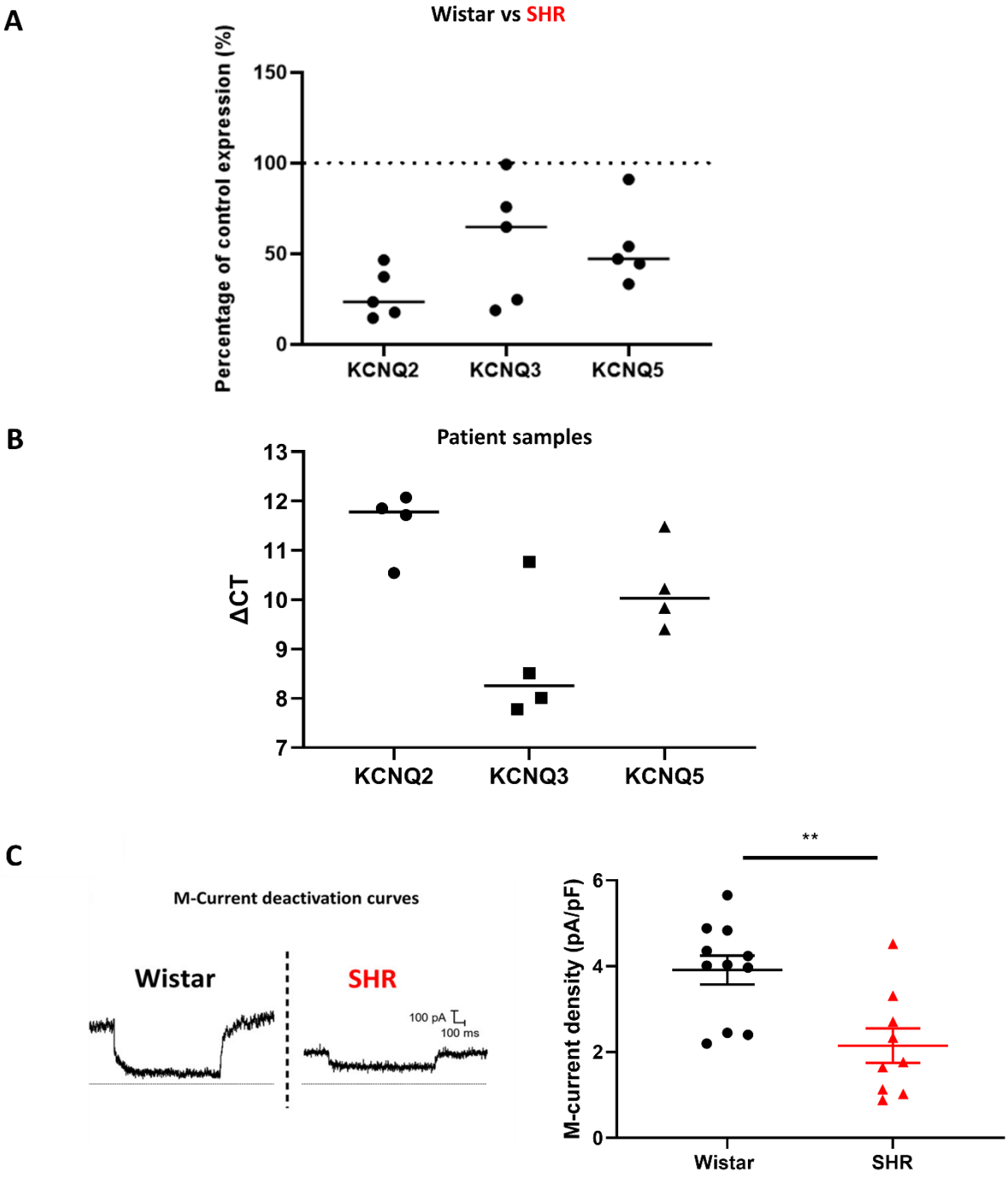



***Figure 4.10 Confirmation of a decrease in functional and transcript expression of M-current, as well as transcript expression in human stellate ganglia*** *RT-qPCR highlighted a decreased in M-current encoding genes KCNQ2, KCNQ3 and KCNQ5 in the SHR relative to Wistar (KCNQ2, 76.58%; KCNQ3, 35.16%; KCNQ5, 52.87%; Wistar, n=8; SHR, n=5) (A). M-current encoding genes were expressed in patient human stellate ganglia tissue (median; ΔCt: KCNQ2, 11.78; KCNQ3, 8.259; KCNQ5, 10.03; n=4) (B). M-current density was reduced in SHR (median±IQR; Wistar, 4.03 pA/pF, n=11; SHR, 1.77 pA/pF) (n=11, n=9; Mann-Whitney test; p=0.0074). Here n refers to cell number, where a culture n of 3 was used, with each culture using 3 animals.*

***Table 4.2 Bulk RNA-sequencing highlights a decrease in KCNQ5 at 15-16 weeks*** Analysed from a published Bulk RNA-sequencing dataset described in Chapter 3 (Davis *et al.*, 2018)***.***

| Gene name | Mean counts | $Log_2$ Fold change | P value | Adjusted P value |
|---|---|---|---|---|
| Kcnq2 | 85.52 | -0.18 | 0.41 | 0.75 |
| Kcnq3 | 1837.72 | 0.30 | 0.082 | 0.37 |
| Kcnq5 | 299.25 | -0.53 | 0.003 | 0.05 |

### 4.3.4 Phenotypic recapitulation

Next the effect of modulating M-current was assessed in terms of neuronal firing, rheobase and membrane potential. First, the effect of inhibiting M-current in Wistar neurons was evaluated through the selective inhibitors XE-991 and linopirdine. Then the effect of the M-current activator Retigabine was tested upon SHR neurons, to see whether this treatment would restore a control phenotype.

M-current inhibition by 3 μM XE-991 significantly increased neuronal firing frequency in Wistar neurons (**Figure 4.11B**), decreased the rheobase (**Figure 4.11C**) and depolarised the membrane potential (**Figure 4.11D**). Viewed qualitatively, 3 μM XE-991 also increased the number of tonic firing neurons. Five cells were excluded from the firing rate dataset due to the use of a shorter 0-150 pA protocol in initial experiments, however this did not affect rheobase or membrane potential recordings.

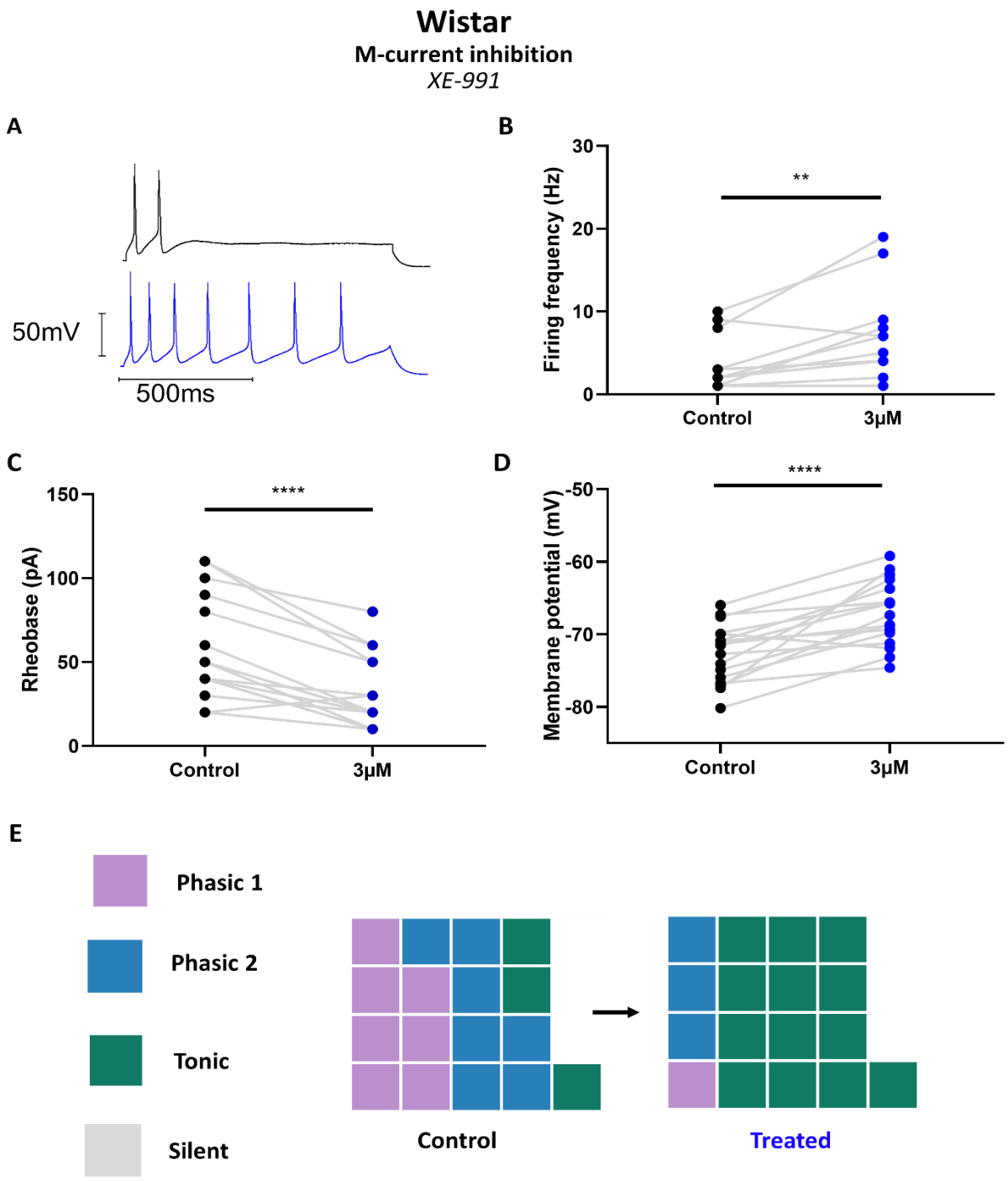



***Figure 4.11 M-current inhibition by XE-991 recapitulated the SHR phenotype in Wistar neurons*** *(A) Example traces of wistar neuron firing before and after M-current inhibtion by XE-991. (B) M-current inhibtion increase Wistar sympathetic neuron firing frequency (Median; control, 3 Hz; treated, 7 Hz) (n=12; Wilcoxon Test; p=0.0059), (C) decreased Wistar neuron rheobase (Median; control, 50 pA; 3 μM XE-991, 20 pA) (n=17; Wilcoxon test; p<0.0001) and (D) depolarised the membrane potential (Mean±SEM; control, −72.59±0.97 mV; 3 μM XE-991, −67.07±1.08 mV) (n=17; Paired t-test; p<0.0001). (E) XE-991 mediated M-current inhibition also increased the number of tonic firing neurons. Here n refers to cell number, where a minimum culture n of 2 was used, with each culture using a minimum of 2 animals.*

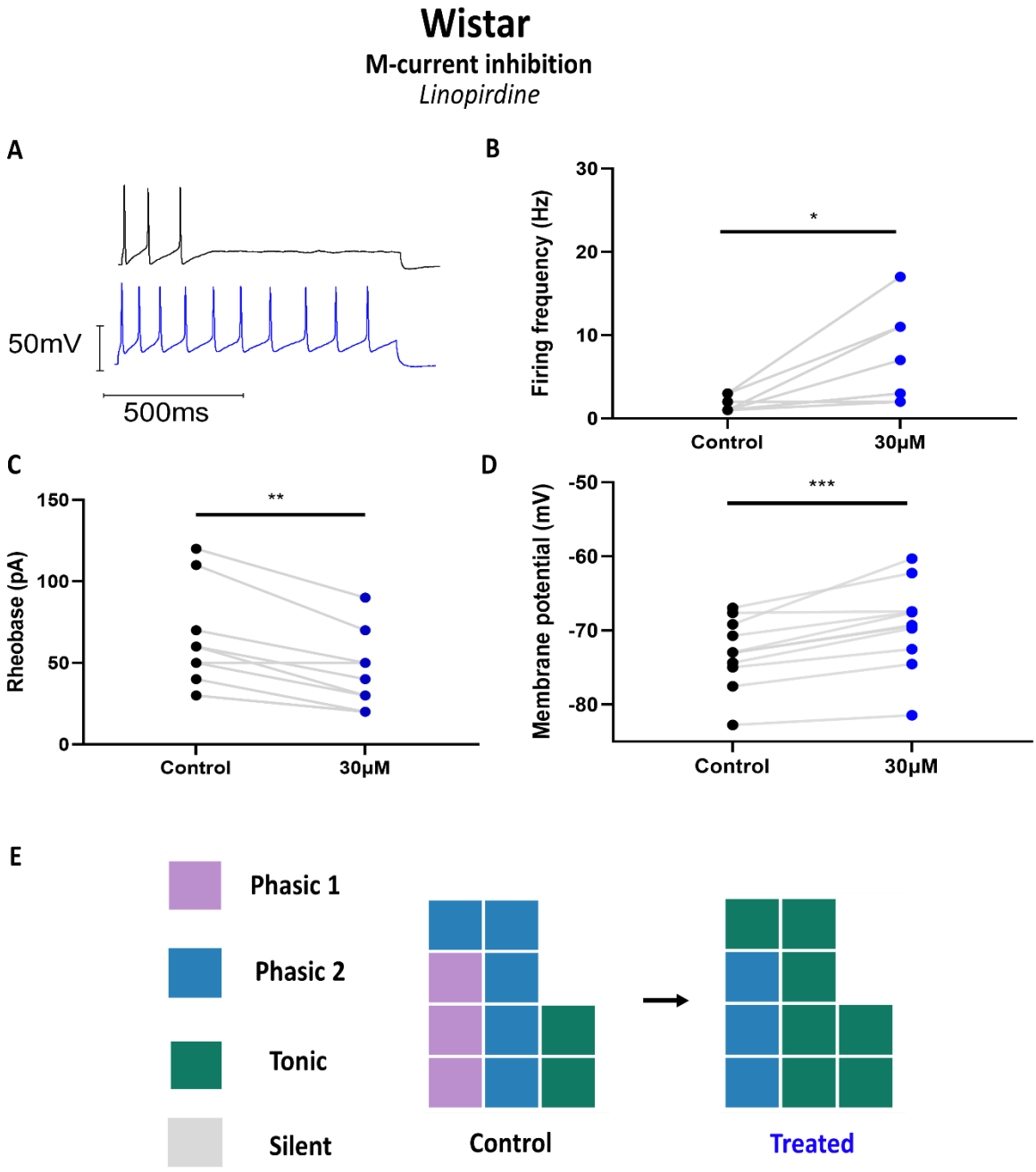



***Figure 4.12 Linopirdine also recapitulated the SHR phenotype in Wistar neurons*** *In Wistar neurons, (B) 30 μM Linopirdine increased neuron firing rate (Median; Wistar 1 Hz; 30 μM Linopirdine, 5 Hz) (n=8; Wilcoxon Test; p=0.016), (C) decreased rheobase (Median; Wistar 55 pA; 30 μM Linopirdine, 35 pA) (n=10; Wilcoxon Test; p=0.0039) and (D) depolarised the neuronal membrane potential (Mean±SEM; Wistar -73.01±1.37 ; 30 μM Linopirdine, 69.29±1.72 mV) (n=10; Paired T-test; p=0.0008). (E) Linopiridine also increased the number of tonic firing neurons. Here n refers to cell number, where a minimum culture n of 2 was used, with each culture using a minimum of 2 animals.*

The observations with XE-991 were replicated with alternate M-current inhibitor Linopirdine (Costa & Brown, 1997). As Linopiridine has a 10-fold lower potency for M-current inhibition relative to XE-991, a 10-fold higher concentration, 30 μM, was used. Linopirdine also increased Wistar neuron firing rate (**Figure 4.12B**), decreased rheobase (**Figure 4.12C**) and depolarised the membrane potential (**Figure 4.12D**). A qualitative view of firing rate classes shows a transition to tonic firing neurons following treatment (**Figure 4.12E**). Two cells were excluded from the firing rate dataset due to the use of a shorter 0-150 pA protocol in initial experiments, however this did not affect rheobase or membrane potential recordings.

M-current activation in SHR neurons by retigabine reduced neuronal excitability (**Figure 4.13**). At three tested doses (3-30 μM), retigabine significantly reduced neuronal firing (**Figure 4.13B**), at the lowest test dose, 3 μM, retigabine also significantly increased SHR neuron rheobase (**Figure 4.13C**). The membrane potential of SHR neurons was significantly hyperpolarised following the addition of 3-30 μM retigabine (**Figure 4.13D**). Following treatment with 3 μM retigabine, the number of tonic firing neurons was reduced in this population (**Figure 4.13E**).

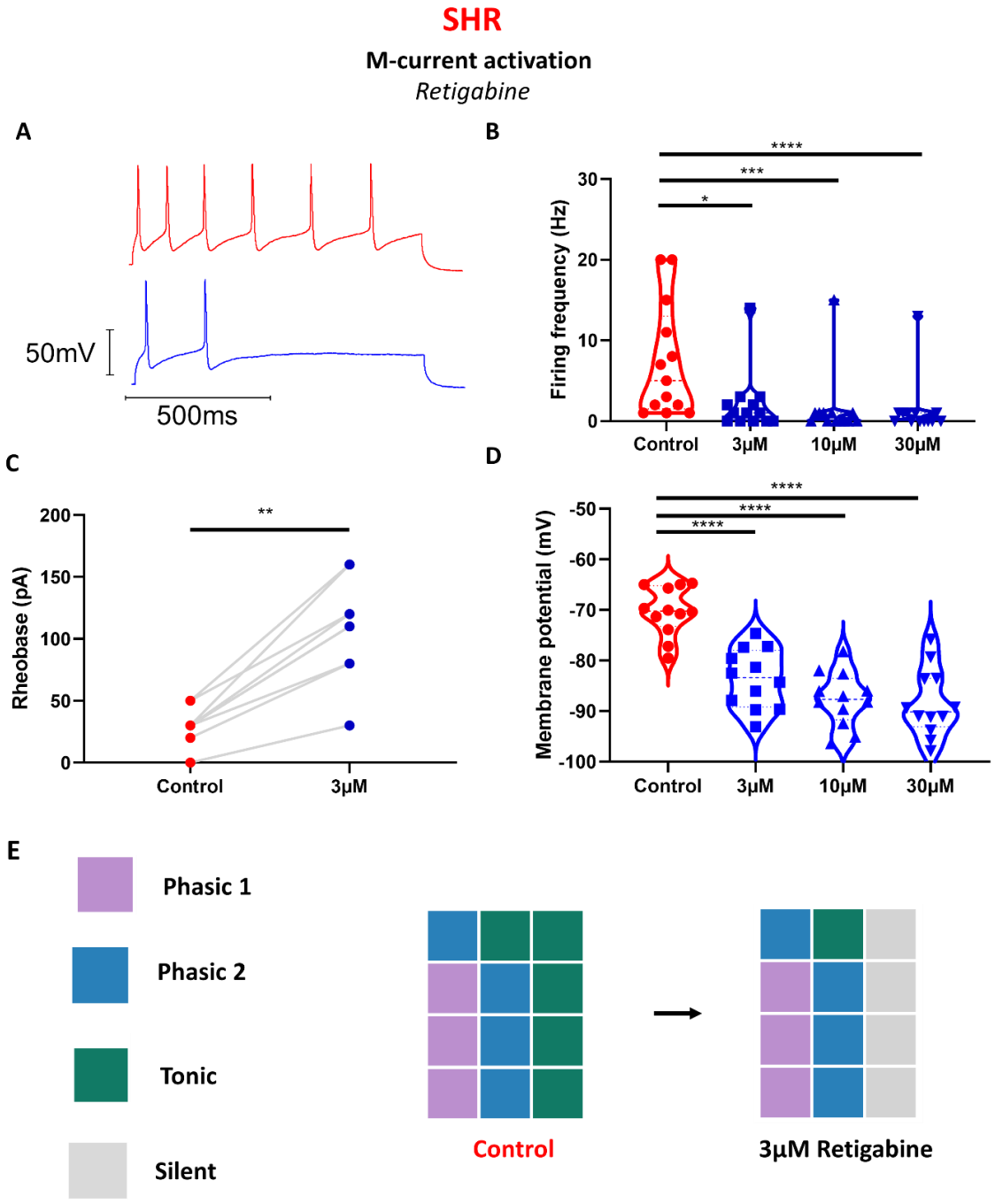



***Figure 4.13 M-current activation by retigabine recapitulated a Wistar phenotype in SHR neurons*** *Firing frequency (B) (Median; control, 5 Hz; 3 μM retigabine, 1 Hz; 10 μM retigabine, 0 Hz; 30 μM retigabine, 0 Hz) (n=13; Friedman test; p<0.0001; Dunn multiple comparisons: control vs 3 μM, p=0.018; control vs 10 μM, p=0.0002; control vs 30 μM, p<0.0001) Rheobase (C) (Median; control, 30 pA; 3 μM retigabine, 110 pA) (n=9; Wilcoxon test; P=0.0039). Membrane potential (D) (Mean±SEM; control, −70.27±1.39 mV; 3 μM, −83.63±1.67 mV; 10 μM, −87.69±1.53 mV; 30 μM, −88.45±1.91 mV) (n=12; 1-way ANOVA; p<0.0001; Dunnett multiple comparisons: control vs 3 μM, p<0.0001; control vs 10 μM, p<0.0001; control vs 30 μM, p<0.0001) (E) Retigabine also reduced the number of tonic firing neurons. Here n refers to cell number, where a minimum culture n of 2 was used, with each culture using a minimum of 2 animals.*

### 4.3.5 $Na_v$ as alternate targets

Having established M-current as a putative mechanism for the hyperexcitable phenotype observed in SHR neurons, the viability of targeting the $Na_v$ family to reduce pathological activity was then assessed. Two general $Na_v$ inhibitors were used; either all $Na_v$ mediated current was inhibited via TTX (**Figure 4.16A**), or the persistent sub-conductance state via was selectively inhibited by riluzole (**Figure 4.16E**). Alongside these data, selective inhibitors for individual $Na_v$ subunits (**Figure 4.16B-D**) were tested following the identification of subtypes in SGNs by scRNAseq (**Figure 4.15**). $Na_V$ voltage-clamp recordings in wistar neurons are provided in appendix figures 16-17.

ScRNAseq revealed transcript expression of *SCN1A*, *SCN2A*, *SCN3A*, *SCN8A* and *SCN9A* in SGNs (**Figure 4.14**), which correspond to $Na_v1.1$, $Na_v1.2$, $Na_v1.3$, $Na_v1.6$ and $Na_v1.7$. This enabled the guided use of selective inhibitors in **Figure 4.16**.

As scRNAseq highlighted a decrease in *SCN1A*, *SCN2A* and *SCN9A* expression (**Table 4.1**) $Na_v$ dependent parameters were assessed to see if this had a functional effect. To this end action potential kinetics, action potential amplitude and action potential upstroke were compared and contrasted between Wistar and SHR neurons. There were no significant differences between Wistar and SHR neuron action potential kinetics (**Figure 4.15**), suggesting similar $Na_v$ function in these populations.

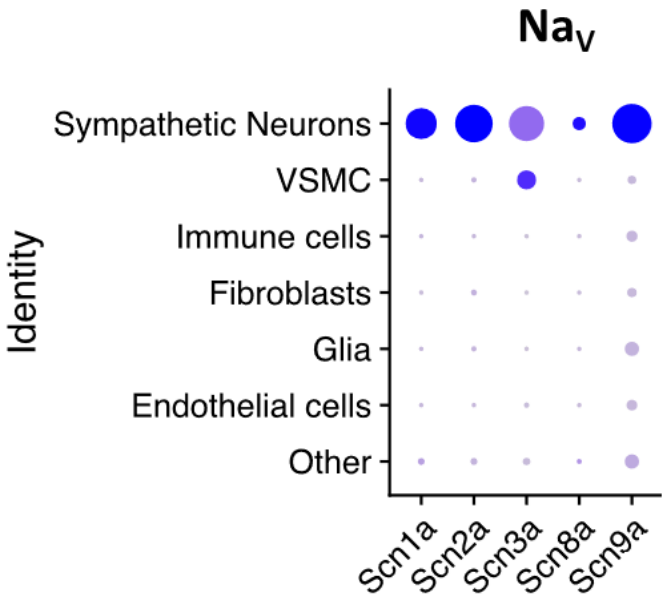



***Figure 4.14 Specific $Na_V$ subunit expression in stellate ganglia cell populations as highlighted by single-cell RNA-sequencing***

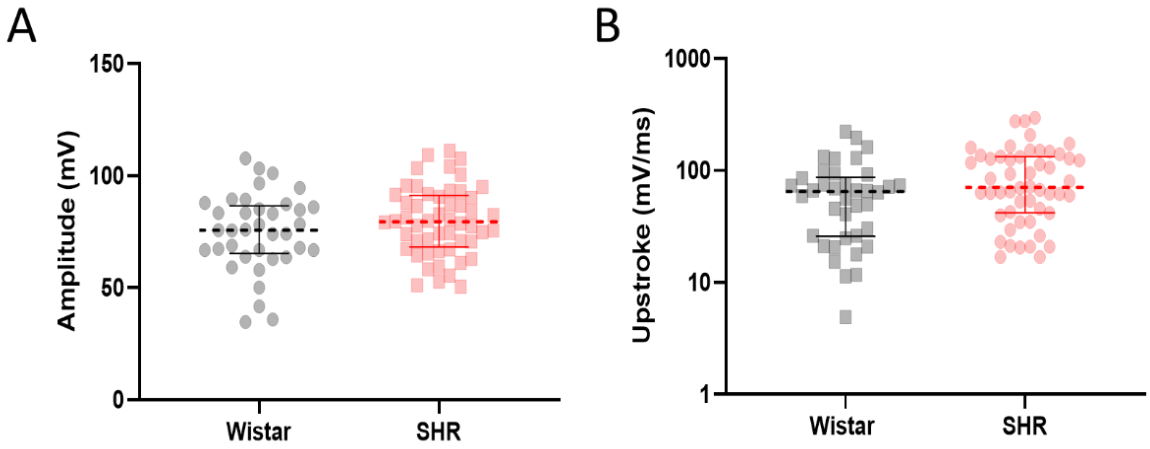



***Figure 4.15 There were no significant difference in $I_{Na}$ dependent action potential kinetics between Wistar and SHR neurons*** *(A) Action potential amplitude (Median; Wistar, 75.74 mV; SHR, 79.39 mV) (Wistar, n=37; SHR,n=52; Mann-Whitney test; p=0.27) and (B) upstroke (Median; Wistar, 64.72 mv/ms SHR 70.54 mv/ms) (Wistar, n=38; SHR, n=52; Mann-Whitney test; p=0.067) were unaltered between Wistar and SHR neurons. Here n refers to cell number, where a minimum culture n of 5 was used, with each culture using a minimum of 2 animals.*

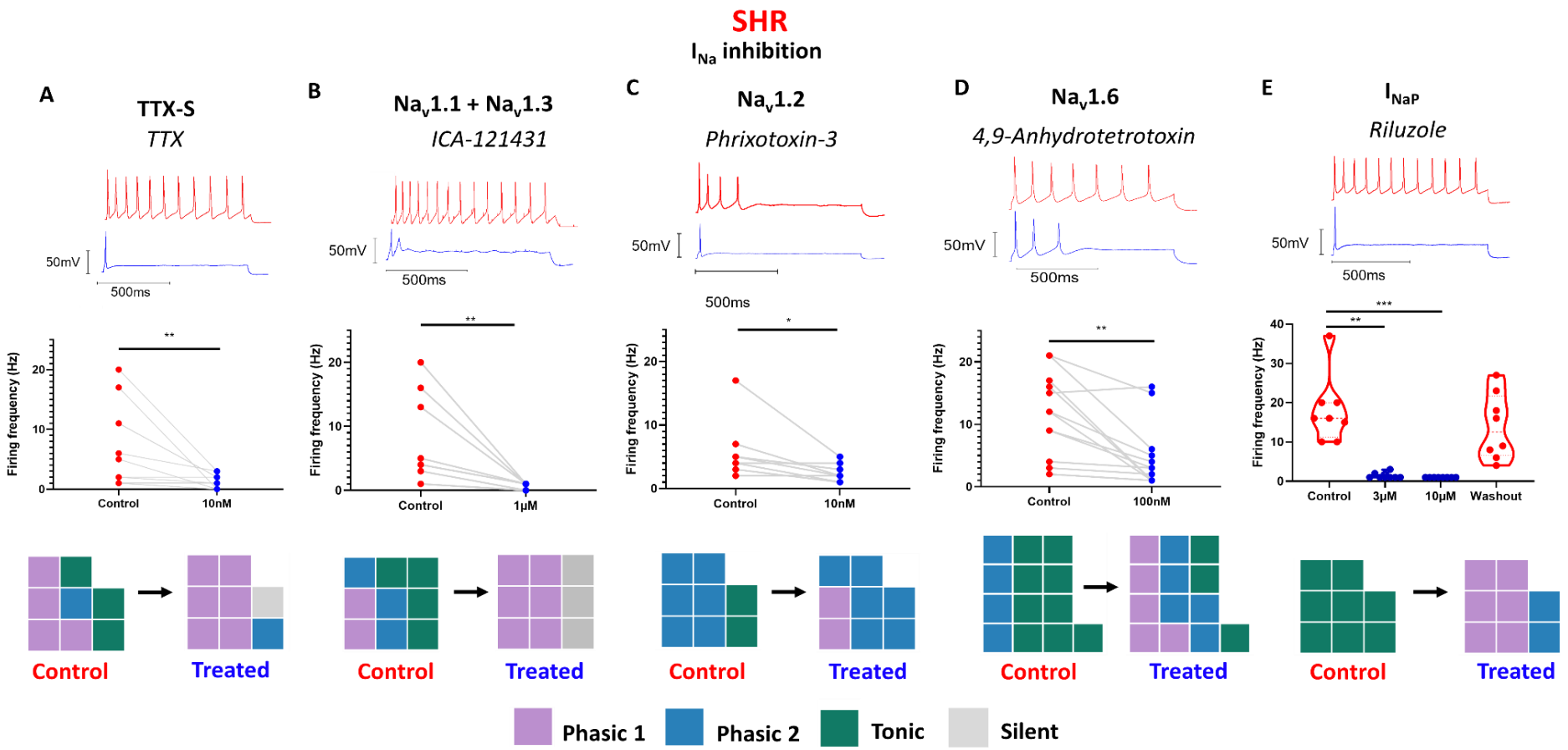



***Figure 4.16 General and selective inhibitors of $Na_v$ subunits reduce SHR neuronal firing*** *Each $Na_v$ inhibitor presented here decreased SHR neuron firing; (A) 10 nM TTX (Median; Control, 2 Hz; TTX 10 nM, 1 Hz) (n=14; Wilcoxon test; P=0.0078), (B) 1 μM ICA-121431 (Median; Control, 4 Hz; 1 μM ICA-121431, 1 Hz) (N=9; Wilcoxon test; p=0.004), (C) 10nM Phrixotoxin-3 (Median; Control, 4.5 Hz; 10nM Phrixotoxin-3, 2 Hz) (n=8; Wilcoxon test; P=0.031), (D) 100 nM 4,9-anhydrotetrodotoxin (Median; Control, 12 Hz; 100 nM 4,9-anhydrotetrodotoxin, 3 Hz) (n=13; Wilcoxon test; P=0.002), (E) Riluzole (Median; Control, 16 Hz; 3 μM, 1 Hz; 10 μM, 1 Hz; Washout, 12.5 Hz) (N=8; Friedman test: P<0.0001) (Dunn multiple comparisons test: Control vs 3 μM, P=0.003; Control vs 10 μM, P=0.007). Here n refers to cell number, where a minimum culture n of 2 was used, with each culture using a minimum of 2 animals.*

All tested subunit-selective and general inhibitors of $I_{Na}$ significantly reduced SHR neuronal firing (**Figure 4.16**), except for the $Na_v1.7$ inhibitors ProTx-III and Huwentoxin IV which had no effect upon firing (**Table 4.3**).

### 4.3.6 $Na_v1.8$ in stellate ganglia neurons?

Prior work suggests that $Na_v1.8$ channels are present in SGNs (Yu *et al.*, 2017), based upon the $Na_v1.8$ selective inhibitor A803467 (Jarvis *et al.*, 2007) ablating pathological stellate ganglia activity *in vivo*. In sensory neurons, $Na_v1.8$ channels conduct a TTX-resistant current crucial to repetitive firing (Bennett *et al.*, 2019). As these channels would play a critical and unexpected role in SGNs, the effect of $Na_v1.8$ inhibitors on SGNs was assessed.

The $Na_v1.8$ inhibitors A803467 (Jarvis *et al.*, 2007) and A887826 (Zhang *et al.*, 2010) both reduced pathological SHR SGN firing (**Figure 4.17A-B**), whereas PF04885614 had no effect. (**Figure 4.17C**). However, no $Na_v1.8$ encoding *SCN10A* transcript expression was in SGNs by scRNAseq (**Figure 4.14**) or stellate ganglia homogenates by RT-qPCR (Data not shown) and only a small number of reads were detected by bulk RNA-sequencing (*SCN10A*; Average reads 25.92) (Davis *et al.*, 2018). These data are supported by the similar $K_v$ I-V curves produced by both TTX subtracted $Na_v$ currents and $Na_v$ isolating solutions (Appendix Figure 19).

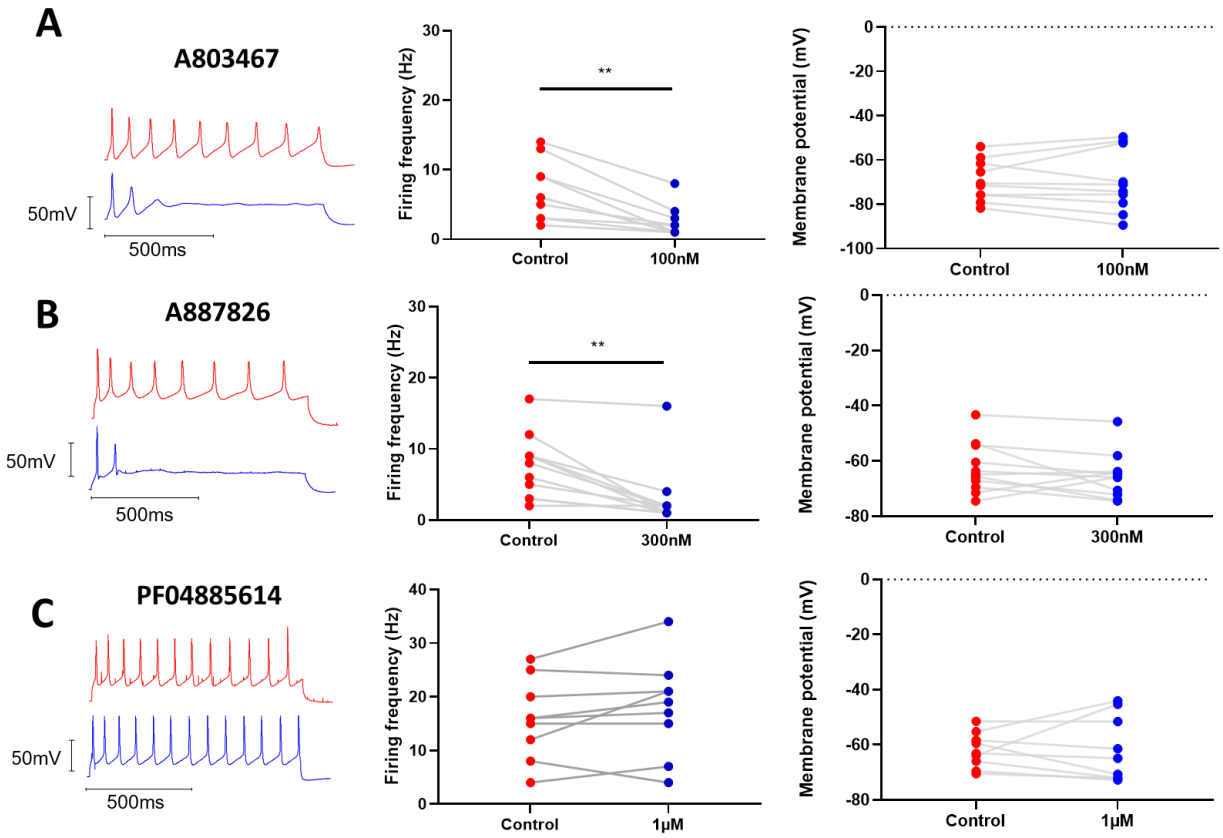



***Figure 4.17 $Na_v1.8$ inhibitors A803467 and A887826 reduced SHR neuron firing, however alternate $Na_v1.8$ inhibitor PF04885614 did not*** *(A) A-803467 reduced SHR neuron firing (n=10; Wilcoxon test; p=0.002), and not affect neuronal membrane potential (n=10; Paired t-test; p=0.88). (B) Likewise, A-887826 reduced neuronal firing in SHR neurons but did not affect the membrane potential. (C) Finally,1 µM PF-04885614 did not effect either the neuronal firing rate (Median; Control, 16 Hz; 1 µM PF04885614, 19 Hz) (n=9; Wilcoxon test; p=0.17) or membrane potential (Mean±SEM; Control -61.97±2.12 mV; 1 µM PF04885614, -61.63±3.93 mV) (n=9; Paired t-test; p=0.92). Here n refers to cell number, where a minimum culture n of 2 was used, with each culture using a minimum of 2 animals.*

### 4.3.7 Physiological role of $Na_v$ and M-current

Having demonstrated the role of both M-current and $Na_v$ in the aberrant SHR SGN phenotype, the relationship between the firing rate phenotype and M-current density was assessed. In addition, proxies for neuronal $Na_v$ current, action potential upstroke and action potential amplitude were also correlated with neuronal firing properties (**Figure 4.18**). Finally, the effect of $Na_v$ inhibition on XE-991 induced excitability in Wistar neurons was assessed.

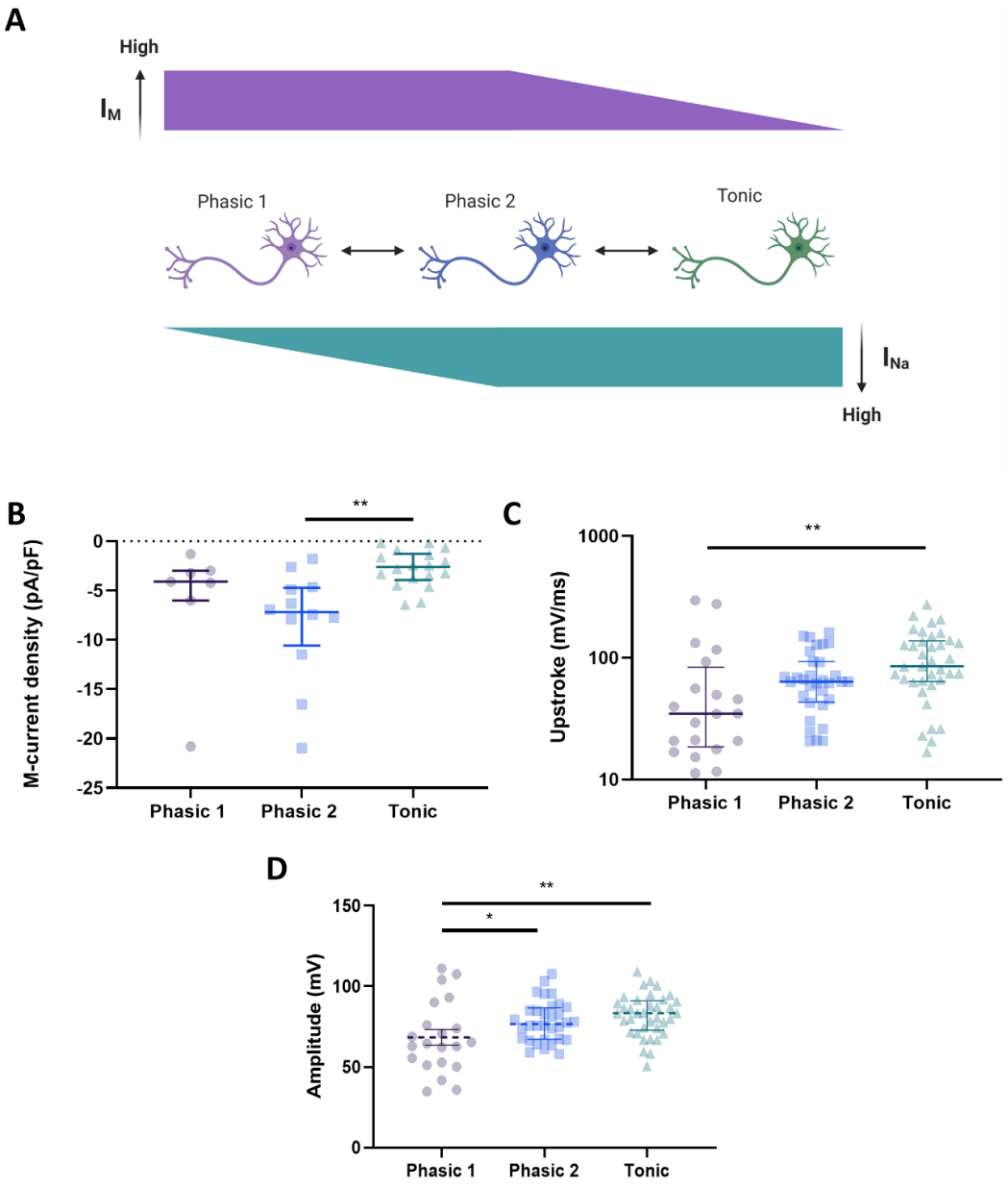



***Figure 4.18 Neuron firing subclasses vary in M-current expression and action potential amplitude and upstroke*** *(A) Scheme of the relationship between M-current and $Na_V$ conductance against neuronal firing type. (B) M-current density was lower in tonic neurons than phasic 2 neurons (n=7, n=12, n=18; Wistar, n=14; SHR, n=23; Kruskal-Wallis test; p=0.0019) (Dunn's multiple comparisons; Phasic 1 vs phasic 2, p=0.38; Phasic 1 vs Tonic, p=0.55; Phasic 2 vs Tonic, p=0.0012). (C) Action potential upstroke was found to be signficantly higher in tonic neurons than phasic neurons (n=20, n=32, n=37; Wistar, n=37, SHR, n=53; Kruskal-Wallis test; p=0.0016)(Dunn's multiple comparisons test; Phasic 1 vs phasic 2, p=0.38; Phasic 1 vs tonic, p=0.55; Phasic 2 vs tonic, p=0.0012) . (D) Action potential amplitude was signficantly greater in phasic 2 and tonic neurons than in Phasic 1 neurons (n=21, n=32, n=37; Wistar, n=38, SHR, n=53; ANOVA; p=0.0071) (Holm-Sidak's multiple comparisons test; Phasic 1 vs phasic 2, p=0.049; Phasic 1 vs tonic, p=0.0054; Phasic 2 vs tonic, p=0.35). Here n refers to cell number, where a minimum culture n of 2 was used, with each culture using a minimum of 2 animals.*

The suggested schema for the distribution of M-current density and $Na_V$ current between the three firing rate classes is graphically represented in **Figure 4.19A**. M-current density here was recorded via deactivation curves as described previously, but without pharmacological subtraction. M-current density was significantly lower in Tonic neurons than phasic 2 neurons, but there was no significant difference between Phasic 1 and Phasic 2 or Tonic neuron M-current density (**Figure 4.18A**). Action potential upstroke was significantly higher in Tonic neurons than Phasic 1 neurons. Phasic 2 neurons also showed a trend towards increased action potential upstroke relative to phasic 1 neurons (**Figure 4.18C**). Action potential amplitude was significantly larger in Phasic 2 and Tonic neurons than in Phasic 1 neurons (**Figure 4.18D**).

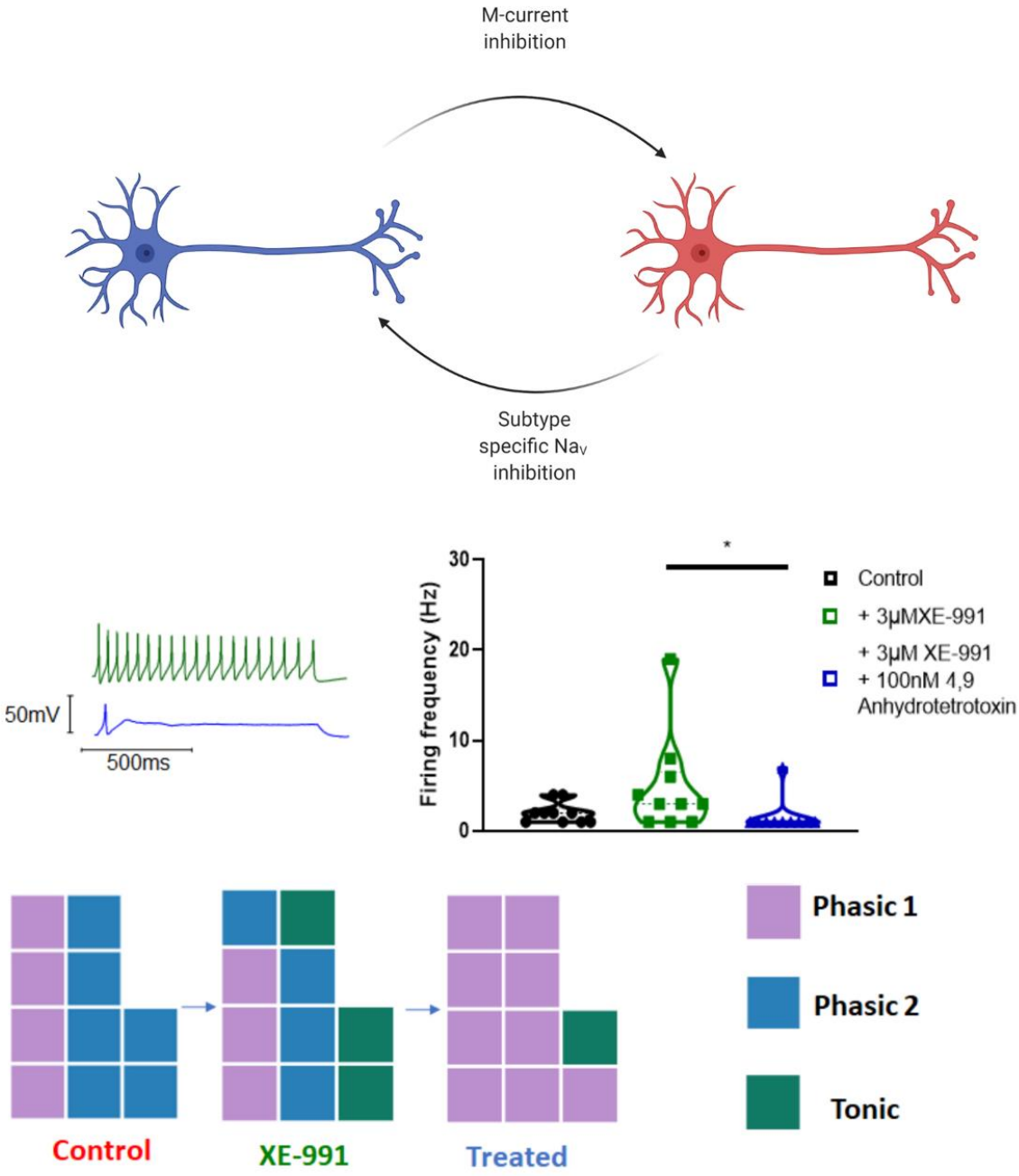



***Figure 4.19 $Na_V1.6$ inhibition by 4,9 Anhydrotetrodotoxin significantly reduced XE-991 induced aberrant firing in wistar neurons*** *Schema of experimental design (Top). $Na_V1.6$ inhibition reduced XE-991 induced abberant firing in Wistar stellate ganglia neurons (Median; Control, 2 Hz; 3 μM XE-991, 3 Hz; 3 μM XE-991 + 100 nM 4,9-Anhydrotetrotoxin, 1 Hz)(n=10 ; Friedman test; p=0.0084) (Dunn's multiple comparisons test; Control vs 3 μM XE-991, p=0.87; 3 μM XE-991 vs 3 μM XE-991 + 100 nM 4,9-Anhydrotetrotoxin, p=0.038)(Middle). The firing rate phenotype of XE-991 treated wistar neurons was also reversed by 100 nM 4,9-Anhydrotetrodotoxin (Bottom). Here n refers to cell number, where a minimum culture n of 2 was used, with each culture using a minimum of 2 animals.*

$Na_v1.6$ inhibition in XE-991 treated Wistar neurons reduced aberrant firing as shown both quantitatively and qualitatively (**Figure 4.19**). A graphical summary of these observation is also shown for clarity.

### 4.3.8 Other channels

Finally, remaining channels were inhibited in SHR neurons to assess their contribution to the aberrant firing phenotype. The molecular identity of these channels was highlighted by scRNAseq (**Figure 4.20**), where the major targets where highlighted to be HCN channels, HCN2 and HCN4, SK channel SK3 (*KCNN3*), BK (*KCNMA1*) and slack $K_{Na}$ (*KCNT1*). In addition, T-type $Ca_v$ channels and TMEM16A (*ANO1*) where inhibited, and in a further experiment $Ca^{2+}$ was excluded to measure the dependence of the SHR phenotype on other $Ca^{2+}$-dependent mechanisms. Finally, the absence of T-type currents is supported by the lack of a LVA $Ba^{2+}$ current in voltage-clamp recordings (Appendix Figure 15).

Of these targets, only SK inhibition by apamin (Kawai & Watanabe, 1986), and $K_v2$ family inhibition by GxTx (Herrington *et al.*, 2006; Li *et al.*, 2013; Kimm *et al.*, 2015*a*) caused a significant change in firing rate (**Figure 4.21**), however, inhibitors that had no significant effect upon firing are shown in **Table 4.3.** Both $K_v2$ and SK channel inhibition significantly increased SHR neuron firing rates (**Figure 4.21**). Whilst BK inhibitor Iberiotoxin (Candia *et al.*, 1992) did not alter firing rate (**Table 4.3**), it did increase action potential width, which is shown in **Figure 4.22.**

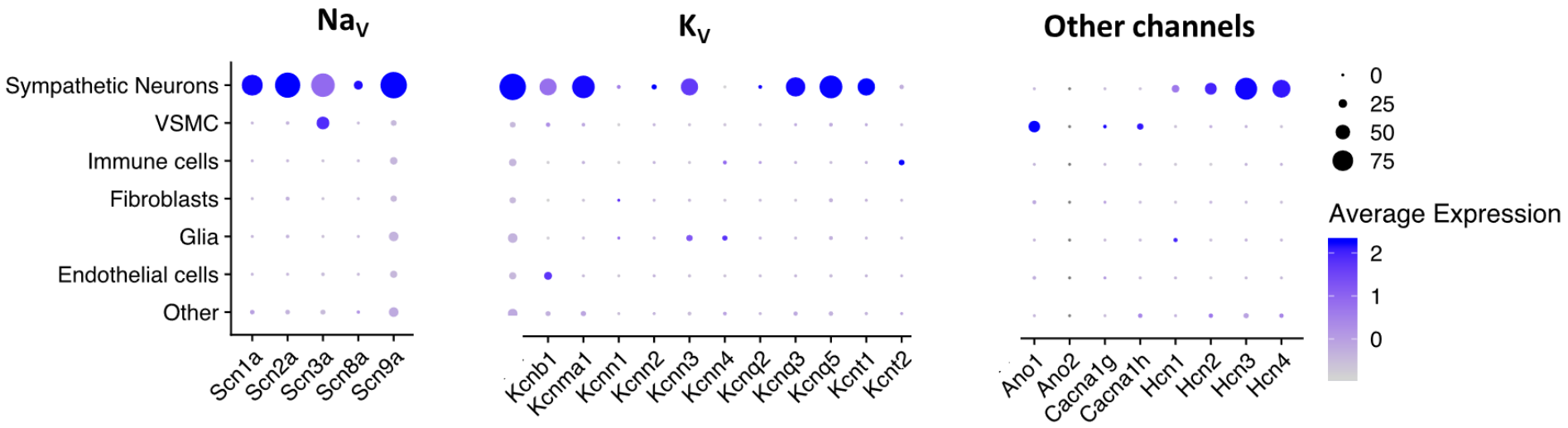



***Figure 4.20 Single-cell RNA-sequencing documents expression of all channel subunits covered within this manuscript, including targets without a significant effect upon firing rate which are documented in Table 2***

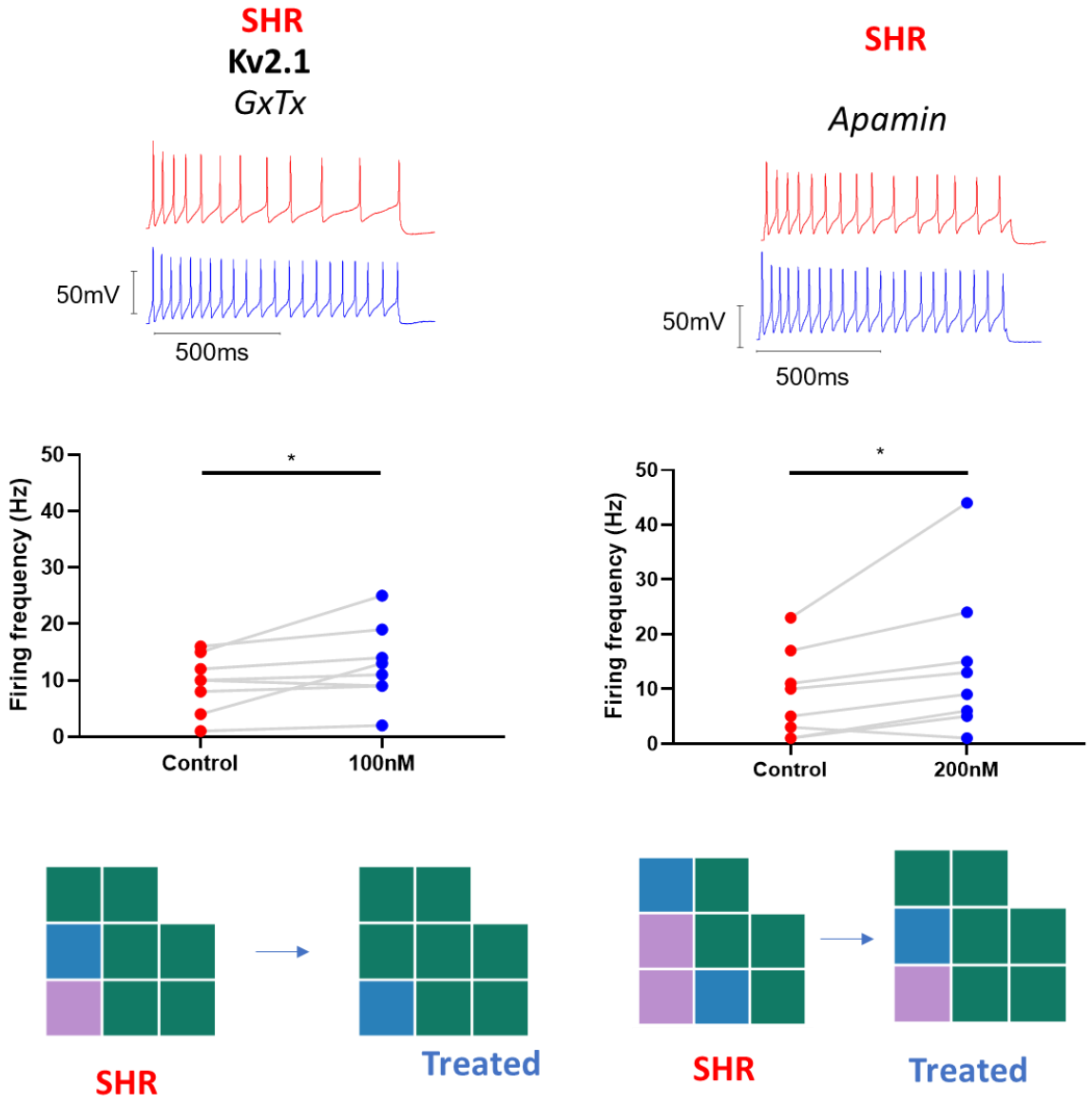



***Figure 4.21 SK and Kv2.1 channels are also involved in determining SHR neuronal firing rate*** *Inhibition of $K_v2.1$ channels by GxTx increased neuronal firing in SHR neurons, and increased the number of tonic firing neurons (n=8; Wilcoxon Test; p=0.039) (Left). Inhibition of SK channels by Apamin increased SHR neuronal firing and increased the number of tonic neurons (n=8; Wilcoxon Test; p=0.016) (Right). Here n refers to cell number, where a minimum culture n of 2 was used, with each culture using a minimum of 2 animals.*

***Table 4.3 Non-signficant inhibitors for other targets.*** *This range of channels is highlighted in* ***Figure 4.21****. Listed here are the target of interest, their inhibitors and the concentrations used as well as the patch-clamp methodology methodology employed. Where applicable a second selective inhibition was utilised. All recordings were performed in SHR neurons. Here n refers to cell number, where a minimum culture n of 2 was used, with each culture using a minimum of 2 animals.*

| | HCN | | T-type | | Ca2+ free | BK | CaCC | Nav1.7 | | KNa |
|---|---|---|---|---|---|---|---|---|---|---|
| **Drug** | Ivabradine | ZD7288 | TTA-A2 | TTA-P2 | EGTA | Iberiotoxin | Ani9 | Protx-III | Huwentoxin-IV | Lithium |
| **Concentration** | 3μM | 1μM | 500nm | 1μM | 5mM | 100nM | 1μM | 50nM | 50nM | N/A |
| **Perforating agent** | Amphotericin | Amphotericin | Amphotericin | Amphotericin | Amphotericin | Amphotericin | Amphotericin | Amphotericin | Amphotericin | Whole cell |
| **Δ Firing rate 150pA** | -1 | 0 | 0 | -1 | -1 | 0 | 0.5 | 0 | 2.5 | 0 |
| *P value* | *0.67* | *0.5* | *>0.99* | *0.60* | *0.59* | *0.81* | *0.87* | *0.38* | *0.11* | *0.84* |
| **Δ Firing rate 100pA** | 0 | 0.5 | 0 | -0.5 | 1 | 0 | 0.5 | 0 | 0.5 | 0 |
| *P value* | *0.75* | *0.95* | *0.25* | *0.89* | *0.22* | *0.94* | *0.55* | *0.44* | *0.19* | *0.5* |
| **Δ Firing rate 50pA** | 0 | 0.5 | 1 | 0 | 0 | 0 | 0.5 | -0.5 | 0 | 0 |
| *P value* | *0.19* | *0.25* | *0.16* | *>0.99* | *0.094* | *>0.9999* | *0.5156* | *0.63* | *0.5* | *0.25* |
| **Δ Maximum firing rate** | 0 | 0 | 0 | -0.5 | 0.5 | 0 | 1 | -0.5 | 1 | 0 |
| *P Value* | *0.13* | *>0.99* | *0.63* | *0.51* | *0.61* | *0.60* | *0.29* | *0.67* | *0.19* | *0.81* |
| **n** | 10 | 8 | 9 | 10 | 12 | 12 | 10 | 8 | 8 | 10 |

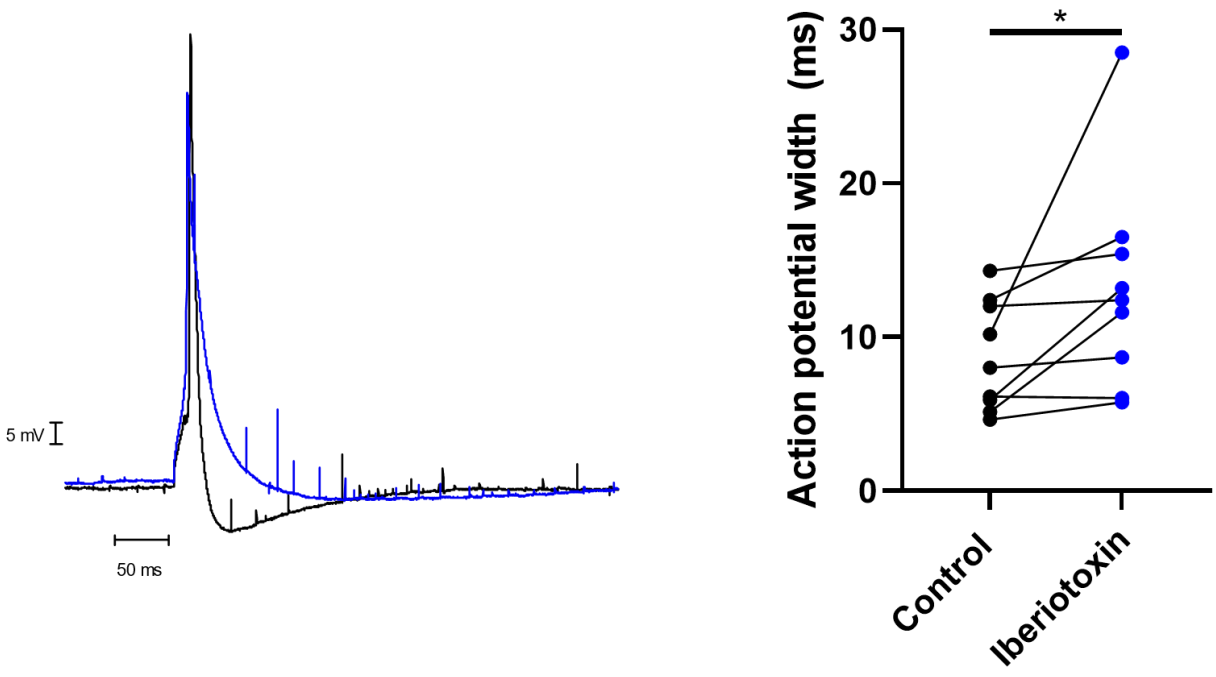



***Figure 4.22 BK channel inhibition caused a significant increase in action potential width*** *A ratio paired t-test showed a significant increase in action potential width in SHR neurons following treatment with iberiotoxin (Mean±SEM; Control, 8.75±1.19 ms; Iberiotoxin, 13.12±2.30 ms) (n=9; Ratio Paired t-test; p=0.025). The outlier was not removed for this analysis; however, statistical significance was still achieved following removal (n=8; Ratio Paired t-test; p=0.047). Here n refers to cell number, where a minimum culture n of 2 was used, with each culture using a minimum of 2 animals.*

To facilitate further discussion, $K_v$ encoding subunits (**Figure 4.23**) with a greater average expression than 0.3 Ln(counts) within the neuronal scRNAseq cluster are shown in **Figure 4.23**. Voltage-clamp recordings of total $K_v$ current from Wistar neurons are provided in appendix figure 19.

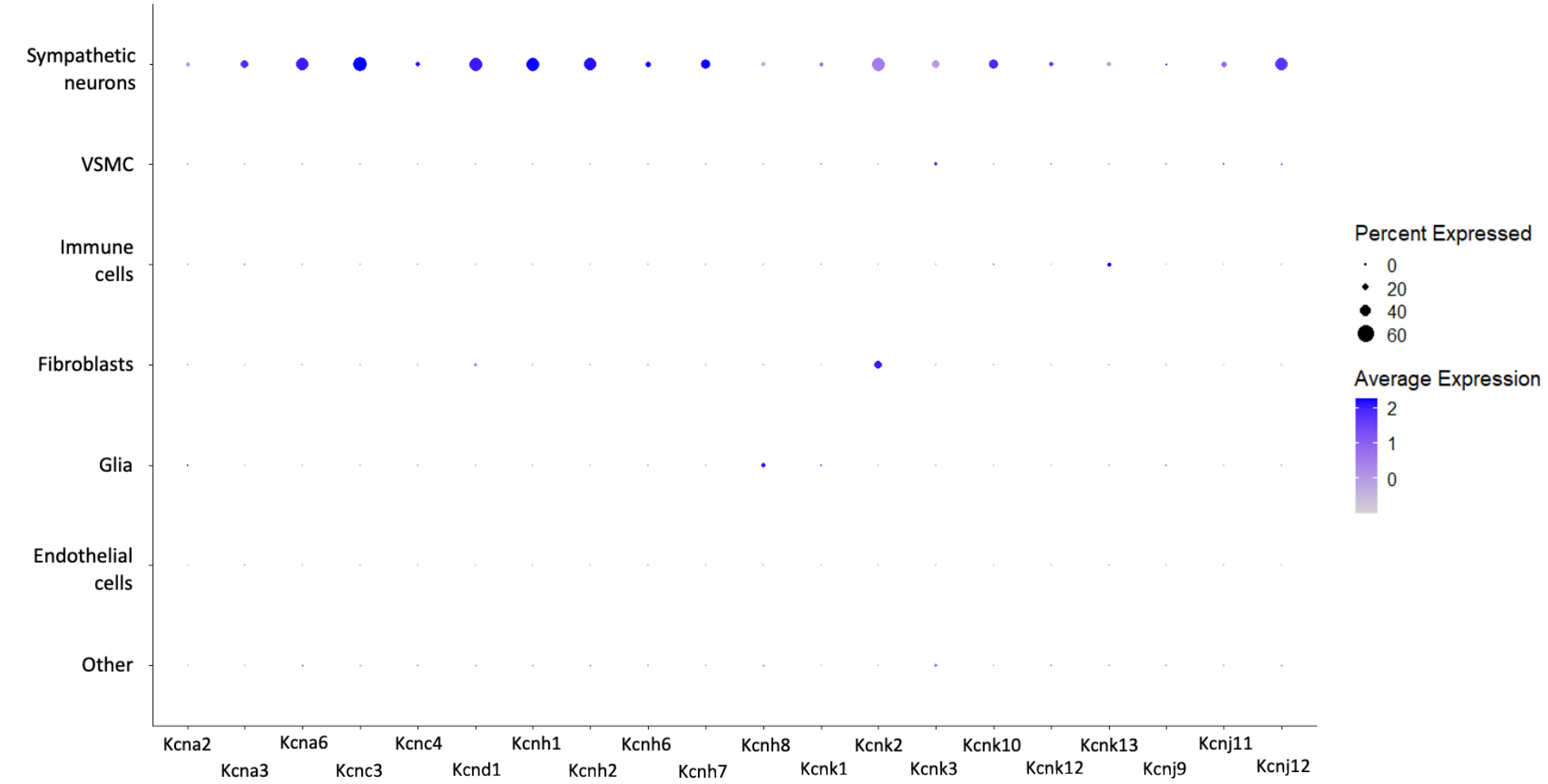



***Figure 4.23 Remaining $K_v$ channel expression for expressed subunits which are not studied in this chapter are visually represented here*** *An expression cut-off level of 0.3 Ln(Average Counts) was used. (KCNA2, $K_v$1.2; KCNA3, $K_v$1.3; KCNA6, $K_v$1.6; KCNC3, $K_v$3.3; KCNC3, $K_v$3.4; KCND1, $K_v$4.1; KCNH1, Kv10.1; KCNH2, Kv11.1; KCNH6, Kv11.2; KCNH7, Kv11.3; KCNH8, Kv12.1; KCNK1, $K_{2P}$1.1; KCNK2, $K_{2P}$2.1; KCNK3, $K_{2P}$3.1; KCNK10, TREK2; KCNK12, THIK-2; KCNK13, THIK-1; KCNJ9, $K_{ir}$3.3; KCNJ11, $K_{ir}$6.2; KCNJ12, $K_{ir}$2.2).*

## 4.4 Discussion

This chapter demonstrates that: SHR SGNs were intrinsically hyperactive in culture. This correlates with a decrease in *KCNQ5* expression and M-current density and that this phenotype was recapitulated with M-current pharmacology. In addition, $Na_v1.1$, $Na_v1.2$, $Na_v1.3$ and $Na_v1.6$, but not $Na_v1.7$ were highlighted as putative molecular targets to counter sympathetic hyperactivity. In addition, an SK channel activator may also be a valid approach. Together, these data lay a foundation for *in vivo* study of pharmacological inhibitors of sympathetic neuron hyperexcitability.

### 4.4.1 The phenotype of SHR stellate ganglia neurons

The phenotype of SHR SGNs described here using perforated patch-clamp recordings is similar to the phenotype described previously by intracellular sharp recordings made in the SCG. These recordings focused upon the prehypertensive 5-6 week age range, given prior work highlighting the postnatal expression in M-current which cease at this age range (Hadley *et al.*, 2003). This age range is comparable to the higher end of recordings made by Jubelin and Kannan (1990), where SHR SCG neurons also presented with a comparable phenotype between 2-5 weeks when recorded via intracellular recordings in culture. However, these authors only report a trend towards depolarisation in SHR neurons, report a trend towards increased rheobase, and do not explore the firing rate phenotype in SHR neurons beyond showing example traces. In this manner, the data presented here expand upon this phenotype in a more physiologically relevant ganglia, using a better controlled age-bracket, a superior electrophysiological technique and a more detailed electrophysiological comparison.

### 4.4.2 M-current as the putative mechanism for SHR hyperexcitability

The phenotype observed in the SHR fits well with the established role of M-current in determining neuronal electrophysiological properties (Brown & Adams, 1980; Brown & Passmore, 2009). As M-current is non-inactivating, and therefore partially activated at potentials similar to the RMP observed here (Wistar, -68.04±0.8123 mV; SHR, -64.97±0.7817 mV) (**Figure 4.3**), it will contribute to the RMP. Therefore, a reduction in M-current density as documented in **Figure 4.10** would also depolarise the membrane potential as observed in **Figure 4.3**. Further, the SHR phenotype involves both an increase in firing rate (**Figure 4.1**), and a loss of time resolved firing (**Figure 4.1-4.2**), which again fits with the characteristics of M-current. As M-current has relatively slow activation kinetics, this permits neuronal firing with the first few hundred milliseconds before full activation of M-current prevents further firing (Brown & Passmore, 2009). This supports my observations of changes in firing rate with M-current pharmacology in **Figures 4.12-4.13**. In addition, the rheobase was decreased in the SHR, and after M-current inhibition (**Figures 4.11-4.12**). Finally, as these data highlight a reduction in M-current density, but not a total loss of current (**Figure 4.10**), it is unsurprising that the M-current activator retigabine could still reduce neuronal excitability in SHR neurons. Overall, a downregulation of M-current appears to replicate the phenotype of intrinsic neuronal hyperexcitability observed in the SHR.

Prior studies have implicated the $K_v7$ family in animal models of hypertension, for example $K_v7.4$ was downregulated in vasculature tissue from the SHR and chronic angiotensin-II induced hypertension models (Jepps *et al.*, 2011; Chadha *et al.*, 2012). This may indicate a wider involvement of the $K_v7$ family in hypertension. Further work has established the role of sympathetic M-current in the

control of cardiomyocytes, utilising in a co-culture model of cardiomyocytes and SCG neurons, to establish that M-current activation by retigabine reduced the excitatory effect of sympathetic neuron stimulation upon cardiomyocyte beating rate (Zaika *et al.*, 2011). This study is in line with our interpretation of sympathetic M-current reducing cardiac stimulation.

Several studies have used *in vivo* methodology to study the role of M-current in Wistar-Kyoto and SHR rats (Berg, 2016, 2018). Here, the M-current activator retigabine reduced SHR heart rate and blood pressure (Berg, 2016), but did not appear to reduce catecholamine levels (Berg, 2018). Conversely, the M-current inhibitor XE-991 increased circulating catecholamines in the SHR (Berg, 2018). Of these two studies, the first suggests that XE-991 increases catecholamine release in the Wistar (Berg, 2016), whilst the second suggests a lack of effect (Berg, 2018), despite being produced by the same author. Further, somewhat surprisingly, XE-991 also decreased blood pressure and heart rate (Berg, 2016). Other authors have reported that in rats that were either normotensive or had pharmacologically induced hypertension, retigabine caused a variable change in heart rate and decreased mean arterial pressure (Fretwell & Woolard, 2013).

The Berg studies are self-contradictory and further report differing effects on heart rate to Fretwell and Woolard (2013). Based on systemic affects alone, Berg also concludes that M-current must be raised in the SHR strain (Berg, 2018), yet this would not support a phenotype of increased sympathetic activity or catecholamine release in the SHR. Additional focused *in vivo* work is required to tease apart the role of M-current in regulating SHR catecholamine release and cardiovascular parameters. *In vivo* interpretation will always be difficult as the vasculature (Jepps *et al.*, 2011; Chadha *et al.*, 2012) and arterial baroreceptors also

express $K_v7$ subunits (Wladyka *et al.*, 2008). Indeed prior work has highlighted that a significant component of vascular responses to $K_v7$ pharmacology were mediated by β-receptors, implying a role for either sympathetic M-current or vascular $K_v7.4$ in this effect (Chadha *et al.*, 2012; Fretwell & Woolard, 2013). These studies may benefit from baroreceptor de-innervation to simplify interpretation. This may reflect the limitations of measuring systemic parameters following the addition of drugs with multi-organ effects.

An early paper suggests that M-current is not implicated in the SCG neuron phenotype (Yarowsky & Weinreich, 1985). Despite the authors claims, M-current has not been adequately excluded. This early work suggests only that SHR SCG neurons can still respond to muscarine, an indirect M-current inhibitor (Yarowsky & Weinreich, 1985). From these data they conclude that M-current was not absent fin the SHR and therefore not implicated in the SHR phenotype, but they do not look for a functional or transcriptional reduction in $K_v7$ gene expression as observed here. This misunderstanding of gene expression changes as an absolute on or off process may merely reflect historic interpretations of gene expression changes, which we now know to be more subtle.

Whilst **Figure 4.10** confirmed the presence of M-current encoding transcripts in human stellate ganglia, this chapter does not provide further translational evidence for the role of M-current in human pathology. However, a recent study has highlighted that KCNQ5 activators are hypotensive (Manville et al. 2019) and have been used in plant-based traditional medicines for this purpose, suggesting a key role for this channel subunit in the maintenance of blood pressure. Additionally, SNPs in KCNQ5 (rs12195276-T) and KCNQ3 (rs138693040-T) have been associated with pulse pressure (Evangelou *et al.*, 2018) and long QT (Méndez-

Giráldez *et al.*, 2017) respectively, suggesting a role for M-current in the maintenance of human cardiovascular parameters associated with the sympathetic nervous system. Finally, in patients, the M-current activator retigabine caused hypotension and long QT syndrome (Ferron *et al.*, 2002)(EMA 2011; Procedure No: EMEA/H/C/001245) as reported side effects. The associations of M-current pharmacology and SNPs with long QT is especially pertinent given the association of cardiac arrhythmias with the sympathetic nervous system, and the lack of *KCNQ2-5* expression in the heart (Schaum *et al.*, 2018). Therefore, the cardiac effects of retigabine must be indirect as retigabine does not affect cardiac $K_v7.1$ (Schenzer *et al.*, 2005). Overall, these data highlight the possibility of sympathetic M-current controlling aspects of cardiac function.

### 4.4.3 Evidence for alternate mechanisms of SHR pathology

SK channels have been suggested as a candidate mechanism for SHR neuronal hyperactivity based upon the ability of SK inhibitor apamin to increase neuronal firing rate, but no evidence of SK channel dysfunction has so far been provided (Jubelin & Kannan, 1990). This studied found no evidence for a decrease in SK alpha or auxiliary subunit expression. Alternatively, decreased $K_{Ca}$ could result from decreased membrane $Ca^{2+}$ conductance (Marrion & Tavalin, 1998). However, prior reports have suggested an increase in the amplitude of $Ca_v$ currents (Larsen *et al.*, 2016) and intracellular $Ca^{2+}$ transients in SHR sympathetic neurons (Li *et al.*, 2012) and so this mechanism is unlikely to occur here.

Alternatively, A-type current was suggested as the molecular mechanism based upon a reported increase in A-type current density in SHR adult neurons.

Here the authors attribute the increase in SHR SCG neuron firing rate to a 6 mV depolarising shift in A-type inactivation kinetics (Robertson & Schofield, 1999). These changes were reported only in neurons from adult SHR neurons, and were not observed in neurons form the prehypertensive SHR. Notably the phenotype of increased firing occurs first in pre-hypertensive rats *in vivo* (Simms *et al.*, 2009) and *in vitro* (Jubelin & Kannan, 1990), as also reported here (**Figure 4.1-4.2**).

The authors provide voltage-clamp recordings of Wistar and SHR neuron A-type current but did not correlate the recorded changes in A-type current with the electrical excitability of the SHR neurons. Prior work in sensory neurons has demonstrated that either a hyperpolarising shift in A-type inactivation kinetics (Qian *et al.*, 2009) or a decrease in A-type current causes increases in neuronal excitability (Viatchenko-Karpinski *et al.*, 2018), and one report suggests that an increase in A-type subunit expression can be compensatory and reduces neuronal excitability in a manner reversible by A-type inhibition (Calvo *et al.*, 2016). Additionally, in SCG neurons, $K_v$4.2 or $K_v$1.5 (A-type) knockout increases the firing rate of tonic firing neurons (Malin & Nerbonne, 2000, 2001). Further, knockout of both $K_v$4.2 and $K_v$1.5 increases the ratio of both tonic and phasic 2 relative to phasic 1 (Malin & Nerbonne, 2001). It is unlikely then that an increase in A-type current would increase neuronal firing. Notably, neither *KCND2* ($K_v$4.2) nor *KCNA5* ($K_v$1.5) are expressed at observable levels in SGNs (**Figure 4.23**), and instead *KCNA3*, *KCNA6, KCNC3* and *KCND1* appear to be the major A-type subunits, providing further evidence of inter-ganglionic electrophysiological differences.

Finally, there were no SNPs or other mutations in the A-type subunits with the highest expression in SGNs, *KCNA3*, *KCNA6*, *KCNC3* and *KCND1* (**Figure 4.23**) when compared with the WKY (Gcrc/N/MCW substrains) and SHR (NHsd

substrain) genomes via Rat genome Database variant browser (Smith *et al.*, 2020). In addition, this study reports no change in A-type subunit expression in either the 5-6 week SHR via scRNAseq (**Table 4.1**), or the adult SHR via bulk RNA-sequencing (Data not shown). However, these methodologies do not exclude other mechanisms of A-type dysregulation via alternative splicing, altered auxiliary subunit binding or channel phosphorylation, and it is possible that these mechanisms may

These data together suggest that A-type is unlikely to be the causative mechanism in the prehypertensive SHR and instead could represent an attempted compensatory mechanism to reduce sympathetic neuron activity in hyperactivity associated with hypertension. This is supported by the apparent emergence of altered A-type current in older SHR animals (Robertson & Schofield, 1999).

### 4.4.4 The role of $Na_V$ subunits

Given the complexity of targeting M-current *in vivo* it was important to identify other targets to limit sympathetic hyperexcitability during hypertension. Selective inhibition of $Na_v$ family subunits has been fervent area of research for the treatment of neuropathic pain (Bennett *et al.*, 2019), however, the feasibility of these targets has not been assessed for sympathetic hyperexcitability.

The expression pattern of $Na_v$ subunits in SGNs has not been previously investigated. Like DRG neurons, *SCN9A* ($Na_v1.7$), *SCN8A* ($Na_v1.6$) and *SCN1A* ($Na_v1.1$) were expressed in SGNs. However, unlike DRG neurons, SGNs also highly expressed genes for $Na_v1.2$ *(SCN2A)* and $Na_v1.3$ (*SCN3A*) and lacked the expression of TTX-insensitive $Na_v1.8$ (*SCN10A*) and $Na_v1.9$ subunits (*SCN11A*)

(Fukuoka *et al.*, 2008; Bennett *et al.*, 2019). Of these subunits, $Na_v1.6$ (*SCN8A*) and $Na_v1.7$ (*SCN9A*) have been previously reported in SCG neurons (Toledo-Aral *et al.*, 1997; Xie *et al.*, 2015), but to my knowledge the presence of $Na_v1.1$-1.3 *(SCN1A*, *SCN2A*, *SCN3A*) in the sympathetic nervous system was previously unknown.

Based upon a combination of scRNAseq and perforated patch-clamp recordings utilising contemporary $Na_v$ pharmacology; $Na_v1.1$, $Na_v1.2$, $Na_v1.3$ and $Na_v1.6$ present as putative targets for reducing SGN firing rate, at least on a cellular level (**Figure 4.17**). The relationships between these channel subunits and neuronal firing is not a new observation, similar have been made in other neuron populations. However, the description of this subunit composition in SGNs is novel, and may help identify targets to reduce sympathetic hyperexcitability, or highlight potential sympathetic off-target effects for $Na_v$ inhibitors. Currently, non-selective block of $Na_v$ channels is utilised to counter SNA in arrythmia patients prior to surgical stellate ganglia blockade (Meng *et al.*, 2017), but a more subtle subunit selective approach may favour long-term treatment.

Interesting, selective $Na_v1.7$ inhibition did not reduce SGN firing rate (**Table 4.3**). As this was surprising, a second pharmacological inhibitor was also employed, but also had no effect. One explanation is that other $Na_v$ channel subtypes confer a functional redundancy on $Na_v1.7$. For example, the role of $Na_v1.7$ appears to be different in sympathetic neurons than DRG neurons, despite being the predominant $Na_v$ isoform in both cell types (**Figure 4.15**; Fukuoka et al. 2008). This is based upon the differing compliment of other $Na_v$ channels in both cell types. For example an inactivation impairing mutation in *SCN9A* ($Na_v1.7$) can render DRG neurons hyperexcitable, but SCG neurons hypoexcitable (Rush *et al.*, 2006). This is because

of the presence of $Na_v1.8$ in DRG neurons, which appears to be absent in SGNs (Rush et al. 2006; $Na_v1.8$ discussed in 4.4.5). It could be that the particular complement of $Na_v$ channels in SGNs can compensate for a functional loss of $Na_v1.7$ in a manner that isn't observed in the DRG, where $Na_v1.7$ knockout decreases firing rate (Habib *et al.*, 2015).

However, despite its differential role in sympathetic neurons, one would still expect $Na_v1.7$ to contribute to neuronal firing. This contradictory observation may also result from the localisation of different $Na_v$ subunits within the neuron which is extremely distinct in central neurons (Vacher *et al.*, 2008). In central neurons, $Na_v1.6$ is present in the distal axon initial segment and nodes of Ranvier and $Na_v1.1$ and $Na_v1.2$ are predominantly present in the proximal action initial segment and somata of adult neurons. As action potentials are initiated in the distal axon initial segment, $Na_v1.6$ is therefore heavily involved in action potential initiation, whereas $Na_v1.1$ and $Na_v1.2$ are involved in the backpropagation of action potentials into the somato-dendritic component. In this way the localisation as well as the kinetics and expression of the channel subunits confers alternate function. Unfortunately, with a few exceptions adult central neurons do not express $Na_v1.3$ and $Na_v1.7$, and DRG neurons have both a different channel complement (Bennett *et al.*, 2019) and a very different morphology from central and sympathetic neurons (Nascimento *et al.*, 2018). Future study looking at the sub-cellular localisation of $Na_v$ subunits in the SGN may explain these data.

The effect of riluzole was unsurprising given the role of persistent $Na_v$ current and prior reports that a riluzole sensitive persistent $Na_v$ current has previously been documented in SCG neurons (Lamas *et al.*, 2009), however it was worth confirming in SGNs as a general mechanism of $Na_v$ inhibition.

Several $Na_v$ encoding genes were downregulated at a transcript level in SHR neurons (**Figure 4.15**), which appears to have little effect on action potential kinetics (**Figure 4.16**). In addition, the SHR has a higher firing rate despite the reduction in $Na_V$ transcript expression, which is relatively surprising given that pharmacological inhibition of several of these subunits individually, or a general reduction in $I_{Na}$ current had a profound effect upon SHR neuron firing rate (**Figure 4.17**). There are several explanations for this difference. Firstly, there may be some functional redundancy in terms of $Na_v$ current in SHR neurons, allowing a slight reduction of $Na_v$ current without a reduction in action potential firing or an alteration in action potential kinetics, followed by a reduction in firing rate with greater inhibition. Alternatively, these changes in $Na_v$ expression may not reflect changes in $Na_v$ protein expression or function. Whilst this may merit further study, this does not appear to have a net effect on SHR function, and so in the interest of time alongside financial and animal costs these experiments were not performed here.

### 4.4.5 Stellate ganglia neuron $Na_v1.8$?

Previous research suggested that $Na_v1.8$ was present in SGNs (Yu *et al.*, 2017), however they did not provide molecular evidence and are instead reliant upon the selectivity of the $Na_v1.8$ inhibitor A-803467 (Jarvis *et al.*, 2007). The presence of $Na_v1.8$ in sympathetic neurons would be interesting for two reasons, firstly, it may present as a druggable target in SGNs, secondly, SNPs in *SCN10A* ($Na_v1.8$) are associated with PR interval lengths (Macri *et al.*, 2018).

It is hotly disputed whether the cardiac $Na_v1.8$ or intracardiac neuron $Na_v1.8$ are responsible for the role of $Na_v1.8$ in determining cardiac parameters. Conflicting

reports have suggested either a presence or absence *SCN10A* ($Na_v1.8$) expression in homogenised human and animal heart tissue or cardiomyocytes (Chambers *et al.*, 2010; Stroud *et al.*, 2016; Casini *et al.*, 2019), which has been further confused by contradictory reports of *SCN10A* ($Na_v1.8$) expression in either intracardiac neurons (Verkerk *et al.*, 2012; Qi *et al.*, 2014; Chen *et al.*, 2016) or cardiomyocytes (Yang *et al.*, 2012; Macri *et al.*, 2018; Casini *et al.*, 2019).

Given this controversary, the presence of $Na_v1.8$ in SGNs would provide an interesting alternate route for a cardiac role of $Na_v1.8$. However, whilst $Na_v1.8$ inhibitors A-803467 and A-887826 reduced SGN firing, this was not replicated via alternate $Na_v1.8$ inhibitor PF-04885614. Further, there was no observable expression of *SCN10A* by scRNAseq or RT-qPCR, and very low expression of *SCN10A* by bulk RNA-sequencing. This is likely attributable to misplaced reads, a known issue with sequencing alignment (Conesa *et al.*, 2016). Finally, there was no TTX-insensitive $Na_v$ current in SGNs (Appendix figure 19), which excludes functional *SCN10A* expression. Despite the prior claims of the selectivity for A-803467 and A-887826, it seems highly likely that this compound is acting upon an off-target ion channel. This is in line with prior *in vivo* observations, where it was reported that A-803467 had an effect in spindle fibers which lack $Na_v1.8$ (Stone *et al.*, 2013) and observations that A-803467 can also inhibit $Ca_v3.2$ *in vitro* (Bladen & Zamponi, 2012).

These observations have wider implications, as the majority of papers studying $Na_v1.8$ rely upon the selectivity of A-803467 (Yang *et al.*, 2012; Qi *et al.*, 2014; Chen *et al.*, 2016; Yu *et al.*, 2017; Casini *et al.*, 2019). Further, this confirms that the changes in cardiac conduction following $Na_v1.8$ mutation or knockout are

not due to changes in sympathetic $I_{Na}$ and that $Na_v1.8$ is not a valid target for reducing SGN activity.

### 4.4.6 Other channels in the stellate ganglia

Alongside these observations there were several interesting finds relating to other channel types. Whilst my own studies rely upon SHR neurons, the following subunits were not differentially expressed in the SHR, allowing for a wider discussion of their functional role in the rat.

*Calcium-activated chloride channels*

Prior studies have suggested that CaCC currents contribute to SCG neuron firing rate (De Castro *et al.*, 1997; Martínez-Pinna *et al.*, 2000; Martinez-Pinna *et al.*, 2018), however, CaCC transcripts were not expressed in SGNs and CaCCs did not appear to contribute to SGN firing rate (**Figure 4.21**; **Table 4.3**).

Previously *ANO1* expression was observed in homogenised whole SCG (Martinez-Pinna *et al.*, 2018), however, *ANO1* expression was absent in SGNs and instead expressed only in stellate ganglia vascular smooth muscle cells. This expression pattern is unsurprising, as *ANO1* is known to be expressed in vascular smooth muscle (Manoury *et al.*, 2010) and sympathetic ganglia are known to be heavily vascularised (Chungcharoen *et al.*, 1952). These observations may explain the appearance of *ANO1* transcripts in homogenised SCG tissue and the limitations of homogenised tissue should be considered for future studies of sympathetic ganglia.

The relatively non-selective inhibitor 9-AC was used to assess CaCC function in the SCG (De Castro *et al.*, 1997; Sacchi *et al.*, 2003; Martinez-Pinna *et al.*, 2018), however, 9-AC also inhibits non-CaCC $Cl^-$ channels and transporters. Instead, as ANO1 was suggested as the putative SCG neuron CaCC channel (Martinez-Pinna *et al.*, 2018), the ANO1 selective inhibitor, Ani-9, was used here instead (Seo *et al.*, 2016), which had no effect upon SGN firing rate (**Table 4.3**).

An 9-AC-sensitive $Cl^-$ current was reported in voltage-clamp recordings of SCG neurons, although $Ca^{2+}$ dependence was not established (Sacchi *et al.*, 1999). The described current had fast activation and inactivation kinetics, which are unlike the slower activation and limited inactivation described for heterologously expressed CaCCs (Schroeder *et al.*, 2008). Notably, there was no other CaCC encoding genes (*BEST1-4; ANO1-2; CALCA1-4*) were expressed by scRNAseq.

It was also suggested that SCG neurons exhibit a small (1.2mV) afterdepolarisation following tetanic stimulation (Martinez-Pinna *et al.*, 2018). These are attributed to excitatory $Cl^-$ currents resulting from a relatively positive $Cl^-$ Nernst potential in sympathetic neurons (Adams & Brown, 1975). This chapter does not exclude the presence of an afterdepolarisation in SGNs; however, based upon the expression data and firing rate data, any contribution by ANO1 seems unlikely.

Notably, previous work on SCG CaCCs utilised intracellular recordings (Martinez-Pinna *et al.*, 2018) which better maintains physiological intracellular [$Cl^-$] than the amphotericin perforated patch-clamp methodology used here. However, whilst intracellular [$Cl^-$] will be dialysed here, potentially altering the direction of $Cl^-$ conductance, a robust ANO1 current would still be expected to influence neuronal firing.

In conclusion, *ANO1* transcripts or Ani-9 function were not observed in SGNs. However, further work is warranted on both SCG and SGNs to study alternative $Cl^-$ currents. If *ANO1* mediated CaCC currents are present in SCG neurons, then this may suggest divergent channel expression between these ganglia.

*$K_v$2 delayed rectifier current*

The data presented in **Figure 4.21** suggest an alternate function for SGN $K_v2$, relative to in the SCG. Here an increase in SHR neuron firing rate was observed following $K_v2$ family inhibition, however, prior work demonstrated that inhibition of $K_v2$ in sympathetic SCG neurons and hippocampal neurons decreased neuronal firing (Liu & Bean, 2014). The authors speculate that this results from depolarised inter-spike membrane potentials which limit the recovery of $Na_v$ channels from inactivation. Perhaps, there is a redundancy in SGN $Na_v$ currents, or inter-spike potentials that prevented this effect here.

In SGNs, *KCNB1* ($K_v2.1$), but not $K_v2.2$ (**Figure 4.20**), were expressed. However, in SCG neurons knockout of either $K_v2.1$ or $K_v2.2$ or both subunits reduced the number of tonic firing neurons (Malin & Nerbonne, 2002). Which suggests a contribution of both subunits to SCG neuron electrophysiology, perhaps suggesting an alternate expression pattern between these ganglia.

*BK channels*

The BK channel inhibitor, Iberiotoxin, widened SHR neurons action potentials (**Figure 4.22**), but had no effect upon firing rate. This is in line with prior reports of the role for BK channels (Kimm *et al.*, 2015*b*), and a wider action potential is expected to result in a larger $Ca^{2+}$ current (Chao & Yang, 2019).

*KCNMB4* which encodes the BK channel $\beta_4$-subunit, was upregulated in neuron population 2 (*NPY* high, *CHRM2* high) relative to neuron population 1 (*NPY* low, *CHRM2* low). This subunit alters BK channel kinetics and calcium dependence (Brenner *et al.*, 2000), but also confers resistance to inhibition by iberiotoxin (Meera *et al.*, 2000). These data would suggest a greater resistance to iberiotoxin inhibition in NPY positive neurons, which may have had a population specific effect here. Whilst, the data from **Figure 4.22** are from the SHR, they suggest that a difference in BK channel current could lead to an altered action potential waveform in neuron population 2 (*NPY* high, *CHRM2* high). However, a NPY dependent difference in action potential width was not observed in the SCG, although NPY positive neurons had an altered afterpotential hyperpolarisation (Li & Horn, 2008). Further investigation is needed to resolve the points discussed here.

*HCN Channels*

Inhibition of HCN channels did not affect neuronal firing rate in SGNs (**Table 4.3**), rheobase, input resistance or membrane potential (Data not shown) despite transcript expression of HCN1-4 in SGNs (**Figure 4.20**). Further, there was no observable HCN current in whole-cell voltage-clamp recordings of Wistar SGNs (Appendix Figure 18) and very little SAG current (Data not shown, but visible in

**figure 4.4**). Whilst the role of HCN channels in neuronal excitability varies based upon subcellular localisation and the presence of other local ion channel populations (Meuth *et al.,* 2006; George *et al.*, 2009; Huang *et al.*, 2011), it was unexpected that inhibition of HCN using either inhibitor would have no effect upon SHR function.

SGNs appear to predominantly express HCN3 and HCN4 transcripts (**Figure 4.20**). However, HCN1 and HCN2 are the predominant isoforms in whole SCG lysates (Kullmann *et al.*, 2016). In the dorsal root ganglia, a peripheral neuron population where HCN channels are better studied, HCN1 and HCN2 are predominant in large diameter neurons, HCN3 in small diameter neurons (Kouranova *et al.*, 2008), with only a small subpopulation expressing HCN4 (Cho *et al.*, 2009). Similarly, HCN2 appears to be the major HCN isoform in most central neurons, followed by HCN1, alongside low-level HCN3 expression and localised HCN4 expression (Moosmang *et al.*, 1999; Notomi *et al.,* 2004). It could be that this unique expression profile of HCN subunits in SGNs also suggests an atypical role for HCN channels in these cells.

It is also possible that HCN expression in SGNs is specific to a non-somatic compartment and had little effect upon somatic HCN recordings. However, this is in contraction with a prior report form the SCG, where HCN currents were recorded via somatic perforated patch-clamp recordings (Kullmann *et al.*, 2016).

*Slack Channels*

Transcript expression of the $K_{Na}$ subunit slack (*KCNT1*) (Kaczmarek, 2013) was detected in SGNs (**Figure 4.20**). Due to the lack of selective pharmacological inhibitors of $K_{Na}$, slack function was assessed by substituting $Li^+$ for $Na^+$. $Li^+$ is conducted by $Na_v$ channels, but is a limited activator of $K_{Na}$ channels (Safronov & Vogel, 1996; Bischoff *et al.*, 1998). This methodology altered firing rate in slack expressing rat motorneurons (Safronov & Vogel, 1996), but did not affect firing rate here. It is possible that slack channels could instead have a more subtle electrophysiological role or form heterodimers with BK subunits produce $K_{Ca}$ currents (Joiner *et al.*, 1998).

### 4.4.7 The stellate ganglia neuron

Previous comparative studies have reported electrophysiological differences between sympathetic ganglia (Wang & McKinnon, 1995; Jobling & Gibbins, 1999), however they did not assess the electrophysiology of SGNs. Based upon my recordings all 3 firing subtypes, phasic 1, phasic 2 and tonic, are present in the stellate ganglia (including 19.7% tonic neurons), however SCG neurons lack a tonic firing phenotype, and the coeliac (~58%) and superior mesenteric (~85%) ganglia have a higher proportion of tonic neurons (Wang & McKinnon, 1995) than reported here in Wistar SGNs (19.7%; **Figure 4.2**).

Wistar SGNs had a middling input resistance (218.2 MΩ) in comparison to recordings from SCG (Mouse 109.7 MΩ, 75-85 MΩ; Rat 389.9, 125.6-143.1 MΩ) neurons, but a higher input resistance in comparison to the thoracic (Mouse 117.9 MΩ) and coeliac (Mouse 161.9 MΩ; Guinea pig 116.9 MΩ) ganglia (Jobling &

Gibbins, 1999; Lamas *et al.*, 2002; Li & Horn, 2008; Martinez-Pinna *et al.*, 2018). Notably intracellular sharp recordings reduce the observed input resistance to a greater degree than patch-clamp recordings, and this may explain the lower values observed by these methods (Li *et al.*, 2004).

In addition these data suggest a more hyperpolarised membrane potential (−68.04 mV) than the majority of recordings from the SCG (Mouse SCG −49.9 mV, −54 mV; Rat SCG −58.3 mV, -54 to -55.2 mV) (Jobling & Gibbins, 1999; Martínez-Pinna *et al.*, 2000; Lamas *et al.*, 2002; Li & Horn, 2008). As an explanation for this discrepancy, previous reports comparing whole patch-clamp and intracellular recordings suggest patch-clamp recordings achieve more hyperpolarised, and more physiological recordings (Li *et al.*, 2004).

Additionally, it is useful to compare these data with a prior intracellular sharp recording of SGNs from the Wistar rat (Mo *et al.*, 1994). In line with my own observations, they report the presence of both tonic and phasic neurons. These authors report a lower input resistance (76-120 MΩ) and more depolarised membrane potential (-58.9 to -60.3 mV) than reported here (218.2 MΩ and −68.04 mV respectively). However, both of these differences are likely attributable to the inferiority of intracellular sharp recordings (Li *et al.*, 2004). Interestingly the authors also report much larger capacitance values (110-121 pF) than reported here (Wistar, 28.05±1 pF; SHR, 27.23±1.56 pF). This may result from SGNs being larger *in situ* than in culture. This effect would be amplified in the low laminin conditions used in my neuronal culture, which has been shown to limit neurite outgrowth (Buettner & Pittman, 1991).

### 4.4.8 Do these data fit with the human hypertensive phenotype?

Does this phenotype fit with observations in patients? Based upon single-unit microneurography measurements, the majority of single sympathetic fibres tend to fire only once per cardiac interval in a healthy patient without sympathetic activity due to the relatively short burst duration of sympathetic stimulation, although a small percentage fire more (Macefield *et al.*, 2002). However, in essential hypertension, there is a demonstrated increase in single-unit and multi-unit SNA which correlates with the severity of the hypertension (Greenwood *et al.*, 1999). This study fits well with the data presented here, as the described phenotype and mechanism correlates well with increase single-unit activity. It would be interesting to observe whether single-unit or multi-unit activity was altered by M-current pharmacology.

### 4.4.9 SNPs in the SHR

Whilst scRNAseq provides a strong hypothesis generator, it is limited in several ways. One of these is that whilst changes in expression can be detected, coverage is not generally high enough to detect SNPs in the genes studied. The rat genome database variant visualiser was used to exclude SNPs in key ion channel genes that were expressed in SGNs (**Figure 4.20** and **Figure 4.23**) (Smith *et al.*, 2020). However, for the sake of completeness it is worth briefly discussing several other ion channel SNPs that have been identified in the SHR. There is an SNP in *KCNJ1* and a frameshift *CACNA1A* (P/Q) in the SHR (Atanur *et al.*, 2010), but neither genes are expressed in the SGN. In addition multiple SNPs in *CACNA1D* ($Ca_v1.3$) were identified previously (Atanur *et al.*, 2010), but are unlikely to be involved in the phenotype present here, although this may be associated with the

increased $Ca_v$ current observed in SHR neurons (Larsen *et al.*, 2016). Overall, it is unlikely that any of these previously identified SNPs will contribute to the SHR SGN phenotype described here.

### 4.4.10 Study limitations

There are several key limitations to this study: the limitations of ion channel pharmacology; the preparation used; the reliance upon sequencing and the SHR model of hypertension. These points will be addressed here.

It is possible that the hypertensive phenotype changes during the process of culturing. However, intracellular sharp recordings from the SCG highlight that a hyperactive phenotype is present *in situ* (Yarowsky & Weinreich, 1985), and prior studies have shown a phenotype of sympathetic hyperactivity *in vivo* (Thoren & Ricksten, 1979). Further, supporting data were obtained from homogenised whole ganglia via RT-qPCR and bulk RNA-sequencing, and scRNAseq was performed on freshly dissociated cells, so these experiments were not subject to culture conditions. Working in culture also has its advantages, patch-clamp in sympathetic ganglia is difficult due to the fibrous tissue surrounding the ganglia and would dramatically increase the financial and animal cost due to the limited number of recordings per animal. Further, freshly dissociated neurons do not have a do not have a mature electrophysiological phenotype (Blaine & Ribera, 2001), in part due to the harsh enzymatic dissociation protocol. Finally, my data shows that the firing rate phenotype does not change during the five-day period following dissociation (**Figure 4.5**) suggesting that culture presents at minimum a stable cell population.

Recordings would have benefited from physiological recording temperatures, due to the reliance of ion channel kinetics upon temperature (Sterratt, 2014). However, SGNs died shortly after entering whole-cell or following perforation at temperatures greater than 30$^{o}$C, and so room temperature was utilised instead.

Observations from the SHR do not necessarily represent the human phenotype. To confirm translatability of this study, a well-controlled comparison between human hypertensive tissue and normotensive controls would have proved useful. Unfortunately, for the tissue used in this study, both the “control” donors and “diseased” patients often exhibitedconfounding cardiovascular symptoms that may influence the transcriptome of the stellate ganglia. This issue was further exacerbated by the difficultly of obtaining a patient cohort who underwent stellectomy for a single pathology. Therefore the “diseased” patients used here represent a cohort of mixed diseases involving dysautonomia (Liu *et al.*, 2018). For these reasons a direct comparison has not been performed, and this tissue was instead used here to demonstrate the presence of M-current subunits in human tissue.

Additionally, alternate animal models of hypertension would have provided additional confirmation of these results. However, due to financial and time constraints, study was restricted to the SHR, which remains the gold-standard of hypertension models (Lerman *et al.*, 2019). Finally, it would have also been interesting to observe if the molecular mechanism described here correlates with increased sympathetic activity in animal models of alternate diseases involving dysautonomia such as heart failure (Cohn *et al.*, 1984), acute myocardial infarction (Graham *et al.*, 2002) and arrythmia (Meredith *et al.*, 1991).

These data rely heavily upon ion channel pharmacology, which although rapidly improving, is relatively poor. A few examples of this are addressed and examined here. Apamin, whilst a relatively selective inhibitor of $K_{Ca}2.2$-2.3 channels, has only a weak effect on $K_{Ca}2.1$ (D'hoedt et al. 2004). However, $K_{Ca}2.1$ does not appear to be expressed in SGNs (**Figure 4.20**), and so the use of apamin was justified here. 10 µM Riluzole also activates SK2 (Cao *et al.*, 2002), SK3 and IK channels (Beltran-Parrazal & Charles, 2003; Liu *et al.*, 2013). 3 µM and 10 µM Riluzole effected SHR firing in this study, and so the effect of SK channel activation should be considered given its role in SHR firing (**Figure 4.21**). However, a $Na_P$ mediated effect upon neuronal firing is not controversial, and there is no reason to suspect that these effects are mediated by other channels.

Unfortunately, the proportion of M-current pharmacologically inhibited by 3 µM XE-991 and 30 µM Linopirdine is likely greater than the decrease in current density observed in the SHR model. However, this would be time consuming, difficult to achieve, and would not representative of a $K_V7.5$ specific reduction in M-current. Instead these data demonstrated that M-current inhibition can cause a similar phenotype to that described in the SHR.

### 4.4.11 Further work

Due to time constraints, this study did not characterise all the electrophysiological differences between Wistar and SHR neurons. For example, this project did not assess the contribution of the $K_{2P}$ family (Gada & Plant, 2019)

which remains uncharacterised in these neurons. Nor did this study, assess the contribution of inwardly rectifying channels (Murata *et al.*, 2016) such as $K_{ATP}$ which has been shown to contribute to sympathetic control of the heart (Mohan & Paterson, 2000). A-type current was not studied here, as it has already been observed to be unaltered in SHR SCG neurons at this age point (Robertson & Schofield, 1999). Additionally, these data would have benefitted from voltage-clamp recordings of major $K_v$ and $Na_v$ current components, to assess whether these currents are altered in pathology. Finally, it would have been prudent to use the SK activator, as 1-ethyl-2-benzimidazolinone (EBIO) (Devor *et al.*, 1996) on SHR neurons, to assess whether this mechanism was a feasible candidate for reducing SHR activity, as has been demonstrated for other neuron types (Pedarzani et al. 2001).

*In vivo* study is an important follow-up to this work; however, it presents a complicated picture. Not only is M-current expressed in sympathetic neurons, sensory neurons, the vasculature and baroreceptors, which all have an involvement in the wider control of blood pressure, but $K_v7.1$ is also expressed in the heart (Bendahhou *et al.*, 2005). Whilst $K_v7.1$ does not produce M-current, it instead conducts cardiac $I_{KS}$ in association with KCNE1 (Also known as minK) (Sanguinetti *et al.*, 1996). $K_v7.1$ can be effect by M-current pharmacology, such as by the M-current inhibitor XE-991 which has weaker but relevant effect upon KCNQ1-KCNE1 complexes (Wang *et al.*, 2000). Studies would therefore benefit from sympathetic neuron specific knockout of $K_v7$ subunits to permit further study, as suggested may also benefit from baroreceptor de-innervation to remove cardiovascular reflexes.

Dynamic clamp would provide an interesting dataset in support of this study which was independent of ion channel pharmacology (Sharp *et al.*, 1992). The

availability of this technique has been improved by the release of build-your-own dynamic clamp amplifiers (Desai *et al.*, 2017), however, it remains a highly specialised technique.

Finally, whilst a molecular mechanism has been provided for neuronal hyperexcitability, these data do not provide evidence for the mechanism underlying the change in *KCNQ5* expression. The discovery of this mechanism would be of fundamental importance to the understanding of sympathetic neuron hyperactivity in hypertension, however this work is beyond the scale of this project. It is possible that this hyperexcitability emerges from a physiological mechanism such as ganglionic long-term potentiation, which has been reported to occur in the SHR (Alkadhi *et al.*, 2001; Martínez *et al.*, 2019) or from otherwise altered input from preganglionic neurons (Magee & Schofield, 1994; Briant *et al.*, 2014). It would be interesting to observe whether the phenotype and M-current downregulation translate to other ganglia such as the coeliac ganglia as this would determine whether M-current downregulation was a global or stellate ganglia-specific mechanism. Further work is required to investigate these points.

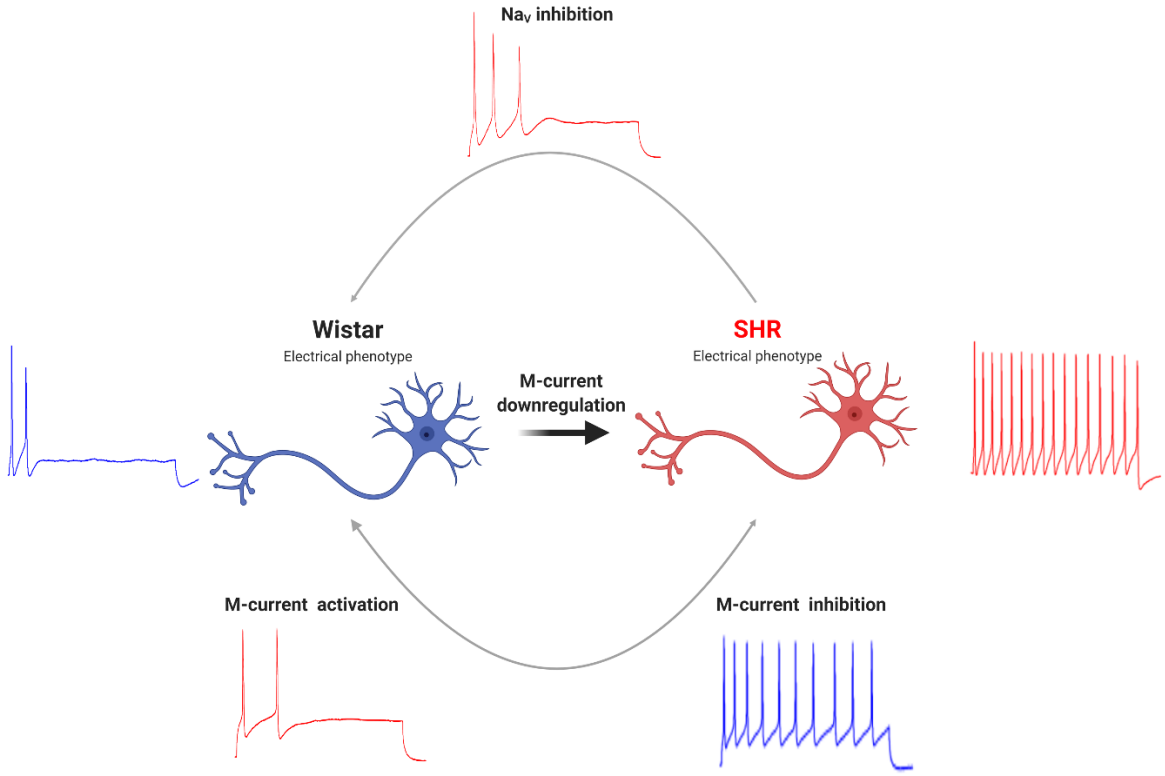



***Figure 4.24 Concluding schematic showing the major findings of this work*** *This project highlighted a downregulation in M-current in the SHR which correlates with an increase in neuronal firing, membrane depolarisation and decreased rheobase. This phenotype can be reversed by M-current activation via retigabine or recapitulated by M-current inhibition in Wistar neurons. A secondary mechanism of reducing this aberrant activity was highlighted via selective inhibition of $Na_V1.1$, $Na_V1.2$, $Na_V1.3$, $Na_V1.6$ or $Na_P$.*

# Chapter 5

## Sodium Sensing in stellate ganglia neurons

## 5.1 Introduction

The association between high blood pressure and dietary salt intake has long been known (Luft *et al.*, 1979), but the exact mechanisms underlying the association are poorly understood. Numerous reports suggest that SNS activity increases in response to elevated serum NaCl concentration in both rodent models (Nomura *et al.*, 2019) and patients (Farquhar *et al.*, 2006), and that this can play a causative role in the development of hypertension (Gomes *et al.*, 2017; Nomura *et al.*, 2019). Indeed, extended periods of elevated dietary sodium can produce a long-lasting sympathetically mediated hypertension in rats (Nomura *et al.*, 2019), which remains after cessation of a high sodium diet (Gomes *et al.*, 2017). This chapter considered a direct role of sympathetic neurons as peripheral $Na^+$ sensors.

### 5.1.1 NaCl sensing – $Na^+$ or osmolarity?

Increased blood pressure can be induced by two general systemic mechanisms following an elevation in NaCl. The first is an osmolarity-dependent increase in midbrain secretion of arginine vasopressin (AVP) (Verney, 1947; Rosenberg & Robertson, 1987; Oliet & Bourque, 1993; Naeini *et al.*, 2006), which appears to be mediated by TRPV1 (Naeini *et al.*, 2006). The second is a $Na^+$-dependent increase in sympathetic activity (Kinsman *et al.*, 2017*b*, 2017*a*; Nomura *et al.*, 2019). It should be noted that, whilst this duality is generally accepted, a contrary report suggests sympathetic and blood pressure changes are also osmolarity-dependent (Antunes *et al.*, 2006). As this is controversial, for the purpose of this chapter the consensus will be taken instead.

AVP (also known as anti-diuretic hormone) is a circulating hormone and neurotransmitter released from magnocellular neurons in the hypothalamic

paraventricular and supraoptic nuclei via the posterior pituitary (Rotondo *et al.*, 2016). Circulating AVP increases blood pressure by increasing water reabsorption in the collecting ducts of the kidneys through $V_2$ mediated aquaporin-II membrane translocation and increasing peripheral vascular resistance through vasoconstriction of arterioles via $V_1$ receptors (Rotondo *et al.*, 2016).

Prior work has highlighted that AVP is involved in the systemic response to high NaCl. Intravenous (IV) delivery of AVP elicits a small effect on blood pressure, without sympathetic activation (Ribeiro *et al.*, 2015) and this pressor response is considerably larger if AVP is delivered directly to the paraventricular nucleus (PVN), and is thought to be activated by a sympathetic and catecholaminergic $\alpha_1$ receptor dependent mechanism (Ribeiro *et al.*, 2015). However, pharmacological inhibition of AVP receptors had no effect on increases in sympathetic activity following high NaCl, and only a minuscule effect on blood pressure (Nomura *et al.*, 2019). Therefore, increased arterial blood pressure and SNA is largely $Na^+$ dependent (Kinsman *et al.*, 2017*a*).

### 5.1.2 Central mechanisms of $Na^+$ sensing

Overwhelmingly, the effect of NaCl elevation has been studied from the perspective of the circumventricular organs. The circumventricular organs, are brain regions which lack a blood brain barrier and are therefore uniquely poised to sense changes in blood constituents (McKinley *et al.*, 2003). To this end extensive *in vivo* study has interrogated the systemic response to isolated central NaCl elevation, with somewhat contradictory results (**Table 5.1**). As the response to central and systemic elevations of NaCl are reliant upon the action of the SNS (Nomura *et al.*,

2019), they are subject to peripheral reflexes such as the baroreflex and renorenal reflex (Morita *et al.*, 1991) and this may explain these discrepancies.

Of the circumventricular organs, the organum vasculosum of the lamina terminalis (OVLT) and the subfornical organ (SFO) are believed to play a critical role in $Na^+$ sensing. Following raised $Na^+$ these nuclei can centrally activate the SNS via descending pathways to the PVN, a major centre for sympathetic control (Coote, 2005). Of these nuclei, the OVLT appears to be the most important region for the central blood pressure response to intracerebroventricular (ICV) NaCl (Nomura *et al.*, 2019), with the SFO primarily involved in regulation of dietary $Na^+$ uptake (Hiyama *et al.*, 2004) and both the OVLT and SFO regulating thirst (Matsuda *et al.*, 2017).

Whilst these studies provide ample evidence for central mechanisms, they fail to exclude additional peripheral mechanisms. This is further compounded by their reliance upon non-physiological mechanisms of central NaCl elevation rather than simply increasing systemic NaCl as would be observed physiologically (**Table 5.1**). As the contemporary narrative has focussed upon central control, little work (**Table 5.2**) has assessed the role of peripheral centres.

***Table 5.1 Summary of the systemic effects observed following elevations of central NaCl*** *Here N/A indicates that this parameter was not measured. ICV refers to intracerebroventricular injection. AV3V refers to Anteroventral third ventricular region*
** (Following sinoaortic denervation).*

| SPECIES | DELIVERY METHOD | CARDIAC SNA | LUMBAR SNA | RENAL SNA | HEART RATE | BLOOD PRESSURE | CITATION |
|---|---|---|---|---|---|---|---|
| **RAT** | ICV | N/A | **Increase** | **Decrease** | **No change** | **Increase** | (Kinsman *et al.*, 2017*b*) |
| **SHEEP** | Intracarotid | **No change** | N/A | **Decrease** | **No change** | **Increase** | (Frithiof *et al.*, 2014) |
| **MOUSE** | ICV | N/A | **Increase** | N/A | N/A | **Increase** | (Nomura *et al.*, 2019) |
| **RAT** | Internal carotid | N/A | N/A | **Transient increase** | **No change** | N/A | (Shi *et al.*, 2007) |
| **RAT** | Internal carotid | N/A | N/A | **Increase** | N/A | **Increase** | (Shi *et al.*, 2008) |
| **RAT** | Intravenous | N/A | **Increase** | **Decrease** | **No change*** | **Increase** | (Weiss *et al.*, 1996) |
| **SHEEP** | ICV | **Increase** | N/A | N/A | **No change** | **Increase** | (Watson *et al.*, 2004) |
| **SHEEP** | ICV | N/A | N/A | **Decrease** | **No change** | **Increase** | (May *et al.*, 2000) |
| **MICE** | Chronic ICV | N/A | N/A | N/A | **Increase** | **Increase** | (van Huysse *et al.*, 2011) |
| **RAT** | ICV | **No change** | **Increase** | **Decrease** | **Increase** | **Increase** | (Kinsman *et al.*, 2017*a*) |
| **RAT** | Intracarotid | N/A | **Increase** | N/A | **No change** | **Increase** | (Kinsman *et al.*, 2017*a*) |
| **RAT** | OLVT microinjection | **Increase (Splanchnic)** | **Increase** | **No change** | **Increase** | **Increase** | (Kinsman *et al.*, 2017*a*) |
| **RAT** | Jugular | N/A | N/A | N/A | **No change** | **Increase** | (Garcia-Estañ *et al.*, 1989) |
| **RAT** | AV3V microinjection | N/A | N/A | **Decrease** | **Decrease** | N/A | (Bealer *et al.*, 1996) |
| **RAT** | Intracarotid | N/A | N/A | **Increase*** | **No change*** | **Increase*** | (Chen & Toney, 2001) |

***Table 5.2 Summary of the systemic effects observed following elevations of serum NaCl*** *Here N/A indicates that this parameter was not measured.*

** (Following sinoaortic denervation).*

*** (Inhibitable by ganglionic blockade)*

| SPECIES | DELIVERY METHOD | CARDIAC SNA | LUMBAR SNA | RENAL SNA | HEART RATE | BLOOD PRESSURE | CITATION |
|---|---|---|---|---|---|---|---|
| **MOUSE** | Intraperitoneal | N/A | N/A | N/A | N/A | **Increase **** | (Nomura *et al.*, 2019) |
| **RAT** | Dietary | N/A | N/A | N/A | N/A | **Increase** | (Walkowska *et al.*, 2015) |
| **RAT** | Dietary | N/A | N/A | N/A | **No change** | **Increase** | (Gomes *et al.*, 2017) |
| **RAT** | Dietary | N/A | N/A | N/A | **Increase** | **Increase** | (Zhu et al., 2004) |
| **RAT** | Intravenous | N/A | N/A | **Decrease** | **Increase** | **Increase** | (Badoer *et al.*, 2003) |
| **RAT** | Dietary | N/A | N/A | N/A | **Decrease** | **No change** | (Pawloski-Dahm & Gordon, 1993) |
| **RAT** | Dietary | N/A | N/A | **Decrease*** | **No change*** | **Increase*** | (Morita *et al.*, 1991) |

### 5.1.3 $Na_x$ - the molecular sodium sensor

The systemic response to elevated $Na^+$ is known to be mediated by a specialised sodium channel, $Na_X$ (also known as $Na_v2.1$, $Na_v2.2$, NaG) encoded by the gene *SCN7A* (George *et al.*, 1992; Hiyama *et al.*, 2002). Indeed, global knockout of *SCN7A* has been shown to abolish both the blood pressure and sympathetic response to elevated dietary and IV NaCl (Nomura *et al.*, 2019). $Na_X$, is extremely unique in that it does not exhibit voltage-dependence and is instead regulated by elevated extracellular $Na^+$ concentration $[Na^+]$ (Hiyama *et al.*, 2002). The $[Na^+]_o$ threshold for $Na_X$ activation is approximately 150 mM after which the channel conducts a relatively selective sodium current with linear activation kinetics (Hiyama *et al.*, 2002). Plasma and central NaCl concentrations above 160 mM have been reported experimentally in wildtype mice (Nomura *et al.*, 2019), suggesting that this channel can be activated under physiological conditions. Finally, in patients several

*SCN7A* SNPs are strongly associated with essential hypertension (Zhang *et al.*, 2015). In combination, these data suggest that $Na_X$ is the primary systemic mechanism for sodium sensitivity.

$Na_x$ is highly expressed in the SFO and OVLT, where it is critical to central $Na^+$ sensing. $Na_x$ in the SFO has been implicated in the control of salt appetite (Matsuda *et al.*, 2017), whereas $Na_x$ in the OVLT appears to involved in the indirect regulation sympathetic outflow (Nomura *et al.*, 2019). Two opposing arguments exist for the sodium sensitivity in the OVLT, one via astrocytic $Na_x$ $Na^+$ sensing (Nomura *et al.*, 2019) or alternatively via OVLT neuron $Na_x$ direct $Na^+$ sensing (Kinsman *et al.*, 2017*b*). Currently some speculation has been placed on additional peripheral or central mechanisms of sodium sensitivity (Nomura *et al.*, 2019; Guyenet, 2019), and it is notable that work on $Na_x$ knockouts has so far focussed upon central responses to ICV NaCl (Nomura *et al.*, 2019), rather than the more physiological serum changes.

### 5.1.4 Renal NaCl response

A prime candidate for a potential peripheral $Na^+$ sensor is the kidney, given its role in renal afferent sympathetic control, RAAS pressor pathway activation and natriuresis (Wadei & Textor, 2012). Here the evidence for a renal role in NaCl mediated blood pressure increases is reviewed.

First, renal denervation did not prevent NaCl induced blood pressure changes in rats (Becker *et al.*, 2017), suggesting that renal afferents do not play an active role in blood pressure changes following increased serum NaCl. In addition, in rats extended periods of elevated dietary $Na^+$ do not appear to cause renal

inflammation (Gomes *et al.*, 2017) or alter renal vascular reactivity (Walkowska *et al.*, 2015), suggesting renal function is not impaired with elevated serum $Na^+$ concentration. This excludes the genesis of NaCl induced hypertension from renal damage.

Secondly, the renin-angiotensin-aldosterone system (RAAS), is the classical systemic blood pressure regulator, and unsurprisingly, RAAS also has a role in the systemic response to NaCl. However, renin synthesis and release is decreased following elevations in NaCl uptake (Kjolby & Bie, 2008; Damkjær *et al.*, 2013; Isaksson *et al.*, 2014) and thus RAAS activity is reduced under these conditions (Schweda, 2015). As RAAS generally has a pressor, and anti-natriuretic effect, a reduction in RAAS activity would be hypotensive (Romero *et al.*, 2015). Therefore, the RAAS axis does not prevent or contribute to the systemic response to increased NaCl.

Finally, *SCN7A* is expressed (Lara *et al.*, 2012) in the kidney, but its role in renal function is poorly understood. Notably, increased protein and transcript expression in the renal medulla follow elevated levels of circulating serum $Na^+$ concentration, implying a relationship with serum $Na^+$ (Lara *et al.*, 2012). However, *SCN7A* knockout does not appear to alter circulating $Na^+$ (Nomura *et al.*, 2019), implying that $Na_X$ has limited involvement in natriuresis. It seems unlikely then that renal $Na_X$ contributes to the phenotype in this manner.

### 5.1.5 Sympathetic $Na_x$?

Both CSF and serum NaCl increase in response to high NaCl (Kawano *et al.*, 1992; Nomura *et al.*, 2019), yet no current study has assessed the response of sympathetic neurons themselves to NaCl, or the role of $Na_x$ in these neurons. The increase in blood pressure following increased systemic or central NaCl, is almost entirely eliminated following ganglionic blockade of the SNS (Nomura *et al.*, 2019). Further, NET activity and TH expression (Habecker *et al.*, 2003; Kreusser *et al.*, 2014) are decreased in response to high NaCl suggesting a link between extracellular NaCl and the sympathetic neuron itself. This mechanism would provide a simple and physiologically intuitive sensor for systemic $Na^+$ sensing to complement central mechanisms. This study utilised scRNAseq, whole cell patch-clamp, calcium imaging, sodium imaging and immunohistochemistry to highlight the role of $Na_x$ in sympathetic neurons, and their potential role in systemic sodium signalling.

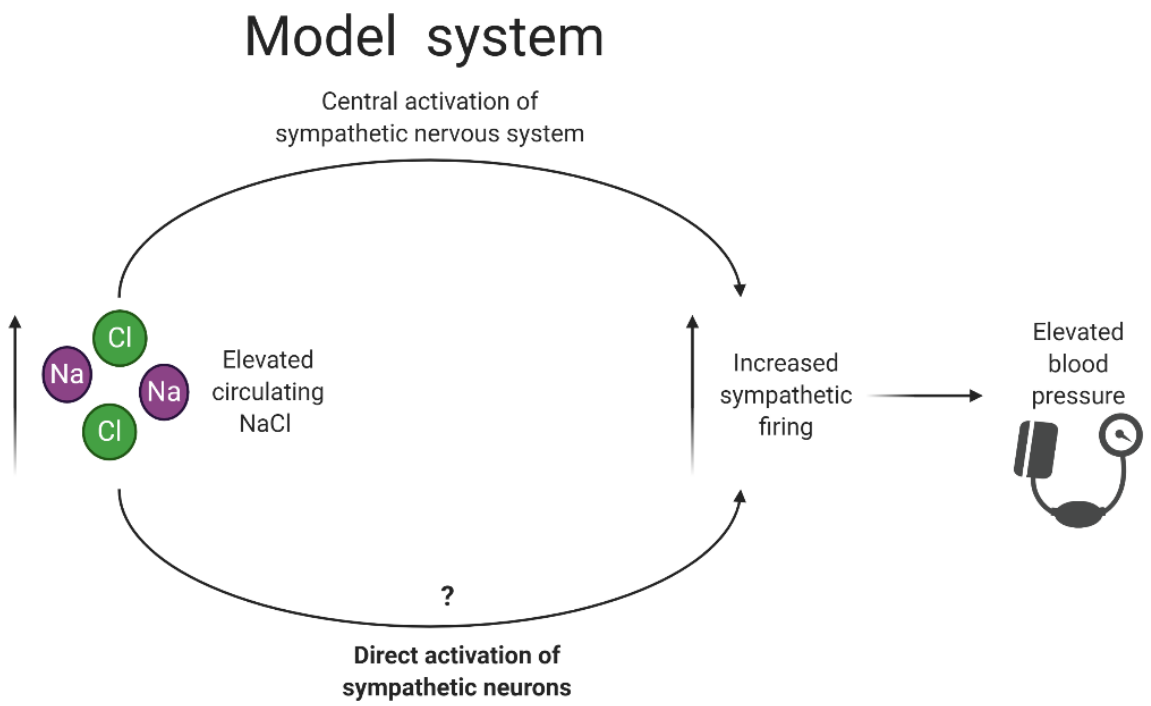



***Figure 5.1 A basic schematic for the hypothesis of this chapter*** *It is already established that central responses to NaCl can elicit a sympathetically mediated increase in blood pressure. However, the contribution of peripheral centres has not been investigated, and research has instead focussed heavily upon artificial methods of directly elevating central nervous system NaCl concentrations. This chapter proposes that sympathetic neurons may additionally be activated by increases in serum NaCl.*

## 5.2 Methods

### 5.2.1 Cell culture and long-term ion adjustments

SCG and superior mesenteric/coeliac ganglia were cultured as previously described for SGNs (Chapter 2)**.** For experiments using a protocol involving extended exposure to high NaCl concentrations, neurobasal media (Thermofisher, US) as ion concentrations were publicly available for this media. For adjustment of ion concentrations 5 M NaCl and 1 M KCl stock solutions were prepared and sterile filtered. For both control and KCl depolarising block experiments, culture media NaCl was adjusted to 140 mM. For KCl depolarising block, KCl was adjusted by 20

mM. For NaCl depolarisation, NaCl was adjusted to 170 mM. Where stated, 2 μM TTX was added directly to the culture media in a similar manner. Following a 24 to 36-hour incubation with the adjusted culture media, neurons were washed for 10 minutes in a standard external recording solution as outlined previously.

### 5.2.2 Whole-cell patch-clamp electrophysiology

Whole-cell patch-clamp recordings were performed as described previously within chapter 2. Drugs, hyperosmotic or hyponatraemic solutions were applied for three minutes before recording firing rate changes. Where applicable drugs were added for a minimum of three minutes prior to the addition of 170 mM NaCl and paired comparisons were made between drug-treated cells and drug-treated cells in 170mM NaCl. Recordings with $R_s$ values above 20 MΩ were discarded. Recordings were not adjusted for the approximately 2-3 mM additional $Na^+$ resulting from pH adjustment with NaOH.

### 5.2.3 Immunohistochemistry

SGNs were dissociated and cultured as outlined previously (Chapter 2). Cells were co-labelled with rabbit anti-SCN7A and sheep anti-TH primary antibodies for a period of an hour at 37$^o$C. Cells were washed three times in PBS. Cells were co-labelled with rabbit anti-SCN7A and sheep anti-TH primary antibodies for a period of an hour at 37$^o$C. Anti-sheep Alexa Flour 488 and anti-rabbit Alexa flour 594 were used as secondary antibodies. Cells were washed three times in PBS. Cells were counterstained Hoescht 33342 stain for one minute. Cells were washed three times

in PBS. Images were acquired at 40x magnification on an inverted Nikon microscope.

### 5.2.4 Fura-2 Imaging

Fura-2 imaging was used to measure changes in $[Ca^{2+}]_i$ as described in chapter 2.

### 5.2.5 Statistics

Firing rate data were treated as non-parametric as explained in chapter 2. For other data, normality was tested as described in the chapter 2, and if the data was found to be normally distributed then parametric statistics were used.

## 5.3 Results

### 5.3.1 NaCl response in sympathetic neurons

Initial experiments focussed upon the effect of elevated NaCl upon sympathetic neurons isolated from a range of sympathetic ganglia; the stellate ganglia, which primarily innervates the heart and vasculature, the SCG, which innervates substructures within the head, including local vascular systems, the carotid body and the thyroid gland; and the combined superior mesenteric and coeliac ganglia, which innervate the kidneys, large intestine and bladder amongst other local tissues (Bankenahally & Krovvidi, 2016).

Neurons from all three ganglia exhibited electrophysiological responses to a 30 mM increase to extracellular NaCl from 140 mM to 170 mM (**Figures 5.1-5.3**), however the nature of this response differs in some respects. In the stellate ganglia and superior mesenteric/coeliac ganglia, neurons both depolarised and had increased firing rates. For the stellate ganglia, neurons depolarised by 4.07±0.75 mV (Mean±SEM of differences) and maximum firing rate increased from 3 Hz to 7 Hz (Median) (**Figure 5.1**), whilst superior mesenteric/coeliac ganglia neurons depolarised by 4.72±1.5 mV and firing increased from 3.5 Hz to 10.5 Hz (**Figure 5.2**). In the SCG, a neuronal depolarisation of 3.68±0.78 mV was observed, but without a significant change in neuronal firing (**Figure 5.3**).

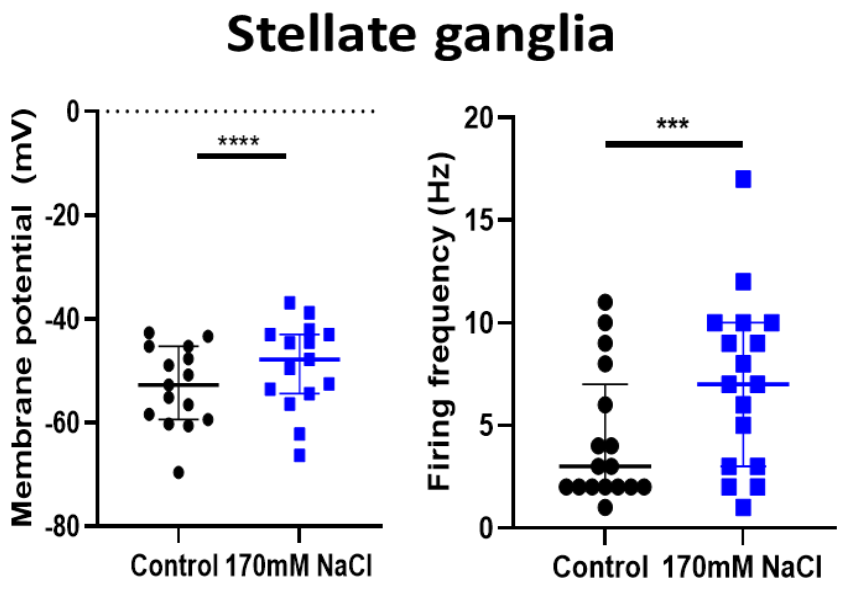



***Figure 5.2 The addition of 170 mM NaCl significantly depolarised cultured stellate ganglia neurons and caused an increase in maximum induced firing.*** *170 mM NaCl induced stellate ganglia neuron membrane depolarisation (n=15; Paired t-test; p<0.0001) (Left) and increased neuron firing (n=17; Wilcoxon test; p=0.0009) (Right). Here n refers to cell number, where a culture n of 3 was used, with each culture using a minimum of 2 animals.*

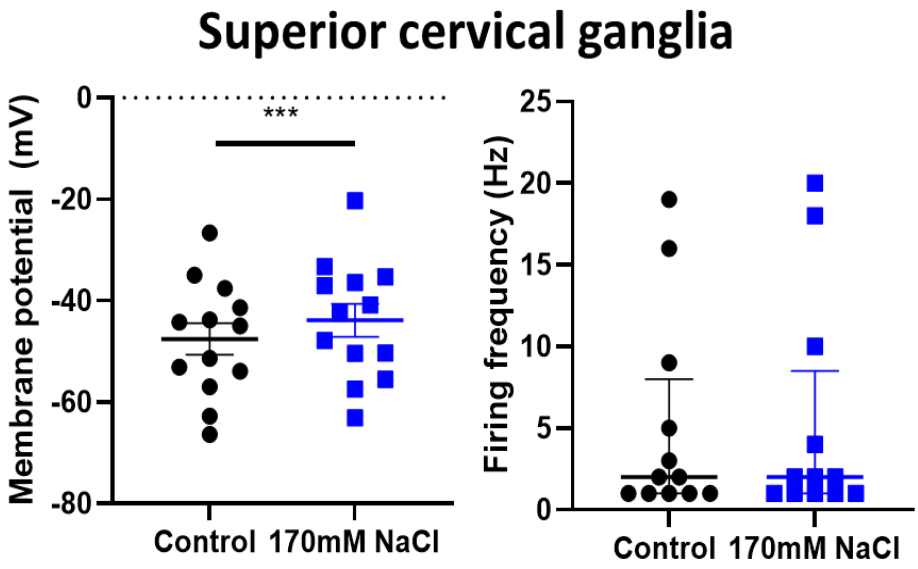



***Figure 5.3 The addition of 170 mM NaCl significantly depolarised cultured superior cervical ganglia neurons and caused an increase in maximum induced firing.*** *170 mM NaCl induced superior cervical ganglia neuron membrane depolarisation (n=13; Paired t-test; p=0.0005) but did not increase neuron firing (n=12; Wilcoxon test; p=0.48) (Right). Here n refers to cell number, where a culture n of 2 was used, with each culture using a minimum of 2 animals.*

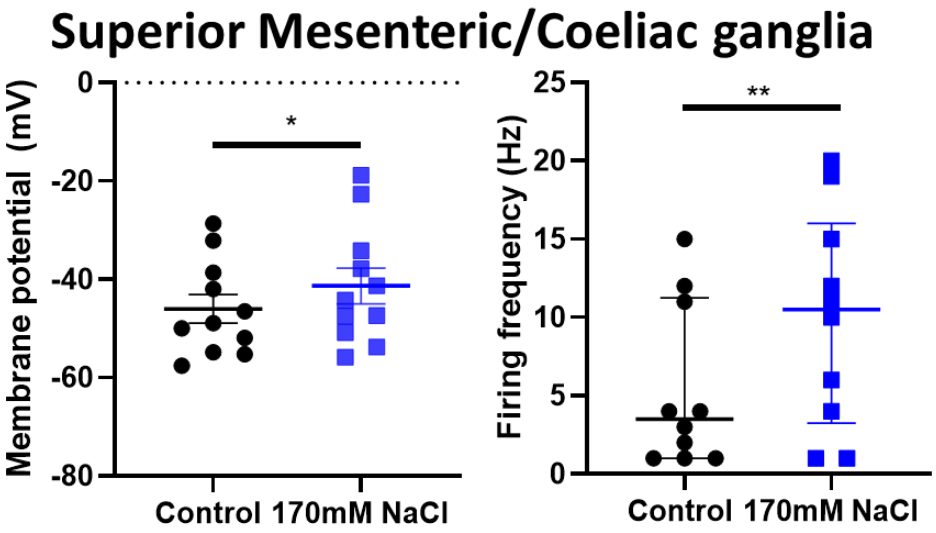



***Figure 5.4 The addition of 170 mM NaCl significantly depolarised cultured superior mesenteric/coeliac ganglia neurons and caused an increase in maximum induced firing.*** *170 mM NaCl induced superior mesenteric/coeliac ganglia neuron membrane depolarisation (n=11; Paired t-test; p=0.01) (Left) and increased neuron firing (n=10; Wilcoxon test; p=0.008) (Right). The superior mesenteric/coeliac ganglia were kindly dissected by Oliver Neely. Here n refers to cell number, where a culture n of 2 was used, with each culture using a minimum of 2 animals.*

SGNs were used for further experiments for three primary reasons: the strong response of SGNs to 170 mM NaCl (**Figure 5.1**), the known phenotype of elevated cardiac sympathetic activity in response to elevated plasma $Na^+$ *in vivo* (**Table 5.1**), and better established protocols for the isolation and culturing SGNs relative to superior mesenteric/coeliac neurons.

It was hypothesised that if the response to NaCl were physiological, then it was likely to be dose dependent and to test this, the membrane potential and firing rate responses to a range of NaCl concentrations (150-200 mM) were recorded in separate populations of neurons (**Figures 5.5-5.6**). SGNs exhibit a dose-dependent membrane depolarisation across the 150-200 mM range of extracellular NaCl,

which appears to saturate between 170-200 mM (**Figure 5.4**). Dose-dependence was found to be significant by a Welch's ANOVA test ($p<0.0001$).

Changes in intracellular or extracellular $Na^+$ and $Cl^-$ concentrations can innately affect the membrane potential as previously outlined. To assess whether changes in NaCl caused a biophysical, rather than physiological alteration in membrane potential, resulting differences in membrane potential expected through altering the Goldman-Hodgkin-Katz equation were calculated and are shown in **figure 5.4**. The calculated depolarisation was both linear and much smaller than the recorded response over the 150-200 mM range. The increase in firing rate elicited by NaCl was also found to be dose dependent within the 150 mM to 200 mM range, where dose-dependence was significant by a Welch's ANOVA test ($p=0.0128$).

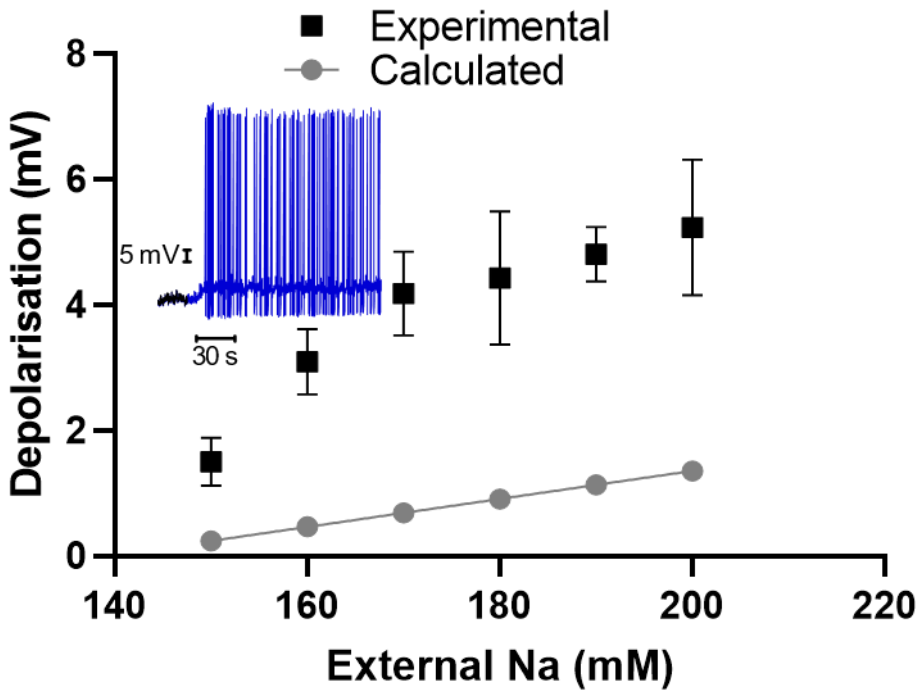



***Figure 5.5 The effect of NaCl on stellate ganglia neuron membrane potential (Black) is dose dependent between the concentration ranges 150mM-200mM and has a greater than that predicted by the Goldman-Hodgkin-Katz equation (grey)*** *Inset data trace shows membrane depolarisation and resulting spontaneous firing following 170 mM NaCl (Blue) relative to 140 mM NaCl (Black) (n=12-22). Here n refers to cell number, where a minimum culture n of 2 was used, with each culture using a minimum of 2 animals.*

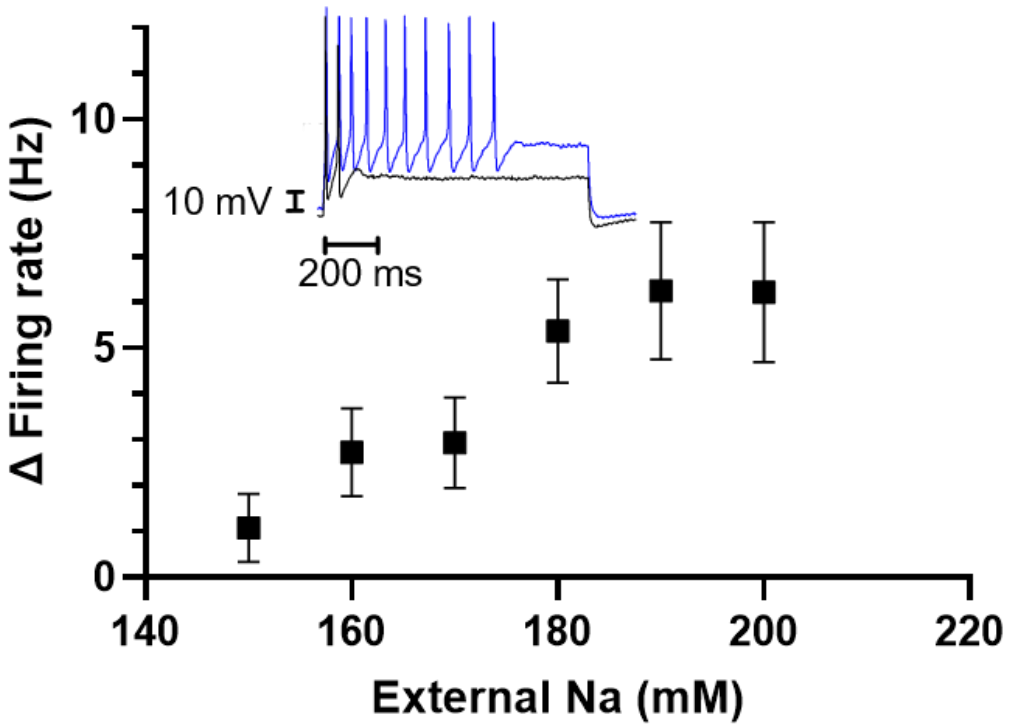



***Figure 5.6 Elevated sodium caused a dose-dependent increase in maximum stellate ganglia neuronal firing rate*** *The increase in firing rate following an increase in extracellular Na is shown as Mean ± SEM (n=8-18). The inset trace shows the evoked response of a stellate ganglia neuron to 150 pA current injection before and after treatment with 170 mM NaCl. The black trace represents a recording at 140mM NaCl, the blue trace is following 170mM NaCl.* Here n refers to cell number, where a minimum culture n of 2 was used, with each culture using a minimum of 2 animals.

### 5.3.2 $Na^+$ dependence

Whilst a direct effect of NaCl upon sympathetic neurons has been demonstrated in **figures 5.1-5.5**, these data do not differentiate between the effect of elevated exogenous $Cl^-$ or $Na^+$, which are both increased during the addition of NaCl. To isolate the effect of $Na^+$, Na-acetate was used to raise extracellular $Na^+$. **Figure 5.6** demonstrates the effect of adding 30 mM Na-acetate, raising external $Na^+$ to 170 mM. Under these conditions, raised $Na^+$ also induced a membrane depolarisation of 2.78±0.75 mV and increased neuronal firing from 1 Hz to 3 Hz.

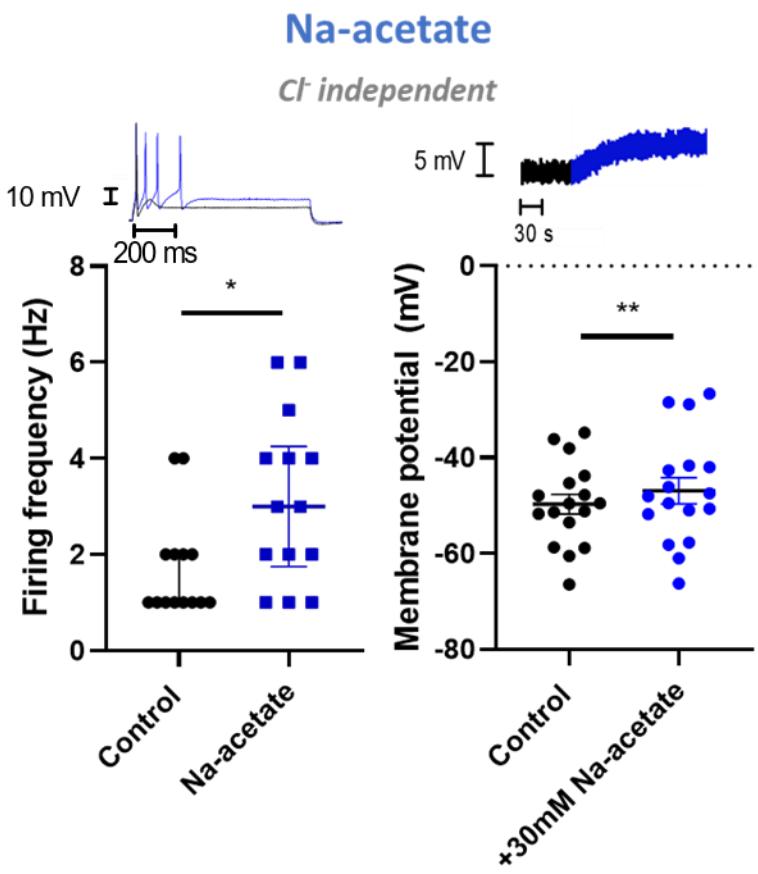



***Figure 5.7 Na-acetate also caused membrane depolarisation and increased maximum firing in stellate ganglia neurons*** *The response was not $Cl^-$ dependent as 30 mM Na-acetate increased stellate ganglia neuron firing rate (n = 14; Wilcoxon test; p = 0.02) and also depolarised the membrane potential (n = 17;Paired t-test ; p = 0.002). Firing rate is shown before (black) and after (blue) 30 mM Na-actetate (Left trace). Membrane depolarisation is shown following 170 mM NaCl. Here n refers to cell number, where a culture n of 3 was used, with each culture using a minimum of 2 animals.*

### 5.3.3 $Na_x$ in stellate ganglia neurons

Based upon the $Na^+$ dependence of the NaCl induced effects, the presence of $Na_x$ was assessed in SGNs. First, these data highlight neuron specific $Na_x$ (*SCN7A*) (Hiyama *et al.*, 2002) transcript expression using scRNAseq (**Figure 5.7**). The expression level for *SCN7A* was found to be comparable to ion channel subunit encoding genes, which are also shown in **Figure 5.7**. This observation was then reinforced by resolving protein level expression of $Na_x$ through

immunohistochemistry (**Figure 5.8**), where $Na_x$ protein was observed to be expressed in *TH* positive neurons.

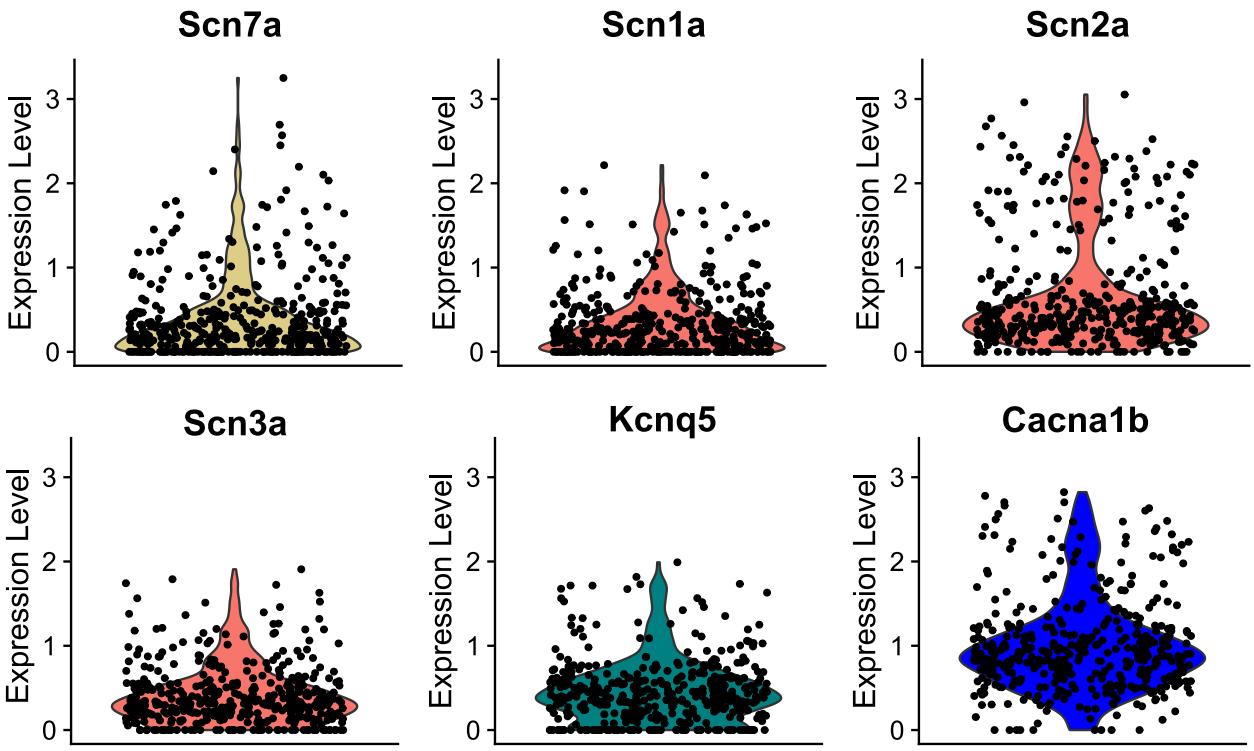



***Figure 5.8 Single-cell RNA-sequencing analysis highlights SCN7A in sympathetic neurons*** *$Na_x$ encoding gene SCN7A (Yellow) was found to be expressed at a transcript level in the sympathetic neuron population highlighted in chapter 2. These data are shown against expression of $Na_v$ encoding genes, SCN1A SCN2A and SCN3A (Red) alongside $K_v$ subunit KCNQ5 (Green) and $Ca_v$ subunit CACNA1B (Blue). Here expression level indicates normalised count data. Here the count data per cell is divided by the total number of counts within that cell, times by a scale factor and then natural-log transformed.*

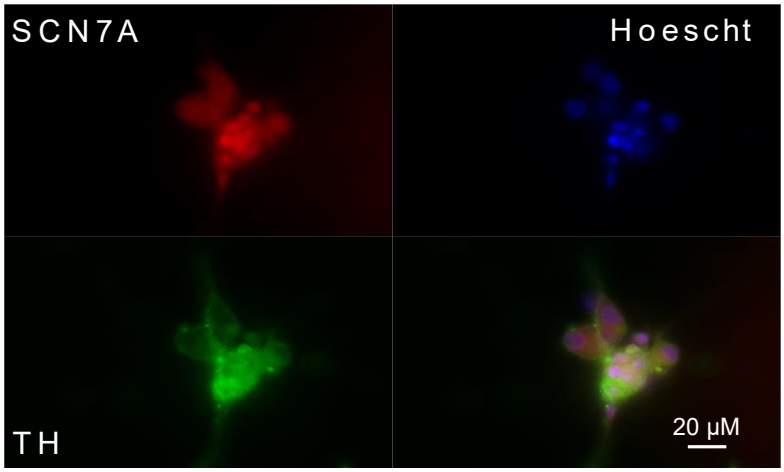



***Figure 5.9 Immunohistochemistry highlights expression of SCN7A ($Na_x$) in TH positive sympathetic neurons*** *Cultured neurons were stained for the sympathetic marker TH (Bottom left), alongside the target of interest SCN7A ($Na_x$) (Top left).The nuclear stain, Hoescht 33342 was used to highlight all cells present (Top right). In the bottom right, all three channels are combined to highlight SCN7A ($Na_x$) expression in TH positive sympathetic neurons.*

### 5.3.4 Exclusion of other $Na^+$ dependent mechanisms

Unfortunately, no selective inhibitors of $Na_x$ are commercially available. This project therefore focussed on excluding other potential mechanisms by which $Na^+$ may cause membrane depolarisation and increased neuronal firing to isolate $Na_x$. First, the contribution of $Na^+$ selective channels and transporters was assessed, namely $Na_v$, $Na^+/K^+$ ATPase and epithelial sodium channels (ENaCs).

**Figure 4.20** highlights the absence of TTX-insensitive $Na_v$ subunits expressed in the SGN, allowing for the use of TTX in these neurons as a global $Na_v$ inhibitor. 1 µM TTX was found to have no effect upon neuronal depolarisation within 150-200 mM NaCl (Two-way Anova; p=0.42) (**Figure 5.9**), firing rate could not be tested under these conditions due to TTX preventing neuronal firing.

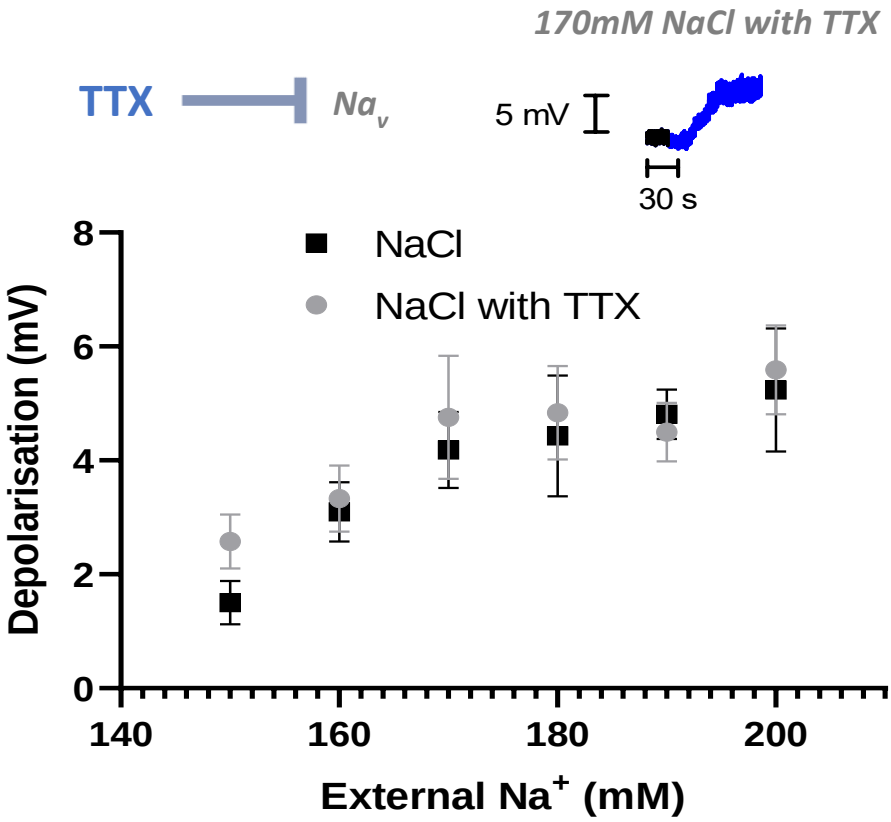



***Figure 5.10 TTX had no effect upon membrane depolarisation induced by 150-200 mM NaCl in stellate ganglia neurons*** *There was no significant difference between membrane depolarisation induced by NaCl in the presence or absence of 1 µM TTX. For raw data trace, physiological extracellular $Na^+$ shown in black and 170 mM NaCl with TTX is shown in blue (Control, n=15-22; 1 µM TTX, n=7-13). Here n refers to cell number, where a minimum culture n of 2 was used, with each culture using a minimum of 2 animals.*

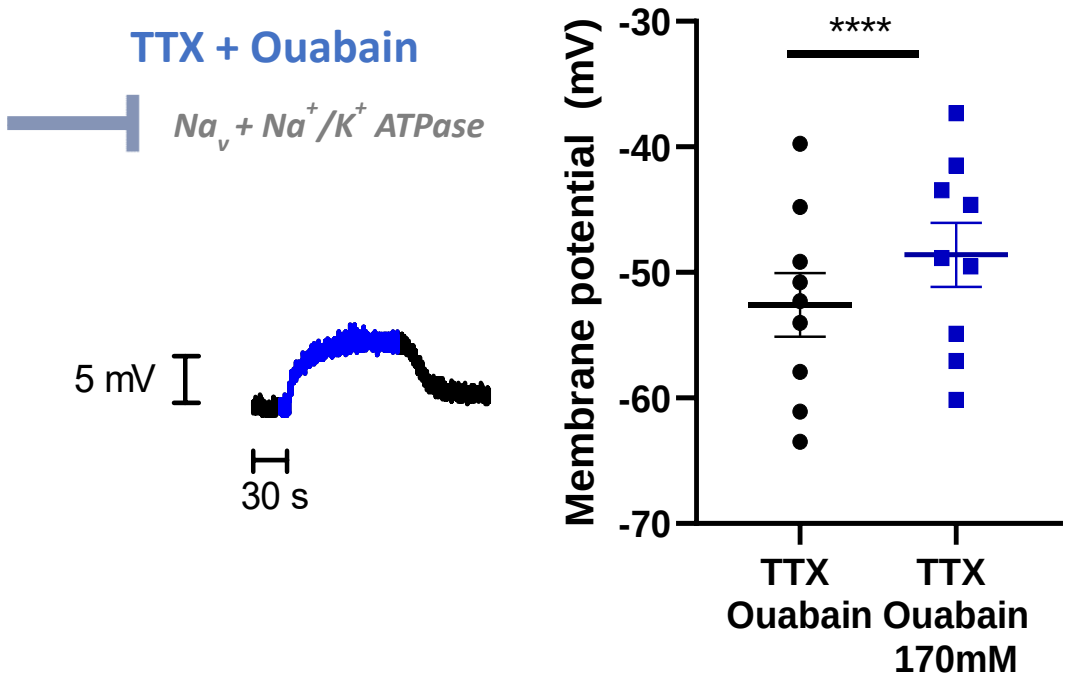



***Figure 5.11 TTX and ouabain did not prevent 170 mM NaCl induced depolarisation*** *170 mM NaCl caused a significant depolarisation of sympathetic neurons in the presence of both 1 µM TTX and 100 µM Ouabain relative to 1 µM TTX and Ouabain alone (n=9; Paired t-test; p<0.0001). On the raw data trace, baseline and washout are shown in black, 170mM NaCl is shown in blue. Here n refers to cell number, where a culture n of 2 was used, with each culture using a minimum of 2 animals.*

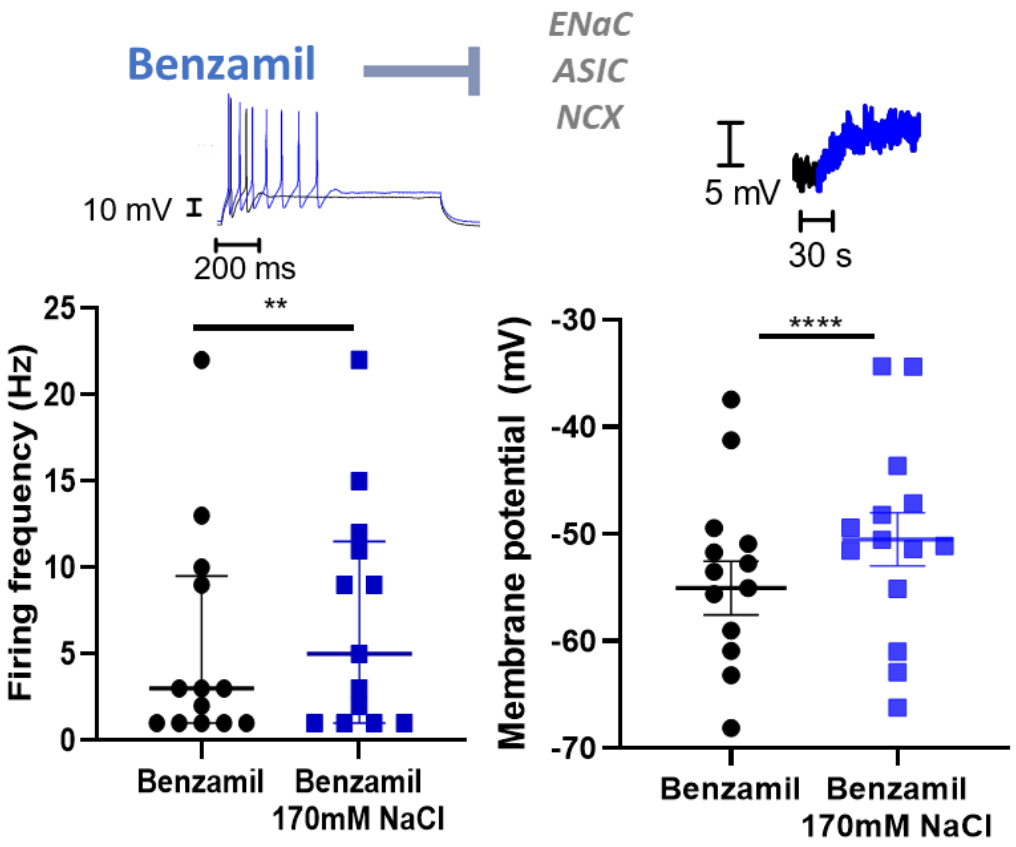



***Figure 5.12 1 µM Benzamil does not prevent NaCl induced firing rate increases or membrane depolarisation in stellate ganglia neurons*** *In the presence of 1 µM Benzamil 170 mM NaCl still increased maximum firing rate (n=13; Wilcoxon test; p=0.0078) and depolarised neuronal membrane potentials (n=14; Paired t-test; p<0.0001). For the raw data trace, 1 µM Benzamil with a physiological extracellular sodium concentration is shown in black, and 1 µM Benzamil with 170 mM NaCl is shown in blue. Here n refers to cell number, where a culture n of 2 was used, with each culture using a minimum of 2 animals.*

Next the effect of Na/K-ATPase inhibitor Ouabain (Schatzmann & Räss, 1965) on NaCl induced depolarisation was tested in the presence of 1 µM TTX. Ouabain/TTX did not prevent 170 mM NaCl induced SGN depolarisation (3.989±0.48 mV).

ENaC, Na-Calcium exchanger (NCX) and acid-sensing ion channel (ASIC) inhibitors 1 µM Amiloride and 1 µM Benzamil (Teiwes & Toto, 2007; Wang *et al.*, 2008; Leng *et al.*, 2016) also did not prevent the depolarising and excitatory effects

of 170 mM NaCl. When added alongside 1 µM Amiloride, 170 mM NaCl elicited a 3.56±0.33 mV depolarisation and increased neuronal firing 4 Hz to 7 Hz. Similarly, 170 mM NaCl in the presence of 1 µM Benzamil evoked a 4.55±0.55 mV depolarisation, increased neuronal firing from 3 Hz to 5 Hz.

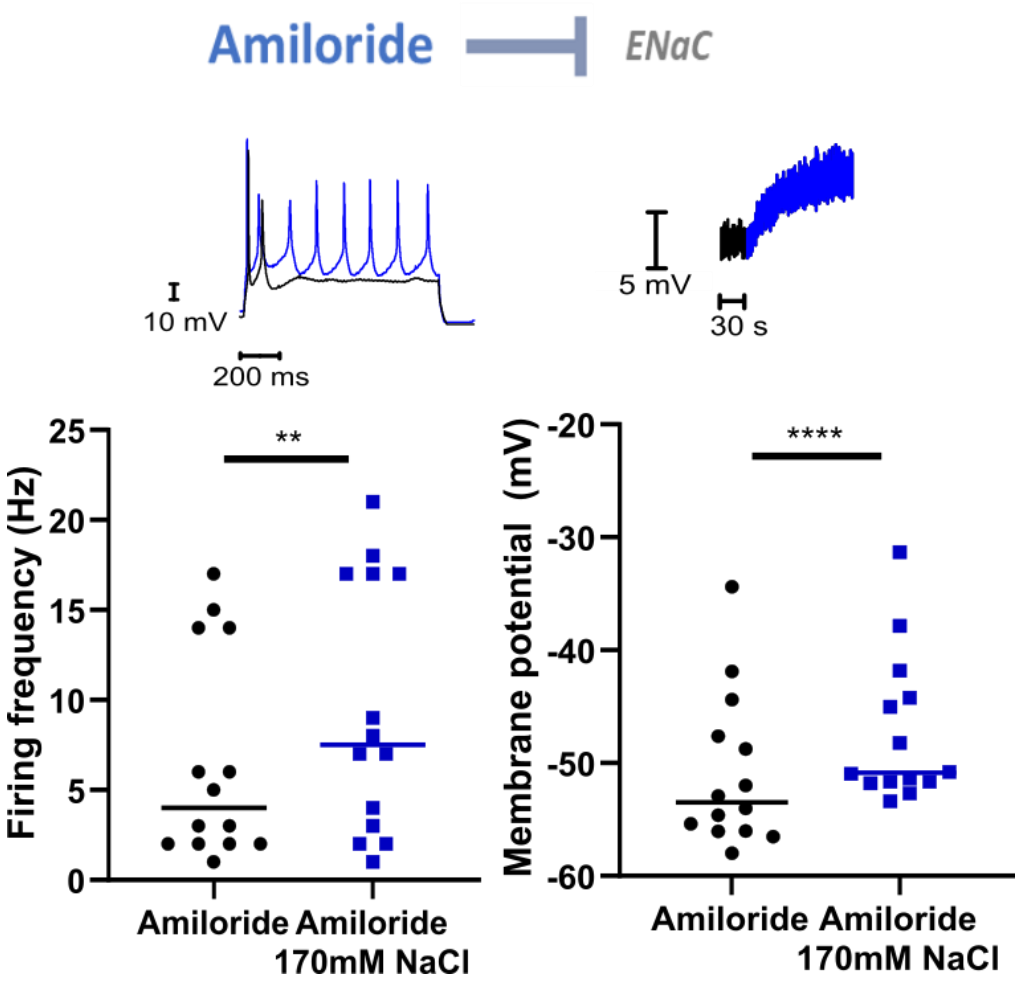



***Figure 5.13 1 µM Amiloride failed to eliminate the effect of 170mM NaCl upon stellate ganglia neuron electrophysiology*** *Maximum firing frequency still increased in the presence of 1 µM amiloride (n=14; Wilcoxon test; p=0.002) and neuronal membrane depolarisation still occurred (n =14; Paired t-test; p<0.0001). For the raw data trace, amiloride with physiological sodium is shown in black, amiloride with 170 mM NaCl is highlighted in blue.* Here n refers to cell number, where a culture n of 3 was used, with each culture using a minimum of 2 animals.

### 5.3.5 $Ca^{2+}$ independence

After excluding known $Na^{+}$ specific mechanisms in **Figures 5.9-5.12**, study then focussed upon $Ca^{2+}$ dependent effects. The approach was two-fold, first the extracellular [$Ca^{2+}$] was lowered to determine if this altered the response to 170 mM NaCl (**Figure 5.13**). Secondly, Fura-2AM (Tsien, 1986) based $Ca^{2+}$ imaging was used to measure whether 170 mM NaCl evoked a rise in $[Ca^{2+}]_i$ (**Figure 5.14**). Low $Ca^{2+}$ Tyrode's solution did not prevent 170 mM evoked increased neuronal firing from 2 Hz to 10 Hz and did not prevent membrane depolarisation (4.32±0.72 mV) (**Figure 5.13**). When measured with Fura-2 AM, 170 mM NaCl did not alter $[Ca^{2+}]_i$.

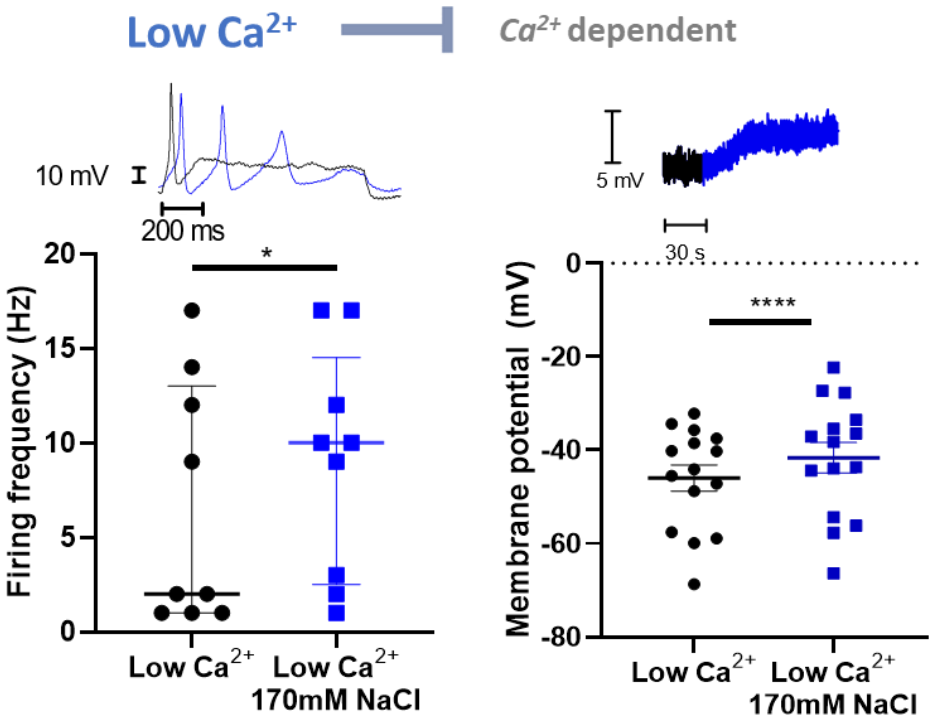



***Figure 5.14 Reducing external calcium from 1.8 mM to 0.2 mM did not prevent the effect of 170 mM NaCl*** *When recording in low $Ca^{2+}$ Tyrode's solution 170 mM NaCl still increased neuronal firing (n=9; Wilcoxon test; p=0.031) and evoked membrane depolarisation in sympathetic stellate ganglia neurons (n=15; Paired t-test; p<0.0001). For the raw data trace, low $Ca^{2+}$ with physiological NaCl is shown in black, low $Ca^{2+}$ with 170 mM NaCl is shown in blue. Here n refers to cell number, where a culture n of 2 was used, with each culture using a minimum of 2 animals.*

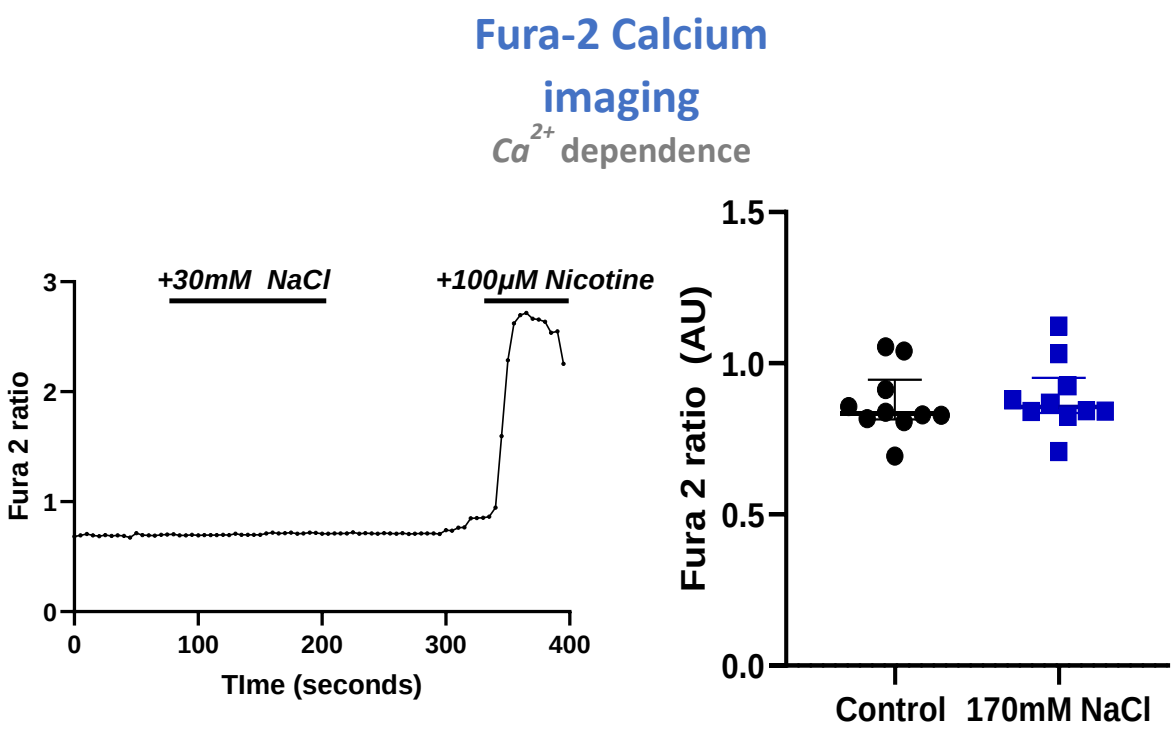



***Figure 5.15 High NaCl does not evoke a $Ca^{2+}$ response in stellate ganglion neurons*** *170 mM extracellular NaCl evoked no significant intracellular $Ca^{2+}$ response in sympathetic stellate ganglia neurons as assessed by Fura-2 live-cell $Ca^{2+}$ imaging (n=10; Paired t-test; p=0.066). Control recordings were taken as the average between 20 and 60 seconds of recording, the response was taken as the peak value between 80 and 200 seconds of recording. Nicotine was added to demonstrate that the tested stellate ganglia neurons were responsive to external stimuli. All tested neurons had a nicotinic response comparable to that shown here. Here n refers to cell number, where a culture n of 2 was used, with each culture using a minimum of 2 animals.*

### 5.3.6 Transient receptor potential channel independence

Transient receptor potential (TRP) channels are often associated with physiological responses to altered osmolarity (Sharif-Naeini *et al.*, 2008) and have previously been associated with NaCl responses in the hypothalamus (Naeini *et al.*, 2006). Therefore, TRP channels were inhibited by two pharmacological methods, first by the TRP vanilloid family inhibitor Ruthenium Red (RuR) (**Figure 5.15**) (Amann & Maggi, 1991), and then by the global TRP channel inhibitor $Gd^{3+}$ (**Figure 5.16**) (Bouron *et al.*, 2015). RuR mediated TRP vanilloid channel inhibition failed to

prevent either increases in firing frequency which increased from 3 Hz to 6 Hz or membrane depolarisation (5.14±1 mV). $Gd^{3+}$ reduced neuronal firing to a phasic 1 state, and so the effect upon neuronal firing was not assessed. However, there was no effect of $Gd^{3+}$ on 170 mM NaCl induced membrane depolarisation (3.61±0.84 mV).

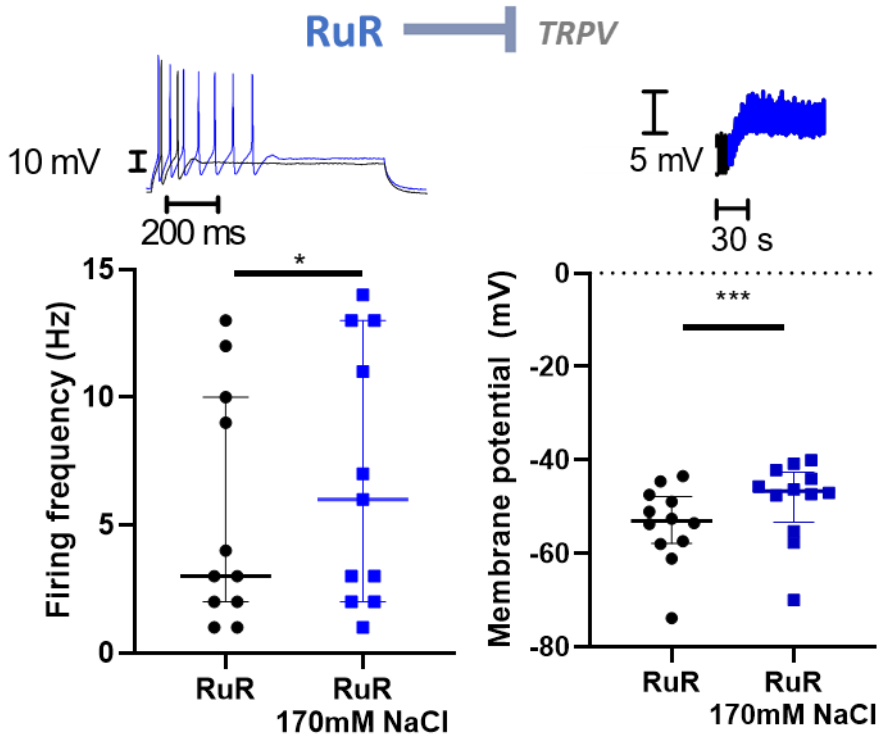



***Figure 5.16 TRPV channel inhibition by ruthenium red does not prevent the effects of high NaCl*** *TRPV inhibitor ruthenium red (10 µM) did not prevent 170 mM induced increased maximum firing frequency (n=11; Wilcoxon test; p=0.016) nor membrane depolarisation (n=11; Wilcoxon test; p<0.0001). Here n refers to cell number, where a culture n of 2 was used, with each culture using a minimum of 2 animals.*

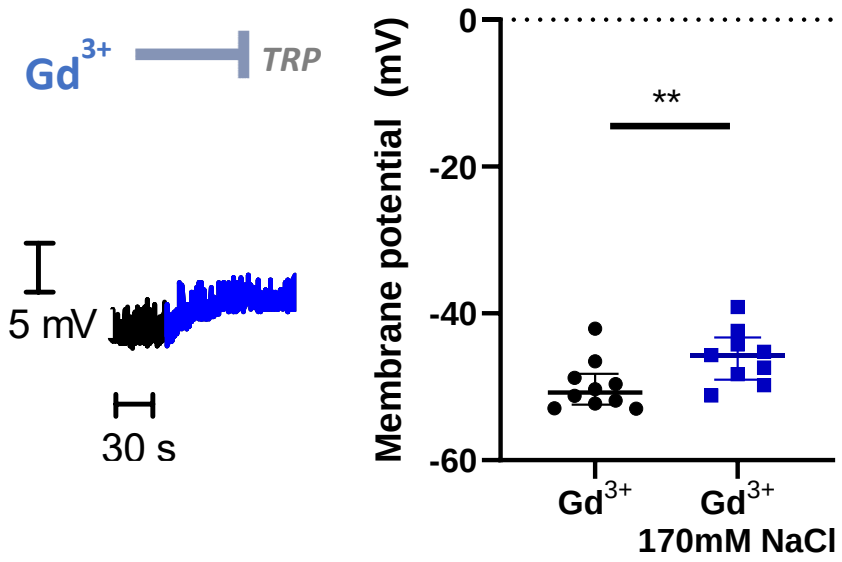



***Figure 5.17 Global TRP channel inhibitor $Gd^{3+}$ did not affect NaCl induced membrane depolarisation*** *170 mM evoked a significant depolarisation in the presence of $Gd^{3+}$ (n=9; Paired t-test; p=0.0025). Raw data trace shown with $Gd^{3+}$ (black) and with $Gd^{3+}$ and 170mM NaCl. Here n refers to cell number, where a culture n of 2 was used, with each culture using a minimum of 2 animals.*

### 5.3.7 Osmolarity independence

It was next prudent to assess whether the effect of $Na^+$ was through osmolarity, which would increase by 20 mM to 120 mM between the tested range of 10 mM to 60 mM NaCl. To assess this, glucose (**Figure 5.17-5.18**) and sucrose (**Figure 5.19**) were used to adjust the extracellular osmolarity to levels comparable to elevated NaCl concentrations. 20-120 mM Glucose, equivalent in osmolarity to an additional 10-60 mM NaCl (150-200 mM NaCl), did not depolarise the membrane potential of SGNs in a manner similar to osmolarity matched NaCl (**Figure 5.17**) (Two-way ANOVA; $p<0.0001$), nor did 60 mM glucose increase neuronal firing in SGNs (**Figure 5.18**), as I previously documented for the equiosmotic 170 mM NaCl (**Figure 5.13**). Equally, the alternative osmotic control, sucrose had no effect upon membrane depolarisation or firing (**Figure 5.19**).

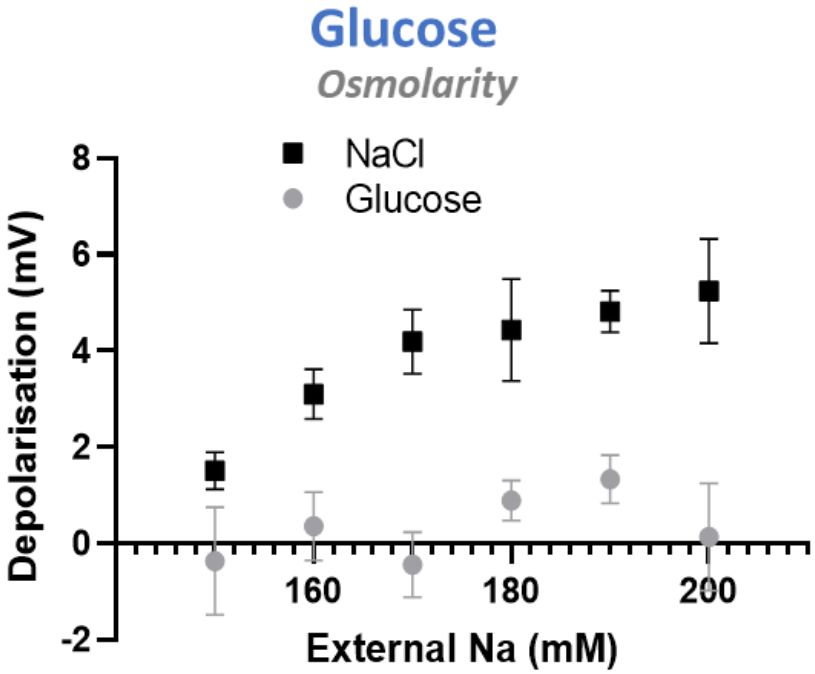



***Figure 5.18 Osmolarity matched glucose controls did not induce membrane depolarisation similar to NaCl*** *Over the range 20 mM to 120 mM glucose, NaCl caused a significantly greater depolarisation than tested concentrations of glucose (Two-way ANOVA; p<0.0001) (NaCl, n=15-22; Glucose, n=8-15). Here n refers to cell number, where a minimum culture n of 2 was used, with each culture using a minimum of 2 animals.*

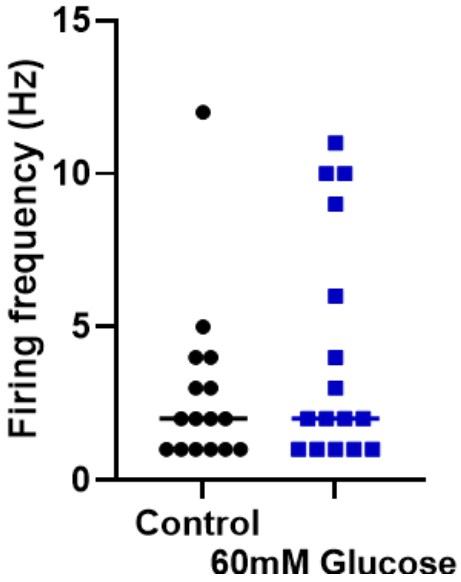



***Figure 5.19 The addition of 60 mM glucose had no effect upon neuronal firing*** *60 mM did not significantly alter stellate ganglia neuron firing (n=16; Wilcoxon test; p=0.094). Here n refers to cell number, where a culture n of 3 was used, with each culture using a minimum of 2 animals.*

To confirm these results, an alternate protocol was used which transitioned from osmolarity matched (60 mM) glucose (**Figure 5.20**) or sucrose (**Figure 5.21**) solutions to 170 mM NaCl to prevent any osmolarity change upon NaCl addition. Under both conditions, 170 mM induced membrane depolarisation, but as recordings were made in TTX, changes in firing could not be recorded. Transitioning from 60mM sucrose to 170 mM NaCl caused a depolarisation of 3.59±0.93 mV and transitioning from 60mM glucose to 170 mM NaCl caused a depolarisation of 2.46±0.45 mV.

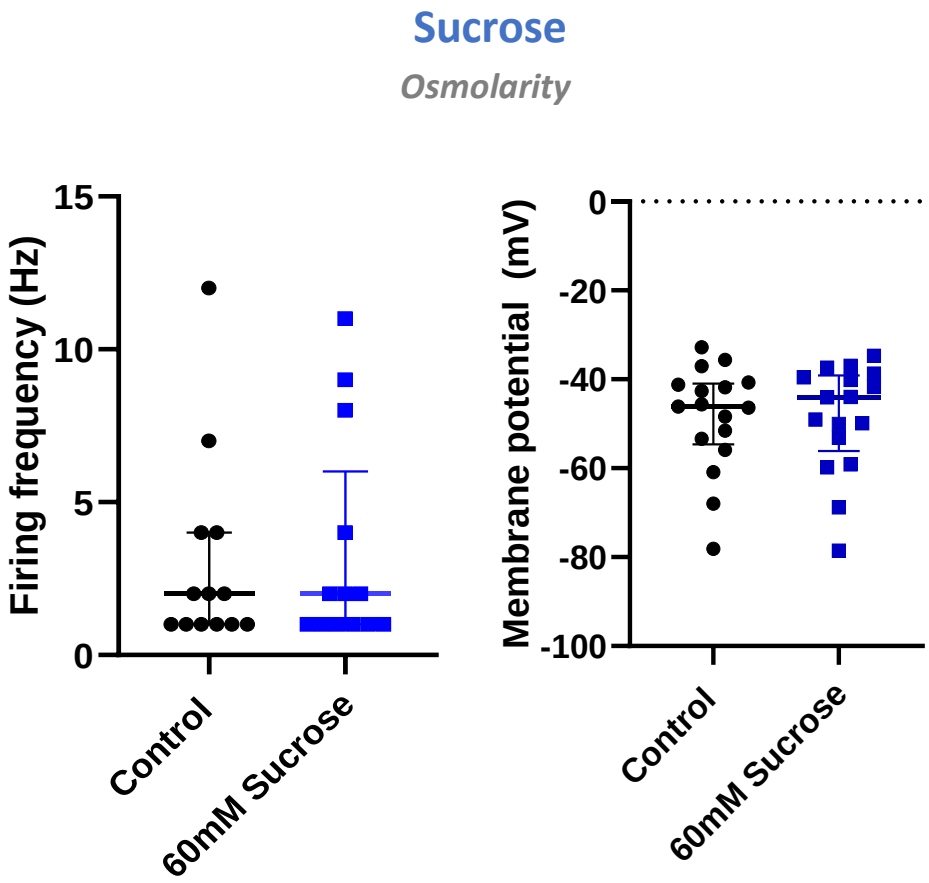



***Figure 5.20 60 mM sucrose had no effect upon induced neuronal firing or membrane potential*** *Firing rate was unaltered following the addition of 60 mM sucrose (n=13 ; Wilcoxon test; p=0.5), as was the neuronal membrane potential (n=17; Paired t-test; p=0.95). Here n refers to cell number, where a culture n of 2 was used, with each culture using a minimum of 2 animals.*

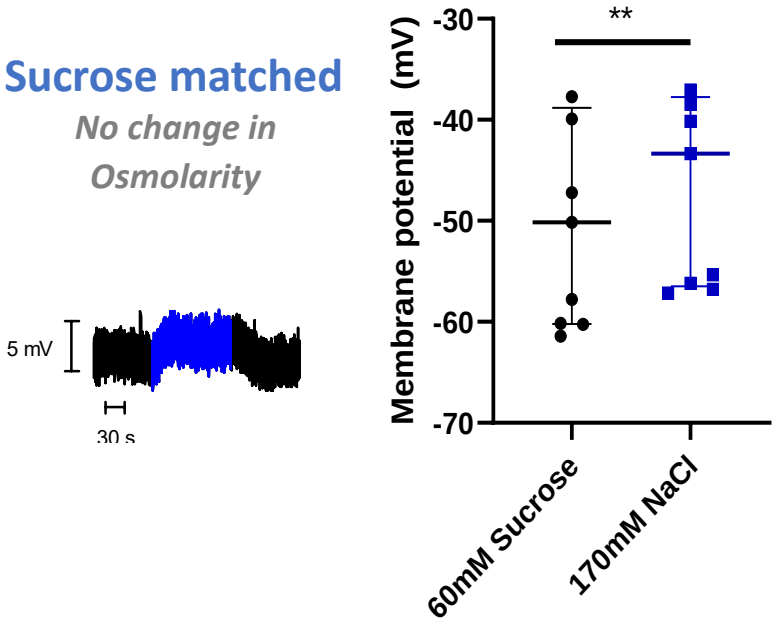



***Figure 5.21 170 mM NaCl induced a response from osmolarity matched solution high sucrose solution*** *Transitioning from 60 mM sucrose control solutions to 170 mM NaCl in the presence of 1 µM TTX still elicited a membrane depolarisation despite balanced osmolarity (n=9; Paired t-test; p=0.005). Here n refers to cell number, where a culture n of 2 was used, with each culture using a minimum of 2 animals.*

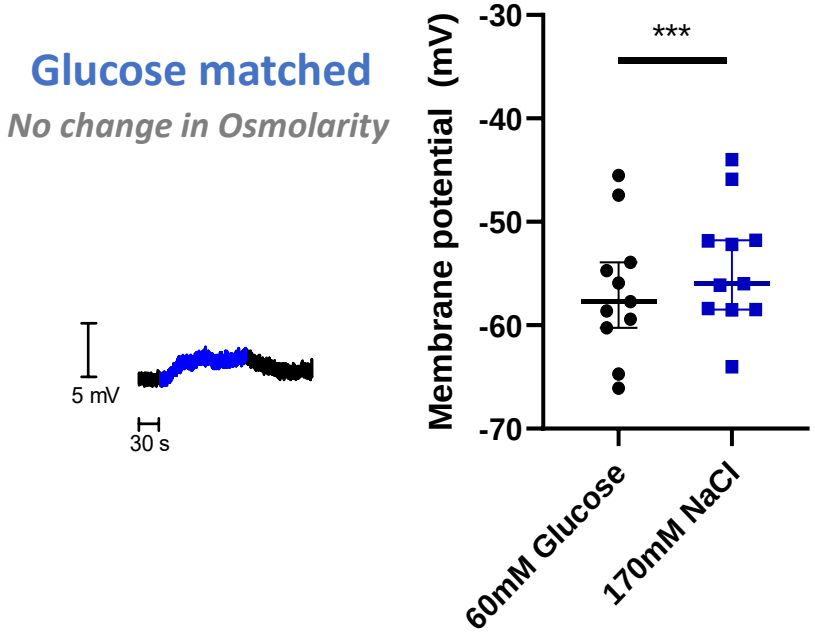



***Figure 5.22 170 mM NaCl induced a response from osmolarity matched solution high glucose solution*** *Transitioning from osmolarity matched glucose solutions to 170 mM NaCl solutions in the presence of 1 µM TTX caused a membrane depolarisation independent of osmolarity (n=11; Paired t-test; p=0.0003). Raw data trace shown with +60 mM glucose (black) and +30mM NaCl (blue). Here n refers to cell number, where a culture n of 2 was used, with each culture using a minimum of 2 animals.*

### 5.3.8 Effects of long term NaCl

Whilst the response of sympathetic neurons to transient increases in NaCl is of importance, it is more likely that these neurons will be exposed to extended elevations of NaCl in physiology. This was achieved by elevating culture media NaCl to either 140 mM or 170 mM, to mimic physiological and supraphysiological extracellular NaCl concentrations. It was plausible that the increase in activity or mild depolarisation induced by 170 mM NaCl could lead to sustained changes in neuronal function, as has been reported with various stimuli in other neuron subtypes.

Neurons were cultured with either 140-170 mM NaCl for 24-36 hours and were washed thoroughly for a minimum period of 10 minutes with a constant perfusion of Tyrode's solution before recording. Neurons exposed to 170 mM NaCl for 24-36 hours had a statistically significant higher firing rate (6 Hz) than the 140 mM controls (2 Hz) (**Figure 5.22**).

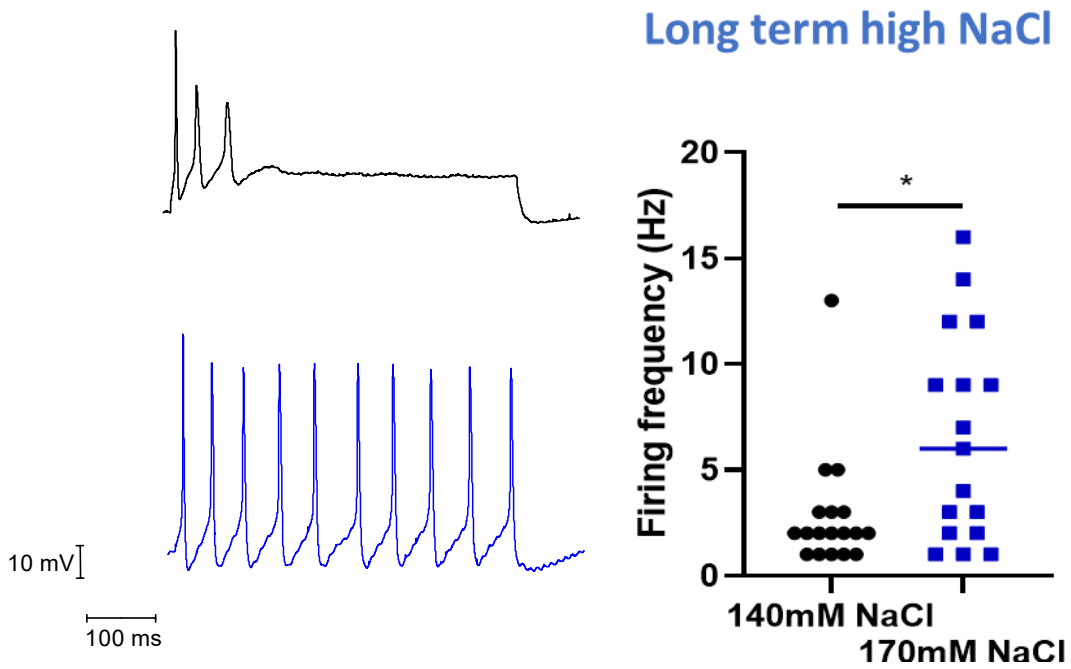



***Figure 5.23 24 hours of high NaCl induces a lasting excitable phenotype*** *Exposure to 170 mM NaCl neurobasal media for 24 hours increased neuronal firing, but not affect neuronal membrane potential (n=18, n=17; Mann-Whitney test; p=0.021). Raw trace from 140 mM shown in black against a 170 mM NaCl trace in blue. Here n refers to cell number, where a culture n of 2 was used, with each culture using a minimum of 2 animals.*

To test for activity dependence, and to separate the NaCl induced depolarisation from activity increases, the next experiments assessed whether the sustained effect of long term 170 mM NaCl could be inhibited by the $Na_v$ inhibitor TTX. Neurons were incubated for 24-36 hours with 170 mM NaCl and 2 µM TTX to allow 170 mM NaCl induced depolarisation (as shown in **Figure 5.9**) whilst preventing concurrent increases in activity. These data show that 2 µM TTX prevented the increase in sustained neuronal firing relative to 170 mM NaCl alone (**Figure 5.23**).

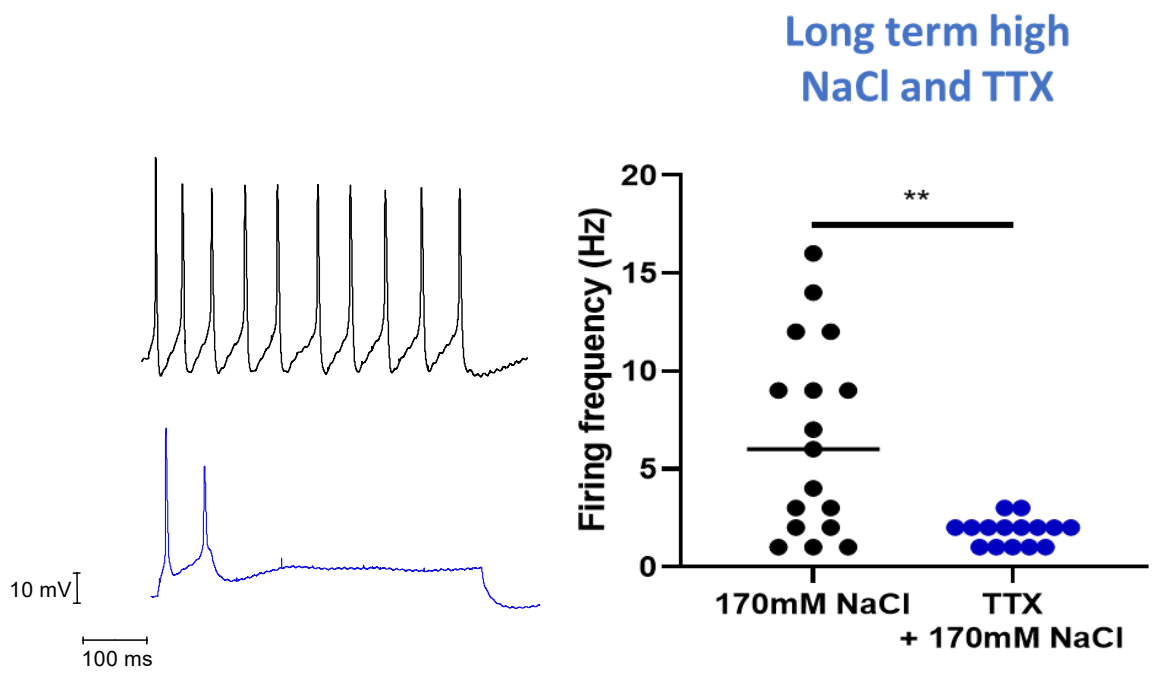



***Figure 5.24 TTX prevents the lasting phenotype resulting from 170mM NaCL*** *24-hour exposure to 170 mM NaCl with 2 µM TTX prevented the sustained increase in neuronal firing observed with 170 mM NaCl alone (n=17, n=15; Mann-Whitney test; p=0.0003). Representative trace for 140 mM NaCl shown in black, representative trace for 170 mM NaCl shown in blue. Here n refers to cell number, where a minimum culture n of 2 was used, with each culture using a minimum of 2 animals.*

To confirm that depolarisation alone does not cause the sustained phenotype induced by 170 mM NaCl, a 20 mM elevation in KCl was used to evoke a large membrane depolarisation and achieve depolarising block. The short-term effect of 20 mM KCl was resolved, via perfusing SGNs with 20 mM KCl for five minutes. 20 mM KCl depolarised neurons by 18.26±1.54 mV and reduced firing rate from a median of 2 Hz to 1 Hz, a 1 Hz decrease (**Figure 5.24**).

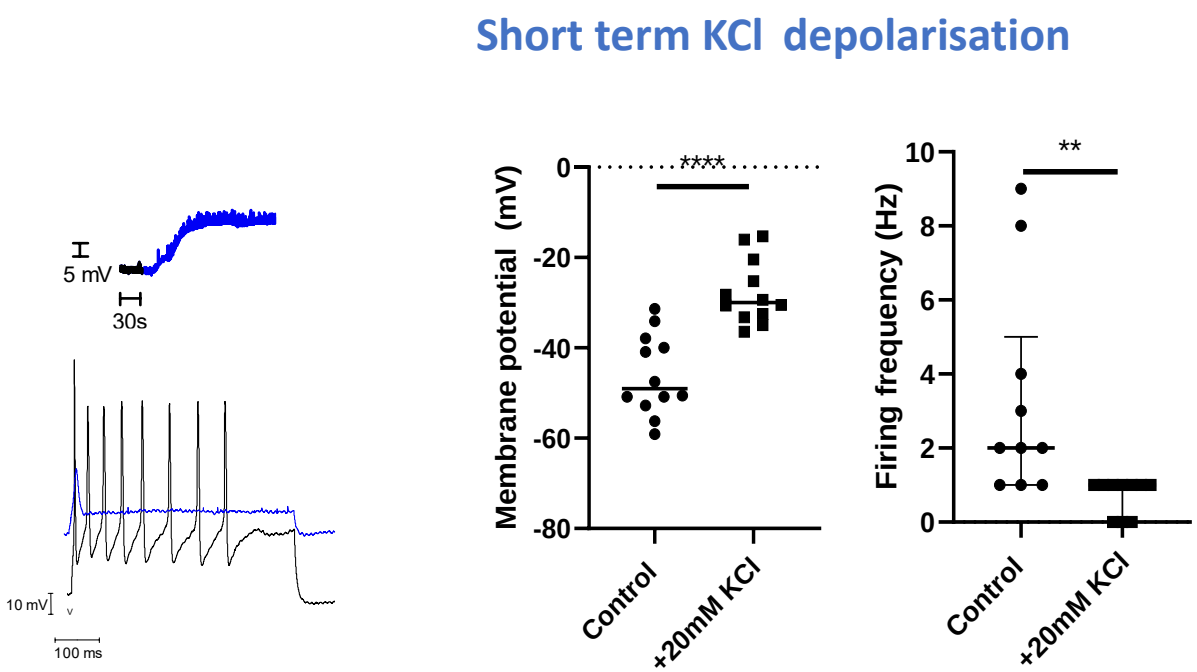



***Figure 5.25 A brief 3-minute addition of 20 mM KCl evoked depolarising block*** *20 mM KCl evoked a significant membrane depolarisation (n=12; Paired t-test; p<0.0001) and KCl limited maximum neuronal firing frequency (n=10; Wilcoxon test; p=0.004). Membrane potential shown before (black) and after an additional 20 mM KCl. Example traces for evoked firing are shown following 150pA under control (Black) and +20mM KCl conditions. Here n refers to cell number, where a culture n of 2 was used, with each culture using a minimum of 2 animals.*

When applied for 24-36 hours, 20 mM induced depolarising block did not alter the sustained neuronal firing phenotype (**Figure 5.26**). To confirm that depolarisation alone did not affect the neuronal firing phenotype, KCl depolarisation was repeated with 2 µM TTX, thus ensuring a large depolarisation with no neuronal firing. This protocol also had no effect upon neuronal firing (**Figure 5.27**).

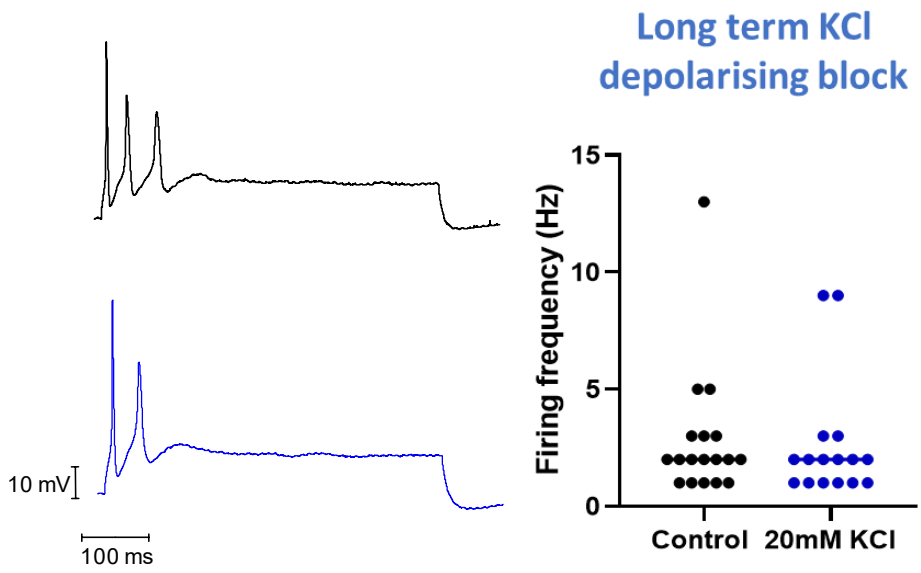



***Figure 5.26 24-hour exposure to depolarising block via 20 mM KCl did not alter sustained the neuronal firing phenotype*** *Example traces shown for culture media with 140 mM NaCl (Black) and 140 mM NaCl with an additional 20 mM KCl (Blue) (n=18, n=16; Mann-whitney test; p=0.55). Here n refers to cell number, where a minimum culture n of 2 was used, with each culture using a minimum of 2 animals.*

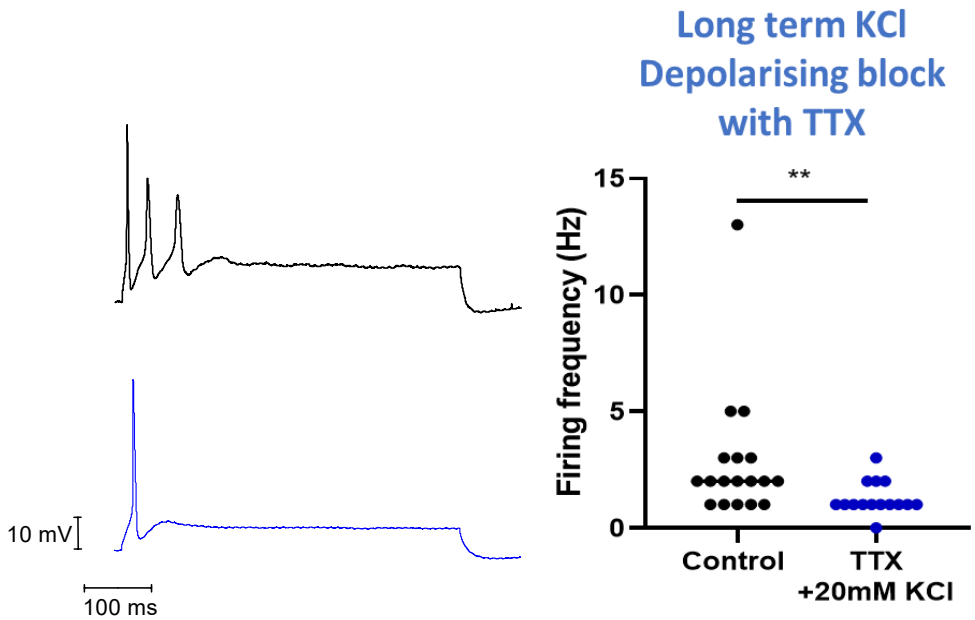



***Figure 5.27 TTX with depolarising block decreased neuronal firing frequency*** *Example traces shown for culture media with 140 mM NaCl (Black) and 140 mM NaCl with an additional 20 mM KCl and 2 µM TTX (Blue)(n=18, n=15; Mann-Whitney test; p=0.0055). Here n refers to cell number, where a minimum culture n of 2 was used, with each culture using a minimum of 2 animals.*

## 5.4 Discussion

This chapter has established three key findings related to the sympathetic response to elevated extracellular NaCl. First, sympathetic neurons can intrinsically respond to elevated extracellular NaCl with both membrane depolarisation and increased induced firing. Secondly, this appears to be mediated by known $Na^+$ sensor, $Na_x$. Finally, sustained increases in NaCl increase sympathetic neuron activity by an activity dependent mechanism. Together these results suggest a role for sympathetic neurons as a secondary $Na^+$ sensor, thereby contributing to the well-established sympathetic response to elevated NaCl.

### 5.4.1 Ganglia-specific effects

Given the well-established role of NaCl in elevated global sympathetic activity, it is interesting to note a pronounced effect on neuronal activity in all three of the tested ganglia (**Figures 5.1-5.3**). Whilst there is some degree of variation between sympathetic neurons in different ganglia (Shanks et al. 2013; Jobling and Gibbins 1999; Wang and McKinnon 1995), the shared mechanism supports a physiologically important mechanism. Notably, all three of these ganglia innervate the vasculature to some degree and this mechanism may contribute to the vasoconstriction that's suggested to follow elevated NaCl (Howe *et al.*, 1990). It is worth noting however, that beyond the effect of NaCl on blood pressure, the effect of NaCl on other measurements was extremely inconsistent between studies (**Tables 5.1-5.2**).

These data report an increase in SGN activity following elevation of extracellular [$Na^+$], however evidence for an increase in heart rate and associated

cardiac SNA *in vivo* is varied. Studies show mixed effects following systemic increases in extracellular NaCl (**Table 5.2**). This discrepancy may be due to the baroreflex, inhibition of which was reported to prevent any observed decrease in heart rate following ICV (Weiss et al., 1996) or IV (Morita *et al.*, 1991) NaCl elevations. Similarly the baroreflex was suggested to resist the sympathetic effects of elevated NaCl in humans (Gianfranco *et al.*, 1996). In rodent models of hypertension, where the baroreflex is impaired (Ricksten & Thoren, 1980; Gordon & Mark, 1984), dietary NaCl causes a more consistent increase in heart rate (Simchon *et al.*, 1989; DiBona & Jones, 1991; Calhoun *et al.*, 1994) which supports the notion that the baroreflex is limiting here. Finally, it is worth noting that interpretation of these data is complicated by additional changes following elevations in dietary sodium. These include an amplified cardiac depressor nerve response (Pawloski-Dahm & Gordon, 1993; Simmonds *et al.*, 2014), increased baroreceptor gain (Trimarco *et al.*, 1991) and a functional association between cardiac and renal sympathetic nerves. Further work *in vivo* is required to assess the role of sympathetic reflexes in restricting cardiac responses.

The increase in superior mesenteric/coeliac ganglia neuron activity following high NaCl is somewhat in contradiction with the decrease in renal activity described *in vivo*. However, Morita, Nishida, and Hosomi (1991) demonstrated that a combination of sinoaortic baroreceptor denervation, vagotomy and sectioning of the anterior and superior hepatic nerves eliminated a major component of the decrease in renal SNA following elevated NaCl. The majority of this response is therefore not centrally mediated, but a small component still appears to be controlled by PVN neurons (Badoer *et al.*, 2003). Overall, this response is physiologically protective, and suppressing renal SNA, thereby favouring natriuresis and negative feedback to

elevated NaCl (Morita *et al.*, 1991; Sata *et al.*, 2018). A physiological delay for this reflex may explain the existence of transient increase in renal SNA observed by Shi et al. (2007).

### 5.4.2 $Na_x$ as the candidate mechanism

In order for these data to have a physiological interpretation, it was important to establish a putative mechanism for the NaCl response. The dose-dependence demonstrated in **Figures 5.4-5.5** is similar in nature to that described for $Na_x$ previously (Asano & Nomura, 2002), and this is further strengthened by the observation that the mechanism is $Na^+$-dependent and $Cl^-$ independent. This is further supported by transcriptomic and protein evidence that *SCN7A*/$Na_x$ was expressed in SGNs, providing crucial evidence that this mechanism is feasible. Whilst it is unfortunate that no selective pharmacology is available for $Na_x$, and *SCN7A* knockouts are not readily available, this chapter utilises a large pharmacological profile to inhibit all other likely candidates and by exclusion it is the last remaining target.

The alternate approach would involve knockdown of *SCN7A* in culture via siRNA (Han, 2018). However, it is difficult to confirm siRNA knockdown in culture, where confirmation can be confirmed by three methods; RT-qPCR, immunohistochemistry and in-situ hybridization. RT-qPCR is not feasible as it is not possible to dissociate SGNs once in culture, where they strongly attach to the glass substrate. This challenge would be further compounded by the low cell yield of sympathetic neurons in culture, and in combination this prevents reliable RNA yields. Finally, it is likely that expression would vary from cell to cell, and this

snapshot would not represent the variation in expression that would result from this method. Immunohistochemistry and in-situ hybridization suffer from the same limitation, in that it is inadvisable to compare expression levels by these methodologies. In conclusion, without a feasible method of confirming siRNA knockdown, this technique was avoided.

Therefore, whilst inconclusive, the pharmacological approach still provides strong functional evidence in support of the $Na_x$ hypothesis. Furthermore, global $Na_x$ knockouts removed almost all increases in SNA in response to high serum NaCl (Nomura *et al.*, 2019). Therefore, if the sympathetic neuron $Na^+$ sensor described here is physiologically important, the best candidate would be $Na_x$.

### 5.4.3 The feasibility of a sympathetic $Na^+$ sensor

The presence of a peripheral $Na^+$ sensor may at first appear controversial given the large swathe of research currently dedicated to central $Na^+$ sensing, however, peripheral mechanisms have not yet been excluded. Indeed, the major work on $Na_x$ in blood pressure control (Nomura *et al.*, 2019), speculates on additional unidentified peripheral and central mechanisms of $Na^+$ sensing. In attempting to prove the mechanism for NaCl mediated blood pressure elevations, or increases in SNA, studies have focussed upon isolated central increases in NaCl (**Table 5.1**). The reasoning for this is confusing, given the difficulty of these perfusion methods in comparison to dietary or IV NaCl and given that central elevations of NaCl are further from physiology than systemic changes. There are two exceptions to this approach. First, ablation of the entire Anteroventral third ventricular region (AV3V) region, which includes the OVLT, limited the impact of

dietary NaCl on sciatic, vagal and aortic nerve induced sympathetic reflexes (Simmonds *et al.*, 2014). Whilst this is an interesting finding, this does not reflect the tonic increase in sympathetic activity observed in other papers. Secondly, high dietary NaCl leads to a larger increase in splanchnic and renal nerve activity following glutamatergic stimulation of central sympathetic centres (Pawloski-Dahm & Gordon, 1993; Adams *et al.*, 2007). Whilst the original authors argue that this suggests increased central activity, these results could equally support increased gain at the level of the sympathetic neuron during dietary elevations. Finally, Antunes et al. (2006) demonstrate a reduction in osmolarity induced SNA following precollicular transection from 21% to 7% which was abolished following removal of the circumventricular organs. However, in this study the authors are using an *in situ* preparation, where the lumbar nerves are exposed to standard Tyrode's solution and not elevated NaCl. This preparation effectively prevents local sympathetic responses to high NaCl, and so it is unsurprising that the phenotype here is only central.

These data cannot rule out a dominant role for central $Na^+$ sensors in NaCl sensing given the ability of ICV NaCl to recapitulate blood pressure elevations and increased SNA (Nomura *et al.*, 2019) and for centrally microinjected pharmacological inhibitors of PVN activity to prevent or alter systemic responses to NaCl (Badoer *et al.*, 2003). However, evidence suggests that in addition to these central mechanisms sympathetic $Na_x$ increases the gain of peripheral sympathetic neurons, and therefore amplifies central input. For example, pharmacological inhibitors of PVN function do not limit the increased heart rate responses to elevated IV NaCl (Badoer *et al.*, 2003). Additional work is clearly required, but these data may highlight an additional mechanism of $Na^+$ sensing as proposed here.

Finally, it is not unprecedented for two complimentary systems to have evolved to meet a physiological problem, and perhaps this is the case here given the importance of $Na^+$ homeostasis for survival. In a similar vein, there are many that believe the autonomic nervous system is an evolutionary predecessor to the central nervous system, and perhaps this cruder mechanism of $Na^+$ sensing is yet more evidence for this.

### 5.4.4 Limitations of $Na_x$ as a $Na^+$ sensor

The concentration used throughout, 170 mM NaCl, is relatively high compared to the typical physiological range. However, we also found that NaCl activates sympathetic neurons at lower physiological concentrations (ie. 150 mM) of serum NaCl concentration (**Figure 5.4**) and 170 mM NaCl produced a large response that was easier to biophysically interrogate. Also, as the mechanism we describe here has similar kinetics to $Na_x$ any limitations regarding NaCl sensitivity of this channel, would also apply to the well-established centrally mediated mechanism of $Na^+$ sensing by $Na_x$.

It is possible that *in vivo* the concentration range for $Na_x$ is shifted under physiological and pathophysiological conditions, as G protein signalling via endothelin-3 receptors has been reported to shift $Na_x$ $Na^+$ sensitivity to a lower concentration range (Hiyama *et al.*, 2013).

### 5.4.5 Long-term effect of high NaCl

Interestingly, NaCl appeared to cause a sustained increase in sympathetic neuron activity *in vitro*. However, it is unknown whether this is relevant to the phenotype *in vivo*. In a rodent model, an increase in blood pressure and sympathetic tone remained after returning to a low sodium diet (Gomes *et al.*, 2017). However, it should be noted that sympathetic tone was measured by heart rate variability (Camm *et al.*, 1996) and the authors relate this entirely to a decreased contribution of the PNS. This explanation seems unlikely given elevated SNA is known to be responsible for elevations in blood pressure (Nomura *et al.*, 2019). Finally heart rate variability remains a controversial method for determining the contribution of a single branch of the autonomic nervous system (Heathers, 2014), so further work is required to confirm this phenotype.

These data may also align with previously reported decreases in noradrenaline transporter gene expression, protein expression and function following exposure of sympathetic neurons *in vitro* or *in vivo* to extended periods of high NaCl (Habecker *et al.*, 2003; Kreusser *et al.*, 2014). Whilst these data do not directly correlate with the results presented here, they do set a precedent for long-term regulation of sympathetic function by NaCl levels.

Still this result was unexpected given that homeostatic neuronal plasticity normally dictates a decline in neuronal activity in response to sustained activity. However, others have demonstrated that increases in $[Ca^{2+}]_i$ are a key signal for homeostatic plasticity (O'Leary *et al.*, 2010), although it is demonstrated here that 170 mM NaCl did not raise $[Ca^{2+}]_i$. This makes it unlikely that inhibitory homeostatic plasticity would occur in this model. We can infer that SGNs can undergo

homeostatic plasticity, as it is invoked here by 20 mM KCl. Whilst not explicitly tested here, 20 mM KCl is likely to evoke $Ca^{2+}$ response, due to depolarising the neuron to potentials within the activation range for $Ca_V$ (**Figure 5.24**).

The long-term effect of NaCl could be evoked by membrane depolarisation or changes in neuronal excitability. We know that it is not merely depolarisation dependent as KCl induced depolarisation of approximately 18.6 mV appeared to invoke inhibitory homeostatic plasticity. Finally, TTX did not prevent transient responses to high NaCl and if, as hypothesised, the described mechanism is $Na_x$ then TTX would not block channel conductance. Therefore, the mechanism of NaCl induced plasticity would be activity-dependent by this schema. An increase in $Na_x$ mediated neuronal activity has been reported in central regions via c-fos expression so an activity-dependent mechanism would also be permissible here. Further investigation is clearly needed to elucidate this mechanism.

### 5.4.6 Limitations of pharmacology

Whilst some of the agents used throughout this work, such as TTX (Narahashi, 2008), show a remarkable selectively at the tested doses, others have poor selectivity with multiple off-target effects. For example, TRP inhibitors RuR and $Gd^{3+}$ are particularly poor pharmacological agents. RuR also blocks $Na_v$ and $Ca_v$ channels (Malécot *et al.*, 1998), and mitochondrial $Ca^{2+}$ transport (Bernardi *et al.*, 1984). $Gd^{3+}$ reduces $Na_v$ current (Li & Baumgarten, 2001) and $K_v$ current (Elinder & Arhem, 1994), and prevented repetitive firing in control experiments (Data not shown), which prevented further firing rate recordings with $Gd^{3+}$. Despite these flaws, none of the tested inhibitors prevented NaCl evoked depolarisation or

increases in neuronal firing, implying that neither the intended target nor off-target effects are involved in NaCl responses. Finally, in some cases the non-specificity of pharmacology has been used to its advantage, such as with benzamil, which was used to inhibit ENaC, NCX and ASICs simultaneously (Wang *et al.*, 2008; Leng *et al.*, 2016).

### 5.4.7 Future work

For this study, operating in culture allowed for a focused study of sympathetic neuron specific mechanisms without the influence of systemic reflexes and other cell types such as glia, which also express *SCN7A* (Watanabe *et al.*, 2006). Still, *in vivo* work is required to fully integrate these observations to a systemic level, and this seems to be the next most important experimental approach. This would be best achieved by a sympathetic neuron specific (TH) knockdown of *SCN7A*, which would allow the parsing out of central and peripheral $Na^+$ sensing mechanisms. Additionally, the baroreflex appears to be limit sympathetic responses to sodium *in vivo* and this requires further investigation. This is a time consuming and expensive experiment, and so was beyond the scope of this focussed project.

For future studies, several key questions remain: 1) Is the long-term mechanism dependent upon $Na^+$? 2) Is this mechanism dependent upon $Na_x$? 3) How long does the effect of long-term NaCl increases remain? 4) What causes the increase in activity? 5) Can any of the described mechanisms be evoked *in vivo*? 6) What is the intracellular mechanism and which membrane channel is regulated?

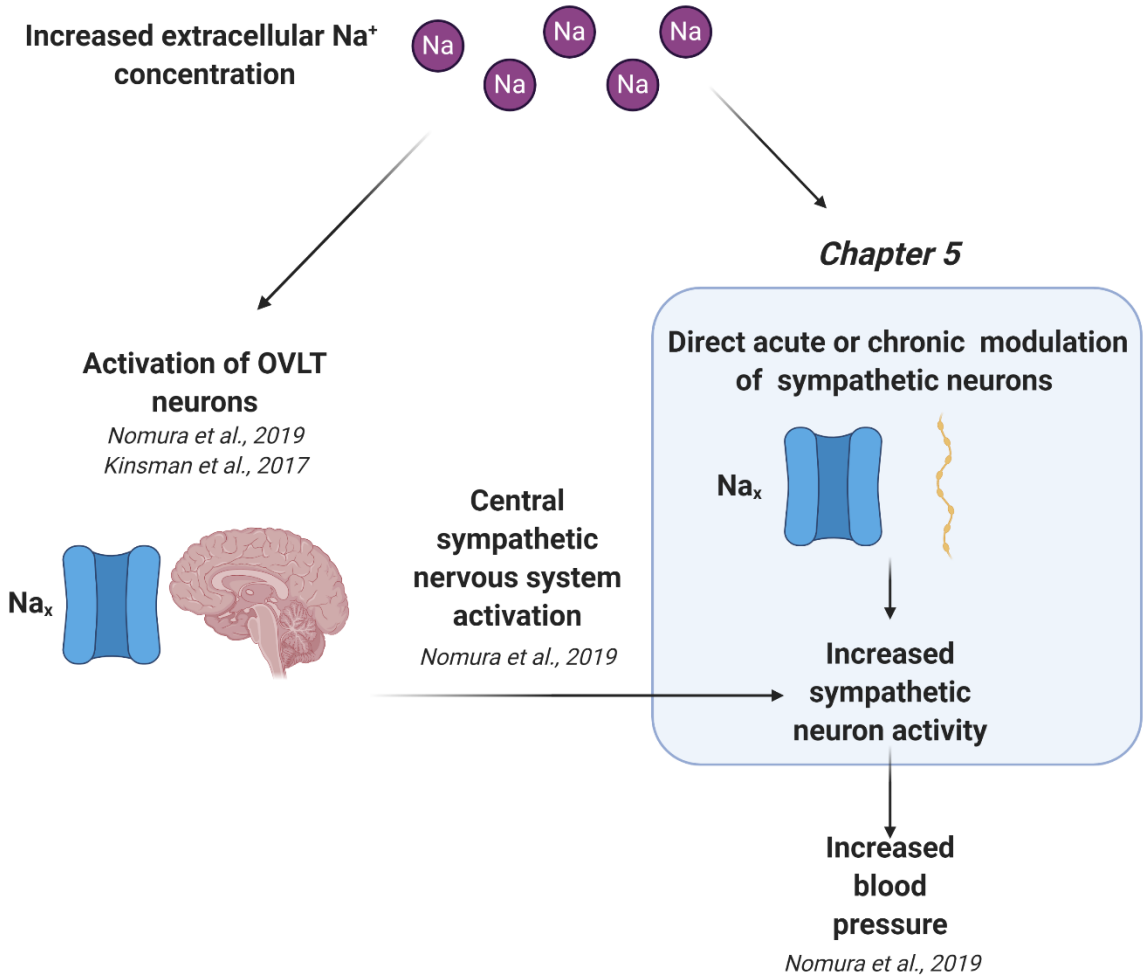



***Figure 5.28 Graphical summary of the key findings of chapter 5*** *The contribution of this chapter to the wider narrative is shown in the blue box. These data highlight that, at least in culture, elevated $Na^+$ can positively modulate electrophysiological activity in sympathetic neurons from the SCG, stellate ganglia and superior mesenteric/coeliac nerve. For the stellate ganglia neurons these data highlighted a long-lasting effect of elevated NaCl on electrically stimulated firing rate. These data are presented here in the wider context of the studies shown in*

# Chapter 6

## Novel signaling pathways

## 6.1 Introduction

The aim of this chapter was to investigate novel signalling mechanisms with the potential to extrinsically regulate stellate ganglia electrical activity. To this end this chapter investigated 1) Transient receptor potential (TRP) channels, 2) GPCRs associated with inflammatory signalling, 3) Glutamatergic receptors and 4) retrograde signalling from cardiomyocytes to SGNs. These areas of investigation were led by both published literature and the scRNAseq study from Chapter 3. The background for each of these projects will now be described, including previous evidence for these signalling mechanisms and the properties of each system.

### 6.1.1 Transient receptor potential channels

TRP channels (Hardie & Minke, 1992) are a diverse family of ligand-gated ion channels which typically exhibit polymodal mechanisms of activation and a high permeability to $Ca^{2+}$ (Ramsey *et al.*, 2006). The heterogenous group of 27 TRP channels found in man can be further subdivided into six identified subfamilies; canonical (TRPC), vanillin (TRPV), polycystin (TRPP), melastatin (TRPM), ankyrin (TRPA) and mucolipin (TRPML), with a similar arrangement found in rodents (Nilius & Owsianik, 2011). Within the cell, TRP channels are localised to either intracellular organelles, or to the plasma membrane, with a pattern of localisation that appears to be subtype specific (Yue *et al.*, 2015). TRP channels can respond to temperature, chemical, mechanical and to a limited extent, electrical stimuli. Therefore they act as important hubs for transducing one or more of these signals into membrane depolarisation and intracellular $Ca^{2+}$ signalling (Holzer & Izzo, 2014).

TRP channels are often associated with sensory neurons, due to their response to noxious stimuli including supra-physiological temperatures (Vandewauw *et al.*, 2018) and inflammation (Schumacher, 2010). However, TRP channels also have an important role in the cardiovascular system, where they are implicated in multiple cardiovascular pathologies (Yue *et al.*, 2015). A range of TRP channels have been identified in cardiomyocytes, cardiac fibroblasts and the vasculature (Yue *et al.*, 2015). Within this system, they perform a number of roles; which including TRPV2 channels sensing mechanical stretch in cardiomyocytes (Muraki *et al.*, 2003) and endothelial nitric oxide sensing by TRPC and TRPV family members (Yoshida *et al.*, 2006).

There are several existing studies reporting TRP channels in sympathetic ganglia. TRPV1 and TRPV2 channels have been identified via immunochemistry in the human stellate ganglia, although the authors did not confirm whether the subpopulation expressing these channels were sympathetic neurons (Kokubun *et al.*, 2015). TRPV2 channels were also identified by immunohistochemistry in rat SCG neurons, where they appear to be upregulated in response to axotomy (Gaudet *et al.*, 2004). However, neither study provides functional data for these channels, and both report immunohistochemical localisation to only a small proportion of neurons. Finally, TRPM7 channels have also been identified in the synaptic vesicles of cultured SCG neurons, where they appear to play a critical role in synaptic release (Krapivinsky *et al.*, 2006). These data suggest the presence of TRP channels in sympathetic neurons, although their functional role has yet to be investigated.

TRP channels already play a critical role in the wider cardiovascular system, but this chapter aims to establish a role for TRP channels in determining SGN responses to external stimuli.

### 6.1.2 Stellate ganglia neuron response to the "inflammatory soup"

In patients with high cardiac SNA associated with ventricular tachycardia storm the stellate ganglion is inflamed (Ajijola *et al.*, 2017), but the ability for SGNs to sense inflammation, in a similar manner to sensory neurons, has not been investigated. Eight putative signalling transmitters were investigated which represent different constituents of the so called "inflammatory soup". The "inflammatory soup" refers to the combined mixture of inflammatory mediators present at a site of tissue injury or inflammation, which activates local sensory neurons (Julius & Basbaum, 2001). The major transmitters in the inflammatory soup are; nerve growth factor (NGF), bradykinin, serotonin (5-HT), histamine, adenosine-triphosphate (ATP), prostaglandin $E_2$ ($PGE_2$), adenosine and protons (Julius & Basbaum, 2001; Antonioli *et al.*, 2013). This study investigated whether the stellate ganglia can acutely transduce inflammatory signals into neuronal excitability as observed in sensory neurons (Julius & Basbaum, 2001). In support of this purpose, a brief description of the inflammatory soup transmitters follows.

*Nerve growth factor (NGF)*

NGF principally signals via TrkA (*NTRK1*) receptors in pain states and inflammation (McKelvey *et al.*, 2013), and is produced in response to inflammatory cytokines by a wide range of cell types (Minnone *et al.*, 2017). The acute signalling

role of NGF is in addition to its established role in TrkA receptor mediated axon outgrowth (Colombo *et al.*, 2014) and sympathetic neuron survival (Levi-Montalcini & Booker, 1997). A second NGF receptor, NGF p75 (*NGFR*) is also present on sympathetic and sensory neurons and appears to be involved in axonal outgrowth (Walsh *et al.*, 1999), development (Edward Hickman *et al.*, 2018), apoptosis (Freidin, 2001), as well as inflammation (Watanabe *et al.*, 2008). Whilst these receptors can function independently, when expressed together both receptors form a high affinity NGF receptor (Hempstead *et al.*, 1991). In the SCG, NGF appears to amplify excitatory responses to other inflammatory transmitters such as bradykinin (Vivas *et al.*, 2014) and increase the excitatory effect of sympathetic neurons upon cardiomyocytes (Lockhart *et al.*, 1997). Previous reports also suggest that NGF decreases SCG firing frequency and increased initial inter-spike interval (Luther & Birren, 2006).

*Bradykinin*

Bradykinin is released by damaged cells and activated mast cells, and acts through $B_1$-receptors (*BDKRB1*) or $B_2$-receptors (*BDKRB2*) (Hall, 1997). In the majority of healthy tissues bradykinin primarily acts through $B_2$-receptors, due to the relatively low expression levels of $B_1$-receptors in most tissues (Golias *et al.*, 2007). $B_1$ expression is instead restricted to specific brain regions (Raidoo & Bhoola, 1997; Shughrue *et al.*, 2003), and during inflammation $B_1$-receptors are also expressed. In SCG neurons, bradykinin has been reported to increase $[Ca^{2+}]_i$ through $B_2$-receptor mediated $G_q$-signalling (Jones *et al.*, 1995) and causes a $Ca^{2+}$-dependent inhibition of M-current (Selyanko & Brown, 1996; Cruzblanca *et al.*, 1998).

*Histamine*

There are four known receptors for the neurotransmitter Histamine, $H_{1\text{-}4}$ *(HRH1-HRH4*), where $H_1$-receptors are $G_q$-coupled, $H_2$ is $G_s$-coupled and $H_{3\text{-}4}$ are $G_i$-coupled (Panula *et al.*, 2015). Histamine decreases SCG neuron noradrenaline release via presynaptic $G_i$-coupled $H_3$-receptors (Silver *et al.*, 2002), and in other neuron populations $H_3$-receptors have also been shown to regulate neuronal firing (Varaschin *et al.*, 2018). $H_1$-receptors have also been demonstrated to depolarise SCG neurons (Field & Newberry, 1991). Finally, a recent report highlights expression of *HRH1-HRH3* in the SCG (Murakami *et al.*, 2015). So far histamine receptors in the stellate ganglia have not been investigated.

*Adenosine*

Adenosine receptors are collectively referred to as $P_1$-receptors, and include $A_1$, $A_{2A\text{-}B}$ and $A_3$-receptors (Burnstock *et al.*, 2011). $A_1$ and $A_3$-receptors are $G_i$ coupled, whereas $A_{2A}$ and $A_{2B}$-receptors are $G_s$-coupled (Borea *et al.*, 2018). In sensory neurons, $A_1$ and $A_{2A}$-receptors mediate adenosine signalling (Carruthers *et al.*, 2001; Schulte *et al.*, 2003), where presynaptic $A_1$-receptors reduce transmitter release (Carruthers *et al.*, 2001), but selective activation of peripheral $A_{2A}$-receptors enhances the response to pain stimuli (Karlsten *et al.*, 1992; Doak & Sawynok, 1995). $A_1$-receptors also inhibit neuronal firing in multiple neuronal populations outside of the SNS (Li *et al.*, 2010; James *et al.*, 2018). Contradictory sympathetic responses to adenosine have also been reported. Acute adenosine elicits a decrease in *in vivo* cardiac SNA in baroreceptor deinnervated rats (Dias da Silva *et al.*, 2012), but increases SNA in man (Biaggioni *et al.*, 1991). In SCG neurons,

adenosine has been reported to reduce $Ca_v$ via $A_1$ receptor $G_i$ mediated signalling (Zhu & Ikeda, 1993) and reduce noradrenaline release (Koh & Hille, 1997).

*$PGE_2$*

$PGE_2$ activates a range of GPCR named $EP_{1-4}$ receptors (*PTGER1-4*), where $EP_1$ is $G_q$-coupled, $EP_2$ and $EP_4$ are $G_s$-coupled and $EP_3$ is $G_i$-coupled (Kawahara *et al.*, 2015). $PGE_2$ can cause spontaneous firing in certain neuronal populations (Baba *et al.*, 2001; Clasadonte *et al.*, 2011), which in dorsal horn spinal neurons is mediated by $EP_2$-receptors (Baba *et al.*, 2001). Further, in sensory neurons $PGE_2$ inhibits $Ca_v$ via an $EP_3$-dependent mechanism, with a similar mechanism described in SCG neurons (Ikeda, 1992). $PGE_2$ has been demonstrated to decrease noradrenaline release in SCG neurons (Koh & Hille, 1997).

*ATP*

ATP signals through either ionotropic P2X receptors (Kolb & Wakelam, 1983; Krishtal *et al.*, 1983; Jahr & Jessell, 1984) or metabotropic P2Y receptors (Erb & Weisman, 2012). There are seven identified P2X receptors termed $P2X_{1-7}$ (North & Surprenant, 2000). ATP has been demonstrated to cause somatic $Ca^{2+}$ transients in SCG neurons and subsequent transmitter release (Boehm *et al.*, 1995; Boehm, 1999). Interestingly, the coeliac and SCG appear to express different P2X isoforms and therefore exhibit alternative P2X kinetics and pharmacology (Khakh *et al.*, 1995). As P2X receptor expression appears to differ between ganglia, it is of physiological interest to document their expression and subunit composition in the SGN.

P2Y receptors are typically arranged into two families, $G_q$-coupled receptors such as $P2Y_{1\text{-}2}$, $P2Y_4$, $P2Y_6$ and $P2Y_{11}$ and $G_i$-coupled $P2Y_{12\text{-}14}$ (Jacobson *et al.*, 2020). Unlike P2X receptors, not all P2Y receptors are preferentially activated by ATP (Burnstock, 2007). For example, $P2Y_6$ is activated by Uridine 5'-diphosphate, but is insensitive to ATP and ADP (Lazarowski *et al.*, 2001; Burnstock, 2007). P2Y receptors can indirectly regulate neuronal electrophysiology, for example activation of $P2Y_1$ and $P2Y_6$ receptors has been demonstrated to inhibit M-current and increased neuronal firing (Filippov *et al.*, 1999, 2006).

*Protons*

Inflamed tissue is typically acidic (Jacobus *et al.*, 1977) and the increased concentration of protons can influence sensory neuron function (Steen *et al.*, 1995; Julius & Basbaum, 2001). For example, protons can directly excite and depolarise dorsal root ganglia neurons via acid-sensing ion channels (ASICs) (Garza *et al.*, 2010; Bray *et al.*, 2013). ASICs have previously been reported to be absent from SCG (Chen *et al.*, 1998). However, SCG and stellate ganglia may differ in their expression of ASICS. Proton-sensing GPCRs have also been characterised (Ludwig *et al.*, 2003; Ihara *et al.*, 2010), and appear to have a role in inflammatory pain (Chen *et al.*, 2009).

These critical inflammatory signalling pathways will be investigated in the context of SGN firing properties. These data will shed light on whether SGNs can respond to the local inflammatory state observed in human stellate ganglia removed for ventricular tachycardia storm treatment (Ajijola *et al.*, 2017).

### 6.1.3 Glutamatergic receptors

Early studies have reported that *in vivo* injections of glutamate into the stellate ganglia elicits an increase in cardiac activity (Butler *et al.*, 1990), and immunohistochemical study has highlighted the presence of glutamate receptor subunits in subpopulations of sympathetic neurons (Carlton *et al.*, 1998). However, no functional cellular evidence has been provided for glutamatergic receptors in sympathetic neurons. The neurotransmitter glutamate activates multiple ionotropic, and metabotropic G-protein coupled receptors. There are three known families of ionotropic glutamate receptors, AMPA receptors (AMPAR), NMDA receptors (NMDAR) and Kainate receptors, and seven metabotropic receptors. These data investigate a functional role for ionotropic glutamatergic signalling in SGNs, which could have wide ranging implications for how sympathetic neurons receive input. The classes of glutamatergic receptors are briefly outlined here.

*AMPA receptors*

AMPAR are generally fast activating cation conducting channels formed from GluA1-4 subunits, which only exhibit $Ca^{2+}$ permeability if the GluA2 subunit is absent. This is due to a Q/R post-transcriptional modification within the *GLUA2* mRNA transcript which occurs under physiological conditions (Sommer *et al.*, 1991; Burnashev *et al.*, 1992; Swanson *et al.*, 1997). GluA2 inclusion also alters AMPAR kinetics to favour slower currents and homomeric GluA2 AMPAR exhibit the unusual ability to conduct when desensitised (Coombs *et al.*, 2019).

*NMDA receptors*

NMDAR are tetramers composed of a heteromeric assembly of GluN1, GluN2A-2D, and GluN3A-3B subunits (Luo *et al.*, 1997). Functional NMDAR are typically expected to require a tetrameric assembly of two GluN1 subunits and a combination of GluN2 and GluN3 subunits (Glasgow *et al.*, 2015). NMDAR are $Ca^{2+}$ permeable (MacDermott *et al.*, 1986) and exhibit slower kinetics than AMPAR(Forsythe & Westbrook, 1988). Unlike other ionotropic glutamate receptors, they not only require the binding of glutamate but also a co-agonist, either glycine (Johnson & Ascher, 1987) or D-serine (Mothet *et al.*, 2000) and require membrane depolarisation to remove $Mg^{2+}$ mediated pore block which is present at the hyperpolarised membrane potentials found in neurons at rest (Mayer *et al.*, 1984). This confers voltage-dependence onto NMDAR and allows them to function as coincidence detectors by requiring both depolarisation and the binding of both agonists (Iacobucci & Popescu, 2017). Physiologically, this tightly controls neuronal $Ca^{2+}$ influx which is potentially excitotoxic (Carvajal *et al.*, 2016).

*Kainate receptors*

Kainate receptors are formed from homomeric or heteromeric assemblies of GLUK1-5 subunits, and typically exhibit slow inward currents. Kainate receptors have similarly low permeability to $Ca^{2+}$ compared to AMPAR. Kainate receptors also have a metabotropic function and have been demonstrated to signal via intracellular signalling pathways (Negrete-Díaz *et al.*, 2018). In the periphery, kainate has been demonstrated to depolarise sensory neurons (Agrawal & Evans, 1986; Huettner, 1990).

*Metabotropic glutamate receptors*

Metabotropic glutamate receptors are a family of 8 GPCRs entitled MGluR1-8, Of these MGluR1 and MGluR5 are $G_q$-coupled, with the remaining receptors primarily coupled to $G_i$-coupled signalling pathways (Niswender & Conn, 2010). There do not appear to be MGluR receptors present in SCG sympathetic neurons based upon functional characterisation (Ikeda *et al.*, 1995).

Functional glutamatergic signalling pathways would be fundamentally important for our fundamental understanding of how the SNS functions. By developing our knowledge of novel systems in the SGN we can identify new targets for modulation of the SNS.

### 6.1.4 The effect of post-synaptic cardiomyocytes upon the neuronal phenotype

Sympathetic neuron and cardiomyocyte co-cultures have often been used as a model of this physiologically important synapse (Bub & Burton, 2015), with previous work primarily focussed upon the effect of neurons on cardiomyocytes. This study instead investigated whether postsynaptic cardiomyocytes impact the electrophysiology of SGNs derived from Wistar and SHR rodents.

An early report suggests that Wistar or SHR neurons significantly increase contraction amplitude in both Wistar and SHR cardiomyocytes, and that SHR cardiomyocytes exhibit a larger increase to either Wistar or SHR neurons (Lloyd & Marvin, 1991). Although notably this study does not directly stimulate sympathetic neurons. A subsequent report established that Wistar cardiomyocytes undergo hypertrophy in co-culture with Wistar sympathetic neurons, to become equal in size

to SHR cardiomyocytes, which are already hypertrophied (Atkins *et al.*, 1992). These studies suggest two important observations about the co-culture model, sympathetic neurons in co-culture causes hypertrophy and increased contractile force without exogenous neuronal stimulation. This suggests that the environment the cardiomyocyte is exposed to is pseudo-physiological, and this may result from the artificial colocalization of cardiomyocytes and sympathetic neurons.

Postsynaptic sino-atrial node cAMP responses to catecholamines are increased in hypertension (Heaton *et al.*, 2006) and a recent report demonstrates that in co-culture both the presynaptic sympathetic and postsynaptic cardiomyocyte must be derived from the SHR to recapitulate the heightened cardiomyocyte cAMP to sympathetic stimulation (Larsen *et al.*, 2016*b*). This study benefits from focussing upon an acute sympathetic stimulation, but does not address the effect of chronic co-culture upon post-synaptic responses as described previously (Lloyd & Marvin, 1991; Atkins *et al.*, 1992).

This study addressed the chronic aphysiological conditions created in a co-culture model. To this end the co-culture preparation is used as a method to assess the chronic effects of post-synaptic cardiomyocytes upon the function of pre-synaptic neurons. Early work suggests that co-culture with cardiomyocytes can affect the relationship between frequency of electrical stimulation and sympathetic neuron noradrenaline release (Wakade & Wakade, 1988). However, no observations of how co-culture affects sympathetic neuron electrophysiology have been made. It was hypothesised that there are two ways in which the post-synaptic cardiomyocyte can influence the pre-synaptic neuron in co-culture. First, sympathetic neurons form physical connections with cardiomyocytes in co-culture (Conforti *et al.*, 1991; Takeuchi *et al.*, 2011; Larsen *et al.*, 2016*a*), and this may

affect the neuronal phenotype. Secondly, cardiomyocytes synthesis and release transmitters (Flynn *et al.*, 1983; Korsching & Thoenen, 1983; Kinnunen *et al.*, 1993), which may have unexplored long-term effects upon neuronal function. Two models were used to explore this, a standard co-culture model, and a neuron only model, where neurons are cultured in media in which cardiomyocytes have been previously been cultured. By comparing the two preparations, and their effects on Wistar and SHR neurons, this preparation allows a crude assay for physical and chemical retrograde signalling.

## 6.2 Methods

### 6.2.1 Single-cell RNA-sequencing

ScRNAseq was performed as described in chapter 3.

### 6.2.2 Whole-cell and perforated patch-clamp

Whole-cell and perforated patch-clamp recordings were performed as described in chapter 2. Recordings with a $R_s$ greater than >20 MΩ were discarded. Similarly, cells with a change of $R_s$ greater than 30% by the end of the recording period were discarded.

For patch-clamp experiments involving a reduction in osmolarity standard whole-cell internal solutions were used as described in chapter 2. External solutions used the same composition as in chapter 2, except that an additional 60 mM of glucose was added and 110 mM NaCl was substituted for 140 mM NaCl. To lower osmolarity the extra 60 mM glucose was removed to cause a 60 mM drop in osmolarity. Inflammatory transmitters were added for a period of three minutes. This time was

chosen because the rundown of GPCR signalling pathways in whole-cell is incomplete (Horn & Marty, 1988).

### 6.2.3 Calcium imaging

Cells were cultured onto poly-d-lysine and laminin coated coverslips, in a manner like that described in chapter 2**.** $[Ca^{2+}]_i$ was measured using the cell permeable fluorescent $Ca^{2+}$ indicator, Fura2-AM (Tsien, 1986). Cells were incubated at 37$^{o}$C with Fura-2AM for 30 minutes, before being washed with Tyrode's solution (Chapter 2). Drugs were applied by 5-6ml/min gravity-fed perfusion of 35-37$^{o}$C Tyrode's solution (**Table 2.9**). The $Ca^{2+}$ response was acquired every two seconds and was measured as the emission ratio of Fura-2 at the ratio of 340/380 (Tsien, 1986). A typical recording had 90 baseline recordings (180 seconds), followed by perfusion with the stated compound for 30 recordings (60 seconds). If inhibitors were specified, they were added for the final 30 baseline recordings (60 seconds) and during agonist perfusion. For $Ca^{2+}$-free recordings, external calcium was omitted from the extracellular solution and 2 mM EDTA was added.

### 6.2.3 siRNA knockdown

Silencer select siRNA (Thermofisher, uS) was used to target GAPDH (Assay ID 4390849), TRPC1 (Assay ID 192793) and TRPV2 (Assay ID 198285). 5 µL of prediluted 10 µM siRNA stock and 15 µL lipofectamine RNAiMAX (Thermofisher, US) were separately dissolved in 25 µL of Optimem media reduced serum media (Thermofisher, US). These two suspensions were then combined and allowed to incubate for five minutes. This suspension was then added to wells containing pre-

cultured neurons (as described in chapter 2) and 2 mL of culture media. This achieved a final siRNA concentration of 12 nM.

### 6.2.4 Immunohistochemistry

Immunohistochemistry was performed on cultured sympathetic SGNs by Dr. Dan Li. Briefly, neurons were cultured in neurobasal plus media as described in chapter 2, before being fixed in 4% paraformaldehyde. To allow for TH and intracellular TRP channel staining cells were blocked and permeabilised in 0.1% triton-x, with donkey serum and 3% BSA for 30 minutes. Rabbit polyclonal primary antibodies were used against TRPC1 (ACC-010, Alomone labs), TRPM7 (ACC-047, Alomone labs) and TRPV2 (ACC-032, Alomone labs). Then cells were incubated with the secondary antibodies 1:200 Donkey anti-mouse Alexa Fluor 555 (A-31570) and 1:200 Donkey anti-rabbit Alexa Fluor 488 (A32790) (Invitrogen, US) for a period of an hour at 37 $^{o}$C. Cells were counterstained with Hoescht 33342 nuclear stain for 1 minute. Labelled cells were imaged on a Zeiss LSM 880 Airy Scan Upright laser-scanning confocal microscope with a 60x objective.

### 6.2.5 Co-culture

Briefly, neonatal cardiomyocytes were dissociated from 1-2day old Wistar ventricles. Cells were cultured in M1 media (**Table 2.10**) for a period of 1 day, before a subsequent day in M2 media (**Table 2.11**). On the third day of culturing, media was exchanged for a 50:50 mix of M2 media and plating media (**Table 2.12**). Where stated Wistar or SHR neurons were dissociated from 5-6 week old rats as described

in chapter 2, and then plated onto the cardiomyocyte layer. Full methods are available in chapter 2.

## 6.3 Results

### 6.3.1 TRP channels

scRNAseq was used to identify expression of *TRPC1*, *TRPM7* and *TRPV2* in most of the stellate ganglia sympathetic neurons sequenced (**Figure 6.1**). Protein expression of these targets was then confirmed, by immunohistochemistry (**Figure 6.2**), which was performed by Dr. Dan Li. From these data we can infer that TRPC1, TRPM7 and TRPV2 are present in SGNs, and appear to be localised in the somata of cultured neurons.

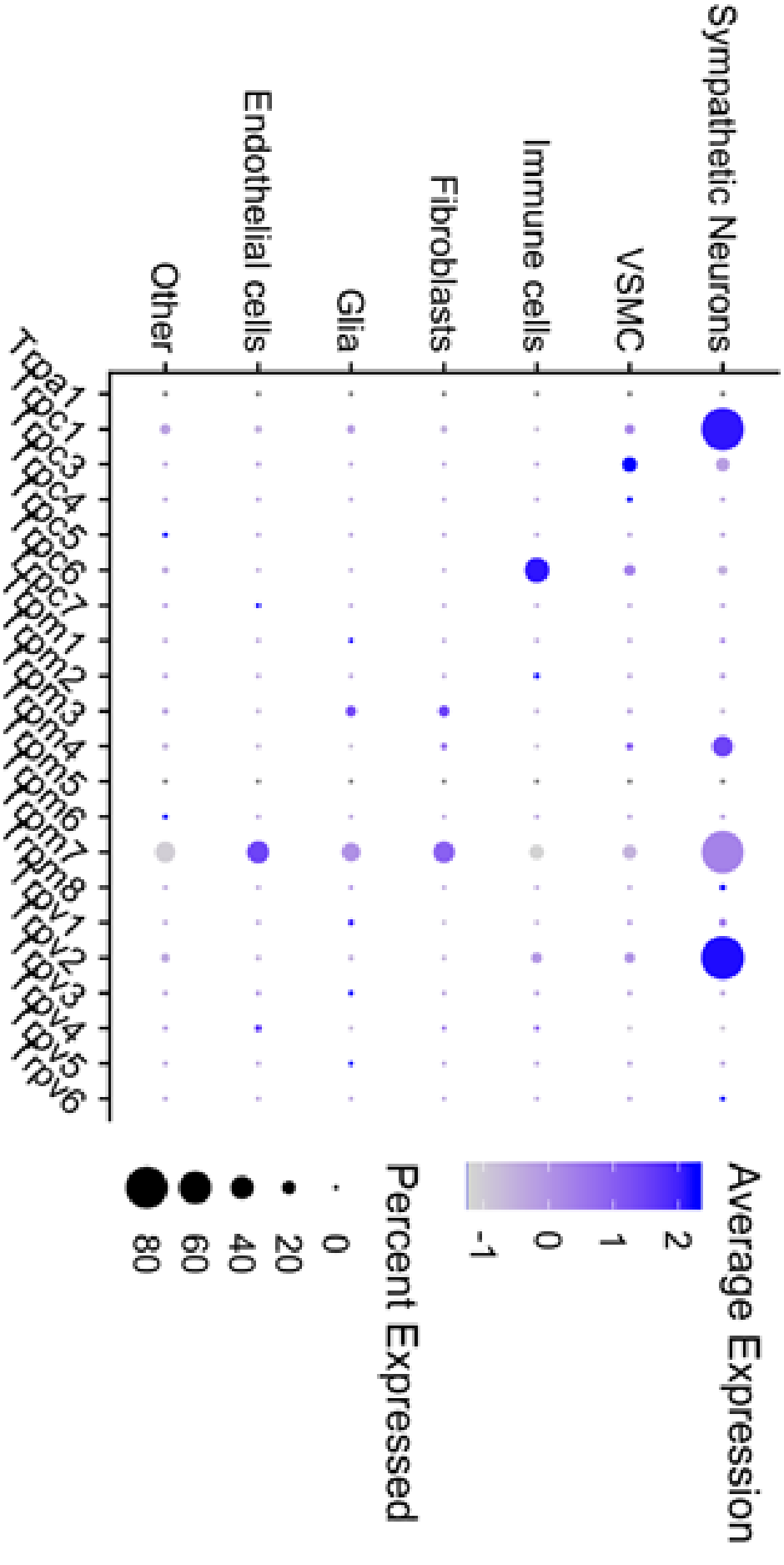



*Figure 6.1 Single-cell RNA-sequencing highlights the expression of TRPC1, TRPM7 and TRPV2 transcripts in stellate ganglia sympathetic neurons.*

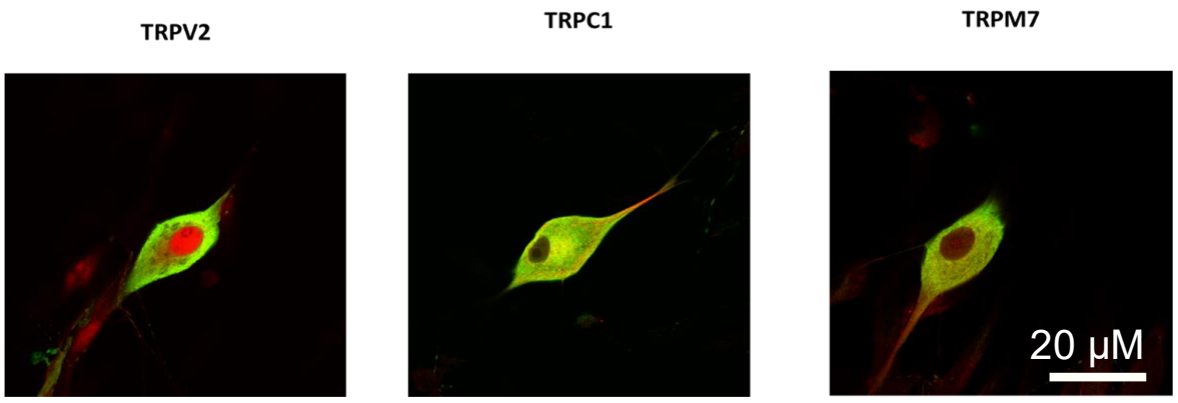



***Figure 6.2 Immunohistochemistry confirms protein expression of TRPV2, TRPC1 and TRPM7.*** *Immunohistochemistry reveals expression of TRPV2, TRPC1 and TRPM7 (Green), in TH positive (Red) cultured sympathetic neurons. Immunohistochemistry and confocal imaging was performed by Dr. Dan Li.*

The function of these channels was then investigated in cultured Wistar SGNs using a panel of known TRP channel agonists (**Figure 6.3**; **Table 6.1**). As TRP channels are $Ca^{2+}$-permeable, the cell-permeable $[Ca^{2+}]_i$ sensor Fura-2AM (Tsien, 1986) was used to screen for TRP channel function. As outlined in **table 6.1**, several of these experiments were performed by an undergraduate project student under my supervision. Of these pharmacological agents, only TRPV and TRPM6 agonist 2-APB (Colton & Zhu, 2007) elicited an increase in $[Ca^{2+}]_i$ (**Figure 6.3A**). 100 μM 2-APB activates TRPV2 channels (Hu *et al.*, 2004; Colton & Zhu, 2007; Iwata *et al.*, 2018), but inhibits TRPC1 (Colton & Zhu, 2007) and TRPM7 channels (Chokshi *et al.*, 2012). This response was then inhibited by TRPV, TRPM6 and TRPA1 channel blocker ruthenium red (Amann & Maggi, 1991; Muraki *et al.*, 2003; Clapham, 2007) to inhibit the 2-APB response. 10 μM Ruthenium red significantly reduced the 2-APB response relative to 2-APB applied alone (**Figure 6.3B**). Finally, the 2-APB response was confirmed via perforated patch-clamp recordings, where 2-APB elicited significant membrane depolarisation (**Figure 6.3C**).

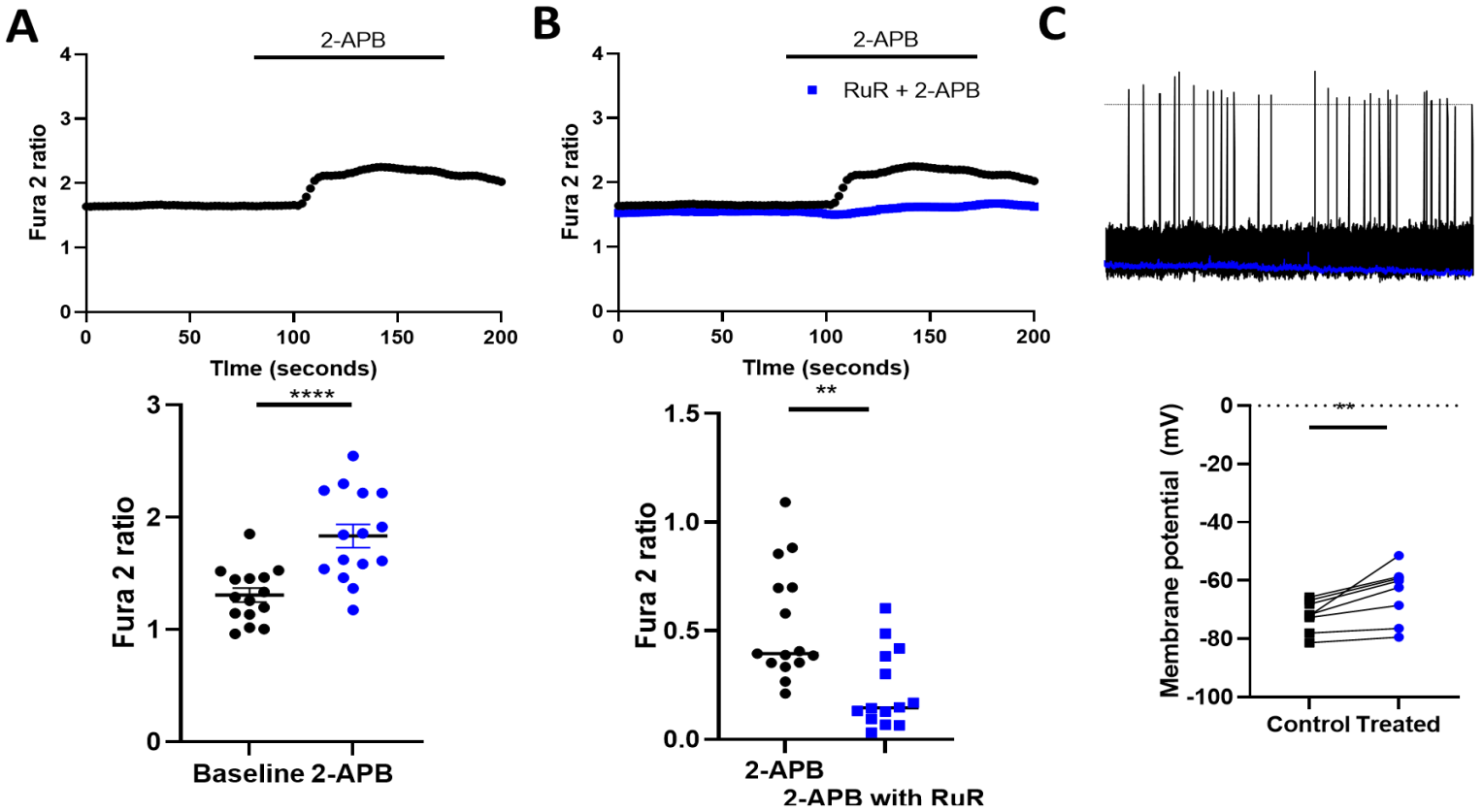



***Figure 6.3 Stellate ganglia neurons exhibited excitatory responses following the addition of TRPV agonist, 2-APB*** *100 μM 2-APB elicited a significant increase in $[Ca^{2+}]_i$ in cultured stellate ganglia neurons when measured by Fura-2 AM (A)(n=15; Paired t-test; p<0.0001). This response was inhibitable by TRP antagonist 10 μM Ruthenium red (B) (n=15, n=14; Mann-Whitney test; p=0.0016). Here an example 2-APB trace is shown in black, and the 100 μM 2-APB response following 10 μM Ruthenium red is shown in blue. The response of stellate ganglia neurons to 100 μM 2-APB with and without Ruthenium red was compared, and the 2-APB response was found to be significantly decreased with ruthenium red. 100 μM 2-APB also elicited a response in the perforated patch clamp configuration, where it caused a significant depolarisation of the membrane potential (C) (7.51 mV) (n=8; Paired t-test; p=0.0093). Here n refers to cell number, where a culture n of 2 was used, with each culture using a minimum of 2 animals.*

***Table 6.1 Summary of data obtained by other TRP channel activators, which had no significant effect upon $[Ca^{2+}]_i$*** *The effect of a range of established TRP channel agonists on $[Ca^{2+}]_i$ was tested via Fura-2AM calcium imaging. Statistical analysis was performed via paired t-tests with the exception of JT010 and carvacrol which were not normally distributed and were tested by Wilcoxon matched-pairs test. (AITC = Allyl isothiocyanate, FPP = Farnesyl Pyrophosphate). Vanillin, Capsaicin, Menthol and AITC recordings were performed by Ayesha Musa, an FHS student under my supervision. Here n refers to cell number, where a culture n of 2 was used, with each culture using a minimum of 2 animals.*

| Drug | Vanillin | Capsaicin | Menthol | Icillin | AITC | JT010 | Naltriben | Carvacrol | FPP |
|---|---|---|---|---|---|---|---|---|---|
| Target | TRPV1/3/ TRPA1 | TRPV1 | TRPM8 | TRPM8 | TRPA1 | TRPA1 | TRPM7 | TRPA1/TRPV3 | TRPV3 |
| Control | 1.316 | 1.409 | 1.143 | 1.058 | 1.220 | 1.223 | 1.069 | 1.128 | 1.177 |
| Response | 1.178 | 1.431 | 1.207 | 1.010 | 1.245 | 1.234 | 1.089 | 1.177 | 1.183 |
| Difference | -0.1378 | 0.022 | 0.06420 | -0.04873 | 0.02567 | 0.01059 | 0.02007 | 0.03978 | 0.006096 |
| n | 14 | 9 | 8 | 11 | **9** | 7 | 16 | 8 | 10 |
| P value | 0.0002 | 0.3925 | 0.1018 | 0.4718 | 0.1036 | 0.2969 | 0.1086 | 0.25 | 0.6312 |

If this response was mediated by a plasma membrane TRP channel, then the effect would be expected to be dependent upon the presence of extracellular $Ca^{2+}$. To confirm this, 100 μM 2-APB was applied in the absence of extracellular $Ca^{2+}$, where it caused no change in $[Ca^{2+}]_i$ (**Figure 6.4**).

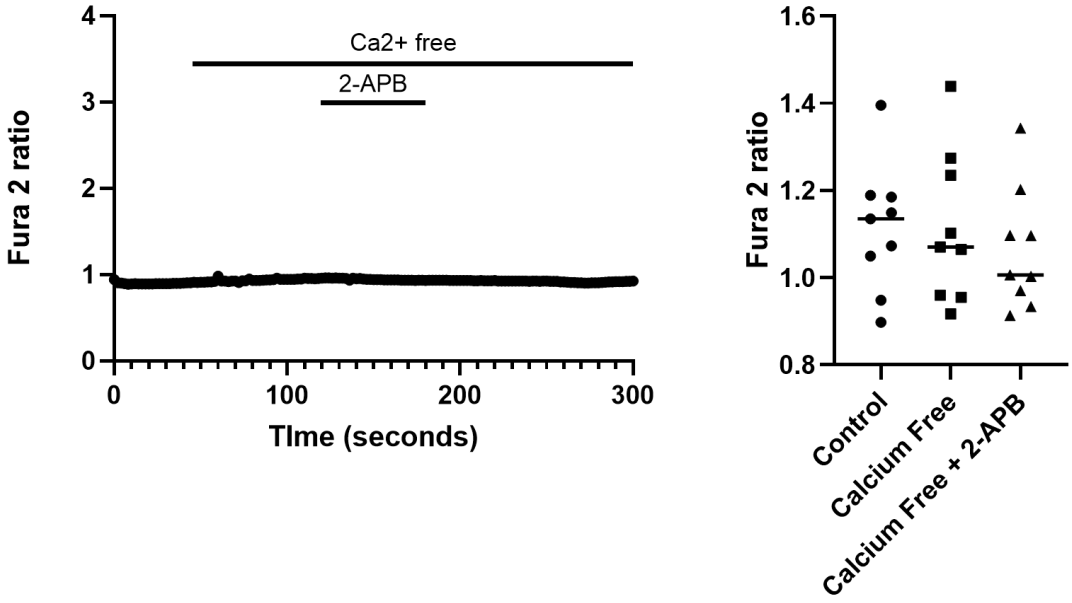



***Figure 6.4 The 2-APB response was dependent upon the presence of extracellular $Ca^{2+}$*** *100 µM 2-APB was applied in $Ca^{2+}$ free Tyrode's solution caused a non-significant decrease in $[Ca^{2+}]_i$. (n=9; Repeated-measures ANOVA; p=0.053). Here n refers to cell number, where a culture n of 2 was used, with each culture using a minimum of 2 animals.*

Only HVA $Ca_v$ are present in SGNs (Appendix Figure 15) and 100 µM 2-APB did not elicit a large enough depolarisation (Mean±SEM 7.51±2.11 mV) (**Figure 6.3C**) to reach their activation threshold of around -40 mV (Appendix Figure 15; Helton, Xu, and Lipscombe 2005). However, 2-APB did cause neuronal firing in a number of tested cells as shown in the example trace of **Figure 6.3C**. Detectable rises in $[Ca^{2+}]$ entry can be elicited by neuronal activity such as that observed in **Figure 6.3C** (Smetters *et al.*, 1999), and so neuronal activity was blocked via 1 µM TTX to isolate direct entry through TRP channels (**Figure 6.5**). Under these conditions 100 µM 2-APB still caused an increase in $[Ca^{2+}]_i$, which was not significantly different from 2-APB alone (**Figure 6.5B**).

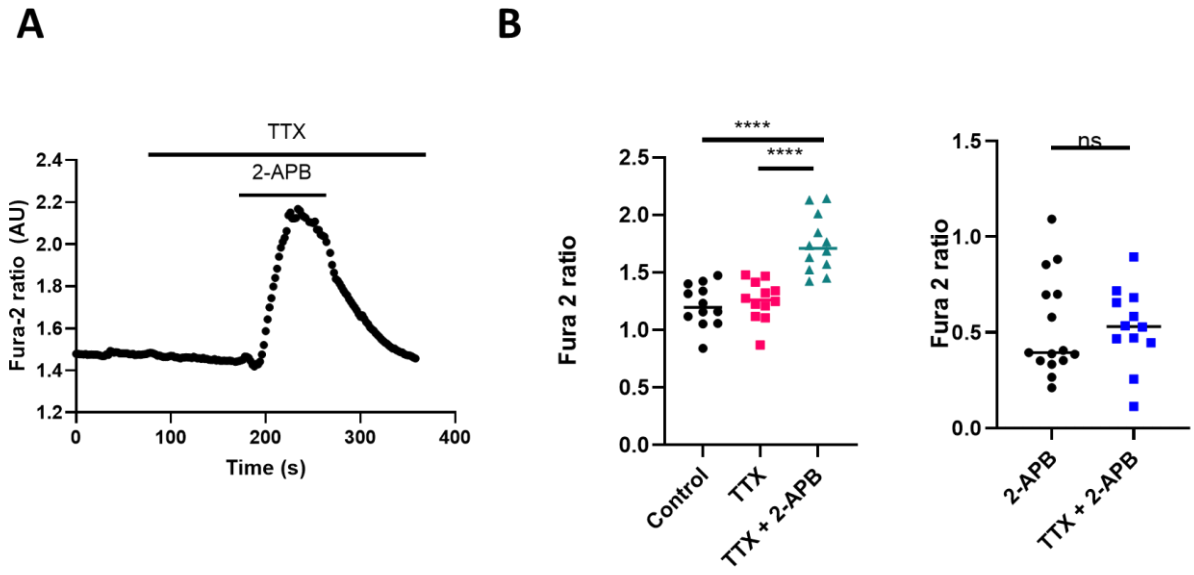



***Figure 6.5 The 2-APB response was independent of neuronal activity*** *Sodium channel inhibitor TTX, did not significantly alter 2-APB $[Ca^{2+}]_i$ responses. 1 μM TTX did not affect baseline $[Ca^{2+}]_i$ and 2-APB still elicited a $Ca^{2+}$ significant response in TTX treated neurons (B) (n=12; Repeated-measures ANOVA; p<0.0001) (Tukey's multiple comparisons test; Control vs TTX, p=0.66; TTX vs TTX with 2-APB, p<0.0001; Control vs TTX with 2-APB, p<0.0001). Here n refers to cell number, where a minimum culture n of 2 was used, with each culture using a minimum of 2 animals.*

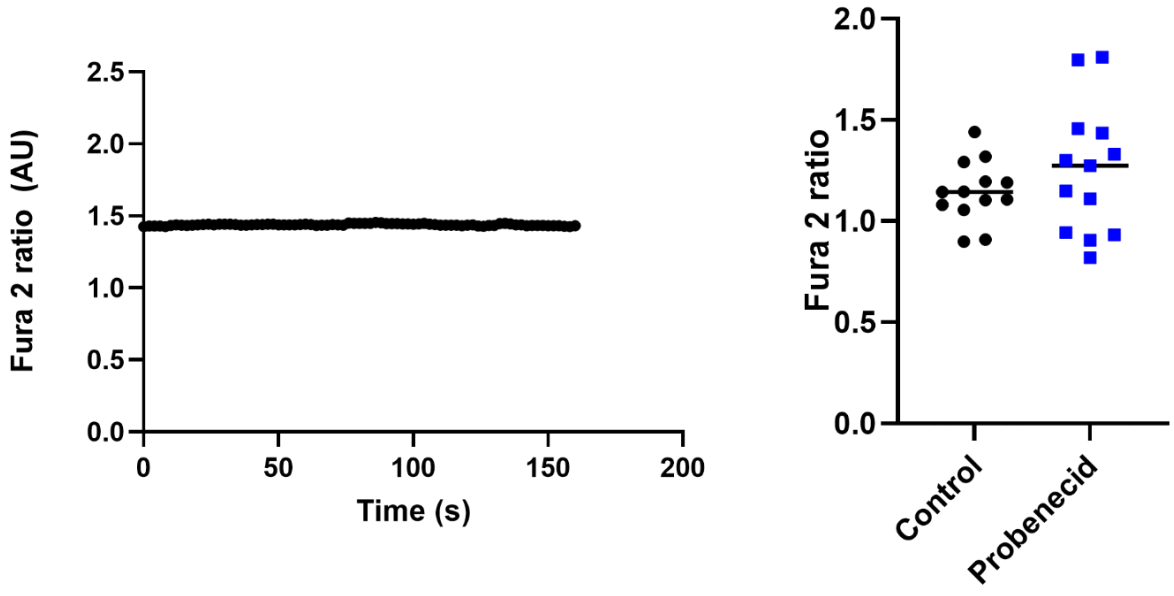



***Figure 6.6 Probenecid had no effect upon*** *$[Ca^{2+}]_i$ Probenecid had no effect upon $[Ca^{2+}]_i$ as measured by Fura-2AM from stellate ganglia neurons (n=13; Paired t-test; p=0.15). Here n refers to cell number, where a culture n of 2 was used, with each culture using a minimum of 2 animals.*

Next, TRPV2 selective pharmacology was assessed. First, the TRPV2 agonists probenecid (Bang *et al.*, 2007) and cannabidiol (Pumroy *et al.*, 2019) were tested. Probenecid had a small non-significant effect (**Figure 6.6**), similar to that previously reported for heterologously expressed TRPV2 (Iwata *et al.*, 2018). 10 µM cannabidiol evoked a significant increase in $[Ca^{2+}]_i$, which was significantly reduced by the TRPV, TRPM6 and TRPA1 antagonist 10 µM ruthenium red (Amann & Maggi, 1991; Muraki *et al.*, 2003; Clapham, 2007) (**Figure 6.7**). Surprisingly, 10 µM cannabidiol did not cause membrane depolarisation in whole-cell patch clamp, and instead caused a significant membrane hyperpolarisation (-1.99±0.69 mV) (**Figure 6.8**). TRPV2 specific antagonist 30 µM tranilast (Iwata *et al.*, 2018) caused a small but significant reduction in 2-APB mediated response (**Figure 6.9**).

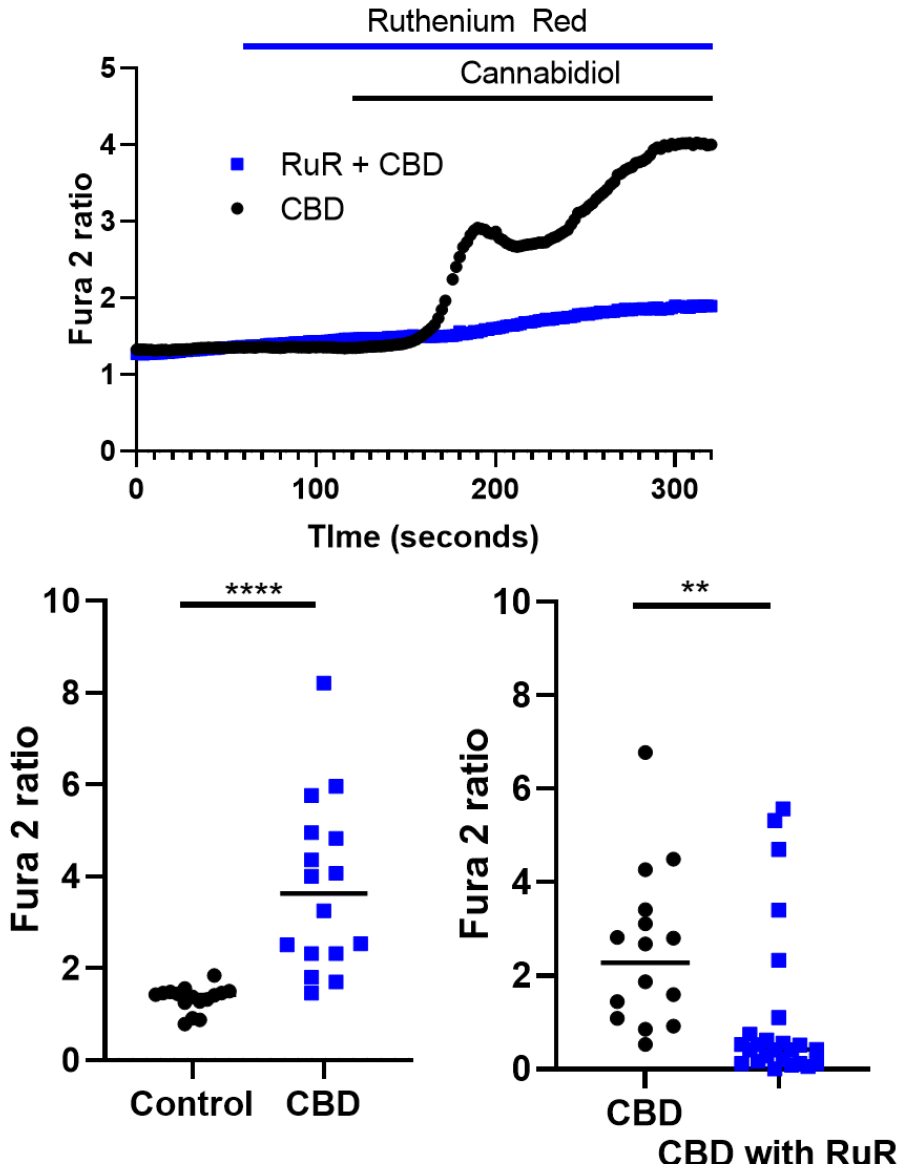



***Figure 6.7 Cannabidiol (CBD) elicited an increase in $[Ca^{2+}]_i$ which was inhibitable by the TRP antagonist Ruthenium red*** *(A) Cannabidiol induced a significant increase in $[Ca^{2+}]_i$ in stellate ganglia neurons (n=16; Paired t-test; p<0.0001). (B) TRP antagonist Ruthenium red significantly reduced the response to cannabidiol relative to cannabidiol alone (n=16, n=24; Mann-Whitney test; p=0.0023). Here n refers to cell number, where a minimum culture n of 2 was used, with each culture using a minimum of 2 animals.*

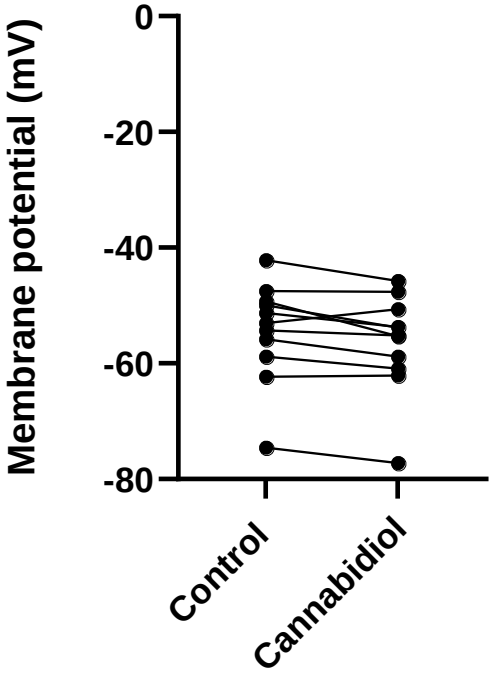



***Figure 6.8 Cannabidiol hyperpolarised neuronal membrane potential*** *Cannabidiol hyperpolarised resting membrane potential as recorded by whole-cell patch-clamp (n=11; Paired t-test; p=0.016). Here n refers to cell number, where a culture n of 2 was used, with each culture using a minimum of 2 animals.*

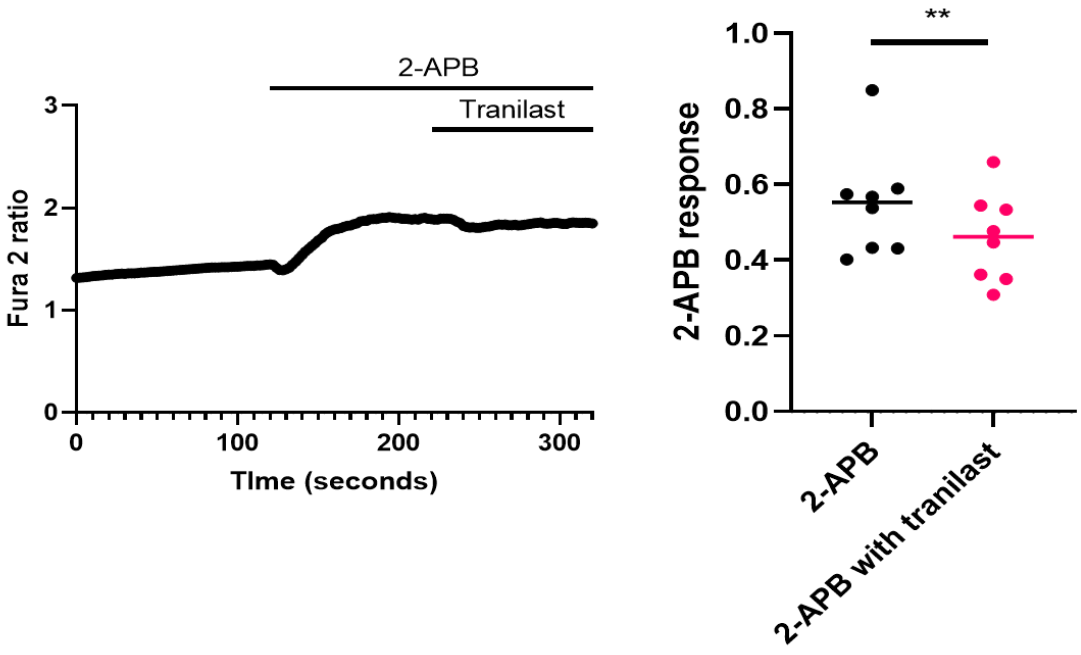



***Figure 6.9 TRPV2 antagonist tranilast caused a small, but significant decrease in 2-APB response*** *When applied after 2-APB, TRPV2 antagonist 30 μM tranilast significantly reduced 2-APB mediated increased $[Ca^{2+}]_i$ (n=8; Paired t-test; p<0.0078). Here n refers to cell number, where a culture n of 2 was used, with each culture using a minimum of 2 animals.*

Next, expression of putative TRP subunits TRPV2 and TRPC1 was reduced via siRNA knockdown (**Figure 6.1**). TRPM7 was not tested for as TRPM7 agonist Naltriben did not elicit a response (**Table 6.1**) and TRPM7 is known to be localised in synaptic vesicles in sympathetic neurons (Krapivinsky *et al.*, 2006). Interestingly, knockdown of both TRPV2 and TRPC1, but not the GAPDH control decreased the 2-APB mediated response (**Figure 6.10**).

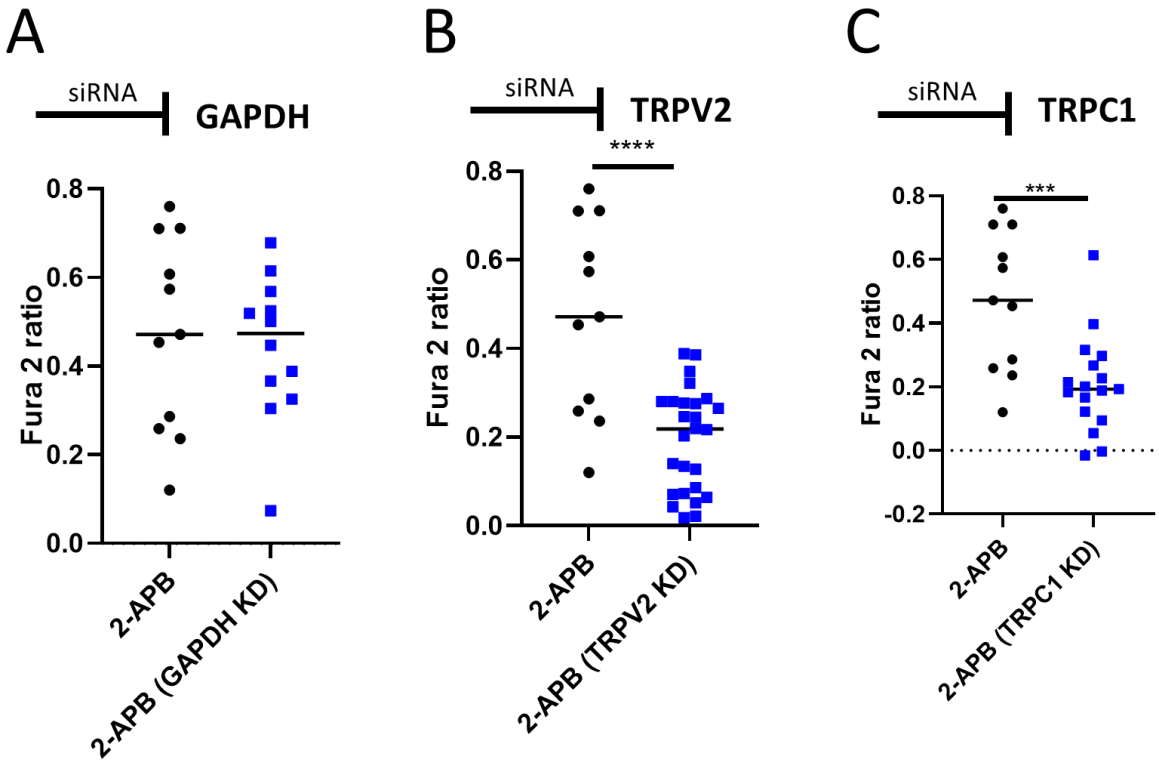



***Figure 6.10 Knockdown of either TRPV2 or TRPC1 reduced the neuronal response to 2-APB*** *siRNA mediated knockdown of TRPV2 (n=11, n=26; Unpaired t-test; p<0.0001) or TRPC1 (n=11, 17; Unpaired t-test; p=0.0008), but not GAPDH (n=11, n=12; Unpaired t-test; 0.72) significantly reduced neuronal $[Ca^{2+}]_i$ response to 100 μM 2-APB as measured by Fura-2AM. Here n refers to cell number, where a culture n of 3 was used, with each culture using a minimum of 2 animals.*

TRPV2 channels are temperature sensitive, but it seems extremely unlikely that the extremes of temperature required to activate TRPV2 (>50ºC) (Caterina *et al.*, 1999; Liu & Qin, 2016) would occur within the stellate ganglia. TRPV2 (Muraki *et al.*, 2003) and TRPC1 (Maroto *et al.*, 2005) are both activated by membrane stretch, such as the activation of cardiomyocyte TRPV2 during contraction

(Katanosaka *et al.*, 2014). It was hypothesised that during strong cardiac contraction this may stretch the sympathetic neurons in a similar manner to that described in cardiomyocytes and aortic myocytes (Muraki *et al.*, 2003; Katanosaka *et al.*, 2014). Membrane stretch simulated here via a reduction in extracellular osmolarity, which is known to activate mechanosensitive TRPV2 channels (Muraki *et al.*, 2003). However, this protocol did not cause depolarisation or alter neuronal excitability (**Figure 6.6**).

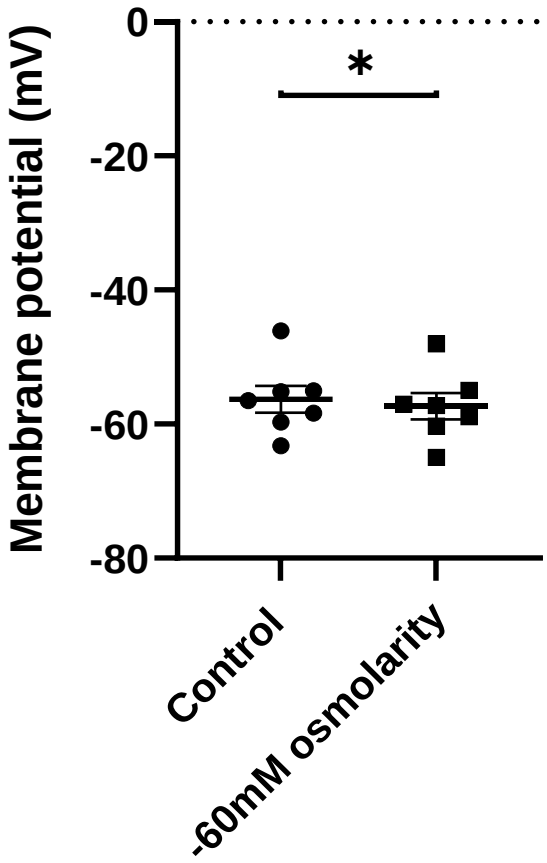



***Figure 6.10 Reducing osmolarity did not significantly alter the resting membrane potential or change firing rate*** *In whole cell recordings, reduction of osmolarity by 60 mM caused a small but significant membrane hyperpolarisation (n=8; Paired t-test; 0.014). Here n refers to cell number, where a culture n of 2 was used, with each culture using a minimum of 2 animals.*

Heterologously expressed TRPV2 2-APB responses are enhanced by low pH (pH 6.5) (Iwata *et al.*, 2018), and addition of 2-APB at pH 6.5 caused a significant increase in $[Ca^{2+}]_i$ (**Figure 6.12A**), which was significantly larger than a paired response for 2-APB at pH 7.4 (**Figure 6.12B**). Next the effect of TRPV2 selective agonist probenecid (Bang *et al.*, 2007) was tested at pH 6.5, which caused a significant increase in $[Ca^{2+}]_i$ under these conditions (**Figure 6.13**). This is consistent with prior reports that the TRPV2 probenecid response is very small at physiological pH (Iwata *et al.*, 2018). Notably, pH 6.5 decreased baseline and nicotinic Fura-2AM responses (Appendix figure 14) and so an increased 2-APB response was not due to a generalised effect of low pH.

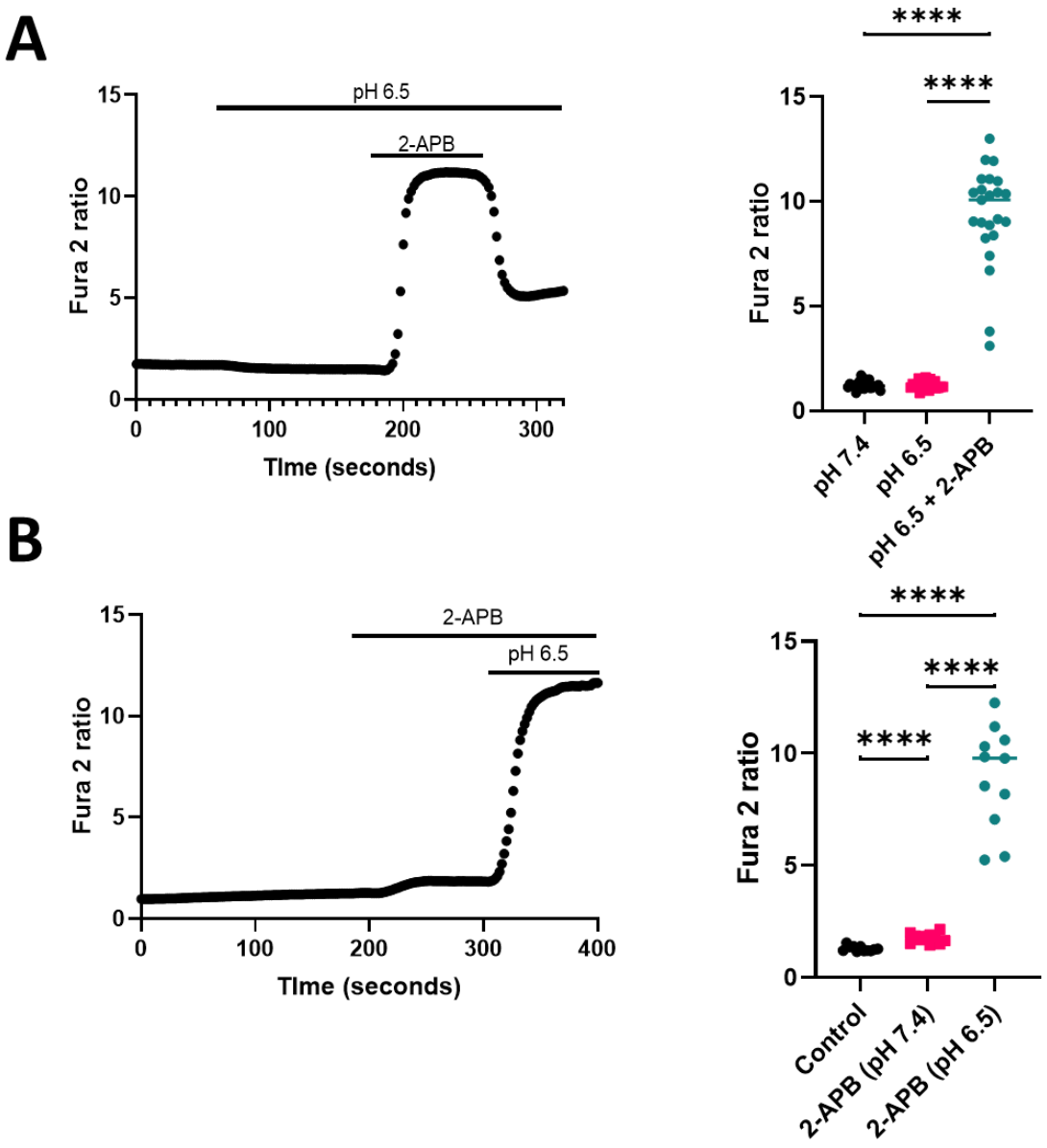



***Figure 6.12 The 2-APB response was modulated by pH*** *Acidic pH amplified the 2-APB response when tested by two alternate protocols. pH 6.5 (A) Tyrode's solution caused a non-significant decrease in $[Ca^{2+}]_i$, but a significant increase in $[Ca^{2+}]_i$ occurred following 2-APB addition at acidic pH (n=23; Repeated-measures ANOVA; p<0.0001) (Tukey's multiple comparisons test; pH 7.4 vs pH 6.5, p=0.41; pH 7.4 vs pH 6.5 with 2-APB, p<0.0001; pH 6.5 vs pH 6.5 with 2-APB, p<0.0001). (B) The 2-APB response was significantly larger at pH 6.5 than at pH 7.4 (n=11; Repeated-measures ANOVA; p<0.0001) (Tukey's multiple comparisons test; Control vs pH 7.4 with 2-APB, p<0.0001; Control vs pH 7.4 with 2-APB, p<0.0001; pH 7.4 with 2-APB vs pH 6.5 with 2-APB, p<0.0001). Here n refers to cell number, where a minimum culture n of 2 was used, with each culture using a minimum of 2 animals.*

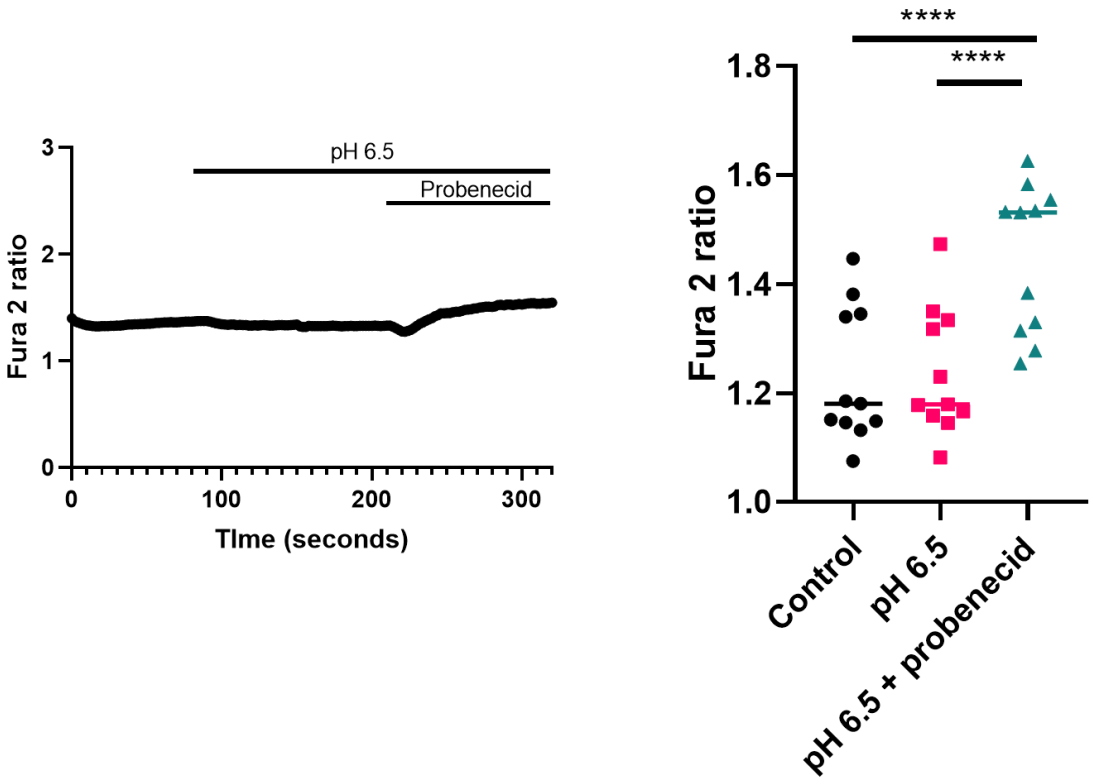



***Figure 6.13 Acidic pH amplifies the probenecid*** *$[Ca^{2+}]_i$* ***response*** *Probenecid induced a statistically significant increase in $[Ca^{2+}]_i$ at pH 6.5 (n=11; Repeated-measures ANOVA; p<0.0001)(Tukey's Multiple comparisons test; Control vs pH 6.5, p=0.65; Control vs pH 6.5 + probenecid, p<0.0001; pH 6.5 vs pH 6.5 with probenecid, p<0.0001). Here n refers to cell number, where a culture n of 2 was used, with each culture using a minimum of 2 animals.*

### 6.3.2 Response to the inflammatory soup

This project assessed the SGNs response to a range of sensory transmitters and environmental conditions which comprise the "inflammatory soup". First transcript expression was investigated by scRNAseq. Sympathetic SGNs express adenosine (*ADORA1*), histamine (*HRH3*), NGF (*NGFR* and *NTRK1*), ATP (*P2RX2*) receptors in a proportion of the sequenced population (**Figure 6.15**).

Ionotropic P2X receptors appear to be the predominant purinergic signalling system in the SGN (**Figure 6.15**). As P2X receptors are $Ca^{2+}$-permeable ion

channels, ATP signalling through P2X can be detected by Fura-2AM intracellular $Ca^{2+}$ imaging (Tsien, 1986; Tenneti *et al.*, 1998). This approach was used here to confirm P2X receptor expression in SGNs. 100 μM ATP induced a significant increase in $[Ca^{2+}]_i$ in SGNs (**Figure 6.15**). The expression of $G_q$-coupled $P2Y_6$ receptors (Chang *et al.*, 1995) was also detected here, although these receptors were not investigated as this receptor is activated by Uridine 5'-diphosphate and not ATP (Lazarowski *et al.*, 2001).

Next, the effect of the neurotransmitter adenosine was tested. Transcript expression of $A_1$-receptors (*ADORA1*) was identified by scRNAseq (**Figure 6.15**)**.** $A_1$-receptors are $G_i$-coupled receptors (Figler *et al.*, 1996), and have demonstrated to reduce SCG $Ca_v$ (Zhu & Ikeda, 1993) and neurotransmitter release (Koh & Hille, 1997). However, their presence in the SGN, or their effect on sympathetic neuron firing properties has not been reported. SGN rheobase increased, but no effect was observed on maximum firing rate (**Figure 6.16C**).

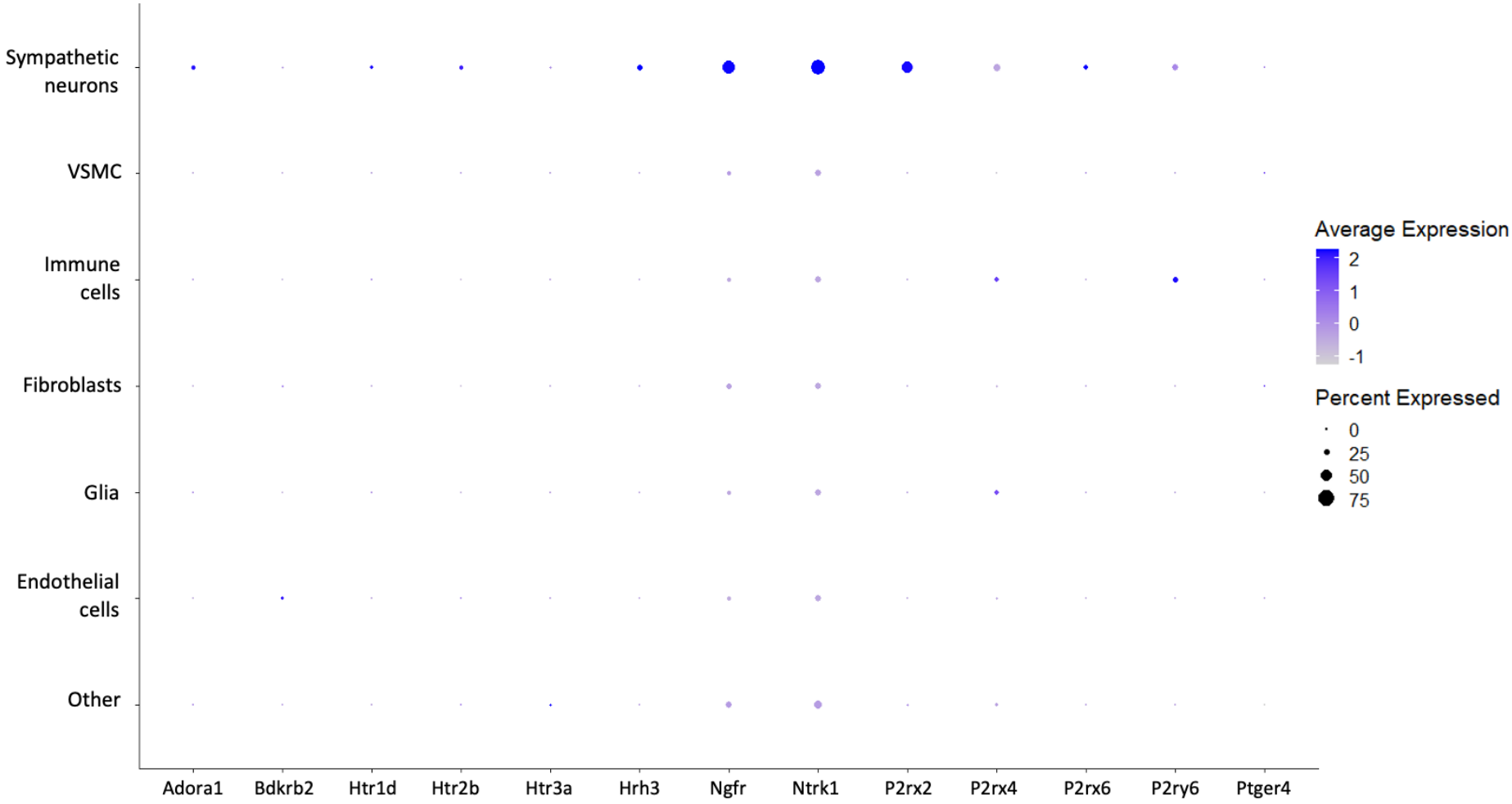



***Figure 6.14 Single-cell RNA sequencing reveals expression of multiple sensory receptors including ADORA1, HRH3, NGFR, NTRK1 and P2RX2***

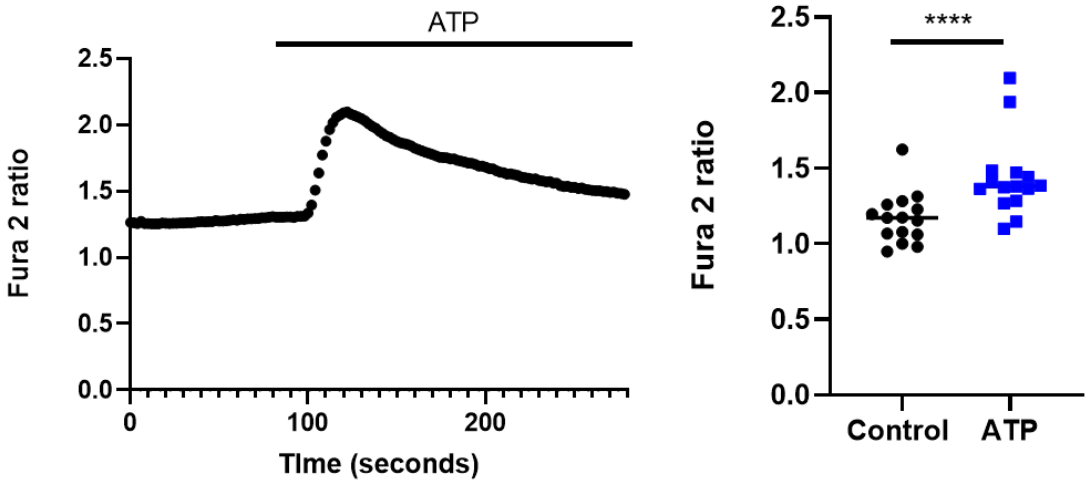



***Figure 6.15 ATP evoked a calcium transient in sympathetic stellate ganglia neurons*** *ATP caused a significant increase (Median; 0.21) in $[Ca^{2+}]_i$ as measured by Fura-2AM imaging. (n=15; Wilcoxon matched-pairs test; p<0.0001). Here n refers to cell number, where a culture n of 2 was used, with each culture using a minimum of 2 animals.*

Low expression of 5-HT receptors 1D and 2B was detected in a proportion of SGNs (**Figure 6.14**). 5-HT1D receptors are $G_i$ coupled (Brys *et al.*, 2000) and 5-HT2B receptors are $G_q$-coupled GPCRs (Roth *et al.*, 1984). Activation of 5-HT receptors by 5-HT, had no effect upon neuronal firing rate or rheobase (**Figure 6.16B**).

Histaminergic $H_3$-receptor encoding gene *HRH3* was expressed in a subset of sympathetic SGNs (**Figure 6.14**). $H_3$-receptors are $G_i$-coupled receptors (Arrang *et al.*, 1983), which would be expected to inhibit neuronal activity based upon their effect in other neuronal populations (Varaschin *et al.*, 2018). Further $H_3$-receptors reduce noradrenaline release from SCG neurons (Silver *et al.*, 2002). An increase in neuronal rheobase was observed, but histamine had no effect upon neuronal firing (**Figure 6.16C**).

NGF receptor encoding *NGFR* and *TRKA* were each expressed in SGNs (**Figure 6.14**). However, NGF had no effect on neuronal maximum firing rate or rheobase (**Figure 6.17A**).

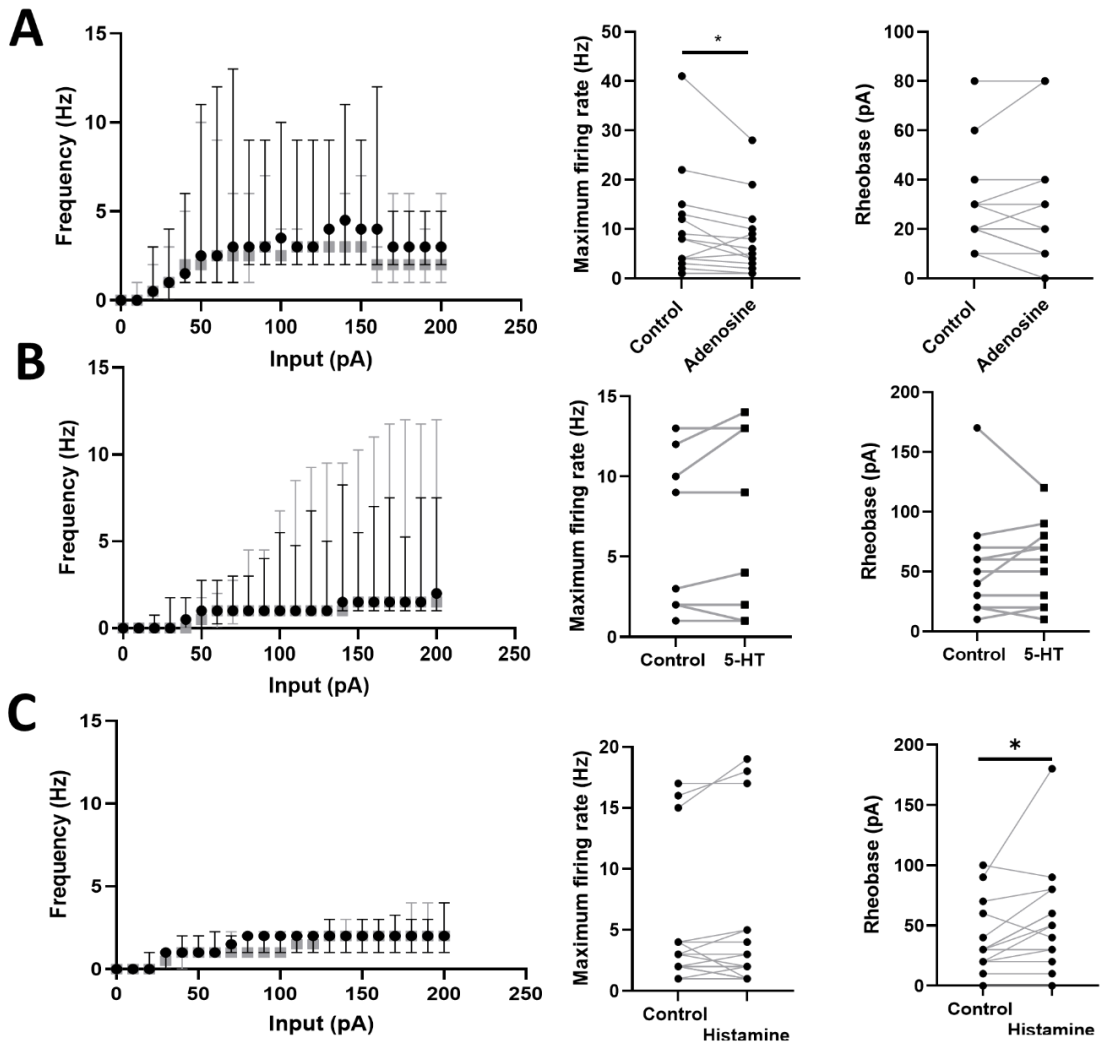



***Figure 6.16 Firing rate responses of stellate ganglia neurons to Adenosine, serotonin and Histamine*** *Adenosine decreased maximum firing rate (n=14; Wilcoxon matched-pairs test; p=0.027), but did not affect rheobase (n=14; Wilcoxon matched-pairs test; p<0.99) (A). 10 μM Serotonin (5-HT) did not affect maximum firing rate (n=12; Wilcoxon matched-pairs test; p=0.38) or rheobase (n=12; Wilcoxon matched-pairs test; p=0.78) (B). Histamine did not affect maximum firing rate (n=17; Wilcoxon matched-pairs test; p=0.44), but significantly increased rheobase (n=17; Wilcoxon matched-pairs test; p=0.033) (C). Here n refers to cell number, where a minimum culture n of 2 was used, with each culture using a minimum of 2 animals.*

Genes encoding ASIC and proton sensitive GPCRs were not expressed in stellate ganglia (**Figure 6.15**), and acidic pH had no effect upon neuronal firing or rheobase (**Figure 6.17B**). Similarly, there was minimal expression of either $PGE_2$ receptors or bradykinin receptors (**Figure 6.15**) and these transmitters had little effect (**Figure 6.17C-D**).

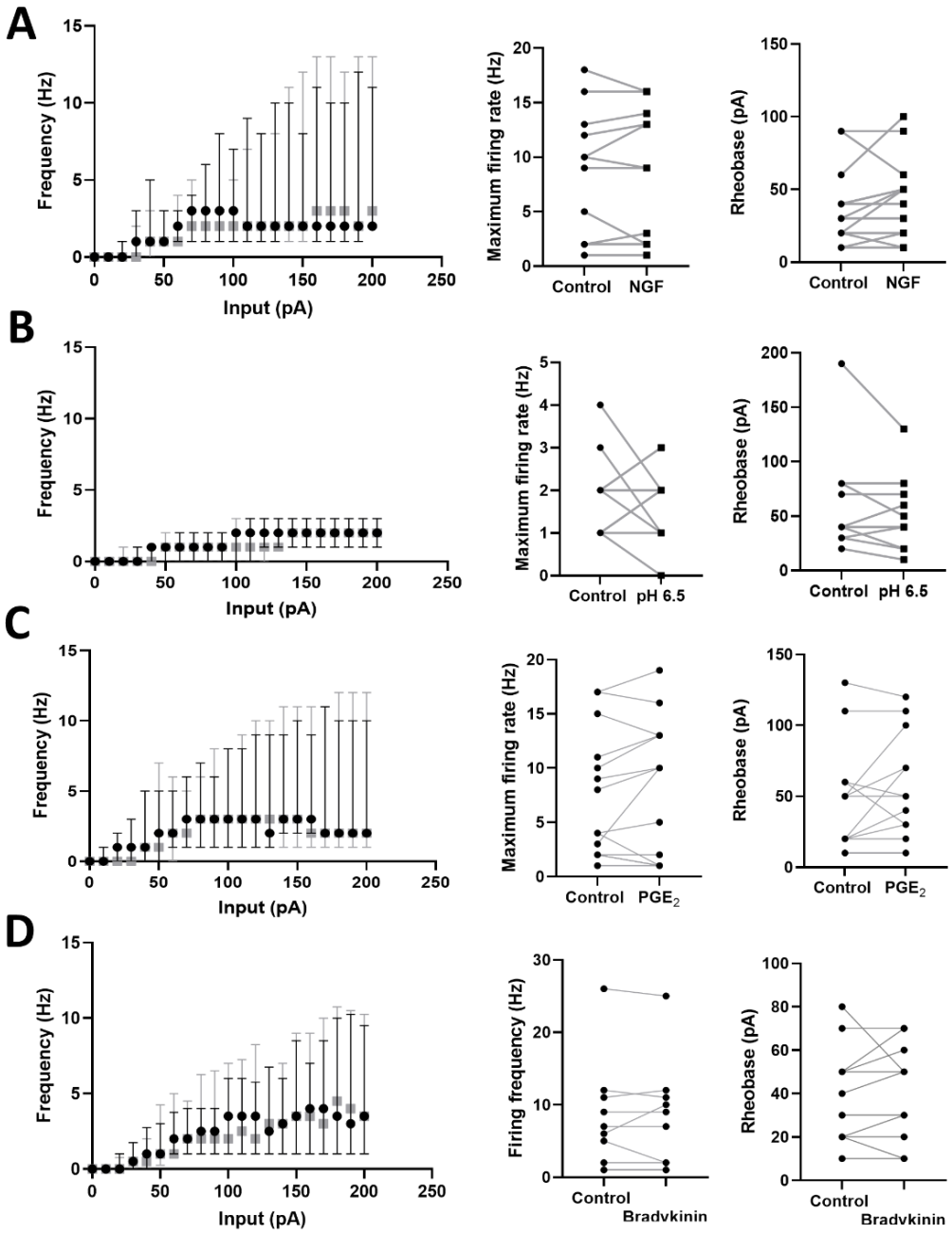



***Figure 6.17 Firing rate responses of stellate ganglia neurons to NGF, pH 6.5, $PGE_2$ and Bradykinin*** *(A)100ng/ml NGF had no effect upon maximal firing rate (n=15; Wilcoxon matched-pairs test; p<0.99) or rheobase (n=15; Wilcoxon matched-pairs test; p=0.24). (B) A change of pH, from 7.4 to 6.5 did not affect firing rate (n=11; Wilcoxon matched-pairs test; p=0.55) or rheobase (n=11; Wilcoxon matched-pairs test; p=0.27). (C) 1 μM PGE2 did not affect maximum neuronal firing rate (n=15; Wilcoxon matched-pairs test; p=0.38) or rheobase (n=15; Wilcoxon matched-pairs test; p=0.30). (D) 10 μM Bradykinin did not affect neuronal maximum firing rate (n=12; Wilcoxon matched-pairs test; p<0.99) or rheobase (n=12; Wilcoxon matched-pairs test; p=0.78). Here n refers to cell number, where a minimum culture n of 2 was used, with each culture using a minimum of 2 animals.*

### 6.3.3 Is there functional evidence for glutamatergic receptors?

Multiple ionotropic glutamatergic subunit encoding genes were expressed in the stellate ganglia (**Figure 6.18**). In addition, $G_i$-coupled Metabotropic glutamate receptor 7 (*GRM7*) (Okamoto *et al.*, 1994) was identified in SGNs (**Figure 6.18**). However, neither glutamate or NMDA with D-Serine and low Magnesium evoked a $Ca^{2+}$ response in SGNs (**Figure 6.19**). $[Ca^{2+}]_i$ significantly decreased following perfusion of glutamate, however, the effect is extremely small and is more likely to represent a miniscule drift during recording.

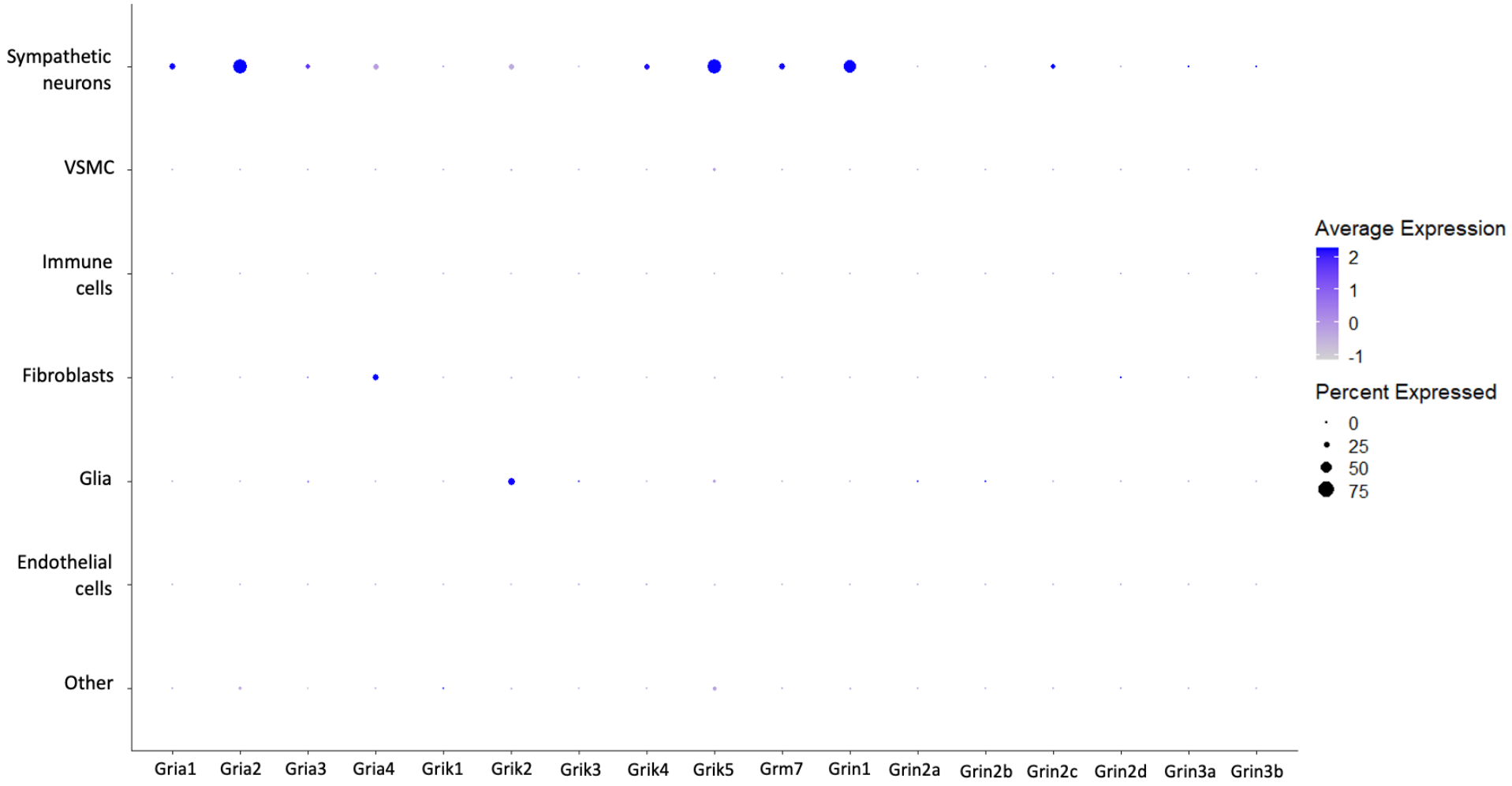



*Figure 6.18 Single-cell RNA-sequencing highlights neuron-specific expression transcript of AMPAR encoding GRIA1, GRIA2, kainate receptor encoding GRIK4 and NMDAR encoding GRIN1 and GRIN2C.*

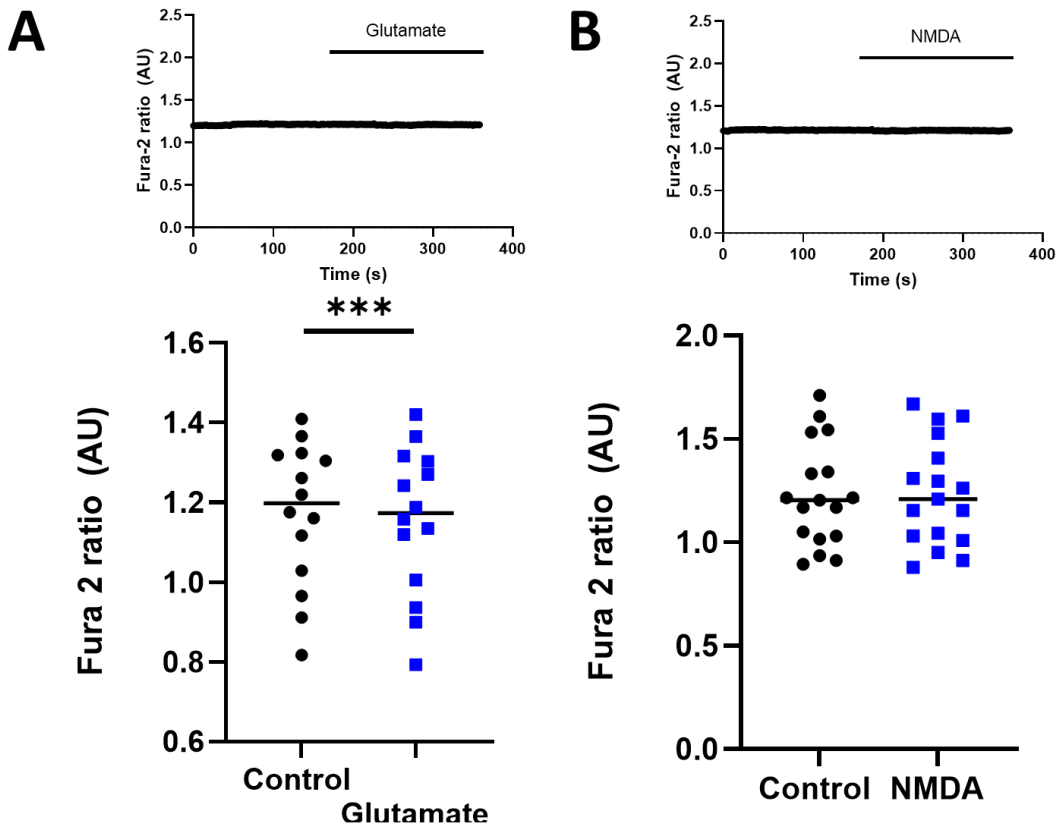



***Figure 6.19 Canonical Glutamatergic receptor agonist Glutamate and NMDA receptor agonist NMDA did not elicit an expected increase in intracellular $Ca^{2+}$concentration*** *(A) Glutamate (1 mM) recordings were performed in normal Tyrode's solution (n=14; Paired t-test; p = 0.0006). (B) NMDA (50 µM) recordings were performed in low (0.2 mM) $Mg^{2+}$solutions with 10 µM D-Serine added as a NMDAR co-agonist (n=17; Paired t-test; p=0.42). These recordings were performed by Ayesha Musa, an FHS student under my supervision. Here n refers to cell number, where a culture n of 4 was used, with each culture using a minimum of 2 animals.*

### 6.3.4 Can cardiomyocytes signal to sympathetic neurons?

Wistar neonatal cardiomyocytes and wistar SGNs were co-cultured together for a minimum of 2 days before the electrical phenotype of the SGNs was assessed by whole-cell patch clamp. Co-culture caused a non-significant trend towards an increased maximum firing rate relative to Wistar neurons alone and caused a non-significant trend towards decreased rheobase (**Figure 6.20**). Cardiomyocytes were then cultured alone, and the media removed after a period of 48 hours. This "conditioned media" was then transferred to dishes containing neurons only, and neurons were cultured in this conditioned media for 24 hours before recording the electrical phenotype. Like in co-culture, wistar neurons cultured in conditioned media also displayed a tendency towards increased maximum firing rate and decreased rheobase (**Figure 6.21**).

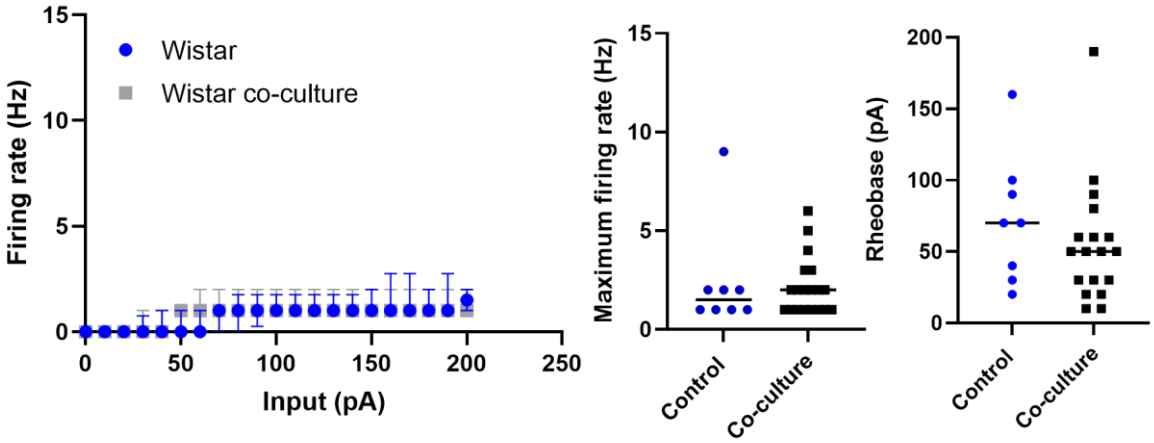



***Figure 6.20 The electrical excitability of Wistar neurons appears to be marginally increased in co-culture*** *(Wistar neuron, 1.5 Hz; Wistar neuron in co-culture, 2 Hz) (n=8, n=19; Mann Whitney test; p=0.68) (Wistar neuron, 70 pA; Wistar neuron in co-culture, 50 pA) (n=8, n=18; Mann Whitney test; p=0.27) Wistar neonatal cardiomyocytes were provided by Dr. Dan Li, Dr. Kun Liu and Dr. Ni Li. Here n refers to cell number, with a culture n of 1 for control recordings and a culture n of 3 for the co-culture recordings. Each culture used a minimum of 2 animals for neurons, and a minimum of 10 animals for cardiomyocytes.*

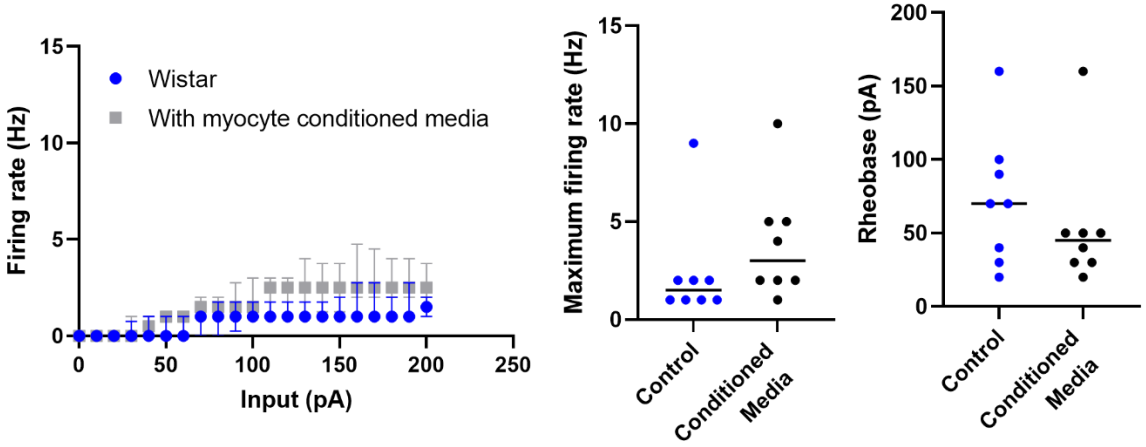



***Figure 6.21 The electrical excitability of Wistar neurons appears to be increased in cardiomyocyte conditioned media*** *(Wistar 1.5 Hz, Wistar neuron with conditioned media, 3 Hz) (n=8, n=8; Mann Whitney test; p=0.10) (Wistar neuron, 70 pA, Wistar neuron with conditioned media, 45 pA) (n=8, n=8; Mann Whitney test; p=0.29). Wistar neonatal cardiomyocytes were provided by Dr. Dan Li, Dr. Kun Liu and Dr. Ni Li. Here n refers to cell number, with a culture n of 1 for control recordings and a culture n of 2 for the conditioned media recordings. Each culture used a minimum of 2 animals for neurons, and a minimum of 10 animals for cardiomyocytes.*

Next SHR neurons were co-cultured with Wistar cardiomyocytes. As these recordings used a different culture media than in chapter 4, the Wistar and SHR phenotypes observed previously were first reconfirmed. As expected SHR neurons had a significantly higher firing rate than Wistar neurons, and SHR neurons had a lower rheobase although this underpowered (p=0.05) (**Figure 6.22**).

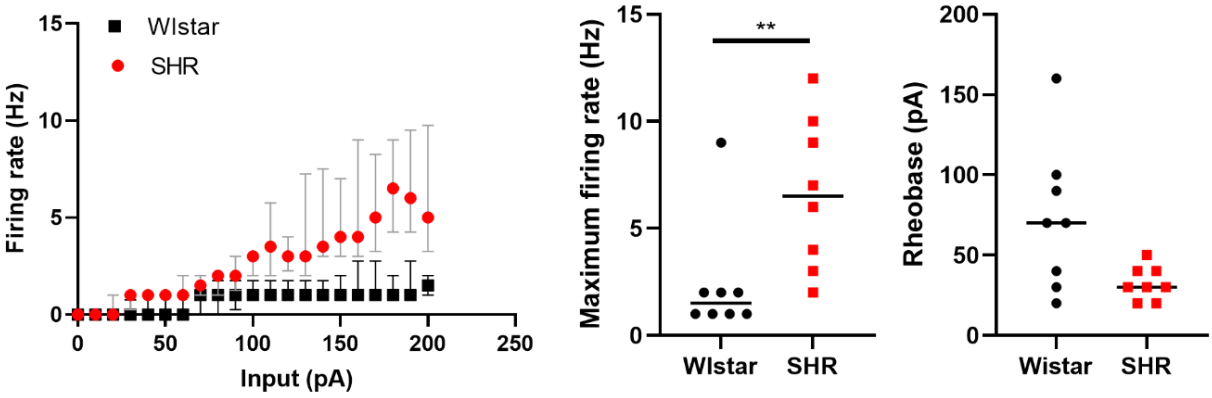



***Figure 6.22 In co-culture media, 5-6 week Wistar and SHR stellate ganglia neurons have a similar electrical phenotype to that described previously*** *SHR stellate ganglia neurons have a significantly greater maximum firing rate than Wistar neurons. (n=8, n=8; Mann Whitney test; p=0.0064) (Wistar 1.5 Hz, SHR 6.5 Hz) Rheobase showed a nonsignificant trend to decrease in SHR neurons. (n=8, n=8; Mann Whitney test; p=0.053) (Wistar 70 pA, SHR 30 pA) Wistar neonatal cardiomyocytes were provided by Dr. Dan Li, Dr. Kun Liu and Dr. Ni Li. Here n refers to cell number, with a culture n of 1 for Wistar recordings and a culture n of 2 for the SHR recordings. Each culture used a minimum of 2 animals.*

Co-culturing SHR neurons with Wistar neonatal cardiomyocytes caused a trend towards reduced SHR neuron firing rate (p=0.05) and significantly increased SHR neuron rheobase relative to SHR neurons cultured alone (**Figure 6.23**). Similar non-significant trends were observed when SHR neurons were cultured in Wistar cardiomyocyte conditioned media (**Figure 6.24**). A summary of the key findings from the co-culture model is shown in **Figure 6.25**.

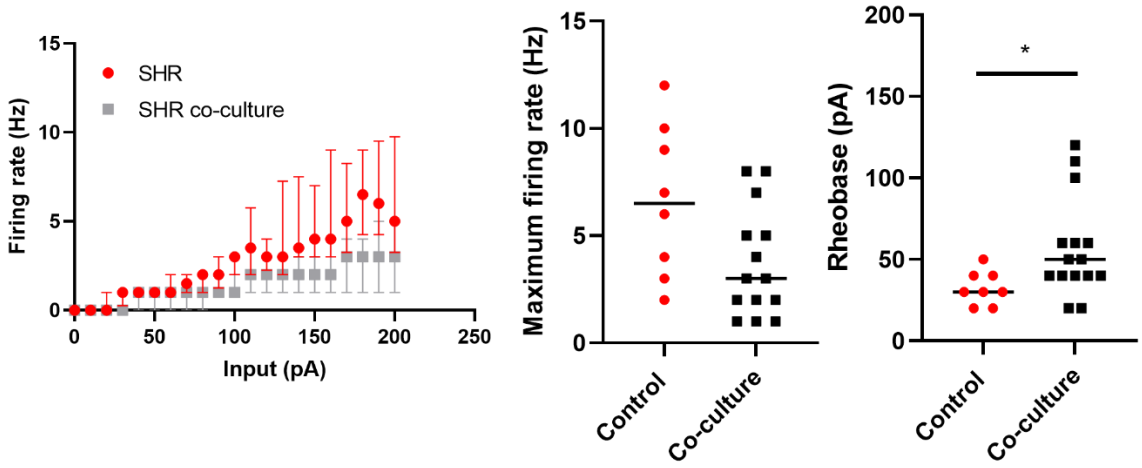



***Figure 6.23 Co-culturing SHR neurons with Wistar cardiomyocytes appears to decrease SHR neuron excitability*** *SHR neurons co-cultured with Wistar cardiomyocytes show a non-significant trend to decrease the median maximum firing rate (SHR neuron in co-culture, 3 Hz) relative to SHR neurons cultured alone (SHR neuron, 6.5 Hz) (n=8, n=15; Mann Whitney test; p=0.051). SHR neurons co-cultured with Wistar cardiomyocytes have a significantly increased median rheobase (SHR neuron in co-culture, 50 pA) relative to SHR neurons cultured alone (SHR neuron, 30 pA) (n=10, n=15; Mann Whitney test; p=0.021). Wistar neonatal cardiomyocytes were provided by Dr. Dan Li, Dr. Kun Liu and Dr. Ni Li. Here n refers to cell number, with a culture n of 1 for control recordings and a culture n of 3 for the co-culture recordings. Each culture used a minimum of 2 animals for neurons, and a minimum of 10 animals for cardiomyocytes.*

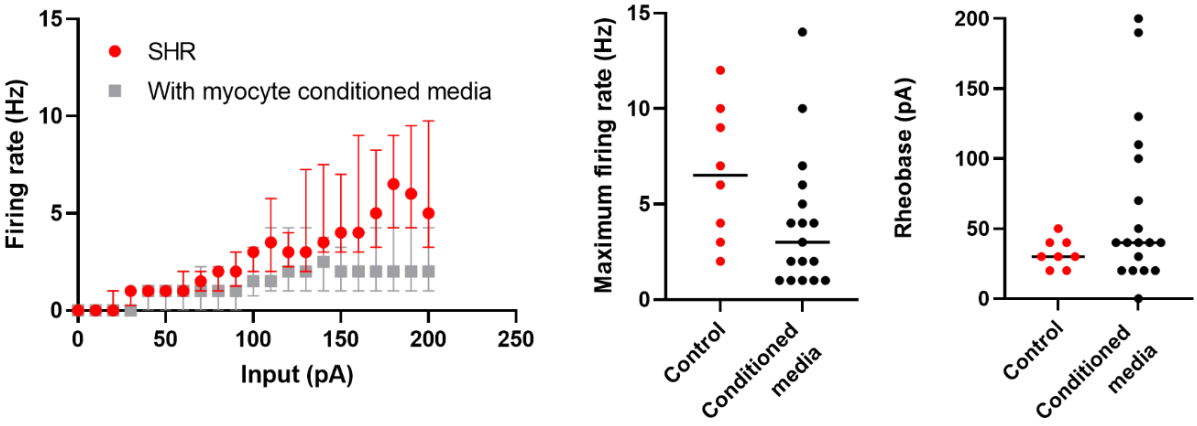



***Figure 6.24 Co-culturing SHR neurons with Wistar myocyte conditioned media appears to replicate the effect observed in co-culture*** *Wistar cardiomyocyte conditioned media caused a non-significant trend towards decreased firing in SHR neurons (SHR neurons with conditioned media, 3 Hz) relative to SHR neurons alone (SHR neuron, 6.5 Hz) (n=8, n=17; Mann Whitney test; p=0.061). Wistar cardiomyocyte treated media caused a non-significant trend towards increased rheobase in SHR neurons (SHR neurons with conditioned media, 40 pA) relative to SHR neurons alone (SHR neuron, 30 pA) (n=8, n=18; Mann Whitney test; p=0.24). Wistar neonatal cardiomyocytes were provided by Dr. Dan Li, Dr. Kun Liu and Dr. Ni Li. Here n refers to cell number, with a culture n of 1 for control recordings and a culture n of 3 for the conditioned media recordings. Each culture used a minimum of 2 animals for neurons, and a minimum of 10 animals for cardiomyocytes.*

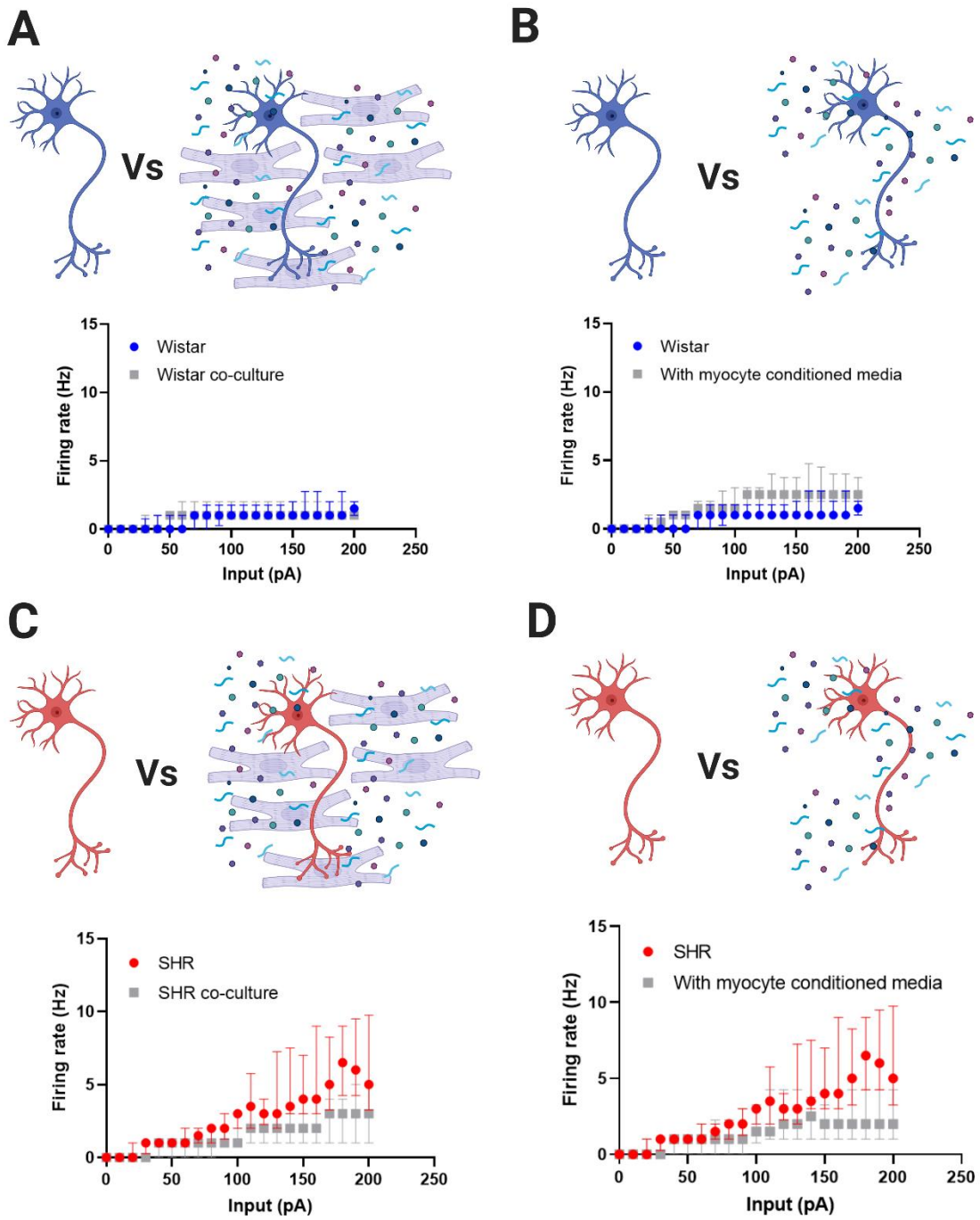



***Figure 6.25 Visual summary of the key findings from the co-culture experiments*** *Here data from figures 6.20-6.24 are summarised together for clarity. Culturing of Wistar 5-6 week old stellate ganglia neurons cultured either (A) directly with neonatal cardiomyocytes or (B) with conditioned media from neonatal cardiomyocytes caused a small trend towards increased neuronal activity. Culturing of SHR 5-6 week old stellate ganglia neurons with either (C) Wistar cardiomyocytes or (D) conditioned media from Wistar cardiomyocytes decreased the increased neuronal firing observed in Figure 6.22 (or chapter 4). For both the diagrams and graphs blue indicates that the cells originated from the Wistar and red originates that the cells were from SHRs. The unidentified factor(s) released from Wistar cardiomyocytes are indicated by the small particles in blue. Neuronal firing data post-treatment are indicated by grey dots for both strains.*

## 6.4 Discussion

### 6.4.1 Observations on TRP channels

Based upon the description provided here, there appears to one or multiple plasma membrane TRP currents present in the Wistar SGN. The pharmacological profile of this channel fits well with TRPV2 currents, an observation which is support by scRNAseq and immunohistochemistry. This is further supported by previous immunohistochemical observations from the rat SCG (Gaudet *et al.*, 2004) and human stellate ganglia (Kokubun *et al.*, 2015). Interestingly, these studies suggest that TRPV2 is present in only a small subpopulation of cells, whereas by scRNAseq, perforated patch clamp and Fura-2AM calcium imaging TRPV2 or at least a very similar current appears to be ubiquitously expressed.

There were however, some inconsistencies with the known characteristics of TRPV2 channels, for example, 10 μM cannabidiol evoked membrane hyperpolarisation, rather than depolarisation, in whole-cell patch-clamp and equally osmolarity induced cell swelling did not activate TRPV2 currents as previously described in other cell types (Muraki *et al.*, 2003). These discrepancies may arise due to the use of the whole-cell configuration, as opposed to perforated patch-clamp which was successfully used to record 2-APB responses. This change in methodology was made due to time constraints. However, it is unlikely as previous reports have suggested that 2-APB (Pumroy *et al.*, 2019), cannabidiol (Pumroy *et al.*, 2019) and cell swelling activated currents (Muraki *et al.*, 2003) were all recordable in the whole-cell configuration. Cannabidiol invoked TRPV2 currents were previously observed to be a lot smaller than 2-APB induced TRPV2 currents (Pumroy *et al.*, 2019), however, this does not explain the membrane hyperpolarisation. This could result from activation of inwardly-rectifying potassium

channels via endogenous cannabinoid receptors (McAllister *et al.*, 1999) thereby counteracting TRPV2 induced depolarisation. For example, functional $CB_1$ receptors were observed in the SCG (Pan *et al.*, 1998); however, scRNAseq did not detect expression of $CB_1$ or $CB_2$ (Data not shown). In addition, CBD is a negative allosteric modulator of $G_i$-coupled $CB_1$ receptors (Laprairie *et al.*, 2015) and would therefore be unlikely to inhibit TRPV2 induced depolarisation. These data could be resolved by voltage-clamp recordings of CBD induced current in either whole-cell or perforated patch-clamp configurations.

A depolarising response to cell swelling was not observed and it is possible that either the morphology of sympathetic neurons, or the properties of their membranes in some way prevents the activation of TRPV2 as observed in aortic myocytes (Muraki *et al.*, 2003). Follow up study could utilised a more regulated mechanised form of cell stretch, such as that recently used to activate sensory neuron TRPV2 channels (Katanosaka *et al.*, 2018). However, given the significant amount of work that this would require, and the unlikelihood of this occurring physiologically these experiments do not seem worthwhile. A notable exclusion from the pharmacological profile tested in this project is the often used TRPV1 and TRPV3 agonist camphor (Xu *et al.*, 2005). This is because this compound would not fully dissolve at the required concentration.

Previous work suggests that TRPV3 was present in the human stellate ganglia by immunohistochemistry (Kokubun *et al.*, 2015), however the data presented here do not support their presence in the rat. Notably, TRPV3 agonists Vanillin (Xu *et al.*, 2006), farnesyl pyrophosphate (Bang *et al.*, 2010) and carvacrol (Xu *et al.*, 2006) caused no change in $[Ca^{2+}]_i$ so it seems unlikely that TRPV3 channels are present in rat SGNs.

ScRNAseq and immunohistochemistry highlighted the expression of TRPV2, TRPC1 and TRPM7 currents in the stellate ganglia sympathetic neurons. However, these data do not provide pharmacological evidence for canonical TRPC1 or TRPM7 channels. For example, TRPM7 channels are activated by protons (Jiang *et al.*, 2005), however low pH had no effect alone, instead amplifying the $[Ca^{2+}]_i$ response to other agonists. This has been previously described for TRPV2 responses in both sensory neurons (Hu *et al.*, 2004) and heterologous expression systems (Iwata *et al.*, 2018). In addition there was not a detectable $[Ca^{2+}]_i$ response to TRPM7 agonist naltriben (Hofmann *et al.*, 2014). Further, TRPM7 (Chokshi *et al.*, 2012) and TRPC1 (Iwata *et al.*, 2018) are both inhibited by 2-APB and so are unlikely to be directly responsible for the 2-APB response alone.

The siRNA study highlighted that TRPV2 and TRPC1 knockdown decreased the 2-APB response. This was surprising given that TRPC1 is inhibited by 2-APB (Iwata *et al.*, 2018). Previous studies highlight that TRPC1 form functional heteromeric assemblies with TRPC4 and TRPC5 channels (Hofmann *et al.*, 2002; Bröker-Lai *et al.*, 2017) and with TRPV4, TRPV6 and TRPP2 channels (Ma *et al.*, 2011; Schindl *et al.*, 2012; Du *et al.*, 2014). However, no study has investigated TRPV2 and TRPC1 heteromeric assembly, and both channels remain poorly studied. Finally, these data may result from a technical issue with siRNA knockdown. GAPDH knockdown had no effect, which suggests that knockdown itself was not having a confounding action. However, without a clear method for confirming the specificity or extent of knockdown in cell culture, it is hard to resolve this issue. For this reason, this technique was not used in other projects, for example chapter 5.

Unfortunately, this project was resolved without a physiological mechanism for TRPV2 activation being highlighted. This in part reflects the poor contemporary understanding of TRPV2's role outside of extreme temperature (Liu & Qin, 2016) and membrane stretch (Muraki *et al.*, 2003) responses, which have not been proven to occur in the stellate ganglia. Further, a response to membrane stretch was not inducible by osmotic swelling here. Since this work was performed a study has highlighted that oxidation of TRPV2 by reactive oxygen species shifts the temperature sensitivity of TRPV2, permitting activation of TRPV2 at temperatures lower than 37$^{o}$C (Fricke *et al.*, 2019). This could suggest that TRPV2 activation is involved in the response to local inflammation or ischaemia and is an interesting line of further investigation

TRPC1 and TRPM7 function was not observed in the SGN (**Table 6.1**). For TRPM7 this is likely due to the localisation of TRPM7 protein on vesicles as observed previously in the SCG (Krapivinsky *et al.*, 2006). There are no selective activators of TRPC1, which is typically activated by $G_q$ coupled GPCRs (Trebak *et al.*, 2007). One possible, unexplored mechanism for TRPC1 activation is via Angiotensin-II, which can activate TRPC1 and TRPM7 channels through activation of $G_q$-coupled $AT_1$-receptors (Saleh *et al.*, 2006; Takahashi *et al.*, 2007). Given the presence of excitatory $AT_1$ signalling in sympathetic neurons (F. *et al.*, 2003; Zaika *et al.*, 2006) and the importance of sympathetic regulation by angiotensin-II in physiology (Tsuda, 2012), this may provide an interesting area of further investigation.

These data provide some of the first evidence of TRP channel electrophysiology in the stellate ganglia. These data support a current resembling TRPV2, with supporting scRNAseq and immunohistochemical data. Further TRPC1

and TRPM7 expression is also highlighted here. A physiological role for these channels is not provided here, but there is a putative role for oxidation in TRPV2 activation and angiotensin II in TRPC1 and/or TRPM7 activation. Further study should focus upon the physiological role of these channels.

### 6.4.2 Observations on sensory G-protein coupled receptors

A robust P2X response to ATP was observed in the SGN by $Ca^{2+}$ imaging, which was similar to that described in SCG neurons previously (Khakh *et al.*, 1995). However, based upon these data it is difficult to discern whether these are auto-receptors, whereby ATP released from the sympathetic neuron acts as a positive feedback mechanism (Hugel & Schlichter, 2000), or heteroreceptors involved in retrograde signalling, and/or communication with other populations in the stellate ganglia. For example, glial cells can release ATP (Kang *et al.*, 2008), and have been found in association with other sympathetic populations (Callahan *et al.*, 2008). This is an interesting line of further inquiry, but was beyond the scope of this study. $P2Y_6$ receptors were expressed in SGNs but were not investigated in this study. Based upon previous studies in SCG and hippocampal neurons it seems likely that $P2Y_6$ receptor would inhibit M-current and N-type $Ca_v$ in SCG neurons as previously described (Filippov *et al.*, 1999, 2006). ATP receptors were specifically focussed upon here given the established role of ATP as a constituent of the inflammatory soup (Julius & Basbaum, 2001). However, it has been suggested that $P2Y_6$ is involved in the immune response (Koizumi *et al.*, 2007), which may suggest a role for $P2Y_6$ in neuronal inflammatory signalling. This receptor may provide a useful route of further investigation.

Across the range of tested inflammatory transmitters, only histamine and adenosine had an effect, where both decreased neuronal excitability by different measures. Adenosine decreased maximum neuronal firing rate and histamine increased neuronal rheobase. Neither effect would support increased sympathetic neuron activity during a state of inflammation. Transcripts for $A_1$ (*ADORA1*) and $H_3$ (*HRH3*) receptors were observed in the SGN by scRNAseq (**Figure 6.15**), albeit in a small proportion of cells. Further, whilst they effects are significant, they are not clearly distinguishable from frequency-plots. As both receptors are $G_i$-coupled it is feasible that they might have an inhibitory effect upon neuronal firing, however these effects are not dramatic, and it is hard to interpret their physiological relevance.

Previous reports from the SCG have demonstrated functional $B_2$-receptors (Jones *et al.*, 1995; Cruzblanca *et al.*, 1998), $H_{1\text{-}3}$-receptors (Field & Newberry, 1991; Silver *et al.*, 2002), an unidentified Gi-coupled $PGE_2$ receptor (Ikeda, 1992) and $A_1$-receptors (Zhu & Ikeda, 1993). It is therefore surprising that there was no or very small effects for these transmitters on firing rate. It may be that the role of these transmitters is more subtle, for example evidence from neonatal SCG neurons suggests that 5-HT can be transported into and released from sympathetic neurons (Sah & Matsumoto, 1987), which would not have been observed in this study. Similarly, in SCG neurons histamine has been suggested to inhibit noradrenaline release via presynaptic $H_3$-receptors (Silver *et al.*, 2002). As *HRH3* is expressed here, it may be that this mechanism can also inhibit noradrenaline release from SGN presynaptic terminals without affecting somatic firing rate. Similar observations could be true for other populations of receptors, as $PGE_2$ (Ikeda, 1992; Koh & Hille, 1997) and adenosine (Zhu & Ikeda, 1993; Koh & Hille, 1997) also appear to inhibit $Ca_v$ and noradrenaline release. It is worth noting that these studies of $Ca_v$ measure

somatic calcium currents, which is not necessarily representative of the environment in the presynaptic terminal.

Two further explanations may explain these discrepancies, which are both dependent upon the methodology used. First, it may be possible that only subpopulations of SGNs express each receptor type as reflected by the scRNAseq dataset (**Figure 6.15**). Therefore, the recording number used here, whilst large enough for a paired comparison of the whole group, is not large enough to reflect responses in small populations. Such diversity is not reflected in prior studies of inflammatory signalling systems for $Ca_v$ recordings in the SCG (Ikeda, 1992; Zhu & Ikeda, 1993; Koh & Hille, 1997; Silver *et al.*, 2002). However, it is possible that the results of these earlier studies reflect exclusion of unresponsive cells. Investigating this further would require a much larger project than originally envisioned, and so the receptor subpopulations were not followed-up in the interest of time. Secondly, the whole cell patch-clamp configuration was used here, which can interfere with intracellular signalling (Ishibashi *et al.*, 2012). This methodology was chosen to facilitate exploratory study into a large number of transmitters with experimental time constraints. Whilst this is a possible explanation, the effects of bradykinin upon M-current (Cruzblanca *et al.*, 1998), and of $PGE_2$ (Ikeda, 1992) and Adenosine (Zhu & Ikeda, 1993) on $Ca_v$ in SCG neurons have also been observed in whole-cell patch-clamp. It is therefore unlikely that this is due purely to a technical difference.

For remaining transmitters this leaves three possibilities; 1) that SCG and stellate ganglia differentially express inflammatory receptors, 2) the inflammatory compounds tested do not affect neuronal firing properties in the SGNs, but affect other parameters, 3) only small populations of SGNs express these receptors. It seems likely that a combination of these will be true, however from the presented

data one can conclude that these transmitters do not have a strong effect upon SGN firing rate.

Stronger conclusions can be drawn for bradykinin and NGF, where firing properties have been studied in the SCG. For both transmitters, they had no effect on firing properties in SGNs as reported here, but large effects in SCG neurons (Cruzblanca *et al.*, 1998; Luther & Birren, 2009; Vivas *et al.*, 2014). These results suggest that there is an inter-ganglia difference for these transmitters.

Overall these data suggest that the SGN is unlikely to respond to the inflammatory soup, or its constituents with an increase in excitatory activity as observed in the sensory neurons (Julius & Basbaum, 2001). Whilst my original aim was to study SGNs responses to inflammatory signals, these data have instead suggested that the SCG neuron may be better equipped for this.

### 6.4.3 Observations on glutamatergic receptors

$Ca^{2+}$ imaging was used as the output measurement for these studies, but GluA2 containing AMPAR are not $Ca^{2+}$ permeable following Q/R RNA-editing. As this process is ubiquitous even *in vitro* (Pachernegg *et al.*, 2015), there was no reason to assume that Q/R RNA-editing would not occur in SGNs. GluA2 appears to be the primary AMPAR subunit expressed in the SGN (**Figure 6.18**), and this subunit would be expected to feature in the majority of any putative AMPAR. At first glance this approach may appear inappropriate, however, this methodology was used for the following reasons.

First, whilst GluA2 AMPAR are not $Ca^{2+}$-permeable, if they were present and functional AMPAR activation would be expected to cause membrane depolarisation

and elicit $Ca^{2+}$ influx via $Ca_v$. Fura-2AM is sensitive enough to detect $[Ca^{2+}]_i$ increases during a single action potential (Foehring *et al.*, 2009) and therefore this approach was justified. This is reinforced by previous work highlighting that AMPAR activation can lead to $Ca^{2+}$ influx via $Ca_v$ (Alberdi *et al.*, 2002). Secondly, these experiments were intended as a fast screening process for an undergraduate project and given the resultant time restraints and technical limitations would not favour patch-clamp electrophysiology.

Further, SBFI-AM, an intracellular $[Na^+]$ sensor with similar spectral properties to Fura-2AM (Minta & Tsien, 1989), emits a relatively small signal and is thus difficult for a student to obtain good quality recordings with low signal-to-noise ratios. From these data, we can infer that either AMPAR and/or Kainate receptor signalling either does not cause a large enough depolarisation to activate $Ca_v$, or that functional AMPAR are not present. Given that it is difficult to fully exclude AMPAR signalling by this approach, further SBFI-AM imaging or patch clamp experiments are required to resolve this project.

From these data it is unlikely that functional NMDAR subunits are present. This is somewhat surprising given that multiple subunits were expressed, theoretically facilitating the expression of functional NMDAR heteromers (Glasgow *et al.*, 2015). The scRNAseq data were consistent with previous immunohistochemical reports of GRIN1 protein in sympathetic neurons (Carlton *et al.*, 1998). Further, the scRNAseq and bulk RNA-sequencing datasets highlight dysregulation of glutamatergic subunits (Chapter 3; Davis et al. 2018; Bardsley et al. 2018a) in the SHR. This was briefly investigated, but no NMDA calcium responses were detected in SHR SGNs (Data not shown).

To resolve this study, a glutamate whole-cell voltage-clamp recording would be sufficient. Interestingly, metabotropic glutamatergic receptors can also activate TRPC1 channels (Kim *et al.*, 2003), which provides a functional association between glutamatergic study and TRP channel study given the presence of metabotropic glutamate receptor 7 encoding *GRM7* transcripts here (**Figure 6.18**). This may also provide an interesting line of further study.

### 6.4.4 Observations on co-culture

Based upon the co-culture study presented here it appears that retrograde signalling between Wistar cardiomyocytes and presynaptic sympathetic neurons occurs in co-culture and that this effect is dependent upon the presynaptic neurons strain.

In co-culture Wistar neurons displayed a small tendency towards increased maximal neuronal firing and decreased rheobase. On the other hand, SHR neurons had a significantly increased rheobase (**Figure 6.23**), and a trend towards reduced maximum neuron firing. Notably, with both conditioned media and co-cultured cardiomyocytes, the reduction in SHR neuron maximum firing rate was identical (Δ3.5 Hz, from 6.5 Hz to 3 Hz). Whilst these data are preliminary and are discussed here with the caveat that they are statistically underpowered; they suggest that retrograde signalling from cardiomyocytes to neurons may occur in co-culture. As this trend was consistent between the conditioned media and the co-culture preparations, these data suggest that any change in neuronal firing properties was based upon chemical transmission and not physical contact.

Beyond increasing the recording number of existing datasets, the most obvious next experiment would be to co-culture Wistar and SHR neurons with SHR cardiomyocytes. However, whilst this has been performed previously within the group (Larsen *et al.*, 2016*a*), significant difficulties were encountered with breeding. SHR are more aggressive than their Wistar counterparts (Potegal & Myers, 1989), and mothers raised locally were observed to frequently kill their litter. This issue was unfortunately not resolved during the time-course of my DPhil and for this reason these experiments were not performed here.

This co-culture preparation suffers from several limitations. First, neonatal cardiomyocytes do not have an adult phenotype, but are used here as adult cardiomyocytes yield extremely low cell numbers in culture (Ehler *et al.*, 2013). Secondly, unlike the artificial situation created here, *in vivo* cardiomyocytes and sympathetic neuron cell bodies are not co-localised and are spatially separated across the thoracic cavity (Rajendran *et al.*, 2019). Prior studies have attempted to address this by a dual chamber co-culture model, in which neurons and cardiomyocytes are cultured in separate chambers connected by small pathways which allow axonal projections (Takeuchi *et al.*, 2009, 2011). However, despite the spatial separation between the myocyte and neuron in this model, neurons are still artificially exposed to cardiomyocyte conditioned media. Therefore, in both models presynaptic neurons are chronically exposed to factors released from the cardiomyocyte such as atrial natriuretic peptide (ANP) (Flynn *et al.*, 1983; Kinnunen *et al.*, 1993) and brain natriuretic peptide (BNP) (Kinnunen *et al.*, 1993). In this study this common artificial condition was intentionally studied, to make general observations about the co-culture model, as well providing a platform to identify any retrograde chemical transmitters.

Overall, whilst these results are preliminary, these data provide a promising early insight into the role of retrograde signalling between cardiomyocytes and sympathetic neurons.

### 6.4.5 Summary

In this chapter, four key points were demonstrated; 1) Functional plasma membrane TRPV2 currents are present in the SGN and can be recorded via perforated patch-clamp and intracellular calcium imaging. 2) Inflammatory mediators do not have a large effect upon the firing properties of SGNs including bradykinin and NGF which affect SCG neurons. 3) Whilst glutamatergic receptor transcripts are present in SGNs, they do not appear to form functional channels. 4) Co-culturing with cardiomyocytes appears to have a mild excitatory effect upon Wistar neurons, but a stronger inhibitory effect upon SHR neurons. There are several points for future follow-up which includes further work on the physiological activation mechanisms for TRPV2, a more direct comparison between SCG and SGNs responses to inflammatory stimuli and a larger scale follow-up of the effect of co-culture upon Wistar and SHR neurons.

# Chapter 7

## Concluding discussion

Hypertension represents the most common cause of cardiovascular disease (Fuchs & Whelton, 2020), yet 15.3% of patients present as treatment resistant (Sim *et al.*, 2013). Emerging evidence suggests a significant component of treatment resistant hypertension results from sympathetic impairment, prompting a need for novel therapeutic target discovery. This thesis addressed three main aims, in order to expand the understanding of sympathetic ganglia in health and disease:

1) *Characterise the transcriptome of the stellate ganglia neuron and any previously unidentified signalling pathways.*

*2) Characterise cellular and molecular pathways underpinning sympathetic electrophysiological hyperactivity in an animal model of hypertension.*

*3) Assess ion channel targets to counteract sympathetic hyperactivity.*

## 7.1 Aim 1

*Characterise the stellate ganglia neuron in terms of its transcriptome and unidentified signalling pathways*

Previous studies of the SGN in health and disease have been focussed on specific *a priori* targets of interest, or have used tissue lysates, limiting neuron-specific observations. A wider proportion of the literature has focussed upon characterising the SCG, which has less cardiac therapeutic relevance. Chapter 3 provides the first large-scale overview of the stellate ganglia, building upon the work of Furlan *et al.* (2016) which characterised a neuron-specific population derived from a larger section of the thoracic sympathetic chain. scRNAseq proved extremely useful for identifying

expression patterns of ion channels specifically in SGNs (Chapter 4), thereby enhancing the fundamental understanding their function, alongside identifying putative targets. Alongside the voltage-clamp studies in appendix figures 15-19, these data have advanced the understanding of stellate ganglia cell populations.

In chapter 3 several signalling pathways were highlighted for experimental interrogation. Many of these are addressed between chapters 5 and 6. For example, chapter 5 studied the role of $Na_x$ in SGNs, and translated these effects to SCG and superior mesenteric/coeliac ganglia neurons. Chapter 6 investigated TRP, inflammatory GPCR and glutamatergic signalling in Wistar neurons. In addition, the effect of co-culturing Wistar cardiomyocytes with Wistar and SHR neurons was investigated.

The ability for sympathetic neurons to directly sense $Na^+$ via $Na_x$ (Chapter 5) is novel and fits with the known increase in SNA following elevations in plasma $Na^+$ (Nomura *et al.*, 2019). This may play an important role in physiology and hypertensive pathophysiology, but *in vivo* confirmation is required. It is likely that a combination of central (Nomura *et al.*, 2019) and peripheral sodium sensing are both important. These data suggest an integrated role for sympathetic neurons within the wider organism, allowing the sympathetic neuron to play a limited sensory role alongside its established efferent signalling.

An afferent role for SGNs was expanded upon in chapter 6. First, a current with similar properties to TRPV2 was described. With the current knowledge of TRPV2 (Santoni & Amantini, 2019), it seems unlikely that this channel will play a sensory role akin to the polymodal signalling exhibited by TRPV1 (Caterina *et al.*, 1999; Caterina & Park, 2006). However, a role for TRPV2 in oxidative stress may prove interesting

(Fricke *et al.*, 2019). Cannabidiol, has a potent agonist effect on TRPV2 (Pumroy *et al.*, 2019) and was shown here to activate a TRPV2-like current in the SGN by calcium imaging. As cannabidiol has been identified as a putative drug for cardiovascular disease (Rajesh *et al.*, 2010; Stanley *et al.*, 2013), TRPV2 in the SGN may be of a wider interest when considering the action of cannabidiol *in vivo*.

Inflammatory mediators did not have a large effect upon firing rate or rheobase when assessed by whole-cell patch-clamp. Whilst this was disappointing, it's interesting that several of these transmitters have been shown to affect SCG neurons (Ikeda, 1992; Zhu & Ikeda, 1993; Koh & Hille, 1997; Cruzblanca *et al.*, 1998; Luther & Birren, 2009). Based upon scRNAseq this could result from receptor expression in a limited number of SGNs, which would not be detected by the experimental design used here. The ability for small populations of sympathetic neurons to detect inflammatory transmitters could be of scientific interest.

The cursory analysis provided in chapter 6 did not identify glutamatergic signalling, which was surprising given scRNAseq and bulk RNA-sequencing highlighted transcript expression of glutamatergic subunits. Further, protein expression of these subunits was reported in sympathetic neurons (Carlton *et al.*, 1998). These calcium imaging data are sufficient to exclude NMDA receptor signalling, but patch-clamp recordings are required to definitively exclude $Ca^{2+}$ impermeable AMPA (Sommer *et al.*, 1991; Burnashev *et al.*, 1992; Swanson *et al.*, 1997) or kainate receptors (Lerma *et al.*, 2001). Given the unconvincing preliminary data the decision remains warranted.

Finally, chapter 6 investigated the possibility of retrograde signalling from cardiomyocytes to neurons. Whilst these data were generally underpowered, there

was an observable trend towards reduced excitability in SHR neurons when co-cultured with Wistar cardiomyocytes. This was observed as a significantly increased rheobase in SHR neurons co-cultured with Wistar cardiomyocytes and a non-significant trend towards reduced firing in SHR neurons cultured with either cardiomyocytes or cardiomyocyte conditioned media. The identity of a putative transmitter remains elusive at this point, however, there are three immediate candidates based upon published literature: NGF, BNP and ANP.

A previous report has suggested that NGF defines the relationship between the cardiomyocyte and neuron (Lockhart *et al.*, 1997). However, these authors only established a relationship between exogenously added NGF and the cardiomyocyte response to nicotinic stimulation of sympathetic neurons. Further, whilst is accepted that NGF is present in the heart (Korsching & Thoenen, 1983), release of NGF from cardiomyocytes is controversial. Whilst NGF mRNA has been reported in cardiomyocytes (Kaye *et al.*, 2000), others have suggested that the primary cardiac NGF source is vascular smooth muscle (Nam *et al.*, 2013; Schaum *et al.*, 2018).

Alternative candidates are ANP and BNP, which both primarily signal through cGMP signalling pathways (Gerzer *et al.*, 1985; Takahashi *et al.*, 2003). Their release from cardiomyocytes is well established, although brain natriuretic peptide release is largely favoured by the ventricular cardiomyocytes used in this study (Nishikimi *et al.*, 2006) and so would be the most likely candidate. BNP is believed to have an acute inhibitory effect upon sympathetic neurons (Li *et al.*, 2015; Buttgereit *et al.*, 2016), although to my knowledge its chronic effect on sympathetic neurons, as would be observed in co-culture, has not been resolved. As BNP is released from ventricular myocytes in response to an increase in stretch stimuli (Kinnunen *et al.*, 1993), a decrease in SNA during sustained ventricular stretch may serve as a cardioprotective

mechanism. Further work is clearly required to resolve the identity of a putative transmitter, with BNP as a primary candidate. A major question remains whether this protective mechanism is present in SHR cardiomyocytes.

These data have highlighted the presence of TRPV2 and a retrograde signalling pathway in the SGN. They have also excluded an effect for inflammatory neurotransmitters on SGN firing. Finally, they have excluded glutamatergic $Ca^{2+}$ signalling in the stellate ganglia.

## 7.2 Aim 2

*Characterise cellular and molecular pathways underpinning sympathetic electrophysiological hyperactivity in an animal model of hypertension*

Chapter 4 identified functional and transcript-level downregulation of *KCNQ5* in SHR neurons, with support from RNA-sequencing described in chapter 3. This observation provides a post-ganglionic mechanism for sympathetic hyperactivity which correlates with the dysfunction of the sympathetic nervous system at the level of a single nerve fibre in hypertensive patients (Greenwood *et al.*, 1999). In addition, it fits with *in vivo* sympathetic dysfunction in pre-hypertensive SHR (4-5 weeks) (Cabassi *et al.*, 1998). Further, work is required to observe whether this exact molecular dysfunction occurs in humans. However, limited availability of human tissue, and the difficulty of obtaining tissue from hypertensive patients without multiple co-morbidities is likely to limit progress. In addition, electrophysiological recordings from *ex vivo* human sympathetic neurons have not been performed to my knowledge.

These data should also be viewed in a systems physiology context. It seems likely that this phenotype will contribute to the phenotype of sympathetic hyperactivity observed *in vivo* (Thoren & Ricksten, 1979), but increased input into the post-ganglionic neuron originating from central sympathetic control centres (Hirooka, 2011), preganglionic neuron dysfunction (Tang *et al.*, 1995; Briant *et al.*, 2014) or baroreceptor dysfunction (Minami *et al.*, 1989) will also drive sympathetic pathology. Additionally, these mechanisms will also play a role in the increased noradrenaline cardiac spill-over observed in the SHR (Esler *et al.*, 1986), but alongside mechanisms such as reduced noradrenaline transporter activity in SGNs (Shanks *et al.*, 2013). Despite these caveats, the mechanism described here will amplify input from

preganglionic neurons, regardless of the any pathological changes to presynaptic input.

Chapter 5 highlighted a lasting increase in sympathetic neuron firing after long-term exposure to high NaCl in culture. Evidence in chapter 5 supported the hypothesis that this was mediated by $Na_x$. Given the association between salt sensitivity and hypertension (Rose *et al.*, 1988; Nomura *et al.*, 2019; Guyenet, 2019), this could present as an additional mechanism for the induction of sympathetic hyperactivity hypertension, although further work is clearly needed. As the phenotype is like that described in chapter 4, it would also be interesting to observe the channel changes underlying this. This is a clear direction for future work.

Chapter 6 identified functional TRPV2 channels in the rat stellate ganglion neuron. Whilst this study failed to identify a physiological mechanism, recent evidence suggests that TRPV2 can be activated by oxidation (Fricke *et al.*, 2019). Whilst this is speculative, it is feasible that this may contribute to the SHR phenotype. Chapter 3 highlighted a dysregulation of multiple mitochondrial genes in the SHR, which is line with prior reports of mitochondrial dysfunction in the SHR (De Cavanagh *et al.*, 2006; Li *et al.*, 2012).

Finally, scRNAseq in chapter 3 highlights many differentially expressed genes between Wistar and SHR non-neuronal populations. Whilst these weren't explored experimentally, they provide interesting targets for future study. For example, glia exhibited multiple differentially expressed genes in the SHR, which could suggest a similar situation to that observed in neuropathic pain models, where glia in sensory ganglia contribute to pathology (Vit *et al.*, 2008; Takeda *et al.*, 2011). Notably, sympathetic glia also appear to be activated in human stellate ganglia tissue in patients with ventricular tachycardia storm (Ajijola *et al.*, 2017).

## 7.3 Aim 3

*Assess ion channel targets to counteract sympathetic hyperactivity*

Chapter 4, supported by scRNAseq from chapter 3, highlighted several $Na_v$ subunits which could provide feasible drug targets for limiting SGN activity. In addition, these data demonstrated that M-current activators such as retigabine decrease SHR neuron firing and restore a control phenotype. However, whilst drugs targeting these channels at a cellular level was efficacious, we do not understand the effects of these drugs *in vivo* and a major concern for both $Na_v$ inhibition and M-current activation is the selectivity of these targets.

For M-current, prior *in vivo* studies are contradictory, with different authors suggesting alternate cardiovascular effects from M-current activation and inhibition (Fretwell & Woolard, 2013; Berg, 2016, 2018). A more thorough *in vivo* approach would remedy this. Based upon cellular studies, M-current is known to be expressed in sensory neurons (Linley *et al.*, 2008), baroreceptors (Wladyka *et al.*, 2008), central neurons (Shah *et al.*, 2002; Santini & Porter, 2010; Bordas *et al.*, 2015) and the vasculature (Jepps *et al.*, 2011; Mani *et al.*, 2016). So whilst it is an interesting observation that retigabine caused hypotension in a proportion of epileptic patients (Ferron *et al.*, 2002)(EMA 2011; Procedure No: EMEA/H/C/001245), we do not know if this effect is due to direct action upon the sympathetic nervous system or other tissues. However, it is worth noting that multiple plant-based traditional medicines used to treat hypertension have been found to target $K_v7.5$ (Manville *et al.*, 2019) and therefore may have some validity as a drug target.

Thoracic epidurals of non-selective $Na_v$ blockers are used for short-term treatment of ventricular tachycardia storm resulting from stellate ganglia hyperactivity

(Do *et al.*, 2017). However, selective $Na_v$ inhibitors have not been investigated in this context. Chapter 4 suggested that $Na_v1.1$-1.3 and $Na_v1.6$ inhibitors may be of interest for this purpose. However, $Na_v1.1$ and $Na_v1.6$ are expressed in populations of sensory neurons (Fukuoka *et al.*, 2008), and inhibitors are likely to have unwanted peripheral effects. However, $Na_v1.2$ and $Na_v1.3$ are generally considered to be central $Na_v$ subunits (Wang *et al.*, 2017; Bennett *et al.*, 2019) and are as such have minimal expression in adult sensory neurons (Ho & O'Leary, 2011). Whilst $Na_v1.3$ it is not the predominant cardiac $Na_v$ subunit, it is present in human and rodent myocytes (Maier *et al.*, 2002, 2003; Lei *et al.*, 2004; Kaufmann *et al.*, 2013) and appears to have a functional role (Maier *et al.*, 2002, 2003; Lei *et al.*, 2004). Therefore, the use of $Na_v1.3$ inhibitors may cause unwanted cardiac effects. $Na_v1.2$ and $Na_v1.3$ are also found in smooth muscle cells (Okabe *et al.*, 1988; James *et al.*, 1995; Platoshyn *et al.*, 2005; Schaum *et al.*, 2018). However, smooth muscle contraction is mediated largely via $Ca_v$ (Knot & Nelson, 1998), and the functional contribution of $Na_v$ is considered to be small (Gershon, 1967). Additionally, any inhibition of smooth muscle vasoconstriction may be beneficial to lowering blood pressure. Based upon these data, a selective $Na_v1.2$ inhibitor which lacked blood-brain-barrier permeability, may present as a relatively selective targets for sympathetic neuron.

It is worth noting that the issues described here are ubiquitous for drug discovery and should not limit attempts at finding viable targets. Overall, this study highlighted the pattern of ion channel expression in SGNs, which should also inform study of other sympathetic neuron populations. Functional and transcriptomic data presented in chapter 4 suggests $Na_v1.2$ and $Na_v1.3$ as possible targets for future studies. However, these targets and M-current should be followed up with thorough *in vivo* study.

## 7.4 Future work and concluding remarks

This body of work has provided 5 key observations about the function of sympathetic ganglia in health and disease: 1) SGNs do not function alone, and are present with an assortment of other cell types, 2) SGNs are not a homogenous population, and differ by other markers than just NPY, 3) Downregulation of M-current has a role in sympathetic dysfunction, 4) Sympathetic neurons can directly sense extracellular $Na^+$ thereby facilitating an increase in sympathetic activity and 5) The electrical phenotype of SGNs is influenced by postsynaptic cardiomyocytes. Together these data suggest that sympathetic neurons are a complex population of cells, with a greater role than mere effectors of the autonomic nervous system.

Further work is required to assess the roles of non-neuronal sympathetic ganglia populations in health and hypertension such as glia, which may be critical to understanding how these neurons function physiologically. Whilst the importance of neuron-glia interactions is well acknowledged in the central nervous system (Allen & Lyons, 2018), and to a certain extent with the sensory nervous system (Harty & Monk, 2017; Abdo *et al.*, 2019), study of neuron-glia within the SNS presents as a important and poorly explored research topic. This is a clear direction for future research, for which chapter 3 provides an important preliminary dataset.

Building upon the prior work of Furlan et al. (2016) and Li & Horn (2006), the data in chapter 3 also suggest that at least two sympathetic neuron populations are present in the stellate ganglia. These data are largely in agreement with the immunohistochemical study provided by Li & Horn (2006) but suggest a much greater divergence in function than had previously been anticipated. As physiologically important functional differences may arise between these populations it is extremely important to resolve this line of enquiry. Future study should incorporate flow

cytometry-based confirmation of these populations as well as functional study of any differences that arise between them. It is possible that targeting a specific population of sympathetic neurons may be of therapeutic interest. For example, selectively targeting the NPY high population to limit the pro-arrhythmic effect of NPY (Kalla *et al.*, 2020) whilst permitting noradrenergic signalling via the NPY low population.

Whilst increased SNS firing is an acknowledged hallmark of hypertension (Greenwood *et al.*, 1999), a direct role for the sympathetic neuron itself has often been ignored. In agreement with previous work (Yarowsky & Weinreich, 1985; Jubelin & Kannan, 1990), the data in chapter 4 suggest that post-ganglionic sympathetic neurons have a more prominent role in the sympathetic hyperactivity observed in hypertension than has recently been allowed for. For example, chapter 4 highlights an electrical phenotype in SGNs in the SHR, that presents in addition to increased input from dysfunctional pre-ganglionic sympathetic neurons (Briant *et al.*, 2014), or from increased central (Johnson & Xue, 2018) or renal afferent input (Ong *et al.*, 2019). Further work is required to elucidate the cause of this dysfunction, but these data suggest that the SGN itself plays a key role in dysautonomia. These data also highlight that sympathetic neuron ion channels may represent targets for treatment of hypertension or other diseases with associated dysautonomia (Herring *et al.*, 2019). This is an important observation, and the inhibitors tested *in vitro* in chapter 4 need to be tested in terms of their effect upon evoked noradrenaline release from sympathetic neurons/ganglia and *in vivo* on sympathetic and cardiovascular parameters.

The discovery in chapter 5 that sympathetic neurons are directly affected by extracellular $Na^+$ in vitro is of physiological interest but needs to be confirmed *in vivo*. It is currently unknown how this system fits with the increase in SNA *in vivo* following elevated plasma [$Na^+$], but the responses observed here are very similar to those

observed in central SNS control centres and appear to be similarly reliant upon the sodium sensor $Na_x$. If these data translate *in vivo*, these data could be of profound importance to our understanding of sodium's role in hypertension and provide a direct association between dietary sodium and increased SNA. If these observations are translational, this could directly implicate the post-ganglionic sympathetic neuron in the development of salt-sensitive hypertension.

Similarly, the suggestion in chapter 6 that cardiomyocytes can reduce aberrant SNA in co-culture indicates that a cardiomyocyte releasable factor could act as an inhibitory clamp on SNA. Identifying the molecular identity of this transmitter may prove an important alternative for reducing dysautonomia. Further to this, assessing whether this inhibitory mechanism is dysfunctional in hypertension is an area of immediate interest to the understanding of hypertensive pathophysiology.

It would be interesting to investigate whether the effect described in chapter 5 has implications for the development of the phenotype presented in chapter 4. To investigate this connection, it would be worthwhile assessing whether the excitatory effect of long-term $[Na^+]$ elevation leads to a transcriptional change in M-current, or whether this sustained change in activity is through an alternate ion channel. Similarly, the effect of the cardiomyocyte's upon SHR neurons (Chapter 6) appears to be long-term and could also be linked to gene transcription. As this mechanism affects firing rate, an SGN ion channel's expression or function is likely affected. It is therefore important to explore this model from the perspective of the SGN. Further work should assess whether M-current or other ion channels are involved in the reduced activity in co-culture.

Together these data provide a firm foundation for further electrophysiological characterisation of the SGN in health and disease. This work has begun to uncover

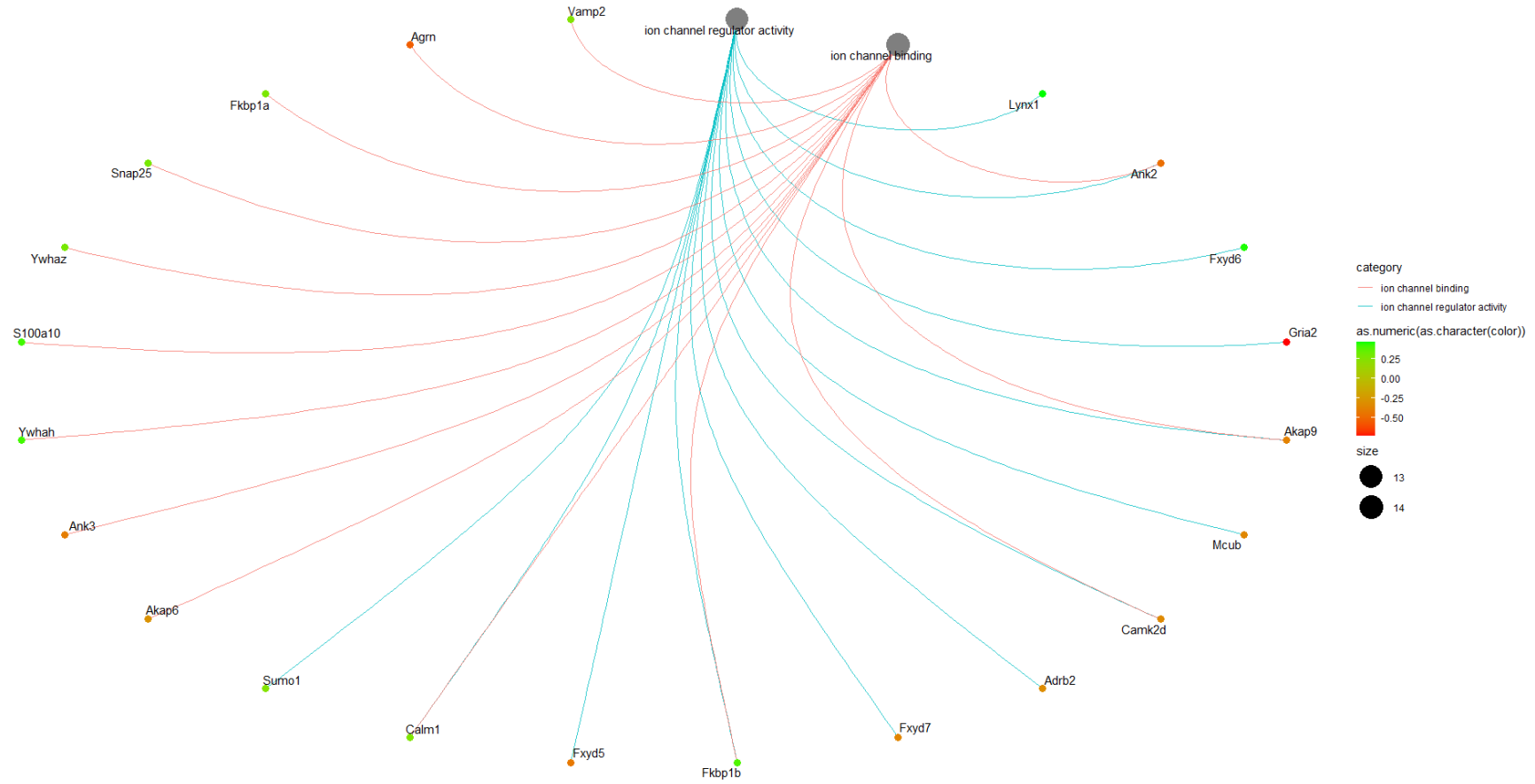
an exciting role for SGNs in pathological SNA as well as providing evidence for the sympathetic neuron as a peripheral sodium sensor. Several ion channel targets of interest have been highlighted in this work that may proof of interest for *in vivo* follow-up and shift the narrative in autonomic research towards directly reducing sympathetic neuron firing, which remains as a key hallmark of hypertensive disease.

# Appendix

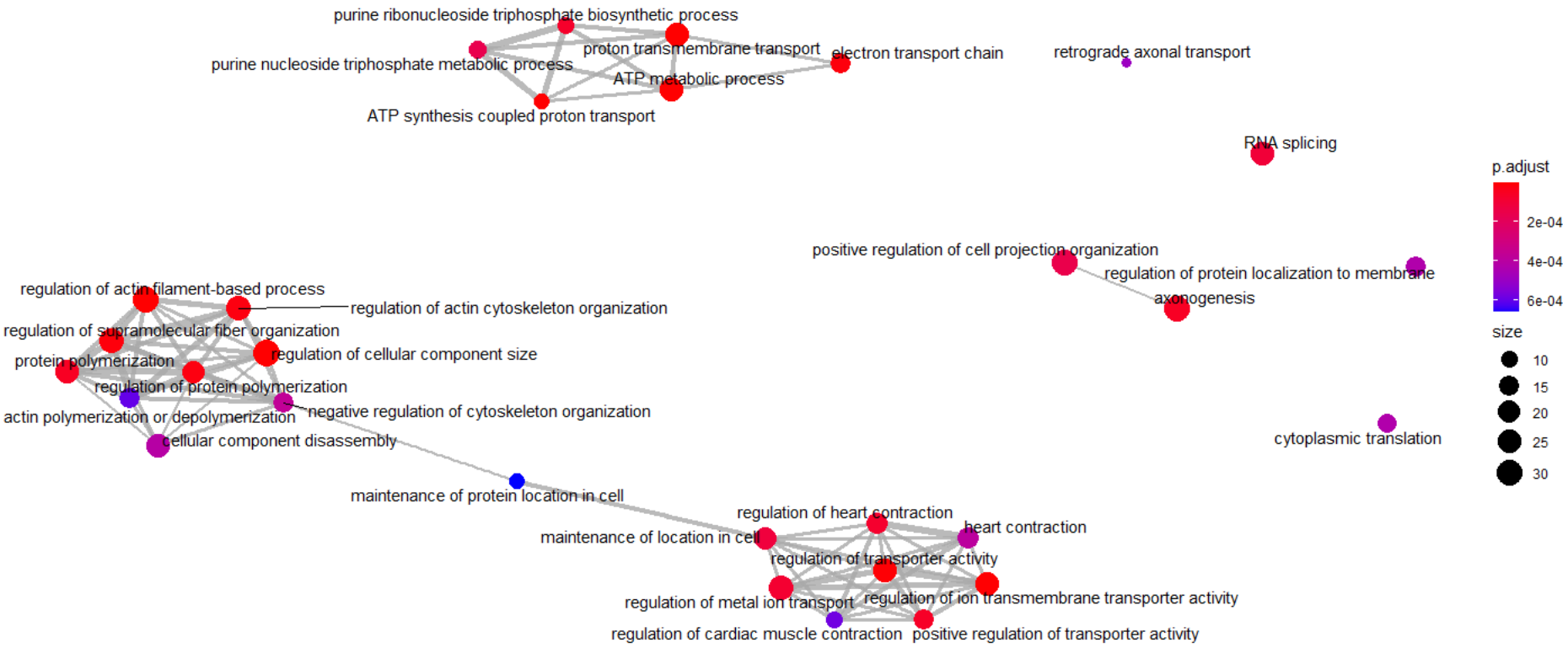
# Chapter 3 Supplementary data



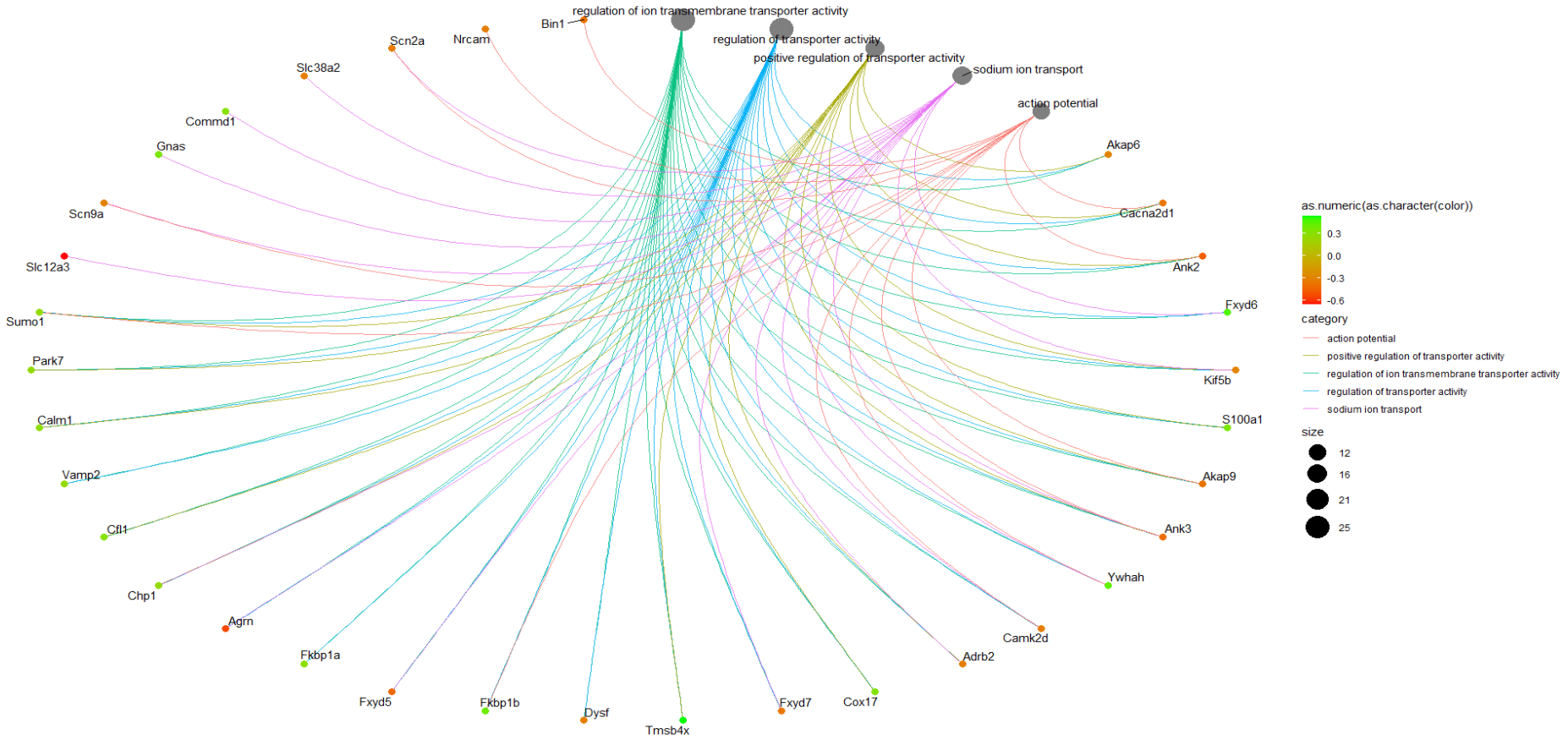

**Appendix Figure 1 Over-represented "Molecular function" gene ontology groups in SHR sympathetic stellate ganglia neurons** Gene ontology over-representation analysis highlighted multiple "Molecular function" gene ontology terms with a larger than expected number of dysregulated genes.



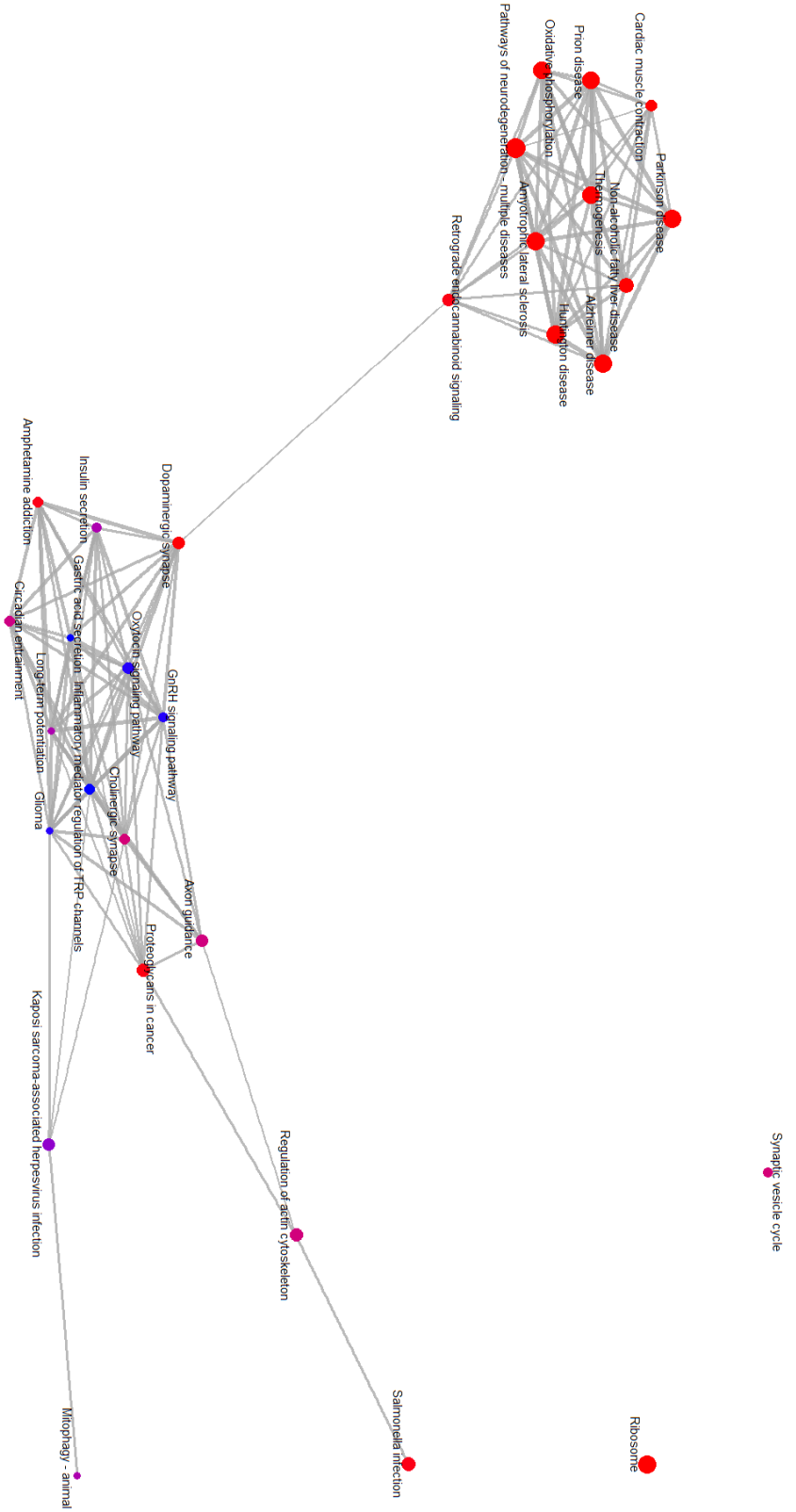

***Appendix Figure 2 A visual breakdown of gene expression changes underpinning 2 physiologically interesting over-represented "Molecular function" gene ontology terms.*** *The differentially expressed genes from the over-represented gene-ontology terms "ion channel regulator activity" and "ion channel binding" are graphically represented here. Lines are colour coded to the gene ontology term of origin. Circles representing genes are coloured based upon the difference in expression between Wistar and SHR neurons, where green indicates an increase in SHR neurons and red indicates a decrease. The size of the circles representing gene ontology terms is proportional to the number of differentially expressed genes associated with this term.*



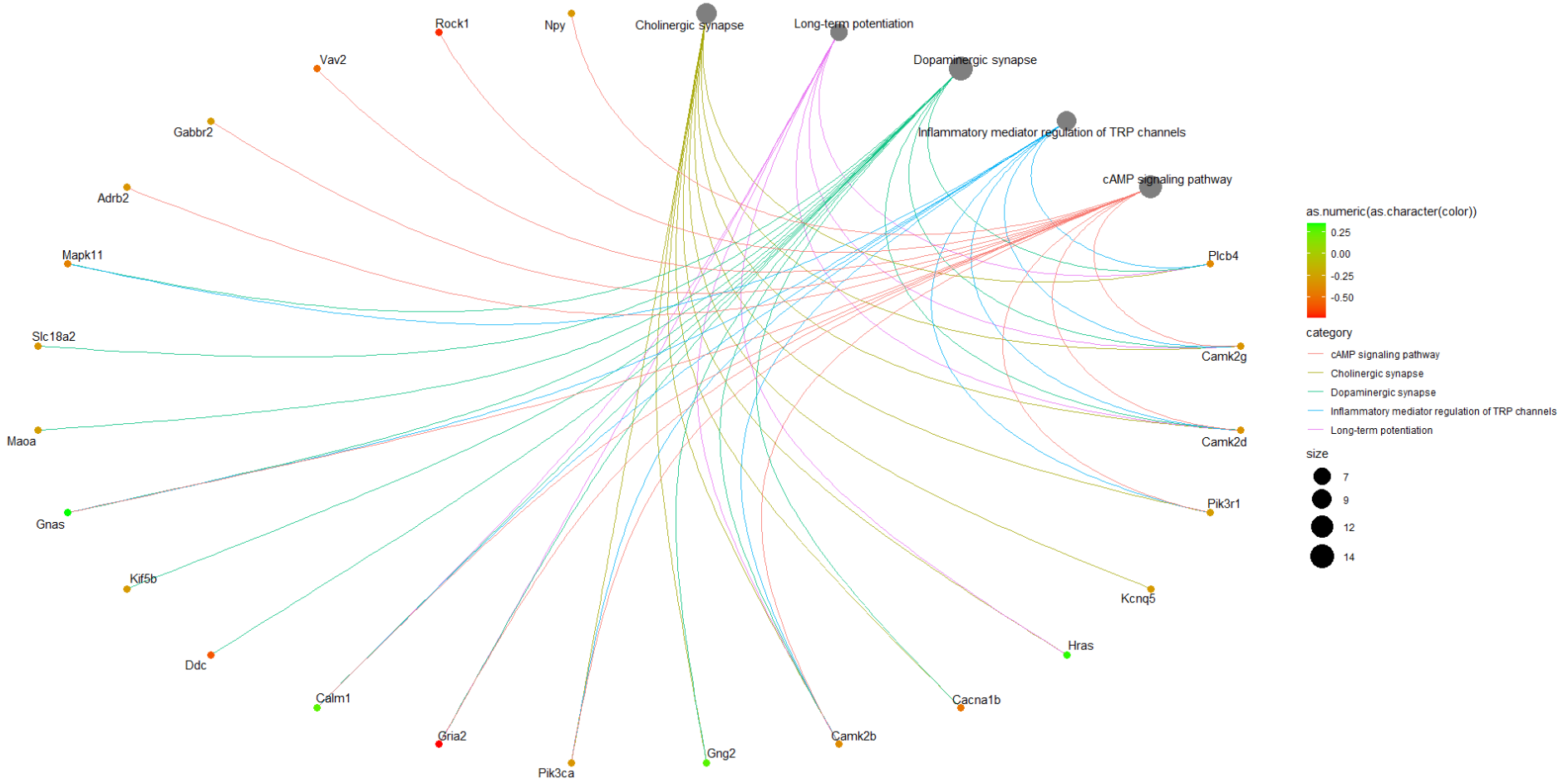

***Appendix Figure 3 Over-represented "Biological process" gene ontology groups in SHR sympathetic stellate ganglia neurons***
*Gene ontology over-representation analysis highlighted multiple "Biological process" gene ontology term with a larger than expected number of dysregulated genes.*




***Appendix Figure 4 A visual breakdown of gene expression changes underpinning 5 physiologically interesting over-represented "Biological process" gene ontology terms*** *The differentially expressed genes from the over-represented gene-ontology groups "regulation of ion transmembrane transporter activity", "regulation of transporter activity", "positive regulation of transporter activity", "sodium ion transport" and "action potential" are graphically represented here. Lines are colour coded to the gene ontology term of origin. Circles representing genes are coloured based upon the difference in expression between Wistar and SHR neurons, where green indicates an increase in SHR neurons and red indicates a decrease. The size of the circles representing gene ontology terms is proportional to the number of differentially expressed genes associated with this term.*




***Appendix Figure 5 Over-represented KEGG terms in SHR sympathetic stellate ganglia neurons*** *KEGG over-representation analysis highlighted multiple KEGG terms with a large number of differentially expressed genes.*

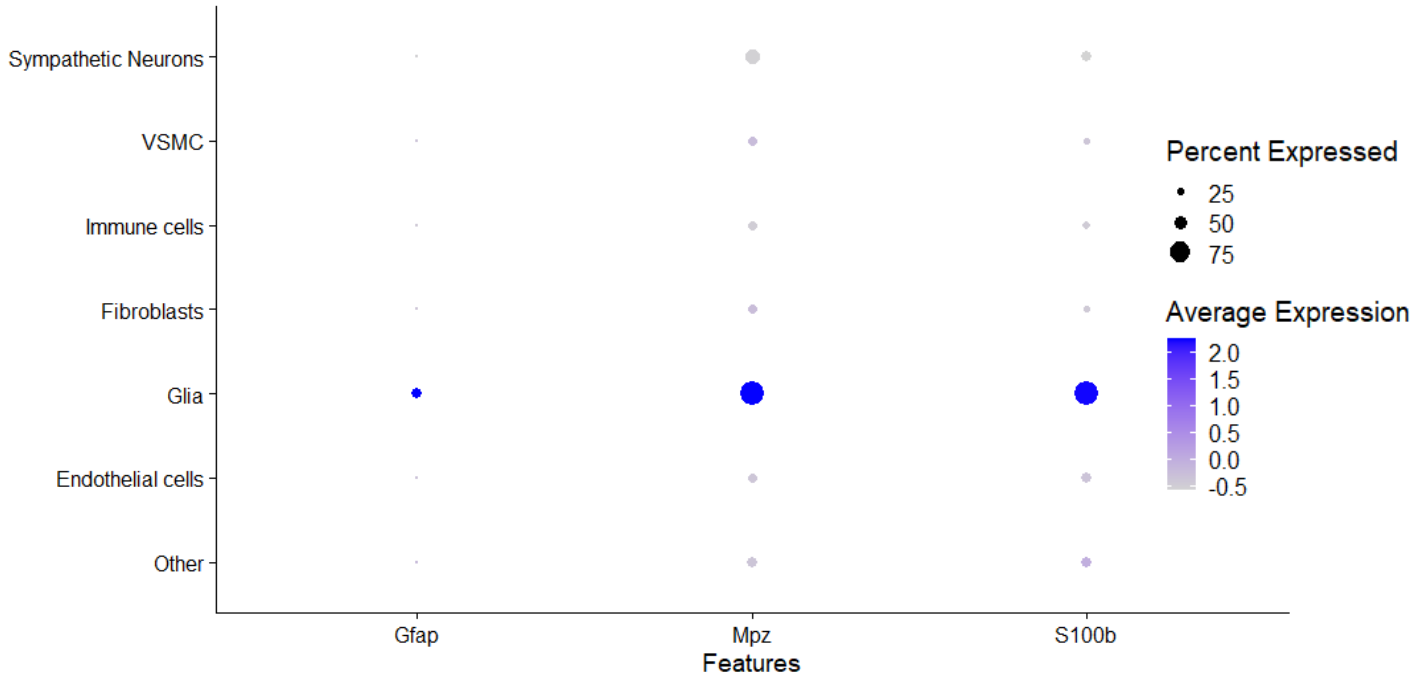



**Appendix Figure 6** ***Visual representation of 5 physiologically interesting KEGG terms which are over-represented in SHR sympathetic stellate ganglia neurons*** *The differentially expressed genes from the over-represented gene-ontology groups "Cholinergic synapse", "Long term potentiation", "Dopaminergic synapse", "Inflammatory mediator regulation of TRP channels" and "cAMP signalling pathway" are graphically represented here. Lines are colour coded to the KEGG term of origin. Circles representing genes are coloured based upon the difference in expression between Wistar and SHR neurons, where green indicates an increase in SHR neurons and red indicates a decrease. The size of the circles representing gene ontology terms is proportional to the number of differentially expressed genes associated with this term.*

## Glia cells

Glia have a major role in both the regulation and support of neuronal function and are increasingly focussed upon for research into the central nervous system (Patel *et al.*, 2019). However, very little is known about sympathetic glia, or peripheral glia in general. In sensory neurons glia have been shown to contribute to pain sensation and are believed to be dysregulated in several disease models of neuropathic pain (Milligan & Watkins, 2009). Glial clusters were identified in the stellate ganglia by expression of established glial markers *GFAP* (Glial Fibrillary Acidic Protein), *MPZ* (Myelin protein Zero) and *S100B* (S100 Calcium Binding Protein B) (Nascimento *et al.*, 2014; Garden & Campbell, 2016; Wang *et al.*, 2019*b*; Avraham *et al.*, 2020) (Appendix figure 7).

As glia are not a focus of functional study within this thesis, only limited analyses are provided here for the purpose of discussion. Analysis shown here was limited to a direct comparison between Wistar and SHR genes. Differential expression analysis was then performed between Wistar and SHR glia (Appendix Table 1).



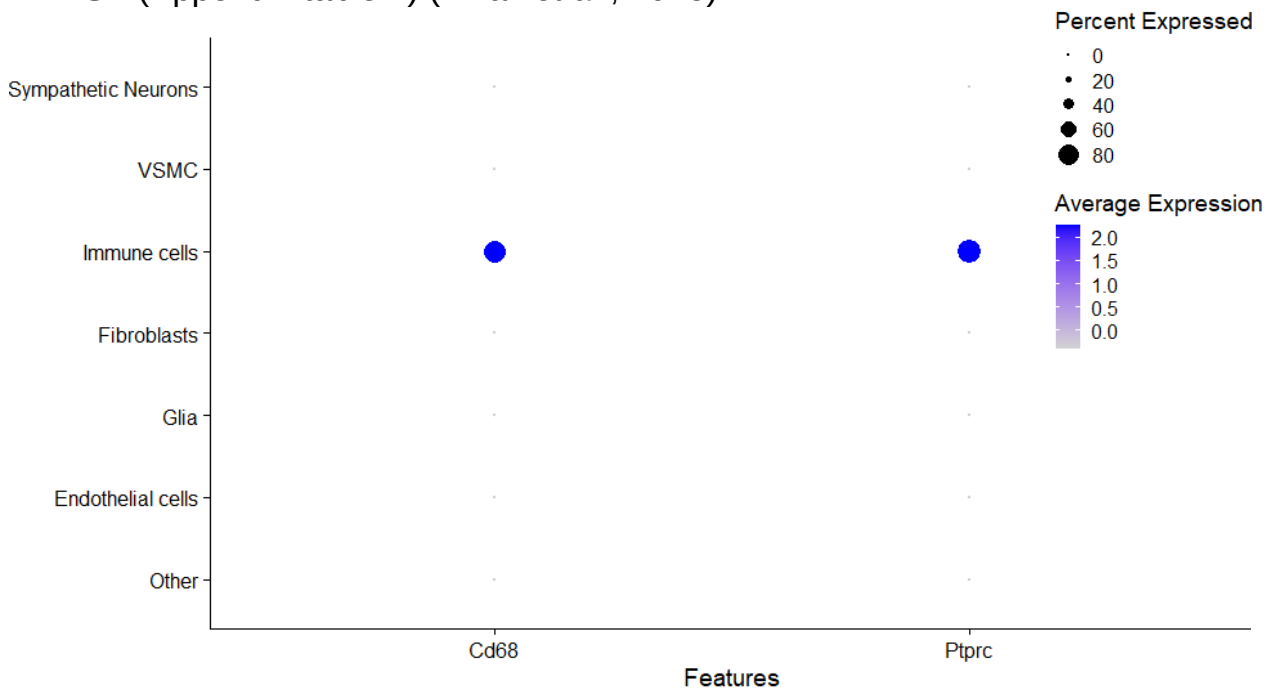

***Appendix Figure 7 Established glial markers were used to identify glia clusters in the stellate ganglia*** *Glia markers* GFAP *(Glial Fibrillary Acidic Protein),* MPZ *(Myelin protein Zero) and* S100B *(S100 Calcium Binding Protein B) were selectively expressed in stellate ganglia glia clusters.*

**Appendix Table 1** ***Top 25 differentially expressed genes between Wistar and SHR glial clusters*** *MAST differential expression highlighted 169 differentially expressed genes between Wistar and SHR stellate ganglia glial cell clusters at the adjusted p < 0.05 cut-off level.*

| Gene | Name | Log Fold change | Adjusted P Value |
|---|---|---|---|
| **RT1-A1** | RT1 class I, A1 | 1.34 | 0 |
| **Prph** | Peripherin | -0.71 | 0 |
| **Uchl1** | Ubiquitin C-Terminal Hydrolase L1 | -0.73 | 0 |
| **Tubb3** | Tubulin Beta 3 | -0.86 | 0 |
| **Stmn2** | Stathmin 2 | -0.88 | 0 |
| **RT1-CE10** | RT1 class I, locus CE10 | -1.30 | 0 |
| **Cst3** | Cystatin C | -2.34 | 0 |
| **Mt-nd3** | Mitochondrially Encoded NADH:Ubiquinone Oxidoreductase Core Subunit 3 | 0.45 | 1.24267992618694e-314 |
| **Tubb2b** | Tubulin Beta 2B Class IIb | -0.74 | 4.22E-289 |
| **Jund** | Transcription Factor Jun-D | 1.16 | 2.71E-288 |
| **Pcp4** | Purkinje Cell Protein 4 | -0.77 | 2.59E-285 |
| **Stmn3** | Stathmin 3 | -0.72 | 9.20E-271 |
| **Ifi27** | Interferon Alpha Inducible Protein 27 | -0.79 | 5.42E-266 |
| **Tubb5** | Tubulin Beta 5 | -0.57 | 6.75E-254 |
| **Nefl** | Neurofilament Light | -0.69 | 5.26E-248 |
| **Map1b** | Microtubule Associated Protein 1B | -0.55 | 5.16E-242 |
| **Syt1** | Synaptotagmin 1 | -0.65 | 4.84E-227 |
| **Moxd1** | Monooxygenase DBH Like 1 | 0.35 | 1.78E-219 |
| **Cd48** | Cluster of Differentiation 48 | 0.49 | 8.61E-217 |
| **Gap43** | Growth Associated Protein 43 | -0.63 | 9.10E-214 |
| **Basp1** | Brain Abundant Membrane Attached Signal Protein 1 | -0.61 | 2.86E-192 |
| **Col28a1** | Collagen Type XXVIII Alpha 1 | 0.67 | 5.99E-190 |
| **Tubb2a** | Tubulin Beta 2A Class IIa | -0.58 | 4.61E-184 |
| **AABR07071891.2** | | -0.52 | 9.70E-182 |
| **Stmn1** | Stathmin 1 | -0.52 | 1.14E-180 |

## Immune cells

Immune cells are a heterogenous group of cells forming the immune system and are involved in cell-cell signalling as well as the immune response. In addition, populations of circulating immune cells have been shown to infiltrate sympathetic ganglia (Pirzgalska *et al.*, 2017). Immune cells were present in Wistar and SHR stellate ganglia and were identified by the markers *PTPRC* (CD45) and *CD68* (Woodward *et al.*, 2004) (Appendix figure 8). To keep these data succinct, this immune population was treated as homogenous. As described for neuron populations, differential expression was assessed via *MAST* (Appendix table 2) (Finak *et al.*, 2015).




***Appendix Figure 8 Immune cells were identified by the expression of 2 established monocyte markers*** *Identified stellate ganglia immune clusters selectively expressed immune markers* PTPRC *(CD45) and* CD68.

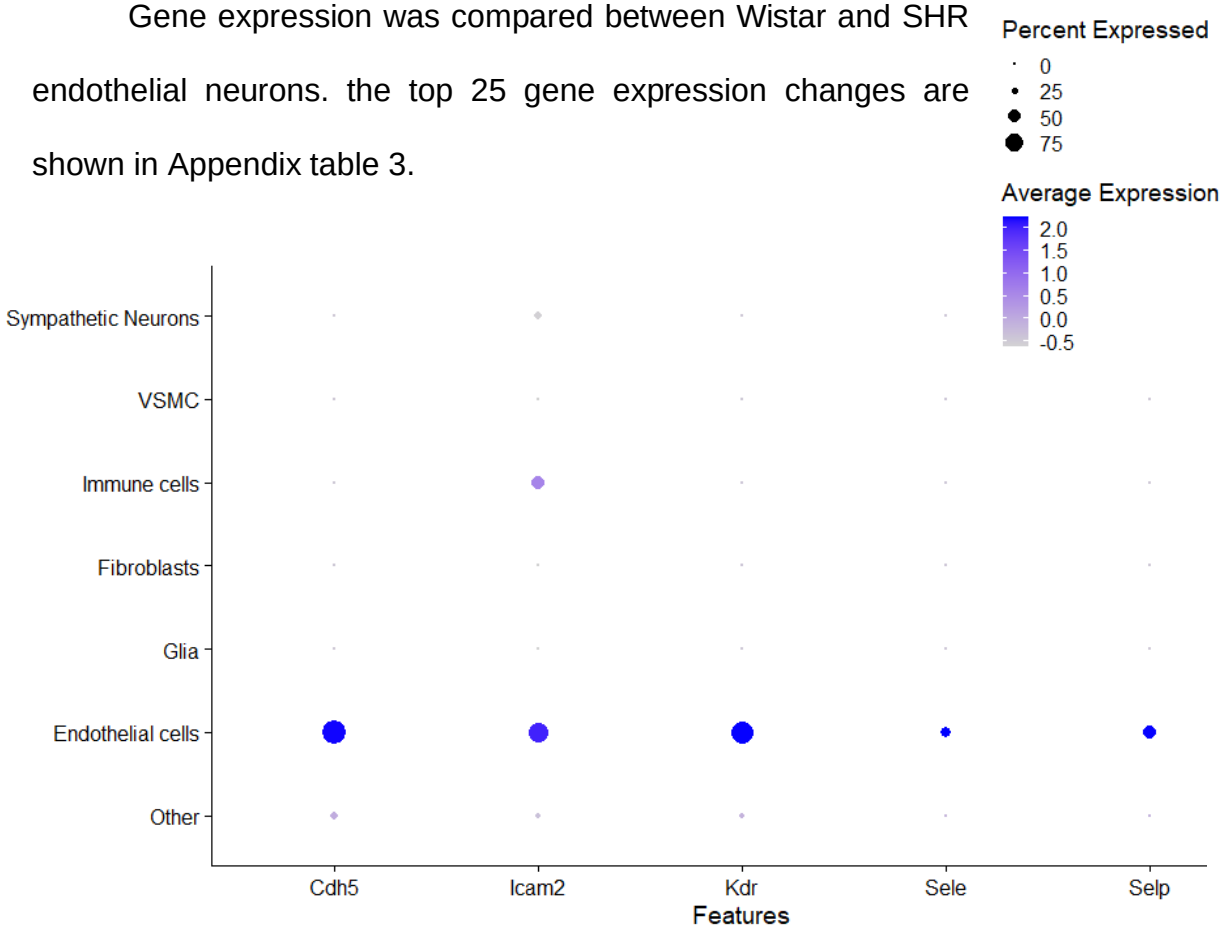
**Appendix Table 2 Top 25 differentially expressed genes between Wistar and SHR Immune cell clusters** MAST differential expression highlighted 167 differentially expressed genes between Wistar and SHR stellate ganglia immune cell clusters at the adjusted $p < 0.05$ cut-off level.

| Gene | Name | Log Fold change | Adjusted P value |
|---|---|---|---|
| **RT1-A1** | RT1 class I, A1 | 1.70 | 7.72E-129 |
| **RT1-CE10** | RT1 class I, A1 | -1.60 | 3.00E-75 |
| **Tuba1a** | Tubulin alpha-1A chain | -0.88 | 3.64E-73 |
| **Stmn2** | Stathmin 2 | -0.99 | 1.13E-57 |
| **Tubb3** | Tubulin, Beta 3 | -0.95 | 9.75E-51 |
| **Uchl1** | Ubiquitin C-Terminal Hydrolase L1 | -0.82 | 1.27E-42 |
| **Sncg** | Synuclein Gamma | -0.83 | 2.00E-41 |
| **Prph** | Peripherin | -0.84 | 9.81E-38 |
| **Map1b** | Microtubule Associated Protein 1B | -0.80 | 2.08E-36 |
| **Jund** | Transcription Factor Jun-D | 1.04 | 2.81E-36 |
| **RGD1559482** | | -1.21 | 1.10E-34 |
| **Stmn3** | Stathmin 3 | -0.83 | 2.91E-34 |
| **Tubb2b** | Tubulin Beta 2B Class IIb | -0.82 | 1.33E-33 |
| **RT1-Bb** | RT1-Bb RT1 class II | -2.21 | 2.34E-30 |
| **Stmn1** | Stathmin 1 | -0.83 | 1.31E-29 |
| **Mt-nd3** | Mitochondrially Encoded NADH:Ubiquinone Oxidoreductase Core Subunit 3 | 0.51 | 4.01E-29 |
| **Pcp4** | Purkinje Cell Protein 4 | -0.79 | 1.94E-27 |
| **Tubb5** | Tubulin, Beta 5 | -0.63 | 2.61E-26 |
| **AABR07071891.2** | | -0.75 | 6.13E-25 |
| **Nefl** | Neurofilament Light | -0.72 | 6.11E-24 |
| **Gap43** | Growth Associated Protein 43 | -0.67 | 1.22E-23 |
| **Lgals1** | Galectin-1 | -0.67 | 1.85E-22 |
| **Slc11a1** | Solute Carrier Family 11 Member 1) | 0.71 | 8.64E-20 |
| **Rps25** | Ribosomal Protein S25 | 0.53 | 2.50E-19 |
| **Ddc** | Dopa Decarboxylase | -0.56 | 1.25E-18 |

## Endothelial cells

Endothelial cells line the inside of blood vessels and regulate blood-tissue exchange as well as the growth of connective tissue (Krüger-Genge *et al.*, 2019). Clusters of endothelial cells were also found in the stellate ganglia using the markers *CDH5* (Vascular endothelial cadherin), *ICAM2* (Intercellular adhesion molecule 2), *KDR* (Vascular endothelial growth factor receptor 2), *SELE* (Selectin-E) and *SELP* (Selectin-P) (Goncharov *et al.*, 2017) (Appendix figure 9). Endothelial cells are treated as a homogenous population here for clarity.

Gene expression was compared between Wistar and SHR endothelial neurons. the top 25 gene expression changes are shown in Appendix table 3.



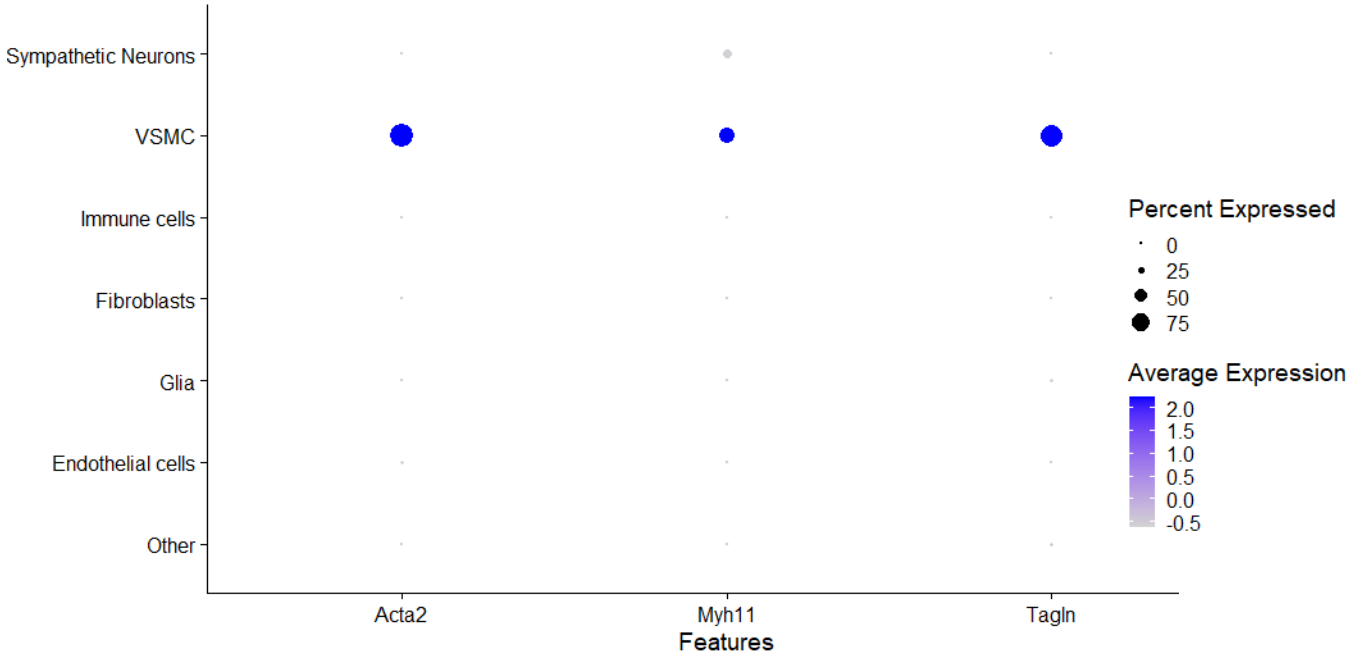

***Appendix Figure 9 Endothelial cell clusters express multiple endothelial markers*** *Cell clusters assigned to the endothelial cell identity expressed endothelial markers* CDH5 *(Vascular endothelial cadherin),* ICAM2 *(Intercellular adhesion molecule 2),* KDR *(Vascular endothelial growth factor receptor 2),* SELE *(Selectin-E) and* SELP *(Selectin-P).*

***Appendix Table 3 Top 25 differentially expressed genes between Wistar and SHR stellate ganglia endothelial cells*** *MAST differential expression highlighted 410 differentially expressed genes between Wistar and SHR stellate ganglia endothelial clusters at the adjusted p < 0.05 cut-off level.*

| Gene | Name | Log Fold change | Adjusted P Value |
|---|---|---|---|
| **RT1-CE10** | RT1 class I, locus CE10 | -1.19 | ######## |
| **Tubb3** | Tubulin, Beta 3 | -0.99 | 8.69E-88 |
| **Stmn2** | Stathmin 2 | -0.96 | 2.64E-86 |
| **Tuba1a** | Tubulin Alpha 1a | -0.69 | 2.64E-70 |
| **Prph** | Peripherin | -0.83 | 7.36E-61 |
| **RT1-T24-4** | RT1 class I, locus T24, gene 4 | -0.95 | 2.39E-59 |
| **Jund** | Transcription Factor Jun-D | 1.13 | 5.62E-58 |
| **RT1-T24-3** | RT1 class I, locus T24, gene 3 | 0.80 | 5.92E-58 |
| **Uchl1** | Ubiquitin C-Terminal Hydrolase L1 | -0.81 | 9.51E-57 |
| **Sphkap** | SPHK1 Interactor, AKAP Domain Containing | -0.66 | 1.93E-56 |
| **Map1b** | Microtubule Associated Protein 1B | -0.71 | 4.55E-54 |
| **Ibsp** | Integrin Binding Sialoprotein | -0.64 | 1.25E-52 |
| **AABR07071891.2** | | -0.67 | 2.19E-50 |
| **Tubb2b** | Tubulin Beta 2B Class IIb | -0.74 | 6.79E-48 |
| **Pcp4** | Purkinje Cell Protein 4 | -0.73 | 6.83E-48 |
| **Stmn3** | Stathmin 3 | -0.72 | 1.94E-47 |
| **Sncg** | Synuclein Gamma | -0.75 | 1.01E-45 |
| **B2m** | Beta-2-Microglobulin | 0.37 | 7.42E-42 |
| **Basp1** | Brain Abundant Membrane Attached Signal Protein 1 | -0.65 | 4.16E-41 |
| **Gap43** | Growth Associated Protein 43 | -0.69 | 8.47E-41 |
| **Nefl** | Neurofilament Light | -0.65 | 2.04E-39 |
| **Ldhb** | Lactate Dehydrogenase B | -0.61 | 5.18E-38 |
| **Tubb5** | Tubulin, Beta 5 | -0.51 | 1.05E-35 |
| **Myof** | Myoferlin | 0.57 | 4.73E-34 |

### Vascular smooth muscle cells

Vascular smooth muscle cells are specialised non-striated muscle cells, that provide the contractile force for vascular constriction. Vascular smooth muscle cells were highlighted by the markers *ACTA2* (Alpha smooth muscle actin), *MYH11* (smooth muscle, myosin heavy chain 11) and *TAGLN* (Transgelin) (Chakraborty *et al.*, 2019) in appendix figure 10. As before, differential expression between Wistar and SHR was then assessed by *MAST* (Finak *et al.*, 2015) and the top 25 changes are shown in Appendix table 4.



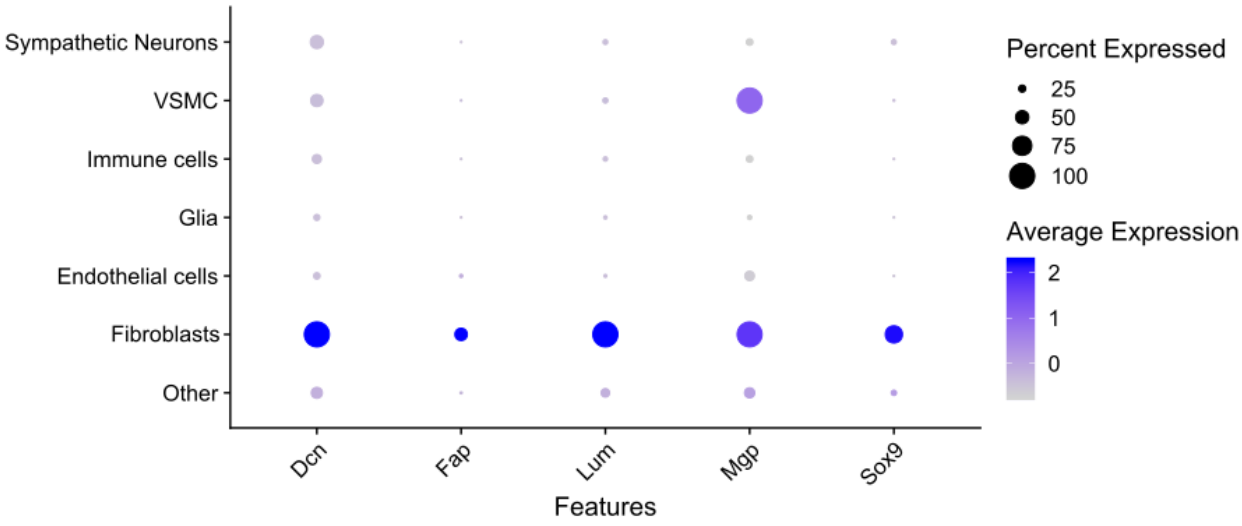

***Appendix figure 10 Established markers were used to identify vascular smooth muscle cell clusters*** *Vascular smooth muscle cells were identified by the selective expression of ACTA2 (Alpha smooth muscle actin), MYH11 (smooth muscle, myosin heavy chain 11) and TAGLN (Transgelin).*

***Appendix Table 4 Top 25 changes in gene expression between Wistar and SHR vascular smooth muscle cells*** *MAST differential expression highlighted 57 differentially expressed genes between Wistar and SHR stellate ganglia vascular smooth muscle cell clusters at the adjusted p < 0.05 cut-off level.*

| Gene | Name | Log Fold change | Adjusted P Value |
|---|---|---|---|
| **Stmn2** | Stathmin 2 | -1.05 | 6.33E-29 |
| **Tubb3** | Tubulin, Beta 3 | -0.91 | 7.18E-25 |
| **Pcp4** | Purkinje Cell Protein 4 | -0.92 | 6.81E-21 |
| **Jund** | Transcription Factor Jun-D | 1.02 | 1.76E-17 |
| **Tubb2b** | Tubulin Beta 2B Class IIb | -0.86 | 3.27E-16 |
| **Uchl1** | Ubiquitin C-Terminal Hydrolase L1 | -0.69 | 8.68E-15 |
| **RT1-A1** | RT1 class I, A1 | 1.21 | 1.81E-14 |
| **Stmn3** | Stathmin 3 | -0.83 | 1.36E-12 |
| **Bcat1** | Branched Chain Amino Acid Transaminase 1 | -0.70 | 2.03E-10 |
| **Tuba1a** | Tubulin Alpha 1a | -0.52 | 9.22E-10 |
| **Syt1** | Synaptotagmin 1 | -0.76 | 1.49E-09 |
| **Tubb5** | Tubulin, Beta 5 | -0.63 | 1.04E-08 |
| **Aldoa** | Aldolase A | -0.53 | 2.51E-08 |
| **Basp1** | Brain Abundant Membrane Attached Signal Protein 1 | -0.70 | 9.56E-08 |
| **Prph** | Peripherin | -0.56 | 1.06E-07 |
| **Stmn1** | Stathmin 1 | -0.61 | 3.46E-07 |
| **Map1b** | Microtubule Associated Protein 1B | -0.53 | 4.05E-07 |
| **Gap43** | Growth Associated Protein 43 | -0.63 | 4.61E-07 |
| **LOC691995** | hypothetical protein LOC691995 | -0.64 | 4.83E-07 |
| **Ndufa4** | NDUFA4 Mitochondrial Complex Associated | -0.61 | 9.55E-07 |
| **Nsg2** | Neuronal Vesicle Trafficking Associated 2 | -0.62 | 1.98E-06 |
| **Rtn1** | Reticulon 1 | -0.71 | 2.54E-06 |
| **LOC108348172.1** | Proprotein convertase subtilisin/kexin type 1 inhibitor | -0.57 | 3.66E-06 |
| **Ddc** | Dopa Decarboxylase | -0.58 | 8.54E-06 |
| **Nefl** | Neurofilament Light | -0.67 | 2.52E-05 |

## Fibroblast cells

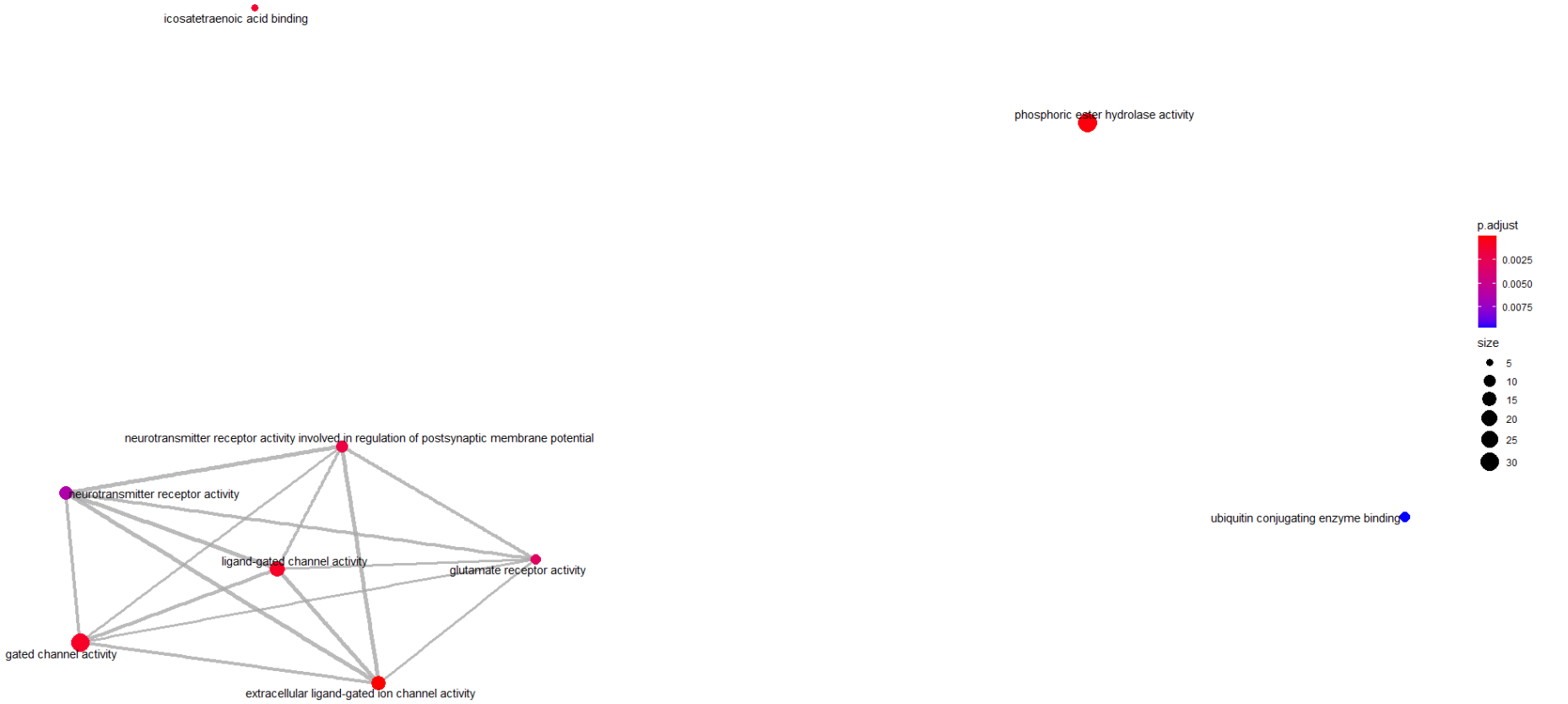
Finally, a population of fibroblasts was identified based upon the markers *DCN* (Decorin), *FAP (*Fibroblast Activation Protein Alpha*)*, *LUM* (Lumican), *MGP* (Matrix Gla Protein) and *SOX9* (SRY-Box Transcription Factor 9) (Philippeos *et al.*, 2018; Kahounová *et al.*, 2018) (Appendix figure 11). A single fibroblast cluster. was identified. Differential expression was again performed by *MAST* and the top 25 differentially expressed genes are shown in Appendix table 5.




***Appendix figure 11 Fibroblasts were identified by expression of known markers***
*Fibroblast markers were identified by expression of* DCN *(Decorin),* FAP (*Fibroblast Activation Protein Alpha*), LUM *(Lumican),* MGP *(Matrix Gla Protein) and* SOX9 *(SRY-Box Transcription Factor 9).*

**Appendix *Table 5 Top 25 changes in gene expression between Wistar and SHR fibroblasts*** *MAST differential expression highlighted 46 differentially expressed genes between Wistar and SHR stellate ganglia fibroblast clusters at the adjusted p < 0.05 cut-off level.*

| Gene | Name | Log Fold change | Adjusted P Value |
|---|---|---|---|
| **RT1-A1** | RT1 class I, A1 | 0.99 | 9.30E-20 |
| **Jund** | Transcription Factor Jun-D | 1.51 | 2.51E-13 |
| **Tubb3** | Tubulin, Beta 3 | -0.80 | 4.16E-12 |
| **Uchl1** | Ubiquitin C-Terminal Hydrolase L1 | -0.77 | 6.79E-12 |
| **Tubb2b** | Tubulin Beta 2B Class IIb | -0.80 | 7.15E-12 |
| **RT1-CE10** | RT1 class I, CE10 | -0.90 | 1.74E-11 |
| **Sncg** | Synuclein Gamma | -1.00 | 4.70E-11 |
| **Ywhag** | Tyrosine 3-Monooxygenase/Tryptophan 5-Monooxygenase | -0.74 | 7.71E-10 |
| **Pcp4** | Purkinje Cell Protein 4 | -0.72 | 9.32E-09 |
| **Stmn2** | Stathmin 2 | -0.78 | 1.15E-08 |
| **AABR07071891.2** | | -0.71 | 1.88E-08 |
| **Stmn3** | Stathmin 3 | -0.69 | 9.17E-08 |
| **Prph** | Peripherin | -0.68 | 1.22E-07 |
| **Stmn1** | Stathmin 1 | -0.99 | 1.27E-07 |
| **Sparcl1** | SPARC Like 1 | 0.82 | 1.48E-07 |
| **Cyr61** | Cysteine-rich angiogenic inducer 61 | 1.82 | 2.34E-07 |
| **Nefl** | Neurofilament Light | -0.76 | 6.13E-07 |
| **RGD1305645** | | 0.80 | 1.26E-06 |
| **Tuba1a** | Tubulin Alpha 1a | -0.54 | 4.35E-06 |
| **Nsg1** | Neuronal Vesicle Trafficking Associated 1 | -0.58 | 2.88E-05 |
| **Aldoa** | Aldolase, Fructose-Bisphosphate A | -0.46 | 0.000132559 |
| **Acp5** | Acid Phosphatase 5, Tartrate Resistant | 0.58 | 0.000271317 |
| **Clec3b** | C-Type Lectin Domain Family 3 Member B | -0.86 | 0.000500569 |
| **Ddc** | Dopa Decarboxylase | -0.47 | 0.000578041 |
| **F3** | Coagulation Factor III, Tissue Factor | 0.72 | 0.00087368 |




***Appendix Figure 12 Over-represented "molecular function" gene ontology terms in SHR sympathetic whole stellate ganglia*** *Gene ontology over-representation analysis highlighted multiple "molecular function" terms with a large number of differentially expressed genes as determined by bulk RNA-sequencing.*




***Appendix Figure 13 Over-represented "biological process" gene ontology terms in SHR sympathetic whole stellate ganglia***
*Gene ontology over-representation analysis highlighted multiple "biological process terms with a large number of differentially expressed genes as determined by bulk RNA-sequencing.*

***Appendix table 6 Genes that weren't expressed in the bulk RNA-sequencing dataset, but were differentially expressed in the single-cell RNA-sequencing dataset***

| | | |
|---|---|---|
| AABR07043389.1 | Atp5f1d | Atp5pd |
| AC134224.1 | Nbeal1 | Bola2 |
| AABR07043510.1 | Atp5md | LOC108348144 |
| LOC100364435 | Vbp1 | Atp5mf |
| AC134224.2 | Heatr5a | Dicer1 |
| RGD1559441 | Ppial4d | LOC100363502 |
| Ank2 | Atp5if1 | LOC103689961 |
| Pcbd2 | LOC100362830 | LOC108348287 |
| Dst | Herc6 | Rps10l1 |
| AABR07053749.2 | Atp5mc3 | Lrp8 |
| Chl1 | Tmem63b | LOC687780 |
| LOC100359583 | Ccdc88a | Cplane1 |
| Pfdn4 | Kmt2d | Mt-nd3 |
| Atp5f1e | Rps18l1 | AABR07056330.1 |
| Nsg2 | AABR07071891.2 | AABR07017145.1 |
| Atp5me | LOC108352650 | AABR07072236.1 |
| LOC108348172.1 | Atp5mg | Serf1 |
| AABR07059380.1 | Samd9 | LOC103693430 |
| Gnas.1 | Kif1a | Dmxl2 |
| Atp5pf | LOC100360522 | Sacs |
| Haghl | Cox7a2l2 | |
| AABR07007032.1 | LOC100364457 | |
| Tmsb15b2 | LOC100362027 | |
| LOC100912195 | Clasp1 | |
| Atp5mc2 | Ubr5 | |
| Herc1 | AABR07028902.1 | |
| Chd9 | Rps27a.1 | |
| LOC100360781 | Smg5 | |

## Discussion points on non-neuronal cells

In addition to the changes reported in the main text, changes in non-neuronal populations were also reported in the SHR and are discussed here. Several of these are discussed here, selected because of the potential physiological importance of these changes.

Interestingly, *PRPH* (Peripherin) was not only expressed in multiple non-neuronal populations in the stellate ganglia, but consistently downregulated in the SHR (Appendix tables 1-5). *PRPH* is traditionally believed to be a selective peripheral neuron marker (Hol & Capetanaki, 2017), so it is surprising that it is expressed in all cell types, albeit at a lower expression level (**Figure 3.7**). This may be artefactual, and result from contamination of other cells with catecholaminergic neuron mRNA during the sequencing process. This notion would be supported by the low-level expression of *TH*, *DBH* and *DDC* in non-neuronal populations (**Figure 3.4**), which was also unexpected.

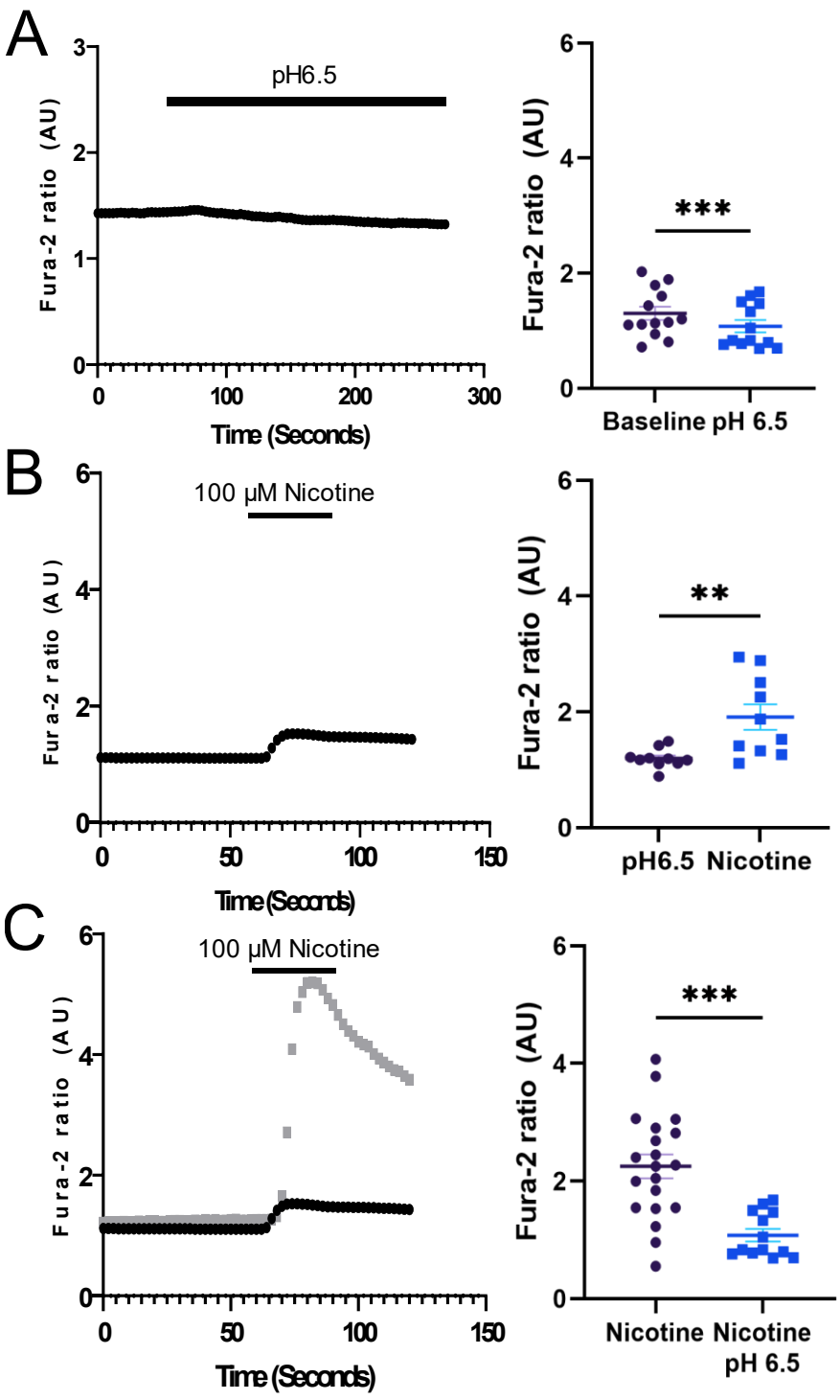
On the contrary, *CACNA1B* and *DLG4* remain neuron specific (**Figure 3.3**) and are also highly expressed in the neuronal population, suggesting that not all highly expressed genes contaminate other populations. In addition, other genes have been labelled as neuron-specific due to extremely high expression in sympathetic neurons, such as the NET transporter (*SLC6A2*) are shown here (**Figure 3.3**). *NET* is used here as a neuronal marker due to its high expression in neurons, there is also expression of *SLC6A2* in non-neuronal populations as previous reported for endothelial (Tseng & Padbury, 1998; Wakayama *et al.*, 2002), vascular smooth muscle cells (Johnson & Watts, 2011), glia (Inazu *et al.*, 2003), fibroblasts (Fang *et al.*, 2013) and immune cells (Pirzgalska *et al.*, 2017). Therefore, it may be that low expression of other sympathetic

genes is broader than expected. Further work is required to resolve these discrepancies, however, for the neuronal changes explored beyond this chapter this should not affect the interpretation of these data.

*JUND* expression was upregulated in every neuronal and non-neuronal cell population (**Tables 3.3-3.5**; Appendix tables 1-5). *JUND* expression has been shown to increase in the central nervous system following seizures (Morgan & Curran, 1991; Elliott & Gall, 2000), water deprivation (Yao *et al.*, 2012) and ischaemia (Kamme & Wieloch, 1996) and alongside other members of the AP-1 complex is regulated by cell activity (Morgan & Curran, 1991), as well as the cellular environment (Hess *et al.*, 2004). These changes in expression could result from previously documented variations in the *JUND* promoter in the SHR (Braun *et al.*, 2014), however the effects of this variations on function and of *JUND* has not been documented. It is unlikely that changes in non-neuronal populations arise from contamination by neuronal mRNA as *JUND* expression was higher in non-neuronal cell clusters (Data not shown). This may be an interesting line of future enquiry.

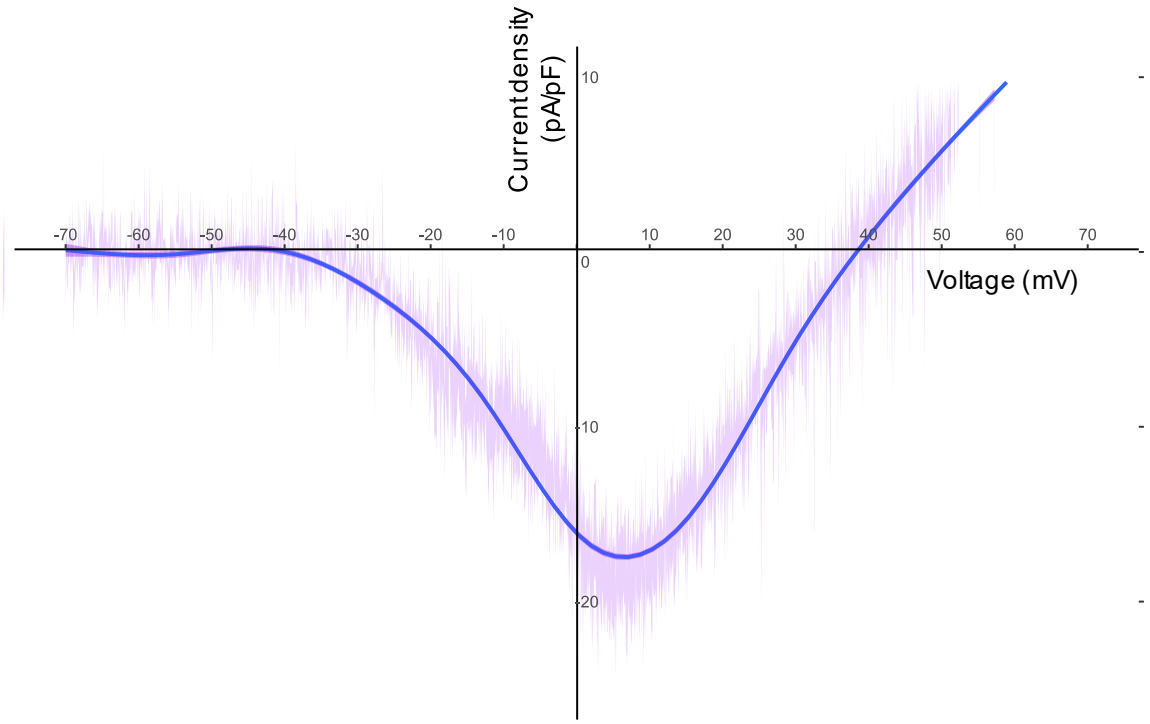
# Chapter 6

# Supplementary data

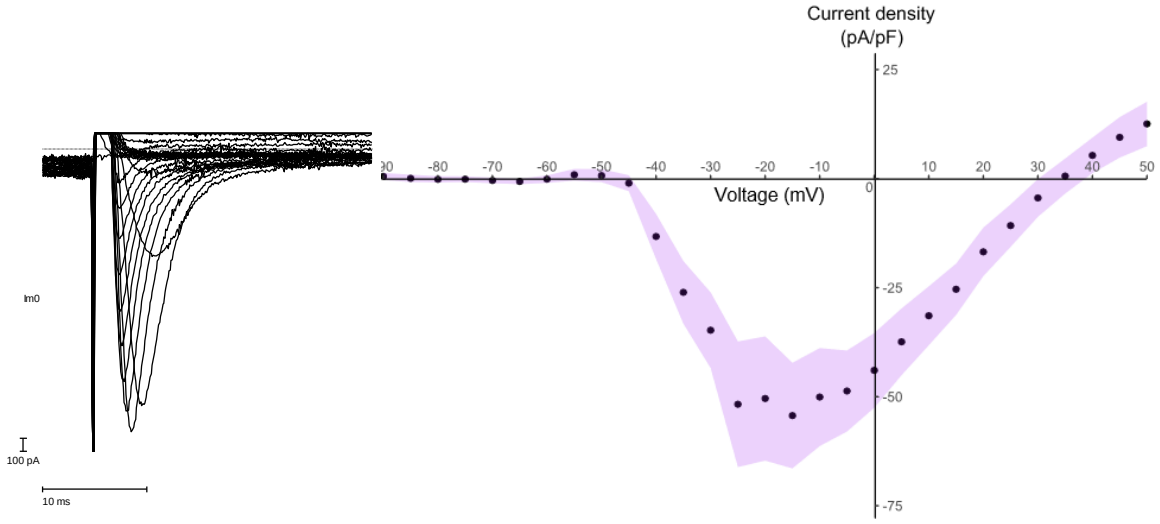



***Appendix figure 14 Effect of pH6.5 on baseline and nicotine responses*** *(A) pH6.5 significantly decreased the baseline fura-2 ratio. The baseline was averaged between 0-60 seconds and the response averaged between 230-270, where the response typically plateaued. (Mean±SEM)(-0.22±0.043) (n=13; Paired t-test, p=0.0002) (B) 100 µM nicotine evoked a small but significant response at pH6.5. (Mean±SEM) (0.72±0.17) (n=11; Paired t-test, p=0.0016) (C) 100 µM nicotine evoked a significantly larger response at pH7.4 than pH6.5. (Mean±SEM) (-1.17 ± 0.26) (n=12; Unpaired t-test, p=0.0005) Grey trace is an example nicotine peak at pH 7.4, black trace represents an example nicotine response at pH6.5.*

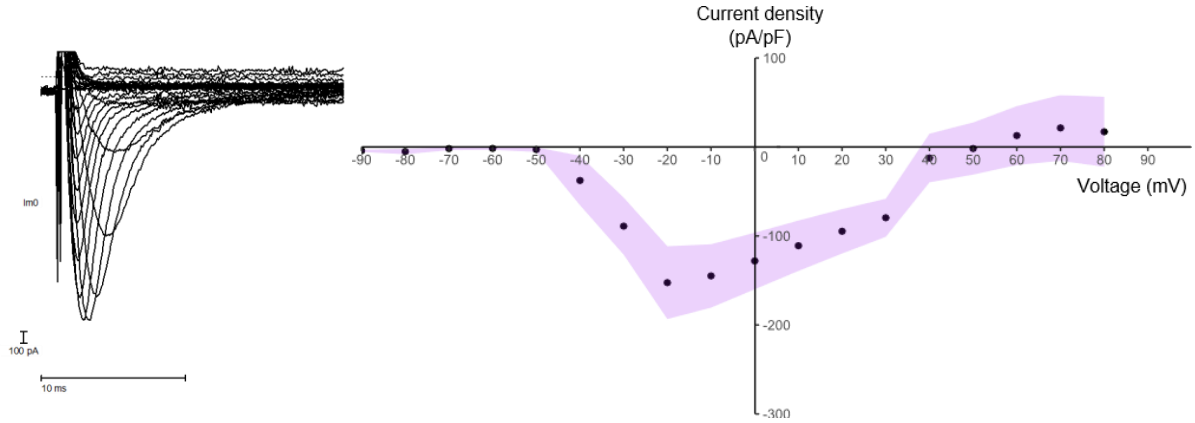
# Voltage clamp Supplementary data



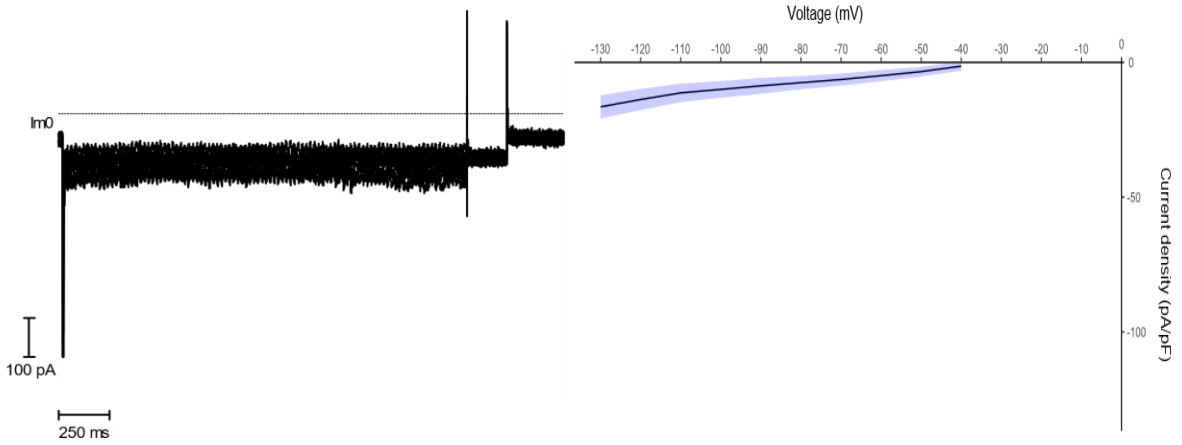

***Appendix Figure 15 Barium current density as determined by perforated patch clamp recordings*** *$Ca_V$ currents were recorded in isolating solutions with $Ba^{2+}$ as the charge carrier (n=11). These currents were elicited by a Voltage ramp from -100 mV to 60 mV at a speed of 0.4 mV/ms. A small linear current was removed from the data and calculated from the linear phase between -100 mV and -70 mV.*



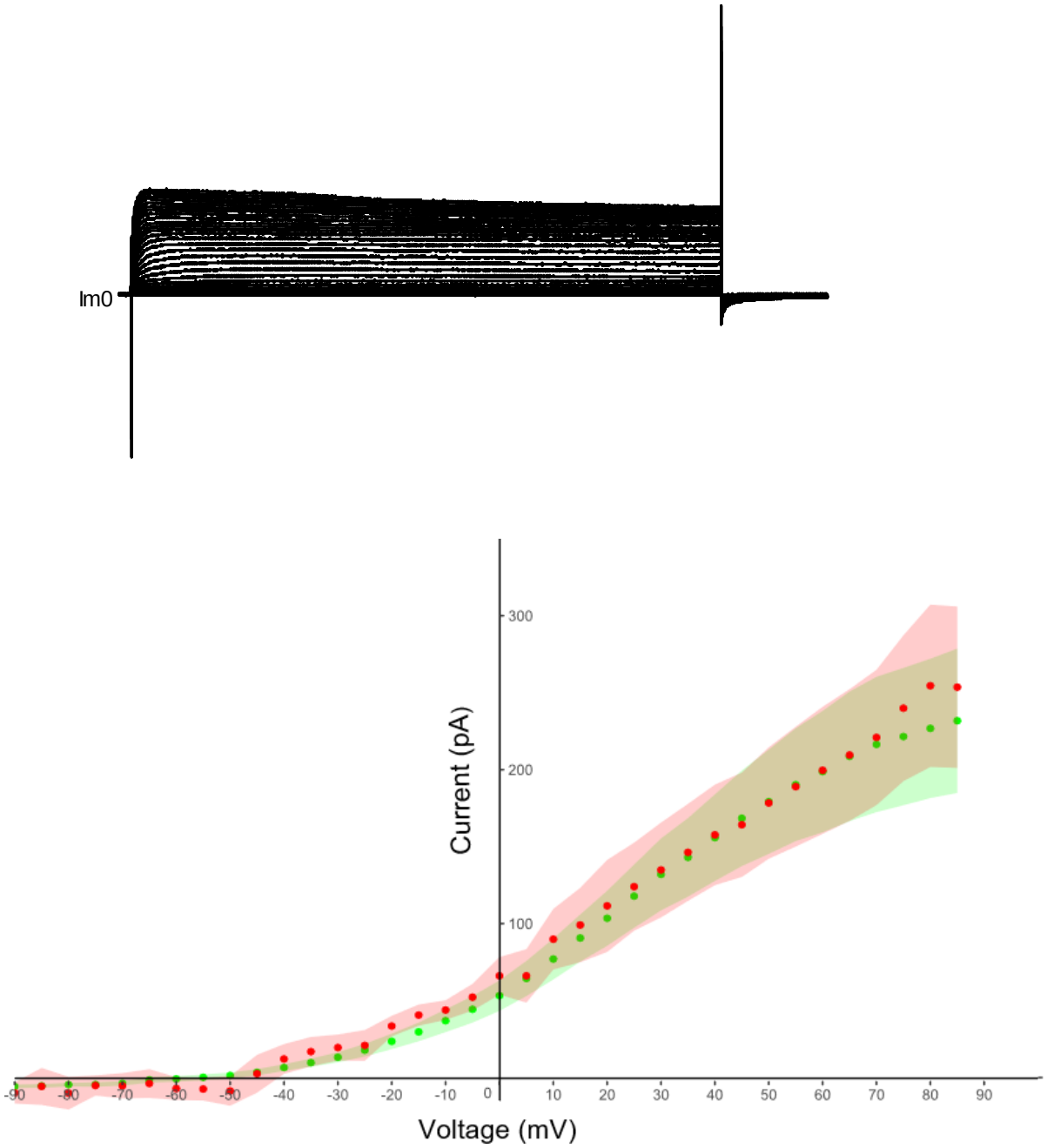

***Appendix Figure 16 Wistar stellate ganglia neuron $Na_V$ currents were recorded in $Na_V$ isolating solutions*** *$Na_V$ isolating solutions are described in **Chapter 2**. Extracellular $Na^+$ was reduced to 35 mM to limit voltage-clamp methods (as described in **Chapter 2**). $Na_V$ currents were elicited by one second 5 mV voltage steps in the range of -90 mV to 50 mV. Error shown as standard error of the mean, n = 15.*




***Appendix Figure 17 Wistar stellate ganglia neuron $Na_v$ currents were derived from TTX-sensitive current subtraction*** *$Na_v$ currents were taken as TTX inhibitable current. (n=13). $Na_v$ currents were elicited by one second 10 mV voltage steps in the range of -90 mV to 80 mV.*




***Appendix Figure 18 Wistar stellate ganglia neuron HCN channel recordings highlight a lack of HCN current in sympathetic neuron somata*** *HCN whole -cell voltage-clamp recordings were performed in the HCN isolating solutions described in Chapter 2. From a holding potential of -40 mV a series of -10mV two second current steps were used in the range of -40 mV to -160 mV followed by a return to -80 mV (n = 10). Only a small linear leak current was observed by this methodology.*




***Appendix Figure 19 Wistar stellate ganglia neuron $K_v$ peak density was similar by whole-cell recordings in $K_v$ isolating solutions (Green) and TTX isolated Kv (Red)*** *I recorded $K_v$ currents by two protocols using solutions outlined in* ***Chapter 2****. The resting membrane potential was held at -90 mV and $K_v$ currents elicited by 5 mV voltage steps from -90 mV to 85 mV. Errors are shown as standard error of the mean, n = 14 for $K_v$ isolating solutions and n = 14 for TTX subtracted currents. Example trace shown for TTX subtracted current.*

# References

Abdo H, Calvo-Enrique L, Lopez JM, Song J, Zhang M-D, Usoskin D, El Manira A, Adameyko I, Hjerling-Leffler J & Ernfors P (2019). Specialized cutaneous Schwann cells initiate pain sensation. *Science (80- )* **365,** 695 LP – 699.

Abe S, Takeda J & Senda M (1980). Resting membrane potential and action potential of Nitella expansa protoplasts. *Plant Cell Physiol* **21,** 537–546.

Adamatzky A (2018). On spiking behaviour of oyster fungi Pleurotus djamor. *Sci Rep* **8,** 7873.

Adams JM, Madden CJ, Sved AF & Stocker SD (2007). Increased dietary salt enhances sympathoexcitatory and sympathoinhibitory responses from the rostral ventrolateral medulla. *Hypertension* **50,** 354–359.

Adams PR & Brown DA (1975). Actions of gamma-aminobutyric acid on sympathetic ganglion cells. *J Physiol* **250,** 85–120.

Adams PR, Brown DA & Constanti A (1982). Pharmacological inhibition of the M-current. *J Physiol* **332,** 223–262.

Aggarwal SK & MacKinnon R (1996). Contribution of the S4 Segment to Gating Charge in the Shaker $K^+$ Channel. *Neuron* **16,** 1169–1177.

Agrawal SG & Evans RH (1986). The primary afferent depolarizing action of kainate in the rat. *Br J Pharmacol* **87,** 345–355.

Aiken SP, Lampe BJ, Murphy PA & Brown BS (1995). Reduction of spike frequency adaptation and blockade of M-current in rat CA1 pyramidal neurones by linopirdine (DuP 996), a neurotransmitter release enhancer. *Br J Pharmacol* **115,** 1163–1168.

Ajijola OA, Hoover DB, Simerly TM, Brown TC, Yanagawa J, Biniwale RM, Lee JM, Sadeghi A, Khanlou N, Ardell JL & Shivkumar K (2017). Inflammation, oxidative stress, and glial cell activation characterize stellate ganglia from humans with electrical storm. *JCI insight* **2,** e94715.

Alaimo A, Gómez-Posada JC, Aivar P, Etxeberrâ A, Rodriguez-Alfaro JA, Areso P & Villaroel A (2009). Calmodulin activation limits the rate of KCNQ2 K+ channel exit from the endoplasmic reticulum. *J Biol Chem* **284,** 20668–20675.

Alberdi E, Sánchez-Gómez MV, Marino A & Matute C (2002). Ca2+ influx through AMPA or kainate receptors alone is sufficient to initiate excitotoxicity in cultured oligodendrocytes. *Neurobiol Dis* **9,** 234–243.

Alcocer L & Cueto L (2008). Hypertension, a health economics perspective. *Ther Adv Cardiovasc Dis* **2,** 147–155.

Alig J, Marger L, Mesirca P, Ehmke H, Mangoni ME & Isbrandt D (2009). Control of heart rate by cAMP sensitivity of HCN channels. *Proc Natl Acad Sci* **106,** 12189 LP – 12194.

Alkadhi KA, Otoom SA, Tanner FL, Sockwell D & Hogan YH (2001). Inhibition of ganglionic long-term potentiation decreases blood pressure in spontaneously hypertensive rats. *Exp Biol Med* **226,** 1024–1030.

Allen NJ & Lyons DA (2018). Glia as architects of central nervous system formation and function. *Science (80- )* **362,** 181 LP – 185.

Altier C & Zamponi GW (2011). Analysis of GPCR/Ion Channel Interactions BT - Signal Transduction Protocols. In, ed. Luttrell LM & Ferguson SSG, pp. 215–225. Humana Press, Totowa, NJ. Available at: https://doi.org/10.1007/978-1-61779-160-4_11.

Altomare C, Terragni B, Brioschi C, Milanesi R, Pagliuca C, Viscomi C, Moroni A, Baruscotti M & DiFrancesco D (2003). Heteromeric HCN1-HCN4 channels: A comparison with native pacemaker channels from the rabbit sinoatrial node. *J Physiol* **549,** 347–359.

Amann R & Maggi CA (1991). Ruthenium red as a capsaicin antagonist. *Life Sci* **49,** 849–856.

Amberg GC, Koh SD, Imaizumi Y, Ohya S & Sanders KM (2003). A-type potassium currents in smooth muscle. *Am J Physiol - Cell Physiol* **284,** C583–C595.

Anderson EA, Sinkey CA, Lawton WJ & Mark AL (1989). Elevated sympathetic nerve activity in borderline hypertensive humans. Evidence from direct intraneural recordings. *Hypertension* **14,** 177–183.

Antonioli L, Blandizzi C, Pacher P & Haskó G (2013). Immunity, inflammation and cancer: A leading role for adenosine. *Nat Rev Cancer* **13,** 842–857.

Antunes VR, Yao ST, Pickering AE, Murphy D & Paton JFR (2006). A spinal vasopressinergic mechanism mediates hyperosmolality-induced sympathoexcitation. *J Physiol* **576,** 569–583.

Arancibia-Cárcamo IL, Ford MC, Cossell L, Ishida K, Tohyama K & Attwell D (2017). Node of Ranvier length as a potential regulator of myelinated axon conduction speed ed. Nave K-A. *Elife* **6,** e23329.

Arbab MA-R, Wiklund L, Delgado T & Svendgaard NA (1988). Stellate ganglion innervation of the vertebro-basilar arterial system demonstrated in the rat with anterograde and retrograde WGA-HRP tracing. *Brain Res* **445,** 175–180.

Armour JA & Butler C (1989). Intrathoracic ganglionic beta-adrenergic receptors involved in efferent sympathetic regulation of the canine heart. *Can J Cardiol* **5,** 275–283.

Armour JA & Hopkins DA (1981). Localization of sympathetic postganglionic neurons of physiologically identified cardiac nerves in the dog. *J Comp Neurol* **202,** 169–184.

Armstrong CM & Bezanilla F (1973). Currents related to movement of the gating particles of the sodium channels. *Nature* **242,** 459–461.

Arrang J-M, Garbarg M & Schwartz J-C (1983). Auto-inhibition of brain histamine release mediated by a novel class (H3) of histamine receptor. *Nature* **302,** 832–837.

Asano M & Nomura Y (2002). Contribution of sarcoplasmic reticulum Ca2+ to the activation of Ca2+ -activated K+ channels in the resting state of arteries from spontaneously hypertensive rats. *J Hypertens* **20,** 447–454.

Atanur SS et al. (2010). The genome sequence of the spontaneously hypertensive rat: Analysis and functional significance. *Genome Res* **20,** 791–803.

Atkins DL, Rosenthal JK, Krumm PA & Marvin WJ (1992). Differential growth of neonatal WKY and SHR ventricular myocytes within sympathetic co-cultures. *J Mol Cell Cardiol* **24,** 1479–1489.

Augustine GJ & Charlton MP (1986). Calcium dependence of presynaptic calcium current and post-synaptic response at the squid giant synapse. *J Physiol* **381,** 619–640.

Augustine GJ, Charlton MP & Smith SJ (1985). Calcium entry into voltage-clamped presynaptic terminals of squid. *J Physiol* **367,** 143–162.

Augustine GJ, Santamaria F & Tanaka K (2003). Local calcium signaling in neurons. *Neuron* **40,** 331–346.

Axelrod J, Hertting G & Potter L (1962). Effect of drugs on the uptake and release of 3H-

norepinephrine in the rat heart. *Nature* **194,** 297.

Baba H, Kohno T, Moore KA & Woolf CJ (2001). Direct Activation of Rat Spinal Dorsal Horn Neurons by Prostaglandin E2. *J Neurosci* **21,** 1750 LP – 1756.

Badoer E, Ng CW & De Matteo R (2003). Glutamatergic input in the PVN is important in renal nerve response to elevations in osmolality. *Am J Physiol - Ren Physiol* **285,** F640–F650.

Baik B, Yoon S & Nam D (2020). Benchmarking RNA-seq differential expression analysis methods using spike-in and simulation data. *PLoS One* **15,** e0232271.

Baker SE, Limberg JK, Dillon GA, Curry TB, Joyner MJ & Nicholson WT (2018). Aging alters the relative contributions of the sympathetic and parasympathetic nervous system to blood pressure control in women. *Hypertension* **72,** 1236–1242.

Bang S, Kim KY, Yoo S, Lee SH & Hwang SW (2007). Transient receptor potential V2 expressed in sensory neurons is activated by probenecid. *Neurosci Lett* **425,** 120–125.

Bang S, Yoo S, Yang T-J, Cho H & Hwang SW (2010). Farnesyl pyrophosphate is a novel pain-producing molecule via specific activation of TRPV3. *J Biol Chem* **285,** 19362–19371.

Bankenahally R & Krovvidi H (2016). Autonomic nervous system: anatomy, physiology, and relevance in anaesthesia and critical care medicine. *BJA Educ* **16,** 381–387.

Bant JS & Raman IM (2010). Control of transient, resurgent, and persistent current by open-channel block by Na channel beta4 in cultured cerebellar granule neurons. *Proc Natl Acad Sci U S A* **107,** 12357–12362.

Bar-Yehuda D & Korngreen A (2008). Space-Clamp Problems When Voltage Clamping Neurons Expressing Voltage-Gated Conductances. *J Neurophysiol* **99,** 1127–1136.

Barajas L, Liu L & Powers K (1992). Anatomy of the renal innervation: intrarenal aspects and ganglia of origin. *Can J Physiol Pharmacol* **70,** 735–749.

Baran-Gale J, Chandra T & Kirschner K (2018). Experimental design for single-cell RNA sequencing. *Brief Funct Genomics* **17,** 233–239.

Bardsley EN, Davis H, Ajijola OA, Buckler KJ, Ardell JL, Shivkumar K & Paterson DJ (2018*a*). RNA sequencing reveals novel transcripts from sympathetic stellate ganglia during cardiac sympathetic hyperactivity. *Sci Rep* **8,** 8633.

Bardsley EN, Davis H, Buckler KJ & Paterson DJ (2018*b*). Neurotransmitter switching coupled to β-adrenergic signaling in sympathetic neurons in prehypertensive states. *Hypertension* **71,** 1226–1238.

Barry EF & Johns EJ (2015). Intrarenal bradykinin elicits reno-renal reflex sympatho-excitation and renal nerve-dependent fluid retention. *Acta Physiol* **213,** 731–739.

Barry PH (1994). JPCalc, a software package for calculating liquid junction potential corrections in patch-clamp, intracellular, epithelial and bilayer measurements and for correcting junction potential measurements. *J Neurosci Methods* **51,** 107–116.

Basting T & Lazartigues E (2017). DOCA-Salt Hypertension: an Update. *Curr Hypertens Rep* **19,** 32.

Bayles RG, Olivas A, Denfeld Q, Woodward WR, Fei SS, Gao L & Habecker BA (2018). Transcriptomic and neurochemical analysis of the stellate ganglia in mice highlights sex differences. *Sci Rep* **8,** 8963.

Bayles RG, Tran J, Olivas A, Woodward WR, Fei SS, Gao L & Habecker BA (2019). Sex differences in

sympathetic gene expression and cardiac neurochemistry in Wistar Kyoto rats. *PLoS One* **14,** e0218133.

Bealer SL, Delle M, Skarphedinsson JO, Carlsson S & Thoren P (1996). Differential responses in adrenal and renal nerves to CNS osmotic stimulation. *Brain Res Bull* **39,** 205–209.

Bean BP (1985). Two kinds of calcium channels in canine atrial cells. Differences in kinetics, selectivity, and pharmacology. *J Gen Physiol* **86,** 1–30.

Bean BP (2007). The action potential in mammalian central neurons. *Nat Rev Neurosci* **8,** 451–465.

Becht E, McInnes L, Healy J, Dutertre CA, Kwok IWH, Ng LG, Ginhoux F & Newell EW (2019). Dimensionality reduction for visualizing single-cell data using UMAP. *Nat Biotechnol* **37,** 38–47.

Beck L (1958). Effect of the autonomic nervous system on arteriolar tone in the experimental animal. *Circulation* **17,** 798–806.

Becker BK, Feagans AC, Chen D, Kasztan M, Jin C, Speed JS, Pollock JS & Pollock DM (2017). Renal denervation attenuates hypertension but not salt sensitivity in ETB receptor-deficient rats. *Am J Physiol - Regul Integr Comp Physiol* **313,** R425–R437.

Beilin LJ, Puddey IB & Burke V (1999). Lifestyle and hypertension. *Am J Hypertens* **12,** 934–945.

Beltran-Parrazal L & Charles A (2003). Riluzole inhibits spontaneous Ca 2+ signaling in neuroendocrine cells by activation of K + channels and inhibition of Na + channels. *Br J Pharmacol* **140,** 881–888.

Bendahhou S, Marionneau C, Haurogne K, Larroque MM, Derand R, Szuts V, Escande D, Demolombe S & Barhanin J (2005). In vitro molecular interactions and distribution of KCNE family with KCNQ1 in the human heart. *Cardiovasc Res* **67,** 529–538.

Bengtson CP & Bading H (2012). Nuclear calcium signaling. In *Synaptic Plasticity*, pp. 377–405. Springer.

Bennett DL, Clark XAJ, Huang J, Waxman SG & Dib-Hajj SD (2019). The role of voltage-gated sodium channels in pain signaling. *Physiol Rev* **99,** 1079–1151.

Bennett MK, Calakos N & Scheller RH (1992). Syntaxin: a synaptic protein implicated in docking of synaptic vesicles at presynaptic active zones. *Science (80- )* **257,** 255 LP – 259.

Berg T (2014). B1-Blockers Lower Norepinephrine Release By Inhibiting Presynaptic, Facilitating B1-Adrenoceptors in Normotensive and Hypertensive Rats. *Front Neurol* **5 APR,** 51.

Berg T (2016). M-currents (Kv7.2-7.3/KCNQ2-KCNQ3) are responsible for dysfunctional autonomic control in hypertensive rats. *Front Physiol* **7,** 584.

Berg T (2018). Kv7(KCNQ)-K+-Channels influence total peripheral resistance in female but not male rats, and hamper catecholamine release in hypertensive rats of both sexes. *Front Physiol* **9,** 117.

Berkefeld H, Sailer CA, Bildl W, Rohde V, Thumfart JO, Eble S, Klugbauer N, Reisinger E, Bischofberger J, Oliver D, Knaus HG, Schultes U & Fakler B (2006). BKCa-Cav channel complexes mediate rapid and localized Ca 2+-activated K+ signaling. *Science (80- )* **314,** 615–620.

Bernardi P, Paradisi V, Pozzan T & Azzone GF (1984). Pathway for Uncoupler-Induced Calcium

Efflux in Rat Liver Mitochondria: Inhibition by Ruthenium Red. *Biochemistry* **23,** 1645–1651.

Berridge MJ, Lipp P & Bootman MD (2000). The versatility and universality of calcium signalling. *Nat Rev Mol Cell Biol* **1,** 11–21.

Bhalla T, Rosenthal JJC, Holmgren M & Reenan R (2004). Control of human potassium channel inactivation by editing of a small mRNA hairpin. *Nat Struct Mol Biol* **11,** 950–956.

Bhatt DL, Kandzari DE, O'Neill WW, D'Agostino R, Flack JM, Katzen BT, Leon MB, Liu M, Mauri L, Negoita M, Cohen SA, Oparil S, Rocha-Singh K, Townsend RR & Bakris GL (2014). A Controlled Trial of Renal Denervation for Resistant Hypertension. *N Engl J Med* **370,** 1393–1401.

Bhattacharjee A, Joiner WJ, Wu M, Yang Y, Sigworth FJ & Kaczmarek LK (2003). Slick (Slo2.1), a Rapidly-Gating Sodium-Activated Potassium Channel Inhibited by ATP. *J Neurosci* **23,** 11681–11691.

Biaggioni I, Killian TJ, Mosqueda-Garcia R, Robertson RM & Robertson D (1991). Adenosine increases sympathetic nerve traffic in humans. *Circulation* **83,** 1668–1675.

Di Biase V, Obermair GJ, Szabo Z, Altier C, Sanguesa J, Bourinet E & Flucher BE (2008). Stable membrane expression of postsynaptic CaV1.2 calcium channel clusters is independent of interactions with AKAP79/150 and PDZ proteins. *J Neurosci* **28,** 13845–13855.

Biel M, Wahl-Schott C, Michalakis S & Zong X (2009). Hyperpolarization-activated cation channels: From genes to function. *Physiol Rev* **89,** 847–885.

Biervert C, Schroeder BC, Kubisch C, Berkovic SF, Propping P, Jentsch TJ & Steinlein OK (1998). A potassium channel mutation in neonatal human epilepsy. *Science (80- )* **279,** 403–406.

Bing OHL, Brooks WW, Robinson KG, Slawsky MT, Hayes JA, Litwin SE, Sens S & Conrad CH (1995). The spontaneously hypertensive rat as a model of the transition from compensated left ventricular hypertrophy to failure. *J Mol Cell Cardiol* **27,** 383–396.

Bischoff U, Vogel W & Safronov B V. (1998). Na+-activated K+ channels in small dorsal root ganglion neurones of rat. *J Physiol* **510,** 743–754.

Bladen C & Zamponi GW (2012). Common mechanisms of drug interactions with sodium and T-type calcium channels. *Mol Pharmacol* **82,** 481–487.

Blaine JT & Ribera AB (2001). Kv2 channels form delayed-rectifier potassium channels in situ. *J Neurosci* **21,** 1473–1480.

Blondel VD, Guillaume JL, Lambiotte R & Lefebvre E (2008). Fast unfolding of communities in large networks. *J Stat Mech Theory Exp* **2008,** P10008.

Blumenfeld JD, Sealey JE, Mann SJ, Bragat A, Marion R, Pecker MS, Sotelo J, August P, Pickering TG & Laragh JH (1999). β-adrenergic receptor blockade as a therapeutic approach for suppressing the renin-angiotensin-aldosterone system in normotensive and hypertensive subjects*. *Am J Hypertens* **12,** 451–459.

Boehm S (1999). ATP stimulates sympathetic transmitter release via presynaptic P2X purinoceptors. *J Neurosci* **19,** 737–746.

Boehm S, Huck S & Illes P (1995). UTP- and ATP-triggered transmitter release from rat sympathetic neurones via separate receptors. *Br J Pharmacol* **116,** 2341–2343.

Böhm M, Kario K, Kandzari DE, Mahfoud F, Weber MA, Schmieder RE, Tsioufis K, Pocock S,

Konstantinidis D & Choi JW (2020). Efficacy of catheter-based renal denervation in the absence of antihypertensive medications (SPYRAL HTN-OFF MED Pivotal): a multicentre, randomised, sham-controlled trial. *Lancet*.

Bolívar JJ (2013). Essential hypertension: An approach to its etiology and neurogenic pathophysiology. *Int J Hypertens* **2013,** 11. Available at: http://dx.doi.org/10.1155/2013/547809 [Accessed August 21, 2018].

Bordas C, Kovacs A & Pal B (2015). The M-current contributes to high threshold membrane potential oscillations in a cell type-specific way in the pedunculopontine nucleus of mice. *Front Cell Neurosci* **9,** 121.

Borea PA, Gessi S, Merighi S, Vincenzi F & Varani K (2018). Pharmacology of Adenosine Receptors: The State of the Art. *Physiol Rev* **98,** 1591–1625.

Borst C & Karemaker JM (1983). Time delays in the human baroreceptor reflex. *J Auton Nerv Syst* **9,** 399–409.

Borst JGG & Sakmann B (1999). Effect of changes in action potential shape on calcium currents and transmitter release in a calyx–type synapse of the rat auditory brainstem. *Philos Trans R Soc London Ser B Biol Sci* **354,** 347–355.

Bourinet E, Soong TW, Sutton K, Slaymaker S, Mathews E, Monteil A, Zamponi GW, Nargeot J & Snutch TP (1999). Splicing of α(1A) subunit gene generates phenotypic variants of P- and Q-type calcium channels. *Nat Neurosci* **2,** 407–415.

Bouron A, Kiselyov K & Oberwinkler J (2015). Permeation, regulation and control of expression of TRP channels by trace metal ions. *Pflugers Arch Eur J Physiol* **467,** 1143–1164.

Brack KE, Coote JH & Ng GA (2006). The effect of direct autonomic nerve stimulation on left ventricular force in the isolated innervated Langendorff perfused rabbit heart. *Auton Neurosci Basic Clin* **124,** 69–80.

Branco T & Staras K (2009). The probability of neurotransmitter release: variability and feedback control at single synapses. *Nat Rev Neurosci* **10,** 373–383.

Bray GE, Ying Z, Baillie LD, Zhai R, Mulligan SJ & Verge VMK (2013). Extracellular pH and neuronal depolarization serve as dynamic switches to rapidly mobilize trkA to the membrane of adult sensory neurons. *J Neurosci* **33,** 8202–8215.

Brennecke P, Anders S, Kim JK, Kołodziejczyk AA, Zhang X, Proserpio V, Baying B, Benes V, Teichmann SA, Marioni JC & Heisler MG (2013). Accounting for technical noise in single-cell RNA-seq experiments. *Nat Methods* **10,** 1093–1095.

Brenner R, Chen QH, Vilaythong A, Toney GM, Noebels JL & Aldrich RW (2005). BK channel β4 subunit reduces dentate gyrus excitability and protects against temporal lobe seizures. *Nat Neurosci* **8,** 1752–1759.

Brenner R, Jegla TJ, Wickenden A, Liu Y & Aldrich RW (2000). Cloning and Functional Characterization of Novel Large Conductance Calcium-activated Potassium Channel β Subunits, hKCNMB3 and hKCNMB4. *J Biol Chem* **275,** 6453–6461.

Briant LJB, Stalbovskiy AO, Nolan MF, Champneys AR & Pickering AE (2014). Increased intrinsic excitability of muscle vasoconstrictor preganglionic neurons may contribute to the elevated sympathetic activity in hypertensive rats. *J Neurophysiol* **112,** 2756–2778.

Bristow MR, Ginsburg R, Umans V, Fowler M, Minobe W, Rasmussen R, Zera P, Menlove R, Shah P & Jamieson S (1986). Beta 1-and beta 2-adrenergic-receptor subpopulations in nonfailing

and failing human ventricular myocardium: coupling of both receptor subtypes to muscle contraction and selective beta 1-receptor down-regulation in heart failure. *Circ Res* **59,** 297–309.

Brock JA & Tan JHC (2004). Selective modulation of noradrenaline release by alpha 2-adrenoceptor blockade in the rat-tail artery in vitro. *Br J Pharmacol* **142,** 267–274.

Brock LG, Coombs JS & Eccles JC (1952). The recording of potentials from motoneurones with an intracellular electrode. *J Physiol* **117,** 431–460.

Bröker-Lai J et al. (2017). Heteromeric channels formed by TRPC1, TRPC4 and TRPC5 define hippocampal synaptic transmission and working memory. *EMBO J* **36,** 2770–2789.

Bronk DW & Stella G (1932). Afferent impulses in the carotid sinus nerve I. The relation of the discharge from single end organs to arterial blood pressure. *J Cell Comp Physiol* **1,** 113–130.

Brose N, Petrenko AG, Sudhof TC & Jahn R (1992). Synaptotagmin: a calcium sensor on the synaptic vesicle surface. *Science (80- )* **256,** 1021–1025.

Brown AM (1967). Cardiac sympathetic adrenergic pathways in which synaptic transmission is blocked by atropine sulfate. *J Physiol* **191,** 271–288.

Brown DA & Adams PR (1980). Muscarinic suppression of a novel voltage-sensitive K+ current in a vertebrate neurone [18]. *Nature* **283,** 673–676. Available at: http://www.nature.com/articles/283673a0 [Accessed September 10, 2018].

Brown DA & Passmore GM (2009). Neural KCNQ (Kv7) channels. *Br J Pharmacol* **156,** 1185–1195.

Brueggemann LI, Haick JM, Cribbs LL & Byron KL (2014). Differential activation of vascular smooth muscle Kv7.4, Kv7.5, and Kv7.4/7.5 channels by ML213 and ICA-069673. *Mol Pharmacol* **86,** 330–341.

Bryant CE, Allcock GH & Warner TD (1995). Comparison of effects of chronic and acute administration of NG-nitro-L-arginine methyl ester to the rat on inhibition of nitric oxide-mediated responses. *Br J Pharmacol* **114,** 1673–1679.

Brys R, Josson K, Castelli MP, Jurzak M, Lijnen P, Gommeren W & Leysen JE (2000). Reconstitution of the Human 5-HT<sub>1D</sub> Receptor-G-Protein Coupling: Evidence for Constitutive Activity and Multiple Receptor Conformations. *Mol Pharmacol* **57,** 1132 LP – 1141.

Bub G & Burton RAB (2015). Macro-micro imaging of cardiac-neural circuits in co-cultures from normal and diseased hearts. *J Physiol* **593,** 3047–3053.

Buerkle H & Yaksh TL (1998). Pharmacological evidence for different alpha 2-adrenergic receptor sites mediating analgesia and sedation in the rat. *Br J Anaesth* **81,** 208–215.

Buettner F, Natarajan KN, Casale FP, Proserpio V, Scialdone A, Theis FJ, Teichmann SA, Marioni JC & Stegle O (2015). Computational analysis of cell-to-cell heterogeneity in single-cell RNA-sequencing data reveals hidden subpopulations of cells. *Nat Biotechnol* **33,** 155–160.

Buettner HM & Pittman RN (1991). Quantitative effects of laminin concentration on neurite outgrowth in vitro. *Dev Biol* **145,** 266–276.

Burnashev N, Monyer H, Seeburg PH & Sakmann B (1992). Divalent ion permeability of AMPA receptor channels is dominated by the edited form of a single subunit. *Neuron* **8,** 189–198.

Burnier M & Brunner HR (2000). Angiotensin II receptor antagonists. *Lancet* **355,** 637–645.

Burnstock G (2004). Cotransmission. *Curr Opin Pharmacol* **4,** 47–52.

Burnstock G (2007). Purine and pyrimidine receptors. *Cell Mol Life Sci* **64,** 1471–1483.

Burnstock G, B Fredholm B & Verkhratsky A (2011). Adenosine and ATP receptors in the brain. *Curr Top Med Chem* **11,** 973–1011.

Butler A, Tsunoda S, McCobb DP, Wei A & Salkoff L (1993). mSlo, a complex mouse gene encoding "maxi" calcium-activated potassium channels. *Science (80- )* **261,** 221 LP – 224.

Butler CK, Smith FM, Nicholson J & Armour JA (1990). Cardiac effects induced by chemically activated neurons in canine intrathoracic ganglia. *Am J Physiol - Hear Circ Physiol* **259,** H1108–H1117.

Buttgereit J, Shanks J, Li D, Hao G, Athwal A, Langenickel TH, Wright H, Da Costa Goncalves AC, Monti J, Plehm R, Popova E, Qadri F, Lapidus I, Ryan B, Özcelik C, Paterson DJ, Bader M & Herring N (2016). C-type natriuretic peptide and natriuretic peptide receptor B signalling inhibits cardiac sympathetic neurotransmission and autonomic function. *Cardiovasc Res* **112,** 637–644.

Cabassi A, Vinci S, Calzolari M, Bruschi G & Borghetti A (1998). Regional sympathetic activity in pre-hypertensive phase of spontaneously hypertensive rats. *Life Sci* **62,** 1111–1118.

Calhoun DA, Zhu S, Wyss JM & Oparil S (1994). Diurnal blood pressure variation and dietary salt in spontaneously hypertensive rats. *Hypertension* **24,** 1–7.

Callahan T, Young HM, Anderson RB, Enomoto H & Anderson CR (2008). Development of satellite glia in mouse sympathetic ganglia: GDNF and GFRα1 are not essential. *Glia* **56,** 1428–1437.

Calvo M, Richards N, Schmid AB, Barroso A, Zhu L, Ivulic D, Zhu N, Anwandter P, Bhat MA, Court FA, McMahon SB & Bennett DLH (2016). Altered potassium channel distribution and composition in myelinated axons suppresses hyperexcitability following injury ed. Mason P. *Elife* **5,** e12661.

Câmara R & Griessenauer CJ (2015). Chapter 27 - Anatomy of the Vagus Nerve. In, ed. Tubbs RS, Rizk E, Shoja MM, Loukas M, Barbaro N & Spinner RJBT-N and NI, pp. 385–397. Academic Press, San Diego. Available at: http://www.sciencedirect.com/science/article/pii/B9780124103900000287.

Camm AJ, Malik M, Bigger JT, Breithardt G, Cerutti S, Cohen RJ, Coumel P, Fallen EL, Kennedy HL & Kleiger RE (1996). Heart rate variability: standards of measurement, physiological interpretation and clinical use. Task Force of the European Society of Cardiology and the North American Society of Pacing and Electrophysiology.

Candia S, Garcia ML & Latorre R (1992). Mode of action of iberiotoxin, a potent blocker of the large conductance Ca(2+)-activated K+ channel. *Biophys J* **63,** 583–590.

Cannon BW (1915). Bodily changes in pain, hunger, fear and rage: An account of recent researches into the function of emotional excitement. *Applet Century Crofts, New York/London*.

Cannon WB (1911). *The mechanical factors of digestion*. Longmans, Green & Company.

Cao YJ, Dreixler JC, Couey JJ & Houamed KM (2002). Modulation of recombinant and native neuronal SK channels by the neuroprotective drug riluzole. *Eur J Pharmacol* **449,** 47–54.

Caplea A, Seachrist D, Daneshvar H, Dunphy G & Ely D (2002). Noradrenergic content and turnover rate in kidney and heart shows gender and strain differences. *J Appl Physiol* **92,**

567–571.

Caputo A, Caci E, Ferrera L, Pedemonte N, Barsanti C, Sondo E, Pfeffer U, Ravazzolo R, Zegarra-Moran O & Galietta LJ V (2008). TMEM16A, a membrane protein associated with calcium-dependent chloride channel activity. *Science (80- )* **322,** 590–594.

Carbon S et al. (2019). The Gene Ontology Resource: 20 years and still GOing strong. *Nucleic Acids Res* **47,** D330–D338.

Carbone E & Lux HD (1984). A low voltage-activated, fully inactivating Ca channel in vertebrate sensory neurones. *Nature* **310,** 501–502.

Carlton SM, Chung K, Ding Z & Coggeshall RE (1998). Glutamate receptors on postganglionic sympathetic axons. *Neuroscience* **83,** 601–605.

Carmeliet E (2019). From Bernstein's rheotome to Neher-Sakmann's patch electrode. The action potential. *Physiol Rep* **7,** e13861–e13861.

Carretero OA & Oparil S (2000). Essential hypertension. Part I: Definition and etiology. *Circulation* **101,** 329–335.

Carrisoza-Gaytán R, Salvador C, Satlin LM, Liu W, Zavilowitz B, Bobadilla NA, Trujillo J & Escobar LI (2010). Potassium secretion by voltage-gated potassium channel Kv1.3 in the rat kidney. *Am J Physiol Renal Physiol* **299,** F255–F264.

Carruthers AM, Sellers LA, Jenkins DW, Jarvie EM, Feniuk W & Humphrey PPA (2001). Adenosine A<sub>1</sub> Receptor-Mediated Inhibition of Protein Kinase A-Induced Calcitonin Gene-Related Peptide Release from Rat Trigeminal Neurons. *Mol Pharmacol* **59,** 1533 LP – 1541.

Carvajal FJ, Mattison HA & Cerpa W (2016). Role of NMDA Receptor-Mediated Glutamatergic Signaling in Chronic and Acute Neuropathologies ed. Kang KD. *Neural Plast* **2016,** 2701526.

Carver CM & Shapiro MS (2019). Gq-coupled muscarinic receptor enhancement of KCNQ2/3 channels and activation of TRPC channels in multimodal control of excitability in dentate gyrus granule cells. *J Neurosci* **39,** 1566–1587.

Casini S, Marchal GA, Kawasaki M, Nariswari FA, Portero V, van den Berg NWE, Guan K, Driessen AHG, Veldkamp MW, Mengarelli I, de Groot JR, Verkerk AO & Remme CA (2019). Absence of Functional Nav1.8 Channels in Non-diseased Atrial and Ventricular Cardiomyocytes. *Cardiovasc Drugs Ther* **33,** 649–660.

Del Castillo J & Katz B (1954). Quantal components of the end-plate potential. *J Physiol* **124,** 560.

Castrén E, Kurihara M, Gutkind JS & Saavedra JM (1987). Specific angiotensin II binding sites in the rat stellate and superior cervical ganglia. *Brain Res* **422,** 347–351.

De Castro F, Geijo-Barrientos E & Gallego R (1997). Calcium-activated chloride current in normal mouse sympathetic ganglion cells. *J Physiol* **498,** 397–408.

Caterina MJ & Park UBT-CT in M (2006). Chapter 4 TRPV1: A Polymodal Sensor in the Nociceptor Terminal. In *The Nociceptive Membrane*, pp. 113–150. Academic Press. Available at: http://www.sciencedirect.com/science/article/pii/S1063582306570036.

Caterina MJ, Rosen TA, Tominaga M, Brake AJ & Julius D (1999). A capsaicin-receptor homologue with a high threshold for noxious heat. *Nature* **398,** 436–441.

Catterall WA (2010). Ion channel voltage sensors: structure, function, and pathophysiology.

*Neuron* **67,** 915–928.

De Cavanagh EMV, Toblli JE, Ferder L, Piotrkowski B, Stella I & Inserra F (2006). Renal mitochondrial dysfunction in spontaneously hypertensive rats is attenuated by losartan but not by amlodipine. *Am J Physiol - Regul Integr Comp Physiol* **290,** R1616–R1625.

Chadha PS, Zunke F, Zhu HL, Davis AJ, Jepps TA, Olesen SP, Cole WC, Moffatt JD & Greenwood IA (2012). Reduced KCNQ4-encoded voltage-dependent potassium channel activity underlies impaired β-adrenoceptor-mediated relaxation of renal arteries in hypertension. *Hypertension* **59,** 877–884.

Chambers JC et al. (2010). Genetic variation in SCN10A influences cardiac conduction. *Nat Genet* **42,** 149–152.

Chang K, Hanaoka K, Kumada M & Takuwa Y (1995). Molecular cloning and functional analysis of a novel P2 nucleotide receptor. *J Biol Chem* **270,** 26152–26158.

Chao OY & Yang YM (2019). Timing constraints of action potential evoked Ca 2+ current and transmitter release at a central nerve terminal. *Sci Rep* **9,** 4448.

Charlton MP, Smith SJ & Zucker RS (1982). Role of presynaptic calcium ions and channels in synaptic facilitation and depression at the squid giant synapse. *J Physiol* **323,** 173–193.

Chen-Izu Y, Xiao RP, Izu LT, Cheng H, Kuschel M, Spurgeon H & Lakatta EG (2000). G(i)-dependent localization of beta(2)-adrenergic receptor signaling to L-type Ca(2+) channels. *Biophys J* **79,** 2547–2556.

Chen CC, England S, Akopian AN & Wood JN (1998). A sensory neuron-specific, proton-gated ion channel. *Proc Natl Acad Sci U S A* **95,** 10240–10245.

Chen QH & Toney GM (2001). AT1-receptor blockade in the hypothalamic PVN reduces central hyperosmolality-induced renal sympathoexcitation. *Am J Physiol Integr Comp Physiol* **281,** R1844–R1853.

Chen XM, Yu LL, Shi SB, Jiang H, Huang CX, Desai M, Li YG, Barajas-Martinez H & Hu D (2016). Neuronal Nav1.8 channels as a novel therapeutic target of acute atrial fibrillation prevention. *J Am Heart Assoc* **5,** e004050.

Chen YJ, Huang CW, Lin CS, Chang WH & Sun WH (2009). Expression and function of proton-sensing G-protein-coupled receptors in inflammatory pain. *Mol Pain* **5,** 39.

Cho HJ, Staikopoulos V, Ivanusic JJ & Jennings EA (2009). Hyperpolarization-activated cyclic-nucleotide gated 4 (HCN4) protein is expressed in a subset of rat dorsal root and trigeminal ganglion neurons. *Cell Tissue Res* **338,** 171–177.

Choate JK, Klemm M & Hirst GDS (1993). Sympathetic and parasympathetic neuromuscular junctions in the guinea-pig sino-atrial node. *J Auton Nerv Syst* **44,** 1–15.

Chokshi R, Fruasaha P & Kozak JA (2012). 2-Aminoethyl diphenyl borinate (2-APB) inhibits TRPM7 channels through an intracellular acidification mechanism. *Channels* **6,** 362–369.

Christian O, Felix M, Axel S, Tilmann D, A. SP, Roland V, Aline S, Christian U, Ulrich L, Michael U, Michael B & E. SR (2013). Renal Denervation in Moderate Treatment-Resistant Hypertension. *J Am Coll Cardiol* **62,** 1880–1886.

Chungcharoen D, Daly M de B & Schweitzer A (1952). The blood supply of the superior cervical sympathetic and the nodose ganglia in cats, dogs and rabbits. *J Physiol* **118,** 528–536.

Cingolani LA, Gymnopoulos M, Boccaccio A, Stocker M & Pedarzani P (2002). Developmental Regulation of Small-Conductance Ca2+-Activated K+ Channel Expression and Function in Rat Purkinje Neurons. *J Neurosci* **22,** 4456–4467.

Clapham DE (2007). SnapShot: mammalian TRP channels. *Cell* **129,** 220-e1.

Clasadonte J, Poulain P, Hanchate NK, Corfas G, Ojeda SR & Prevot V (2011). Prostaglandin E 2 release from astrocytes triggers gonadotropin-releasing hormone (GnRH) neuron firing via EP2 receptor activation. *Proc Natl Acad Sci U S A* **108,** 16104–16109.

Cohn JN, Levine TB, Olivari MT, Garberg V, Lura D, Francis GS, Simon AB & Rector T (1984). Plasma Norepinephrine as a Guide to Prognosis in Patients with Chronic Congestive Heart Failure. *N Engl J Med* **311,** 819–823.

Collett JA, Paulose JK, Cassone VM & Osborn JL (2013). Maternally derived mitochondria in SHR exhibit significant reduction in oxidative phosphorylation gene expression. *FASEB J* **27,** 955.4-955.4.

Colombo F, Racchetti G & Meldolesi J (2014). Neurite outgrowth induced by NGF or L1CAM via activation of the TrkA receptor is sustained also by the exocytosis of enlargeosomes. *Proc Natl Acad Sci U S A* **111,** 16943–16948.

Colton CK & Zhu MX (2007). 2-aminoethoxydiphenyl borate as a common activator of TRPV1, TRPV2, and TRPV3 channels. *Handb Exp Pharmacol* **179,** 173–187.

Conesa A, Madrigal P, Tarazona S, Gomez-Cabrero D, Cervera A, McPherson A, Szcześniak MW, Gaffney DJ, Elo LL, Zhang X & Mortazavi A (2016). A survey of best practices for RNA-seq data analysis. *Genome Biol* **17,** 13.

Conforti L, Tohse N & Sperelakis N (1991). Influence of sympathetic innervation on the membrane electrical properties of neonatal rat cardiomyocytes in culture. *J Dev Physiol* **15,** 237–246.

Connor JA & Stevens CF (1971). Voltage clamp studies of a transient outward membrane current in gastropod neural somata. *J Physiol* **213,** 21–30.

Conrad CH, Brooks WW, Hayes JA, Sen S, Robinson KG & Bing OHL (1995). Myocardial fibrosis and stiffness with hypertrophy and heart failure in the spontaneously hypertensive rat. *Circulation* **91,** 161–170.

Constanti A & Brown DA (1981). M-currents in voltage-clamped mammalian sympathetic neurones. *Neurosci Lett* **24,** 289–294.

Conway J (1983). Hypotensive mechanisms of beta blockers. *Eur Heart J* **4,** 43–51.

Coombs ID, Soto D, McGee TP, Gold MG, Farrant M & Cull-Candy SG (2019). Homomeric GluA2(R) AMPA receptors can conduct when desensitized. *Nat Commun* **10,** 4312.

Coombs JS, Eccles JC & Fatt P (1953). *The action of the inhibitory synaptic transmitter*. Australasian Medical Publishing Company.

Coombs JS, Eccles JC & Fatt P (1955). The specific ionic conductances and the ionic movements across the motoneuronal membrane that produce the inhibitory post-synaptic potential. *J Physiol* **130,** 326–374.

Coons AH, Creech HJ, Jones RN & Berliner E (1942). The demonstration of pneumococcal antigen in tissues by the use of fluorescent antibody. *J Immunol* **45,** 159–170.

Coote JH (2005). A role for the paraventricular nucleus of the hypothalamus in the autonomic

control of heart and kidney. *Exp Physiol* **90,** 169–173.

Costa AMN & Brown BS (1997). Inhibition of M-current in cultured rat superior cervical ganglia by linopirdine: Mechanism of action studies. *Neuropharmacology* **36,** 1747–1753.

Cragg BG & Thomas PK (1957). The relationships between conduction velocity and the diameter and internodal length of peripheral nerve fibres. *J Physiol* **136,** 606–614.

Craig MT & McBain CJ (2014). The emerging role of GABAB receptors as regulators of network dynamics: fast actions from a "slow" receptor? *Curr Opin Neurobiol* **26,** 15–21.

Cramer M, Siegal M, Bigger Jr JT & Hoffman BF (1977). Characteristics of extracellular potentials recorded from the sinoatrial pacemaker of the rabbit. *Circ Res* **41,** 292–300.

Crill WE (1996). Persistent Sodium Current in Mammalian Central Neurons. *Annu Rev Physiol* **58,** 349–362.

Cruzblanca H, Koh DS & Hille B (1998). Bradykinin inhibits M current via phospholipase C and Ca2+ release from IP3-sensitive Ca2+ stores in rat sympathetic neurons. *Proc Natl Acad Sci U S A* **95,** 7151–7156.

Cuevas J, Roth AL & Berg DK (2000). Two distinct classes of functional 7-containing nicotinic receptor on rat superior cervical ganglion neurons. *J Physiol* **525 Pt 3,** 735–746.

Curtis HJ & Cole KS (1938). Transverse electric impedance of the squid giant axon. *J Gen Physiol* **21,** 757–765.

Dalbey R & von Heijne G (2002). *Protein targeting, transport, and translocation*. Elsevier.

Dale HH & Dudley HW (1929). The presence of histamine and acetylcholine in the spleen of the ox and the horse. *J Physiol* **68,** 97–123.

Dale HH, Feldberg W & Vogt M (1936). Release of acetylcholine at voluntary motor nerve endings. *J Physiol* **86,** 353–380.

Damkjær M, Isaksson GL, Stubbe J, Jensen BL, Assersen K & Bie P (2013). Renal renin secretion as regulator of body fluid homeostasis. *Pflugers Arch Eur J Physiol* **465,** 153–165.

Dampney RAL (2016). Central neural control of the cardiovascular system: current perspectives. *Adv Physiol Educ* **40,** 283–296.

Dang S, Feng S, Tien J, Peters CJ, Bulkley D, Lolicato M, Zhao J, Zuberbühler K, Ye W, Qi L, Chen T, Craik CS, Jan YN, Minor DL, Cheng Y & Jan LY (2017). Cryo-EM structures of the TMEM16A calciumactivated chloride channel. *Nature* **552,** 426–429.

Davis H, Bardsley EN & Paterson DJ (2018). Data Descriptor: Transcriptional profiling of stellate ganglia from normotensive and spontaneously hypertensive rat strains. *Sci Data*; DOI: 10.1038/sdata.2018.123.

Davis H, Herring N & Paterson DJ (2020). Downregulation of M Current Is Coupled to Membrane Excitability in Sympathetic Neurons before the Onset of Hypertension. *Hypertension* **76,** 1915–1923.

Davletov BA & Südhof TC (1993). A single C2 domain from synaptotagmin I is sufficient for high affinity Ca2+/phospholipid binding. *J Biol Chem* **268,** 26386–26390.

Delmas P, Abogadie FC, Milligan G, Buckley NJ & Brown DA (1999). betagamma dimers derived from Go and Gi proteins contribute different components of adrenergic inhibition of Ca2+ channels in rat sympathetic neurones. *J Physiol* **518,** 23–36.

Deng Y & Rapp JP (1992). Cosegregation of blood pressure with angiotensin converting enzyme and atrial natriuretic peptide receptor genes using Dahl salt–sensitive rats. *Nat Genet* **1,** 267–272.

Deng LY & Schiffrin EL (1992). Effects of endothelin on resistance arteries of DOCA-salt hypertensive rats. *Am J Physiol - Hear Circ Physiol* **262,** H1782–H1787.

Denton D, Weisinger R, Mundy NI, Wickings EJ, Dixson A, Moisson P, Pingard AM, Shade R, Carey D, Ardaillou R, Paillard F, Chapman J, Thillet J & Baptiste Michel J (1995). The effect of increased salt intake on blood pressure of chimpanzees. *Nat Med* **1,** 1009–1016.

Desai NS, Gray R & Johnston D (2017). A Dynamic Clamp on Every Rig. *eNeuro* **4,** ENEURO.0250-17.2017.

Desjardins P & Conklin D (2010). NanoDrop microvolume quantitation of nucleic acids. *J Vis Exp*2565.

Devereux RB, Palmieri V, Liu JE, Wachtell K, Bella JN, Boman K, Gerdts E, Nieminen MS, Papademetriou V & Dahlöf B (2002). Progressive hypertrophy regression with sustained pressure reduction in hypertension: the Losartan Intervention For Endpoint Reduction study. *J Hypertens* **20,** 1445–1450.

Devor DC, Singh AK, Frizzell RA & Bridges RJ (1996). Modulation of Cl- secretion by benzimidazolones. I. Direct activation of a Ca2+-dependent K+ channel. *Am J Physiol - Lung Cell Mol Physiol* **271,** L775–L784.

Dias da Silva VJ, Gnecchi-Ruscone T, Bellina V, Oliveira M, Maciel L, Campos de Carvalho AC, Cesar Salgado H, Bergamaschi CM, Tobaldini E & Porta A (2012). Acute adenosine increases cardiac vagal and reduces sympathetic efferent nerve activities in rats. *Exp Physiol* **97,** 719–729.

DiBona GF & Jones SY (1991). Renal manifestations of NaCl sensitivity in borderline hypertensive rats. *Hypertension* **17,** 44–53.

Dickhout JG & Lee RMKW (1998). Blood pressure and heart rate development in young spontaneously hypertensive rats. *Am J Physiol - Hear Circ Physiol* **274,** H794–H800.

Difrancesco D (1986). Characterization of single pacemaker channels in cardiac sino-atrial node cells. *Nature* **324,** 470–473.

DiFrancesco D (2005). Letter regarding article by Michels et al, “Single-channel properties support a potential contribution of hyperpolarization-activated cyclic nucleotide-gated channels and If to cardiac arrhythmias”. *Circulation* **112,** 399–404.

DiFrancesco D & Tortora P (1991). Direct activation of cardiac pacemaker channels by intracellular cyclic AMP. *Nature* **351,** 145–147.

Do DH, Bradfield J, Ajijola OA, Vaseghi M, Le J, Rahman S, Mahajan A, Nogami A, Boyle NG & Shivkumar K (2017). Thoracic Epidural Anesthesia Can Be Effective for the Short-Term Management of Ventricular Tachycardia Storm. *J Am Heart Assoc* **6,** e007080.

Doak GJ & Sawynok J (1995). Complex role of peripheral adenosine in the genesis of the response to subcutaneous formalin in the rat. *Eur J Pharmacol* **281,** 311–318.

Dobin A, Davis CA, Schlesinger F, Drenkow J, Zaleski C, Jha S, Batut P, Chaisson M & Gingeras TR (2013). STAR: Ultrafast universal RNA-seq aligner. *Bioinformatics* **29,** 15–21.

Dodge Jr FA & Rahamimoff R (1967). Co-operative action a calcium ions in transmitter release at the neuromuscular junction. *J Physiol* **193,** 419–432.

Dohlman HG, Caron MG & Lefkowitz RJ (1987). A family of receptors coupled to guanine nucleotide regulatory proteins. *Biochemistry* **26,** 2657–2664.

Dolphin AC (2016). Voltage-gated calcium channels and their auxiliary subunits: physiology and pathophysiology and pharmacology. *J Physiol* **594,** 5369–5390.

Dominiak P & Grobecker H (1982). Elevated plasma catecholamines in young hypertensive and hyperkinetic patients: effect of pindolol. *Br J Clin Pharmacol* **13,** 381S-390S.

Doyle DA, Cabral JM, Pfuetzner RA, Kuo A, Gulbis JM, Cohen SL, Chait BT & MacKinnon R (1998). The Structure of the Potassium Channel: Molecular Basis of K<sup>+</sup> Conduction and Selectivity. *Science (80- )* **280,** 69 LP – 77.

Dryer SE (1991). Na(+)-activated K+ channels and voltage-evoked ionic currents in brain stem and parasympathetic neurones of the chick. *J Physiol* **435,** 513–532.

Du J, Ma X, Shen B, Huang Y, Birnbaumer L & Yao X (2014). TRPV4, TRPC1, and TRPP2 assemble to form a flow-sensitive heteromeric channel. *FASEB J* **28,** 4677–4685.

Du Y, Huang Q, Arisdakessian C & Garmire LX (2020). Evaluation of STAR and kallisto on single cell RNA-seq data alignment. *G3 Genes, Genomes, Genet* **10,** 1775–1783.

Dulubova I, Khvotchev M, Liu S, Huryeva I, Südhof TC & Rizo J (2007). Munc18-1 binds directly to the neuronal SNARE complex. *Proc Natl Acad Sci U S A* **104,** 2697–2702.

e Silva LFS, Brito MD, Yuzawa JMC & Rosenstock TR (2019). Mitochondrial Dysfunction and Changes in High-Energy Compounds in Different Cellular Models Associated to Hypoxia: Implication to Schizophrenia. *Sci Rep* **9,** 18049.

Edvinsson L, Hara H & Uddman R (1989). Retrograde tracing of nerve fibers to the rat middle cerebral artery with true blue: colocalization with different peptides. *J Cereb Blood Flow Metab* **9,** 212–218.

Edward Hickman F, Stanley EM & Carter BD (2018). Neurotrophin responsiveness of sympathetic neurons is regulated by rapid mobilization of the p75 receptor to the cell surface through trka activation of arf6. *J Neurosci* **38,** 5606–5619.

Eguchi Y, Shimizu S & Tsujimoto Y (1997). Intracellular ATP levels determine cell death fate by apoptosis or necrosis. *Cancer Res* **57,** 1835–1840.

Ehler E, Moore-Morris T & Lange S (2013). Isolation and culture of neonatal mouse cardiomyocytes. *J Vis Exp*50154.

Elinder F & Arhem P (1994). Effects of gadolinium on ion channels in the myelinated axon of Xenopus laevis: four sites of action. *Biophys J* **67,** 71–83.

Elliott P, Stamler J, Nichols R, Dyer AR, Stamler R, Kesteloot H & Marmot M (1996). Intersalt revisited: further analyses of 24 hour sodium excretion and blood pressure within and across populations. Intersalt Cooperative Research Group. *BMJ* **312,** 1249–1253.

Elliott TR (1905). The action of adrenalin. *J Physiol* **32,** 401–467.

Enyedi P & Czirják G (2010). Molecular Background of Leak K+ Currents: Two-Pore Domain Potassium Channels. *Physiol Rev* **90,** 559–605.

Erb L & Weisman GA (2012). Coupling of P2Y receptors to G proteins and other signaling pathways. *Wiley Interdiscip Rev Membr Transp Signal* **1,** 789–803.

Ernsberger U & Rohrer H (2018). Sympathetic tales: Subdivisons of the autonomic nervous system

and the impact of developmental studies. *Neural Dev* **13,** 20.

Esler M, Jennings G, Biviano B, Lambert G & Hasking G (1986). Mechanism of elevated plasma noradrenaline in the course of essential hypertension. *J Cardiovasc Pharmacol* **8,** S39–S43.

Esler MD et al. (2010*a*). Renal sympathetic denervation in patients with treatment-resistant hypertension (The Symplicity HTN-2 Trial): A randomised controlled trial. *Lancet* **376,** 1903–1909.

Esler MD et al. (2010*b*). Renal sympathetic denervation in patients with treatment-resistant hypertension (The Symplicity HTN-2 Trial): A randomised controlled trial. *Lancet* **376,** 1903–1909.

Esler MD, Krum H, Schlaich M, Schmieder RE, Böhm M & Sobotka PA (2012). Renal sympathetic denervation for treatment of drug-resistant hypertension: one-year results from the Symplicity HTN-2 randomized, controlled trial. *Circulation* **126,** 2976–2982.

Esunge PM (1991). From blood pressure to hypertension: The history of research. *J R Soc Med* **84,** 621.

Etxeberria A, Aivar P, Rodriguez-Alfaro JA, Alaimo A, Villace P, Gomez-Posada JC, Areso P & Villarroel A (2008). Calmodulin regulates the trafficking of KCNQ2 potassium channels. *FASEB J* **22,** 1135–1143.

Euler US von & Hillarp N-Å (1956). Evidence for the Presence of Noradrenaline in Submicroscopic Structures of Adrenergic Axons. *Nature* **177,** 44–45.

Evangelou E et al. (2018). Genetic analysis of over 1 million people identifies 535 new loci associated with blood pressure traits. *Nat Genet* **50,** 1412–1425.

Evans JA & Bartels CC (1949). Results of high dorsolumbar sympathectomy for hypertension. *Ann Intern Med* **30,** 307–329.

Evilsizor MN, Ray-Jones HF, Lifshitz J & Ziebell J (2015). Primer for immunohistochemistry on cryosectioned rat brain tissue: Example staining for microglia and neurons. *J Vis Exp* **2015,** e52293.

Fan J-S & Palade P (1998). Perforated Patch Recording with β-escin. *Pflügers Arch* **436,** 1021–1023.

Fares A (2013). Winter Hypertension: Potential mechanisms. *Int J Health Sci (Qassim)* **7,** 210–219.

Farquhar WB, Wenner MM, Delaney EP, Prettyman A V. & Stillabower ME (2006). Sympathetic neural responses to increased osmolality in humans. *Am J Physiol - Hear Circ Physiol* **291,** H2181–H2186.

Feldberg W & Gaddum JH (1934). The chemical transmitter at synapses in a sympathetic ganglion. *J Physiol* **81,** 305.

De Felice LJ (2016). Chloride requirement for monoamine transporters. *Pflugers Arch Eur J Physiol* **468,** 503–511.

Fenwick EM, Marty A & Neher E (1982). A patch-clamp study of bovine chromaffin cells and of their sensitivity to acetylcholine. *J Physiol* **331,** 577–597.

Fernandez-Chacon R, Königstorfer A, Gerber SH, García J, Matos MF, Stevens CF, Brose N, Rizo J, Rosenmund C & Südhof TC (2001). Synaptotagmin I functions as a calcium regulator of release probability. *Nature* **410,** 41–49.

Fernández JM, Bezanilla F & Taylor RE (1982). Distribution and kinetics of membrane dielectric polarization. II. Frequency domain studies of gating currents. *J Gen Physiol* **79,** 41–67.

Fernandez SM & Berlin RD (1976). Cell surface distribution of lectin receptors determined by resonance energy transfer. *Nature* **264,** 411–415.

Fernandez SF, Huang MH, Davidson BA, Knight PR & Izzo JL (2003). Modulation of Angiotensin II Responses in Sympathetic Neurons by Cytosolic Calcium. *Hypertension* **41,** 56–63.

Ferron GM, Paul J, Fruncillo R, Richards L, Knebel N, Getsy J & Troy S (2002). Multiple-dose, linear, dose-proportional pharmacokinetics of retigabine in healthy volunteers. *J Clin Pharmacol* **42,** 175–182.

Field JL & Newberry NR (1991). On the histamine-induced depolarization of the isolated superior cervical ganglion of the rat. *Br J Pharmacol* **103,** 1752–1756.

Figler RA, Graber SG, Lindorfer MA, Yasuda H, Linden J & Garrison JC (1996). Reconstitution of recombinant bovine A1 adenosine receptors in Sf9 cell membranes with recombinant G proteins of defined composition. *Mol Pharmacol* **50,** 1587–1595.

Filippov AK, Choi RCY, Simon J, Barnard EA & Brown DA (2006). Activation of P2Y1 nucleotide receptors induces inhibition of the M-type K+ current in rat hippocampal pyramidal neurons. *J Neurosci* **26,** 9340–9348.

Filippov AK, Webb TE, Barnard EA & Brown DA (1999). Dual coupling of heterologously-expressed rat P2Y6 nucleotide receptors to N-type Ca2+ and M-type K+ currents in rat sympathetic neurones. *Br J Pharmacol* **126,** 1009–1017.

Finak G, McDavid A, Yajima M, Deng J, Gersuk V, Shalek AK, Slichter CK, Miller HW, McElrath MJ, Prlic M, Linsley PS & Gottardo R (2015). MAST: A flexible statistical framework for assessing transcriptional changes and characterizing heterogeneity in single-cell RNA sequencing data. *Genome Biol* **16,** 278.

Fink GD, Haywood JR, Bryan WJ, Packwood W & Brody MJ (1980). Central site for pressor action of blood-borne angiotensin in rat. *Am J Physiol Integr Comp Physiol* **239,** R358–R361.

Fischer G (1982). Cultivation of mouse cerebellar cells in serum free, hormonally defined media: Survival of neurons. *Neurosci Lett* **28,** 325–329.

Flaa A, Mundal HH, Eide I, Kjeldsen S & Rostrup M (2006). Sympathetic activity and cardiovascular risk factors in young men in the low, normal, and high blood pressure ranges. *Hypertension* **47,** 396–402.

Flack M (1910). An investigation of the sino-auricular node of the mammalian heart. *J Physiol* **41,** 64.

Flacke W & Gillis RA (1968). IMPULSE TRANSMISSION VIA NICOTINIC AND MUSCARINIC PATHWAYS IN THE STELLATE GANGLION OF THE DOG. *J Pharmacol Exp Ther* **163,** 266 LP – 276.

Floras JS, Jones JV, Osman Hassan M & Sleight P (1988). Effects of acute and chronic β-adrenoceptor blockade on baroreflex sensitivity in humans. *J Auton Nerv Syst* **25,** 87–94.

Flynn TG, Mercedes L & Adolfo J (1983). The amino acid sequence of an atrial peptide with potent diuretic and natriuretic properties. *Biochem Biophys Res Commun* **117,** 859–865.

Foehring RC, Zhang XF, Lee JCF & Callaway JC (2009). Endogenous calcium buffering capacity of substantia nigral dopamine neurons. *J Neurophysiol* **102,** 2326–2333.

Förster T (1948). Zwischenmolekulare energiewanderung und fluoreszenz. *Ann Phys* **437,** 55–75.

Forsythe ID & Westbrook GL (1988). Slow excitatory postsynaptic currents mediated by N-methyl-D-aspartate receptors on cultured mouse central neurones. *J Physiol* **396,** 515–533.

Forte JG, Miguel JM, Miguel MJ, De Padua F & Rose G (1989). Salt and blood pressure: a community trial. *J Hum Hypertens* **3,** 179–184.

Frame AA, Carmichael CY & Wainford RD (2016). Renal Afferents. *Curr Hypertens Rep* **18,** 69.

Freedman DA & Petitti DB (2001). Salt and blood pressure: Conventional wisdom reconsidered. *Eval Rev* **25,** 267–287.

Fregly MJ (1954). Effects of extremes of temperature on hypertensive rats. *Am J Physiol* **176,** 275–281.

Freidin MM (2001). Antibody to the extracellular domain of the low affinity NGF receptor stimulates p75NGFR-mediated apoptosis in cultured sympathetic neurons. *J Neurosci Res* **64,** 331–340.

Fretwell L V. & Woolard J (2013). Cardiovascular responses to retigabine in conscious rats - Under normotensive and hypertensive conditions. *Br J Pharmacol* **169,** 1279–1289.

Fricke TC, Echtermeyer F, Zielke J, de la Roche J, Filipovic MR, Claverol S, Herzog C, Tominaga M, Pumroy RA, Moiseenkova-Bell VY, Zygmunt PM, Leffler A & Eberhardt MJ (2019). Oxidation of methionine residues activates the high-threshold heat-sensitive ion channel TRPV2. *Proc Natl Acad Sci U S A* **116,** 24359–24365.

Frithiof R, Xing T, McKinley MJ, May CN & Ramchandra R (2014). Intracarotid hypertonic sodium chloride differentially modulates sympathetic nerve activity to the heart and kidney. *Am J Physiol - Regul Integr Comp Physiol* **306,** R567–R575.

Fuchs FD & Whelton PK (2020). High Blood Pressure and Cardiovascular Disease. *Hypertension* **75,** 285–292.

Fukuoka T, Kobayashi K, Yamanaka H, Obata K, Dai Y & Noguchi K (2008). Comparative study of the distribution of the α-subunits of voltage-gated sodium channels in normal and axotomized rat dorsal root ganglion neurons. *J Comp Neurol* **510,** 188–206.

Fuller BC, Sumner AD, Kutzler MA & Ruiz-Velasco V (2004*a*). A novel approach employing ultrasound guidance for percutaneous cardiac muscle injection to retrograde label rat stellate ganglion neurons. *Neurosci Lett* **363,** 252–256.

Fuller BC, Sumner AD, Kutzler MA & Ruiz-Velasco V (2004*b*). A novel approach employing ultrasound guidance for percutaneous cardiac muscle injection to retrograde label rat stellate ganglion neurons. *Neurosci Lett* **363,** 252–256.

Furberg C, Wright JT, Davis BR, Cutler JA, Alderman M & Black H (2002). The ALLHAT Officers and Coordinators for the ALLHAT Collaborative Research Group, et al. Major outcomes in high-risk hypertensive patients randomized to angiotensinconverting enzyme inhibitor or calcium channel blocker vs diuretic. The antihypertensive an. *JAMA* **288,** 2981–2997.

Furlan A, La Manno G, Lübke M, Häring M, Abdo H, Hochgerner H, Kupari J, Usoskin D, Airaksinen MS, Oliver G, Linnarsson S & Ernfors P (2016). Visceral motor neuron diversity delineates a cellular basis for nipple- and pilo-erection muscle control. *Nat Neurosci* **19,** 1331–1340.

Furuhashi M, Moniwa N, Mita T, Fuseya T, Ishimura S, Ohno K, Shibata S, Tanaka M, Watanabe Y, Akasaka H, Ohnishi H, Yoshida H, Takizawa H, Saitoh S, Ura N, Shimamoto K & Miura T

(2015). Urinary Angiotensin-Converting Enzyme 2 in Hypertensive Patients May Be Increased by Olmesartan, an Angiotensin II Receptor Blocker. *Am J Hypertens* **28,** 15–21.

Gada K & Plant LD (2019). Two-pore domain potassium channels: emerging targets for novel analgesic drugs: IUPHAR Review 26. *Br J Pharmacol* **176,** 256–266.

Galis ZS, Thrasher T, Reid DM, Stanley D V & Oh YS (2013). Investing in high blood pressure research: a national institutes of health perspective. *Hypertens (Dallas, Tex 1979)* **61,** 757–761.

Gamba G (2012). Regulation of the renal Na+-Cl- cotransporter by phosphorylation and ubiquitylation. *Am J Physiol - Ren Physiol* **303,** F1573–F1583.

Gamper N & Shapiro MS (2003). Calmodulin Mediates Ca 2+ -dependent Modulation of M-type K + Channels. *J Gen Physiol* **122,** 17–31.

Gamper N, Li Y & Shapiro MS (2005). Structural requirements for differential sensitivity of KCNQ K+ channels to modulation by Ca2+/calmodulin. *Mol Biol Cell* **16,** 3538–3551.

Garcia-Estañ J, Carbonell LF, Garcia-Salom M, Salazar FJ & Quesada T (1989). Hemodynamic effects of hypertonic saline in the conscious rat. *Life Sci* **44,** 1343–1350.

Garcia-Sevilla JA, Dubocovich ML & Langer SZ (1979). Angiotensin II facilitates the potassium-evoked release of 3H-noradrenaline from the rabbit hypothalamus. *Eur J Pharmacol* **56,** 173–176.

Garrett S & Rosenthal JJC (2012). RNA editing underlies temperature adaptation in K+ channels from polar octopuses. *Science* **335,** 848–851.

Garza A, López-Ramírez O, Vega R & Soto E (2010). The aminoglycosides modulate the acid-sensing ionic channel currents in dorsal root ganglion neurons from the rat. *J Pharmacol Exp Ther* **332,** 489–499.

Gattone VH (1986). Body Weight of the Spontaneously Hypertensive Rat during the Suckling and Weanling Periods. *Jpn Heart J* **27,** 881–884.

Gattone VH, Marfurt CF & Dallie S (1986). Extrinsic innervation of the rat kidney: a retrograde tracing study. *Am J Physiol Physiol* **250,** F189–F196.

Gaudet AD, Williams SJ, Hwi LPR & Ramer MS (2004). Regulation of TRPV2 by axotomy in sympathetic, but not sensory neurons. *Brain Res* **1017,** 155–162.

Gayet-Primo J, Yaeger DB, Khanjian RA & Puthussery T (2018). Heteromeric K<sub>V</sub>2/K<sub>V</sub>8.2 Channels Mediate Delayed Rectifier Potassium Currents in Primate Photoreceptors. *J Neurosci* **38,** 3414 LP – 3427.

Geiger JRP & Jonas P (2000). Dynamic Control of Presynaptic Ca2+ Inflow by Fast-Inactivating K+ Channels in Hippocampal Mossy Fiber Boutons. *Neuron* **28,** 927–939.

Gentet LJ, Stuart GJ & Clements JD (2000). Direct Measurement of Specific Membrane Capacitance in Neurons. *Biophys J* **79,** 314–320.

George AL, Knittle TJ & Tamkun MM (1992). Molecular cloning of an atypical voltage-gated sodium channel expressed in human heart and uterus: evidence for a distinct gene family. *Proc Natl Acad Sci* **89,** 4893–4897.

George MS, Abbott LF & Siegelbaum SA (2009). HCN hyperpolarization-activated cation channels inhibit EPSPs by interactions with M-type K+ channels. *Nat Neurosci* **12,** 577.

Geppert M, Goda Y, Hammer RE, Li C, Rosahl TW, Stevens CF & Südhof TC (1994). Synaptotagmin I: A major $Ca^{2+}$ sensor for transmitter release at a central synapse. *Cell* **79,** 717–727.

Gershon MD (1967). Effects of tetrodotoxin on innervated smooth muscle preparations. *Br J Pharmacol Chemother* **29,** 259.

Gerzer R, Witzgall H, Tremblay J, Gutkowska J & Hamet P (1985). Rapid increase in plasma and urinary cyclic gmp after bolus injection of atrial natriuretic factor in man. *J Clin Endocrinol Metab* **61,** 1217–1219.

Gianfranco P, Carmela B, Michele D, Elvira S, R. MM, Mauro C & Vincenzo M (1996). Heart Rate and Blood Pressure Variabilities in Salt-Sensitive Hypertension. *Hypertension* **28,** 944–952.

Glasgow NG, Siegler Retchless B & Johnson JW (2015). Molecular bases of NMDA receptor subtype-dependent properties. *J Physiol* **593,** 83–95.

Go AS et al. (2013). Executive summary: Heart disease and stroke statistics-2013 update: A Report from the American Heart Association. *Circulation* **127,** 143–152.

Go AS, Hylek EM, Phillips KA, Chang Y, Henault LE, Selby J V & Singer DE (2001). Prevalence of Diagnosed Atrial Fibrillation in AdultsNational Implications for Rhythm Management and Stroke Prevention: the AnTicoagulation and Risk Factors In Atrial Fibrillation (ATRIA) Study. *JAMA* **285,** 2370–2375.

Golias C, Charalabopoulos A, Stagikas D, Charalabopoulos K & Batistatou A (2007). The kinin system--bradykinin: biological effects and clinical implications. Multiple role of the kinin system--bradykinin. *Hippokratia* **11,** 124–128.

Gomes PM, Sá RWM, Aguiar GL, Paes MHS, Alzamora AC, Lima WG, De Oliveira LB, Stocker SD, Antunes VR & Cardoso LM (2017). Chronic high-sodium diet intake after weaning lead to neurogenic hypertension in adult Wistar rats. *Sci Rep* **7,** 5655.

Gomez-Ospina N & Dolmetsch R (2008). L-type Channel Regulation of Gene Expression BT - Transcriptional Regulation by Neuronal Activity: To the Nucleus and Back. In, ed. Dudek SM, pp. 111–123. Springer US, Boston, MA. Available at: https://doi.org/10.1007/978-0-387-73609-9_6.

Gordon FJ & Mark AL (1984). Mechanism of impaired baroreflex control in prehypertensive Dahl salt-sensitive rats. *Circ Res* **54,** 378–387.

Gordon RD, Küchel O, Liddle GW & Island DP (1967). Role of the sympathetic nervous system in regulating renin and aldosterone production in man. *J Clin Invest* **46,** 599–605.

Graham RM, Perez PM, Hwa John & Piascik TM (1996). α1-Adrenergic Receptor Subtypes. *Circ Res* **78,** 737–749.

Graham LN, Smith PA, Stoker JB, Mackintosh AF & Mary DASG (2002). Time course of sympathetic neural hyperactivity after uncomplicated acute myocardial infarction. *Circulation* **106,** 793–797.

Granger JP, Alexander BT & Llinas M (2002). Mechanisms of pressure natriuresis. *Curr Hypertens Rep* **4,** 152–159.

Grant AO (2009). Cardiac ion channels. *Circ Arrhythmia Electrophysiol* **2,** 185–194.

Grassi G (2009). Assessment of sympathetic cardiovascular drive in human hypertension: Achievements and perspectives. *Hypertension* **54,** 690–697.

Grassi G, Cattaneo BM, Seravalle G, Lanfranchi A & Mancia G (1998). Baroreflex control of sympathetic nerve activity in essential and secondary hypertension. *Hypertension* **31,** 68–72.

Green SA, Holt BD & Liggett SB (1992). Beta 1-and beta 2-adrenergic receptors display subtype-selective coupling to Gs. *Mol Pharmacol* **41,** 889–893.

Greenwood JP, Stoker JB & Mary DASG (1999). Single-unit sympathetic discharge: Quantitative assessment in human hypertensive disease. *Circulation* **100,** 1305–1310.

Griffin KA, Churchill PC, Picken M, Webb RC, Kurtz TW & Bidani AK (2001). Differential salt-sensitivity in the pathogenesis of renal damage in SHR and stroke prone SHR*. *Am J Hypertens* **14,** 311–320.

Grynkiewicz G, Poenie M & Tsien RY (1985). A new generation of Ca2+ indicators with greatly improved fluorescence properties. *J Biol Chem* **260,** 3440–3450.

Guido G, M. CB, Gino S, Antonio L, Massimo P, Alberto M, Stefano C & Giuseppe M (1997). Effects of Chronic ACE Inhibition on Sympathetic Nerve Traffic and Baroreflex Control of Circulation in Heart Failure. *Circulation* **96,** 1173–1179.

Guild SJ, McBryde FD, Malpas SC & Barrett CJ (2012). High dietary salt and angiotensin II chronically increase renal sympathetic nerve activity: A direct telemetric study. *Hypertension* **59,** 614–620.

Guy HR & Seetharamulu P (1986). Molecular model of the action potential sodium channel. *Proc Natl Acad Sci U S A* **83,** 508–512.

Guyenet PG (2006). The sympathetic control of blood pressure. *Nat Rev Neurosci* **7,** 335–346.

Guyenet PG (2019). Sodium Is Detected by the OVLT to Regulate Sympathetic Tone. *Neuron* **101,** 3–5.

Guyenet PG, Stornetta RL, Souza GMPR, Abbott SBG & Brooks VL (2020). Neuronal Networks in Hypertension: Recent Advances. *Hypertension* **0,** 300–311.

Haas E & Goldblatt H (1960). Effects of various ganglionic blocking agents on blood pressure and on activity of pressor agents. *Am J Physiol Content* **198,** 1023–1028.

Habecker BA, Grygielko ET, Huhtala TA, Foote B & Brooks VL (2003). Ganglionic tyrosine hydroxylase and norepinephrine transporter are decreased by increased sodium chloride in vivo and in vitro. *Auton Neurosci* **107,** 85–98.

Habermeier-Muth A & Muscholl E (1988). Short- and long-latency muscarinic inhibition of noradrenaline release from rabbit atria induced by vagal stimulation. *J Physiol* **401,** 277–293.

Habib AM, Wood JN & Cox JJ (2015). Sodium channels and pain. In *Handbook of Experimental Pharmacology*, ed. Schaible H-G, pp. 39–56. Springer Berlin Heidelberg, Berlin, Heidelberg. Available at: https://doi.org/10.1007/978-3-662-46450-2_3.

Hadley JK, Passmore GM, Tatulian L, Al-Qatari M, Ye F, Wickenden AD & Brown DA (2003). Stoichiometry of expressed KCNQ2/KCNQ3 potassium channels and subunit composition of native ganglionic M channels deduced from block by tetraethylammonium. *J Neurosci* **23,** 5012–5019.

Hafemeister C & Satija R (2019). Normalization and variance stabilization of single-cell RNA-seq data using regularized negative binomial regression. *Genome Biol* **20,** 296.

Hagiwara S, Kusano K & Saito N (1961). Membrane changes of Onchidium nerve cell in potassium-

rich media. *J Physiol* **155,** 470–489.

Hagiwara S, Ozawa S & Sand O (1975). Voltage clamp analysis of two inward current mechanisms in the egg cell membrane of a starfish. *J Gen Physiol* **65,** 617–644.

Hall JE, Mizelle HL, Woods LL & Montani J-P (1988). Pressure natriuresis and control of arterial pressure during chronic norepinephrine infusion. *J Hypertens* **6,** 723–731.

Hall JM (1997). Bradykinin receptors. *Gen Pharmacol* **28,** 1–6.

Hallworth NE, Wilson CJ & Bevan MD (2004). Erratum: Apamin-Sensitive Small Conductance Calcium-Activated Potassium Channels, through their Selective Coupling to Voltage-Gated Calcium Channels, Are Critical Determinants of the Precision, Pace, and Pattern of Action Potential Generation in Rat Subth. *J Neurosci* **24,** 7525–7542.

Hamer DW & Santer RM (1981). Anatomy and blood supply of the coeliac-superior mesenteric ganglion complex of the rat. *Anat Embryol (Berl)* **162,** 353–362.

Hamill OP, Marty A, Neher E, Sakmann B & Sigworth FJ (1981). Improved patch-clamp techniques for high-resolution current recording from cells and cell-free membrane patches. *Pflügers Arch* **391,** 85–100.

Han H (2018). RNA interference to knock down gene expression. *Methods Mol Biol* **1706,** 293–302.

Hanani M (2010). Satellite glial cells in sympathetic and parasympathetic ganglia: In search of function. *Brain Res Rev* **64,** 304–327. Available at: https://www.sciencedirect.com/science/article/pii/S0165017310000524?via%3Dihub [Accessed April 30, 2018].

Hanemaaijer NAK, Popovic MA, Wilders X, Grasman S, Pavón Arocas O & Kole MHP (2020). Ca2+ entry through NaV channels generates submillisecond axonal Ca2+ signaling ed. Maduke M, Aldrich RW, Maduke M, Sabatini BL & Trimmer JS. *Elife* **9,** e54566.

Hanna P, Rajendran PS, Ajijola OA, Vaseghi M, Andrew Armour J, Ardell JL & Shivkumar K (2017). Cardiac neuroanatomy - Imaging nerves to define functional control. *Auton Neurosci* **207,** 48–58.

Hanson PI, Roth R, Morisaki H, Jahn R & Heuser JE (1997). Structure and Conformational Changes in NSF and Its Membrane Receptor Complexes Visualized by Quick-Freeze/Deep-Etch Electron Microscopy. *Cell* **90,** 523–535.

Hardie RC & Minke B (1992). The trp gene is essential for a light-activated $Ca^{2+}$ channel in Drosophila photoreceptors. *Neuron* **8,** 643–651.

Harding EK, Boivin B & Salter MW (2020). Intracellular Calcium Responses Encode Action Potential Firing in Spinal Cord Lamina I Neurons. *J Neurosci* **40,** 4439 LP – 4456.

Harrap SB, Van der Merwe WM, Griffin SA, Macpherson F & Lever AF (1990). Brief angiotensin converting enzyme inhibitor treatment in young spontaneously hypertensive rats reduces blood pressure long-term. *Hypertension* **16,** 603–614.

Harty BL & Monk KR (2017). Unwrapping the unappreciated: recent progress in Remak Schwann cell biology. *Curr Opin Neurobiol* **47,** 131–137.

Hata Y, Slaughter CA & Südhof TC (1993). Synaptic vesicle fusion complex contains unc-18 homologue bound to syntaxin. *Nature* **366,** 347–351.

Haynes W (2013*a*). Bonferroni Correction. In *Encyclopedia of Systems Biology*, ed. Dubitzky W, Wolkenhauer O, Cho K-H & Yokota H, pp. 154–154. Springer New York, New York, NY. Available at: https://doi.org/10.1007/978-1-4419-9863-7_1213.

Haynes W (2013*b*). Benjamini–Hochberg Method. In *Encyclopedia of Systems Biology*, ed. Dubitzky W, Wolkenhauer O, Cho K-H & Yokota H, pp. 78–78. Springer New York, New York, NY. Available at: https://doi.org/10.1007/978-1-4419-9863-7_1215.

He FJ, Li J & MacGregor GA (2013). Effect of longer term modest salt reduction on blood pressure: Cochrane systematic review and meta-analysis of randomised trials. *Bmj*.

Head GA (1994). CARDIAC BAROREFLEXES AND HYPERTENSION. *Clin Exp Pharmacol Physiol* **21,** 791–802.

Heathers JAJ (2014). Everything Hertz: methodological issues in short-term frequency-domain HRV . *Front Physiol* **5,** 177. Available at: https://www.frontiersin.org/article/10.3389/fphys.2014.00177.

Heaton DA, Lei M, Li D, Golding S, Dawson TA, Mohan RM & Paterson DJ (2006). Remodeling of the cardiac pacemaker L-type calcium current and its β-adrenergic responsiveness in hypertension after neuronal NO synthase gene transfer. *Hypertension* **48,** 443–452.

Hein L, Altman JD & Kobilka BK (1999). Two functionally distinct α2-adrenergic receptors regulate sympathetic neurotransmission. *Nature* **402,** 181–184.

Heller J, Hellerová S, Dobesková Z, Kunes J & Zicha J (1993). The Prague hypertensive rat: A new model of genetic hypertension. *Clin Exp Hypertens* **15,** 807–818.

Helton TD, Xu W & Lipscombe D (2005). Neuronal L-Type Calcium Channels Open Quickly and Are Inhibited Slowly. *J Neurosci* **25,** 10247 LP – 10251.

Hempstead BL, Martin-Zanca D, Kaplan DR, Parada LF & Chao M V (1991). High-affinity NGF binding requires coexpression of the trk proto-oncogene and the low-affinity NGF receptor. *Nature* **350,** 678–683.

Henry JP, Sagné C, Botton D, Isambert MF & Gasnier B (1997). Molecular Pharmacology of the Vesicular Monoamine Transporter. In, ed. Goldstein DS, Eisenhofer G & McCarty RBT-A in P, pp. 236–239. Academic Press. Available at: http://www.sciencedirect.com/science/article/pii/S105435890860736X.

Herring N (2015). Autonomic control of the heart: going beyond the classical neurotransmitters. *Exp Physiol* **100,** 354–358.

Herring N, Kalla M & Paterson DJ (2019). The autonomic nervous system and cardiac arrhythmias: current concepts and emerging therapies. *Nat Rev Cardiol*; DOI: 10.1038/s41569-019-0221-2.

Herring N & Paterson DJ (2018). *Levick's introduction to cardiovascular physiology*. CRC Press.

Herrington J et al. (2006). Blockers of the delayed-rectifier potassium current in pancreatic β-cells enhance glucose-dependent insulin secretion. *Diabetes* **55,** 1034–1042.

Hess P, Lansman JB & Tsien RW (1984). Different modes of Ca channel gating behaviour favoured by dihydropyridine Ca agonists and antagonists. *Nature* **311,** 538–544.

Hicks MJ, Shigekawa M & Katz AM (1979). Mechanism by which cyclic adenosine 3':5'-monophosphate-dependent protein kinase stimulates calcium transport in cardiac sarcoplasmic reticulum. *Circ Res* **44,** 384–391.

Higuchi R, Fockler C, Dollinger G & Watson R (1993). Kinetic PCR analysis: real-time monitoring of DNA amplification reactions. *Bio/technology* **11,** 1026–1030.

Hillman D, Chen S, Aung TT, Cherksey B, Sugimori M & Llinas RR (1991). Localization of P-type calcium channels in the central nervous system. *Proc Natl Acad Sci U S A* **88,** 7076–7080.

Hines ML & Carnevale NT (2001). NEURON: A tool for neuroscientists. *Neuroscientist* **7,** 123–135.

Hirooka Y (2011). Oxidative stress in the cardiovascular center has a pivotal role in the sympathetic activation in hypertension. *Hypertens Res* **34,** 407–412.

Hiyama TY, Watanabe E, Okado H & Noda M (2004). The subfornical organ is the primary locus of sodium-level sensing by Nax sodium channels for the control of salt-intake behavior. *J Neurosci* **24,** 9276–9281.

Hiyama TY, Watanabe E, Ono K, Inenaga K, Tamkun MM, Yoshida S & Noda M (2002). Nax channel involved in CNS sodium-level sensing. *Nat Neurosci* **5,** 511–512.

Hiyama TY, Yoshida M, Matsumoto M, Suzuki R, Matsuda T, Watanabe E & Noda M (2013). Endothelin-3 expression in the subfornical organ enhances the sensitivity of Nax, the brain sodium-level sensor, to suppress salt intake. *Cell Metab* **17,** 507–519.

Ho C & O'Leary ME (2011). Single-cell analysis of sodium channel expression in dorsal root ganglion neurons. *Mol Cell Neurosci* **46,** 159–166.

Hodgkin AL & Huxley AF (1952*a*). A quantitative description of membrane current and its application to conduction and excitation in nerve. *J Physiol* **117,** 500–544.

Hodgkin AL & Huxley AF (1952*b*). Currents carried by sodium and potassium ions through the membrane of the giant axon of Loligo. *J Physiol* **116,** 449–472.

Hodgkin AL & Huxley AF (1952*c*). The components of membrane conductance in the giant axon of Loligo. *J Physiol* **116,** 473–496.

Hodgkin AL & Huxley AF (1952*d*). Propagation of electrical signals along giant nerve fibres. *Proc R Soc London Ser B-Biological Sci* **140,** 177–183.

Hodgkin AL & Katz B (1949). The effect of sodium ions on the electrical activity of the giant axon of the squid. *J Physiol* **108,** 37–77.

Hoffman JA, Papas BN, Trotter KW & Archer TK (2020). Single-cell RNA sequencing reveals a heterogeneous response to Glucocorticoids in breast cancer cells. *Commun Biol* **3,** 126.

Hofmann T, Schaefer M, Schultz G & Gudermann T (2002). Subunit composition of mammalian transient receptor potential channels in living cells. *Proc Natl Acad Sci U S A* **99,** 7461–7466.

Hofmann T, Schäfer S, Linseisen M, Sytik L, Gudermann T & Chubanov V (2014). Activation of TRPM7 channels by small molecules under physiological conditions. *Pflügers Arch - Eur J Physiol* **466,** 2177–2189.

Holland PM, Abramson RD, Watson R & Gelfand DH (1991). Detection of specific polymerase chain reaction product by utilizing the 5'----3'exonuclease activity of Thermus aquaticus DNA polymerase. *Proc Natl Acad Sci* **88,** 7276–7280.

Hollenberg NK (2003). Nephron number in patients with primary hypertension. *Curr Hypertens Rep* **5,** 285–286.

Holzer P & Izzo AA (2014). The pharmacology of TRP channels. *Br J Pharmacol* **171,** 2469–2473.

Hoopengardner B, Bhalla T, Staber C & Reenan R (2003). Nervous System Targets of RNA Editing Identified by Comparative Genomics. *Science (80- )* **301,** 832 LP – 836.

Horn R & Marty A (1988). Muscarinic activation of ionic currents measured by a new whole-cell recording method. *J Gen Physiol* **92,** 145–159.

Hotelling H (1933). Analysis of a complex of statistical variables into principal components. *J Educ Psychol* **24,** 417.

Houseley J & Tollervey D (2009). The Many Pathways of RNA Degradation. *Cell* **136,** 763–776.

Howe PRC, Rogers PF & Minson JB (1990). Dietary sodium loading elevates blood pressure in baroreceptor denervated rats. *J Auton Nerv Syst* **29,** 151–156.

Hu HZ, Gu Q, Wang C, Colton CK, Tang J, Kinoshita-Kawada M, Lee LY, Wood JD & Zhu MX (2004). 2-Aminoethoxydiphenyl borate is a common activator of TRPV1, TRPV2, and TRPV3. *J Biol Chem* **279,** 35741–35748.

Hu W & Bean BP (2018). Differential Control of Axonal and Somatic Resting Potential by Voltage-Dependent Conductances in Cortical Layer 5 Pyramidal Neurons. *Neuron* **97,** 1315-1326.e3.

Huang Z, Lujan R, Kadurin I, Uebele VN, Renger JJ, Dolphin AC & Shah MM (2011). Presynaptic HCN1 channels regulate Cav3.2 activity and neurotransmission at select cortical synapses. *Nat Neurosci* **14,** 478–486.

Huang WC, Xiao S, Huang F, Harfe BD, Jan YN & Jan LY (2012). Calcium-Activated Chloride Channels (CaCCs) Regulate Action Potential and Synaptic Response in Hippocampal Neurons. *Neuron* **74,** 179–192.

Huettner JE (1990). Glutamate receptor channels in rat DRG neurons: Activation by kainate and quisqualate and blockade of desensitization by con A. *Neuron* **5,** 255–266.

Hugel S & Schlichter R (2000). Presynaptic P2X Receptors Facilitate Inhibitory GABAergic Transmission between Cultured Rat Spinal Cord Dorsal Horn Neurons. *J Neurosci* **20,** 2121 LP – 2130.

Huidobro-Toro PJ & Donoso MV (2004). Sympathetic co-transmission: the coordinated action of ATP and noradrenaline and their modulation by neuropeptide Y in human vascular neuroeffector junctions. *Eur J Pharmacol* **500,** 27–35.

Humphries ESA & Dart C (2015). Neuronal and Cardiovascular Potassium Channels as Therapeutic Drug Targets: Promise and Pitfalls. *J Biomol Screen* **20,** 1055–1073.

Hutter OF & Noble D (1960). Rectifying properties of heart muscle. *Nature* **188,** 495.

van Huysse JW, Dostanic I, Lingrel JB, Hou X & Wu H (2011). Hypertension from chronic central sodium chloride in mice is mediated by the ouabain-binding site on the Na, K-ATPase α 2-isoform. *Am J Physiol - Hear Circ Physiol* **301,** H2147–H2153.

Iacobucci GJ & Popescu GK (2017). NMDA receptors: Linking physiological output to biophysical operation. *Nat Rev Neurosci* **18,** 236–249.

Ihara Y, Kihara Y, Hamano F, Yanagida K, Morishita Y, Kunita A, Yamori T, Fukayama M, Aburatani H, Shimizu T & Ishii S (2010). The G protein-coupled receptor T-cell death-associated gene 8 (TDAG8) facilitates tumor development by serving as an extracellular pH sensor. *Proc Natl Acad Sci U S A* **107,** 17309–17314.

Ikeda SR (1992). Prostaglandin modulation of Ca2+ channels in rat sympathetic neurones is

mediated by guanine nucleotide binding proteins. *J Physiol* **458,** 339–359.

Ikeda SR, Lovinger DM, McCool BA & Lewis DL (1995). Heterologous expression of metabotropic glutamate receptors in adult rat sympathetic neurons: Subtype-specific coupling to ion channels. *Neuron* **14,** 1029–1038.

Ilicic T, Kim JK, Kolodziejczyk AA, Bagger FO, McCarthy DJ, Marioni JC & Teichmann SA (2016). Classification of low quality cells from single-cell RNA-seq data. *Genome Biol* **17,** 29.

Irie T, Yamakawa K, Hamon D, Nakamura K, Shivkumar K & Vaseghi M (2017). Cardiac sympathetic innervation via middle cervical and stellate ganglia and antiarrhythmic mechanism of bilateral stellectomy. *Am J Physiol Heart Circ Physiol* **312,** H392–H405.

Isacoff EY, Jan YN & Jan LY (1990). Evidence for the formation of heteromultimeric potassium channels in Xenopus oocytes. *Nature* **345,** 530–534.

Isaksson GL, Stubbe J, Lyngs Hansen P, Jensen BL & Bie P (2014). Salt sensitivity of renin secretion, glomerular filtration rate and blood pressure in conscious Sprague-Dawley rats. *Acta Physiol* **210,** 446–454.

Ishibashi H, Moorhouse AJ & Nabekura J (2012). Perforated Whole-Cell Patch-Clamp Technique: A User's Guide BT - Patch Clamp Techniques: From Beginning to Advanced Protocols. In, ed. Okada Y, pp. 71–83. Springer Japan, Tokyo. Available at: https://doi.org/10.1007/978-4-431-53993-3_4.

Ishii TM, Silvia C, Hirschberg B, Bond CT, Adelman JP & Maylie J (1997). A human intermediate conductance calcium-activated potassium channel. *Proc Natl Acad Sci U S A* **94,** 11651–11656.

Ishii TM, Takano M & Ohmori H (2001). Determinants of activation kinetics in mammalian hyperpolarization-activated cation channels. *J Physiol* **537,** 93–100.

Itri JN, Michel S, Vansteensel MJ, Meijer JH & Colwell CS (2005). Fast delayed rectifier potassium current is required for circadian neural activity. *Nat Neurosci* **8,** 650–656.

Itter G, Jung W, Juretschke P, Schoelkens BA & Linz W (2004). A model of chronic heart failure in spontaneous hypertensive rats (SHR). *Lab Anim* **38,** 138–148.

Iwata Y, Katayama Y, Okuno Y & Wakabayashi S (2018). Novel inhibitor candidates of TRPV2 prevent damage of dystrophic myocytes and ameliorate against dilated cardiomyopathy in a hamster model. *Oncotarget* **9,** 14042–14057.

Jacobson KA, Delicado EG, Gachet C, Kennedy C, von Kügelgen I, Li B, Miras-Portugal MT, Novak I, Schöneberg T, Perez-Sen R, Thor D, Wu B, Yang Z & Müller CE (2020). Update of P2Y receptor pharmacology: IUPHAR Review 27. *Br J Pharmacol* **177,** 2413–2433.

Jacobus WE, Taylor IV GJ, Hollis DP & Nunnally RL (1977). Phosphorus nuclear magnetic resonance of perfused working rat hearts [32]. *Nature* **265,** 756–758.

Jahr CE & Jessell TM (1984). ATP excites a subpopulation of rat dorsal horn neurones. *Prog Neuropsychopharmacol Biol Psychiatry* **8,** 503–505.

James AF, Okada T & Horie M (1995). A fast transient outward current in cultured cells from human pulmonary artery smooth muscle. *Am J Physiol - Hear Circ Physiol* **268,** H2358–H2365.

James SD, Hawkins VE, Falquetto B, Ruskin DN, Masino SA, Moreira TS, Olsen ML & Mulkey DK (2018). Adenosine signaling through A1 receptors inhibits chemosensitive neurons in the

retrotrapezoid nucleus. *eNeuro* **5,** ENEURO.0404-18.2018.

Janes RD, Brandys JC, Hopkins DA, Johnstone DE, Murphy DA & Armour JA (1986). Anatomy of human extrinsic cardiac nerves and ganglia. *Am J Cardiol* **57,** 299–309.

Jarvis MF et al. (2007). A-803467, a potent and selective Nav1.8 sodium channel blocker, attenuates neuropathic and inflammatory pain in the rat. *Proc Natl Acad Sci U S A* **104,** 8520–8525.

Jenkins MA, Christel CJ, Jiao Y, Abiria S, Kim KY, Usachev YM, Obermair GJ, Colbran RJ & Lee A (2010). Ca2+-Dependent facilitation of cav1.3 ca2+ channels by densin and ca2+/calmodulin-dependent protein kinase II. *J Neurosci* **30,** 5125–5135.

Jensen BC, O'Connell TD & Simpson PC (2011). Alpha-1-adrenergic receptors: targets for agonist drugs to treat heart failure. *J Mol Cell Cardiol* **51,** 518–528.

Jentsch TJ, Poët M, Fuhrmann JC & Zdebik AA (2005). Physiological functions of CLC Cl− channels gleaned from human genetic disease and mouse models. *Annu Rev Physiol* **67,** 779–807.

Jepps TA, Chadha PS, Davis AJ, Harhun MI, Cockerill GW, Olesen SP, Hansen RS & Greenwood IA (2011). Downregulation of Kv7.4 channel activity in primary and secondary hypertension. *Circulation* **124,** 602–611.

Ji W, Foo JN, O'Roak BJ, Zhao H, Larson MG, Simon DB, Newton-Cheh C, State MW, Levy D & Lifton RP (2008). Rare independent mutations in renal salt handling genes contribute to blood pressure variation. *Nat Genet* **40,** 592–599.

Jiang J, Li M & Yue L (2005). Potentiation of TRPM7 inward currents by protons. *J Gen Physiol* **126,** 137–150.

Jobling P & Gibbins IL (1999*a*). Electrophysiological and morphological diversity of mouse sympathetic neurons. *J Neurophysiol* **82,** 2747–2764.

Jobling P & Gibbins IL (1999*b*). Electrophysiological and morphological diversity of mouse sympathetic neurons. *J Neurophysiol* **82,** 2747–2764.

Johnson JW & Ascher P (1987). Glycine potentiates the NMDA response in cultured mouse brain neurons. *Nature* **325,** 529–531.

Johnson ML, Ely DL & Turner ME (1992). Genetic divergence between the Wistar-Kyoto rat and the spontaneously hypertensive rat. Hypertension 19, 425–427.

Johnson AK & Xue B (2018). Central nervous system neuroplasticity and the sensitization of hypertension. *Nat Rev Nephrol* **14,** 750–766.

Joiner WJ, Tang MD, Wang LY, Dworetzky SI, Boissard CG, Gan L, Gribkoff VK & Kaczmarek LK (1998). Formation of intermediate-conductance calcium-activated potassium channels by interaction of Slack and Slo subunits. *Nat Neurosci* **1,** 462–469.

Joiner WJ, Wang LUY, Tang MD & Kaczmarek LK (1997). hSK4, a member of a novel subfamily of calcium-activated potassium channels. *Proc Natl Acad Sci U S A* **94,** 11013–11018.

Jones S, Brown DA, Milligan G, Willer E, Buckley NJ & Caulfield MP (1995). Bradykinin excites rat sympathetic neurons by inhibition of M current through a mechanism involving B2 receptors and Gαq/11. *Neuron* **14,** 399–405.

Ju YK & Allen DG (1999). How does beta-adrenergic stimulation increase the heart rate? The role of intracellular Ca2+ release in amphibian pacemaker cells. *J Physiol* **516 ( Pt 3,** 793–804.

Jubelin BC & Kannan MS (1990). Neurons from neonatal hypertensive rats exhibit abnormal membrane properties in vitro. *Am J Physiol - Cell Physiol* **259,** C389–C396.

Julius D & Basbaum AI (2001). Molecular mechanisms of nociception. *Nature* **413,** 203–210.

Just A, Wittmann U, Nafz B, Wagner CD, Ehmke H, Kirchheim HR & Persson PB (1994). The blood pressure buffering capacity of nitric oxide by comparison to the baroreceptor reflex. *Am J Physiol Circ Physiol* **267,** H521–H527.

Kaczmarek LK (2013). Slack, Slick, and Sodium-Activated Potassium Channels. *ISRN Neurosci* **2013,** 1–14.

Kaeser PS, Deng L, Wang Y, Dulubova I, Liu X, Rizo J & Südhof TC (2011). RIM proteins tether Ca2+ channels to presynaptic active zones via a direct PDZ-domain interaction. *Cell* **144,** 282–295.

Kalla M, Hao G, Tapoulal N, Tomek J, Liu K, Woodward L, Study' 'Oxford Acute Myocardial Infarction (OxAMI), Dall'Armellina E, Banning AP, Choudhury RP, Neubauer S, Kharbanda RK, Channon KM, Ajijola OA, Shivkumar K, Paterson DJ & Herring N (2020). The cardiac sympathetic co-transmitter neuropeptide Y is pro-arrhythmic following ST-elevation myocardial infarction despite beta-blockade. *Eur Heart J* **41,** 2168–2179.

Kameyama M, Kakei M, Sato R, Shibasaki T, Matsuda H & Irisawa H (1984). Intracellular Na+ activates a K+ channel in mammalian cardiac cells. *Nature* **309,** 354–356.

Kandzari DE et al. (2018). Effect of renal denervation on blood pressure in the presence of antihypertensive drugs: 6-month efficacy and safety results from the SPYRAL HTN-ON MED proof-of-concept randomised trial. *Lancet* **391,** 2346–2355.

Kanehisa M, Sato Y, Kawashima M, Furumichi M & Tanabe M (2016). KEGG as a reference resource for gene and protein annotation. *Nucleic Acids Res* **44,** D457–D462.

Kaneko H, Putzier I, Frings S & Gensch TBT-CT in M (2002). Determination of intracellular chloride concentration in dorsal root ganglion neurons by fluorescence lifetime imaging. In *Calcium-Activated Chloride Channels*, pp. 167–189. Academic Press. Available at: http://www.sciencedirect.com/science/article/pii/S1063582302530337.

Kang J, Kang N, Lovatt D, Torres A, Zhao Z, Lin J & Nedergaard M (2008). Connexin 43 hemichannels are permeable to ATP. *J Neurosci* **28,** 4702–4711.

Kannel WB, Wolf PA, Benjamin EJ & Levy D (1998). Prevalence, incidence, prognosis, and predisposing conditions for atrial fibrillation: population-based estimates 11Reprints are not available. *Am J Cardiol* **82,** 2N-9N.

Karam H, Heudes D, Gonzales MF, Loffler BM, Clozel M & Clozel JP (1996). Respective role of humoral factors and blood pressure in aortic remodeling of DOCA hypertensive rats. *Am J Hypertens* **9,** 991–998.

Karasek R, Baker D, Marxer F, Ahlbom A & Theorell T (1981). Job decision latitude, job demands, and cardiovascular disease: a prospective study of Swedish men. *Am J Public Health* **71,** 694–705.

Karlsten R, Gordh T & Post C (1992). Local Antinociceptive and Hyper algesic Effects in the Formalin Test after Peripheral Administration of Adenosine Analogues in Mice. *Pharmacol Toxicol* **70,** 434–438.

Katanosaka K, Takatsu S, Mizumura K, Naruse K & Katanosaka Y (2018). TRPV2 is required for mechanical nociception and the stretch-evoked response of primary sensory neurons. *Sci Rep* **8,** 16782.

Katanosaka Y, Iwasaki K, Ujihara Y, Takatsu S, Nishitsuji K, Kanagawa M, Sudo A, Toda T, Katanosaka K, Mohri S & Naruse K (2014). TRPV2 is critical for the maintenance of cardiac structure and function in mice. *Nat Commun* **5,** 3932.

Katholi RE (1983). Renal nerves in the pathogenesis of hypertension in experimental animals and humans. *Am J Physiol Physiol* **245,** F1–F14.

Katholi RE, Hageman GR, Whitlow PL & Woods WT (1983). Hemodynamic and afferent renal nerve responses to intrarenal adenosine in the dog. *Hypertension* **5,** I149.

Katz B & Miledi R (1967). Ionic requirements of synaptic transmitter release. *Nature* **215,** 651.

Katz B & Miledi R (1972). The statistical nature of the acetylcholine potential and its molecular components. *J Physiol* **224,** 665–699.

Kaufmann SG, Westenbroek RE, Maass AH, Lange V, Renner A, Wischmeyer E, Bonz A, Muck J, Ertl G, Catterall WA, Scheuer T & Maier SKG (2013). Distribution and function of sodium channel subtypes in human atrial myocardium. *J Mol Cell Cardiol* **61,** 133–141.

Kawahara K, Hohjoh H, Inazumi T, Tsuchiya S & Sugimoto Y (2015). Prostaglandin E2-induced inflammation: Relevance of prostaglandin E receptors. *Biochim Biophys Acta - Mol Cell Biol Lipids* **1851,** 414–421.

Kawai T & Watanabe M (1986). Blockade of Ca-activated K conductance by apamin in rat sympathetic neurones. *Br J Pharmacol* **87,** 225–232.

Kawano Y, Yoshida K, Kawamura M, Yoshimi H, Ashida T, Abe H, Imanishi M, Kimura G, Kojima S, Kuramochi M & Omae T (1992). Sodium and Noradrenaline in Cerebrospinal Fluid and Blood in Salt-Sensitive and Non-Salt-Sensitive Essential Hypertension. *Clin Exp Pharmacol Physiol* **19,** 235–241.

Kaye DM, Vaddadi G, Gruskin SL, Du XJ & Esler MD (2000). Reduced myocardial nerve growth factor expression in human and experimental heart failure. *Circ Res* **86,** e80–e84.

Kearney PM, Whelton M, Reynolds K, Muntner P, Whelton PK & He J (2005). Global burden of hypertension: analysis of worldwide data. *Lancet* **365,** 217–223.

Khakh BS, Humphrey PP & Surprenant A (1995). Electrophysiological properties of P2X-purinoceptors in rat superior cervical, nodose and guinea-pig coeliac neurones. *J Physiol* **484,** 385–395.

Kiedrowski L, Wroblewski JT & Costa E (1994). Intracellular sodium concentration in cultured cerebellar granule cells challenged with glutamate. *Mol Pharmacol* **45,** 1050 LP – 1054.

Kim DM & Nimigean CM (2016). Voltage-Gated Potassium Channels: A Structural Examination of Selectivity and Gating. *Cold Spring Harb Perspect Biol* **8,** a029231.

Kim SJ, Kim YS, Yuan JP, Petralia RS, Worley PF & Linden DJ (2003). Activation of the TRPC1 cation channel by metabotropic glutamate receptor mGluR1. *Nature* **426,** 285–291.

Kim TH, Zhou X & Chen M (2020). Demystifying “drop-outs” in single-cell UMI data. *Genome Biol* **21,** 196.

Kimm T, Khaliq ZM & Bean BP (2015*a*). Differential regulation of action potential shape and burst-frequency firing by BK and Kv2 channels in substantia nigra dopaminergic neurons. *J Neurosci* **35,** 16404–16417.

Kimm T, Khaliq ZM & Bean BP (2015*b*). Differential regulation of action potential shape and burst-

frequency firing by BK and Kv2 channels in substantia nigra dopaminergic neurons. *J Neurosci* **35,** 16404–16417.

Kinnunen P, Vuolteenaho O & Ruskoaho H (1993). Mechanisms of atrial and brain natriuretic peptide release from rat ventricular myocardium: effect of stretching. *Endocrinology* **132,** 1961–1970.

Kinsman BJ, Browning KN & Stocker SD (2017*a*). NaCl and osmolarity produce different responses in organum vasculosum of the lamina terminalis neurons, sympathetic nerve activity and blood pressure. *J Physiol* **595,** 6187–6201.

Kinsman BJ, Simmonds SS, Browning KN & Stocker SD (2017*b*). Organum Vasculosum of the Lamina Terminalis Detects NaCl to Elevate Sympathetic Nerve Activity and Blood Pressure. *Hypertension* **69,** 163–170.

Kirshner N (1962). Uptake of catecholamines by a particulate fraction of the adrenal medulla. *Science (80- )* **135,** 107–108.

Kjolby M & Bie P (2008). Chronic activation of plasma renin is log-linearly related to dietary sodium and eliminates natriuresis in response to a pulse change in total body sodium. *Am J Physiol - Regul Integr Comp Physiol* **294,** R17–R25.

Klingbeil AU, Schneider M, Martus P, Messerli FH & Schmieder RE (2003). A meta-analysis of the effects of treatment on left ventricular mass in essential hypertension. *Am J Med* **115,** 41–46.

Klocke FJ, Kaiser GA, Ross J & Braunwald E (1965). An Intrinsic Adrenergic Vasodilator Mechanism in the Coronary Vascular. *Circ Res* **16,** 376–382.

Knight DR, Kirby DA & Vatner SF (1985). Effects of a calcium channel blocker on cardiac output distribution in conscious hypertensive dogs. *Hypertension* **7,** 380–385.

Knot HJ & Nelson MT (1998). Regulation of arterial diameter and wall [Ca2+] in cerebral arteries of rat by membrane potential and intravascular pressure. *J Physiol* **508 ( Pt 1,** 199–209.

Kobayashi K & Nagatsu T (2012). Tyrosine Hydroxylase. In *Primer on the Autonomic Nervous System*, ed. Robertson D, Biaggioni I, Burnstock G, Low PA & Paton JFRBT-P on the ANS (Third E, pp. 45–47. Academic Press, San Diego. Available at: http://www.sciencedirect.com/science/article/pii/B978012386525000007X.

Koch C, Rapp M & Segev I (1996). A brief history of time (constants). *Cereb cortex* **6,** 93–101.

Koester HJ & Johnston D (2005). Target Cell-Dependent Normalization of Transmitter Release at Neocortical Synapses. *Science (80- )* **308,** 863 LP – 866.

Koh DS & Hille B (1997). Modulation by neurotransmitters of catecholamine secretion from sympathetic ganglion neurons detected by amperometry. *Proc Natl Acad Sci U S A* **94,** 1506–1511.

Köhler M, Hirschberg B, Bond CT, Kinzie JM, Marrion N V., Maylie J & Adelman JP (1996). Small-conductance, calcium-activated potassium channels from mammalian brain. *Science (80- )* **273,** 1709–1714.

Koizumi S, Shigemoto-Mogami Y, Nasu-Tada K, Shinozaki Y, Ohsawa K, Tsuda M, Joshi B V., Jacobson KA, Kohsaka S & Inoue K (2007). UDP acting at P2Y6 receptors is a mediator of microglial phagocytosis. *Nature* **446,** 1091–1095.

Kokubun S, Sato T, Ogawa C, Kudo K, Goto K, Fujii Y, Shimizu Y & Ichikawa H (2015). Distribution

of TRPV1 and TRPV2 in the human stellate ganglion and spinal cord. *Neurosci Lett* **590,** 6–11.

Kolb HA & Wakelam MJO (1983). Transmitter-like action of ATP on patched membranes of cultured myoblasts and myotubes. *Nature* **303,** 621–623.

Kole MHP & Cooper EC (2014). Axonal Kv7.2/7.3 channels. *Channels* **8,** 288–289.

Kole MHP, Hallermann S & Stuart GJ (2006). Single Ih channels in pyramidal neuron dendrites: Properties, distribution, and impact on action potential output. *J Neurosci* **26,** 1677–1687.

Kole MHP, Letzkus JJ & Stuart GJ (2007). Axon Initial Segment Kv1 Channels Control Axonal Action Potential Waveform and Synaptic Efficacy. *Neuron* **55,** 633–647.

Koncz C & Daugirdas JT (1994). Use of MQAE for measurement of intracellular [Cl-] in cultured aortic smooth muscle cells. *Am J Physiol Circ Physiol* **267,** H2114–H2123.

Korsching S & Thoenen H (1983). Nerve growth factor in sympathetic ganglia and corresponding target organs of the rat: correlation with density of sympathetic innervation. *Proc Natl Acad Sci* **80,** 3513–3516.

Kosenko A & Hoshi N (2013). A change in configuration of the calmodulin-KCNQ channel complex underlies Ca2+-dependent modulation of KCNQ channel activity. *PLoS One* **8,** e82290.

Kostyuk PG (1984). Intracellular perfusion of nerve cells and its effects on membrane currents. *Physiol Rev* **64,** 435–454.

Kouranova E V., Strassle BW, Ring RH, Bowlby MR & Vasilyev D V. (2008). Hyperpolarization-activated cyclic nucleotide-gated channel mRNA and protein expression in large versus small diameter dorsal root ganglion neurons: Correlation with hyperpolarization-activated current gating. *Neuroscience* **153,** 1008–1019.

Krapivinsky G, Mochida S, Krapivinsky L, Cibulsky SM & Clapham DEE (2006). The TRPM7 Ion Channel Functions in Cholinergic Synaptic Vesicles and Affects Transmitter Release. *Neuron* **52,** 485–496.

Kreitzer AC, Gee KR, Archer EA & Regehr WG (2000). Monitoring presynaptic calcium dynamics in projection fibers by in vivo loading of a novel calcium indicator. *Neuron* **27,** 25–32.

Kreusser MM, Lehmann LH, Riffel JH, Haass M, Maser-Gluth C, Backs J, Katus HA & Buss SJ (2014). Aldosterone augments Na+-induced reduction of cardiac norepinephrine reuptake. *Am J Physiol - Hear Circ Physiol* **307,** H1169–H1177.

Krishna GG, Riley LJ, Deuter G, Kapoor SC & Narins RG (1991). Natriuretic Effect of Calcium-Channel Blockers in Hypertensives. *Am J Kidney Dis* **18,** 566–572.

Krishtal OA, Marchenko SM & Pidoplichko VI (1983). Receptor for ATP in the membrane of mammalian sensory neurones. *Neurosci Lett* **35,** 41–45.

Krum H, Schlaich M, Whitbourn R, Sobotka PA, Sadowski J, Bartus K, Kapelak B, Walton A, Sievert H, Thambar S, Abraham WT & Esler M (2009). Catheter-based renal sympathetic denervation for resistant hypertension: a multicentre safety and proof-of-principle cohort study. *Lancet* **373,** 1275–1281.

Krum H, Schlaich MP, Sobotka PA, Böhm M, Mahfoud F, Rocha-Singh K, Katholi R & Esler MD (2014). Percutaneous renal denervation in patients with treatment-resistant hypertension: final 3-year report of the Symplicity HTN-1 study. *Lancet* **383,** 622–629.

Kshatri AS, Gonzalez-Hernandez A & Giraldez T (2018). Physiological Roles and Therapeutic

Potential of Ca2+ Activated Potassium Channels in the Nervous System. *Front Mol Neurosci* **11,** 258. Available at: https://www.frontiersin.org/article/10.3389/fnmol.2018.00258.

Kubota J, Nishimura H, Ueyama M & Kawamura K (1993). Effects of renal denervation on pressure-natriuresis in spontaneously hypertensive rats. *Jpn Circ J* **57,** 1097–1105.

Kukwa W, Macioch T & Szulczyk PJ (1998). Stellate neurones innervating the rat heart express N, L and P/Q calcium channels. *J Auton Nerv Syst* **74,** 143–151.

Kullmann PHM, Sikora KM, Clark KL, Arduini I, Springer MG & Horn JP (2016). HCN hyperpolarization-activated cation channels strengthen virtual nicotinic EPSPs and thereby elevate synaptic amplification in rat sympathetic neurons. *J Neurophysiol* **116,** 438–447.

Kummer W (1987). Galanin and neuropeptide Y-like immunoreactivities coexist in paravertebral sympathetic neurones of the cat. *Neurosci Lett* **78,** 127–131.

Kummer W, Fischer A, Kurkowski R & Heym C (1992). The sensory and sympathetic innervation of guinea-pig lung and trachea as studied by retrograde neuronal tracing and double-labelling immunohistochemistry. *Neuroscience* **49,** 715–737.

Kuner T & Augustine GJ (2000). A Genetically Encoded Ratiometric Indicator for Chloride: Capturing Chloride Transients in Cultured Hippocampal Neurons. *Neuron* **27,** 447–459.

Kuo C-C & Bean BP (1994). Na+ channels must deactivate to recover from inactivation. *Neuron* **12,** 819–829.

Lamas JA, Reboreda A & Codesido V (2002). Ionic basis of the resting membrane potential in cultured rat sympathetic neurons. *Neuroreport* **13,** 585–591.

Lamas JA, Romero M, Reboreda A, Sánchez E & Ribeiro SJ (2009). A riluzole- and valproate-sensitive persistent sodium current contributes to the resting membrane potential and increases the excitability of sympathetic neurones. *Pflugers Arch Eur J Physiol* **458,** 589–599.

Lanfranchi PA & Somers VK (2002). Arterial baroreflex function and cardiovascular variability: interactions and implications. *Am J Physiol Integr Comp Physiol* **283,** R815–R826.

Langley JN (1898). On the Union of Cranial Autonomic (Visceral) Fibres with the Nerve Cells of the Superior Cervical Ganglion. *J Physiol* **23,** 240–270.

Laprairie RB, Bagher AM, Kelly MEM & Denovan-Wright EM (2015). Cannabidiol is a negative allosteric modulator of the cannabinoid CB1 receptor. *Br J Pharmacol* **172,** 4790–4805.

Lara LS, Satou R, Bourgeois CRT, Gonzalez AA, Zsombok A, Prieto MC & Gabriel Navar L (2012). The sodium-activated sodium channel is expressed in the rat kidney thick ascending limb and collecting duct cells and is upregulated during high salt intake. *Am J Physiol - Ren Physiol* **303,** F105–F109.

Larsen HE, Bardsley EN, Lefkimmiatis K & Paterson DJ (2016*a*). Dysregulation of neuronal Ca2+ channel linked to heightened sympathetic phenotype in prohypertensive states. *J Neurosci* **36,** 8562–8573.

Larsen HE, Lefkimmiatis K & Paterson DJ (2016*b*). Sympathetic neurons are a powerful driver of myocyte function in cardiovascular disease. *Sci Rep* **6,** 38898.

Lau DH, Shipp NJ, Kelly DJ, Thanigaimani S, Neo M, Kuklik P, Lim HS, Zhang Y, Drury K, Wong CX, Chia NH, Brooks AG, Dimitri H, Saint DA, Brown L & Sanders P (2013). Atrial Arrhythmia in Ageing Spontaneously Hypertensive Rats: Unraveling the Substrate in Hypertension and Ageing. *PLoS One* **8,** e72416.

Lazarowski ER, Rochelle LG, O'Neal WK, Ribeiro CMP, Grubb BR, Zhang V, Harden TK & Boucher RC (2001). Cloning and functional characterization of two murine uridine nucleotide receptors reveal a potential target for correcting ion transport deficiency in cystic fibrosis gallbladder. *J Pharmacol Exp Ther* **297,** 43–49.

Lechner SG, Mayer M & Boehm S (2003). Activation of M1 muscarinic receptors triggers transmitter release from rat sympathetic neurons through an inhibition of M-type K+ channels. *J Physiol* **553,** 789–802.

Lei M, Jones SA, Liu J, Lancaster MK, Fung SS-M, Dobrzynski H, Camelliti P, Maier SKG, Noble D & Boyett MR (2004). Requirement of neuronal- and cardiac-type sodium channels for murine sinoatrial node pacemaking. *J Physiol* **559,** 835–848.

Leng TD, Si HF, Li J, Yang T, Zhu M, Wang B, Simon RP & Xiong ZG (2016). Amiloride Analogs as ASIC1a Inhibitors. *CNS Neurosci Ther* **22,** 468–476.

Lerche C, Scherer CR, Seebohm G, Derst C, Wei AD, Busch AE & Steinmeyer K (2000). Molecular cloning and functional expression of KCNQ5, a potassium channel subunit that may contribute to neuronal M-current diversity. *J Biol Chem* **275,** 22395–22400.

Lerma J, Paternain A V, Rodríguez-Moreno A & López-García JC (2001). Molecular Physiology of Kainate Receptors. *Physiol Rev* **81,** 971–998.

Lerman LO, Kurtz TW, Touyz RM, Ellison DH, Chade AR, Crowley SD, Mattson DL, Mullins JJ, Osborn J, Eirin A, Reckelhoff JF, Iadecola C & Coffman TM (2019). Animal Models of Hypertension: A Scientific Statement From the American Heart Association. *Hypertens (Dallas, Tex 1979)* **73,** e87–e120.

Levi-Montalcini R & Booker B (1997). Destruction of the Sympathetic Ganglia in Mammals By an Antiserum To a Nerve-Growth Protein. *Proc Natl Acad Sci* **46,** 180–187.

Levy BI, Ambrosio G, Pries AR & Struijker-Boudier HAJ (2001). Microcirculation in hypertension: A new target for treatment? *Circulation* **104,** 735–740.

Levy D, Larson MG, Vasan RS, Kannel WB & Ho KKL (1996). The Progression From Hypertension to Congestive Heart Failure. *JAMA* **275,** 1557–1562.

Lewis GP & Reit E (1965). The action of angiotensin and bradykinin on the superior cervical ganglion of the cat. *J Physiol* **179,** 538.

Lewis T, Oppenheimer BS & Oppenheimer A (1910). The site of origin of the mammalian heart beat: the pacemaker in the dog. *Heart* **2,** 1910–1911.

Li C & Horn JP (2006). Physiological Classification of Sympathetic Neurons in the Rat Superior Cervical Ganglion. *J Neurophysiol* **95,** 187–195.

Li C & Horn JP (2008). Differential inhibition of Ca2+ channels by α2- adrenoceptors in three functional subclasses of rat sympathetic neurons. *J Neurophysiol* **100,** 3055–3063.

Li D, Lee CW, Buckler K, Parekh A, Herring N & Paterson DJ (2012). *Abnormal intracellular calcium homeostasis in sympathetic neurons from young prehypertensive rats*.

Li D, Lu CJ, Hao G, Wright H, Woodward L, Liu K, Vergari E, Surdo NC, Herring N, Zaccolo M & Paterson DJ (2015*a*). Efficacy of B-type natriuretic peptide is coupled to phosphodiesterase 2A in cardiac sympathetic neurons. *Hypertension* **66,** 190–198.

Li D & Paterson DJ (2016). Cyclic nucleotide regulation of cardiac sympatho-vagal responsiveness. *J Physiol* **594,** 3993–4008.

Li DP, Chen SR & Pan HL (2010). Adenosine inhibits paraventricular pre-sympathetic neurons through ATP-dependent potassium channels. *J Neurochem* **113,** 530–542.

Li GR & Baumgarten CM (2001). Modulation of cardiac Na+ current by gadolinium, a blocker of stretch-induced arrhythmias. *Am J Physiol - Hear Circ Physiol* **280,** H272–H279.

Li J, Kemp BA, Howell NL, Massey J, Mińczuk K, Huang Q, Chordia MD, Jack Roy R, Patrie JT, Davogustto GE, Kramer CM, Epstein FH, Carey RM, Taegtmeyer H, Keller SR & Kundu BK (2019). Metabolic changes in spontaneously hypertensive rat hearts precede cardiac dysfunction and left ventricular hypertrophy. *J Am Heart Assoc* **8,** e010926.

Li Q & Yan J (2016). Modulation of BK Channel Function by Auxiliary Beta and Gamma Subunits. *Int Rev Neurobiol* **128,** 51–90.

Li Q, Youn J-Y & Cai H (2015*b*). Mechanisms and consequences of endothelial nitric oxide synthase dysfunction in hypertension. *J Hypertens* **33,** 1128–1136.

Li S, Wang Z, Yang X, Hu B, Huang Y & Fan S (2017). Association between circulating angiotensin-converting enzyme 2 and cardiac remodeling in hypertensive patients. *Peptides* **90,** 63–68.

Li W & Aldrich RW (2004). Unique inner pore properties of BK channels revealed by quaternary ammonium block. *J Gen Physiol* **124,** 43–57.

Li WC, Soffe SR & Roberts A (2004). A direct comparison of whole cell patch and sharp electrodes by simultaneous recording from single spinal neurons in frog tadpoles. *J Neurophysiol* **92,** 380–386.

Li XN, Herrington J, Petrov A, Ge L, Eiermann G, Xiong Y, Jensen M V., Hohmeier HE, Newgard CB, Garcia ML, Wagner M, Zhang BB, Thornberry NA, Howard AD, Kaczorowski GJ & Zhou YP (2013). The role of voltage-gated potassium channels Kv2.1 and Kv2.2 in the regulation of insulin and somatostatin release from pancreatic isletss. *J Pharmacol Exp Ther* **344,** 407–416.

Linley JE (2013). Perforated whole-cell patch-clamp recording. In *Methods in Molecular Biology*, ed. Gamper N, pp. 149–157. Humana Press, Totowa, NJ. Available at: https://doi.org/10.1007/978-1-62703-351-0_11.

Linley JE, Rose K, Patil M, Robertson B, Akopian AN & Gamper N (2008). Inhibition of M current in sensory neurons by exogenous proteases: a signaling pathway mediating inflammatory nociception. *J Neurosci* **28,** 11240–11249.

Lipman NS, Jackson LR, Trudel LJ & Weis-Garcia F (2005). Monoclonal Versus Polyclonal Antibodies: Distinguishing Characteristics, Applications, and Information Resources. *ILAR J* **46,** 258–268.

Lipscombe D, Madison D V., Poenie M, Reuter H, Tsien RY & Tsien RW (1988). Spatial distribution of calcium channels and cytosolic calcium transients in growth cones and cell bodies of sympathetic neurons. *Proc Natl Acad Sci U S A* **85,** 2398–2402.

Liu B & Qin F (2016). Use Dependence of Heat Sensitivity of Vanilloid Receptor TRPV2. *Biophys J* **110,** 1523–1537.

Liu BS, Ferreira R, Lively S & Schlichter LC (2013). Microglial SK3 and SK4 currents and activation state are modulated by the neuroprotective drug, riluzole. *J Neuroimmune Pharmacol* **8,** 227–237.

Liu K, Li D, Hao G, McCaffary D, Neely O, Woodward L, Ioannides D, Lu C-J, Brescia M, Zaccolo M, Tandri H, Ajijola OA, Ardell JL, Shivkumar K & Paterson DJ (2018). Phosphodiesterase 2A as a therapeutic target to restore cardiac neurotransmission during sympathetic hyperactivity.

*JCI Insight*; DOI: 10.1172/jci.insight.98694.

Liu PW & Bean BP (2014). Kv2 channel regulation of action potential repolarization and firing patterns in superior cervical ganglion neurons and hippocampal CA1 pyramidal neurons. *J Neurosci* **34,** 4786–4800.

Livak KJ & Schmittgen TD (2001). Analysis of relative gene expression data using real-time quantitative PCR and the 2-ΔΔCT method. *Methods* **25,** 402–408.

Llinás R & Nicholson C (1975). Calcium role in depolarization-secretion coupling: an aequorin study in squid giant synapse. *Proc Natl Acad Sci U S A* **72,** 187–190.

Llinás R, Steinberg IZ & Walton K (1981). Presynaptic calcium currents in squid giant synapse. *Biophys J* **33,** 289–321.

Lloyd TR & Marvin WJ (1991). Contractile response to sympathetic innervation in neonatal ventricular cardiomyocytes of the spontaneously hypertensive rat. *Pediatr Res* **30,** 207–210.

Lock JT, Parker I & Smith IF (2015). A comparison of fluorescent $Ca^{2+}$ indicators for imaging local $Ca^{2+}$ signals in cultured cells. *Cell Calcium* **58,** 638–648.

Lockhart ST, Turrigiano GG & Birren SJ (1997). Nerve growth factor modulates synaptic transmission between sympathetic neurons and cardiac myocytes. *J Neurosci* **17,** 9573–9582.

Loewi O (1921). Über humorale übertragbarkeit der Herznervenwirkung. *Pflüger's Arch für die gesamte Physiol des Menschen und der Tiere* **189,** 239–242.

Loewi O & Navratil E (1926). Über humorale übertragbarkeit der herznervenwirkung. *Pflüger's Arch für die gesamte Physiol des Menschen und der Tiere* **214,** 678–688.

Löffelholz K & Muscholl E (1969). A muscarinic inhibition of the noradrenaline release evoked by postganglionic sympathetic nerve stimulation. *Naunyn Schmiedebergs Arch Pharmakol* **265,** 1–15.

Logothetis DE, Movahedi S, Satler C, Lindpaintner K & Nadal-Ginard B (1992). Incremental reductions of positive charge within the S4 region of a voltage-gated K+ channel result in corresponding decreases in gating charge. *Neuron* **8,** 531–540.

Logsdon NJ, Kang J, Togo JA, Christian EP & Aiyar J (1997). A novel gene, hKCa4, encodes the calcium-activated potassium channel in human T lymphocytes. *J Biol Chem* **272,** 32723–32726.

Lohmeier TE, Haque A, McManus WJ & Hildebrandt DA (2000). Long-term influence of basal renal nerve activity on arterial pressure. In *FASEB JOURNAL*, pp. A373–A373. FEDERATION AMER SOC EXP BIOL 9650 ROCKVILLE PIKE, BETHESDA, MD 20814-3998 USA.

Lohmeier TE, Reinhart GA, Mizelle HL, Han M & Dean MM (1998). Renal denervation supersensitivity revisited. *Am J Physiol Integr Comp Physiol* **275,** R1239–R1246.

Louis WJ & Howes LG (1990). Genealogy of the Spontaneously Hypertensive Rat and Wistar-Kyoto Rat Strains: Implications for Studies of Inherited Hypertension. *J Cardiovasc Pharmacol* **16,** S1???S5.

Love MI, Huber W & Anders S (2014). Moderated estimation of fold change and dispersion for RNA-seq data with DESeq2. *Genome Biol* **15,** 550.

Lozano R et al. (2012). Global and regional mortality from 235 causes of death for 20 age groups

in 1990 and 2010: a systematic analysis for the Global Burden of Disease Study 2010. *Lancet* **380,** 2095–2128.

Ludwig A, Zong X, Jeglitsch M, Hofmann F & Biel M (1998). A family of hyperpolarization-activated mammalian cation channels. *Nature* **393,** 587–591.

Ludwig A, Zong X, Stieber J, Hullin R, Hofmann F & Biel M (1999). Two pacemaker channels from human heart with profoundly different activation kinetics. *EMBO J* **18,** 2323–2329.

Ludwig M-G, Vanek M, Guerini D, Gasser JA, Jones CE, Junker U, Hofstetter H, Wolf RM & Seuwen K (2003). Proton-sensing G-protein-coupled receptors. *Nature* **425,** 93–98.

Luebke JI, Weight FF & Aguayo LG (1992). Labelling and recording from dissociated target-specific rat superior cervical ganglion neurons. *Neurosci Lett* **135,** 210–214.

Luff SE (1996). Ultrastructure of sympathetic axons and their structural relationship with vascular smooth muscle. *Anat Embryol (Berl)* **193,** 515–531.

Luft FC, Rankin LI, Bloch R, Weyman AE, Willis LR, Murray RH, Grim CE & Weinberger MH (1979). Cardiovascular and humoral responses to extremes of sodium intake in normal black and white men. *Circulation* **60,** 697–706.

Lundberg JM, Rudehill A, Sollevi A & Hamberger B (1989). Evidence for co-transmitter role of neuropeptide Y in the pig spleen. *Br J Pharmacol* **96,** 675–687.

Lundberg JM, Terenius L, HÖkfelt T, Martling CR, Tatemoto K, Mutt V, Polak J, Bloom S & Goldstein M (1982). Neuropeptide Y (NPY)-like immunoreactivity in peripheral noradrenergic neurons and effects of NPY on sympathetic function. *Acta Physiol Scand* **116,** 477–480.

Luo D, Cheng Y, Zhang H, Ba M, Chen P, Li H, Chen K, Sha W, Zhang C & Chen H (2020). Association between high blood pressure and long term cardiovascular events in young adults: systematic review and meta-analysis. *BMJ* **370,** m3222.

Luo J, Wang Y, Yasuda RP, Dunah AW & Wolfe BB (1997). The majority of N-methyl-D-aspartate receptor complexes in adult rat cerebral cortex contain at least three different subunits (NR1/NR2A/NR2B). *Mol Pharmacol* **51,** 79–86.

Luther JA & Birren SJ (2006). Nerve growth factor decreases potassium currents and alters repetitive firing in rat sympathetic neurons. *J Neurophysiol* **96,** 946–958.

Luther JA & Birren SJ (2009). p75 and TrkA signaling regulates sympathetic neuronal firing patterns via differential modulation of voltage-gated currents. *J Neurosci* **29,** 5411–5424.

Luttrell LM & Lefkowitz RJ (2002). The role of β-arrestins in the termination and transduction of G-protein-coupled receptor signals. *J Cell Sci* **115,** 455 LP – 465.

Ma X, Cheng K-T, Wong C-O, O'Neil RG, Birnbaumer L, Ambudkar IS & Yao X (2011). Heteromeric TRPV4-C1 channels contribute to store-operated Ca(2+) entry in vascular endothelial cells. *Cell Calcium* **50,** 502–509.

Van Der Maaten L & Hinton G (2008). Visualizing data using t-SNE. *J Mach Learn Res* **9,** 2579–2625.

MacDermott AB, Mayer ML, Westbrook GL, Smith SJ & Barker JL (1986). NMDA-receptor activation increases cytoplasmic calcium concentration in cultured spinal cord neurones. *Nature* **321,** 519–522.

MacDougall AI, Addis GJ, MacKay N, Dymock IW, Turpie AGG, Ballingall DLK, MacLennan WJ, Whiting B & MacArthur JG (1970). Treatment of hypertension with clonidine. *Br Med J* **3,** 440–442.

Macefield VG, Elam M & Wallin BG (2002). Firing properties of single postganglionic sympathetic neurones recorded in awake human subjects. *Auton Neurosci Basic Clin* **95,** 146–159.

Mackenzie PJ, Umemiya M & Murphy TH (1996). $Ca^{2+}$ Imaging of CNS Axons in Culture Indicates Reliable Coupling between Single Action Potentials and Distal Functional Release Sites. *Neuron* **16,** 783–795.

Macosko EZ, Basu A, Satija R, Nemesh J, Shekhar K, Goldman M, Tirosh I, Bialas AR, Kamitaki N, Martersteck EM, Trombetta JJ, Weitz DA, Sanes JR, Shalek AK, Regev A & McCarroll SA (2015). Highly Parallel Genome-wide Expression Profiling of Individual Cells Using Nanoliter Droplets. *Cell* **161,** 1202–1214.

Macri V et al. (2018). Common Coding Variants in SCN10A Are Associated With the Nav1.8 Late Current and Cardiac Conduction. *Circ Genomic Precis Med* **11,** e001663.

Magee JC (1998). Dendritic hyperpolarization-activated currents modify the integrative properties of hippocampal CA1 pyramidal neurons. *J Neurosci* **18,** 7613–7624.

Magee JC & Schofield GG (1994). Alterations of synaptic transmission in sympathetic ganglia of spontaneously hypertensive rats. *Am J Physiol - Regul Integr Comp Physiol* **267,** R1397–R1407.

Maier SKG, Westenbroek RE, Schenkman KA, Feigl EO, Scheuer T & Catterall WA (2002). An unexpected role for brain-type sodium channels in coupling of cell surface depolarization to contraction in the heart. *Proc Natl Acad Sci U S A* **99,** 4073–4078.

Maier SKG, Westenbroek RE, Yamanushi TT, Dobrzynski H, Boyett MR, Catterall WA & Scheuer T (2003). An unexpected requirement for brain-type sodium channels for control of heart rate in the mouse sinoatrial node. *Proc Natl Acad Sci U S A* **100,** 3507–3512.

Major G, Larkman AU, Jonas P, Sakmann B & Jack JJ 7 (1994). Detailed passive cable models of whole-cell recorded CA3 pyramidal neurons in rat hippocampal slices. *J Neurosci* **14,** 4613–4638.

Maki BA, Cummings KA, Paganelli MA, Murthy SE & Popescu GK (2014). One-channel cell-attached patch-clamp recording. *J Vis Exp*51629.

Malécot CO, Bito V & Argibay JA (1998). Ruthenium red as an effective blocker of calcium and sodium currents in guinea-pig isolated ventricular heart cells. *Br J Pharmacol* **124,** 465–472.

Malgaroli A, Milani D, Meldolesi J & Pozzan T (1987). Fura-2 measurement of cytosolic free Ca2+ in monolayers and suspensions of various types of animal cells. *J Cell Biol* **105,** 2145–2155.

Malin SA & Nerbonne JM (2000). Elimination of the fast transient in superior cervical ganglion neurons with expression of Kv4.2W362F: Molecular dissection of I(A). *J Neurosci* **20,** 5191–5199.

Malin SA & Nerbonne JM (2001). Molecular heterogeneity of the voltage-gated fast transient outward K+ current, IAf, in mammalian neurons. *J Neurosci* **21,** 8004–8014.

Malin SA & Nerbonne JM (2002). Delayed rectifier K+ currents, IK, are encoded by Kv2 α-subunits and regulate tonic firing in mammalian sympathetic neurons. *J Neurosci* **22,** 10094–10105.

Mancia G, Ferrari A, Gregorini L, Ferrari MC, Bianchini C, Terzoli L, Leonetti G & Zanchettie A

(1980). Effects of prazosin on autonomic control of circulation in essential hypertension. *Hypertension* **2,** 700–707.

Mandela P & Ordway GA (2006). The norepinephrine transporter and its regulation. *J Neurochem* **97,** 310–333.

Mani BK, Robakowski C, Brueggemann LI, Cribbs LL, Tripathi A, Majetschak M & Byron KL (2016). Kv7.5 Potassium Channel Subunits Are the Primary Targets for PKA-Dependent Enhancement of Vascular Smooth Muscle Kv7 Currents. *Mol Pharmacol* **89,** 323–334.

Mannuzzu LM, Moronne MM & Isacoff EY (1996). Direct Physical Measure of Conformational Rearrangement Underlying Potassium Channel Gating. *Science (80- )* **271,** 213 LP – 216.

Manolis AJ, Poulimenos LE, Kallistratos MS, Gavras I & Gavras H (2014). Sympathetic Overactivity in Hypertension and Cardiovascular Disease. *Curr Vasc Pharmacol* **12,** 4–15.

Manoury B, Tamuleviciute A & Tammaro P (2010). TMEM16A/Anoctamin 1 protein mediates calcium-activated chloride currents in pulmonary arterial smooth muscle cells. *J Physiol* **588,** 2305–2314.

Mantegazza M, Frank HY, Powell AJ, Clare JJ, Catterall WA & Scheuer T (2005). Molecular determinants for modulation of persistent sodium current by G-protein βγ subunits. *J Neurosci* **25,** 3341–3349.

Manville RW, Papanikolaou M & Abbott GW (2018). Direct neurotransmitter activation of voltage-gated potassium channels. *Nat Commun* **9,** 1847.

Manville RW, Van Der Horst J, Redford KE, Katz BB, Jepps TA & Abbott GW (2019). KCNQ5 activation is a unifying molecular mechanism shared by genetically and culturally diverse botanical hypotensive folk medicines. *Proc Natl Acad Sci U S A* **116,** 21236–21245.

Maroto R, Raso A, Wood TG, Kurosky A, Martinac B & Hamill OP (2005). TRPC1 forms the stretch-activated cation channel in vertebrate cells. *Nat Cell Biol* **7,** 179–185.

Marrion N V. & Tavalin SJ (1998). Selective activation of Ca2+-activated K+ channels by co-localized Ca2+ channels in hippocampal neurons. *Nature* **395,** 900–905.

Marrion N V, Smart TG, Marsh SJ & Brown DA (1989). Muscarinic suppression of the M-current in the rat sympathetic ganglion is mediated by receptors of the M1-subtype. *Br J Pharmacol* **98,** 557–573.

Marshall JM (1982). The influence of the sympathetic nervous system on individual vessels of the microcirculation of skeletal muscle of the rat. *J Physiol* **332,** 169–186.

Martinello K, Huang Z, Lujan R, Tran B, Watanabe M, Cooper EC, Brown DA & Shah MM (2015). Cholinergic afferent stimulation induces axonal function plasticity in adult hippocampal granule cells. *Neuron* **85,** 346–363.

Martinello K, Giacalone E, Migliore M, Brown DA & Shah MM (2019). The subthreshold-active K(V)7 current regulates neurotransmission by limiting spike-induced Ca(2+) influx in hippocampal mossy fiber synaptic terminals. *Commun Biol* **2,** 145.

Martínez-Pinna J, Antonio Lamas J & Gallego R (2002). Calcium current components in intact and dissociated adult mouse sympathetic neurons. *Brain Res* **951,** 227–236.

Martínez-Pinna J, McLachlan EM & Gallego R (2000). Distinct mechanisms for activation of Cl- and K+ currents by Ca2+ from different sources in mouse sympathetic neurones. *J Physiol* **527,** 249–264.

Martinez-Pinna J, Soriano S, Tudurí E, Nadal A & de Castro F (2018). A calcium-dependent chloride current increases repetitive firing in mouse sympathetic neurons. *Front Physiol* **9,** 508.

Martínez LA, Cifuentes F & Morales MA (2019). Ganglionic Long-Term Potentiation in Prehypertensive and Hypertensive Stages of Spontaneously Hypertensive Rats Depends on GABA Modulation. *Neural Plast* **2019,** 7437894.

Marty A (1981). Ca-dependent K channels with large unitary conductance in chromaffin cell membranes. *Nature* **291,** 497–500.

Matsuda T, Hiyama TY, Niimura F, Matsusaka T, Fukamizu A, Kobayashi K, Kobayashi K & Noda M (2017). Distinct neural mechanisms for the control of thirst and salt appetite in the subfornical organ. *Nat Neurosci* **20,** 230–241.

Matthews EA, Bee LA, Stephens GJ & Dickenson AH (2007). The Cav2.3 calcium channel antagonist SNX-482 reduces dorsal horn neuronal responses in a rat model of chronic neuropathic pain. *Eur J Neurosci* **25,** 3561–3569.

May CN, McAllen RM & McKinley MJ (2000). Renal nerve inhibition by central NaCl and ANG II is abolished by lesions of the lamina terminalis. *Am J Physiol - Regul Integr Comp Physiol* **279,** R1827–R1833.

May DC, Ross EM, Gilman AG & Smigel MD (1985). Reconstitution of catecholamine-stimulated adenylate cyclase activity using three purified proteins. *J Biol Chem* **260,** 15829–15833.

Mayer ML (1985). A calcium-activated chloride current generates the after-depolarization of rat sensory neurones in culture. *J Physiol* **364,** 217–239.

Mayer ML, Westbrook GL & Guthrie PB (1984). Voltage-dependent block by Mg2+ of NMDA responses in spinal cord neurones. *Nature* **309,** 261–263.

McAllister SD, Griffin G, Satin LS & Abood ME (1999). Cannabinoid receptors can activate and inhibit G protein-coupled inwardly rectifying potassium channels in a xenopus oocyte expression system. *J Pharmacol Exp Ther* **291,** 618–626.

McCrossan ZA, Billeter R & White E (2004). Transmural changes in size, contractile and electrical properties of SHR left ventricular myocytes during compensated hypertrophy. *Cardiovasc Res* **63,** 283–292.

McDavid A, Finak G, Chattopadyay PK, Dominguez M, Lamoreaux L, Ma SS, Roederer M & Gottardo R (2013). Data exploration, quality control and testing in single-cell qPCR-based gene expression experiments. *Bioinformatics* **29,** 461–467.

McDougal DH & Gamlin PD (2015). Autonomic control of the eye. *Compr Physiol* **5,** 439–473.

McInnes L, Healy J & Melville J (2018). UMAP: Uniform manifold approximation and projection for dimension reduction. *arXiv*.

McKelvey L, Shorten GD & O'Keeffe GW (2013). Nerve growth factor-mediated regulation of pain signalling and proposed new intervention strategies in clinical pain management. *J Neurochem* **124,** 276–289.

McKinley MJ, McAllen RM, Davern P, Giles ME, Penschow J, Sunn N, Uschakov A & Oldfield BJ (2003). *The sensory circumventricular organs of the mammalian brain.* Springer Science & Business Media.

Minami N, Imai Y, Munakata M, Sasaki S, Sekino H, Abe K & Yoshinaga K (1989). Age-Related Changes in Blood Pressure, Heart Rate and Baroreflex Sensitivity in Shr. *Clin Exp Pharmacol*

*Physiol* **16,** 85–87.

Meera P, Wallner M & Toro L (2000). A neuronal β subunit (KCNMB4) makes the large conductance, voltage- and Ca<sup>2+</sup>-activated K<sup>+</sup> channel resistant to charybdotoxin and iberiotoxin. *Proc Natl Acad Sci* **97,** 5562 LP – 5567.

Mehta JL & Lopez LM (1987). Rebound Hypertension Following Abrupt Cessation of Clonidine and Metoprolol: Treatment With Labetalol. *Arch Intern Med* **147,** 389–390.

Mei Q & Liang BT (2001). P2 purinergic receptor activation enhances cardiac contractility in isolated rat and mouse hearts. *Am J Physiol Circ Physiol* **281,** H334–H341.

Méndez-Giráldez R et al. (2017). GWAS of the electrocardiographic QT interval in Hispanics/Latinos generalizes previously identified loci and identifies population-specific signals. *Sci Rep* **7,** 17075.

Meng L, Tseng CH, Shivkumar K & Ajijola O (2017). Efficacy of Stellate Ganglion Blockade in Managing Electrical Storm: A Systematic Review. *JACC Clin Electrophysiol* **3,** 942–949.

Meredith IT, Broughton A, Jennings GL & Esler MD (1991). Evidence of a Selective Increase in Cardiac Sympathetic Activity in Patients with Sustained Ventricular Arrhythmias. *N Engl J Med* **325,** 618–624.

Meuth SG, Kanyshkova T, Meuth P, Landgraf P, Munsch T, Ludwig A, Hofmann F, Pape H-C & Budde T (2006). Membrane resting potential of thalamocortical relay neurons is shaped by the interaction among TASK3 and HCN2 channels. *J Neurophysiol* **96,** 1517–1529.

Mikala G, Klöckners U, Varadi M, Eisfeld J, Schwartz A & Varadi G (1998). cAMP-dependent phosphorylation sites and macroscopic activity of recombinant cardiac L-type calcium channels. *Mol Cell Biochem* **185,** 95–109.

Millar BC, Schluter KD, Zhou XJ, McDermott BJ & Piper HM (1994). Neuropeptide Y stimulates hypertrophy of adult ventricular cardiomyocytes. *Am J Physiol Physiol* **266,** C1271–C1277.

Min S, Chang RB, Prescott SL, Beeler B, Joshi NR, Strochlic DE & Liberles SD (2019). Arterial baroreceptors sense blood pressure through decorated aortic claws. *Cell Rep* **29,** 2192–2201.

Minami N, Imai Y, Munakata M, Sasaki S, Sekino H, Abe K & Yoshinaga K (1989). Age-Related Changes in Blood Pressure, Heart Rate and Baroreflex Sensitivity in Shr. *Clin Exp Pharmacol Physiol* **16,** 85–87.

Minnone G, De Benedetti F & Bracci-Laudiero L (2017). NGF and its receptors in the regulation of inflammatory response. *Int J Mol Sci* **18,** 1028.

Minta A & Tsien RY (1989). Fluorescent indicators for cytosolic sodium. *J Biol Chem* **264,** 19449–19457.

Mintz IM, Adams ME & Bean BP (1992*a*). P-type calcium channels in rat central and peripheral neurons. *Neuron* **9,** 85–95.

Mintz IM, Venema VJ, Swiderek KM, Lee TD, Bean BP & Adams ME (1992*b*). P-type calcium channels blocked by the spider toxin ω-Aga-IVA. *Nature* **355,** 827–829.

Mo N, Wallis DI & Watson A (1994). Properties of putative cardiac and non-cardiac neurones in the rat stellate ganglion. *J Auton Nerv Syst* **47,** 7–22.

Mobley AS, Miller AM, Araneda RC, Maurer LR, Müller F & Greer CA (2010). Hyperpolarization-activated cyclic nucleotide-gated channels in olfactory sensory neurons regulate axon extension and glomerular formation. J Neurosci 30, 16498–16508.

Mohan RM & Paterson DJ (2000). Activation of sulphonylurea-sensitive channels and the NO-cGMP pathway decreases the heart rate response to sympathetic nerve stimulation. *Cardiovasc Res* **47,** 81–89.

Moosmang S, Biel M, Hofmann F & Ludwig A (1999). Differential Distribution of Four Hyperpolarization-Activated Cation Channels in Mouse Brain. **380,** 975–980.

Morales P, Garneau L, Klein H, Lavoie M-F, Parent L & Sauvé R (2013). Contribution of the KCa3.1 channel-calmodulin interactions to the regulation of the KCa3.1 gating process. *J Gen Physiol* **142,** 37–60.

Moran Y, Barzilai MG, Liebeskind BJ & Zakon HH (2015). Evolution of voltage-gated ion channels at the emergence of Metazoa. *J Exp Biol* **218,** 515 LP – 525.

Morita H, Nishida Y & Hosomi H (1991). Neural control of urinary sodium excretion during hypertonic NaCl load in conscious rabbits: role of renal and hepatic nerves and baroreceptors. *J Auton Nerv Syst* **34,** 157–169.

Mothet J-P, Parent AT, Wolosker H, Brady RO, Linden DJ, Ferris CD, Rogawski MA & Snyder SH (2000). D-serine is an endogenous ligand for the glycine site of the N-methyl-D-aspartate receptor. *Proc Natl Acad Sci* **97,** 4926–4931.

Murakami M, Yoshikawa T, Nakamura T, Ohba T, Matsuzaki Y, Sawamura D, Kuwasako K, Yanagisawa T, Ono K, Nakaji S & Yanai K (2015). Involvement of the histamine H1 receptor in the regulation of sympathetic nerve activity. *Biochem Biophys Res Commun* **458,** 584–589.

Muraki K, Iwata Y, Katanosaka Y, Ito T, Ohya S, Shigekawa M & Imaizumi Y (2003). TRPV2 Is a Component of Osmotically Sensitive Cation Channels in Murine Aortic Myocytes. *Circ Res* **93,** 829–838.

Murata Y, Yasaka T, Takano M & Ishihara K (2016). Neuronal and glial expression of inward rectifier potassium channel subunits Kir2.x in rat dorsal root ganglion and spinal cord. *Neurosci Lett* **617,** 59–65.

Myagmar B-E, Flynn JM, Cowley PM, Swigart PM, Montgomery MD, Thai K, Nair D, Gupta R, Deng DX, Hosoda C, Melov S, Baker AJ & Simpson PC (2017). Adrenergic Receptors in Individual Ventricular Myocytes: The Beta-1 and Alpha-1B Are in All Cells, the Alpha-1A Is in a Subpopulation, and the Beta-2 and Beta-3 Are Mostly Absent. *Circ Res* **120,** 1103–1115.

Myers VB & Haydon DA (1972). Ion transfer across lipid membranes in the presence of gramicidin A: II. The ion selectivity. *Biochim Biophys Acta - Biomembr* **274,** 313–322.

Naeini RS, Witty MF, Séguéla P & Bourque CW (2006). An N-terminal variant of Trpv1 channel is required for osmosensory transduction. *Nat Neurosci* **9,** 93–98.

Nam J, Onitsuka I, Hatch J, Uchida Y, Ray S, Huang S, Li W, Zang H, Ruiz-Lozano P & Mukouyama Y (2013). Coronary veins determine the pattern of sympathetic innervation in the developing heart. *Development* **140,** 1475 LP – 1485.

Narahashi T (2008). Tetrodotoxin - A brief history. *Proc Japan Acad Ser B Phys Biol Sci* **84,** 147–154.

Nascimento AI, Mar FM & Sousa MM (2018). The intriguing nature of dorsal root ganglion neurons: Linking structure with polarity and function. *Prog Neurobiol* **168,** 86–103.

Navar LG, Champion WJ & Thomas CE (1986). Effects of calcium channel blockade on renal vascular resistance responses to changes in perfusion pressure and angiotensin-converting enzyme inhibition in dogs. *Circ Res* **58,** 874–881.

Neal B, MacMahon S & Chapman N (2000). Collaboration BPLTT. Effects of ACE inhibitors, calcium antagonists, and other blood-pressure-lowering drugs: results of prospectively designed overviews of randomised trials. *Blood Press Low Treat trialists' Collab Lancet* **356,** 1955–1964.

Negrete-Díaz J V, Sihra TS, Flores G & Rodríguez-Moreno A (2018). Non-canonical Mechanisms of Presynaptic Kainate Receptors Controlling Glutamate Release . *Front Mol Neurosci* **11,** 128. Available at: https://www.frontiersin.org/article/10.3389/fnmol.2018.00128.

Neher E (1971). Two fast transient current components during voltage clamp on snail neurons. *J Gen Physiol* **58,** 36–53.

Neher E (1998). Vesicle pools and Ca2+ microdomains: New tools for understanding their roles in neurotransmitter release. *Neuron* **20,** 389–399.

Neher E & Sakmann B (1976). Single-channel currents recorded from membrane of denervated frog muscle fibres. *Nature* **260,** 799–802.

Ng GA, Brack KE & Coote JH (2001). Effects of direct sympathetic and vagus nerve stimulation on the physiology of the whole heart - A novel model of isolated Langendorff perfused rabbit heart with intact dual autonomic innervation. *Exp Physiol* **86,** 319–329.

Nguyen Q, Dominguez J, Nguyen L & Gullapalli N (2010). Hypertension management: an update. *Am Heal drug benefits* **3,** 47–56.

Nguyen TP, Sovari AA, Pezhouman A, Iyer S, Cao H, Ko CY, Bapat A, Vahdani N, Ghanim M, Fishbein MC & Karagueuzian HS (2016). Increased susceptibility of spontaneously hypertensive rats to ventricular tachyarrhythmias in early hypertension. *J Physiol* **594,** 1689–1707.

NICE (2019). National Institute for Health and Care Excellence. Hypertension in adults: diagnosis and management [NG136].

Nicholl SM, Bell D, Paul Spiers J & McDermott BJ (2002). Neuropeptide Y Y1 receptor regulates protein turnover and constitutive gene expression in hypertrophying cardiomyocytes. *Eur J Pharmacol* **441,** 23–34.

Nilius B & Owsianik G (2011). The transient receptor potential family of ion channels. *Genome Biol* **12,** 218.

Nishikimi T, Maeda N & Matsuoka H (2006). The role of natriuretic peptides in cardioprotection. *Cardiovasc Res* **69,** 318–328.

Niswender CM & Conn PJ (2010). Metabotropic glutamate receptors: physiology, pharmacology, and disease. *Annu Rev Pharmacol Toxicol* **50,** 295–322.

Noble D & Stein RB (1966). The threshold conditions for initiation of action potentials by excitable cells. *J Physiol* **187,** 129–162.

Noble D & Tsien RW (1969). Outward membrane currents activated in the plateau range of potentials in cardiac Purkinje fibres. *J Physiol* **200,** 205–231.

Noda M, Ikeda T, Suzuki H, Takeshima H, Takahashi T, Kuno M & Numa S (1986). Expression of functional sodium channels from cloned cDNA. *Nature* **322,** 826–828.

Noda M, Shimizu S, Tanabe T, Takai T, Kayano T, Ikeda T, Takahashi H, Nakayama H, Kanaoka Y & Minamino N (1984). Primary structure of Electrophorus electricus sodium channel deduced from cDNA sequence. *Nature* **312,** 121–127.

Noma A & Irisawa H (1976). Membrane currents in the rabbit sinoatrial node cell as studied by the double microelectrode method. *Pflügers Arch Eur J Physiol* **364,** 45–52.

Nomura K, Hiyama TY, Sakuta H, Matsuda T, Lin CH, Kobayashi K, Kobayashi K, Kuwaki T, Takahashi K, Matsui S & Noda M (2019). [Na + ] Increases in Body Fluids Sensed by Central Na x Induce Sympathetically Mediated Blood Pressure Elevations via H + -Dependent Activation of ASIC1a. *Neuron* **101,** 60-75.e6.

North RA & Surprenant A (2000). Pharmacology of cloned P2X receptors. *Annu Rev Pharmacol Toxicol* **40,** 563–580.

Notomi T & Shigemoto R (2004). Immunohistochemical localization of Ih channel subunits, HCN1–4, in the rat brain. J Comp Neurol 471, 241–276.

Nowycky MC, Fox AP & Tsien RW (1985). Three types of neuronal calcium channel with different calcium agonist sensitivity. *Nature* **316,** 440–443.

Nunes VW, Fortes ZB, Nigro D, Carvalho MHC, Zorn TMT & Scivoletto R (2000). Influence of enalapril on the endothelial function of DOCA-salt hypertensive rats. *Gen Pharmacol* **34,** 117–125.

O'Connell TD, Jensen BC, Baker AJ & Simpson PC (2013). Cardiac alpha1-adrenergic receptors: novel aspects of expression, signaling mechanisms, physiologic function, and clinical importance. *Pharmacol Rev* **66,** 308–333.

O'Leary T, van Rossum MCW & Wyllie DJA (2010). Homeostasis of intrinsic excitability in hippocampal neurones: Dynamics and mechanism of the response to chronic depolarization. *J Physiol* **588,** 157–170.

Ogawa K, Hirooka Y, Kishi T & Sunagawa K (2011). Brain AT1 receptor activates the sympathetic nervous system through toll-like receptor 4 in mice with heart failure. *J Cardiovasc Pharmacol* **58,** 543–549.

Oh GC & Cho H-J (2020). Blood pressure and heart failure. *Clin Hypertens* **26,** 1.

Okabe K, Kitamura K & Kuriyama H (1988). The existence of a highly tetrodotoxin sensitive Na channel in freshly dispersed smooth muscle cells of the rabbit main pulmonary artery. *Pflügers Arch* **411,** 423–428.

Okamoto K & Aoki K (1963). Development of a strain of spontaneously hypertensive rats. *Jpn Circ J* **27,** 282–293.

Okamoto N, Hori S, Akazawa C, Hayashi Y, Shigemoto R, Mizuno N & Nakanishi S (1994). Molecular characterization of a new metabotropic glutamate receptor mGluR7 coupled to inhibitory cyclic AMP signal transduction. *J Biol Chem* **269,** 1231–1236.

Oliet SHR & Bourque C (1993). Mechanosensitive channels transduce osmosensitivity in supraoptic neurons. *Nature* **364,** 341–343.

Oliva C, Cohen IS & Mathias RT (1988). Calculation of time constants for intracellular diffusion in whole cell patch clamp configuration. *Biophys J* **54,** 791–799.

Ong J, Kinsman BJ, Sved AF, Rush BM, Tan RJ, Carattino MD & Stocker SD (2019). Renal sensory nerves increase sympathetic nerve activity and blood pressure in 2-kidney 1-clip

hypertensive mice. *J Neurophysiol* **122,** 358–367.

Orimo S, Uchihara T, Kanazawa T, Itoh Y, Wakabayashi K, Kakita A & Takahashi H (2011). Unmyelinated axons are more vulnerable to degeneration than myelinated axons of the cardiac nerve in Parkinson's disease. *Neuropathol Appl Neurobiol* **37,** 791–802.

Osborn JL, Plato CF, Gordin E & He XR (1997). LONG-TERM INCREASES IN RENAL SYMPATHETIC NERVE ACTIVITY AND HYPERTENSION. *Clin Exp Pharmacol Physiol* **24,** 72–76.

Pachernegg S, Münster Y, Muth-Köhne E, Fuhrmann G & Hollmann M (2015). GluA2 is rapidly edited at the Q/R site during neural differentiation in vitro . *Front Cell Neurosci* **9,** 69. Available at: https://www.frontiersin.org/article/10.3389/fncel.2015.00069.

Pahor M, Giudice P Lo, Bernabei R, Di Gennaro M, Pacifici L, Ramacci MT & Carbonin PU (1989). Age-related increase in the incidence of ventricular arrhythmias in isolated hearts from spontaneously hypertensive rats. *Cardiovasc drugs Ther* **3,** 163–169.

Paál B, Oór Á, Szücs G, Kovács I & Rusznák Z (2003). HCN channels contribute to the intrinsic activity of cochlear pyramidal cells. Cell Mol Life Sci C 60, 2189–2199.

Pan X, Ikeda SR & Lewis DL (1998). SR 141716A Acts as an Inverse Agonist to Increase Neuronal Voltage-Dependent Ca<sup>2+</sup> Currents by Reversal of Tonic CB1 Cannabinoid Receptor Activity. *Mol Pharmacol* **54,** 1064 LP – 1072.

Pan Z, Selyanko AA, Hadley JK, Brown DA, Dixon JE & McKinnon D (2001). Alternative splicing of KCNQ2 potassium channel transcripts contributes to the functional diversity of M-currents. *J Physiol* **531,** 347–358.

Panula P, Chazot PL, Cowart M, Gutzmer R, Leurs R, Liu WLS, Stark H, Thurmond RL & Haas HL (2015). International Union of Basic and Clinical Pharmacology. XCVIII. Histamine Receptors. *Pharmacol Rev* **67,** 601–655.

Papahadjopoulos D, Nir S & Ohki S (1972). Permeability properties of phospholipid membranes: Effect of cholesterol and temperature. *Biochim Biophys Acta - Biomembr* **266,** 561–583.

Parajuli LK, Nakajima C, Kulik A, Matsui K, Schneider T, Shigemoto R & Fukazawa Y (2012). Quantitative regional and ultra structural localization of the Ca v2.3 subunit of R-type calcium channel in mouse brain. *J Neurosci* **32,** 13555–13567.

Paredes RM, Etzler JC, Watts LT, Zheng W & Lechleiter JD (2008). Chemical calcium indicators. *Methods* **46,** 143–151.

Park D & Dunlap K (1998). Dynamic Regulation of Calcium Influx by G-Proteins, Action Potential Waveform, and Neuronal Firing Frequency. *J Neurosci* **18,** 6757 LP – 6766.

Parker JP, F. SL, A. KG, Jens J, R. SJ, A. QR & R. SD (2001). Altered Autonomic Support of Arterial Blood Pressure With Age in Healthy Men. *Circulation* **104,** 2424–2429.

Parkington HC & Coleman HA (2012). Intracellular 'Sharp' Microelectrode Recording. *Essent Guid to Read Biomed Pap*77–84. Available at: https://doi.org/10.1002/9781118402184.ch9.

Parsons RL & Merriam LA (1993). Galanin activates an inwardly rectifying potassium conductance in mudpuppy atrial myocytes. *Pflügers Arch* **422,** 410–412.

Patro R, Duggal G, Love MI, Irizarry RA & Kingsford C (2017). Salmon provides fast and bias-aware quantification of transcript expression. *Nat Methods* **14,** 417–419.

Patton DE, Silva T & Bezanilla F (1997). RNA editing generates a diverse array of transcripts encoding squid Kv2 K+ channels with altered functional properties. *Neuron* **19,** 711–722.

Pawloski-Dahm CM & Gordon FJ (1993). Increased dietary salt sensitizes vasomotor neurons of the rostral ventrolateral medulla. *Hypertension* **22,** 929–933.

Pearson K (1901). LIII. On lines and planes of closest fit to systems of points in space . *London, Edinburgh, Dublin Philos Mag J Sci* **2,** 559–572.

Peet MM & Isberg EM (1949). The Treatment of Hypertensive Cerebrovascular Disease by Splanchnicectomy. *N Engl J Med* **240,** 319–323.

Peng YJ, Yuan G, Khan S, Nanduri J, Makarenko V V., Reddy VD, Vasavda C, Kumar GK, Semenza GL & Prabhakar NR (2014). Regulation of hypoxia-inducible factor-α isoforms and redox state by carotid body neural activity in rats. *J Physiol* **592,** 3841–3858.

Penney DG & Robinson MC (1990). Effects of verapamil and carbon monoxide on blood pressure and heart mass in the spontaneously hypertensive rat. *Eur J Pharmacol* **182,** 29–36.

Perez-Reyes E (2003). Molecular physiology of low-voltage-activated T-type calcium channels. *Physiol Rev* **83,** 117–161.

Peters HC, Hu H, Pongs O, Storm JF & Isbrandt D (2005). Conditional transgenic suppression of M channels in mouse brain reveals functions in neuronal excitability, resonance and behavior. *Nat Neurosci* **8,** 51–60.

Pirzgalska RM et al. (2017). Sympathetic neuron-associated macrophages contribute to obesity by importing and metabolizing norepinephrine. *Nat Med* **23,** 1309–1318.

Platoshyn O, Remillard C V, Fantozzi I, Sison T & Yuan JX-J (2005). Identification of functional voltage-gated Na(+) channels in cultured human pulmonary artery smooth muscle cells. *Pflugers Arch* **451,** 380–387.

Potegal M & Myers MM (1989). Spontaneously hypertensive Wistar-derived male rats are more aggressive than those of their normotensive progenitor strain. *Behav Neural Biol* **51,** 247–261.

Poulter NR, Khaw KT, Hopwood BE, Mugambi M, Peart WS, Rose G & Sever PS (1990). The Kenyan Luo migration study: observations on the initiation of a rise in blood pressure. *Br Med J* **300,** 967 LP – 972.

Pumroy RA, Samanta A, Liu Y, Hughes TET, Zhao S, Yudin Y, Rohacs T, Han S & Moiseenkova-Bell VY (2019). Molecular mechanism of TRPV2 channel modulation by cannabidiol ed. Boudker O, Islas LD, Islas LD & Herzik M. *Elife* **8,** e48792.

Puzserova A, Ilovska V, Balis P, Slezak P & Bernatova I (2014). Age-related alterations in endothelial function of femoral artery in young SHR and WKY rats ed. Andriantsitohaina R. *Biomed Res Int* **2014,** 658479.

Qi B, Wei Y, Chen S, Zhou G, Li H, Xu J, Ding Y, Lu X, Zhao L, Zhang F, Chen G, Zhao J & Liu S (2014). Nav1.8 channels in ganglionated plexi modulate atrial fibrillation inducibility. *Cardiovasc Res* **102,** 480–486.

Qian AH, Liu XQ, Yao WY, Wang HY, Sun J, Zhou L & Yuan YZ (2009). Voltage-gated potassium channels in IB4-positive colonic sensory neurons mediate visceral hypersensitivity in the rat. *Am J Gastroenterol* **104,** 2014–2027.

Qian Z, Okuhara D, Abe MK & Rosner MR (1999). Molecular cloning and characterization of a

mitogen-activated protein kinase-associated intracellular chloride channel. *J Biol Chem* **274,** 1621–1627.

Raba M, Palgi J, Lehtivaara M & Arumäe U (2016). Microarray analysis reveals increased transcriptional repression and reduced metabolic activity but not major changes in the core apoptotic machinery during maturation of sympathetic neurons. *Front Cell Neurosci* **10,** 66.

Rae J, Cooper K, Gates P & Watsky M (1991). Low access resistance perforated patch recordings using amphotericin B. *J Neurosci Methods* **37,** 15–26.

Raia Jr JJ, Barone JA, Byerly WG & Lacy CR (1990). Angiotensin-converting enzyme inhibitors: a comparative review. *DICP* **24,** 506–525.

Raidoo DM & Bhoola KD (1997). Kinin receptors on human neurones. *J Neuroimmunol* **77,** 39–44.

Rajendran PS, Challis RC, Fowlkes CC, Hanna P, Tompkins JD, Jordan MC, Hiyari S, Gabris-Weber BA, Greenbaum A, Chan KY, Deverman BE, Münzberg H, Ardell JL, Salama G, Gradinaru V & Shivkumar K (2019). Identification of peripheral neural circuits that regulate heart rate using optogenetic and viral vector strategies. *Nat Commun* **10,** 1944.

Rajesh M, Mukhopadhyay P, Bátkai S, Patel V, Saito K, Matsumoto S, Kashiwaya Y, Horváth B, Mukhopadhyay B, Becker L, Haskó G, Liaudet L, Wink DA, Veves A, Mechoulam R & Pacher P (2010). Cannabidiol attenuates cardiac dysfunction, oxidative stress, fibrosis, and inflammatory and cell death signaling pathways in diabetic cardiomyopathy. *J Am Coll Cardiol* **56,** 2115–2125.

Rall TW & Sutherland EW (1958). Formation of a cyclic adenine ribonucleotide by tissue particles. *J Biol Chem* **232,** 1065–1076.

Rall W (1969). Time constants and electrotonic length of membrane cylinders and neurons. *Biophys J* **9,** 1483–1508.

Ramsey IS, Delling M & Clapham DE (2006). An introduction to TRP channels. *Annu Rev Physiol* **68,** 619–647.

Randall A & Tsien RW (1995). Pharmacological dissection of multiple types of Ca2+ channel currents in rat cerebellar granule neurons. *J Neurosci* **15,** 2995–3012.

Ranjan R, Logette E, Marani M, Herzog M, Tâche V, Scantamburlo E, Buchillier V & Markram H (2019). A Kinetic Map of the Homomeric Voltage-Gated Potassium Channel (Kv) Family . *Front Cell Neurosci* **13,** 358. Available at: https://www.frontiersin.org/article/10.3389/fncel.2019.00358.

Raplee ID, Evsikov A V & Marín de Evsikova C (2019). Aligning the Aligners: Comparison of RNA Sequencing Data Alignment and Gene Expression Quantification Tools for Clinical Breast Cancer Research. *J Pers Med* **9,** 18.

Rapoport RM & Soleimani M (2019). Mechanism of Thiazide Diuretic Arterial Pressure Reduction: The Search Continues . *Front Pharmacol* **10,** 815. Available at: https://www.frontiersin.org/article/10.3389/fphar.2019.00815.

Rapp JP & Dene H (1985). Development and characteristics of inbred strains of Dahl salt-sensitive and salt-resistant rats. *Hypertension* **7,** 340–349.

Ray-Chaudhuri K, Thomaides T, Maule S, Watson L, Lowe S & Mathias CJ (1993). The effect of captopril on the superior mesenteric artery and portal venous blood flow in normal man. *Br J Clin Pharmacol* **35,** 517–524.

Reichard A & Asosingh K (2019). Best Practices for Preparing a Single Cell Suspension from Solid Tissues for Flow Cytometry. *Cytometry A* **95,** 219–226.

Reid JE & Wernisch L (2016). Pseudotime estimation: deconfounding single cell time series. *Bioinformatics* **32,** 2973–2980.

Ren D (2011). Sodium leak channels in neuronal excitability and rhythmic behaviors. *Neuron* **72,** 899–911.

Rettig J, Heinemann SH, Wunder F, Lorra C, Parcej DN, Oliver Dolly J & Pongs O (1994). Inactivation properties of voltage-gated K+ channels altered by presence of β-subunit. *Nature* **369,** 289–294.

Reuter H & Scholz H (1977). The regulation of the calcium conductance of cardiac muscle by adrenaline. *J Physiol* **264,** 49–62.

Ribeiro N, Panizza H do N, dos Santos KM, Ferreira-Neto HC & Antunes VR (2015). Salt-induced sympathoexcitation involves vasopressin V1a receptor activation in the paraventricular nucleus of the hypothalamus. *Am J Physiol - Regul Integr Comp Physiol* **309,** R1369–R1379.

Ricksten S & Thoren P (1980). Reflex inhibition of sympathetic activity during volume load in awake normotensive and spontaneously hypertensive rats. *Acta Physiol Scand* **110,** 77–82.

Rimoldi SF, Scherrer U & Messerli FH (2014). Secondary arterial hypertension: when, who, and how to screen? *Eur Heart J* **35,** 1245–1254.

Rizo J & Xu J (2015). The Synaptic Vesicle Release Machinery. *Annu Rev Biophys* **44,** 339–367.

Robbins J, Marsh SJ & Brown DA (2006). Probing the regulation of M (Kv7) potassium channels in intact neurons with membrane-targeted peptides. *J Neurosci* **26,** 7950–7961.

Robertson WP & Schofield GG (1999). Primary and adaptive changes of A-type K+ currents in sympathetic neurons from hypertensive rats. *Am J Physiol - Regul Integr Comp Physiol* **276,** R1758–R1765.

Rocchini AP, Key J, Bondie D, Chico R, Moorehead C, Katch V & Martin M (1989). The Effect of Weight Loss on the Sensitivity of Blood Pressure to Sodium in Obese Adolescents. *N Engl J Med* **321,** 580–585.

Rocco AG, Palombi D & Raeke D (1995). Anatomy of the lumbar sympathetic chain. *Reg Anesth Pain Med* **20,** 13–19.

Roden DM & Kupershmidt S (1999). From genes to channels: normal mechanisms. *Cardiovasc Res* **42,** 318–326.

Roe MW, Lemasters JJ & Herman B (1990). Assessment of Fura-2 for measurements of cytosolic free calcium. *Cell Calcium* **11,** 63–73.

Romero CA, Orias M & Weir MR (2015). Novel RAAS agonists and antagonists: Clinical applications and controversies. *Nat Rev Endocrinol* **11,** 242–252.

Rose CR & Ransom BR (1997). Regulation of intracellular sodium in cultured rat hippocampal neurones. *J Physiol* **499,** 573–587.

Rose G, Stamler J, Stamler R, Elliott P, Marmot M, Pyorala K, Kesteloot H, Joossens J, Hansson L, Mancia G, Dyer A, Kromhout D, Laaser U & Sans S (1988). Intersalt: An international study of electrolyte excretion and blood pressure. Results for 24 hour urinary sodium and potassium excretion. *Br Med J* **297,** 319–328.

Rosenberg GA & Robertson GL (1987). Mannitol-induced hyperosmolality and cerebrospinal fluid vasopressin in anesthetized cats. *Neurosci Lett* **75,** 60–64.

Rosenthal JJC & Bezanilla F (2002). Extensive editing of mRNAs for the squid delayed rectifier K+ channel regulates subunit tetramerization. *Neuron* **34,** 743–757.

Roth BL, Nakaki T, Chuang D-M & Costa E (1984). Aortic recognition sites for serotonin (5HT) are coupled to phospholipase C and modulate phosphatidylinositol turnover. *Neuropharmacology* **23,** 1223–1225.

Roth GA et al. (2017). Global, Regional, and National Burden of Cardiovascular Diseases for 10 Causes, 1990 to 2015. *J Am Coll Cardiol* **70,** 1–25.

Rothberg BS & Magleby KL (2000). Voltage and Ca2+ Activation of Single Large-Conductance Ca2+-Activated K+ Channels Described by a Two-Tiered Allosteric Gating Mechanism . *J Gen Physiol* **116,** 75–100.

Rotondo F, Butz H, Syro L V., Yousef GM, Di Ieva A, Restrepo LM, Quintanar-Stephano A, Berczi I & Kovacs K (2016). Arginine vasopressin (AVP): a review of its historical perspectives, current research and multifunctional role in the hypothalamo-hypophysial system. *Pituitary* **19,** 345–355.

Roufa D, Bunge MB, Johnson MI & Cornbrooks CJ (1986). Variation in content and function of non-neuronal cells in the outgrowth of sympathetic ganglia from embryos of differing age. *J Neurosci* **6,** 790–802.

Rubinstein JL (2017). Cryo-EM Captures the Dynamics of Ion Channel Opening. *Cell* **168,** 341–343.

Rugiero F, Mistry M, Sage D, Black JA, Waxman SG, Crest M, Clerc N, Delmas P & Gola M (2003). Selective expression of a persistent tetrodotoxin-resistant Na+ current and NaV1.9 subunit in myenteric sensory neurons. *J Neurosci* **23,** 2715–2725.

Ruit KG, Osborne PA, Schmidt RE, Johnson EM & Snider WD (1990). Nerve growth factor regulates sympathetic ganglion cell morphology and survival in the adult mouse. *J Neurosci* **10,** 2412 LP – 2419.

Rule (2011). Association of kidney function and metabolic risk factors with density glomeruli on renal biopsy samples from living donors (Mayo Clinic Proceedings (2011) 86, 4 (282-290)). In *Mayo Clinic Proceedings*, p. 469. Elsevier.

Ruppersberg JP, Schröter KH, Sakmann B, Stocker M, Sewing S & Pongs O (1990). Heteromultimeric channels formed by rat brain potassium-channel proteins. *Nature* **345,** 535–537.

Rush AM, Dib-Hajj SD, Liu S, Cummins TR, Black JA & Waxman SG (2006). A single sodium channel mutation produces hyper- or hypoexcitability in different types of neurons. *Proc Natl Acad Sci U S A* **103,** 8245–8250.

Russ R, Abdel-Rahman ARA & Wooles WR (1991). Role of the sympathetic nervous system in ethanol-induced hypertension in rats. *Alcohol* **8,** 301–307.

Sabatini BL & Regehr WG (1996). Timing of neurotransmission at fast synapses in the mammalian brain. *Nature* **384,** 170–172.

Sabatini BL & Regehr WG (1997). Control of Neurotransmitter Release by Presynaptic Waveform at the Granule Cell to Purkinje Cell Synapse. *J Neurosci* **17,** 3425 LP – 3435.

Sacchi O, Rossi ML, Canella R & Fesce R (1999). Participation of a chloride conductance in the

subthreshold behavior of the rat sympathetic neuron. *J Neurophysiol* **82,** 1662–1675.

Sacchi O, Rossi ML, Canella R & Fesce R (2003). Voltage- and activity-dependent chloride conductance controls the resting status of the intact rat sympathetic neuron. *J Neurophysiol* **90,** 712–722.

Saelens W, Cannoodt R, Todorov H & Saeys Y (2019). A comparison of single-cell trajectory inference methods. *Nat Biotechnol* **37,** 547–554.

Safronov B V. & Vogel W (1996). Properties and functions of Na+-activated K+ channels in the soma of rat motoneurones. *J Physiol* **497,** 727–734.

Sagvolden T, Metzger MA, Schiorbeck HK, Rugland A-L, Spinnangr I & Sagvolden G (1992). The spontaneously hypertensive rat (SHR) as an animal model of childhood hyperactivity (ADHD): changed reactivity to reinforcers and to psychomotor stimulants. *Behav Neural Biol* **58,** 103–112.

Sah DWY & Matsumoto SG (1987). Evidence for serotonin synthesis, uptake, and release in dissociated rat sympathetic neurons in culture. *J Neurosci* **7,** 391–399.

Saiki RK, Gelfand DH, Stoffel S, Scharf SJ, Higuchi R, Horn GT, Mullis KB & Erlich HA (1988). Primer-directed enzymatic amplification of DNA with a thermostable DNA polymerase. *Science (80-)* **239,** 487–491.

Sakmann B & Neher E (1984). Patch Clamp Techniques for Studying Ionic Channels in Excitable Membranes. *Annu Rev Physiol* **46,** 455–472.

Saleem F, Rowe ICM & Shipston MJ (2009). Characterization of BK channel splice variants using membrane potential dyes. *Br J Pharmacol* **156,** 143–152.

Saleh SN, Albert AP, Peppiatt CM & Large WA (2006). Angiotensin II activates two cation conductances with distinct TRPC1 and TRPC6 channel properties in rabbit mesenteric artery myocytes. *J Physiol* **577,** 479–495.

Sandhu M, Touma AM, Dysthe M, Sadler F, Sivaramakrishnan S & Vaidehi N (2019). Conformational plasticity of the intracellular cavity of GPCR−G-protein complexes leads to G-protein promiscuity and selectivity. *Proc Natl Acad Sci* **116,** 11956 LP – 11965.

Sanguinetti MC, Curran ME, Zou A, Shen J, Spector PS, Atkinson DL & Keating MT (1996). Coassembly of K(V)LQT1 and minK (IsK) proteins to form cardiac I(Ks) potassium channel. *Nature* **384,** 80–83.

Santini E & Porter JT (2010). M-type potassium channels modulate the intrinsic excitability of infralimbic neurons and regulate fear expression and extinction. *J Neurosci* **30,** 12379–12386.

Santoni G & Amantini C (2019). The Transient Receptor Potential Vanilloid Type-2(TRPV2) Ion Channels in Neurogenesis andGliomagenesis: Cross-Talk between TranscriptionFactors and Signaling Molecules. *Cancers (Basel)* **11,** 322.

Santoro B, Liu DT, Yao H, Bartsch D, Kandel ER, Siegelbaum SA & Tibbs GR (1998). Identification of a gene encoding a hyperpolarization-activated pacemaker channel of brain. *Cell* **93,** 717–729.

Sarantopoulos C, McCallum JB, Kwok W-M & Hogan Q (2004). β-escin diminishes voltage-gated calcium current rundown in perforated patch-clamp recordings from rat primary afferent neurons. *J Neurosci Methods* **139,** 61–68.

Sata Y, Head GA, Denton K, May CN & Schlaich MP (2018). Role of the sympathetic nervous system and its modulation in renal hypertension. *Front Med* **5,** 82.

Sather WA & McCleskey EW (2003). Permeation and Selectivity in Calcium Channels. *Annu Rev Physiol* **65,** 133–159.

Scala F, Kobak D, Bernabucci M, Bernaerts Y, Cadwell CR, Castro JR, Hartmanis L, Jiang X, Laturnus S, Miranda E, Mulherkar S, Tan ZH, Yao Z, Zeng H, Sandberg R, Berens P & Tolias AS (2020). Phenotypic variation of transcriptomic cell types in mouse motor cortex. *Nature*; DOI: 10.1038/s41586-020-2907-3.

Schatzmann HJ & Räss B (1965). Inhibition of the active Na-K-transport and Na-K-activated membrane ATP-ase of erythrocyte stroma by ouabain. *Helv Physiol Pharmacol Acta* **65,** C47-9.

Schaum N et al. (2018). Single-cell transcriptomics of 20 mouse organs creates a Tabula Muris. *Nature* **562,** 367–372.

Schenzer A, Friedrich T, Pusch M, Saftig P, Jentsch TJ, Grötzinger J & Schwake M (2005). Molecular determinants of KCNQ (KV7) K+ channel sensitivity to the anticonvulsant retigabine. *J Neurosci* **25,** 5051–5060.

Schikorski T & Stevens CF (1997). Quantitative ultrastructural analysis of hippocampal excitatory synapses. *J Neurosci* **17,** 5858–5867.

Schindl R, Fritsch R, Jardin I, Frischauf I, Kahr H, Muik M, Riedl MC, Groschner K & Romanin C (2012). Canonical transient receptor potential (TRPC) 1 acts as a negative regulator for vanilloid TRPV6-mediated Ca2+ influx. *J Biol Chem* **287,** 35612–35620.

Schlaich MP, Kaye DM, Lambert E, Sommerville M, Socratous F & Esler MD (2003). Relation between cardiac sympathetic activity and hypertensive left ventricular hypertrophy. *Circulation* **108,** 560–565.

Schlaich MP, Lambert E, Kaye DM, Krozowski Z, Campbell DJ, Lambert G, Hastings J, Aggarwal A & Esler MD (2004). Sympathetic Augmentation in Hypertension: Role of Nerve Firing, Norepinephrine Reuptake, and Angiotensin Neuromodulation. *Hypertension* **43,** 169–175.

Schramm LP & Chornoboy ES (1982). Sympathetic activity in spontaneously hypertensive rats after spinal transection. *Am J Physiol Integr Comp Physiol* **243,** R506–R511.

Schroeder BC, Cheng T, Jan YN & Jan LY (2008). Expression Cloning of TMEM16A as a Calcium-Activated Chloride Channel Subunit. *Cell* **134,** 1019–1029.

Schroeder BC, Hechenberger M, Weinreich F, Kubisch C & Jentsch TJ (2000). KCNQ5, a Novel Potassium Channel Broadly Expressed in Brain, Mediates M-type Currents. *J Biol Chem* **275,** 24089–24095.

Schuetze SM (1983). The discovery of the action potential. *Trends Neurosci* **6,** 164–168.

Schulte G, Robertson B, Fredholm BB, DeLander GE, Shortland P & Molander C (2003). Distribution of antinociceptive adenosine a1 receptors in the spinal cord dorsal horn, and relationship to primary afferents and neuronal subpopulations. *Neuroscience* **121,** 907–916.

Schulz DJ, Goaillard JM & Marder E (2006). Variable channel expression in identified single and electrically coupled neurons in different animals. *Nat Neurosci* **9,** 356–362.

Schumacher MA (2010). Transient receptor potential channels in pain and inflammation: Therapeutic opportunities. *Pain Pract* **10,** 185–200.

Schweda F (2015). Salt feedback on the renin-angiotensin-aldosterone system. *Pflugers Arch Eur J Physiol* **467,** 565–576.

Schwindt PC, Spain WJ & Crill WE (1989). Long-lasting reduction of excitability by a sodium-dependent potassium current in cat neocortical neurons. *J Neurophysiol* **61,** 233–244.

Seagard JL, F van BJ, Dean C, Hopp FA, Gallenberg LA & Kampine JP (1990). Firing characteristics of single-fiber carotid sinus baroreceptors. *Circ Res* **66,** 1499–1509.

Segev A, Garcia-Oscos F & Kourrich S (2016). Whole-cell Patch-clamp Recordings in Brain Slices. *J Vis Exp*54024.

Selyanko AA & Brown DA (1996). Intracellular calcium directly inhibits potassium M channels in excised membrane patches from rat sympathetic neurons. *Neuron* **16,** 151–162.

Selyanko AA, Hadley JK, Wood IC, Abogadie FC, Jentsch TJ & Brown DA (2000). Inhibition of KCNQ1-4 potassium channels expressed in mammalian cells via M1 muscarinic acetylcholine receptors. *J Physiol* **522,** 349–355.

Seo Y, Lee HK, Park J, Jeon DK, Jo S, Jo M & Namkung W (2016). Ani9, a novel potent small-molecule ANO1 inhibitor with negligible effect on ANO2. *PLoS One* **11,** e0155771.

Shafi S, Welzel D, Weidinger G, Brown J & Born GVR (2000). Effect of Reserpine Treatment on Low-Density Lipoproteins in Arterial Wall and Internal Organs of Rats. *J Cardiovasc Pharmacol*. Available at: https://journals.lww.com/cardiovascularpharm/Fulltext/2000/05000/Effect_of_Reserpine_Treatment_on_Low_Density.2.aspx.

Shah MM (2014). Cortical HCN channels: Function, trafficking and plasticity. *J Physiol* **592,** 2711–2719.

Shah MM, Migliore M, Valencia I, Cooper EC & Brown DA (2008). Functional significance of axonal Kv7 channels in hippocampal pyramidal neurons. *Proc Natl Acad Sci* **105,** 7869–7874.

Shah MM, Mistry M, Marsh SJ, Brown DA & Delmas P (2002). Molecular correlates of the M-current in cultured rat hippocampal neurons. *J Physiol* **544,** 29–37.

Shamon SD & Perez MI (2016). Blood pressure-lowering efficacy of reserpine for primary hypertension. *Cochrane Database Syst Rev*; DOI: 10.1002/14651858.CD007655.pub3.

Shanker S, Paulson A, Edenberg HJ, Peak A, Perera A, Alekseyev YO, Beckloff N, Bivens NJ, Donnelly R & Gillaspy AF (2015). Evaluation of commercially available RNA amplification kits for RNA sequencing using very low input amounts of total RNA. *J Biomol Tech JBT* **26,** 4.

Shanks J, Mane S, Ryan R & Paterson DJ (2013). Ganglion-specific impairment of the norepinephrine transporter in the hypertensive rat. *Hypertension* **61,** 187–193.

Shapiro MS, Wollmuth LP & Hille B (1994). Angiotensin II inhibits calcium and M current channels in rat sympathetic neurons via G proteins. *Neuron* **12,** 1319–1329.

Sharif-Naeini R, Ciura S, Zhang Z & Bourque CW (2008). Contribution of TRPV channels to osmosensory transduction, thirst, and vasopressin release. *Kidney Int* **73,** 811–815.

Sharp AA, Abbott LF & Marder E (1992). Artificial electrical synapses in oscillatory networks. *J Neurophysiol* **67,** 1691–1694.

Shcherbakova OG, Hurt CM, Xiang Y, Dell'Acqua ML, Zhang Q, Tsien RW & Kobilka BK (2007). Organization of beta-adrenoceptor signaling compartments by sympathetic innervation of

cardiac myocytes. *J Cell Biol* **176,** 521–533.

Sheng Y & Zhu L (2018). The crosstalk between autonomic nervous system and blood vessels. *Int J Physiol Pathophysiol Pharmacol* **10,** 17–28.

Shi P, Martinez MA, Calderon AS, Chen Q, Cunningham JT & Toney GM (2008). Intra-carotid hyperosmotic stimulation increases Fos staining in forebrain organum vasculosum laminae terminalis neurones that project to the hypothalamic paraventricular nucleus. *J Physiol* **586,** 5231–5245.

Shi P, Stocker SD & Toney GM (2007). Organum vasculosum laminae terminalis contributes to increased sympathetic nerve activity induced by central hyperosmolality. *Am J Physiol - Regul Integr Comp Physiol* **293,** R2279–R2289.

Shughrue PJ, Ky B & Austin CP (2003). Localization of B1 bradykinin receptor mRNA in the primate brain and spinal cord: An in situ hybridization study. *J Comp Neurol* **465,** 372–384.

Sigworth FJ (1995). Electronic design of the patch clamp. In *Single-channel recording*, pp. 95–127. Springer.

Sikora KM, Kullmann PHM & Horn JP (2017). Differential gene expression in populations of sympathetic neurons purified from a neuropeptide Y reporter mouse. *bioRxiv*; DOI: 10.1101/128074. Available at: http://europepmc.org/abstract/PPR/PPR28785.

Silver RB, Poonwasi KS, Seyedi N, Wilson SJ, Lovenberg TW & Levi R (2002). Decreased intracellular calcium mediates the histamine H3-receptor-induced attenuation of norepinephrine exocytosis from cardiac sympathetic nerve endings. *Proc Natl Acad Sci U S A* **99,** 501–506.

Sim JJ, Bhandari SK, Shi J, Liu ILA, Calhoun DA, McGlynn EA, Kalantar-Zadeh K & Jacobsen SJ (2013). Characteristics of resistant hypertension in a large, ethnically diverse hypertension population of an integrated health system. *Mayo Clin Proc* **88,** 1099–1107.

Simchon S, Manger WM, Carlin RD, Peeters LL, Rodriguez J, Batista D, Brown T, Merchant NB, Jan K-M & Chien S (1989). Salt-Induced Hypertension in Dahi Salt-Sensitive Rats.

Simeone TA, Rho JM & Baram TZ (2005). Single channel properties of hyperpolarization-activated cation currents in acutely dissociated rat hippocampal neurones. *J Physiol* **568,** 371–380.

Simmonds SS, Lay J & Stocker SD (2014). Dietary salt intake exaggerates sympathetic reflexes and increases blood pressure variability in normotensive rats. *Hypertension* **64,** 583–589.

Simms AE, Paton JFR, Pickering AE & Allen AM (2009). Amplified respiratory-sympathetic coupling in the spontaneously hypertensive rat: Does it contribute to hypertension? *J Physiol* **587,** 597–610.

Sinnott S-J, Douglas IJ, Smeeth L, Williamson E & Tomlinson LA (2020). First line drug treatment for hypertension and reductions in blood pressure according to age and ethnicity: cohort study in UK primary care. *BMJ* **371,** m4080.

Skou JC (1957). The influence of some cations on an adenosine triphosphatase from peripheral nerves. *Biochim Biophys Acta* **23,** 394–401.

Slater CR (2017). The Structure of Human Neuromuscular Junctions: Some Unanswered Molecular Questions. *Int J Mol Sci* **18,** 2183.

Smetters D, Majewska A & Yuste R (1999). Detecting action potentials in neuronal populations with calcium imaging. *Methods* **18,** 215–221.

Smirk FH & Hall WH (1958). Inherited hypertension in rats. *Nature* **182,** 727–728.

Smith JR, Hayman GT, Wang SJ, Laulederkind SJF, Hoffman MJ, Kaldunski ML, Tutaj M, Thota J, Nalabolu HS, Ellanki SLR, Tutaj MA, De Pons JL, Kwitek AE, Dwinell MR & Shimoyama ME (2020). The Year of the Rat: The Rat Genome Database at 20: A multi-species knowledgebase and analysis platform. *Nucleic Acids Res* **48,** D731–D742.

Smith MR, Smith RD, Plummer NW, Meisler MH & Goldin AL (1998). Functional analysis of the mouse Scn8a sodium channel. *J Neurosci* **18,** 6093–6102.

Smith NJ, Hone AJ, Memon T, Bossi S, Smith TE, McIntosh JM, Olivera BM & Teichert RW (2013). Comparative functional expression of nAChR subtypes in rodent DRG neurons. *Front Cell Neurosci* **7,** 225.

Smith SJ, MacDermott AB & Weight FF (1983). Detection of intracellular Ca2+ transients in sympathetic neurones using arsenazo III. *Nature* **304,** 350–352.

Smits JF & Brody MJ (1984). Activation of afferent renal nerves by intrarenal bradykinin in conscious rats. *Am J Physiol Integr Comp Physiol* **247,** R1003–R1008.

Soh H & Park CS (2001). Inwardly rectifying current-voltage relationship of small-conductance Ca2+-activated K+ channels rendered by intracellular divalent cation blockade. *Biophys J* **80,** 2207–2215.

Söllner T, Bennett MK, Whiteheart SW, Scheller RH & Rothman JE (1993*a*). A protein assembly-disassembly pathway in vitro that may correspond to sequential steps of synaptic vesicle docking, activation, and fusion. *Cell* **75,** 409–418.

Söllner T, Whiteheart SW, Brunner M, Erdjument-Bromage H, Geromanos S, Tempst P & Rothman JE (1993*b*). SNAP receptors implicated in vesicle targeting and fusion. *Nature* **362,** 318–324.

Sommer B, Köhler M, Sprengel R & Seeburg PH (1991). RNA editing in brain controls a determinant of ion flow in glutamate-gated channels. *Cell* **67,** 11–19.

Soneson C, Love MI & Robinson MD (2016). Differential analyses for RNA-seq: Transcript-level estimates improve gene-level inferences [version 2; referees: 2 approved]. *F1000Research* **4,** 1521.

Spruill TM (2010). Chronic psychosocial stress and hypertension. *Curr Hypertens Rep* **12,** 10–16.

Spruston N & Johnston D (1992). Perforated patch-clamp analysis of the passive membrane properties of three classes of hippocampal neurons. *J Neurophysiol* **67,** 508–529.

Stanley CP, Hind WH & O'Sullivan SE (2013). Is the cardiovascular system a therapeutic target for cannabidiol? *Br J Clin Pharmacol* **75,** 313–322.

Steen KH, Steen AE & Reeh PW (1995). A dominant role of acid pH in inflammatory excitation and sensitization of nociceptors in rat skin, in vitro. *J Neurosci* **15,** 3982–3989.

Steinberg SF, Bilezikian JP & Al-Awqati Q (1987). Fura-2 fluorescence is localized to mitochondria in endothelial cells. *Am J Physiol Physiol* **253,** C744–C747.

Steinfath M, Chen YY, Lavický J, Magnussen O, Nose M, Rosswag S, Schmitz W & Scholz H (1992). Cardiac alpha 1-adrenoceptor densities in different mammalian species. *Br J Pharmacol* **107,** 185–188.

Sterratt DC (2014). Q10: The Effect of Temperature on Ion Channel Kinetics. In *Encyclopedia of Computational Neuroscience*, ed. Jaeger D & Jung R, pp. 1–3. Springer New York, New York,

NY. Available at: https://doi.org/10.1007/978-1-4614-7320-6_236-1.

Stieber J, Stöckl G, Herrmann S, Hassfurth B & Hofmann F (2005). Functional expression of the human HCN3 channel. *J Biol Chem* **280,** 34635–34643.

Stimberg M, Brette R & Goodman DFM (2019). Brian 2, an intuitive and efficient neural simulator ed. Skinner FK, Calabrese RL, Skinner FK, Zeldenrust F & Gerkin RC. *Elife* **8,** e47314.

Stocker M (2004). Ca2+-activated K+ channels: Molecular determinants and function of the SK family. *Nat Rev Neurosci* **5,** 758–770.

Stöhr H, Heisig JB, Benz PM, Schöberl S, Milenkovic VM, Strauss O, Aartsen WM, Wijnholds J, Weber BHF & Schulz HL (2009). TMEM16B, a novel protein with calcium-dependent chloride channel activity, associates with a presynaptic protein complex in photoreceptor terminals. *J Neurosci* **29,** 6809–6818.

Stojilkovic SS (2012). Molecular mechanisms of pituitary endocrine cell calcium handling. *Cell Calcium* **51,** 212–221.

Stone AJ, Kim JS, Yamauchi K, Ruiz-Velasco V & Kaufman MP (2013). Attenuation of autonomic reflexes by A803467 may not be solely caused by blockade of NaV 1.8 channels. *Neurosci Lett* **543,** 177–182.

Stout AK & Reynolds IJ (1999). High-affinity calcium indicators underestimate increases in intracellular calcium concentrations associated with excitotoxic glutamate stimulations. *Neuroscience* **89,** 91–100.

Street K, Risso D, Fletcher RB, Das D, Ngai J, Yosef N, Purdom E & Dudoit S (2018). Slingshot: Cell lineage and pseudotime inference for single-cell transcriptomics. *BMC Genomics* **19,** 477.

Stroud DM, Yang T, Bersell K, Kryshtal DO, Nagao S, Shaffer C, Short L, Hall L, Atack TC, Zhang W, Knollmann BC, Baudenbacher F & Roden DM (2016). Contrasting Nav1.8 activity in Scn10a-/- ventricular myocytes and the intact heart. *J Am Heart Assoc* **5,** e002946.

Stuart T, Butler A, Hoffman P, Hafemeister C, Papalexi E, Mauck WM, Hao Y, Stoeckius M, Smibert P & Satija R (2019). Comprehensive Integration of Single-Cell Data. *Cell* **177,** 1888-1902.e21.

Su C, Bevan JA & Burnstock G (1971). [3H] adenosine triphosphate: release during stimulation of enteric nerves. *Science (80- )* **173,** 336–338.

Suchyna TM, Markin VS & Sachs F (2009). Biophysics and structure of the patch and the gigaseal. *Biophys J* **97,** 738–747.

Südhof TC (2013). Neurotransmitter release: the last millisecond in the life of a synaptic vesicle. *Neuron* **80,** 675–690.

Suh BC & Hille B (2002). Recovery from muscarinic modulation of M current channels requires phosphatidylinositol 4,5-bisphosphate synthesis. *Neuron* **35,** 507–520.

Suh BC, Inoue T, Meyer T & Hille B (2006). Rapid chemically induced changes of PtdIns(4,5)P2 gate KCNQ ion channels. *Science (80- )* **314,** 1454–1457.

Sun XP, Yazejian B & Grinnell AD (2004). Electrophysiological properties of BK channels in Xenopus motor nerve terminals. *J Physiol* **557,** 207–228.

Sutherland EW, Robison GA & Butcher RW (1968). Some Aspects of the Biological Role of Adenosine 3',5'-monophosphate (Cyclic AMP). *Circulation* **37,** 279–306.

Sutton RB, Fasshauer D, Jahn R & Brunger AT (1998). Crystal structure of a SNARE complex

involved in synaptic exocytosis at 2.4 Å resolution. *Nature* **395,** 347–353.

Swanson GT, Kamboj SK & Cull-Candy SG (1997). Single-channel properties of recombinant AMPA receptors depend on RNA editing, splice variation, and subunit composition. *J Neurosci* **17,** 58–69.

Taanman J-W (1999). The mitochondrial genome: structure, transcription, translation and replication. *Biochim Biophys Acta - Bioenerg* **1410,** 103–123.

Tabei R, Spector S, Louis WJ & Sjoerdsma A (1970). Effects of antihypertensive drugs in the spontaneously hypertensive rat. *Clin Pharmacol Ther* **11,** 269–274.

Takahashi M, Takeda S, Kurokawa S, Kubo T, Fukuda N & Izumi T (2003). **Cyclic GMP Production by ANP, BNP, and NO during Worsening and Improvement of Chronic Heart Failure**. *Jpn Heart J* **44,** 713–724.

Takahashi Y, Watanabe H, Murakami M, Ohba T, Radovanovic M, Ono K, Iijima T & Ito H (2007). Involvement of transient receptor potential canonical 1 (TRPC1) in angiotensin II-induced vascular smooth muscle cell hypertrophy. *Atherosclerosis* **195,** 287–296.

Takeda K & Buñag RD (1980). Augmented sympathetic nerve activity and pressor responsiveness in DOCA hypertensive rats. *Hypertension* **2,** 97–101.

Takeda M, Takahashi M, Nasu M & Matsumoto S (2011). Peripheral inflammation suppresses inward rectifying potassium currents of satellite glial cells in the trigeminal ganglia. *Pain* **152,** 2147–2156.

Takeuchi A, Moriguchi H, Kotani K, Miwa K, Lee JK, Noshiro M & Jimbo Y (2009). Development of semi-separated co-culture system of sympathetic neuron and cardiomyocyte. *Proc 31st Annu Int Conf IEEE Eng Med Biol Soc Eng Futur Biomed EMBC 2009* **129,** 1832–1835.

Takeuchi A, Nakafutami S, Tani H, Mori M, Takayama Y, Moriguchi H, Kotani K, Miwa K, Lee JK, Noshiro M & Jimbo Y (2011). Device for co-culture of sympathetic neurons and cardiomyocytes using microfabrication. *Lab Chip* **11,** 2268–2275.

Tang FR, Tan CK & Ling EA (1995). An ultrastructural study of the sympathetic preganglionic neurons that innervate the superior cervical ganglion in spontaneously hypertensive rats and Wistar-Kyoto rats. *J Hirnforsch* **36,** 411–420.

Tang X, Huang Y, Lei J, Luo H & Zhu X (2019). The single-cell sequencing: New developments and medical applications. *Cell Biosci* **9,** 53.

Tapia L, Kuryatov A & Lindstrom J (2007). Ca2+ permeability of the (α4) 3 (β2) 2 stoichiometry greatly exceeds that of (α4) 2 (β2) 3 human acetylcholine receptors. *Mol Pharmacol* **71,** 769–776.

Taylor SC, Nadeau K, Abbasi M, Lachance C, Nguyen M & Fenrich J (2019). The Ultimate qPCR Experiment: Producing Publication Quality, Reproducible Data the First Time. *Trends Biotechnol* **37,** 761–774.

Teiwes J & Toto RD (2007). Epithelial Sodium Channel Inhibition in Cardiovascular Disease. A Potential Role for Amiloride. *Am J Hypertens* **20,** 109–117.

Tenneti L, Gibbons SJ & Talamo BR (1998). Expression and trans-synaptic regulation of P(2x4) and P(2z) receptors for extracellular ATP in parotid acinar cells: Effects of parasympathetic denervation. *J Biol Chem* **273,** 26799–26808.

Terashima T, Xu Q, Yamaguchi S & Yaksh TL (2013). Intrathecal P/Q- and R-type calcium channel

blockade of spinal substance P release and c-Fos expression. *Neuropharmacology* **75,** 1–8.

Thompson SH (1977). Three pharmacologically distinct potassium channels in molluscan neurones. *J Physiol* **265,** 465–488.

Thoren P & Ricksten SE (1979). Recordings of renal and splanchnic sympathetic nervous activity in normotensive and spontaneously hypertensive rats. *Clin Sci* **57,** 197–199.

Thurbon D, Lüscher H-R, Hofstetter T & Redman SJ (1998). Passive electrical properties of ventral horn neurons in rat spinal cord slices. *J Neurophysiol* **79,** 2485–2502.

Tien J, Peters CJ, Wong XM, Cheng T, Jan YN, Jan LY & Yang H (2014). A comprehensive search for calcium binding sites critical for TMEM16A calcium-activated chloride channel activity ed. Aldrich R. *Elife* **3,** e02772.

Toledo-Aral JJ, Moss BL, He ZJ, Koszowski AG, Whisenand T, Levinson SR, Wolf JJ, Silos-Santiago I, Halegoua S & Mandel G (1997). Identification of PN1, a predominant voltage-dependent sodium channel expressed principally in peripheral neurons. *Proc Natl Acad Sci U S A* **94,** 1527–1532.

Trebak M, Lemonnier L, Smyth JT, Vazquez G & Putney JW (2007). Phospholipase C-Coupled Receptors and Activation of TRPC Channels BT - Transient Receptor Potential (TRP) Channels. In, ed. Flockerzi V & Nilius B, pp. 593–614. Springer Berlin Heidelberg, Berlin, Heidelberg. Available at: https://doi.org/10.1007/978-3-540-34891-7_35.

Trimarco B, Lembo G, Ricciardelli B, N DL, Rendina V, Condorelli G & Volpe M (1991). Salt-induced plasticity in cardiopulmonary baroreceptor reflexes in salt-resistant hypertensive patients. *Hypertension* **18,** 483–493.

Trimble WS, Cowan DM & Scheller RH (1988). VAMP-1: a synaptic vesicle-associated integral membrane protein. *Proc Natl Acad Sci* **85,** 4538–4542.

Trippodo NC & Frohlich ED (1981). Similarities of genetic (spontaneous) hypertension. Man and rat. *Circ Res* **48,** 309–319.

Tsien RY (1981). A non-disruptive technique for loading calcium buffers and indicators into cells. *Nature* **290,** 527–528.

Tsien RY (1986). New tetracarboxylate chelators for fluorescence measurement and photochemical manipulation of cytosolic free calcium concentrations. *Soc Gen Physiol Ser* **40,** 327–345.

Tsuda K (2012). Renin-Angiotensin system and sympathetic neurotransmitter release in the central nervous system of hypertension. *Int J Hypertens* **2012,** 474870.

Tucker DC (1985). Components of functional sympathetic control of heart rate in neonatal rats. *Am J Physiol Integr Comp Physiol* **248,** R601–R610.

Tyzio R, Cossart R, Khalilov I, Minlebaev M, Hübner CA, Represa A, Ben-Ari Y & Khazipov R (2006). Maternal Oxytocin Triggers a Transient Inhibitory Switch in GABA Signaling in the Fetal Brain During Delivery. *Science (80- )* **314,** 1788 LP – 1792.

Vacher H, Mohapatra DP & Trimmer JS (2008). Localization and targeting of voltage-dependent ion channels in mammalian central neurons. *Physiol Rev* **88,** 1407–1447.

Vandewauw I, De Clercq K, Mulier M, Held K, Pinto S, Van Ranst N, Segal A, Voet T, Vennekens R, Zimmermann K, Vriens J & Voets T (2018). A TRP channel trio mediates acute noxious heat sensing. *Nature* **555,** 662–666.

Vanhoutte PM (1974). Inhibition by acetylcholine of adrenergic neurotransmission in vascular smooth muscle. *Circ Res* **34,** 317–326.

Varaschin RK, Osterstock G, Ducrot C, Leino S, Bourque MJ, Prado MAM, Prado VF, Salminen O, Rannanpää (née Nuutinen) S & Trudeau LE (2018). Histamine H3 Receptors Decrease Dopamine Release in the Ventral Striatum by Reducing the Activity of Striatal Cholinergic Interneurons. *Neuroscience* **376,** 188–203.

Vargas G, Akhtar M & Damato AN (1975). Electrophysiologic effects of isoproterenol on cardiac conduction system in man. *Am Heart J* **90,** 25–34.

Velazquez H & Wright FS (1986). Effects of diuretic drugs on Na, Cl, and K transport by rat renal distal tubule. *Am J Physiol Physiol* **250,** F1013–F1023.

Vergara RC, Jaramillo-Riveri S, Luarte A, Moënne-Loccoz C, Fuentes R, Couve A & Maldonado PE (2019). The Energy Homeostasis Principle: Neuronal Energy Regulation Drives Local Network Dynamics Generating Behavior. *Front Comput Neurosci* **13,** 49.

Verkerk AO, Remme CA, Schumacher CA, Scicluna BP, Wolswinkel R, De Jonge B, Bezzina CR & Veldkamp MW (2012). Functional NaV1.8 channels in intracardiac neurons: The link between SCN10A and cardiac electrophysiology. *Circ Res* **111,** 333–343.

Verney EB (1947). The antidiuretic hormone and the factors which determine its release. *Proc R Soc London Ser B, Contain Pap* **135,** 25–106.

Viatchenko-Karpinski V, Ling J & Gu JG (2018). Down-regulation of kv4.3 channels and a-type kþ currents in v2 trigeminal ganglion neurons of rats following oxaliplatin treatment. *Mol Pain* **14,** 1744806917750995.

Vincent M, Bornet H, Berthezene F, Dupont J & Sassard J (1978). Thyroid function and blood pressure in two new strains of spontaneously hypertensive and normotensive rats. *Clin Sci Mol Med* **54,** 391–395.

Virani SS et al. (2020). Heart disease and stroke statistics—2020 update: A report from the American Heart Association. *Circulation* **141,** E139–E596.

Vit J-P, Ohara PT, Bhargava A, Kelley K & Jasmin L (2008). Silencing the Kir4. 1 potassium channel subunit in satellite glial cells of the rat trigeminal ganglion results in pain-like behavior in the absence of nerve injury. *J Neurosci* **28,** 4161–4171.

Vivas O, Kruse M & Hille B (2014). Nerve growth factor sensitizes adult sympathetic neurons to the proinflammatory peptide bradykinin. *J Neurosci* **34,** 11959–11971.

Wadei HM & Textor SC (2012). The role of the kidney in regulating arterial blood pressure. *Nat Rev Nephrol* **8,** 602–609.

Wakade AR & Wakade TD (1988). Comparison of transmitter release properties of embryonic sympathetic neurons growing in vivo and in vitro. *Neuroscience* **27,** 1007–1019.

Walch-Solimena C, Takei K, Marek KL, Midyett K, Sudhof TC, De Camilli P & Jahn R (1993). Synaptotagmin: a membrane constituent of neuropeptide-containing large dense-core vesicles. *J Neurosci* **13,** 3895–3903.

Walkowska A, Kuczeriszka M, Sadowski J, Olszyñski KH, Dobrowolski L, Červenka L, Hammock BD & Kompanowska-Jezierska E (2015). High salt intake increases blood pressure in normal rats: putative role of 20-HETE and no evidence on changes in renal vascular reactivity. *Kidney Blood Press Res* **40,** 323–334.

Wallace AG & Sarnoff SJ (1964). Effects of cardiac sympathetic nerve stimulation on conduction in the heart. *Circ Res* **14,** 86–92.

Wallner M, Meera P & Toro L (1999). Molecular basis of fast inactivation in voltage and Ca2+-activated K+ channels: a transmembrane β-subunit homolog. *Proc Natl Acad Sci* **96,** 4137–4142.

Walsh GS, Krol KM & Kawaja MD (1999). Absence of the p75 neurotrophin receptor alters the pattern of sympathosensory sprouting in the trigeminal ganglia of mice overexpressing nerve growth factor. *J Neurosci* **19,** 258–273.

Wang HS, Brown BS, Mckinnon D & Cohen IS (2000). Molecular basis for differential sensitivity of KCNQ and I(Ks) channels to the cognitive enhancer XE991. *Mol Pharmacol* **57,** 1218–1223.

Wang HS & McKinnon D (1995). Potassium currents in rat prevertebral and paravertebral sympathetic neurones: control of firing properties. *J Physiol* **485,** 319–335.

Wang HS, Pan Z, Shi W, Brown BS, Wymore RS, Cohen IS, Dixon JE & McKinnon D (1998). KCNQ2 and KCNQ3 potassium channel subunits: Molecular correlates of the M-channel. *Science (80-)* **282,** 1890–1893.

Wang FC, Parcej DN & Dolly JO (1999). α Subunit compositions of Kv1.1-containing K+ channel subtypes fractionated from rat brain using dendrotoxins. *Eur J Biochem* **263,** 230–237.

Wang J, Ou S-W & Wang Y-J (2017). Distribution and function of voltage-gated sodium channels in the nervous system. *Channels (Austin)* **11,** 534–554.

Wang SS-H, Shultz JR, Burish MJ, Harrison KH, Hof PR, Towns LC, Wagers MW & Wyatt KD (2008*a*). Functional Trade-Offs in White Matter Axonal Scaling. *J Neurosci* **28,** 4047 LP – 4056.

Wang T, Li B, Nelson CE & Nabavi S (2019). Comparative analysis of differential gene expression analysis tools for single-cell RNA sequencing data. *BMC Bioinformatics* **20,** 40.

Wang X, Takeya K, Aaronson PI, Loutzenhiser K & Loutzenhiser R (2008*b*). Effects of amiloride, benzamil, and alterations in extracellular Na + on the rat afferent arteriole and its myogenic response. *Am J Physiol - Ren Physiol* **295,** F272–F282.

Wang Z & Qiu P (2018). Count data monitoring: Parametric or nonparametric? *Qual Reliab Eng Int* **34,** 1763–1774.

Warner MR & Levy MN (1990). Sinus and atrioventricular nodal distribution of sympathetic fibers that contain neuropeptide Y. *Circ Res* **67,** 713–721.

Watanabe E, Hiyama TY, Shimizu H, Kodama R, Hayashi N, Miyata S, Yanagawa Y, Obata K & Noda M (2006). Sodium-level-sensitive sodium channel Nax is expressed in glial laminate processes in the sensory circumventricular organs. *Am J Physiol - Regul Integr Comp Physiol* **290,** R568–R576.

Watanabe T, Ito T, Inoue G, Ohtori S, Kitajo K, Doya H, Takahashi K & Yamashita T (2008). The p75 receptor is associated with inflammatory thermal hypersensitivity. *J Neurosci Res* **86,** 3566–3574.

Watson AMD, Mogulkoc R, McAllen RM & May CN (2004). Stimulation of cardiac sympathetic nerve activity by central angiotensinergic mechanisms in conscious sheep. *Am J Physiol - Regul Integr Comp Physiol* **286,** R1051–R1056.

Weiss ML, Claassen DE, Hirai T & Kenney MJ (1996). Nonuniform sympathetic nerve responses to

intravenous hypertonic saline infusion. *J Auton Nerv Syst* **57,** 109–115.

van Weperen VY-SH, Contreras J, Littman R & Ajijola OA (2020). Single-cell RNA Sequencing reveals molecular heterogeneity of glia within mouse sympathetic ganglia. *FASEB J* **34,** 1–1.

West AE, Chen WG, Dalva MB, Dolmetsch RE, Kornhauser JM, Shaywitz AJ, Takasu MA, Tao X & Greenberg ME (2001). Calcium regulation of neuronal gene expression. *Proc Natl Acad Sci* **98,** 11024 LP – 11031.

Whelton PK, Carey RM, Aronow WS, Casey DE, Collins KJ, Himmelfarb CD, DePalma SM, Gidding S, Jamerson KA & Jones DW (2018). 2017 ACC/AHA/AAPA/ABC/ACPM/AGS/APhA/ASH/ASPC/NMA/PCNA guideline for the prevention, detection, evaluation, and management of high blood pressure in adults: a report of the American College of Cardiology/American Heart Association Task Force on Clinical Pr. *J Am Coll Cardiol* **71,** e127–e248.

Wickenden AD, Zou A, Wagoner PK & Jegla T (2001). Characterization of KCNQ5/Q3 potassium channels expressed in mammalian cells. *Br J Pharmacol* **132,** 381–384.

Williams SR & Mitchell SJ (2008). Direct measurement of somatic voltage clamp errors in central neurons. *Nat Neurosci* **11,** 790.

Wise AK, Pujol R, Landry TG, Fallon JB & Shepherd RK (2017). Structural and Ultrastructural Changes to Type I Spiral Ganglion Neurons and Schwann Cells in the Deafened Guinea Pig Cochlea. *J Assoc Res Otolaryngol* **18,** 751–769.

Wiysonge CS, Bradley HA, Volmink J, Mayosi BM & Opie LH (2017). Beta-blockers for hypertension. *Cochrane Database Syst Rev*; DOI: 10.1002/14651858.CD002003.pub5.

Wladyka CL, Feng B, Glazebrook PA, Schild JH & Kunze DL (2008). The KCNQ/M-current modulates arterial baroreceptor function at the sensory terminal in rats. *J Physiol* **586,** 795–802.

Wong GWK, Boyda HN & Wright JM (2014). Blood pressure lowering efficacy of partial agonist beta blocker monotherapy for primary hypertension. *Cochrane database Syst Rev* **2014,** CD007450–CD007450.

Wright SH (2004). Generation of resting membrane potential. *Adv Physiol Educ* **28,** 139–142.

Xia X-M, Zeng X & Lingle CJ (2002). Multiple regulatory sites in large-conductance calcium-activated potassium channels. *Nature* **418,** 880–884.

Xia XM, Fakler B, Rivard A, Wayman G, Johnson-Pais T, Keen JE, Ishii T, Hirschberg B, Bond CT, Lutsenko S, Maylie J & Adelman JP (1998). Mechanism of calcium gating in small-conductance calcium-activated potassium channels. *Nature* **395,** 503–507.

Xiao Q, Yu K, Perez-Cornejo P, Cui Y, Arreola J & Hartzell HC (2011). Voltage- and calcium-dependent gating of TMEM16A/Ano1 chloride channels are physically coupled by the first intracellular loop. *Proc Natl Acad Sci* **108,** 8891 LP – 8896.

Xiao RP & Lakatta EG (1993). Beta 1-adrenoceptor stimulation and beta 2-adrenoceptor stimulation differ in their effects on contraction, cytosolic Ca2+, and Ca2+ current in single rat ventricular cells. *Circ Res* **73,** 286–300.

Xie J & McCobb DP (1998). Control of Alternative Splicing of Potassium Channels by Stress Hormones. *Science (80- )* **280,** 443 LP – 446.

Xie W, Strong JA & Zhang JM (2015). Local knockdown of the NaV1.6 sodium channel reduces pain behaviors, sensory neuron excitability, and sympathetic sprouting in rat models of

neuropathic pain. *Neuroscience* **291,** 317–330.

Xiong L, Liu Y, Zhou M, Wang G, Quan D, Shen C, Shuai W, Kong B, Huang C & Huang H (2018). Targeted ablation of cardiac sympathetic neurons improves ventricular electrical remodelling in a canine model of chronic myocardial infarction. *EP Eur* **20,** 2036–2044.

Xiuying M, W. CM, A. WC, M. AF & Klaus B (2001). Angiotensin Selectively Activates a Subpopulation of Postganglionic Sympathetic Neurons in Mice. *Circ Res* **88,** 787–793.

Xu H, Blair NT & Clapham DE (2005). Camphor Activates and Strongly Desensitizes the Transient Receptor Potential Vanilloid Subtype 1 Channel in a Vanilloid-Independent Mechanism. *J Neurosci* **25,** 8924 LP – 8937.

Xu H, Delling M, Jun JC & Clapham DE (2006). Oregano, thyme and clove-derived flavors and skin sensitizers activate specific TRP channels. *Nat Neurosci* **9,** 628–635.

Xu J, Mashimo T & Südhof TC (2007). Synaptotagmin-1,-2, and-9: Ca2+ sensors for fast release that specify distinct presynaptic properties in subsets of neurons. *Neuron* **54,** 567–581.

Yamada-Hanff J & Bean BP (2015). Activation of I h and TTX-sensitive sodium current at subthreshold voltages during CA1 pyramidal neuron firing. *J Neurophysiol* **114,** 2376–2389.

Yan L, Figueroa DJ, Austin CP, Liu Y, Bugianesi RM, Slaughter RS, Kaczorowski GJ & Kohler MG (2004). Expression of Voltage-Gated Potassium Channels in Human and Rhesus Pancreatic Islets. *Diabetes* **53,** 597 LP – 607.

Yang E-K, Alvira MR, Levitan ES & Takimoto K (2001). Kvβ Subunits Increase Expression of Kv4.3 Channels by Interacting with Their C Termini *. *J Biol Chem* **276,** 4839–4844.

Yang H, Zhang G & Cui J (2015). BK channels: Multiple sensors, one activation gate. *Front Physiol* **6,** 29. Available at: https://www.frontiersin.org/article/10.3389/fphys.2015.00029.

Yang N & Horn R (1995). Evidence for voltage-dependent S4 movement in sodium channels. *Neuron* **15,** 213–218.

Yang Q, Sumner AD, Puhl HL & Ruiz-Velasco V (2006). M1 and M2 muscarinic acetylcholine receptor subtypes mediate Ca2+ channel current inhibition in rat sympathetic stellate ganglion neurons. *J Neurophysiol* **96,** 2479–2487.

Yang R & Liang BT (2012). Cardiac P2X 4 receptors: Targets in ischemia and heart failure? *Circ Res* **111,** 397–401.

Yang T, Atack TC, Stroud DM, Zhang W, Hall L & Roden DM (2012). Blocking Scn10a channels in heart reduces late sodium current and is antiarrhythmic. *Circ Res* **111,** 322–332.

Yang YD, Cho H, Koo JY, Tak MH, Cho Y, Shim W-S, Park SP, Lee J, Lee B, Kim B-M, Raouf R, Shin YK & Oh U (2008). TMEM16A confers receptor-activated calcium-dependent chloride conductance. *Nature* **455,** 1210–1215.

Yarowsky P & Weinreich D (1985). Loss of accommodation in sympathetic neurons from spontaneously hypertensive rats. *Hypertension* **7,** 268–276.

Yatabe MS, Yatabe J & Yoneda M (2010). Salt sensitivity is associated with insulin resistance, sympathetic overactivity, and decreased suppression of circulating renin activity in lean patients with essential hypertension (American Journal of Clinical Nutrition (2010) 92, (77-82)). *Am J Clin Nutr* **92,** 1002.

Yokoyama T, Settai K, Nakamuta N & Yamamoto Y (2019). Distribution and morphology of

baroreceptors in the rat carotid sinus as revealed by immunohistochemistry for P2X3 purinoceptors. *Histochem Cell Biol* **151,** 161–173.

Yoshida T, Inoue R, Morii T, Takahashi N, Yamamoto S, Hara Y, Tominaga M, Shimizu S, Sato Y & Mori Y (2006). Nitric oxide activates TRP channels by cysteine S-nitrosylation. *Nat Chem Biol* **2,** 596–607.

You D, Loufrani L, Baron C, Levy BI, Widdop RE & Henrion D (2005). High blood pressure reduction reverses angiotensin II type 2 receptor–mediated vasoconstriction into vasodilation in spontaneously hypertensive rats. *Circulation* **111,** 1006–1011.

Yu G, Wang LG, Han Y & He QY (2012). ClusterProfiler: An R package for comparing biological themes among gene clusters. *Omi A J Integr Biol* **16,** 284–287.

Yu L, Wang M, Hu D, Huang B, Zhou L, Zhou X, Wang Z, Wang S & Jiang H (2017). Blocking the Nav1.8 channel in the left stellate ganglion suppresses ventricular arrhythmia induced by acute ischemia in a canine model. *Sci Rep* **7,** 534.

Yuan A, Santi CM, Wei A, Wang ZW, Pollak K, Nonet M, Kaczmarek L, Crowder CM & Salkoff L (2003). The sodium-activated potassium channel is encoded by a member of the Slo gene family. *Neuron* **37,** 765–773.

Yue Z, Xie J, Yu AS, Stock J, Du J & Yue L (2015). Role of trp channels in the cardiovascular system. *Am J Physiol - Hear Circ Physiol* **308,** H157–H182.

Zaccolo M & Pozzan T (2002). Discrete microdomains with high concentration of cAMP in stimulated rat neonatal cardiac myocytes. *Science (80- )* **295,** 1711–1715.

Zaglia T & Mongillo M (2017). Cardiac sympathetic innervation, from a different point of (re)view. *J Physiol* **595,** 3919–3930.

Zagotta WN, Olivier NB, Black KD, Young EC, Olson R & Gouaux E (2003). Structural basis for modulation and agonist specificity of HCN pacemaker channels. *Nature* **425,** 200–205.

Zaika O, Lara LS, Gamper N, Hilgemann DW, Jaffe DB & Shapiro MS (2006). Angiotensin II regulates neuronal excitability via phosphatidylinositol 4,5-bisphosphate-dependent modulation of Kv7 (M-type) K+ channels. *J Physiol* **575,** 49–67.

Zaika O, Zhang J & Shapiro MS (2011). Functional role of M-type (KCNQ) K+ channels in adrenergic control of cardiomyocyte contraction rate by sympathetic neurons. *J Physiol* **589,** 2559–2568.

Zandany N, Marciano S, Magidovich E, Frimerman T, Yehezkel R, Shem-Ad T, Lewin L, Abdu U, Orr I & Yifrach O (2015). Alternative splicing modulates Kv channel clustering through a molecular ball and chain mechanism. *Nat Commun* **6,** 6488.

Zemel BM, Ritter DM, Covarrubias M & Muqeem T (2018). A-Type KV Channels in Dorsal Root Ganglion Neurons: Diversity, Function, and Dysfunction. *Front Mol Neurosci* **11,** 253. Available at: https://www.frontiersin.org/article/10.3389/fnmol.2018.00253.

Zeng W-Z, Marshall KL, Min S, Daou I, Chapleau MW, Abboud FM, Liberles SD & Patapoutian A (2018). PIEZOs mediate neuronal sensing of blood pressure and the baroreceptor reflex. *Science* **362,** 464–467.

Zhang B, Li M, Wang L, Li C, Lou Y, Liu J, Liu Y, Wang Z & Wen S (2015). The Association between the Polymorphisms in a Sodium Channel Gene SCN7A and Essential Hypertension: A Case-Control Study in the Northern Han Chinese. *Ann Hum Genet* **79,** 28–36.

Zhang DY & Anderson AS (2014). The Sympathetic Nervous System and Heart Failure. *Cardiol Clin* **32,** 33–45.

Zhang H, Craciun LC, Mirshahi T, Rohács T, Lopes CMB, Jin T & Logothetis DE (2003). PIP2 activates KCNQ channels, and its hydrolysis underlies receptor-mediated inhibition of M currents. *Neuron* **37,** 963–975.

Zhang L, Zhang X, Zhang G, Pang CP, Leung YF, Zhang M & Zhong W (2017). Expression profiling of the retina of pde6c, a zebrafish model of retinal degeneration. *Sci Data* **4,** 1–9.

Zhang S, Li X, Lin Q & Wong KC (2020). Review of single-cell RNA-seq data clustering for cell type identification and characterization. *arXiv*.

Zhang XF, Shieh CC, Chapman ML, Matulenko MA, Hakeem AH, Atkinson RN, Kort ME, Marron BE, Joshi S, Honore P, Faltynek CR, Krafte DS & Jarvis MF (2010). A-887826 is a structurally novel, potent and voltage-dependent Nav1.8 sodium channel blocker that attenuates neuropathic tactile allodynia in rats. *Neuropharmacology* **59,** 201–207.

Zhang Z (2016). Introduction to machine learning: K-nearest neighbors. *Ann Transl Med* **4,** 218.

Zheng GXY et al. (2017). Massively parallel digital transcriptional profiling of single cells. *Nat Commun* **8,** 14049.

Zhou B et al. (2017). Worldwide trends in blood pressure from 1975 to 2015: a pooled analysis of 1479 population-based measurement studies with 19·1 million participants. *Lancet* **389,** 37–55.

Zhou B et al. (2019). Long-term and recent trends in hypertension awareness, treatment, and control in 12 high-income countries: an analysis of 123 nationally representative surveys. *Lancet* **394,** 639–651.

Zhou Q, Hu J, Guo Y, Zhang F, Yang X, Zhang L, Xu X, Wang L, Wang H & Hou Y (2013). Effect of the stellate ganglion on atrial fibrillation and atrial electrophysiological properties and its left-right asymmetry in a canine model. *Exp Clin Cardiol* **18,** 38–42.

Zhu Y & Ikeda SR (1993). Adenosine modulates voltage-gated Ca2+ channels in adult rat sympathetic neurons. *J Neurophysiol* **70,** 610–620.

Zimmerman BG, Brody MJ & Beck L (1960). Mechanism of the cardiac output reduction by hexamethonium. *Am J Physiol Content* **199,** 319–324.